X-RAY DIFFRACTION

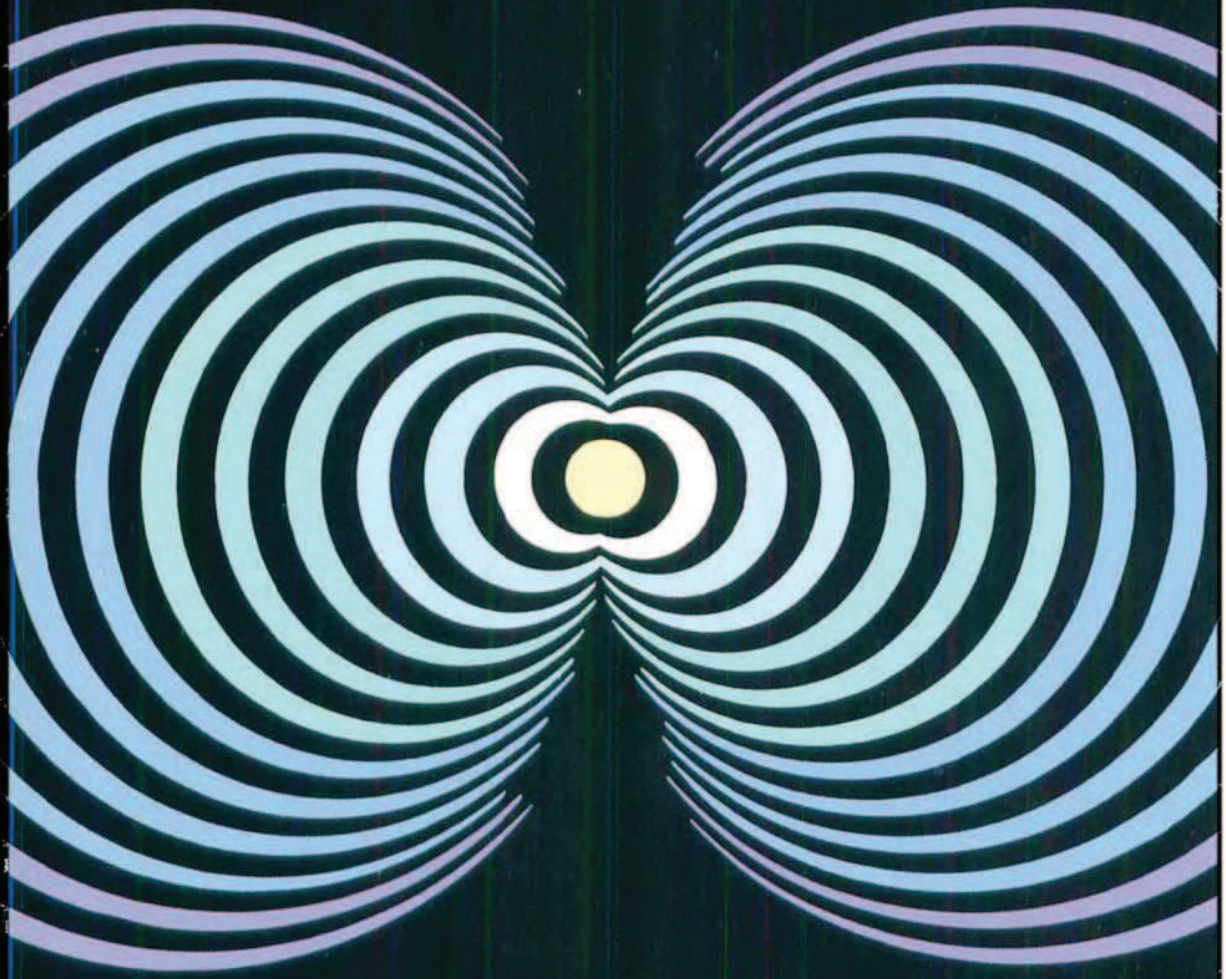

B.E. Warren

DOVER BOOKS ON PHYSICS

METHODS OF QUANTUM FIELD THEORY IN STATISTICAL PHYSICS, A.A. Abrikosov et al. (63228-8)

ELECTRODYNAMICS AND CLASSICAL THEORY OF FIELDS AND PARTICLES, A.O. Barut. (64038-8)

DYNAMIC LIGHT SCATTERING: WITH APPLICATIONS TO CHEMISTRY, BIOLOGY, AND PHYSICS, Bruce J. Berne and Robert Pecora. (41155-9)

QUANTUM THEORY, David Bohm. (65969-0)

ATOMIC PHYSICS (8TH EDITION), Max Born. (65984-4)

EINSTEIN'S THEORY OF RELATIVITY, Max Born. (60769-0)

INTRODUCTION TO HAMILTONIAN OPTICS, H.A. Buchdahl. (67597-1)

MATHEMATICS OF CLASSICAL AND QUANTUM PHYSICS, Frederick W. Byron, Jr. and Robert W. Fuller. (67164-X)

MECHANICS, J.P. Den Hartog. (60754-2)

INVESTIGATIONS ON THE THEORY OF THE BROWNIAN MOVEMENT, Albert Einstein. (60304-0)

THE PRINCIPLE OF RELATIVITY, Albert Einstein, et al. (60081-5)

THE PHYSICS OF WAVES, William C. Elmore and Mark A. Heald. (64926-1)

THERMODYNAMICS, Enrico Fermi. (60361-X)

INTRODUCTION TO MODERN OPTICS, Grant R. Fowles. (65957-7)

DIALOGUES CONCERNING TWO NEW SCIENCES, Galileo Galilei. (60099-8)

GROUP THEORY AND ITS APPLICATION TO PHYSICAL PROBLEMS, Morton Hamermesh. (66181-4)

ELECTRONIC STRUCTURE AND THE PROPERTIES OF SOLIDS: THE PHYSICS OF THE CHEMICAL BOND, Walter A. Harrison. (66021-4)

SOLID STATE THEORY, Walter A. Harrison. (63948-7)

PHYSICAL PRINCIPLES OF THE QUANTUM THEORY, Werner Heisenberg. (60113-7)

ATOMIC SPECTRA AND ATOMIC STRUCTURE, Gerhard Herzberg. (60115-3)

AN INTRODUCTION TO STATISTICAL THERMODYNAMICS, Terrell L. Hill. (65242-4)

EQUILIBRIUM STATISTICAL MECHANICS, E. Atlee Jackson (41185-0)

OPTICS AND OPTICAL INSTRUMENTS: AN INTRODUCTION, B.K. Johnson. (60642-2)

THEORETICAL SOLID STATE PHYSICS, VOLS. I & II, William Jones and Norman H. March. (65015-4, 65016-2)

THEORETICAL PHYSICS, Georg Joos, with Ira M. Freeman. (65227-0)

THE VARIATIONAL PRINCIPLES OF MECHANICS, Cornelius Lanczos. (65067-7)

A GUIDE TO FEYNMAN DIAGRAMS IN THE MANY-BODY PROBLEM, Richard D. Mattuck. (67047-3)

MATTER AND MOTION, James Clerk Maxwell. (66895-9)

FUNDAMENTAL FORMULAS OF PHYSICS, VOLS. I & II, Donald H. Menzel (ed.). (60595-7, 60596-5)

OPTICKS, Sir Isaac Newton. (60205-2)

THEORY OF RELATIVITY, W. Pauli. (64152-X)

(continued on back flap)

X-RAY DIFFRACTION

B. E. WARREN
Professor Emeritus of Physics
Massachusetts Institute of Technology

DOVER PUBLICATIONS, INC., NEW YORK

Copyright © 1969, 1990 by B. E. Warren.
All rights reserved under Pan American and International Copyright Conventions.

This Dover edition, first published in 1990, is an unabridged and corrected republication of the work originally published in 1969 by Addison-Wesley Publishing Company, Inc., Reading, Mass., as part of the Addison-Wesley Series in Metallurgy and Materials.

Manufactured in the United States of America
Dover Publications, Inc., 31 East 2nd Street, Mineola, N.Y. 11501

Library of Congress Cataloging-in-Publication Data

Warren, B. E. (Bertram Eugene), 1902-
X-ray diffraction / B. E. Warren.
p. cm.
Reprint. Originally published: Reading, Mass. : Addison-Wesley Pub. Co., 1969. Originally published in series: Addison-Wesley series in metallurgy and materials.
Includes bibliographical references.
ISBN 0-486-66317-5
1. X-rays—Diffraction. 2. X-ray crystallography. I. Title.
QD945.W33 1990
548'.83—dc20 89-78470
CIP

PREFACE

The material presented in this book is the outgrowth of a series of lectures given to graduate students in physics and metallurgy at the Massachusetts Institute of Technology. The emphasis is on a rigorous development of the basic diffraction theory. Throughout the book, the treatment is carried far enough to relate to experimentally observable quantities, even though this often requires rather long and wearisome manipulations. Although the elements of crystal structure determination are presented, the book is not intended to cover the details of structure determination. The main part of the book is devoted to the application of x-ray diffraction methods to non-structural problems such as temperature vibration effects, order-disorder, crystal imperfections, the structure of amorphous materials, and the diffraction of x-rays in perfect crystals. The treatment of perfect crystal theory is not intended for the specialists in this field, but rather for the large group of x-ray diffraction people who are only interested in a simple survey which can be easily understood. For this reason the treatment is based on the Darwin approach rather than on the more elegant Ewald-von Laue formulation, since the former is much more closely related to the kinematical theory, and more readily applied to various related problems.

Discussions of experimental apparatus and procedures have been minimized, since this subject is thoroughly covered in books such as that of Klug and Alexander, *X-Ray Diffraction Procedures.* Similarly the subject of small angle x-ray scattering has been omitted, since it is already well covered in the several books by Guinier. Various applications of metallurgical interest, such as stress analysis and texture studies, are omitted because they are already covered in books such as Cullity, *Elements of X-Ray Diffraction.*

It is not possible to get a real understanding of a subject unless one does something with it himself, preferably something involving a little originality. Hence for the benefit of the serious student, problems are given at the end of each chapter; some of them are rather involved.

It has been well said, "If you would a teacher be, by your students you will be taught." This is correct, and I take this opportunity to express my thanks to a large group of graduate students from whom I have learned a great deal. In particular, I am indebted to Dr. C. B. Walker who kindly

wrote Section 11.9, to Drs. B. W. Batterman and H. Cole for many valuable discussions of perfect crystal theory, and to Dr. B. Borie for making available to me in advance his Darwin formulation of the Borrmann effect and for many valuable discussions. My thanks are due to Dr. Norman Henry, editor of the *International Tables for X-Ray Crystallography*, for permission to take from these tables the numerical data in Appendices II–VI. Finally, it is a pleasure to express my thanks to Mrs. Elaine Cook for her patience and diligence in preparing the typed manuscript.

Cambridge, Massachusetts B. E. W.
August 1968

CONTENTS

Chapter 1 X-Ray Scattering by Atoms

1.1 Classical scattering by a free electron 1
1.2 Polarization by scattering 4
1.3 Scattering from several centers, complex representation . . 5
1.4 Scattering by an atom 7

Chapter 2 Crystal Axes and the Reciprocal Lattice

2.1 Crystal axes 15
2.2 The crystallographic planes *hkl* 16
2.3 Reciprocal vectors and the reciprocal lattice 16
2.4 The sphere of reflection 19
2.5 Spacing formulae 20
2.6 The 14 Bravais lattices 22
2.7 Transforming axes and indices 24

Chapter 3 Diffraction by a Small Crystal

3.1 Intensity from a small crystal 27
3.2 The 3 Laue equations 30
3.3 Structure factor for a Bragg reflection 31
3.4 Effect of temperature vibration on the intensity from a small crystal 35

Chapter 4 The Integrated Intensity

4.1 Integrated intensity from a small single crystal 41
4.2 The extended face imperfect crystal 45
4.3 The integrated intensity for a powder sample 47

Chapter 5 The Powder Method

5.1 Powder patterns by film recording 51
5.2 Diffractometer recording of power patterns 54
5.3 Analysis of a cubic powder pattern by diffractometer recording 57
5.4 Analysis of a hexagonal powder pattern 62

5.5 Analysis of orthorhombic powder patterns 66
5.6 Precision axial length measurements 67

Chapter 6 The Laue Method

6.1 The transmission Laue pattern 75
6.2 The back reflection Laue pattern 77

Chapter 7 The Rotation Method

7.1 The simple rotation pattern 85
7.2 Indexing of rotation patterns 88
7.3 The Weissenberg pattern 89
7.4 Fiber diagrams as rotation patterns 92

Chapter 8 The Use of Space Groups in Structure Determination

8.1 The space group Cmcm 95
8.2 Space group methods applied to Uranium 100

Chapter 9 Fourier Series Methods in Structure Determinations

9.1 Representation by Fourier series 105
9.2 Fourier series representation of the electron density 108
9.3 The Patterson function 112

Chapter 10 Scattering by Noncrystalline Forms of Matter

10.1 The general scattering equation for a random orientation . . 116
10.2 Gas of polyatomic molecules 117
10.3 Application to a crystalline powder 119
10.4 Liquid or amorphous solid with one kind of atom 120
10.5 Application to a simple liquid 123
10.6 Convergence factor and termination errors 127
10.7 Fourier inversion with the Beevers-Lipson strips 131
10.8 Approximate method for sample with more than one kind of atom 132
10.9 Exact method for an amorphous sample with more than one kind of atom 135

10.10 Amorphous scattering from a flat-faced diffractometer sample . 142
10.11 Multiple scattering from amorphous samples 145

Chapter 11 The Effect of Temperature Vibration on X-Ray Diffraction

11.1 Introduction 151
11.2 Long wavelength elastic waves in a cubic crystal 152
11.3 Restrictions due to the lattice nature and finite size of the sample 156
11.4 Intensity from a cubic crystal with one atom per cell . . . 159
11.5 The first-order temperature diffuse scattering 163
11.6 The second-order temperature diffuse scattering 165
11.7 The measurement of temperature diffuse scattering 169
11.8 Interpretation of temperature diffuse scattering measurements . 174
11.9 Determination of the interatomic force constants from temperature scattering 178
11.10 Evaluation of $2M$ 189
11.11 Temperature diffuse scattering for cubic powder patterns . . 193
11.12 Existence of an inversion temperature for the diffuse scattering 201

Chapter 12 X-Ray Studies of Order-Disorder

12.1 Introduction 206
12.2 Long-range order in binary compositions 208
12.3 Antiphase domains 216
12.4 Short-range order diffuse intensity 227
12.5 Effect of temperature vibration on short-range order intensities 237
12.6 Size effect in disordered binary compositions 241
12.7 Experimental measurements of short-range order intensity . . 245

Chapter 13 Diffraction by Imperfect Crystals

13.1 Particle size broadening 251
13.2 Corrections for instrumental broadening 257
13.3 Powder pattern power theorem 262
13.4 Small coherent domains and strains 264

13.5 Effects of deformation and twin faulting in FCC metals . . 275
13.6 Effects of deformation and twin faulting in HCP metals . . 298
13.7 Effect of deformation and twin faults in BCC metals . . . 305
13.8 General remarks 312

Chapter 14 Perfect Crystal Theory

14.1 Introduction 315
14.2 The Darwin treatment for Bragg reflection 316
14.3 Bragg reflection for a thick crystal with negligible absorption . 324
14.4 Width of a Bragg reflection 329
14.5 Extinction 331
14.6 Bragg reflection when the reflecting power is small 333
14.7 Bragg reflection with absorption 335
14.8 The symmetrical Laue case and the Borrmann effect . . . 339
14.9 Asymmetric Bragg reflection 348

Appendix I The Kinematical Integrated Intensity By Fresnel Diffraction 359

Appendix II Wavelengths (in Angstroms) of Some Characteristic Emission Lines and Absorption Edges . . . 364

Appendix III Mass Absorption Coefficients μ_m of the Elements (Z = 1 to 83) For a Selection of Wavelengths . . 366

Appendix IV Atomic Scattering Factors 369

Appendix V Dispersion Corrections for Atomic Scattering Factors 372

Appendix VI Compton-Scattering Intensities I_{inc}/R with Exchange Terms Based on Hartree-Fock Wave Functions . . 374

Index 377

X-RAY SCATTERING BY ATOMS

1.1 CLASSICAL SCATTERING BY A FREE ELECTRON

When an x-ray beam falls on an atom, two processes may occur: (1) the beam may be absorbed with an ejection of electrons from the atom, or (2) the beam may be scattered. We shall first consider the scattering process in terms of classical theory. The primary beam is an electromagnetic wave with electric vector varying sinusoidally with time and directed perpendicular to the direction of propagation of the beam. This electric field exerts forces on the electrons of the atom producing accelerations of the electrons. Following classical electromagnetic theory, an accelerated charge radiates. This radiation, which spreads out in all directions from the atom, has the same frequency as the primary beam, and it is called scattered radiation.

We shall first consider the scattering from a single free electron following classical theory. One might suppose that this is a waste of time, since we know that x-ray scattering does not follow classical theory. Experimentally we observe both an unmodified scattering with the same wavelength as the primary beam, and a Compton modified scattering with a longer wavelength. Classical theory predicts only the unmodified scattering. However, there are several reasons why the intensity of classical scattering is extremely important for much of what we shall do. (1) The correct wave mechanical treatment of scattering shows that the sum of the intensities of unmodified and modified scattering from each individual electron in the atom is closely equal to the classical intensity per electron. (2) The quantitative unit in which it is convenient to express the scattered intensity from a sample is the electron unit. An intensity in electron units I_{eu} is the intensity from a sample divided by the classical intensity from a single electron. (3) The polarization of both the unmodified and the modified scattering is given correctly by the classical treatment.

Let us consider a single free electron at the origin of Fig. 1.1, with an unpolarized primary beam directed along the X-axis. We are interested in the intensity of scattered radiation at a point P which is at a distance R from the electron at an angle ϕ with the X-axis. We choose the other axes so that the point P is in the XY-plane. Since the primary beam is unpolarized, the electric vector takes with equal probability all orientations in the YZ-plane.

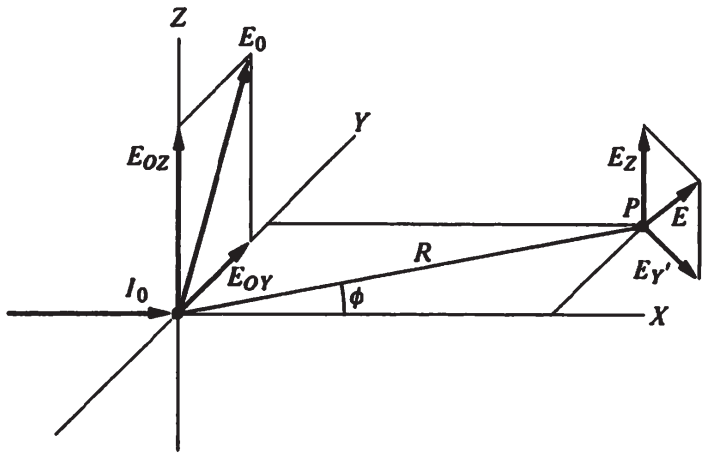

Fig. 1.1 Classical scattering of an unpolarized primary beam by a single free electron at the origin.

We can choose one direction E_0 and later average over all directions. Since it is a vector, E_0 can be resolved into components $E_{0Y'}$ and E_{0Z}. If ν is the frequency of the primary beam, the instantaneous values of the electric fields are

$$\epsilon_{0Y'} = E_{0Y'} \sin 2\pi\nu t, \qquad \epsilon_{0Z} = E_{0Z} \sin 2\pi\nu t.$$

Considering first the component $\epsilon_{0Y'}$, a force is exerted on the electron which produces a Y-component of acceleration

$$a_{Y'} = \frac{f_{Y'}}{m} = \frac{eE_{0Y'}}{m} \sin 2\pi\nu t,$$

where e and m are the charge and mass of the electron.

From electromagnetic theory an accelerated charge radiates. Figure 1.2 illustrates a charge q with an acceleration **a**, and at distance R, the electric field ϵ which results from the acceleration. In terms of cgs units, which for x-ray scattering are the simplest, the electric field is given by

$$\epsilon = \frac{qa \sin \alpha}{c^2 R}, \tag{1.1}$$

where c is the velocity of light. The electric field is in the plane of R and a, and its magnitude depends upon the component $a \sin \alpha$. This leads to a very

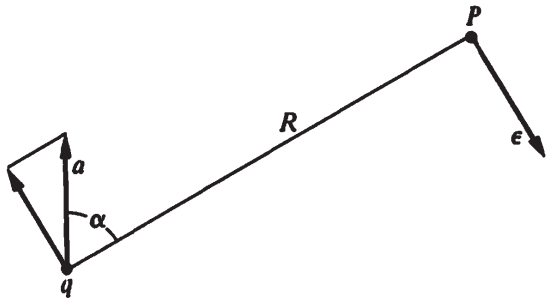

Fig. 1.2 Illustration of the electric field ϵ, produced by a charge q with acceleration a, according to classical electromagnetic theory.

simple and useful rule in considering problems of scattering and polarization. With the eye placed at the point of observation P, the component of acceleration $a \sin \alpha$, which is seen, determines the electric field produced.

By means of Eq. (1.1), we can now express the instantaneous value of the electric field due to the acceleration $a_{1'}$:

$$\epsilon_{1'} = \frac{e^2 E_{0Y}}{mc^2 R} \sin 2\pi\nu t \cos \phi.$$

Expressed in terms of an amplitude, $\epsilon_{1'} = E_{1'} \sin 2\pi\nu t$ where the amplitude is given by

$$E_{1'} = \frac{e^2 E_{01}}{mc^2 R} \cos \phi.$$

Similar reasoning applied to the initial amplitude E_{0Z} leads to

$$E_Z = \frac{e^2 E_{0Z}}{mc^2 R}.$$

The resultant amplitude E at the point of observation is then given by

$$E^2 = E_Z^2 + E_{1'}^2 = \frac{e^4}{m^2 c^4 R^2} (E_{0Z}^2 + E_{0Y}^2 \cos^2 \phi).$$

We now let E_0 take with equal probability all orientations in the YZ-plane and consider the appropriate averages

$$\langle E_{01'}^2 \rangle + \langle E_{0Z}^2 \rangle = \langle E_0^2 \rangle.$$

Since the Y- and Z-axes are equivalent,

$$\langle E_{01'}^2 \rangle = \langle E_{0Z}^2 \rangle = \tfrac{1}{2} \langle E_0^2 \rangle$$

and

$$\langle E^2 \rangle = \langle E_0^2 \rangle \frac{e^4}{m^2 c^4 R^2} \left(\frac{1 + \cos^2 \phi}{2} \right). \tag{1.2}$$

The observable quantity is the intensity I, where by intensity we shall always mean energy per unit area per unit time. In cgs units, the intensity is given by

$$I = \frac{c}{8\pi} \langle E^2 \rangle,$$

where E is the amplitude or maximum value of a sinusoidally varying field. Multiplying both sides of Eq. (1.2) by $c/8\pi$, we obtain

$$I = I_0 \frac{e^4}{m^2 c^4 R^2} \left(\frac{1 + \cos^2 \phi}{2} \right). \tag{1.3}$$

Equation (1.3) gives the intensity of classical scattering by a single free electron, and it is often called the Thomson scattering equation. The factor $(1 + \cos^2 \phi)/2$ is called the polarization factor for an unpolarized primary beam. If the primary beam is not unpolarized, the polarization factor takes a different form. The numerical value involved in Eq. (1.3) is important. Since we are using cgs units, R is in cms, and

$$\frac{e^4}{m^2c^4} = \frac{(4.802 \times 10^{-10})^4}{(9.107 \times 10^{-28})^2(2.998 \times 10^{10})^4} = 7.94 \times 10^{-26} \text{ cm}^2.$$

At a few centimeters from a single electron, the ratio I/I_0 is therefore of the order 10^{-26}, and one might think that the intensity of scattered x-rays would be far too small to measure. However when we recall that in even 1 milligram of matter the number of electrons is approximately 10^{20}, we see that the intensity of scattered radiation from a sample of matter is not necessarily too small to measure.

1.2 POLARIZATION BY SCATTERING

For x-rays there are no Nicol prisms or polaroid sheets to produce polarization. However, scattering at any angle will produce partial polarization, and scattering at 90° produces complete linear polarization. An example of a polarizer and analyzer is given by Fig. 1.3. An unpolarized x-ray beam directed along the X-axis falls on a scatterer such as a block of carbon at O.

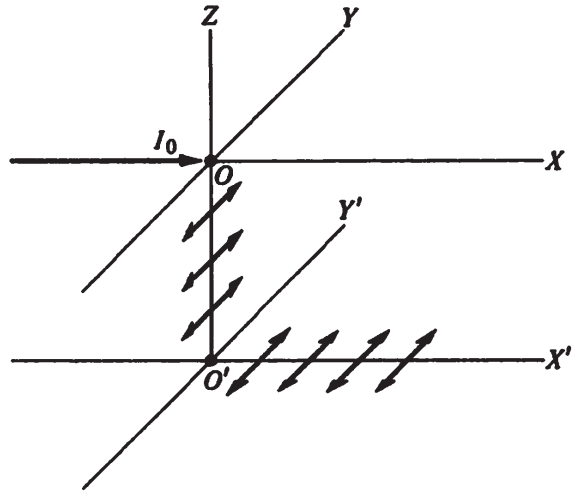

Fig. 1.3 A double scattering experiment which illustrates the production of a polarized beam by scattering at 90°, and the analysis of the polarized beam by a second scattering at 90°.

The electrons in the block are accelerated in all directions in the YZ-plane. To determine the nature of the scattered radiation from O to O', we use the rule which was discussed in connection with Eq. (1.1). Placing the eye at O' and looking back toward the scatterer at O, we see only the Y-component of the electron accelerations. Hence the scattered radiation from O to O' will be linearly polarized with electric field in the Y-direction. The scattering at 90° has produced a polarized beam.

To analyze the polarization, imagine a second scatterer at O'. The electrons at O' will be accelerated only in the Y'-direction. With the eye placed at X', we see the full component of the Y'-acceleration, and hence there will be a scattered beam along the X'-axis, which is polarized with electric field in the Y'-direction. Placing the eye at Y', we see no component of the Y'-acceleration of the electrons and hence the intensity of scattering along the Y'-axis is zero. A recorder pivoted at O' and moving in the $X'Y'$-plane, would record a maximum at X' and zero at Y'. The second scattering at 90° plays the role of an analyzer.

Since the Bragg reflections from a crystal are nothing but sharp maxima in the scattered radiation, any Bragg reflection at approximately $2\theta = 90°$ is a linearly polarized beam. Scattering is often done with blocks of low atomic number such as carbon. In this case an appreciable fraction of the scattered intensity is due to the Compton modified component. However, the polarization of both the unmodified and the Compton modified scattering follows exactly the same rules that have been developed here for classical scattering.

1.3 SCATTERING FROM SEVERAL CENTERS, COMPLEX REPRESENTATION

Our next problem is to formulate a simple procedure for handling the scattering from several centers. In Fig. 1.4 we have a plane parallel beam directed toward the right. Scattering takes place from several centers, 1, 2, 3, n, and we are interested in the intensity of scattering at a point of observation P.

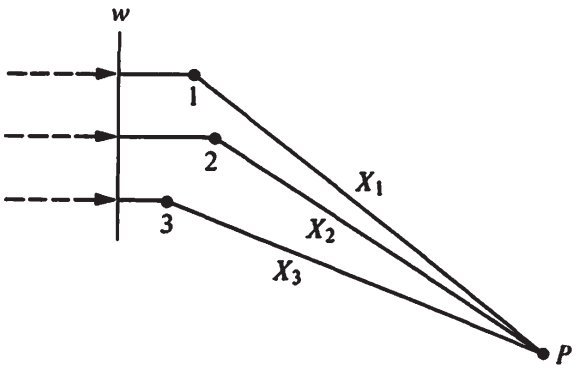

Fig. 1.4 Scattering of a plane parallel primary beam by several scattering centers. The lengths X_n are the total distances from a wave front W in the primary beam to the point of observation P.

The relative phases at P are determined by the path lengths X_1, X_2, X_3, X_n from a wave front W in the primary beam to the point P. The instantaneous value of the electric field at P, in each of the scattered waves, is given by the usual expression for a traveling wave:

$$\epsilon_n = E_n \cos\left(2\pi\nu t - \frac{2\pi X_n}{\lambda}\right), \tag{1.4}$$

where ν is the frequency, λ the wavelength, and the amplitudes E_1, E_2, E_n are, in general, different from one another. Expanded, the equations are written

$$\epsilon_n = E_n \cos 2\pi\nu t \cos 2\pi X_n/\lambda + E_n \sin 2\pi\nu t \sin 2\pi X_n/\lambda.$$

The resultant instantaneous field at P is given by the sum

$$\epsilon = \sum \epsilon_n = \cos 2\pi\nu t \sum E_n \cos \frac{2\pi X_n}{\lambda} + \sin 2\pi\nu t \sum E_n \sin \frac{2\pi X_n}{\lambda}.$$

Let

$$\begin{aligned} \sum E_n \cos \frac{2\pi X_n}{\lambda} &= E \cos \phi, \\ \sum E_n \sin \frac{2\pi X_n}{\lambda} &= E \sin \phi. \end{aligned} \tag{1.5}$$

With these abbreviations, the instantaneous field at P is given by

$$\epsilon = E(\cos 2\pi\nu t \cos \phi + \sin 2\pi\nu t \sin \phi) = E \cos (2\pi\nu t - \phi).$$

Hence the quantity E, which was introduced in Eqs. (1.5), is the amplitude of the resultant field at P. But the only quantity that we can observe at P is the intensity, and in cgs units this is given by

$$I = \frac{cE^2}{8\pi}.$$

Hence it is only E^2 that is of interest to us, and from Eqs. (1.5) this is given by

$$E^2 = \left(\sum E_n \cos \frac{2\pi X_n}{\lambda}\right)^2 + \left(\sum E_n \sin \frac{2\pi X_n}{\lambda}\right)^2. \tag{1.6}$$

To obtain the intensity, we need only the quantity E^2 given by Eq. (1.6). We shall now develop the method of the complex exponential, which is much simpler to use in diffraction problems, and which can be justified by showing that it leads to the same value of E^2. In terms of $i = \sqrt{-1}$, we write Eq. (1.4) in the complex exponential form

$$\epsilon_n = E_n e^{i[2\pi\nu t - (2\pi X_n/\lambda)]}.$$

Since $e^{-ix} = \cos x - i \sin x$, we can write

$$\epsilon_n = e^{i2\pi\nu t}\left(E_n \cos \frac{2\pi X_n}{\lambda} - iE_n \sin \frac{2\pi X_n}{\lambda}\right).$$

Forming the sum,

$$\epsilon = \sum \epsilon_n = e^{i2\pi\nu t}\left(\sum E_n \cos \frac{2\pi X_n}{\lambda} - i \sum E_n \sin \frac{2\pi X_n}{\lambda}\right).$$

We next write the complex conjugate ϵ^*, which for any complex quantity is obtained by replacing i by $-i$:

$$\epsilon^* = e^{-i2\pi\nu t}\left(\sum E_n \cos\frac{2\pi X_n}{\lambda} + i\sum E_n \sin\frac{2\pi X_n}{\lambda}\right).$$

The product $\epsilon\epsilon^*$ is then given by

$$\epsilon\epsilon^* = \left(\sum E_n \cos\frac{2\pi X_n}{\lambda}\right)^2 + \left(\sum E_n \sin\frac{2\pi X_n}{\lambda}\right)^2. \tag{1.7}$$

Comparing Eqs. (1.6) and (1.7), we see that

$$\epsilon\epsilon^* = E^2. \tag{1.8}$$

Hence by proper use of the complex exponential, we arrive at the quantity E^2, and this is all that we need to obtain the intensity I.

We shall use the complex exponential representation since it generally simplifies the mathematical manipulations. What we have just proved can be formulated as a set of rules. For each scatterer write in complex form the instantaneous value of the electric field at the point of observation. Sum these values, and form the complex conjugate of the sum. The product of the sum and its complex conjugate is then equal to E^2 the square of the amplitude. The intensity at the point of observation is given by $I = cE^2/8\pi$.

1.4 SCATTERING BY AN ATOM

We first consider the classical scattering from a group of electrons confined to a small volume such as the volume of an atom. The conditions are shown by Fig. 1.5. The primary beam, of amplitude E_0 polarized so that E_0 is normal to the plane of the paper, has a direction represented by the unit vector $\mathbf{s}_0$. The electrons are clustered about point O, the position of each represented by a vector $\mathbf{r}_n$. We consider scattering at a point of observation P, at a large distance R from the electrons, in a direction given by a unit vector $\mathbf{s}$.

In terms of a wave front through O, the instantaneous value of the field in the primary beam acting on electron n is given by

$$\epsilon_0 = E_0 \cos\left(2\pi\nu t - \frac{2\pi X_1}{\lambda}\right).$$

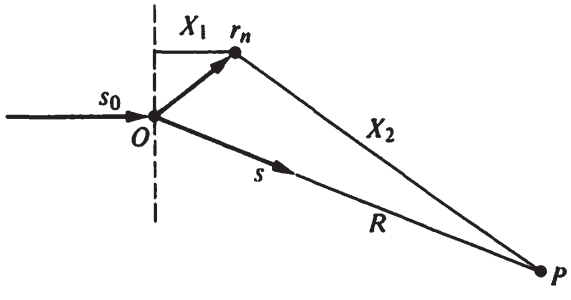

Fig. 1.5 Scattering by a group of electrons at positions $\mathbf{r}_n$. The unit vectors $\mathbf{s}_0$ and $\mathbf{s}$ give the direction of the primary beam and the direction to the point of observation P.

To represent the magnitude and phase of the scattered beam at P due to electron n, we can multiply by the classical factor for an electron and

consider the total path as $X_1 + X_2$:

$$\epsilon_n = \frac{E_0 e^2}{mc^2 X_2} \cos\left[2\pi\nu t - \frac{2\pi}{\lambda}(X_1 + X_2)\right].$$

This neglects a 180° jump in phase in the scattering, but this is of no importance to the present problem since it is the same for all the electrons. Considering that the source and the point of observation are both at distances very large compared to the length $|\mathbf{r}_n|$, we can make the usual plane wave approximations. In the denominator $X_2 \to R$, and in the cosine

$$X_1 + X_2 \to \mathbf{r}_n \cdot \mathbf{s}_0 + R - \mathbf{r}_n \cdot \mathbf{s} = R - (\mathbf{s} - \mathbf{s}_0) \cdot \mathbf{r}_n.$$

Expressed in terms of the complex exponential, the sum of the instantaneous fields at P is given by

$$\epsilon = \frac{E_0 e^2}{mc^2 R} e^{2\pi i[\nu t - (R/\lambda)]} \sum_n e^{(2\pi i/\lambda)(\mathbf{s}-\mathbf{s}_0)\cdot\mathbf{r}_n}. \tag{1.9}$$

However, electrons do not scatter in the manner predicted by classical theory. From both theory and experiment we know that there are two kinds of scattering: (a) unmodified scattering (same wavelength) and (b) Compton modified scattering (longer wavelength). In scattering from a crystal, it is the unmodified scattering which gives rise to the Bragg reflections. The modified scattering from the different electrons is completely incoherent because of the change in wavelength, and accordingly it produces only a diffuse background. A correct treatment of x-ray scattering involves wave mechanical methods which we are not in position to consider here. However, the results of the wave mechanical treatment can be expressed as simple rules which allow us to calculate the unmodified and modified scattering from an atom.

To calculate the unmodified scattering from an atom, we consider that each electron is spread out into a diffuse cloud of negative charge, characterized by a charge density ρ expressed in electron units. The quantity $\rho\, dV$ is the ratio of the charge in volume dV to the charge of one electron, so that for each electron $\int \rho\, dV = 1$. The wave mechanical treatment then says that the amplitude of unmodified scattering from the element $\rho\, dV$ is equal to $\rho\, dV$ times the amplitude of classical scattering from a single electron. To get the total amplitude of unmodified scattering from one electron, we must integrate over the volume occupied by the electron, and in doing this make proper allowance for the phase of the contribution from each element $\rho\, dV$.

The instantaneous value of electric field for the unmodified scattering, due to one of the electrons in an atom, is then given directly by Eq. (1.9), by considering that instead of electrons at positions $\mathbf{r}_n$ we have charge

elements $\rho\, dV$ at positions r, and by replacing the sum by an integral:

$$\epsilon_e = \frac{E_0 e^2}{mc^2 R} e^{2\pi i[\nu t - (R/\lambda)]} \int e^{(2\pi i/\lambda)(\mathbf{s}-\mathbf{s}_0)\cdot\mathbf{r}} \rho\, dV. \tag{1.10}$$

The quantity represented by the integral is called f_e, the scattering factor per electron

$$f_e = \int e^{(2\pi i/\lambda)(\mathbf{s}-\mathbf{s}_0)\cdot\mathbf{r}} \rho\, dV. \tag{1.11}$$

Evidently f_e is the ratio of the amplitude of unmodified scattering from one electron to the amplitude scattered by an electron according to classical theory. Stated in another way, f_e is the amplitude of unmodified scattering per electron, expressed in electron units.

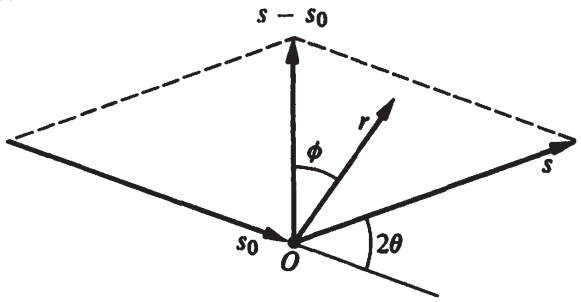

Fig. 1.6 Relation between the $\mathbf{s} - \mathbf{s}_0$ vector and the vector r for an atom centered at O.

Of course it is not true that the charge distribution has spherical symmetry for each electron in the atom. However for closed groups of inner electrons, spherical symmetry exists, and we can work with the combined charge distribution for the electrons of a closed group. By assuming spherical symmetry for the charge distribution $\rho = \rho(r)$, and taking the origin at the center of the atom, we obtain a simple expression for f_e. In terms of the quantities represented by Fig. 1.6, $(\mathbf{s} - \mathbf{s}_0) \cdot \mathbf{r} = 2 \sin\theta\, r \cos\phi$, and with the abbreviation

$$k = \frac{4\pi \sin\theta}{\lambda}, \tag{1.12}$$

we can write

$$f_e = \int_{r=0}^{\infty} \int_{\phi=0}^{\pi} e^{ikr\cos\phi} \rho(r) 2\pi r^2 \sin\phi\, d\phi\, dr.$$

The integration with respect to ϕ is readily performed, and we obtain

$$f_e = \int_0^{\infty} 4\pi r^2 \rho(r) \frac{\sin kr}{kr}\, dr. \tag{1.13}$$

For an atom containing several electrons, the amplitude of unmodified scattering per atom is the sum of the amplitudes per electron:

$$f = \sum_n f_{en} = \sum_n \int_0^{\infty} 4\pi r^2 \rho_n(r) \frac{\sin kr}{kr}\, dr. \tag{1.14}$$

The quantity f plays an important role in x-ray diffraction theory, and it is usually called the atomic scattering factor. Evidently f is the amplitude of unmodified scattering per atom expressed in electron units (amplitude in units of the amplitude from a single electron according to classical theory). To compute f, we need only to know the radial dependence of the electron density in the atom $\sum_n \rho_n(r)$. For any atom, f is a function of $(\sin\theta)/\lambda$, since it is a function of k. Calling Z the number of electrons in the atom,

$$\sum_n \int_0^\infty 4\pi r^2 \rho_n(r)\, dr = Z,$$

and f approaches Z at small values of $(\sin\theta)/\lambda$.

The simple treatment of the atomic scattering factor, which we have given here, is based on two assumptions: (a) the x-ray wavelength is much smaller than any of the absorption edge wavelengths in the atom, and (b) the electron distribution in the atom has spherical symmetry. If the first condition is not satisfied, a dispersion correction is necessary. The correction can be expressed in the form

$$f = f_0 + \Delta f' + i\,\Delta f'', \tag{1.15}$$

where f is the corrected scattering factor, f_0 is the value found in the tables, and $\Delta f'$, $\Delta f''$ are the real and imaginary parts of the dispersion correction. The imaginary part $\Delta f''$ represents a small shift in phase of the scattered radiation. The angular dependance of $\Delta f'$ and $\Delta f''$ is much smaller than that of f_0. An example in which the second condition is not satisfied is given by the diamond crystal. The lack of complete spherical symmetry in the electron distribution in carbon allows weak Bragg reflections from diamond which could not exist if the distributions had complete spherical symmetry.

To compute the intensity of modified scattering from an atom, we use another result from the wave mechanical treatment. For each electron considered individually, the intensity of unmodified scattering plus the intensity of modified scattering is equal to the intensity of classical scattering per electron. Written in terms of an unpolarized primary beam, and calling i_e the intensity of modified scattering per electron expressed in electron units:

$$I_0 \frac{e^4}{m^2c^4R^2}\left(\frac{1+\cos^2 2\theta}{2}\right) f_e^2 + I_0 \frac{e^4}{m^2c^4R^2}\left(\frac{1+\cos^2 2\theta}{2}\right) i_e = I_0 \frac{e^4}{m^2c^4R^2}\left(\frac{1+\cos^2 2\theta}{2}\right)$$

and hence $i_e = 1 - f_e^2$. Since the modified scattering from the different electrons is incoherent, the intensity of modified scattering per atom is the sum of the intensities of modified scattering from the electrons:

$$i(M) = \sum_n i_{en} = Z - \sum_{n=1}^{Z} f_{en}^2. \tag{1.16}$$

To illustrate the use of Eqs. (1.14) and (1.16), let us suppose that the electron density for each of the three electrons in neutral Li can be represented by a hydrogen-like expression of the form

$$\rho = \frac{e^{-(2r/a)}}{\pi a^3},$$

where for each K electron $a_K = 0.20$ A and for the L electron $a_L = 1.60$ A. The expression is already normalized so that

$$\int_0^\infty 4\pi r^2 \frac{e^{-(2r/a)}}{\pi a^3}\, dr = 1.$$

From Eq. (1.13),

$$f_e = \int_0^\infty 4\pi r^2 \frac{e^{-(2r/a)}}{\pi a^3} \frac{\sin kr}{kr}\, dr = \frac{1}{[1 + (2\pi a \sin\theta/\lambda)^2]^2}$$

and hence

$$f_{eK} = \frac{1}{[1 + (2\pi a_K \sin\theta/\lambda)^2]^2}, \qquad f_{eL} = \frac{1}{[1 + (2\pi a_L \sin\theta/\lambda)^2]^2}.$$

From Eq. (1.14), the atomic scattering factor for Li is given by

$$f_{\mathrm{Li}} = 2f_{eK} + f_{eL}.$$

Using Eq. (1.16), the intensity of modified scattering in electron units is given by

$$i(M) = 3 - 2f_{eK}^2 - f_{eL}^2.$$

Figure 1.7 shows plots of f_{eK}, f_{eL}, f, and $i(M)$ against $(\sin\theta)/\lambda$ for a neutral Li atom, which for purposes of illustration is supposed to have the assumed charge distribution.

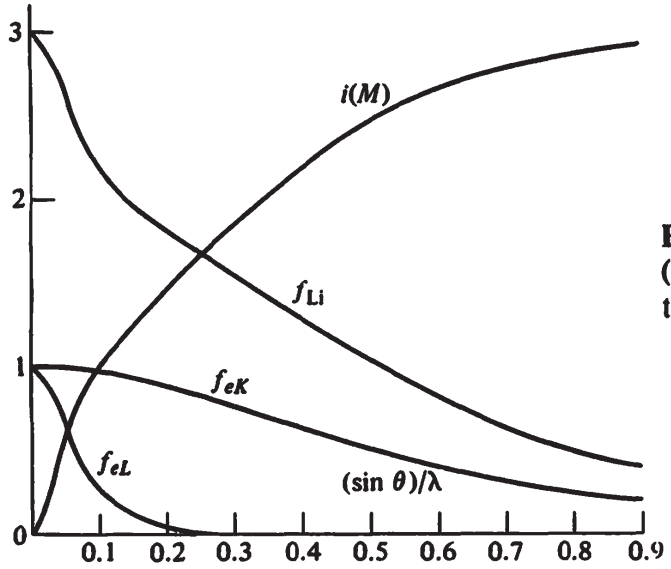

Fig. 1.7 Values of f_{eL}, f_{eK}, f, and (iM) for an assumed charge distribution in neutral Li.

The above treatment is oversimplified. For the modified scattering there is an additional small term coming from cross interaction between the charge densities of different electrons. There is also the Breit Dirac factor $R = (\nu'/\nu)^3$, where ν' is the frequency of the modified scattering and ν is the frequency of the primary beam. The intensity of modified scattering is obtained by multiplying $i(M)$ by the Breit Dirac factor R.

In general it is not necessary to evaluate the various quantities from first principles. Tables of the atomic scattering factor f_0, the dispersion corrections $\Delta f'$ and $\Delta f''$, and the modified scattering per atom $i(M)$ are given in the International Tables.[1] For K electrons only, the dispersion correction terms $\Delta f'$ and $\Delta f''$ are given in James.[2] Dispersion corrections for all the electrons have been tabulated by Dauben and Templeton.[3] For a thorough treatment of the x-ray scattering by atoms, reference should be made to James.[2]

REFERENCES

1. *International Tables for X-Ray Crystallography*, Vol. III, 1962.
2. R. W. JAMES: *The Optical Principles of the Diffraction of X-Rays*, G. Bell and Sons Ltd., London, 1948, Chaps. III and IV and p. 608.
3. C. H. DAUBEN and D. H. TEMPLETON: *Acta Cryst.* **8**, 841 (1955).

PROBLEMS

1.1 a) An unpolarized primary beam of intensity I_0 is scattered according to classical theory by a single electron. Show that the total scattered power (integral of intensity over area) is given by

$$P = \frac{8\pi}{3}\left(\frac{e^4}{m^2c^4}\right) I_0.$$

b) What is the total scattered power if the primary beam has an intensity I_0 and is linearly polarized?

1.2 Assuming classical scattering and incoherency (the intensity from n electrons is n times the intensity from one electron), show that for elements of low atomic number the total scattered power per gram P_{gm} is given by $P_{gm} = 0.20I_0$.

1.3 A parallel x-ray beam limited by an opening of area 0.50 cm^2 falls upon a 0.10 gm carbon block close to the opening, as shown by Fig. 1.8. The window of the ionization chamber is 2 × 2 cm, and 5 cm from the carbon block. Assume that for scattering at 90°, the electrons scatter according to classical theory and incoherently (the intensity from n electrons is n times the intensity from one electron). In position A with the block removed, the ionization current is found to be about 2500 times greater than in position B with the block in place. Making reasonable approximations, calculate the number of electrons in the carbon atom.

1.4 A primary beam of wavelength $\lambda = 1.0$ A, intensity I_0, small cross-sectional area a_0, and power $P_0 = I_0a_0$, falls upon a large flat-faced carbon block. Scattered

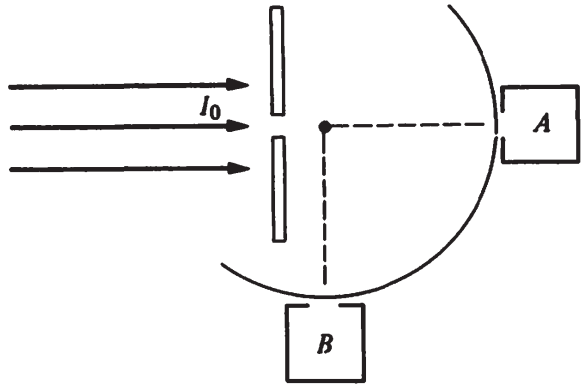

Fig. 1.8 Scattering by a carbon block of an unpolarized primary beam, as considered in Problem 1.3.

radiation is observed at 10 cm from the point of impact. The primary and scattered beams are at 90° to one another, and each makes 45° with the face of the block. Assume that the electrons scatter according to classical theory and incoherently. Making reasonable approximations, what is the value of I/P_0? [*Hint:* Set up the contribution dI from a small volume $a_0\,dx$, and allow for absorption. For carbon, and $\lambda = 1.0$ A, the mass abs. coef. is $\mu_m = 1.37\ \text{cm}^2\ \text{gm}^{-1}$. Answer: $I/P_0 = 4.4 \times 10^{-5}\ \text{cm}^{-2}$.]

1.5 The unpolarized x-ray beam of Fig. 1.9 is directed in the XZ-plane at an angle 2θ to the X-axis. It is scattered by a carbon block at O. The scattered radiation arriving at O' is partially polarized and we call its intensity I_0 at point O'. This partially polarized beam is scattered classically by an electron at O'. The intensity of the scattering from O' is measured at a point P distance R from O' and at an angle ϕ with the X-axis. Deduce an expression for I in terms of I_0, R, θ, and ϕ,

a) if P is in the XY'-plane;
b) if P is in the XZ'-plane.

Answer part (b):

$$I = I_0 \frac{e^4}{m^2c^4R^2}\left(\frac{1 + \cos^2 2\theta \cos^2 \phi}{1 + \cos^2 2\theta}\right).$$

[*Note:* The angular factor illustrates the polarization factor for a crystal monochromated beam obtained by using a crystal at O.]

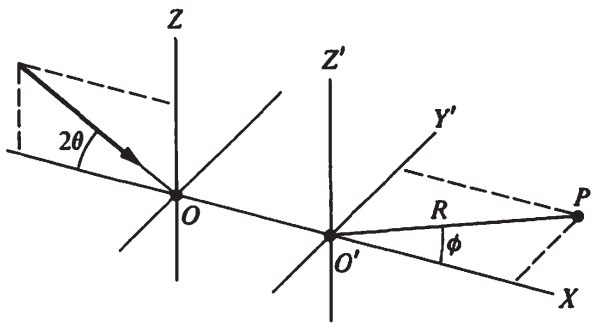

Fig. 1.9 Double scattering of an initially unpolarized beam. The beam scattered by O which falls on an electron at O' is partially polarized. Illustration of Problem 1.5.

1.6 The instantaneous value of the electric field, at the point of observation, due to a number of beams, is

$$\epsilon = \sum_n \epsilon_n = \sum_n E_n e^{i(2\pi\nu t - \phi_n)}.$$

The frequencies ν of the beams are all the same, but the phases ϕ_n are independent of each other and vary randomly with time. This is one example of a set of beams which can be called incoherent with respect to one another. Show that the average intensity is the sum of the individual intensities:

$$\langle I \rangle = \sum_n I_n.$$

1.7 Show that for any atom at very small values of $(\sin\theta)/\lambda$, both the scattering factor f and the intensity of modified scattering $i(M)$ are parabolic functions of $(\sin\theta)/\lambda$, and hence both curves intersect the axis of ordinates with zero slope.

1.8 For the hydrogen atom in the normal state, wave mechanics gives the electron density as

$$\rho = (e^{-2r/a})/\pi a^3, \qquad a = 0.53 \text{ A}, \qquad \int \rho \, dV = 1.$$

a) Derive expressions for f and $i(M)$ as functions of $(\sin\theta)/\lambda$.
b) Compute values of f and $i(M)$ for $(\sin\theta)/\lambda = 0.0, 0.2, 0.4$, and compare with the tabulated values.

1.9 Assume that for each of the two electrons in He, the electron density is given by

$$\rho = (e^{-(2r/a)})/\pi a^3, \qquad a = 0.32 \text{ A}, \qquad \int \rho \, dV = 1.$$

If a beam of Cu$K\alpha$ ($\lambda = 1.54$ A) falls on a single He atom, at what scattering angle 2θ is the intensity of unmodified scattering equal to that of the modified scattering?

1.10 A beam of Mo$K\alpha$ ($\lambda = 0.71$ A) falls on a single carbon atom. Using values from the tables, compute the ratio of the total intensity (unmodified plus modified) to that expected if the six electrons scattered according to classical theory and incoherently. Evaluate for $(\sin\theta)/\lambda = 1.1$.

1.11 Assume a model for the carbon atom which is far from reality. Assume that the two K electrons are spread uniformly over the surface of a sphere of radius $r_K = 0.20$ A and that the four L electrons are spread uniformly over the surface of a sphere of radius $r_L = 1.50$ A. Compute and plot f_e as a function of $(\sin\theta)/\lambda$ from 0.0 to 0.6 in steps of 0.1. What incorrect feature in f has been produced by the assumption of spherical shells?

CRYSTAL AXES AND THE RECIPROCAL LATTICE

2.1 CRYSTAL AXES

A crystal is a three-dimensional repetition of some unit of atoms or molecules. The essential feature is illustrated in two dimensions by Fig. 2.1. Two different kinds of atoms or molecules represented by circles and triangles are shown repeated identically. The scheme of repetition is defined by three vectors $\mathbf{a}_1\mathbf{a}_2\mathbf{a}_3$, called the crystal axes. It is only the magnitude and direction of the repeating displacements that is of importance, and hence for present purposes, the position chosen as origin is immaterial. The parallelopipedon defined by the three axes $\mathbf{a}_1\mathbf{a}_2\mathbf{a}_3$ is the smallest volume which repeated will make up the crystal. This smallest volume is called the unit cell. The unit cell volume is given by $v_a = \mathbf{a}_1 \cdot \mathbf{a}_2 \times \mathbf{a}_3$.

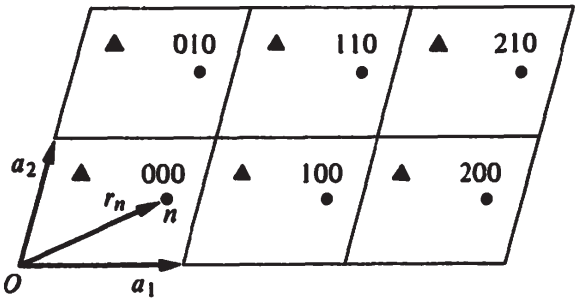

Fig. 2.1 Two-dimensional representation of the periodic property of a crystal.

We suppose that the different atoms in the unit cell are numbered $1, 2, 3, \ldots, n$, and that the positions of the atoms relative to the cell origin are given by cell vectors $\mathbf{r}_1, \mathbf{r}_2, \mathbf{r}_3, \ldots, \mathbf{r}_n$. We shall designate the different unit cells by three integers m_1, m_2, m_3, such that cell $m_1m_2m_3$ is the one whose origin is displaced from the crystal origin by $m_1\mathbf{a}_1 + m_2\mathbf{a}_2 + m_3\mathbf{a}_3$. Finally the position of the atom of type n in the unit cell $m_1m_2m_3$ is given by the vector

$$\mathbf{R}_m^n = m_1\mathbf{a}_1 + m_2\mathbf{a}_3 + m_3\mathbf{a}_3 + \mathbf{r}_n. \tag{2.1}$$

2.2 THE CRYSTALLOGRAPHIC PLANES *hkl*

In using the Bragg law, we consider diffraction in terms of a set of crystallographic planes *hkl*. A precise definition of this concept is indicated by Fig. 2.2. By the set of crystallographic planes *hkl*, we mean a set of parallel equidistant planes, one of which passes through the origin, and the next nearest makes intercepts a_1/h, a_2/k, and a_3/l on the three crystallographic axes. The integers *hkl* are usually called the Miller indices.

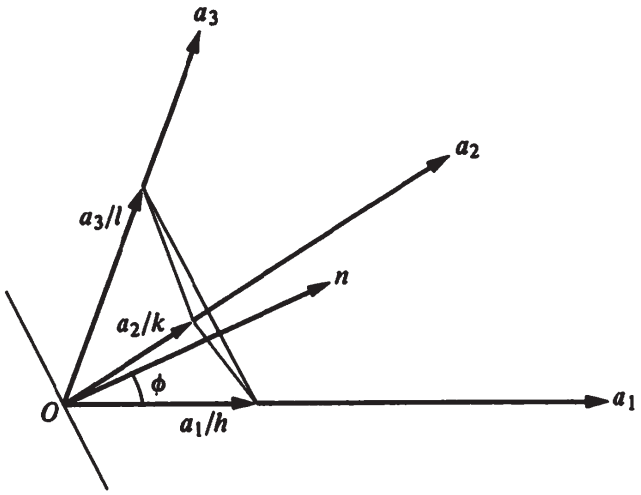

Fig. 2.2 Representation of the crystallographic planes *hkl*.

Two properties of a set of *hkl* planes are involved in using the Bragg law: the orientation of the planes and their spacing. A simple representation of both properties is obtained by introducing a vector $\mathbf{H}_{hkl}$, which is perpendicular to the planes *hkl*, and whose magnitude is the reciprocal of the spacing. We first introduce a set of reciprocal vectors $\mathbf{b}_1\mathbf{b}_2\mathbf{b}_3$, and in terms of these a vector $\mathbf{H}_{hkl}$ which will have the desired properties.

2.3 RECIPROCAL VECTORS AND THE RECIPROCAL LATTICE

In terms of the crystal axes $\mathbf{a}_1\mathbf{a}_2\mathbf{a}_3$, we define a set of reciprocal vectors $\mathbf{b}_1\mathbf{b}_2\mathbf{b}_3$:

$$\mathbf{b}_1 = \frac{\mathbf{a}_2 \times \mathbf{a}_3}{\mathbf{a}_1 \cdot \mathbf{a}_2 \times \mathbf{a}_3}, \qquad \mathbf{b}_2 = \frac{\mathbf{a}_3 \times \mathbf{a}_1}{\mathbf{a}_1 \cdot \mathbf{a}_2 \times \mathbf{a}_3}, \qquad \mathbf{b}_3 = \frac{\mathbf{a}_1 \times \mathbf{a}_2}{\mathbf{a}_1 \cdot \mathbf{a}_2 \times \mathbf{a}_3}. \tag{2.2}$$

Each reciprocal vector is perpendicular to the plane defined by the two crystal axes having different indices. The definitions are easily remembered from the fact that for the reciprocal vector and the two crystal axes in the numerator, the indices run cyclically. An important relation between the two sets of vectors is expressed by the scalar products. If the indices are the same,

$$\mathbf{a}_1 \cdot \mathbf{b}_1 = \mathbf{a}_1 \cdot \frac{\mathbf{a}_2 \times \mathbf{a}_3}{\mathbf{a}_1 \cdot \mathbf{a}_2 \times \mathbf{a}_3} = 1.$$

If the indices are different,

$$\mathbf{a}_1 \cdot \mathbf{b}_2 = \mathbf{a}_1 \cdot \frac{\mathbf{a}_3 \times \mathbf{a}_1}{\mathbf{a}_1 \cdot \mathbf{a}_2 \times \mathbf{a}_3} = 0,$$

since the vector $\mathbf{a}_3 \times \mathbf{a}_1$ is a vector perpendicular to $\mathbf{a}_1$ and hence the scalar product of $\mathbf{a}_1$ and $\mathbf{a}_3 \times \mathbf{a}_1$ involves cos 90°. These results can be generalized by writing

$$\mathbf{a}_i \cdot \mathbf{b}_j = \begin{cases} 1, & i = j, \\ 0, & i \neq j. \end{cases} \tag{2.3}$$

The relations expressed by Eq. (2.3) can be called the normal and orthogonal conditions between the primary and reciprocal vectors. We shall make considerable use of these relations.

We next define a vector $\mathbf{H}_{hkl}$ in terms of the reciprocal vectors and the Miller indices:

$$\mathbf{H}_{hkl} = h\mathbf{b}_1 + k\mathbf{b}_2 + l\mathbf{b}_3. \tag{2.4}$$

From Fig. 2.2 it is evident that $(\mathbf{a}_1/h - \mathbf{a}_2/k)$ and $(\mathbf{a}_2/k - \mathbf{a}_3/l)$ are vectors which are parallel to the *hkl*-planes. But from the relations expressed by Eq. (2.3),

$$\left(\frac{\mathbf{a}_1}{h} - \frac{\mathbf{a}_2}{k}\right) \cdot \mathbf{H}_{hkl} = \left(\frac{\mathbf{a}_1}{h} - \frac{\mathbf{a}_2}{k}\right) \cdot (h\mathbf{b}_1 + k\mathbf{b}_2 + l\mathbf{b}_3) = 1 - 1 = 0,$$

$$\left(\frac{\mathbf{a}_2}{k} - \frac{\mathbf{a}_3}{l}\right) \cdot \mathbf{H}_{hkl} = \left(\frac{\mathbf{a}_2}{k} - \frac{\mathbf{a}_3}{l}\right) \cdot (h\mathbf{b}_1 + k\mathbf{b}_2 + l\mathbf{b}_3) = 1 - 1 = 0.$$

Hence the vector $\mathbf{H}_{hkl}$ is perpendicular to the set of *hkl*-planes, since it is perpendicular to two vectors which are parallel to the planes. The spacing of the planes d_{hkl} is the perpendicular distance between planes. If $\mathbf{n}$ is a unit vector perpendicular to the planes, we see from Fig. 2.2 that

$$d_{hkl} = \frac{|\mathbf{a}_1|}{h} \cos\phi = \frac{\mathbf{a}_1}{h} \cdot \mathbf{n}.$$

Since $\mathbf{H}_{hkl}$ is perpendicular to the *hkl*-planes, we can make up a unit vector $\mathbf{n}$ by using $\mathbf{H}_{hkl}/|\mathbf{H}_{hkl}|$. Hence the spacing is given by

$$d_{hkl} = \frac{\mathbf{a}_1}{h} \cdot \frac{(h\mathbf{b}_1 + k\mathbf{b}_2 + l\mathbf{b}_3)}{|\mathbf{H}_{hkl}|} = \frac{1}{|\mathbf{H}_{hkl}|}.$$

We have now proved that the vector $\mathbf{H}_{hkl}$ defined by Eq. (2.4) is perpendicular to the planes *hkl* and of length equal to the reciprocal of the spacing.

If vectors $\mathbf{H}_{hkl}$ are drawn for all values of the indices *hkl*, the terminal points of these vectors form a new lattice with repetition vectors $\mathbf{b}_1$, $\mathbf{b}_2$, $\mathbf{b}_3$. This lattice is called the reciprocal lattice, and it will turn out to be extremely

useful in the treatment of crystal diffraction problems. One simple use for the reciprocal lattice is already obvious. From the crystal axes $\mathbf{a}_1\mathbf{a}_2\mathbf{a}_3$, we can obtain the reciprocal vectors by use of Eq. (2.2), and hence lay out the reciprocal lattice by repetitions of $\mathbf{b}_1\mathbf{b}_2\mathbf{b}_3$. The vector from the origin to any point *hkl* of the lattice is then the vector $\mathbf{H}_{hkl}$, and this vector is normal to the planes *hkl* and of length equal to the reciprocal of the spacing.

It is convenient to express the Bragg law in vector form by use of the vector $\mathbf{H}_{hkl}$. If $\mathbf{s}_0$ and $\mathbf{s}$ are unit vectors in the directions of the primary and diffracted beams, we construct vectors $\mathbf{s}_0/\lambda$ and $\mathbf{s}/\lambda$ making angles θ with the diffracting planes as illustrated by Fig. 2.3. The Bragg law in vector form is then given by

$$\frac{\mathbf{s} - \mathbf{s}_0}{\lambda} = \mathbf{H}_{hkl} \qquad (2.5)$$

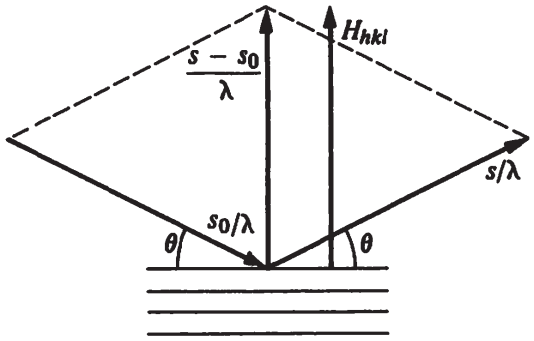

Fig. 2.3 Relations involved in the vector representation of the Bragg law.

To see that Eq. (2.5) is equivalent to the Bragg law, we note that it is a vector equation and hence two conditions are implied: (1) the vectors on either side must be parallel, and (2) the magnitudes on either side must be equal. The first condition says that the primary and diffracted beams make equal angles with the diffracting planes. The second condition requires that

$$\left|\frac{\mathbf{s} - \mathbf{s}_0}{\lambda}\right| = \frac{2 \sin \theta}{\lambda} = |\mathbf{H}_{hkl}| = \frac{1}{d_{hkl}},$$

and this is equivalent to the usual form of the Bragg law $\lambda = 2d_{hkl} \sin \theta$.

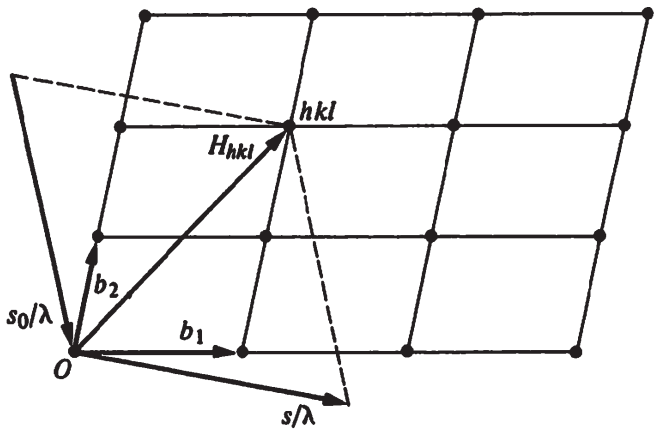

Fig. 2.4 Reciprocal lattice representation of the satisfying of the Bragg law for a set of planes *hkl*. The diffraction vector $(\mathbf{s} - \mathbf{s}_0)/\lambda$ must terminate on the point *hkl* of the reciprocal lattice.

The reciprocal lattice provides a simple graphical representation of the satisfying of the Bragg law. This is illustrated by Fig. 2.4. For the set of planes *hkl* we draw the vector $\mathbf{H}_{hkl}$ to the point *hkl* in the reciprocal lattice. For a given λ, a set of possible directions for the primary and diffracted beams is then constructed to satisfy Eq. (2.5). The plane of the $\mathbf{s}_0/\lambda$ and $\mathbf{s}/\lambda$ vectors can, of course, take any orientation by rotating about the $\mathbf{H}_{hkl}$ vector.

2.4 THE SPHERE OF REFLECTION

A very powerful and useful way of representing the satisfying of the Bragg law is given by the sphere of reflection (Ewald sphere). The reciprocal lattice is represented schematically in 2 dimensions by Fig. 2.5. The direction of the primary beam is shown by the vector $\mathbf{s}_0/\lambda$, a vector of length $1/\lambda$ terminating on the origin of the reciprocal lattice. A sphere of radius $1/\lambda$ centered on the initial end of $\mathbf{s}_0/\lambda$ passes through the origin. Any reciprocal lattice point *hkl* which happens to fall on the surface of the sphere, represents a set of planes *hkl* for which the Bragg law is satisfied. The direction of the diffracted beam is given by the vector $\mathbf{s}/\lambda$ from the center of the sphere to the point *hkl*. It is evident that the relation of the three vectors $\mathbf{s}_0/\lambda$, $\mathbf{s}/\lambda$, and $\mathbf{H}_{hkl}$ shown by Fig. 2.5 is that of the Bragg law expressed by Eq. (2.5). Although Fig. 2.5 shows the relations schematically in two dimensions, the sphere of reflection construction is valid in three dimensions, and the point *hkl* can be anywhere on the surface of the sphere.

In terms of the sphere of reflection, the satisfying of the Bragg law for a set of planes *hkl* is simply the condition that the reciprocal lattice point *hkl* falls on the surface of the sphere. Problems such as how much must the crystal turn to allow a certain set of planes to diffract, and for a certain range of oscillation which *hkl*-planes will have the chance to diffract, are all readily visualized in terms of the sphere of reflection.

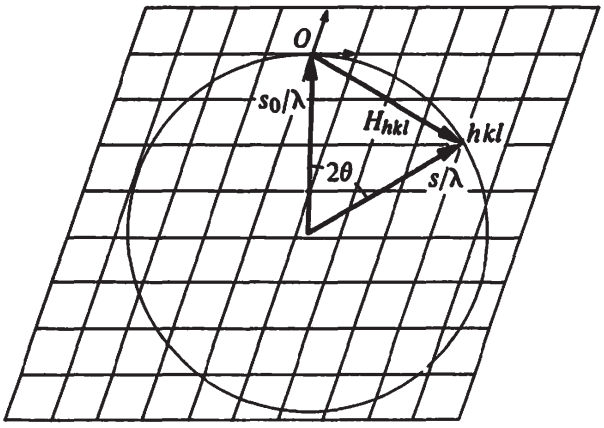

Fig. 2.5 Two-dimensional representation of the sphere of reflection in the reciprocal lattice. The Bragg law is satisfied for any set of planes whose point *hkl* falls on the surface of the sphere.

2.5 SPACING FORMULAE

In using the Bragg law, we need the value of the planar spacing d_{hkl}. Assuming that we know the lengths of the three crystal axes and the angles between them, we wish to express the spacing in the form

$$d_{hkl} = f(a_1, a_2, a_3, \alpha_{12}, \alpha_{23}, \alpha_{31}, h, k, l).$$

The obvious starting point is to write

$$\frac{1}{d_{hkl}^2} = |\mathbf{H}_{hkl}|^2 = (h\mathbf{b}_1 + k\mathbf{b}_2 + l\mathbf{b}_3) \cdot (h\mathbf{b}_1 + k\mathbf{b}_2 + l\mathbf{b}_3),$$

$$\frac{1}{d_{hkl}^2} = h^2\mathbf{b}_1 \cdot \mathbf{b}_1 + k^2\mathbf{b}_2 \cdot \mathbf{b}_2 + l^2\mathbf{b}_3 \cdot \mathbf{b}_3 + 2hk\mathbf{b}_1 \cdot \mathbf{b}_2 + 2kl\mathbf{b}_2 \cdot \mathbf{b}_3 + 2lh\mathbf{b}_3 \cdot \mathbf{b}_1.$$

Using Eqs. (2.2) and factoring out $v_a = \mathbf{a}_1 \cdot \mathbf{a}_2 \times \mathbf{a}_3$,

$$\begin{aligned}\frac{1}{d_{hkl}^2} = \frac{1}{v_a^2}\{&h^2 |\mathbf{a}_2 \times \mathbf{a}_3|^2 + k^2 |\mathbf{a}_3 \times \mathbf{a}_1|^2 + l^2 |\mathbf{a}_1 \times \mathbf{a}_2|^2 \\ &+ 2hk(\mathbf{a}_2 \times \mathbf{a}_3) \cdot (\mathbf{a}_3 \times \mathbf{a}_1) + 2kl(\mathbf{a}_3 \times \mathbf{a}_1) \cdot (\mathbf{a}_1 \times \mathbf{a}_2) \\ &+ 2lh(\mathbf{a}_1 \times \mathbf{a}_2) \cdot (\mathbf{a}_2 \times \mathbf{a}_3)\}.\end{aligned}$$

From the equations of vector analysis

$$\begin{aligned}(\mathbf{a}_i \times \mathbf{a}_j) \cdot (\mathbf{a}_j \times \mathbf{a}_k) &= \mathbf{a}_i \cdot \mathbf{a}_j \mathbf{a}_j \cdot \mathbf{a}_k - \mathbf{a}_i \cdot \mathbf{a}_k a_j^2 \\ &= a_i a_j^2 a_k (\cos \alpha_{ij} \cos \alpha_{jk} - \cos \alpha_{ik}), \\ |\mathbf{a}_i \times \mathbf{a}_j|^2 &= a_i^2 a_j^2 \sin^2 \alpha_{ij}.\end{aligned}$$

Using these relations and factoring out $a_1^2 a_2^2 a_3^2$, we obtain

$$\begin{aligned}\frac{1}{d_{hkl}^2} = \frac{a_1^2 a_2^2 a_3^2}{v_a^2}\Bigg\{&\frac{h^2 \sin^2 \alpha_{23}}{a_1^2} + \frac{k^2 \sin^2 \alpha_{31}}{a_2^2} + \frac{l^2 \sin^2 \alpha_{12}}{a_3^2} \\ &+ \frac{2hk}{a_1 a_2}(\cos \alpha_{23} \cos \alpha_{31} - \cos \alpha_{12}) + \frac{2kl}{a_2 a_3}(\cos \alpha_{31} \cos \alpha_{12} - \cos \alpha_{23}) \\ &+ \frac{2lh}{a_3 a_1}(\cos \alpha_{12} \cos \alpha_{23} - \cos \alpha_{31})\Bigg\}.\end{aligned} \tag{2.6}$$

The square of the triple scalar product is conveniently expressed in determinant form in terms of simple scalar products:

$$v_a^2 = (\mathbf{a}_1 \cdot \mathbf{a}_2 \times \mathbf{a}_3)^2 = \begin{vmatrix} \mathbf{a}_1 \cdot \mathbf{a}_1 & \mathbf{a}_1 \cdot \mathbf{a}_2 & \mathbf{a}_1 \cdot \mathbf{a}_3 \\ \mathbf{a}_2 \cdot \mathbf{a}_1 & \mathbf{a}_2 \cdot \mathbf{a}_2 & \mathbf{a}_2 \cdot \mathbf{a}_3 \\ \mathbf{a}_3 \cdot \mathbf{a}_1 & \mathbf{a}_3 \cdot \mathbf{a}_2 & \mathbf{a}_3 \cdot \mathbf{a}_3 \end{vmatrix},$$

$$v_a^2 = a_1^2 a_2^2 a_3^2 (1 + 2 \cos \alpha_{12} \cos \alpha_{23} \cos \alpha_{31} - \cos^2 \alpha_{12} - \cos^2 \alpha_{23} - \cos^2 \alpha_{31}). \tag{2.7}$$

To conform to the usual crystallographic notation, we let

$$\begin{aligned} a_1 &= a, & \alpha_{23} &= \alpha, \\ a_2 &= b, & \alpha_{31} &= \beta, \\ a_3 &= c, & \alpha_{12} &= \gamma. \end{aligned}$$

Combining Eqs. (2.6) and (2.7) and changing to the usual crystallographic notation, we obtain

$$\frac{1}{d_{hkl}^2} = \frac{1}{(1 + 2\cos\alpha\cos\beta\cos\gamma - \cos^2\alpha - \cos^2\beta - \cos^2\gamma)} \times \left\{\frac{h^2\sin^2\alpha}{a^2} + \frac{k^2\sin^2\beta}{b^2} + \frac{l^2\sin^2\gamma}{c^2} + \frac{2hk}{ab}(\cos\alpha\cos\beta - \cos\gamma) + \frac{2kl}{bc}(\cos\beta\cos\gamma - \cos\alpha) + \frac{2lh}{ac}(\cos\gamma\cos\alpha - \cos\beta)\right\}. \quad (2.8)$$

Equation (2.8) is the spacing formula for the general triclinic crystal. The formulae simplify considerably for the other systems.

Rhombohedral, $a = b = c$, $\alpha = \beta = \gamma$:

$$\frac{1}{d_{hkl}^2} = \frac{(h^2 + k^2 + l^2)\sin^2\alpha + 2(hk + kl + lh)(\cos^2\alpha - \cos\alpha)}{a^2(1 + 2\cos^3\alpha - 3\cos^2\alpha)}. \quad (2.9)$$

Hexagonal, $a = b$, $\alpha = \beta = 90°$, $\gamma = 120°$:

$$\frac{1}{d_{hkl}^2} = \frac{4}{3}\left(\frac{h^2 + hk + k^2}{a^2}\right) + \frac{l^2}{c^2}. \quad (2.10)$$

Monoclinic, $\alpha = \gamma = 90°$:

$$\frac{1}{d_{hkl}^2} = \frac{1}{\sin^2\beta}\left(\frac{h^2}{a^2} + \frac{k^2\sin^2\beta}{b^2} + \frac{l^2}{c^2} - \frac{2hl\cos\beta}{ac}\right). \quad (2.11)$$

Orthorhombic, $\alpha = \beta = \gamma = 90°$:

$$\frac{1}{d_{hkl}^2} = \frac{h^2}{a^2} + \frac{k^2}{b^2} + \frac{l^2}{c^2}. \quad (2.12)$$

Tetragonal, $a = b$, $\alpha = \beta = \gamma = 90°$:

$$\frac{1}{d_{hkl}^2} = \frac{h^2 + k^2}{a^2} + \frac{l^2}{c^2}. \quad (2.13)$$

Cubic, $a = b = c$, $\alpha = \beta = \gamma = 90°$:

$$\frac{1}{d_{hkl}^2} = \frac{h^2 + k^2 + l^2}{a^2}. \quad (2.14)$$

2.6 THE 14 BRAVAIS LATTICES

By the Bravais lattice of a crystal we mean the spacial scheme of repetition, this scheme of repetition being completely expressed by the lengths and directions of the three primary translation vectors $\mathbf{a}_1$, $\mathbf{a}_2$, $\mathbf{a}_3$. In the most general lattice, the three lengths and the three angles are wholly arbitrary. This type of lattice is known as triclinic, and it is represented by the symbol Γ_{tr}. Now it is a matter of observation that crystals tend to display symmetry elements such as symmetry centers, rotation axes, and reflection planes. It is evident that in the general triclinic lattice rotation axes and reflection planes cannot exist. A triclinic lattice can allow a center of symmetry but no more than this.

In order that a lattice may allow other symmetry elements in addition to the center of symmetry, certain restrictions must be imposed upon the six quantities a_1, a_2, a_3, α_{12}, α_{23}, α_{31}. By considering one after another of the various symmetry elements and combinations of symmetry elements which comprise the 32 symmetry classes of crystals, and finding the restrictions which must be imposed upon a_1, a_2, a_3, α_{12}, α_{23}, α_{31}, we tabulate the various special types of lattices which are compatible with the 32 classes of symmetry. The tabulation leads to 14 essentially different restrictions, known as the 14 Bravais lattices.

Consider the restrictions that must be imposed in order that a lattice may have a 2-fold rotation axis. It is evident that this is possible if one axis is perpendicular to the other two axes, $\alpha_{12} = \alpha_{23} = 90°$, the lengths of the three axes being arbitrary. This lattice is called the simple monoclinic lattice represented by Γ_m.

However a little consideration will show that a 2-fold axis is also possible in a lattice with the following restrictions: $a_1 = a_2$ and $\alpha_{13} = \alpha_{23}$. Such a lattice with the appropriate smallest unit cell is shown by Fig. 2.6. However, it is possible to choose another set of axes $\mathbf{A}_1\mathbf{A}_2\mathbf{a}_3$ such that $\mathbf{A}_2$ is perpendicular to $\mathbf{A}_1$ and $\mathbf{a}_3$. In practice it is much easier to work with the second set of axes, and moreover they display more clearly the true monoclinic symmetry of the lattice. However, in choosing the new set, we encounter the serious difficulty that the translation $\mathbf{a}_2$ which makes point C equivalent to point O is no longer contained and expressed by the system of axes. To express the true spacial scheme of repetition, if we decide to use the axes $\mathbf{A}_1\mathbf{A}_2\mathbf{a}_3$, we must specify that in addition there is a translation $\mathbf{a}_2 = (\mathbf{A}_1 + \mathbf{A}_2)/2$. Axes which for convenience have been arbitrarily taken in such a way that the unit cell which they define is larger than the true elementary unit cell, and for which an additional translation must be specified, are spoken of as defining a unit cell which is side-centered, or body-centered, or face-centered. The lattice defined by $\mathbf{A}_1\mathbf{A}_2\mathbf{a}_3$ is known as the monoclinic side-centered lattice Γ'_m. The volume of the cell defined by $\mathbf{A}_1\mathbf{A}_2\mathbf{a}_3$ is twice the volume of the true unit cell defined by $\mathbf{a}_1\mathbf{a}_2\mathbf{a}_3$. For every atom at position $\mathbf{r}_n$ there must be an identical atom at $\mathbf{r}_n + (\mathbf{A}_1 + \mathbf{A}_2)/2$.

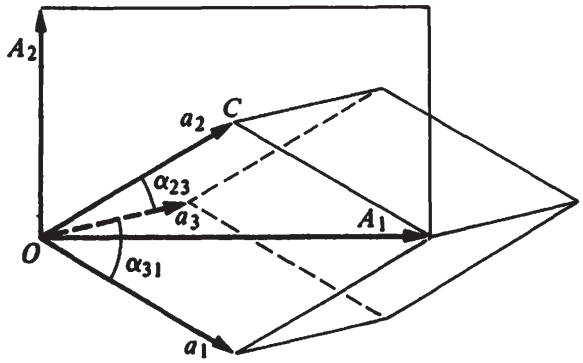

Fig. 2.6 Relations between the axes $\mathbf{a}_1\mathbf{a}_2\mathbf{a}_3$ of the true unit cell and the more convenient axes $\mathbf{A}_1\mathbf{A}_2\mathbf{a}_3$, defining a cell of double the volume, for the monoclinic side-centered lattice.

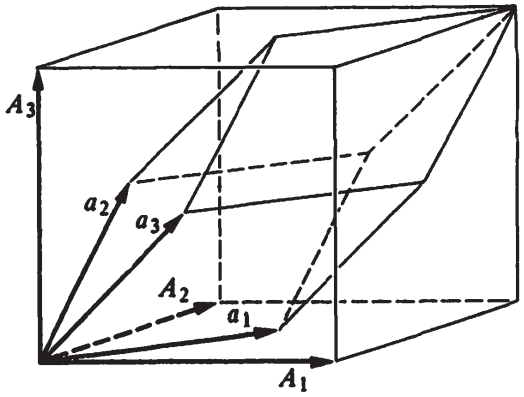

Fig. 2.7 Relation between the axes $\mathbf{a}_1\mathbf{a}_2\mathbf{a}_3$ of the true unit cell and the more convenient axes $\mathbf{A}_1\mathbf{A}_2\mathbf{A}_3$, defining a cell of four times the volume, for the face-centered cubic lattice.

Instead of tabulating all of the 14 Bravais lattices we will next consider the restrictions which must be imposed to allow cubic symmetry. It is evident that the restrictions $a_1 = a_2 = a_3$ and $\alpha_{12} = \alpha_{23} = \alpha_{31} = 90°$ are ones which will allow cubic symmetry. This lattice is known as the simple cubic lattice Γ_c.

However the restrictions $a_1 = a_2 = a_3$ and $\alpha_{12} = \alpha_{23} = \alpha_{31} = 60°$ can also allow cubic symmetry. The true unit cell defined by the axes $\mathbf{a}_1\mathbf{a}_2\mathbf{a}_3$ is shown by Fig. 2.7. By combinations of the $\mathbf{a}_1\mathbf{a}_2\mathbf{a}_3$, we can obtain a new set of orthogonal axes:

$$\mathbf{A}_1 = \mathbf{a}_1 - \mathbf{a}_2 + \mathbf{a}_3,$$
$$\mathbf{A}_2 = \mathbf{a}_1 + \mathbf{a}_2 - \mathbf{a}_3,$$
$$\mathbf{A}_3 = -\mathbf{a}_1 + \mathbf{a}_2 + \mathbf{a}_3.$$

Although the orthogonal axes are much more convenient to use, they do not specify the complete scheme of repetition. In addition to the repetitions given directly by the axes $\mathbf{A}_1\mathbf{A}_2\mathbf{A}_3$, we must specify three additional repetitions $(\mathbf{A}_1 + \mathbf{A}_2)/2$, $(\mathbf{A}_2 + \mathbf{A}_3)/2$, and $(\mathbf{A}_3 + \mathbf{A}_1)/2$. The orthogonal cell has a volume four times that of the true cell, and for every atom at position $\mathbf{r}_n$ there must be three identical atoms at positions

$$\mathbf{r}_n + (\mathbf{A}_1 + \mathbf{A}_2)/2,$$
$$\mathbf{r}_n + (\mathbf{A}_2 + \mathbf{A}_3)/2,$$
$$\mathbf{r}_n + (\mathbf{A}_3 + \mathbf{A}_1)/2.$$

This lattice is known as the face-centered cubic lattice Γ_c' and the words "face-centered" can be considered as just shorthand terminology for specifying the additional three translations. In a crystal whose Bravais lattice

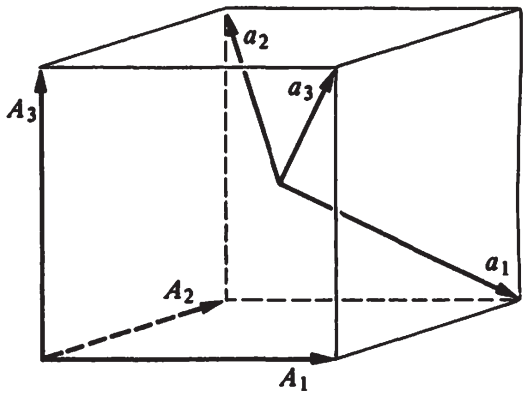

Fig. 2.8 Relation between the axes $\mathbf{a}_1\mathbf{a}_2\mathbf{a}_3$ of the true unit cell and the more convenient axes $\mathbf{A}_1\mathbf{A}_2\mathbf{A}_3$, defining a cell of twice the volume, for the body-centered cubic lattice.

is face-centered cubic, there can be many different kinds of atoms, but for each kind, the number of atoms per cell must be some multiple of four.

The restrictions $a_1 = a_2 = a_3$ and $\alpha_{12} = \alpha_{23} = \alpha_{31} = 109°28'$ will also allow cubic symmetry. In Fig. 2.8 the axes are shown, drawn from the center of a cube to three of the corners. Again it is possible by linear combinations to form a new set of orthogonal axes:

$$\mathbf{A}_1 = \mathbf{a}_1 + \mathbf{a}_3,$$
$$\mathbf{A}_2 = \mathbf{a}_1 + \mathbf{a}_2,$$
$$\mathbf{A}_3 = \mathbf{a}_2 + \mathbf{a}_3.$$

In using the new axes $\mathbf{A}_1\mathbf{A}_2\mathbf{A}_3$ it is necessary to specify the additional translation $(\mathbf{A}_1 + \mathbf{A}_2 + \mathbf{A}_3)/2$. This lattice is known as the body-centered cubic lattice Γ_c'', and the words "body-centered" can be considered as shorthand notation for specifying the additional translation. The volume of the orthogonal cell is twice that of the true unit cell and for each atom at position $\mathbf{r}_n$ there must be an identical atom at $\mathbf{r}_n + (\mathbf{A}_1 + \mathbf{A}_2 + \mathbf{A}_3)/2$. There may be many kinds of atoms in the cell, but for each kind the number must be some multiple of two.

2.7 TRANSFORMING AXES AND INDICES

Having considered a structure in terms of a set of axes $\mathbf{a}_1\mathbf{a}_2\mathbf{a}_3$ and having determined the corresponding indices *hkl*, we sometimes find it necessary to change to a new set of axes $\mathbf{A}_1\mathbf{A}_2\mathbf{A}_3$. We then have the problem of transforming the indices *hkl* to the corresponding new set *HKL*. To illustrate let us consider two such transformations of axes.

a) Hexagonal to Orthorhombic

The usual hexagonal axes with $\mathbf{a}_3$ perpendicular to $\mathbf{a}_1$ and $\mathbf{a}_2$, $|\mathbf{a}_1| = |\mathbf{a}_2|$, and $\alpha_{12} = 120°$ are shown by Fig. 2.9. To transform to a set of orthorhombic axes, we let

$$\mathbf{A}_1 = \mathbf{a}_1,$$
$$\mathbf{A}_2 = \mathbf{a}_1 + 2\mathbf{a}_2,$$
$$\mathbf{A}_3 = \qquad\qquad \mathbf{a}_3.$$

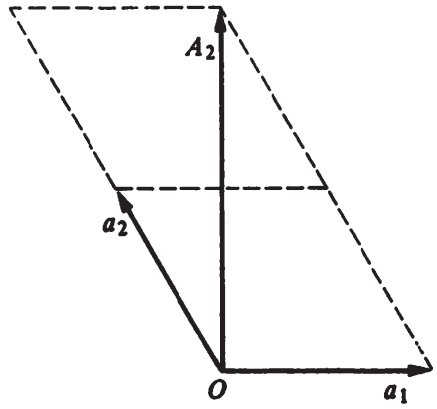

Fig. 2.9 The transformation from hexagonal axes $\mathbf{a}_1\mathbf{a}_2\mathbf{a}_3$ to orthorhombic axes.

b) Face-Centered Cubic to Rhombohedral

If the Bravais lattice is face-centered cubic, and we have indexed in terms of cubic axes $\mathbf{a}_1\mathbf{a}_2\mathbf{a}_3$, it is sometimes desirable to change to the smaller rhombohedral cell. The relation between the two sets of axes is given by

$$\begin{aligned}\mathbf{A}_1 &= \tfrac{1}{2}\mathbf{a}_1 + \tfrac{1}{2}\mathbf{a}_2 + 0,\\ \mathbf{A}_2 &= 0 + \tfrac{1}{2}\mathbf{a}_2 + \tfrac{1}{2}\mathbf{a}_3,\\ \mathbf{A}_3 &= \tfrac{1}{2}\mathbf{a}_1 + 0 + \tfrac{1}{2}\mathbf{a}_3.\end{aligned}$$

From these two examples, it can be seen that in general the transformation is represented by a set of equations such as

$$\begin{aligned}\mathbf{A}_1 &= \alpha_{11}\mathbf{a}_1 + \alpha_{12}\mathbf{a}_2 + \alpha_{13}\mathbf{a}_3,\\ \mathbf{A}_2 &= \alpha_{21}\mathbf{a}_1 + \alpha_{22}\mathbf{a}_2 + \alpha_{23}\mathbf{a}_3,\\ \mathbf{A}_3 &= \alpha_{31}\mathbf{a}_1 + \alpha_{32}\mathbf{a}_2 + \alpha_{33}\mathbf{a}_3,\end{aligned} \tag{2.15}$$

where the α_{ij} are integers or simple fractions. In terms of the original axes $\mathbf{a}_1\mathbf{a}_2\mathbf{a}_3$, the indices were called *hkl*. We are now interested in determining the indices *HKL* corresponding to the new axes. In terms of the two sets of axes $\mathbf{a}_1\mathbf{a}_2\mathbf{a}_3$ and $\mathbf{A}_1\mathbf{A}_2\mathbf{A}_3$, there are reciprocal vectors $\mathbf{b}_1\mathbf{b}_2\mathbf{b}_3$ and $\mathbf{B}_1\mathbf{B}_2\mathbf{B}_3$ defined by Eqs. (2.2). Since the orientation and spacing of a set of planes is the same in either set of axes, we can write

$$H\mathbf{B}_1 + K\mathbf{B}_2 + L\mathbf{B}_3 = h\mathbf{b}_1 + k\mathbf{b}_2 + l\mathbf{b}_3. \tag{2.16}$$

Multiplying the first line of Eq. (2.15) by Eq. (2.16), we have

$$\mathbf{A}_1 \cdot (H\mathbf{B}_1 + K\mathbf{B}_2 + L\mathbf{B}_3) = (\alpha_{11}\mathbf{a}_1 + \alpha_{12}\mathbf{a}_2 + \alpha_{13}\mathbf{a}_3) \cdot (h\mathbf{b}_1 + k\mathbf{b}_2 + l\mathbf{b}_3),$$

and this reduces to $H = \alpha_{11}h + \alpha_{12}k + \alpha_{13}l$. Treating each line of Eq. (2.15) in this way, we obtain

$$\begin{aligned}H &= \alpha_{11}h + \alpha_{12}k + \alpha_{13}l,\\ K &= \alpha_{21}h + \alpha_{22}k + \alpha_{23}l,\\ L &= \alpha_{31}h + \alpha_{32}k + \alpha_{33}l.\end{aligned} \tag{2.17}$$

Having set up a matrix of coefficients α_{ij} to transform the axes, the indices are then transformed by the same matrix.

PROBLEMS

2.1 If $v_a = \mathbf{a}_1 \cdot \mathbf{a}_2 \times \mathbf{a}_3$ and $v_b = \mathbf{b}_1 \cdot \mathbf{b}_2 \times \mathbf{b}_3$, by use of the vector relation $\mathbf{a} \times (\mathbf{b} \times \mathbf{c}) = \mathbf{b}(\mathbf{a} \cdot \mathbf{c}) - \mathbf{c}(\mathbf{a} \cdot \mathbf{b})$ show that $v_b = 1/v_a$.

2.2 Two crystallographic directions are represented by the vectors $\mathbf{A}_u = u_1\mathbf{a}_1 + u_2\mathbf{a}_2 + u_3\mathbf{a}_3$ and $\mathbf{A}_v = v_1\mathbf{a}_1 + v_2\mathbf{a}_2 + v_3\mathbf{a}_3$. If ϕ is the angle between the two directions, $\cos\phi = \mathbf{A}_u \cdot \mathbf{A}_v/|\mathbf{A}_u|\,|\mathbf{A}_v|$. Deduce expressions for $\cos\phi$ for (a) orthorhombic system (b) cubic system.

2.3 Represent a crystallographic direction by $\mathbf{A}_{uvw} = u\mathbf{a}_1 + v\mathbf{a}_2 + w\mathbf{a}_3$ and the normal to the *hkl* planes by $\mathbf{H}_{hkl} = h\mathbf{b}_1 + k\mathbf{b}_2 + l\mathbf{b}_3$. Let ϕ be the angle between $\mathbf{A}_{uvw}$ and $\mathbf{H}_{hkl}$. For the orthorhombic system deduce an expression for $\cos\phi$ in terms of $u, v, w, h, k, l, a_1, a_2, a_3$.

2.4 The zone axis *uvw* is defined by the vector $\mathbf{A}_{uvw} = u\mathbf{a}_1 + v\mathbf{a}_2 + w\mathbf{a}_3$. All planes *hkl* which contain the direction $\mathbf{A}_{uvw}$ are said to belong to the zone *uvw*. Deduce an expression for the indices *hkl* of planes belonging to the zone *uvw*.

2.5 If β_{12} is the angle between $\mathbf{b}_1$ and $\mathbf{b}_2$, $\cos\beta_{12} = \mathbf{b}_1 \cdot \mathbf{b}_2/|\mathbf{b}_1|\,|\mathbf{b}_2|$. Using the vector relation $(\mathbf{a}_i \times \mathbf{a}_j) \cdot (\mathbf{a}_j \times \mathbf{a}_k) = a_i a_j^2 a_k (\cos\alpha_{ij}\cos\alpha_{jk} - \cos\alpha_{ik})$, derive an expression for $\cos\beta_{12}$ in terms of $\alpha_{12}\alpha_{23}\alpha_{31}$.

2.6 Let $|\mathbf{a}_1| = 3.0$, $|\mathbf{a}_2| = 2.0$, $|\mathbf{a}_3| = 1.0$, $\alpha_{12} = 60°$, $\mathbf{a}_1$ and $\mathbf{a}_2$ in the plane of the paper, and $\mathbf{a}_3$ perpendicular to the paper. Draw accurately to scale the axes $\mathbf{a}_1$ and $\mathbf{a}_2$, and from definition $\mathbf{b}_1$ and $\mathbf{b}_2$. From the definition of the indices *hkl*, show the sets of planes (110), (210), and (310). From the definition $\mathbf{H}_{hkl} = h\mathbf{b}_1 + k\mathbf{b}_2 + l\mathbf{b}_3$, show the vectors $\mathbf{H}_{110}$, $\mathbf{H}_{210}$, and $\mathbf{H}_{310}$.

2.7 For metals having the FCC Bravais lattice with 4 atoms per cell, it is sometimes convenient to change to hexagonal axes $\mathbf{A}_1\mathbf{A}_2\mathbf{A}_3$, where $\mathbf{A}_1$ and $\mathbf{A}_2$ are parallel to a 111 plane and at 120° to one another; $\mathbf{A}_3$ is perpendicular to the 111 plane. The hexagonal cell contains 3 atoms. Set up expressions for the new indices *HKL* in terms of the cubic indices *hkl*.

DIFFRACTION BY A SMALL CRYSTAL

3.1 INTENSITY FROM A SMALL CRYSTAL

We consider an unpolarized monochromatic beam, of intensity I_0 and wavelength λ, falling on a very small single crystal. The conditions are illustrated by Fig. 3.1. We first consider that the primary beam is plane polarized with the electric field normal to the plane of the paper, and then later remove the restriction. The direction of the primary beam is represented by the unit vector $\mathbf{s}_0$. Relative to a crystal origin at O, the position of the atom of type n in unit cell $m_1m_2m_3$ is given by the vector $\mathbf{R}_m^n = m_1\mathbf{a}_1 + m_2\mathbf{a}_2 + m_3\mathbf{a}_3 + \mathbf{r}_n$. We consider the scattered intensity at a point of observation P, at a distance R from the crystal, in a direction specified by a unit vector $\mathbf{s}$. The crystal is assumed to be so small, relative to the distance from the x-ray source, that the primary beam can be treated by the plane-wave approximation. In terms of a wave front through O, the phase of the electric field in the primary beam acting on atom (m, n) depends upon the distance x_1. The total distance from the initial wave front to the point of observation is $x_1 + x_2$. Following the treatment of Chapter 1, and neglecting a 180° jump in phase in the scattering process, the instantaneous value of the electric field at the point of observation due to the unmodified scattering from the atom (m, n) is given by

$$\epsilon_p = \frac{E_0 e^2}{mc^2 R} f_n \cos\left[2\pi\nu t - \frac{2\pi}{\lambda}(x_1 + x_2)\right].$$

We assume that the crystal is so small, relative to the distance R to the point of observation, that the scattered beam can also be treated by the plane-wave

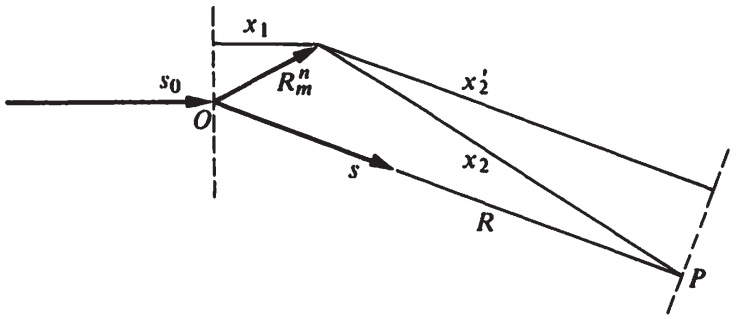

Fig. 3.1 Diffraction of a parallel primary beam by a small crystal.

approximation, and hence $(x_1 + x_2) \to (x_1 + x_2')$. Written in terms of the complex exponential, the instantaneous field at P due to unmodified scattering from the atom (m, n) is given by

$$\epsilon_p = \frac{E_0 e^2}{mc^2 R} f_n e^{i\{2\pi\nu t - (2\pi/\lambda)[R - (\mathbf{s}-\mathbf{s}_0)\cdot(m_1\mathbf{a}_1 + m_2\mathbf{a}_2 + m_3\mathbf{a}_3 + \mathbf{r}_n)]\}}.$$

The resultant field at P due to all the atoms in the crystal is then obtained by summing over n to include all the atoms in a unit cell, and summing over $m_1 m_2 m_3$ to include all the unit cells. For simplicity we shall assume that the crystal has the shape of a parallelopipedon with edges $N_1 a_1$, $N_2 a_2$, $N_3 a_3$ parallel to the crystal axes $\mathbf{a}_1\mathbf{a}_2\mathbf{a}_3$. This restriction will be removed when we consider the integrated intensity. Separating the four summations, the instantaneous field is expressed by

$$\epsilon_p = \frac{E_0 e^2}{mc^2 R} e^{2\pi i[\nu t - (R/\lambda)]} \sum_n f_n e^{(2\pi i/\lambda)(\mathbf{s}-\mathbf{s}_0)\cdot\mathbf{r}_n} \sum_{m_1=0}^{N_1-1} e^{(2\pi i/\lambda)(\mathbf{s}-\mathbf{s}_0)\cdot m_1\mathbf{a}_1} \times \sum_{m_2=0}^{N_2-1} e^{(2\pi i/\lambda)(\mathbf{s}-\mathbf{s}_0)\cdot m_2\mathbf{a}_2} \sum_{m_3=0}^{N_3-1} e^{(2\pi i/\lambda)(\mathbf{s}-\mathbf{s}_0)\cdot m_3\mathbf{a}_3}. \quad (3.1)$$

The summation over n involves the positions $\mathbf{r}_n$ of the different atoms in the unit cell, and hence it varies from one structure to another. It is called the structure factor and designated by F, where

$$F = \sum_n f_n e^{(2\pi i/\lambda)(\mathbf{s}-\mathbf{s}_0)\cdot\mathbf{r}_n}. \quad (3.2)$$

For purposes of crystal structure determinations, the structure factor F plays a very important role, since it is only in the structure factor that the atomic positions appear.

The summations over $m_1 m_2 m_3$ have the form of geometric progressions for which the sum is given by

$$S = a + ar + ar^2 + \cdots + l = \frac{rl - a}{r - 1}, \quad (3.3)$$

where a is the first term, l is the last term, and r is the ratio. Using Eq. (3.3), the sum over m_1 becomes

$$\sum_{m_1=0}^{N_1-1} e^{(2\pi i/\lambda)(\mathbf{s}-\mathbf{s}_0)\cdot m_1\mathbf{a}_1} = \frac{e^{(2\pi i/\lambda)(\mathbf{s}-\mathbf{s}_0)\cdot N_1\mathbf{a}_1} - 1}{e^{(2\pi i/\lambda)(\mathbf{s}-\mathbf{s}_0)\cdot\mathbf{a}_1} - 1}.$$

With similar expressions for the sums over m_2 and m_3, the instantaneous field at P can be written

$$\epsilon_p = \frac{E_0 e^2}{mc^2 R} e^{2\pi i[\nu t - (R/\lambda)]} F \frac{e^{(2\pi i/\lambda)(\mathbf{s}-\mathbf{s}_0)\cdot N_1\mathbf{a}_1} - 1}{e^{(2\pi i/\lambda)(\mathbf{s}-\mathbf{s}_0)\cdot\mathbf{a}_1} - 1} \frac{e^{(2\pi i/\lambda)(\mathbf{s}-\mathbf{s}_0)\cdot N_2\mathbf{a}_2} - 1}{e^{(2\pi i/\lambda)(\mathbf{s}-\mathbf{s}_0)\cdot\mathbf{a}_2} - 1} \times \frac{e^{(2\pi i/\lambda)(\mathbf{s}-\mathbf{s}_0)\cdot N_3\mathbf{a}_3} - 1}{e^{(2\pi i/\lambda)(\mathbf{s}-\mathbf{s}_0)\cdot\mathbf{a}_3} - 1}.$$

Following the rules set up in Chapter 1, we now write the complex conjugate ϵ_p^*:

$$\epsilon_p^* = \frac{E_0 e^2}{mc^2 R} e^{-2\pi i[\nu t-(R/\lambda)]F^*} \frac{e^{-(2\pi i/\lambda)(\mathbf{s}-\mathbf{s}_0)\cdot N_1\mathbf{a}_1}-1}{e^{-(2\pi i/\lambda)(\mathbf{s}-\mathbf{s}_0)\cdot\mathbf{a}_1}-1} \frac{e^{-(2\pi i/\lambda)(\mathbf{s}-\mathbf{s}_0)\cdot N_2\mathbf{a}_2}-1}{e^{-(2\pi i/\lambda)(\mathbf{s}-\mathbf{s}_0)\cdot\mathbf{a}_2}-1} \times \frac{e^{-(2\pi i/\lambda)(\mathbf{s}-\mathbf{s}_0)\cdot N_3\mathbf{a}_3}-1}{e^{-(2\pi i/\lambda)(\mathbf{s}-\mathbf{s}_0)\cdot\mathbf{a}_3}-1},$$

where by the complex conjugate of the structure factor we mean

$$F^* = \sum_n f_n^* e^{-(2\pi i/\lambda)(\mathbf{s}-\mathbf{s}_0)\cdot\mathbf{r}_n}. \tag{3.4}$$

In taking the product $\epsilon_p\epsilon_p^*$, there will be products of the form

$$\left(\frac{e^{iNx}-1}{e^{ix}-1}\right)\left(\frac{e^{-iNx}-1}{e^{-ix}-1}\right) = \frac{2-2\cos Nx}{2-2\cos x} = \frac{\sin^2 Nx/2}{\sin^2 x/2}$$

and hence

$$\epsilon_p\epsilon_p^* = \frac{E_0^2 e^4}{m^2c^4R^2} FF^* \frac{\sin^2(\pi/\lambda)(\mathbf{s}-\mathbf{s}_0)\cdot N_1\mathbf{a}_1}{\sin^2(\pi/\lambda)(\mathbf{s}-\mathbf{s}_0)\cdot\mathbf{a}_1} \frac{\sin^2(\pi/\lambda)(\mathbf{s}-\mathbf{s}_0)\cdot N_2\mathbf{a}_2}{\sin^2(\pi/\lambda)(\mathbf{s}-\mathbf{s}_0)\cdot\mathbf{a}_2} \times \frac{\sin^2(\pi/\lambda)(\mathbf{s}-\mathbf{s}_0)\cdot N_3\mathbf{a}_3}{\sin^2(\pi/\lambda)(\mathbf{s}-\mathbf{s}_0)\cdot\mathbf{a}_3}. \tag{3.5}$$

Following the results of Chapter 1, $\epsilon_p\epsilon_p^* = E^2$, where E is the amplitude at the point of observation. Multiplying both sides of the equation by $c/8\pi$, we obtain the intensity at the point of observation $I_p = E^2c/8\pi$ in terms of the intensity in the primary beam $I_0 = E_0^2c/8\pi$. Our derivation has been carried through for a primary beam polarized with electric field perpendicular to the plane of the paper in Fig. 3.1. If we had assumed a primary beam polarized with the electric field in the plane of the paper, we would have obtained Eq. (3.5) with an additional factor $\cos^2 2\theta$. For an unpolarized beam, E_0 takes all orientations perpendicular to $\mathbf{s}_0$. We resolve into two components, and average the value of E^2 at point P exactly as was done in deriving Eq. (1.2). This introduces a polarization factor $(1+\cos^2 2\theta)/2$. For an unpolarized primary beam of intensity I_0, the intensity I_p from a small parallelopipedon crystal is given by

$$I_p = I_e F^2 \frac{\sin^2(\pi/\lambda)(\mathbf{s}-\mathbf{s}_0)\cdot N_1\mathbf{a}_1}{\sin^2(\pi/\lambda)(\mathbf{s}-\mathbf{s}_0)\cdot\mathbf{a}_1} \frac{\sin^2(\pi/\lambda)(\mathbf{s}-\mathbf{s}_0)\cdot N_2\mathbf{a}_2}{\sin^2(\pi/\lambda)(\mathbf{s}-\mathbf{s}_0)\cdot\mathbf{a}_2} \times \frac{\sin^2(\pi/\lambda)(\mathbf{s}-\mathbf{s}_0)\cdot N_3\mathbf{a}_3}{\sin^2(\pi/\lambda)(\mathbf{s}-\mathbf{s}_0)\cdot\mathbf{a}_3}, \tag{3.6}$$

where

$$I_e = I_0 \frac{e^4}{m^2c^4R^2}\left(\frac{1+\cos^2 2\theta}{2}\right)$$

and FF^* has been abbreviated by F^2.

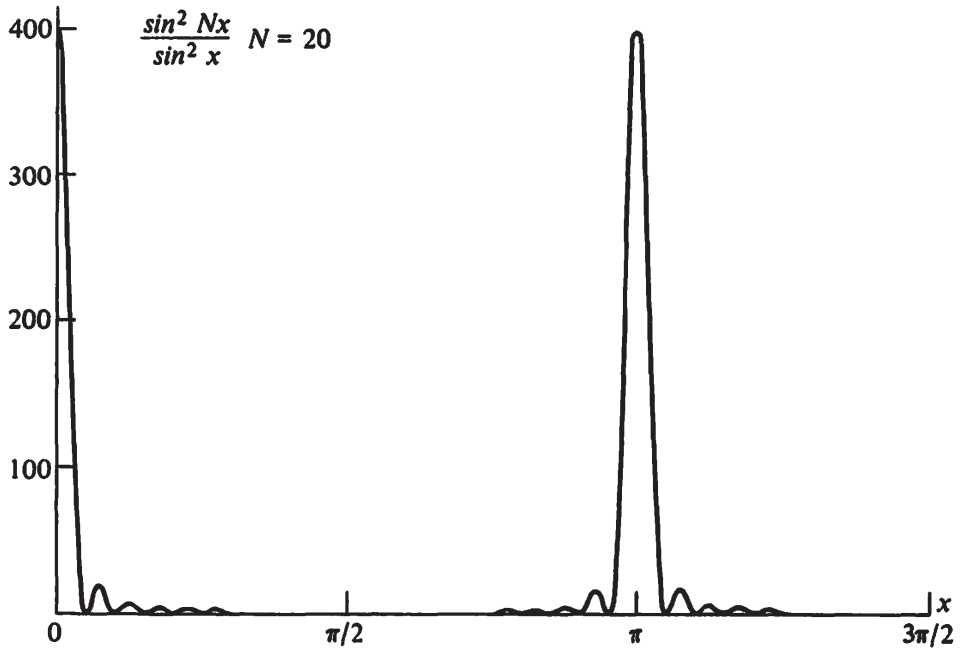

Fig. 3.2 The function $(\sin^2 Nx)/\sin^2 x$ for $N = 20$. The function peaks at values of x which are integral multiples of π, and it is essentially zero everywhere else.

3.2 THE 3 LAUE EQUATIONS

The value of the intensity at the point of observation depends sharply upon the three quotients of Eq. (3.6). These are of the form

$$y = \frac{\sin^2 Nx}{\sin^2 x},$$

where $x_i = (\pi/\lambda)(\mathbf{s} - \mathbf{s}_0) \cdot \mathbf{a}_i$. Figure 3.2 shows the function

$$y = \frac{\sin^2 Nx}{\sin^2 x}$$

for $N = 20$. The function rises to high maxima $y = N^2$ at the positions $x = n\pi$. For the average crystal which we shall be considering, N is considerably greater than 20, and the peaks are accordingly much higher and sharper than those of Fig. 3.2. We can say that the function $y = (\sin^2 Nx)/\sin^2 x$ is essentially zero everywhere except in the immediate vicinity of $x = n\pi$, where it rises to high maxima. Hence the intensity I_p will be essentially zero unless the three quotients are simultaneously close to their maximum values. For I_p to be a maximum, we must simultaneously satisfy the three conditions

$$(\pi/\lambda)(\mathbf{s} - \mathbf{s}_0) \cdot \mathbf{a}_1 = h'\pi,$$

$$(\pi/\lambda)(\mathbf{s} - \mathbf{s}_0) \cdot \mathbf{a}_2 = k'\pi,$$

$$(\pi/\lambda)(\mathbf{s} - \mathbf{s}_0) \cdot \mathbf{a}_3 = l'\pi,$$

where h', k', l' are three integers. Rearranged and written in the form below, these are called the 3 Laue equations:

$$\begin{aligned}(\mathbf{s} - \mathbf{s}_0) \cdot \mathbf{a}_1 &= h'\lambda, \\ (\mathbf{s} - \mathbf{s}_0) \cdot \mathbf{a}_2 &= k'\lambda, \\ (\mathbf{s} - \mathbf{s}_0) \cdot \mathbf{a}_3 &= l'\lambda.\end{aligned} \tag{3.7}$$

Since a diffracted beam exists only if the 3 Laue equations are simultaneously satisfied, these three equations together must be equivalent to the Bragg law. To show that this is so, let any arbitrary vector $\mathbf{r}$ be represented in terms of the three reciprocal vectors:

$$\mathbf{r} = p_1\mathbf{b}_1 + p_2\mathbf{b}_2 + p_3\mathbf{b}_3.$$

To determine the coefficient p_1, take the scalar product with $\mathbf{a}_1$:

$$\mathbf{r} \cdot \mathbf{a}_1 = (p_1\mathbf{b}_1 + p_2\mathbf{b}_2 + p_3\mathbf{b}_3) \cdot \mathbf{a}_1 = p_1.$$

With p_2 and p_3 determined in a similar way, we can write the general relation for expressing a vector $\mathbf{r}$ in terms of the reciprocal vectors $\mathbf{b}_1\mathbf{b}_2\mathbf{b}_3$:

$$\mathbf{r} = (\mathbf{r} \cdot \mathbf{a}_1)\mathbf{b}_1 + (\mathbf{r} \cdot \mathbf{a}_2)\mathbf{b}_2 + (\mathbf{r} \cdot \mathbf{a}_3)\mathbf{b}_3. \tag{3.8}$$

We now let $\mathbf{r}$ be the vector $(\mathbf{s} - \mathbf{s}_0)$, and combine Eq. (3.8) with the 3 Laue equations:

$$\begin{aligned}(\mathbf{s} - \mathbf{s}_0) = (\mathbf{s} - \mathbf{s}_0) \cdot \mathbf{a}_1\mathbf{b}_1 + (\mathbf{s} - \mathbf{s}_0) \cdot \mathbf{a}_2\mathbf{b}_2 + (\mathbf{s} - \mathbf{s}_0) \cdot \mathbf{a}_3\mathbf{b}_3 \\ = \lambda(h'\mathbf{b}_1 + k'\mathbf{b}_2 + l'\mathbf{b}_3), \\ \mathbf{s} - \mathbf{s}_0 = \lambda\mathbf{H}_{h'k'l'}.\end{aligned} \tag{3.9}$$

Comparing with Eq. (2.5), it is seen that Eq. (3.9) is simply the Bragg law for the plane $h'k'l'$, and hence the three integers $h'k'l'$ of the Laue equations are the Miller indices hkl of the corresponding reflection.

3.3 STRUCTURE FACTOR FOR A BRAGG REFLECTION

The structure factor depends upon the atomic positions and these were represented by the cell vectors $\mathbf{r}_n$. It is convenient to express the cell vectors in terms of components along $\mathbf{a}_1\mathbf{a}_2\mathbf{a}_3$ by means of fractional coordinates x_n, y_n, z_n, which are numbers between zero and unity. As illustrated by Fig. 3.3, $\mathbf{r}_n = x_n\mathbf{a}_1 + y_n\mathbf{a}_2 + z_n\mathbf{a}_3$. For an hkl-reflection, we are interested in the value of the structure factor when the Bragg law is satisfied for this set of planes, and hence when $\mathbf{s} - \mathbf{s}_0 = \lambda\mathbf{H}_{hkl}$. Expressing the cell vectors in terms of fractional coordinates, and using the $(\mathbf{s} - \mathbf{s}_0)$ value which corresponds to an hkl-reflection, Eq. (3.2) becomes

$$F_{hkl} = \sum_n f_n e^{2\pi i(h\mathbf{b}_1 + k\mathbf{b}_2 + l\mathbf{b}_3) \cdot (x_n\mathbf{a}_1 + y_n\mathbf{a}_2 + z_n\mathbf{a}_3)} = \sum_n f_n e^{2\pi i(hx_n + ky_n + lz_n)}. \tag{3.10}$$

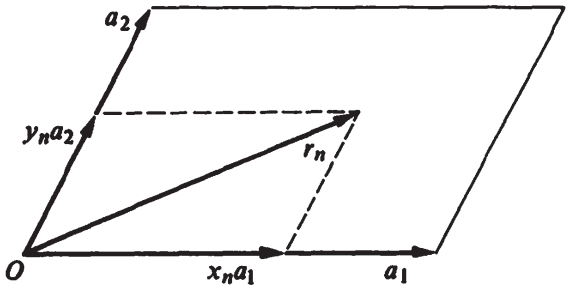

Fig. 3.3 Representation of the basis vector $\mathbf{r}_n$ in terms of the fractional coordinates x_n, y_n, and z_n.

Equation (3.10) expresses the structure factor for a reflection *hkl* in the simplest and most useful form.

If the structure factor F_{hkl} is zero for a certain reflection *hkl*, the intensity of that reflection will be zero. It is by means of systematically vanishing intensities that we decide between the side-centered, face-centered, and body-centered Bravais lattices discussed in Section 2.6.

In a crystal whose Bravais lattice is face-centered, for every atom with fractional coordinates $x_n y_n z_n$, there must be three identical atoms with coordinates $x_n + \frac{1}{2}, y_n + \frac{1}{2}, z_n$; $x_n + \frac{1}{2}, y_n, z_n + \frac{1}{2}$; and $x_n, y_n + \frac{1}{2}, z_n + \frac{1}{2}$. If the cell contains n atoms, there are $n/4$ groups of four, all four atoms in each group having the same scattering factor. The structure factor can be expressed as a sum over such groups of 4 atoms:

$$F_{hkl} = \sum_{n/4} f_n \{ e^{2\pi i(hx_n+ky_n+lz_n)} + e^{2\pi i(h[x_n+1/2]+k[y_n+1/2]+lz_n)} + e^{2\pi i(h[x_n+1/2]+ky_n+l[z_n+1/2])} + e^{2\pi i(hx_n+k[y_n+1/2]+l(z_n+1/2])} \}.$$

This can be written in the simpler form

$$F_{hkl} = [1 + e^{\pi i(h+k)} + e^{\pi i(h+l)} + e^{\pi i(k+l)}] \sum_{n/4} f_n e^{2\pi i(hx_n+ky_n+lz_n)}. \quad (3.11)$$

If m is an integer, $e^{\pi i m} = (-1)^m$, and hence the first factor takes the value 4 if *hkl* are unmixed (all odd or all even) and the value zero if *hkl* are mixed:

$$hkl \text{ unmixed: } F_{hkl} = 4 \sum_{n/4} f_n e^{2\pi i(hx_n+ky_n+lz_n)}; \quad (3.12)$$

$$hkl \text{ mixed: } \quad F_{hkl} = 0.$$

Regardless of the atomic coordinates $x_n y_n z_n$, $F_{hkl} = 0$ for all reflections with mixed *hkl*. Hence the face-centered Bravais lattice is recognized by the fact that all reflections with mixed indices are missing.

In a crystal whose Bravais lattice is body-centered, for every atom with fractional coordinates $x_n y_n z_n$, there must be an identical atom with coordinates $x_n + \frac{1}{2}, y_n + \frac{1}{2}$, and $z_n + \frac{1}{2}$. The structure factor is expressed as a sum over such groups of 2 atoms:

$$F_{hkl} = [1 + e^{\pi i(h+k+l)}] \sum_{n/2} f_n e^{2\pi i(hx_n+ky_n+lz_n)}$$

and hence

$$\begin{aligned} h+k+l = \text{even}: &\qquad F_{hkl} = 2\sum_{n/2} f_n e^{2\pi i(hx_n+ky_n+lz_n)}, \\ h+k+l = \text{odd}: &\qquad F_{hkl} = 0. \end{aligned} \tag{3.13}$$

The body-centered Bravais lattice is recognized from the fact that all reflections will be missing for $h + k + l =$ odd.

We next consider the evaluation of the structure factor for two common structures having the face-centered cubic Bravais lattice. In rock salt, the cubic cell contains 4 Na and 4 Cl at the following positions:

$$\text{Cl}: \begin{matrix} 0 & 0 & 0 \\ \frac{1}{2} & \frac{1}{2} & 0 \\ \frac{1}{2} & 0 & \frac{1}{2} \\ 0 & \frac{1}{2} & \frac{1}{2} \end{matrix} \qquad \text{Na}: \begin{matrix} \frac{1}{2} & \frac{1}{2} & \frac{1}{2} \\ 0 & 0 & \frac{1}{2} \\ 0 & \frac{1}{2} & 0 \\ \frac{1}{2} & 0 & 0 \end{matrix}$$

To evaluate the structure factor using Eq. (3.12), we can choose any one of the positions in each group of 4 atoms. Using 0 0 0 for Cl and $\frac{1}{2}\,\frac{1}{2}\,\frac{1}{2}$ for Na, the structure factor is given by

$$\begin{aligned} hkl \text{ mixed}: &\qquad F_{hkl} = 0 \\ hkl \text{ unmixed}: &\qquad F_{hkl} = 4[f_{\text{Cl}} + f_{\text{Na}} e^{\pi i(h+k+l)}]. \end{aligned}$$

For rock salt, the structure factor takes the three forms:

$$\begin{aligned} hkl \quad \text{all even}: &\qquad F_{hkl} = 4(f_{\text{Cl}} + f_{\text{Na}}), \\ hkl \quad \text{all odd}: &\qquad F_{hkl} = 4(f_{\text{Cl}} - f_{\text{Na}}), \\ hkl \quad \text{mixed}: &\qquad F_{hkl} = 0. \end{aligned} \tag{3.14}$$

In the zinc blende form of ZnS, the face-centered cubic cell contains 4 Zn and 4 S at the following positions:

$$\text{Zn}: \begin{matrix} 0 & 0 & 0 \\ \frac{1}{2} & \frac{1}{2} & 0 \\ \frac{1}{2} & 0 & \frac{1}{2} \\ 0 & \frac{1}{2} & \frac{1}{2} \end{matrix} \qquad \text{S}: \begin{matrix} \frac{1}{4} & \frac{1}{4} & \frac{1}{4} \\ \frac{3}{4} & \frac{3}{4} & \frac{1}{4} \\ \frac{3}{4} & \frac{1}{4} & \frac{3}{4} \\ \frac{1}{4} & \frac{3}{4} & \frac{3}{4} \end{matrix}$$

Using Eq. (3.12) with the positions 0 0 0 for Zn and $\frac{1}{4}\,\frac{1}{4}\,\frac{1}{4}$ for S, the structure factor is given by

$$hkl \text{ unmixed}: F_{hkl} = 4[f_{\text{Zn}} + f_{\text{S}} e^{(\pi i/2)(h+k+l)}].$$

In this case, the expression may be either real or complex, and hence we consider the square $F_{hkl}^2 = F_{hkl} F_{hkl}^*$:

$$\begin{aligned} F_{hkl}^2 &= 16[f_{\text{Zn}} + f_{\text{S}} e^{(\pi i/2)(h+k+l)}][f_{\text{Zn}} + f_{\text{S}} e^{-(\pi i/2)(h+k+l)}] \\ &= 16\left[f_{\text{Zn}}^2 + f_{\text{S}}^2 + 2f_{\text{Zn}} f_{\text{S}} \cos\frac{\pi}{2}(h+k+l)\right] \end{aligned}$$

For zinc blende, the structure factor takes the four forms:

$$\begin{aligned} &h + k + l = 4n && F_{hkl}^2 = 16(f_{Zn} + f_S)^2, \\ &h + k + l = (2n + 1)2: && F_{hkl}^2 = 16(f_{Zn} - f_S)^2, \\ &hkl \text{ all odd:} && F_{hkl}^2 = 16(f_{Zn}^2 + f_S^2), \\ &hkl \text{ mixed:} && F_{hkl}^2 = 0. \end{aligned} \tag{3.15}$$

We next consider the three common metal structures. Copper has a face-centered cubic Bravais lattice with 4 atoms per cubic cell at positions: 0 0 0, $\frac{1}{2}\frac{1}{2}0$, $\frac{1}{2}0\frac{1}{2}$, and $0\frac{1}{2}\frac{1}{2}$. Using Eq. (3.12) and the position 0 0 0, the structure factor takes the two forms:

$$\begin{aligned} &hkl \text{ unmixed:} && F_{hkl} = 4f, \\ &hkl \text{ mixed:} && F_{hkl} = 0. \end{aligned} \tag{3.16}$$

Tungsten has a body-centered cubic Bravais lattice with 2 atoms per cubic cell at positions: 0 0 0 and $\frac{1}{2}\frac{1}{2}\frac{1}{2}$. Using Eq. (3.13) and the position 0 0 0, the structure factor takes the two forms:

$$\begin{aligned} &h + k + l = \text{even:} && F_{hkl} = 2f, \\ &h + k + l = \text{odd:} && F_{hkl} = 0. \end{aligned} \tag{3.17}$$

Zinc has the hexagonal close-packed structure with 2 atoms per hexagonal cell at the positions 0 0 0 and $\frac{1}{3}\frac{2}{3}\frac{1}{2}$. The structure factor is expressed by

$$F_{hkl} = f[1 + e^{2\pi i\{[(h+2k)/3]+(l/2)\}}].$$

Since the expression can be either real or complex, we change to the square

$$\begin{aligned} F_{hkl}^2 &= f^2[1 + e^{2\pi i\{[(h+2k)/3]+(l/2)\}}][1 + e^{-2\pi i\{[(h+2k)/3]+(l/2)\}}] \\ &= 4f^2 \cos^2 \pi\left(\frac{h + 2k}{3} + \frac{l}{2}\right). \end{aligned}$$

For the hexagonal close-packed structure, the structure factor takes the four forms:

$$\begin{aligned} &h + 2k = 3n,\ l = \text{even:} && F_{hkl}^2 = 4f^2, \\ &h + 2k = 3n \pm 1,\ l = \text{odd:} && F_{hkl}^2 = 3f^2, \\ &h + 2k = 3n \pm 1,\ l = \text{even:} && F_{hkl}^2 = f^2, \\ &h + 2k = 3n,\ l = \text{odd:} && F_{hkl}^2 = 0. \end{aligned} \tag{3.18}$$

The hexagonal close-packed structure can be recognized from the fact that all reflections are missing for which l = odd and either $h + 2k = 3n$ or $2h + k = 3n$. The condition can be stated either way since if $h + 2k = 3n$, $2h + k = 6n - 3k = 3n'$.

For copper and tungsten the vanishings were a result of the Bravais lattice. The cubic cell was not the true smallest unit cell. If we had indexed in terms of the axes defining the one-atom cell, there would have been no vanishings. In the hexagonal close-packed structure it is not possible to find a new set of axes which will allow only one atom per cell. In this case the vanishings have to do with a particular structure.

It is important to notice carefully the distinction between a structure and a Bravais lattice. Structures are generally named after some common substance having that kind of structure. Any substance AB based on the face-centered cubic Bravais lattice, with a cubic cell containing $4A$ and $4B$ at the positions listed above for rock salt, is said to have the NaCl or rock salt structure. Similarly any substance AB with a cubic cell containing $4A$ and $4B$ at the positions listed above for ZnS is said to have the zinc blende structure. In both cases the Bravais lattice was face-centered cubic, but they were two different structures. The metals based on a face-centered cubic Bravais lattice with 4 atoms per cubic cell are said to have the copper structure. The metals whose structure is based upon a body-centered cubic Bravais lattice with 2 atoms per cubic cell are said to have the tungsten structure. Metals having the hexagonal close-packed structure with 2 atoms per hexagonal cell are said to have the magnesium structure. Silicon and germanium have face-centered cubic Bravais lattices with 8 atoms per cubic cell and are said to have the diamond structure. The common metal structures with only one kind of atom in the cell are degenerate cases and the general terminology is not followed in every day discussion. Instead of saying that Ag, Au, and Al have the copper structure we say that they are face-centered cubic, and instead of saying that αFe and Mo have the tungsten structure we say that they are body-centered cubic. This is not correct terminology, but since the practice has become widely established, and since we all know what is meant, there is probably no harm in following the common practice.

3.4 EFFECT OF TEMPERATURE VIBRATION ON THE INTENSITY FROM A SMALL CRYSTAL

Equation (3.6) was derived on the assumption that the atoms occupy definite positions in the crystal. These definite positions are however only average positions about which the atoms oscillate. Even at room temperature, an atom may at any instant be displaced appreciably from its average position as a result of the thermal vibrations in the crystal. We shall now repeat the derivation of Eq. (3.6), but this time include the temperature vibration of the atoms. In carrying through the derivation, we shall use the reduced notation which is customary for this type of calculation. Instead of speaking of the atom of type n in the unit cell $m_1m_2m_3$, we shall speak of the atom l

at the average position $\mathbf{R}_l$. At any instant the atom is at $\mathbf{R}'_l = \mathbf{R}_l + \boldsymbol{\delta}_l$, where $\boldsymbol{\delta}_l$ is the instantaneous displacement due to thermal vibration.

Omitting the nonessential terms which drop out on multiplying by the complex conjugate, the intensity is obtained by summing over all atoms to form the complex amplitude, and then multiplying this by its complex conjugate:

$$I = I_e \sum_l f_l e^{(2\pi i/\lambda)(\mathbf{s}-\mathbf{s}_0)\cdot(\mathbf{R}_l+\boldsymbol{\delta}_l)} \sum_{l'} f_{l'}^* e^{-(2\pi i/\lambda)(\mathbf{s}-\mathbf{s}_0)\cdot(\mathbf{R}_{l'}+\boldsymbol{\delta}_{l'})}.$$

What we observe experimentally is the time average of the intensity:

$$I = I_e \sum_l \sum_{l'} f_l f_{l'}^* e^{(2\pi i/\lambda)(\mathbf{s}-\mathbf{s}_0)\cdot(\mathbf{R}_l-\mathbf{R}_{l'})} \langle e^{(2\pi i/\lambda)(\mathbf{s}-\mathbf{s}_0)\cdot(\boldsymbol{\delta}_l-\boldsymbol{\delta}_{l'})} \rangle \tag{3.19}$$

Let $(2\pi i/\lambda)(\mathbf{s} - \mathbf{s}_0) \cdot \boldsymbol{\delta}_l = iku_{sl}$, where $k = 4\pi \sin\theta/\lambda$ and u_{sl} is the component of $\boldsymbol{\delta}_l$ along $\mathbf{s} - \mathbf{s}_0$, and hence the component of displacement normal to the diffracting planes. The average which we need is expressed by

$$\langle e^{(2\pi i/\lambda)(\mathbf{s}-\mathbf{s}_0)\cdot(\boldsymbol{\delta}_l-\boldsymbol{\delta}_{l'})} \rangle = \langle e^{ik(u_{sl}-u_{sl'})} \rangle.$$

If x is small and has equal probability of being positive or negative, we can obtain the average $\langle e^{ix} \rangle$ by expanding and using the fact that odd power averages are zero:

$$\langle e^{ix} \rangle = 1 + i\langle x \rangle - \tfrac{1}{2}\langle x^2 \rangle - \tfrac{1}{6}i\langle x^3 \rangle = e^{-(1/2)\langle x^2 \rangle}.$$

If x follows a Gaussian distribution, this result is exact even if x is not confined to small values. A Gaussian probability is expressed by

$$p(x) = \frac{\alpha}{\sqrt{\pi}} e^{-\alpha^2 x^2},$$

where

$$\int_{-\infty}^{+\infty} p(x)\, dx = 1.$$

Since $\langle e^{ix} \rangle = \langle \cos x \rangle + i\langle \sin x \rangle = \langle \cos x \rangle$, the average $\langle e^{ix} \rangle$ is given by

$$\langle e^{ix} \rangle = \int_{-\infty}^{+\infty} \frac{\alpha}{\sqrt{\pi}} e^{-\alpha^2 x^2} \cos x\, dx = e^{-(1/4\alpha^2)}.$$

Also

$$\langle x^2 \rangle = \int_{-\infty}^{+\infty} \frac{\alpha}{\sqrt{\pi}} e^{-\alpha^2 x^2} x^2\, dx = \frac{1}{2\alpha^2}.$$

From these two expressions

$$\langle e^{ix} \rangle = e^{-(1/2)\langle x^2 \rangle}. \tag{3.20}$$

Hence if either $k(u_{sl} - u_{sl'})$ is small, or if it follows a Gaussian distribution

$$\langle e^{ik(u_{sl}-u_{sl'})}\rangle = e^{-(1/2)k^2\langle(u_{sl}-u_{sl'})^2\rangle} = e^{-(1/2)k^2\langle u_{sl}{}^2\rangle}e^{-(1/2)k^2\langle u_{sl'}{}^2\rangle}e^{k^2\langle u_{sl}u_{sl'}\rangle}.$$

Introduce the abbreviations

$$e^{-(1/2)k^2\langle u_{sl}{}^2\rangle} = e^{-M_l}, \qquad e^{-(1/2)k^2\langle u_{sl'}{}^2\rangle} = e^{-M_{l'}}, \tag{3.21}$$

and write

$$e^{k^2\langle u_{sl}u_{sl'}\rangle} = 1 + (e^{k^2\langle u_{sl}u_{sl'}\rangle} - 1).$$

Incorporating these results, Eq. (3.19) can be split into two terms

$$I = I_e \sum_l \sum_{l'} f_l e^{-M_l} f_{l'}^* e^{-M_{l'}} e^{(2\pi i/\lambda)(\mathbf{s}-\mathbf{s}_0)\cdot(\mathbf{R}_l-\mathbf{R}_{l'})}$$
$$+ I_e \sum_l \sum_{l'} f_l e^{-M_l} f_{l'}^* e^{-M_{l'}} e^{(2\pi i/\lambda)(\mathbf{s}-\mathbf{s}_0)\cdot(\mathbf{R}_l-\mathbf{R}_{l'})}\{e^{k^2\langle u_{sl}u_{sl'}\rangle} - 1\}. \tag{3.22}$$

Since $\langle u_{sl}u_{sl'}\rangle$ approaches zero for positions l and l' which are not near one another, the second term of Eq. (3.22) will not contain any contributions for large values of $|\mathbf{R}_l - \mathbf{R}_{l'}|$, and hence it will not give rise to sharp peaks since it is the large values of $|\mathbf{R}_l - \mathbf{R}_{l'}|$ which produce sharpness. It represents a diffuse contribution which is called the temperature diffuse scattering. The first term in Eq. (3.22) represents the sharp crystalline reflection reduced in intensity by the factors e^{-M_l} and $e^{-M_{l'}}$. Except for these two factors, the first term of Eq. (3.22) is exactly equivalent to Eq. (3.6). To include temperature vibration in the intensity from a small crystal we replace Eq. (3.6) by

$$I = I_e F_T^2 \frac{\sin^2(\pi/\lambda)(\mathbf{s}-\mathbf{s}_0)\cdot N_1\mathbf{a}_1}{\sin^2(\pi/\lambda)(\mathbf{s}-\mathbf{s}_0)\cdot\mathbf{a}_1} \frac{\sin^2(\pi/\lambda)(\mathbf{s}-\mathbf{s}_0)\cdot N_2\mathbf{a}_2}{\sin^2(\pi/\lambda)(\mathbf{s}-\mathbf{s}_0)\cdot\mathbf{a}_2}$$
$$\times \frac{\sin^2(\pi/\lambda)(\mathbf{s}-\mathbf{s}_0)\cdot N_3\mathbf{a}_3}{\sin^2(\pi/\lambda)(\mathbf{s}-\mathbf{s}_0)\cdot\mathbf{a}_3}, \tag{3.23}$$

where

$$F_T = \sum_n f_n e^{-M_n} e^{2\pi i(hx_n+ky_n+lz_n)}. \tag{3.24}$$

To separate the angular part, we often write $M = B\sin^2\theta/\lambda^2$. Since the $\langle u_{sl}^2\rangle$ may be different for the different kinds of atoms in the crystal, Eq. (3.24) allows for different values of B_n. In addition the $\langle u_{sl}^2\rangle$ may be different for *hkl*-planes with different orientation, so that for each kind of atom, the B_n may vary with the *hkl*-orientation.

When there is only one kind of atom, so that all of the M_n are the same,

$$F_T^2 = F^2 e^{-2M}. \tag{3.25}$$

For this case, the effect of temperature vibration on the sharp crystalline peaks is adequately expressed by a factor e^{-2M} which is usually called the Debye temperature factor. From Eq. (3.21), $2M = 16\pi^2\langle u_s^2\rangle(\sin^2\theta)/\lambda^2$ and hence the reduction in intensity becomes more pronounced for high temperatures where $\langle u_s^2\rangle$ is large, and for reflections at high values of $(\sin\theta)/\lambda$.

PROBLEMS

3.1 Show that the difference in the distances x_2 and x_2' of Fig. 3.1 can be approximated by

$$x_2 - x_2' = (\mathbf{R}_m^n \times \mathbf{s})^2/2R.$$

For a distance $R = 10$ cm and wavelength $\lambda = 1.5$ A what is the maximum permissible value for $|\mathbf{R}_m^n|$ to allow the approximation $(x_1 + x_2) \to (x_1 + x_2')$ with an error of less than $\lambda/30$ (Regardless of the angle between $\mathbf{R}_m^n$ and s)?

3.2 In the vicinity of $x = 0$, the function $y = \sin^2 Nx/\sin^2 x$ can be approximated by $y = N^2\sin^2\phi/\phi^2$, where $\phi = Nx$. Derive an expression for the full peak breadth at half maximum ordinate. Derive an expression for the area under the peak. What are the dependences upon N: of the maximum ordinate, of the full peak breadth at half maximum ordinate, and of the area under the peak?

3.3 In the vicinity of a Bragg reflection, the Laue equations are nearly satisfied and we can write $(\mathbf{s} - \mathbf{s}_0)\cdot\mathbf{a}_1 = h'\lambda + \epsilon\cdot\mathbf{a}_1$, where $\epsilon\cdot\mathbf{a}_1$ is sufficiently small to allow the sum to be replaced by an integral:

$$\sum_{m_1=0}^{N_1-1} e^{(2\pi i/\lambda)(\mathbf{s}-\mathbf{s}_0)\cdot m_1\mathbf{a}_1} = \sum_{m_1=0}^{N_1-1} e^{(2\pi i/\lambda)\epsilon\cdot m_1\mathbf{a}_1} \to \int_{m_1=0}^{N_1} e^{(2\pi i/\lambda)\epsilon\cdot\mathbf{a}_1 m_1}\, dm_1.$$

Derive an equation corresponding to Eq. (3.6) and show that the two equations are equivalent.

3.4 For a crystal with the side-centered lattice represented by the axes A_1, A_2, a_3, of Fig. 2.6, show that all reflections with $h + k =$ odd will be missing.

3.5 Cesium chloride (CsCl) is simple cubic with one CsCl per unit cell; Cs 0 0 0, Cl $\frac{1}{2}\frac{1}{2}\frac{1}{2}$. Derive simplified expressions for the structure factor F. Will there be any systematic vanishings?

3.6 Diamond is face-centered cubic (FCC) with 8 atoms per unit cell, coordinates 0 0 0; $\frac{1}{4}\frac{1}{4}\frac{1}{4}$ and the other 6 given by the face-centering translations.

a) Derive simplified expressions for the structure factor F.
b) What class of reflections will be missing?
c) What should be the intensity of the 2 2 2 reflection from diamond?

3.7 Fluorite (CaF_2) is face-centered cubic a =5.45 A, with 4 CaF_2 per unit cell at Ca 0 0 0; F $\frac{1}{4}\frac{1}{4}\frac{1}{4}$, $\frac{3}{4}\frac{3}{4}\frac{3}{4}$, and the other positions given by the face-centering translations.

a) Derive simplified expressions for the structure factor F.
b) From the f tables evaluate F^2 for the reflections 1 1 1 and 2 2 2.
c) Set up an expression for F^2 including dispersion corrections $\Delta f'$ and $\Delta f''$ for Ca.

3.8 Graphite is hexagonal with 4 atoms per cell in the positions 0 0 0; $\frac{1}{3}\,\frac{2}{3}\,0$; $0\,0\,\frac{1}{2}$; $\frac{2}{3}\,\frac{1}{3}\,\frac{1}{2}$. Show that the structure factor is given by

$$l = \text{even}: \quad F = 4f\cos^2 \pi(h + 2k)/3,$$

$$l = \text{odd}: \quad F = i2f\sin 2\pi(h + 2k)/3.$$

For what combinations of *hkl* will the structure factor vanish?

3.9 The Wurtzite form of ZnS is hexagonal with 2 ZnS per unit cell at positions Zn 0 0 0, $\frac{1}{3}\,\frac{2}{3}\,\frac{1}{2}$; S 0 0 $\frac{3}{8}$, $\frac{1}{3}\,\frac{2}{3}\,\frac{7}{8}$. Derive simplified expressions for the structure factor *F*. For what *hkl* combinations will *F* vanish?

3.10 Cu_3Au is cubic with 1 unit of Cu_3Au per unit cell. In the ordered form the positions are Au 000 and Cu $\frac{1}{2}\,\frac{1}{2}\,0$, $\frac{1}{2}\,0\,\frac{1}{2}$, $0\,\frac{1}{2}\,\frac{1}{2}$. In the disordered form the same positions are occupied at random; consider this to be statistically equivalent to $\frac{1}{4}$ Au and $\frac{3}{4}$ Cu at each position.

a) Derive simplified expressions for *F* for the ordered form.
b) Derive simplified expressions for *F* for the disordered form.
c) For what reflections will *F* be the same in the two forms, and for what reflections will they differ?
d) Set up an expression for F^2 for the ordered form, allowing for dispersion corrections $\Delta f'$ and $\Delta f''$ for Cu and Au.

3.11 Uranium is orthorhombic with 4 atoms per cell in the positions $0, y, \frac{1}{4}$; $0 - y, \frac{3}{4}$; $\frac{1}{2}, \frac{1}{2} + y, \frac{1}{4}$; and $\frac{1}{2}, \frac{1}{2} - y, \frac{3}{4}$.

a) Derive simplified expressions for *F*.
b) For what reflections will *F* vanish regardless of the value of the parameter *y*?
c) What is the orthorhombic Bravais lattice: simple, body-centered, face-centered, or side-centered?

3.12 The Rutile form of TiO_2 is tetragonal with $2TiO_2$ per unit cell in the following positions:

Ti 000; $\frac{1}{2}\quad\frac{1}{2}\quad\frac{1}{2}$
O $uu0$; $-u, -u, 0$; $\frac{1}{2} - u, u + \frac{1}{2}, \frac{1}{2}$; $u + \frac{1}{2}, \frac{1}{2} - u, \frac{1}{2}$

a) Give simplified expressions for the structure factor *F*.
b) For what reflections will *F* vanish, regardless of *u*?
c) Is the Bravais lattice simple tetragonal or body-centered tetragonal?

3.13 Including the dispersion correction, the atomic scattering factor is written

$$f = f_0 + \Delta f' + i\Delta f'',$$

where f_0 is the value found in the tables, and $\Delta f'$, $\Delta f''$ are the real and imaginary parts of the correction. Using Mo$K\alpha$ ($\lambda = 0.711$ A) with a Zinc Blende crystal, the correction for S is negligible, but for Zn, $\Delta f' = 0.3$ and $\Delta f'' = 1.6$.

a) Generalize the expressions of Eq. (3.15) to allow for a dispersion correction for Zn.
b) Reflecting off opposite sides of a Zinc Blende crystal cut parallel to 111 (reflections 111 and $\bar{1}\bar{1}\bar{1}$) what should be the ratio of the integrated intensities for the two measurements?

Zinc Blende $a = 5.44$ A, $\quad \sin\theta/\lambda = 0.16$, $\quad f_0(\text{S}) = 12.4$; $\quad f_0(\text{Zn}) = 25.8$.

3.14 If a primary beam is reflected from a set of planes $h_1k_1l_1$, it is sometimes possible for the reflected beam to have the right direction to be reflected from another set of planes $h_2k_2l_2$.

a) Show that the direction of the second reflected beam is the same as that of a beam reflected directly by the planes $h_3k_3l_3$ where

$$h_3 = h_1 + h_2, \qquad k_3 = k_1 + k_2, \qquad l_3 = l_1 + l_2.$$

b) Using Cu$K\alpha$ ($\lambda = 1.542$ A), it is possible by a double reflection $(\bar{1}\bar{1}1)$ and $(h_2k_2l_2)$ to give an apparent (222) reflection from diamond ($a = 3.568$ A). What are the planes $h_2k_2l_2$? What must be the direction of the primary beam (direction cosines of $\mathbf{s}_0$ with the three orthogonal axes $\mathbf{a}_1\mathbf{a}_2\mathbf{a}_3$)?

THE INTEGRATED INTENSITY

4.1 INTEGRATED INTENSITY FROM A SMALL SINGLE CRYSTAL

The intensity from a small single crystal is given by Eq. (3.23). Since we are in the habit of saying that intensities are observable quantities even though amplitudes are not, we might think that Eq. (3.23) represents an observable quantity. For the special case of crystals so small that particle size broadening is appreciable, the predicted intensity can be observed, but for the general case of crystals large enough to give sharp diffraction peaks, the intensity represented by Eq. (3.23) is not an observable quantity.

If the three Laue equations were exactly satisfied, Eq. (3.23) would predict a maximum intensity:

$$(I_p)_{\max} = I_e F_T^2 N_1^2 N_2^2 N_3^2.$$

However, the peaks in the function $y = (\sin^2 Nx)/\sin^2 x$ have a finite breadth, so that there is an appreciable intensity in the diffracted beam at values of $(\mathbf{s} - \mathbf{s}_0)$ which differ slightly from $\lambda \mathbf{H}_{hkl}$. The primary beam is never perfectly parallel, and hence it is never true that all of the primary beam has the correct direction $\mathbf{s}_0$ to exactly satisfy the three Laue equations. In general, a crystal is slightly mosaic, different parts of the same small crystal are not exactly parallel, and hence an exact setting on one part of the crystal would not be correct for other parts. Even if the primary beam could be made perfectly parallel and set to exactly the correct angle for a single perfect crystal, there would be diffracted radiation over a range of angle on either side of the exact Bragg law direction. To measure $(I_p)_{\max}$ would require an extremely narrow slit set exactly on the peak of the diffracted beam. We conclude that $(I_p)_{\max}$ is not a measurable quantity, and turn to a more useful quantity, the "integrated intensity," which can be both calculated and measured.

We consider now a roughly collimated primary beam falling upon a small single crystal so oriented that the beam makes roughly the right angle θ for the set of planes *hkl*. During the measurement, the crystal will be rotated continuously at the constant angular velocity ω about an axis parallel to the planes *hkl* and normal to the primary beam. The crystal will be started one or two degrees on one side of the Bragg law setting and rotated to one or

two degrees on the other side, thus covering the whole range of orientation in which there is any contribution to the reflection. At the receiving surface, we will imagine a photographic film or an ionization chamber with slit set so wide that all the diffracted radiation from the reflection *hkl* is recorded. We will measure the total diffracted energy E given out from the crystal during its rotation through the Bragg law setting for the reflection *hkl*. This is an arrangement which can be experimentally realized; we measure total diffracted energy rather than an intensity, and due to the rotation of the crystal, all parts of the crystal make the Bragg law angle with each direction in the primary beam at some time during the rotation.

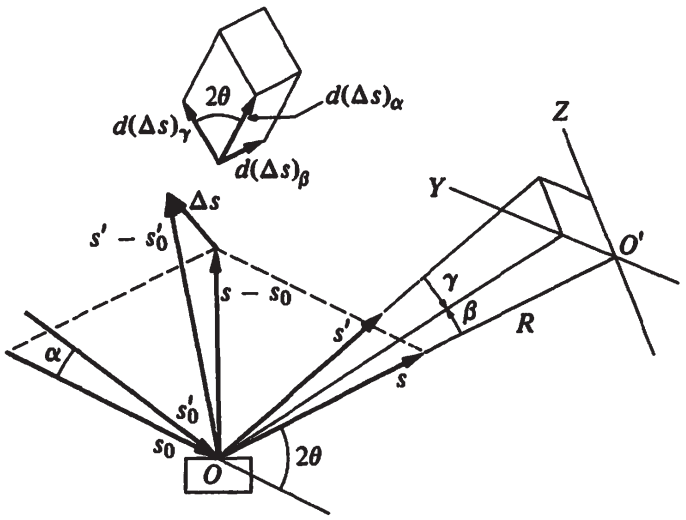

Fig. 4.1 The geometry involved in calculating the integrated intensity from a small single crystal which is rotated at constant angular velocity ω about an axis normal to the paper.

The small crystal with planes *hkl* horizontal is shown in Fig. 4.1. The direction of primary beam which makes the correct angle θ to satisfy the Bragg law is represented by the vector $\mathbf{s}_0$. The corresponding direction of diffracted beam at angle θ is represented by the vector s. The diffracted beam s falls normally upon a receiving surface O' at distance R from the crystal. Since we are considering all directions in which there is any diffracted energy, let s' be a vector whose direction differs from the Bragg law direction s by the small angles β normal to the paper and γ in the plane of the paper. Since intensity is energy per unit area per unit time, the total energy E striking the receiving surface is obtained by integrating I_p over time and over the area of the receiving surface:

$$E = \iint I_p \, dt \, dA = \iiint I_p \, dt R^2 \, d\beta \, d\gamma.$$

We are interested in finding the total diffracted energy when the crystal is rotated with constant angular velocity ω about an axis through O normal

to the paper. In practice we actually rotate the crystal, but for the present calculation it is more convenient to think of the crystal as fixed, and to imagine that the direction of the primary beam rotates at velocity ω. Let the instantaneous direction of the primary beam be represented by the vector $\mathbf{s}_0'$ making an angle α with the Bragg law direction $\mathbf{s}_0$. The time during which the direction of the primary beam will be found between the values α and $\alpha + d\alpha$ is

$$dt = (d\alpha)/\omega.$$

The total diffracted energy is then given by

$$E = \frac{R^2}{\omega} \iiint I_p \, d\alpha \, d\beta \, d\gamma. \tag{4.1}$$

Since we are considering directions of primary and diffracted beams which differ from the Bragg law directions, I_p is given by Eq. (3.23) with $\mathbf{s} - \mathbf{s}_0$ replaced by $\mathbf{s}' - \mathbf{s}_0'$. Let $\mathbf{s}' - \mathbf{s}_0' = \mathbf{s} - \mathbf{s}_0 + \Delta\mathbf{S}$, where $\mathbf{s} - \mathbf{s}_0 = \lambda\mathbf{H}_{hkl}$. Considering one of the sine functions from Eq. (3.23) with $(\mathbf{s} - \mathbf{s}_0)$ replaced by $\lambda\mathbf{H}_{hkl} + \Delta\mathbf{S}$,

$$\sin^2 \frac{\pi}{\lambda}(\lambda\mathbf{H}_{hkl} + \Delta\mathbf{S}) \cdot N_1\mathbf{a}_1 = \sin^2 \pi\left(hN_1 + \frac{\Delta\mathbf{S} \cdot N_1\mathbf{a}_1}{\lambda}\right) = \sin^2 \frac{\pi}{\lambda} \Delta\mathbf{S} \cdot N_1\mathbf{a}_1. \tag{4.2}$$

It is convenient to represent $\Delta\mathbf{S}$ as a vector in reciprocal space

$$\Delta\mathbf{S} = \lambda(p_1\mathbf{b}_1 + p_2\mathbf{b}_2 + p_3\mathbf{b}_3), \tag{4.3}$$

where $\mathbf{b}_1\mathbf{b}_2\mathbf{b}_3$ are the reciprocal vectors and the coefficients $p_1p_2p_3$ are the new variables. The sine function of Eq. (4.2) becomes

$$\sin^2 \frac{\pi}{\lambda} \Delta\mathbf{S} \cdot N_1\mathbf{a}_1 = \sin^2 \pi(p_1\mathbf{b}_1 + p_2\mathbf{b}_2 + p_3\mathbf{b}_3) \cdot N_1\mathbf{a}_1 = \sin^2 \pi N_1 p_1.$$

The total diffracted energy given by Eq. (4.1) can now be expressed by

$$E = I_e \frac{R^2}{\omega} F_T^2 \iiint \frac{\sin^2 \pi N_1 p_1}{\sin^2 \pi p_1} \frac{\sin^2 \pi N_2 p_2}{\sin^2 \pi p_2} \frac{\sin^2 \pi N_3 p_3}{\sin^2 \pi p_3} \, d\alpha \, d\beta \, d\gamma. \tag{4.4}$$

Changes $d\alpha \, d\beta \, d\gamma$ produce changes in the vectors $-\mathbf{s}_0'$ and $\mathbf{s}'$, the changes being perpendicular to $\mathbf{s}_0$ and $\mathbf{s}$. These are also changes in the vector $\Delta\mathbf{S}$, and the three contributions

$$|d(\Delta\mathbf{S})_\alpha| = d\alpha, \qquad |d(\Delta\mathbf{S})_\beta| = d\beta, \qquad |d(\Delta\mathbf{S})_\gamma| = d\gamma$$

are shown by Fig. 4.1. As a result of these three changes, the terminal point of the vector $\Delta\mathbf{S}$ traces out a volume element in reciprocal space:

$$dV = d(\Delta\mathbf{S})_\beta \cdot d(\Delta\mathbf{S})_\gamma \times d(\Delta\mathbf{S})_\alpha = \sin 2\theta \, d\alpha \, d\beta \, d\gamma.$$

The triple integral over $\alpha\beta\gamma$ given by Eq. (4.4) can now be expressed as a volume integral in reciprocal space:

$$E = I_e \frac{R^2 F_T^2}{\omega \sin 2\theta} \iiint \frac{\sin^2 \pi N_1 p_1}{\sin^2 \pi p_1} \frac{\sin^2 \pi N_2 p_2}{\sin^2 \pi p_2} \frac{\sin^2 \pi N_3 p_3}{\sin^2 \pi p_3} dV. \qquad (4.5)$$

With a volume integral we are at liberty to choose any convenient element of volume. Using Eq. (4.3), a convenient volume element for the terminal point of the ΔS vector is given by

$$dV = \lambda \mathbf{b}_1 \, dp_1 \cdot \lambda \mathbf{b}_2 \, dp_2 \times \lambda \mathbf{b}_3 \, dp_3 = \lambda^3 v_b \, dp_1 \, dp_2 \, dp_3 = (\lambda^3 / v_a) \, dp_1 \, dp_2 \, dp_3.$$

The Bragg law is exactly satisfied when $p_1 = p_2 = p_3 = 0$, and hence the integrand of Eq. (4.5) is of interest only for very small values of $p_1 p_2 p_3$. In the denominators we replace $\sin^2 \pi p_i$ by $(\pi p_i)^2$ and then since there is only one peak, the integrals are taken from $-\infty$ to $+\infty$:

$$E = I_e \frac{R^2 \lambda^3 F_T^2}{\omega v_a \sin 2\theta} \int_{-\infty}^{+\infty} \frac{\sin^2 \pi N_1 p_1}{(\pi p_1)^2} dp_1 \int_{-\infty}^{+\infty} \frac{\sin^2 \pi N_2 p_2}{(\pi p_2)^2} dp_2 \times \int_{-\infty}^{+\infty} \frac{\sin^2 \pi N_3 p_3}{(\pi p_3)^2} dp_3.$$

The three integrals give values N_1, N_2, N_3, and letting $N = N_1 N_2 N_3$ be the number of unit cells in the crystal, the diffracted energy is given by

$$E = \frac{I_e R^2 \lambda^3 N F_T^2}{\omega v_a \sin 2\theta}.$$

Letting $N v_a = \delta V$, where δV is the volume of the small crystal, and introducing the value for I_e:

$$I_e = I_0 \frac{e^4}{m^2 c^4 R^2} \left(\frac{1 + \cos^2 2\theta}{2} \right),$$

we obtain a final expression for the total diffracted energy when a small single crystal is rotated at velocity ω through the Bragg law position:

$$E = \frac{I_0}{\omega} \left(\frac{e^4}{m^2 c^4} \right) \frac{\lambda^3 \delta V F_T^2}{v_a^2} \left(\frac{1 + \cos^2 2\theta}{2 \sin 2\theta} \right). \qquad (4.6)$$

The factor $(1 + \cos^2 2\theta)/2 \sin 2\theta$ is the Lorentz-polarization factor for a single crystal in an unpolarized primary beam. Notice that the total diffracted energy E depends only upon the volume δV of the crystal. The restriction which we made when we assumed the crystal to have the shape of a parallelopipedon was a real restriction as long as we talked about intensity. As soon as we change to the experimentally observable quantity "total energy" or "integrated intensity," the restriction vanishes. A small single crystal, which does not have the shape of a parallelopipedon, could be imagined to be

composed of small parallelopipedon blocks, to each of which Eq. (4.6) applies. Absorption has been neglected, and hence there is still the restriction that the crystal is so small that absorption effects are negligible. For a very strong reflection, the primary beam loses intensity as it passes through the crystal due to energy being diffracted out of the beam. This effect is called extinction. Our neglect of extinction effects is justified for either a very small crystal or a weak Bragg reflection.

Equation (4.6) applies to a practical experimental arrangement. A small crystal of known volume δV is rotated at a known angular velocity ω. If an ionization chamber is used, the slit is so wide that all the diffracted energy in the particular reflection can get in, and E is proportional to the total charge measured. In this way relative values of E for different hkl-reflections are readily obtained. The quantitative ratio E/I_0 can also be obtained but with more difficulty. After having measured a charge proportional to E, the chamber is put into the position of the crystal, and the slit closed down to a small area. The primary beam, reduced to a known fraction by the use of absorbing screens, enters the chamber for a time t sec. The intensity I_0 is proportional to the collected charge, corrected for reduction by the absorbing screens, and divided by the slit area and the time t. The corrected ratio of the two charges gives E/I_0. From Eq. (4.6) we then obtain $F_T^2(hkl)$, since all the other quantities are known or can be measured. Values of $F_T^2(hkl)$ obtained in this way can be used to determine the structure of the crystal or, in the case of simple structures, to determine the atomic scattering factors.

In deriving Eq. (3.23) for the intensity from a single crystal, we assumed that the crystal was small enough to treat the primary and diffracted beams by the plane wave approximation. However, the restrictions imposed by the plane wave approximation disappear when we change from an intensity to the integrated intensity E, since the errors in the peak height and peak width cancel one another to give a correct peak area. To show that Eq. (4.6) is independent of the plane wave approximation, and that it is correct even when the crystal is not exceedingly small, the derivation is repeated in Appendix I where the plane wave approximation is avoided by using the method of Fresnel integrals.

4.2 THE EXTENDED FACE IMPERFECT CRYSTAL

Although measurements of the diffracted energy E can be made with a small crystal to which Eq. (4.6) applies, it is sometimes more convenient to use the technique of the extended face imperfect crystal. The average crystal is imperfect, and has what is called a mosaic structure. This means that instead of being one large perfect crystal, it can be considered as an assemblage of mosaic blocks. Each little mosaic block can have a high degree of

perfection, but there are slight variations in orientation in going from one block to the next. The variation in orientation can be thought of as due to small angle grain boundaries or to some other kind of dislocation array. A crystal is said to be "ideally imperfect" if it can be approximated by very small mosaic blocks, differing enough in orientation, so that the diffraction by each block can be considered as incoherent with respect to the diffraction from other blocks. Many crystals are intermediate between the perfect and the ideally imperfect state. Such crystals are made to approach the ideally imperfect state by rough treatment such as grinding the surface, pounding with a hammer, or heating and dipping quickly into liquid air. By getting the crystal into the ideally imperfect state, we can then apply Eq. (4.6) to each little mosaic block of the crystal.

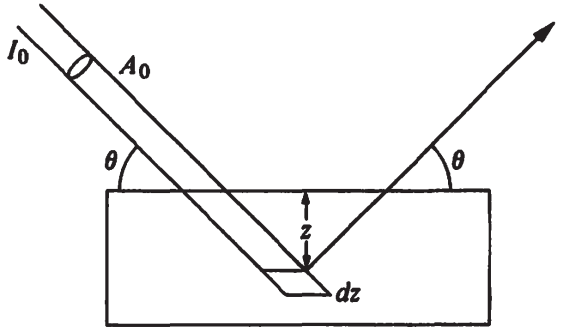

Fig. 4.2 The geometry involved in calculating the integrated intensity for an extended face mosaic crystal.

The extended face imperfect crystal technique is illustrated by Fig. 4.2. A primary beam of intensity I_0 and cross-sectional area A_0, falls upon a crystal whose dimensions are greater than the cross-sectional area of the primary beam. We will assume that the diffracting planes are parallel to the face of the crystal, so that the primary and diffracted beams each make angles θ with the face of the crystal. We will also assume that the crystal is so thick that there is no appreciable transmitted beam.

We consider a volume element between depths z and $z + dz$, irradiated by the primary beam. If δV is the average volume of a mosaic block, the number of blocks in the volume element will be $(A_0\, dz)/(\delta V \sin\theta)$. For the radiation diffracted by this volume element, there is an absorption factor $\exp[-2\mu z/\sin\theta]$, where μ is the linear absorption coefficient. Applying Eq. (4.6) to each little mosaic block, the total diffracted energy is given by

$$E = \frac{I_0}{\omega}\left(\frac{e^4}{m^2c^4}\right)\frac{\lambda^3 \delta V F_T^2}{v_a^2}\left(\frac{1 + \cos^2 2\theta}{2 \sin 2\theta}\right)\int_{z=0}^{\infty} e^{-2\mu z/\sin\theta}\frac{A_0\, dz}{\delta V \sin\theta}.$$

Let $I_0 A_0 = P_0$, where P_0 is the power in the primary beam. The total diffracted energy for an extended face imperfect crystal is given by

$$E = \frac{P_0}{\omega}\left(\frac{e^4}{m^2c^4}\right)\frac{\lambda^3 F_T^2}{2\mu v_a^2}\left(\frac{1 + \cos^2 2\theta}{2 \sin 2\theta}\right). \tag{4.7}$$

The validity of Eq. (4.7) is limited by the requirement that extinction effects are negligible. This means that as the primary beam penetrates the sample, the reduction in intensity due to energy being diffracted out of the beam must be small compared to the reduction by absorption. For an ideally imperfect sample, with very small mosaic blocks having a wide range of disorientation, or for a weak Bragg reflection, this condition will be well fulfilled. From a quantitative measurement of the ratio E/P_0, we can obtain an absolute value for F_T^2 since the other quantities in Eq. (4.7) are known.

4.3 THE INTEGRATED INTENSITY FOR A POWDER SAMPLE

In the powder method, a monochromatic beam falls upon a powder sample containing an enormous number of very small crystals having completely random orientations. For any set of planes *hkl* with spacing d_{hkl}, there will be a few crystals whose planes *hkl* make the correct angle with the primary beam to allow a Bragg reflection. The diffracted beams make a fixed angle $2\theta_{hkl}$ with the primary beam, but since they can have any orientation around the primary beam, they form the elements of a cone of half apex angle $2\theta_{hkl}$. From a powder sample, there is a cone of diffracted radiation for each spacing d_{hkl}.

We now consider a monochromatic beam falling upon a small powder sample. Let M be the number of crystals in the sample, and δV the average volume per crystal. If θ is the correct Bragg law angle for a set of planes *hkl*, we are interested in finding the number of crystals having a set of planes *hkl* making an angle between $\theta + \alpha$ and $\theta + \alpha + d\alpha$ with the primary beam. Suppose that vectors $\mathbf{H}_{hkl}$ are constructed for each crystal, normal to the *hkl*-planes. For the powder sample, the effective number of these vectors will be Mm_{hkl}, where m_{hkl} is the *hkl*-multiplicity. The multiplicity factor arises from the fact that in general there will be several sets of *hkl*-planes, having different orientations in the crystal, but equivalent in that they have the same d and F^2 values. The multiplicity factor is evaluated by finding the number of variations in position and sign which can be given to $\pm h$, $\pm k$, $\pm l$, and have planes with the same d and F^2. Evidently the value depends upon *hkl* and the crystal symmetry. For the highest cubic symmetry, a few equivalent sets of planes are the following:

$100, \bar{1}00, 010, 0\bar{1}0, 001, 00\bar{1}$	$m_{100} = 6,$
$110, \bar{1}10, 1\bar{1}0, \bar{1}\bar{1}0, 101, \bar{1}01, 10\bar{1}, \bar{1}0\bar{1}, 011, 0\bar{1}1, 01\bar{1}, 0\bar{1}\bar{1}$	$m_{110} = 12,$
$111, 11\bar{1}, 1\bar{1}1, \bar{1}11, 1\bar{1}\bar{1}, \bar{1}1\bar{1}, \bar{1}\bar{1}1, \bar{1}\bar{1}\bar{1}$	$m_{111} = 8.$

In the cubic system the highest multiplicity is 48, in the tetragonal system it is 16, and in the orthorhombic system it is 8.

The terminal points of the Mm_{hlk} vectors cover uniformly the surface of the sphere of radius H, shown by Fig. 4.3. The number of crystals having an

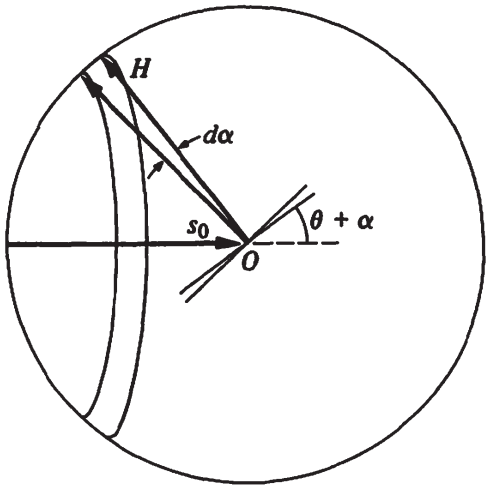

Fig. 4.3 Representation of the number of crystals in a powder sample whose *hkl* planes make angles between $\theta + \alpha$ and $\theta + \alpha + d\alpha$ with the primary beam.

hkl-plane between $\theta + \alpha$ and $\theta + \alpha + d\alpha$ with the primary beam is given by

$$dM = \frac{Mm}{4\pi H^2} 2\pi H^2 \cos(\theta + \alpha)\, d\alpha = \frac{Mm}{2} \cos\theta\, d\alpha. \tag{4.8}$$

The intensity from one crystal is given by Eq. (3.23). By means of two orthogonal angles β and γ equivalent to those of Fig. 4.1, an element of area on the receiving surface is given by

$$dA = R^2\, d\beta\, d\gamma.$$

For a reflection *hkl*, the total diffracted power from the powder sample is given by multiplying the intensity from one crystal by the number of crystals in the orientation range $\theta\, d\alpha$, and by the element of area dA, and then integrating over all orientations and over the whole area of the receiving surface:

$$P = \iiint I_p \frac{Mm}{2} \cos\theta\, d\alpha R^2\, d\beta\, d\gamma. \tag{4.9}$$

The changes $d\alpha\ d\beta\ d\gamma$ have exactly the same significance as in Section 4.1, and the triple integration can be expressed as a volume integration in reciprocal space in terms of the same variables $p_1 p_2 p_3$:

$$P = I_0\left(\frac{e^4}{m^2c^4}\right)\left(\frac{1 + \cos^2 2\theta}{2}\right)\frac{M\lambda^3 m F_T^2}{4v_a \sin\theta} \int_{-\infty}^{+\infty} \frac{\sin^2 \pi N_1 p_1}{(\pi p_1)^2} dp_1$$
$$\times \int_{-\infty}^{+\infty} \frac{\sin^2 \pi N_2 p_2}{(\pi p_2)^2} dp_2 \int_{-\infty}^{+\infty} \frac{\sin^2 \pi N_3 p_3}{(\pi p_3)^2} dp_3.$$

The product of the three integrals is $N_1 N_2 N_3 = N$, where N is the number of unit cells in a single crystal. Let $MNv_a = V$, where V is the effective volume of crystalline material in the powder sample. The total diffracted power in a reflection *hkl* is then given by

$$P = I_0\left(\frac{e^4}{m^2c^4}\right)\frac{V\lambda^3 m F_T^2}{4v_a^2}\left(\frac{1 + \cos^2 2\theta}{2 \sin\theta}\right). \tag{4.10}$$

But this is the total power belonging to the reflection, and this power is spread uniformly over the elements of a cone of half apex angle 2θ. In comparing the blackening of two powder pattern lines recorded on a film, or comparing the area of the two peaks recorded by a diffractometer, it is not the total power in the whole cone which we are comparing, but rather the power per unit length of the diffraction circle on the receiving surface. At a distance R from the sample, the circumference of this circle is $2\pi R \sin 2\theta$. The useful quantity is the power per unit length of diffraction circle P', where

$$P' = \frac{P}{2\pi R \sin 2\theta}.$$

For a powder sample of volume V, bathed in an unpolarized primary beam of intensity I_0, the power per unit length of diffraction circle at a distance R from the sample is given by

$$P' = \frac{I_0}{16\pi R}\left(\frac{e^4}{m^2c^4}\right)\frac{V\lambda^3 m F_T^2}{v_a^2}\left(\frac{1+\cos^2 2\theta}{\sin\theta \sin 2\theta}\right). \tag{4.11}$$

If the receiving surface is at a constant distance R from the sample, the Lorentz-polarization factor is $\mathrm{LP} = (1+\cos^2 2\theta)/(\sin\theta \sin 2\theta)$. In comparing different hkl-reflections on the same powder pattern, the power per unit length of diffraction circle is proportional to the product

$$m_{hkl}(F_T^2)_{hkl}(\mathrm{LP})_{hkl}.$$

Quantitative measurements of powder patterns are usually made with a diffractometer using a large flat-faced briquet of powder. The briquet is maintained in a symmetrical position, so that the primary and diffracted beams make equal angles θ with the face of the briquet. The arrangement is illustrated by Fig. 4.2 by replacing the single mosaic crystal by a briquet of powder. The volume V of Eq. (4.11) is replaced by

$$V \to \int_{z=0}^{\infty} e^{-(2\mu z)/\sin\theta}\frac{A_0\,dz}{\sin\theta} = \frac{A_0}{2\mu}.$$

For the flat-faced briquet sample, symmetrically placed relative to the primary and diffracted beams, the power per unit length of diffraction circle at a distance R from the briquet, is given by

$$P' = \frac{P_0}{16\pi R}\left(\frac{e^4}{m^2c^4}\right)\frac{\lambda^3 m F_T^2}{2\mu v_a^2}\left(\frac{1+\cos^2 2\theta}{\sin\theta \sin 2\theta}\right). \tag{4.12}$$

If the sample has a completely random orientation and there is no extinction trouble, the peak areas on a diffractometer pattern are directly proportional to the P' of Eq. (4.12).

PROBLEMS

4.1 A primary beam of Mo$K\alpha$ ($\lambda = 0.711$ A) falls upon a crystal of NaCl ($a = 5.64$ A) whose large extended face is parallel to the 400 planes. The crystal is rotated at 1° per minute through the range for a 400 reflection. An ionization chamber placed to catch the diffracted beam records a total charge which is 0.18 times as much as the chamber records when placed to pick up the primary beam for 2.0 sec. What is the value of $F(400)$? Compare with the value computed from the scattering factor tables, $F = 4(f_{\text{Na}} + f_{\text{Cl}})$. By what percentage was the intensity reduced by extinction and temperature effect?

4.2 Suppose that the external face of a large mosaic crystal is not parallel to the diffracting planes so that in the plane of the two beams, the primary and diffracted beams make angles ϕ_1 and ϕ_2 with the external face. Deduce an expression corresponding to Eq. (4.7) for the diffracted energy. If $\phi_1 = \theta + \epsilon$ and $\phi_2 = \theta - \epsilon$ where ϵ is small, show that the effect is to add a correction factor $(1 - \epsilon \operatorname{ctn} \theta)$ to Eq. (4.7). If $\epsilon = 1°$ and $\theta = 15°$, what is the percentage change in E from the symmetrical case?

4.3 In the transmission case we diffract from a set of planes which are normal to the surface of a thin slab of mosaic crystal of thickness t. The slab is perpendicular to the plane of the primary and diffracted beams. The primary beam has an intensity I_0 and cross-sectional area A_0, and the crystal rotates at velocity ω about an axis normal to the plane of the two beams. Deduce an expression for the diffracted energy E. For what thickness t will E be a maximum? How does $E_{\max}$ for the transmission case compare with the value from Eq. (4.7)?

4.4 The powder pattern from a very small sample of volume V is recorded on a flat film at distance D from the sample, the film being perpendicular to the primary beam. In terms of D, deduce an expression for P' the power per unit length of diffraction circle on the flat film.

4.5 A powder pattern is recorded in transmission from a thin slab of powder of mass per unit area m. The primary and diffracted beams make equal angles with the face of the slab. In terms of $I_0 A_0 = P_0$, the power in the primary beam, deduce an expression for P', the power per unit length of diffraction circle at distance R from the sample? For what value of m will P' be a maximum?

4.6 A Laue pattern is made using a parallel beam of continuous spectrum, and a parallelopipedon crystal of volume δV small enough to be completely bathed in the beam and to neglect absorption in the crystal. Let $I(\lambda)\, d\lambda$ be the intensity in the primary beam between wavelengths λ and $\lambda + d\lambda$, and assume that $I(\lambda)$ varies slowly with λ. For the Laue case, $\mathbf{s}_0$ has a fixed direction relative to the planes hkl; it is λ and the direction s which vary. Hence it is best to work with the vectors $\mathbf{s}_0/\lambda$, $\mathbf{s}'/\lambda$, and $\Delta\mathbf{S}/\lambda = p_1\mathbf{b}_1 + p_2\mathbf{b}_2 + p_3\mathbf{b}_3$. Show that the diffracted power for an hkl-reflection is given by

$$P = I(\lambda_{hkl}) \frac{e^4}{m^2c^4} \frac{\lambda_{hkl}^4 \, \delta V F^2}{4v_a^2} \left(\frac{1 + \cos^2 2\theta}{\sin^2 \theta} \right).$$

5

THE POWDER METHOD

The ideal powder sample consists of an enormous number of very tiny crystals of size 10^{-3} cm or smaller with completely random orientation. Suitable samples may be obtained as fine grained precipitates, or by grinding coarse crystalline material, or in the case of metals by making filings. The monochromatic radiation required for the powder method is usually the $K\alpha_1\alpha_2$ doublet, monochromated by crystal reflection, or by the use of a filter whose K absorption wavelength falls between the $K\alpha$ and $K\beta$ wavelengths. The Cu$K\alpha_1\alpha_2$ doublet ($\lambda = 1.542$ A) with a Ni filter ($\lambda_K = 1.488$ A) is probably used more than any other source. A wavelength of radiation which is just shorter than an absorption edge wavelength in the sample is always to be avoided, since these conditions lead to a high absorption coefficient and strong fluorescence radiation. For example, Cu$K\alpha$ ($\lambda = 1.542$ A) would never be used with a sample of iron ($\lambda_K = 1.743$ A).

For any set of planes with spacing $d(hkl)$, there are many crystals oriented so that their hkl-planes make the correct Bragg law angle θ with the primary beam. Since the correctly oriented crystals have all orientations about the primary beam, the diffracted beams form a cone of half apex angle 2θ. For each planar spacing $d(hkl)$, there is a cone of angle $2\theta(hkl)$. Powder patterns are usually registered by film recording or by counter diffractometers.

5.1 POWDER PATTERNS BY FILM RECORDING

A typical powder pattern camera is illustrated by Fig. 5.1. The primary beam enters through the collimator A, which has a bore of 1 mm or less, and a relief at the end to prevent scattering from the end. The beam leaves the camera through the exit port E. The powder sample at O is a cylinder of diameter 1 mm or less. Centering adjustments for the sample are usually provided, and the sample is often rotated during the exposure to help provide crystals with all possible orientations. Figure 5.1 shows the Straumanis method of loading the film in the camera. The ends of the film are at B and C, and holes at A and E are provided for the entrance collimator and the exit port. With the Straumanis type loading, the center of the small-angle cone 1

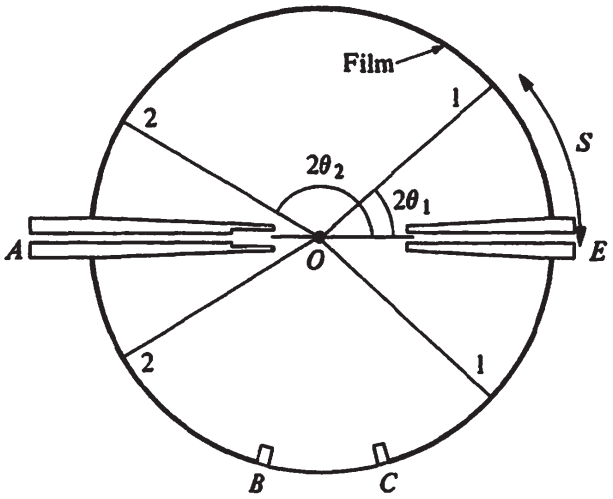

Fig. 5.1 Powder pattern camera with Straumanis type of film loading.

gives the position for $2\theta = 0$, and the center of the high-angle cone 2 gives the position on the film for $2\theta = 180°$. These two reference positions are fixed on the film independent of film shrinkage or uncertainty in the radius of the camera. Examples of simple powder patterns are given by Fig. 5.2.

With the film spread out flat, it is a simple matter to measure the distance S from the exit midpoint to each line in the pattern. Expressed in degrees, the angle θ is given by

$$\theta^0 = \frac{S180}{2R\pi}. \tag{5.1}$$

To simplify the use of Eq. (5.1), it is customary to provide convenient camera diameters such as $2R = 180/\pi = 57.3$ mm, or twice this value. For the camera diameter $D = 57.3$ mm, which is in common use, Eq. (5.1) takes the simple form $\theta^0 = S$ (mm).

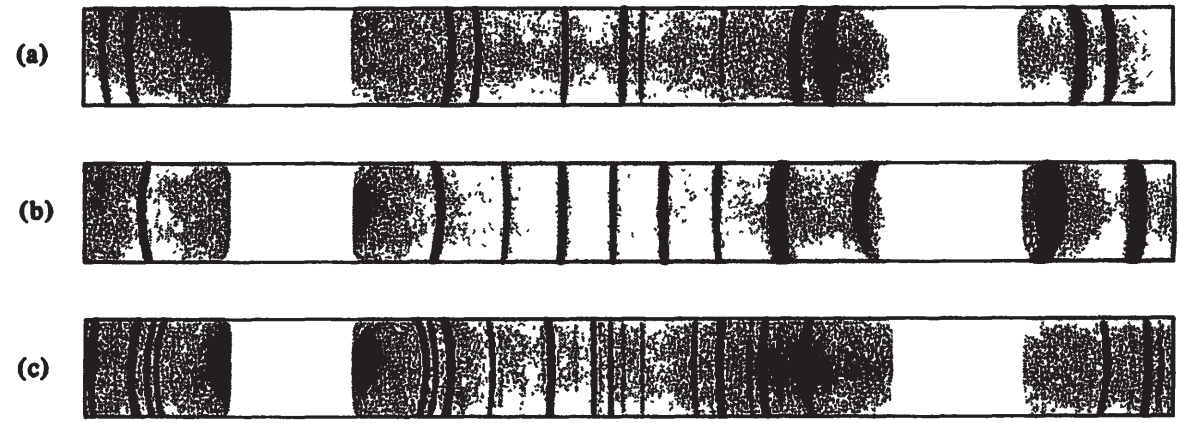

Fig. 5.2 Powder patterns made with the camera illustrated by Fig. 5.1; radiation Cu$K\alpha$ with Ni filter: (a) Copper, (b) Molybdenum, (c) Zinc. $2\theta = 0$ at the left.

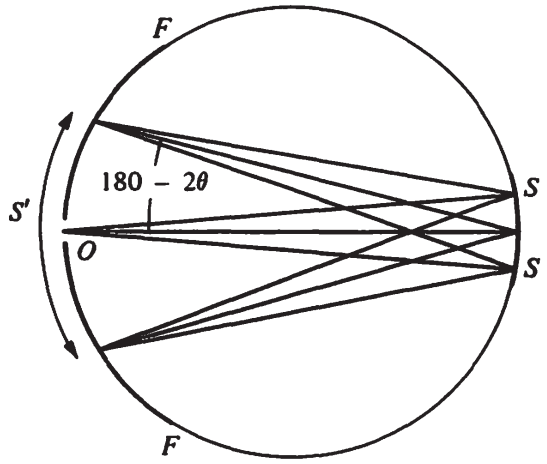

Fig. 5.3 The symmetrical back reflection focusing camera with film centered on the entrance slit.

When the interest is in precision measurements of sharp high-angle reflections, the symmetrical back reflection focusing camera is often used. The camera is shown schematically by Fig. 5.3. The sample *SS* and the film *FF* are both on the focusing circle. The primary beam enters through a very narrow and short slit at *O*, and a certain amount of divergence is allowed. For each *d*(*hkl*) the diffracted beams are focused at the film. However, it is very important that the length of the entrance slit shall be very small and that the primary beam be confined to a thin layer parallel to the plane of the paper to prevent an error in line position which could become serious for very high angle reflections. From the distance S' between corresponding reflections,

$$90 - \theta^0 = 180S'/8\pi R. \tag{5.2}$$

The power per unit length of diffraction circle P' given by Eq. (4.11) is often estimated qualitatively from the apparent blackening of the recorded diffraction lines. However, quantitative measurements of P' can be obtained from film recorded powder patterns by microphotometering.

In the typical recording microphotometer, a narrow pencil of light falls normally upon the film. The transmitted light is received by a thermopile or a photocell. The deflection of the chart recorder is proportional to the generated emf and hence is proportional to the intensity of the transmitted light. The film is scanned by an automatic drive which moves both the film and the chart. A typical microphotometer record of a diffraction line is illustrated by Fig. 5.4.

Horizontal distances on the chart are proportional to distances on the film. The horizontal line at the top of the record represents zero deflection of the recorder and hence corresponds to zero light intensity coming through the film. Distances down from the zero line are proportional to the intensity of light coming through the film; D_0 is the deflection when the beam of light

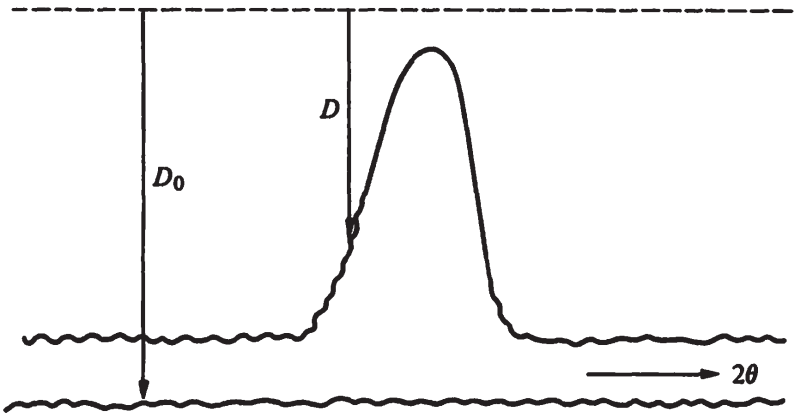

Fig. 5.4 Microphotometer recording of a powder pattern peak and the background on either side. The upper reference line corresponds to a completely opaque film, and the lower reference line corresponds to a clear film with zero blackening.

passes through an unblackened part of the film, and D is the deflection when the light falls on a blackened part of the film.

The blackening of a film B is defined as

$$B = \log \frac{D_0}{D}. \tag{5.3}$$

For a given type of development, it is a good approximation to consider that the blackening depends only on the product of the x-ray intensity and the time of exposure. Doubling the intensity and halving the time gives the same blackening (reciprocity law). By exposing different parts of a film for times proportional to 1, 2, 3, 4, etc., and measuring the blackening B of the different regions, it is found that for x-ray film the blackening B is closely a linear function of the exposure ($I \times t$) up to blackenings a little less than unity.

For a diffraction pattern with a low blackening, the x-ray intensity can be taken as proportional to the measured blackening B. If the blackening is not small, the experimentally determined calibration curve B vs. (kIt) must be used to transform the microphotometer curve into a curve whose ordinate is proportional to the x-ray intensity. The peak area above background on this intensity curve is then proportional to P' the power per unit length of diffraction circle. Although quantitative x-ray intensity measurements can be obtained from microphotometer records, the trend in recent years is toward the use of counter diffractometers for quantitative intensity measurements.

5.2 DIFFRACTOMETER RECORDING OF POWDER PATTERNS

The counter diffractometer is illustrated schematically by Fig. 5.5. The sample O is a flat-faced briquet of powder. Monochromatic radiation diverges from the entrance slit E, which in some cases is just the line focus on the target. The diffracted radiation is selected by a narrow receiving slit R.

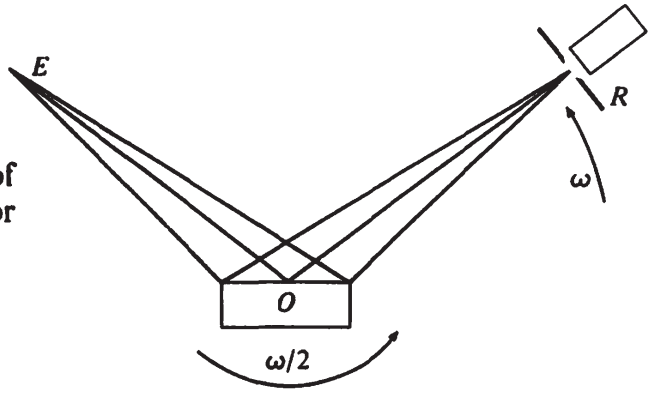

Fig. 5.5 Schematic representation of the counter diffractometer as used for recording powder patterns.

The appropriate filter is usually placed in the diffracted beam at the receiving slit. The distances *EO* and *OR* are made equal, and since the sample face is maintained symmetrical with respect to the primary and diffracted beams, there is an approximate focusing condition. The radiation passed by the receiving slit is detected by some type of counter, such as a Geiger counter, gas proportional counter, or crystal scintillation counter. The pulses produced in the counter are amplified and fed to a chart recorder. During the measurement the counter turns at an angular velocity ω, and the sample turns at a velocity $\omega/2$ to maintain focusing conditions and a simple absorption geometry. A Geiger counter diffractometer recording of the powder pattern of rock salt (NaCl) is shown by Fig. 5.6. The 2θ-values for each reflection are read directly from such a recording.

For a diffractometer recording such as that of Fig. 5.6, the integrated intensity or power per unit length of diffraction circle is given by Eq. (4.12).

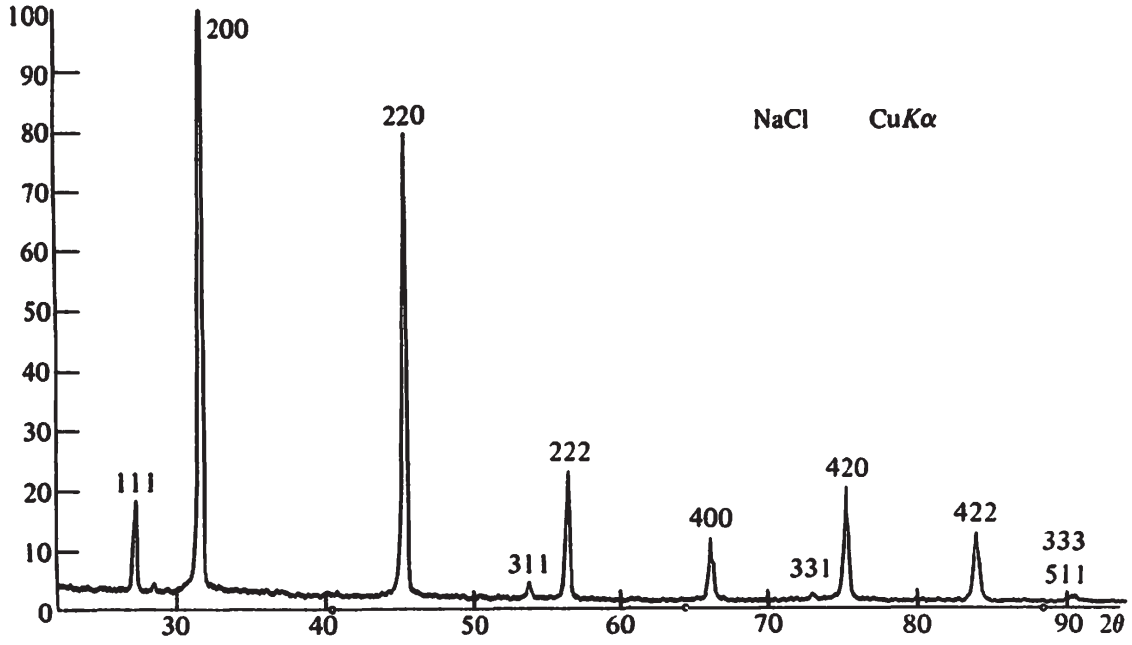

Fig. 5.6 Diffractometer recording of the powder pattern of NaCl using Ni filtered Cu$K\alpha$ radiation.

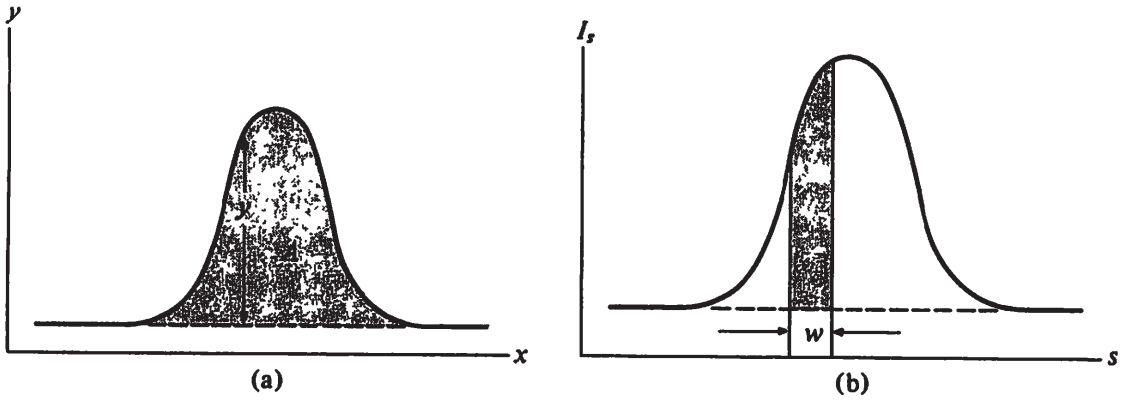

Fig. 5.7 (a) Diffractometer recording of powder pattern peak. (b) Distribution of intensity in the plane of the receiving slit.

The receiving slit is usually very narrow compared to the width of an *hkl*-reflection, and the total peak contribution is recorded as the receiving slit scans across the diffracted beam. We are now interested in obtaining the relation between the observable area of diffraction peaks, such as those of Fig. 5.6, and the corresponding power per unit length P' of Eq. (4.12).

Let Fig. 5.7(a) represent the crystalline peak as it is recorded on the chart, and let Fig. 5.7(b) represent the distribution of intensity in the peak in the plane of the receiving slit.

We define the following quantities:

w = width of receiving slit (cm),
l = length of receiving slit (cm),
s = position coordinate of the receiving slit in a direction perpendicular to its length (cm),
I_s = intensity at the receiving slit (power/cm^2),
$V = ds/dt$ = speed of receiving slit (cm/sec),
$V = R\omega$ where ω is the counter speed (rad/sec) and R is the distance from sample to slit (cm),
$v = dx/dt$ = chart speed (cm/sec) or (in./sec),
y = ordinate distance on chart (cm) or (in.),
x = abscissa distance on chart (cm) or (in.),
A = peak area above background on chart (cm^2) or (in.^{2}),
k = proportionality constant between chart ordinate and power entering receiving slit (cm/unit power) or (in./unit power).

For linear recording, the chart ordinate is given by

$$y = k\int_s^{s+w} I_s l \, ds.$$

If we are interested in a peak area, it is understood that y and I_s are both measured above background. The peak area above background on the chart

is given by

$$A = \int y\,dx = \int \left[k \int_s^{s+w} I_s l\,ds \right] dx.$$

Since $dx = v\,dt = v\,ds/R\omega$,

$$A = \frac{v}{R\omega} \int \left[k \int_s^{s+w} I_s l\,ds \right] ds. \tag{5.4}$$

The power per unit length of diffraction circle is given by

$$P' = \int I_s(1)\,ds.$$

We can reverse the order of integration in Eq. (5.4) and obtain

$$A = \frac{klv}{R\omega} \int_s^{s+w} P'\,ds = \frac{klvwP'}{R\omega}. \tag{5.5}$$

Equation (5.5) shows that the peak area on the chart recording is proportional to the power per unit length P'. In some cases we are interested in the factor of proportionality. For example, suppose that we are considering a diffuse intensity such as the Compton modified scattering, and we wish to compare the chart ordinate for the diffuse intensity with the area of a crystalline peak. The sample composition is of the form $A_pB_qC_r$ and we can refer to this as a unit of composition. If v_c is the volume per unit of composition, the intensity of Compton modified scattering for a flat-faced sample is given by

$$I(\text{mod}) = \frac{P_0}{2\mu v_c} \left(\frac{e^4}{m^2c^4R^2} \right) \left(\frac{1 + \cos^2 2\theta}{2} \right) \sum i(M), \tag{5.6}$$

where the sum is over the atoms making up the unit of composition. The chart ordinate due to the Compton modified scattering is then

$$y(\text{mod}) = klwI(\text{mod}),$$

and it is a simple matter to compare the chart ordinate due to the diffuse intensity with the area on the chart due to a crystalline peak.

5.3 ANALYSIS OF A CUBIC POWDER PATTERN BY DIFFRACTOMETER RECORDING

As an example of the interpretation of a very simple powder pattern, we will consider the diffractometer recording of rock salt (NaCl) shown by Fig. 5.6. Only the reflections up to $2\theta = 94°$ are shown, but this is enough to illustrate the procedure. The sample was a flat-faced briquet made from a mixture of Duco cement and rock salt powder which had been ground to a size of about 5×10^{-4} cm. The pattern was recorded on a Norelco diffractometer using

Cu$K\alpha_{12}$ radiation ($\lambda = 1.542$ A) with a Ni filter at the receiving slit, and the counter turning at 1°/min. For the measurements recorded below, each peak was enlarged by running at a slower speed, and using a scale factor which magnified the ordinates. The calculations involved in the interpretation of a diffraction pattern should always be recorded in tabular form as illustrated by Table 5.1.

The 2θ-values for the different reflections are read directly from the chart recording and tabulated in column 1. The corresponding values of $1/d^2 = 4 \sin^2 0/\lambda^2$ are computed and recorded in column 2. Rock salt is a cubic crystal, but even when the crystal system is unknown, we would start out by trying to index the pattern in terms of a cubic lattice. If it is not cubic, this will quickly turn out to be impossible, and we would then fall back on the various schemes for handling systems of lower symmetry.

From Eq. (2.14) for a cubic crystal,

$$\frac{4 \sin^2 \theta}{\lambda^2} = \frac{1}{d^2} = \frac{h^2 + k^2 + l^2}{a^2}; \tag{5.7}$$

hence column 2 divided by $(1/a^2)$ will give $(h^2 + k^2 + l^2)$. Accordingly we look for some divisor for column 2 which will give small integers. We start, of course, with 0.0940, and then half of this, and so on until a suitable divisor is found. In this case, one third of 0.0940 is apparently the proper divisor, since the numbers obtained are close to small integers. The integral values of $h^2 + k^2 + l^2$ are listed in column 3. Numbers such as 7, 15, 23, 28, 31, which are derived from $4^p(8q + 7)$ with p and q any integers, including zero, cannot be produced as the sum of the squares of three integers. A partial check on the work at this stage is obtained by noting that such numbers do not occur in column 3.

The *hkl*-values of column 4 are easily obtained by inspection. In a few cases the same value of $h^2 + k^2 + l^2$ leads to more than one set of *hkl*-indices. This means that the diffraction cones from two different sets of planes are superimposed. Dividing column 3 by 2 gives a^2, and the corresponding values of a are listed in column 5. The higher angle values are the more accurate, and they are given a higher weight in taking an average.

The number of Na and Cl atoms per unit cell can be computed from the density, the Avogadro number, and the molecular weight by expressing the mass of the unit cell in two ways $\rho a^3 = nM/N$:

$$n = \frac{N\rho a^3}{M} = \frac{0.602 \times 10^{24} \times 2.17 \times (5.64 \times 10^{-8})^3}{(23.0 + 35.5)} = 4.00.$$

There are accordingly 4 Na and 4 Cl per cubic unit cell. The only *hkl*-indices appearing in column 4 are unmixed, and hence the Bravais lattice is face-centered cubic. We have seen that for a face-centered cubic lattice, the

Table 5.1

POWDER DIFFRACTOMETER PATTERN OF NaCl ($\lambda = 1.542$ A)

1	2	3	4	5	6	7	8	9	10	11	12	13	14
2θ	$\frac{4\sin^2\theta}{\lambda^2}$	$h^2+k^2+l^2$	hkl	$a(A)$	$\frac{\sin\theta}{\lambda}$	f_{Cl}	f_{Na}	F^2	m	(LP)	$\frac{F^2m(LP)}{1000}$	A, arb. unit	Col. 12 corrected
27.3	0.0940	3	111	5.65	0.154	13.50	8.90	338	8	33.5	91	116	102
31.7	0.1255	4	200	5.65	0.177	12.70	8.70	7330	6	24.0	1057	1260	1160
45.5	0.2516	8	220	5.64	0.251	10.50	7.65	5280	12	10.9	690	694	697
53.9	0.3455	11	311	5.64	0.294	9.60	7.00	107	24	7.4	19	23	18
56.5	0.3768	12	222	5.64	0.307	9.35	6.75	4150	8	6.6	219	200	201
66.3	0.503	16	400	5.64	0.354	8.65	6.10	3490	6	4.7	98	92	82
73.2	0.598	19	331	5.64	0.386	8.30	5.65	112	24	3.8	10	13	8
75.4	0.629	20	420	5.64	0.396	8.20	5.50	3010	24	3.60	260	198	195
84.1	0.755	24	422	5.64	0.434	7.85	5.05	2660	24	3.05	195	136	136
90.6	0.849	27	511 333	5.64	0.461	7.60	4.75	130	24 8	2.80	12	10	8

number of atoms of each kind must be a multiple of 4. Hence there is a self-consistency check by finding 4 Na and 4 Cl per unit cell.

For a face-centered cubic lattice, we have seen that for every atom with coordinates xyz there must be three identical atoms at coordinates $x + \frac{1}{2}$, $y + \frac{1}{2}$, z; $x + \frac{1}{2}$, y, $z + \frac{1}{2}$; and x, $y + \frac{1}{2}$, $z + \frac{1}{2}$. Hence if we choose as origin the position of one of the Cl, the coordinates of the four Cl atoms will be 0 0 0, $\frac{1}{2}\frac{1}{2}$ 0, $\frac{1}{2}$ 0 $\frac{1}{2}$, 0 $\frac{1}{2}\frac{1}{2}$. If we place one of the Na at xyz, the positions of the other three Na are fixed at $x + \frac{1}{2}$, $y + \frac{1}{2}$, z; $x + \frac{1}{2}$, y, $z + \frac{1}{2}$; and x, $y + \frac{1}{2}$, $z + \frac{1}{2}$. But there are only 3 unoccupied sets of xyz-values which will allow cubic symmetry in a crystal with the 4 Cl already placed. These three possible sets of Na positions are $\frac{1}{2}\frac{1}{2}\frac{1}{2}$; $\frac{1}{4}\frac{1}{4}\frac{1}{4}$; and $\frac{3}{4}\frac{3}{4}\frac{3}{4}$. Since the third can be obtained from the second by rotating the crystal 90°, we need consider only the first two sets.

Substances of composition AB whose structures are based on the first set of positions are said to have the "rock salt" structure, and those involving the second set of positions are said to have the "zinc blende" structure. Simplified expressions for the structure factor for these two structures are given by Eqs. (3.14) and (3.15). To complete the structure determination, and also to illustrate the calculation of integrated intensities, we will now show that the observed intensities are in good agreement with those predicted by the rock salt structure, and in strong disagreement with those for the zinc blende structure.

The atomic scattering factors are listed in the Tables as a function of $\sin\theta/\lambda$. The appropriate values of f_{Cl} and f_{Na} are entered in columns 7 and 8. The values of F^2 are calculated from Eq. (3.14) and listed in column 9. For the high cubic symmetry involved in the rock salt and the zinc blende structures, the powder pattern multiplicities are given by the number of ways of interchanging $\pm h$, $\pm k$, $\pm l$. The multiplicity values m are listed in column 10. The Lorentz-polarization factor (LP) for powder patterns is proportional to either $(1 + \cos^2 2\theta)/\sin\theta \sin 2\theta$ or $(1 + \cos^2 2\theta)/\sin^2\theta \cos\theta$. Values are tabulated in various references such as the International Tables for X-ray Crystallography. The appropriate numbers are listed in column 11.

For the flat-faced powder sample, the integrated intensity is given by Eq. (4.12). Except for the Debye temperature factor, it is proportional to F^2m (LP). The product of columns 9, 10, and 11 divided by 1000 is tabulated in column 12. The peak areas in arbitrary units taken from the enlarged version of Fig. 5.6 are listed in column 13. It is evident that the measured areas fall off more rapidly with increasing θ than the computed values of column 12. The discrepancy is due to neglecting the Debye temperature factor. As an approximation, we can follow Eq. (3.25) and use the same value of

$$2M = 2B\frac{\sin^2\theta}{\lambda^2}$$

for both kinds of atoms. With this approximation the peak areas should be given by

$$A = K(F^2 m\mathrm{LP}/1000) \exp\,[-2B \sin^2 \theta/\lambda^2]$$

and hence

$$\ln\left(\frac{1000\,A}{F^2 m\mathrm{LP}}\right) = \ln K - 2B\frac{\sin^2\theta}{\lambda^2}. \tag{5.8}$$

A plot of $\ln (1000\,A/F^2 m\mathrm{LP})$ against $\sin^2\theta/\lambda^2$ gives the values $K = 1.210$ and $2B = 2.94\ \mathrm{A}^2$. The values of column 12 multiplied by $1.210 \times \exp\,[-2.94 \sin^2\theta/\lambda^2]$ are listed in column 14.

Except for two interesting discrepancies, there is satisfactory agreement between the measured areas of column 13 and the computed areas of column 14. For all reflections with odd indices, the measured area is higher than the computed value. These reflections involve the difference of the two scattering factors, and it is a poor approximation to use the same temperature factor for both atoms. For the reflections 200 and 400, the measured area is larger than the computed value. This is due to a slight 200 preferred orientation in the sample surface. The crystal fragments produced by grinding tend to have a cubic shape and pressing with a flat plate gives a slight surface orientation.

A theoretical expression for the Debye factor $2M = 2B \sin^2\theta/\lambda^2$ is developed in Chapter 11. For a cubic element

$$2B = \frac{12h^2T}{mk\Theta^2}\left\{\Phi(x) + \frac{x}{4}\right\}, \tag{5.9}$$

where h is Planck's constant, T is the absolute temperature, m is the mass of the atom, k is the Boltzmann constant, Θ is the Debye characteristic temperature of the substance, $x = \Theta/T$, and $\{\Phi(x) + x/4\}$ is a tabulated function which is approximately unity for $T > \Theta$. Approximating NaCl as an element with average atom mass, $m = (23.0 + 35.5)/(2 \times 0.602 \times 10^{24})$ and using $h = 6.62 \times 10^{-27}$, $T = 300°\mathrm{K}$, $k = 1.38 \times 10^{-16}$, $\Theta = 281°\mathrm{K}$, and $\{\Phi(x) + x/4\} = 1.02$, we obtain $2B = 3.02\ \mathrm{A}^2$. The value $2B = 2.94\ \mathrm{A}^2$ which we obtained from the logarithmic plot is in satisfactory agreement.

For a more accurate treatment it is necessary to allow for different values of $M(\mathrm{Cl})$ and $M(\mathrm{Na})$:

$$\frac{A(\mathrm{meas})}{m(\mathrm{LP})} = K^2\{f_{\mathrm{Cl}}e^{-M(\mathrm{Cl})} \pm f_{\mathrm{Na}}e^{-M(\mathrm{Na})}\}^2.$$

With the abbreviation $Q^2 = A(\mathrm{meas})/m(\mathrm{LP})$, we have two cases:

$$hkl \text{ all even:}\quad Q(\mathrm{even}) = K[f_{\mathrm{Cl}}e^{-M(\mathrm{Cl})} + f_{\mathrm{Na}}e^{-M(\mathrm{Na})}],$$

$$hkl \text{ all odd}\quad Q(\mathrm{odd}) = K[f_{\mathrm{Cl}}e^{-M(\mathrm{Cl})} - f_{\mathrm{Na}}e^{-M(\mathrm{Na})}].$$

Table 5.2
INTERPRETATION OF NaCl PATTERN IN TERMS OF ZINC BLENDE STRUCTURE

hkl	f_{Cl}	f_{Na}	F^2	m	(LP)	$\frac{F^2 m(\text{LP})}{1000}$	A arb. units
111	13.50	8.90	4180	8	33.5	1120	116
200	12.70	8.70	256	6	24.0	37	1260
220	10.50	7.65	5270	12	10.9	690	694

By plotting the measured values of Q against $\sin\theta/\lambda$, we can treat Q(even) and Q(odd) as continuous functions of $\sin\theta/\lambda$. From the sums and differences, we obtain

$$\ln\left[\frac{Q(\text{even})+Q(\text{odd})}{2f(\text{Cl})}\right] = \ln K - B(\text{Cl})\left(\frac{\sin\theta}{\lambda}\right)^2,$$
$$\ln\left[\frac{Q(\text{even})-Q(\text{odd})}{2f(\text{Na})}\right] = \ln K - B(\text{Na})\left(\frac{\sin\theta}{\lambda}\right)^2. \tag{5.10}$$

From plots of the left-hand side of Eq. (5.10) against $(\sin\theta/\lambda)^2$, the slopes give directly the values of B(Cl) and B(Na).

To complete the discussion, it is of interest to show that the zinc blende structure would predict intensities in strong disagreement with those observed. The structure factors for the zinc blende structure are given by Eq. (3.15). The calculations for the first three reflections are given in Table 5.2. The disagreement is most pronounced. The zinc blende structure predicts a very strong 111 and a very weak 200, just the opposite to what is observed.

Our structure determination for NaCl is now complete. The unit cell is cubic with dimensions $a = 5.64$ A. The Bravais lattice is face-centered cubic and there are 4 Cl and 4 Na per unit cell in the positions 0 0 0, $\frac{1}{2}\frac{1}{2}$ 0, $\frac{1}{2}$ 0 $\frac{1}{2}$, 0 $\frac{1}{2}\frac{1}{2}$, and $\frac{1}{2}\frac{1}{2}\frac{1}{2}$, 0 0 $\frac{1}{2}$, 0 $\frac{1}{2}$ 0, $\frac{1}{2}$ 0 0. All AB compounds whose atoms are arranged in this way are said to have the rock salt structure.

5.4 ANALYSIS OF A HEXAGONAL POWDER PATTERN

For the powder patterns of noncubic materials, the simple procedure of looking for a common divisor for the values of $4\sin^2\theta/\lambda^2$ no longer suffices. For the tetragonal and hexagonal systems, there are two unknowns (a and c) to be determined. Several graphical methods for indexing such patterns have been developed by Hull and Davey,[1] Bjurström,[2] and Bunn.[3] Of these, the method of the Hull-Davey charts is probably the simplest in principle. To illustrate, we will now develop the Hull-Davey chart for the hexagonal system.

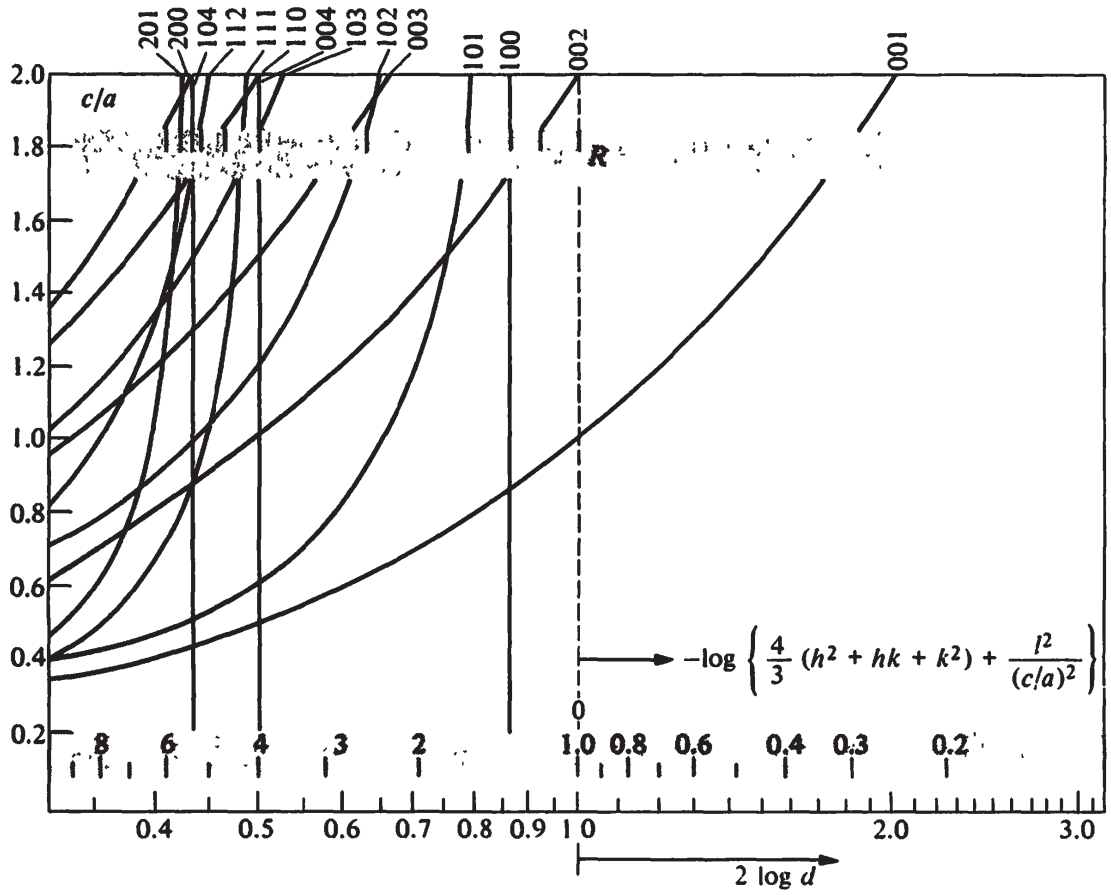

Fig. 5.8 Construction of the Hull-Davey Chart for the hexagonal system.

The spacing formula for the hexagonal system is given by Eq. (2.10). This can be put into the form

$$2\log d = 2\log a - \log\left\{\tfrac{4}{3}(h^2 + hk + k^2) + \frac{l^2}{(c/a)^2}\right\}. \qquad (5.11)$$

The construction of the chart on 2 range semilog paper is illustrated by Fig. 5.8. The ordinate is the linear scale c/a, and the abscissa is $-\log\{(h^2 + hk + k^2)\frac{4}{3} + l^2/(c/a)^2\}$ measured from the origin at $\log\{1\} = 0$. A curve is plotted for each index combination hkl. Reflections of the type $hk0$ are vertical lines since they are independent of c/a, the other reflections are represented by curved lines. Figure 5.8 shows curves for only the low index combinations 100, 110, 200, 001, 002, 003, 004, 101, 102, 103, 104, 111, 112, 201. Below the set of curves is provided a 2 log d-scale, this is a logarithmic scale measured from the same origin but increasing toward the right and plotted to twice the scale factor to provide the factor of 2.

To use the chart, a strip of paper is placed along the 2 log d-scale, and a mark is made on the strip at each measured d-value. Moving the strip up onto the chart, we look for a fit where each mark on the strip falls on a curve. Moving the strip up and down varies c/a, and moving it horizontally varies 2 log a. Having found a fit, we read off directly the indices for each of the

reflections. The (c/a)-value is read from the ordinate position of the strip. The a-value can be obtained by making a reference mark on the strip at the position of the origin line O. Putting the strip back in its original position on the 2 log d-scale, the position of the reference mark gives the value of a. The a- and c-values are also readily obtained from the spacing values for $hk0$- and $00l$-reflections. Figure 5.8 shows a fit for the powder pattern of zinc.

In the hexagonal system, it is convenient to introduce a fourth index i, whose significance is illustrated by Fig. 5.9. Since there are three equivalent axes at 120° to one another, it is arbitrary which two are chosen for a_1 and a_2. The fourth index i is the index with respect to the axis a'. From the geometry of lines at 60° to one another, the intercepts by an hkl-plane satisfy the relation

$$\frac{1}{(-a'/i)} = \frac{1}{(a_1/h)} + \frac{1}{(a_2/k)},$$

from which

$$h + k + i = 0.$$

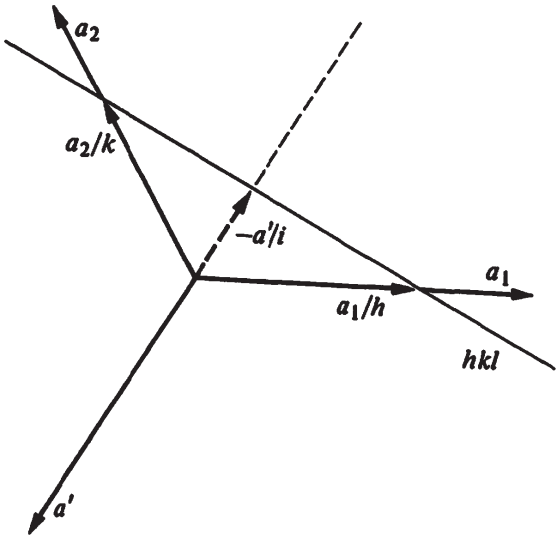

Fig. 5.9 Significance of the fourth index which is used in the hexagonal system.

Equation (2.10) gives the same spacing value d if for h and k we use any two of the three indices hki. Suppose we choose to use h and i. Since

$$(h^2 + hi + i^2) = h^2 + h(-h - k) + (-h - k)^2 = h^2 + hk + k^2,$$

h and i give the same d-value as h and k.

The multiplicity of planes with equal spacing in the hexagonal system is readily handled by means of the fourth index. We can interchange the positions of hki, change the sign of all three indices hki, and independently change the sign of l, and maintain the same d-value. To illustrate, consider the plane 132 which with a fourth index would be written $13\bar{4}2$. The 24 equivalent planes with the same spacing are given in Table 5.3. For any combination of positive and negative indices, there is always one member of the group of equivalent planes for which the hkl are all positive. It is for this reason that only positive indices appear on the Hull-Davey charts.

Since the charts are logarithmic, the curves get very close together on the left-hand side, and we are apt to underestimate the usefulness of the chart. The trouble arises from the fact that the charts are always reduced far too much for reproduction on textbook pages. Magnified by at least a factor of

Table 5.3
A SET OF EQUIVALENT PLANES IN THE HEXAGONAL SYSTEM

$13\bar{4}2$	$\bar{1}342$	$13\bar{4}\bar{2}$	$\bar{1}34\bar{2}$
$31\bar{4}2$	$\bar{3}142$	$31\bar{4}\bar{2}$	$\bar{3}14\bar{2}$
$1\bar{4}32$	$\bar{1}432$	$1\bar{4}\bar{3}2$	$\bar{1}43\bar{2}$
$3\bar{4}12$	$\bar{3}412$	$3\bar{4}\bar{1}2$	$\bar{3}41\bar{2}$
$\bar{4}132$	$4\bar{1}32$	$\bar{4}13\bar{2}$	$4\bar{1}3\bar{2}$
$\bar{4}312$	$43\bar{1}2$	$\bar{4}31\bar{2}$	$43\bar{1}\bar{2}$

Table 5.4
CALCULATIONS FOR POWDER PATTERN OF ZINC

1	2	3	4	5	6	7	8	9
$s = \theta°$	$d(A)$	hkl	f_{Zn}	F^2	m	(LP)	$\frac{F^2m(LP)}{1000}$	P' obs
18.4	2.44	002	23.8	2260	2	17.5	79	*MS*
19.7	2.29	100	23.0	530	6	15.0	48	*M*
21.8	2.08	101	22.2	1479	12	12.0	213	*VS*
27.4	1.675	102	20.1	404	12	7.20	35	*M*
35.3	1.333	110 103	17.5	1224 918	6 12	4.10	75	*S*
38.7	1.235	004	16.9	1140	2	3.50	8	*W*
41.3	1.169	112	16.0	1024	12	3.10	38	*M*
42.2	1.151	200	15.7	246	6	3.05	4	*VW*
43.4	1.121	201	15.4	711	12	3.00	26	*M*
45.4	1.082	104	15.1	228	12	2.85	8	*W*

4 over the usual size, their usefulness is greatly increased, since the accuracy of the experimental d-values is very high in the region where the curves crowd together.

We now illustrate the interpretation of a hexagonal powder pattern by considering the film recorded pattern of Zn shown in Fig. 5.2. The camera diameter was $D = 57.3$ mm and the radiation was Cu$K\alpha(\lambda = 1.542$ A). The distances S in mm are directly the $\theta°$ values, and these are recorded in column 1 of Table 5.4 for the first 10 reflections. The d-spacings computed from the $\theta°$-values are tabulated in column 2. The d-values fitted on the Hull-Davey chart are shown by Fig. 5.8. The indices of the reflections are read from the chart and recorded in column 3. Replacing the strip on the 2 log d-scale, the position of the reference mark R gives $a = 2.66$ A. From the spacing values for 200 and 004, we obtain $a = 2.66$ A and $c = 4.94$ A. The number of

atoms in the hexagonal cell is given by

$$n = \frac{N\rho V}{A} = \frac{0.602 \times 10^{24} \times 7.14 \times (2.66)^2 \times 4.94 \times 0.866 \times 10^{-24}}{65.4} = 1.99.$$

Within experimental error there are 2 atoms per unit cell. The missing reflections indicated on Fig. 5.8 are 001, 003, and 111. From Eq. (3.18) these are the missing reflections for the hexagonal close-packed structure. Hence the 2 atoms are at the positions 0 0 0 and $\frac{1}{3}\ \frac{2}{3}\ \frac{1}{2}$.

Although this completes the structure determination for zinc, it is instructive to carry through a qualitative comparison of the integrated intensities. The atomic scattering factors for Zn are listed in column 4. Using the appropriate relations from Eqs. (3.18), the values of the structure factor squared are recorded in column 5. The multiplicity values are readily determined with the help of the fourth index. They are tabulated in column 6. From a plot of the Lorentz-polarization factor $(1 + \cos^2 2\theta)/\sin^2 \theta \cos \theta$ against $\theta°$, the appropriate LP values are obtained and recorded in column 7. The values of $(F^2m\text{LP})/1000$ are listed in column 8. If we neglect the effect of temperature vibration and the θ dependent absorption effect, the values of $(F^2m\text{LP})/1000$ should be proportional to the integrated intensities P'. Since these two effects depend in opposite ways upon θ, they tend to compensate one another, so that neglecting them is often not serious. Column 9 lists the observed integrated intensities P' obtained as qualitative estimates of the blackening per unit length. They are recorded on the qualitative scale: very strong, strong, medium strong, medium, weak, and very weak. The agreement between columns 8 and 9 is quite satisfactory.

Our structure determination is now complete. Zinc has a hexagonal cell with axes $a = 2.66$ A, $c = 4.94$ A and 2 atoms per cell. We can either specify the atomic positions 0 0 0, $\frac{1}{3}\ \frac{2}{3}\ \frac{1}{2}$, or state that zinc has the hexagonal close-packed structure. For spheres in hexagonal close packing the axial ratio is $c/a = 1.63$. Zinc has the abnormal value $c/a = 1.86$, and we could describe zinc as a hexagonal close packing of ellipsoids.

5.5 ANALYSIS OF ORTHORHOMBIC POWDER PATTERNS

Following the cubic, tetragonal, and hexagonal systems, the next in order of increasing difficulty is the orthorhombic system. For orthorhombic crystals there are three axes, a, b, c, and graphical methods are not practical. A numerical method described by Lipson[4] can, however, be used. We start with the spacing formula:

$$\frac{1}{d^2(hkl)} = \frac{h^2}{a^2} + \frac{k^2}{b^2} + \frac{l^2}{c^2}.$$

For all pairs of reflections with the same h and k but different l,

$$\frac{1}{d^2(hkl_1)} - \frac{1}{d^2(hkl_2)} = (l_1^2 - l_2^2)(1/c^2) = (1, 3, 4, 5, 8, \ldots)(1/c^2).$$

Similarly for pairs of reflections with the same k and l but different h there will be differences $(h_1^2 - h_2^2)(1/a^2)$, and for pairs of reflections with the same l and h but different k there will be differences $(k_1^2 - k_2^2)(1/b^2)$.

We now tabulate the differences of all pairs of experimental $1/d^2$ values and plot the frequency of occurrence. Differences which occur several times are likely to include the numbers $(1, 3, 4, 5, 8, \ldots)(1/a^2)$ or $(1, 3, 4, 5, 8, \ldots)(1/b^2)$ or $(1, 3, 4, 5, 8, \ldots)(1/c^2)$. With a little trial and error consideration, it is often possible to obtain the axes from these occurrences. Since spurious multiple occurrences are to be expected, it is very important to have extremely accurate $(1/d^2)$-values. The method works best for simple orthorhombic lattices; for centered lattices, the number of coincidences is reduced.

5.6 PRECISION AXIAL LENGTH MEASUREMENTS

Powder patterns are very often used for a precision measurement of the crystal axes. An important application is to solid solutions where the crystal axes usually vary slightly with composition, and a precision measurement of the axial lengths suffices to determine the composition. The measurements are readily made from powder patterns to an accuracy of better than 1 part in 10,000. The procedures are best adapted to cubic materials, but lower symmetry samples can also be handled.

The first step in obtaining high precision is to use reflections where θ approaches 90°, since it is sin θ that appears in the Bragg law, and near 90° a rough value of θ suffices to give a precise value of sin θ. If in addition, the systematic error decreases to zero as θ approaches 90°, and varies linearly with some function of θ, a linear extrapolation to $\theta = 90°$ gives an axial length which is independent of the systematic error. Although in principle various systematic errors can be handled by extrapolation, or by applying computed corrections, it is a general principle that everything possible should be done to eliminate the error by proper design of the apparatus and proper choice of procedure.

We assume that the sample gives reasonably sharp reflections, since there is generally no point to considering high precision measurements from distorted and imperfect structures. The question of whether the measurements should be made on the peak (mid-chord at say $\frac{4}{5}$ height) or on the center of gravity of the peak has been discussed by Parrish and Wilson.[5] For purposes of theoretical derivations, the center of gravity is very attractive, since in this form the effects of the different errors are directly additive. However,

the center of gravity depends heavily on the ordinate values in the tails of the peaks, and for high-angle reflections the tails spread out appreciably, and they are difficult to separate from the effects of overlap and the background resulting from Compton modified and temperature diffuse scattering. Wholly apart from truncation devices, the center of gravity is not a truly objective quantity for an experimental peak, since it depends on how the background is estimated. On the other hand, the peak position (mid-chord at, say, $\frac{4}{5}$ height) is a truly objective quantity, it is independent of slow background changes and several observers will independently choose the same value. Slowly varying quantities in the intensity expressions have an appreciable effect on the center of gravity, but only a very small effect on the peak positions of sharp peaks. The most recent tabulated x-ray wavelengths are those of Bearden,[6] and these relate to the peak position. We conclude that the center of gravity is not a useful quantity for experimental peaks, and in the following discussion it will be understood that we are discussing peak positions of reasonably sharp peaks.

a) Film Recording

Let us first consider the systematic errors for the Debye-Scherrer type powder camera, in which the film is loaded for back reflection as illustrated by Fig. 5.10. For a high angle reflection, if we measure the distance s' between two lines on opposite sides of the entrance port, $s' = 4R\phi$ where $\theta + \phi = 90°$. Since $\lambda = 2d \sin\theta$, and λ is assumed known,

$$\frac{\Delta d}{d} = -\frac{\Delta \sin\theta}{\sin\theta} = \frac{\sin\phi}{\cos\phi}\Delta\phi. \tag{5.12}$$

But the measured ϕ is given by $\phi = s'/4R$, and hence the fractional error in ϕ due to film shrinkage and error in the effective radius is expressed by

$$\frac{\Delta\phi}{\phi} = \frac{\Delta s'}{s'} - \frac{\Delta R}{R}. \tag{5.13}$$

A displacement of the sample from the camera center can be decomposed into longitudinal and transverse components. A small transverse displacement introduces no error in ϕ since for a high angle reflection the line on one side moves out and the line on the other side moves in by the same amount. Calling Δx the longitudinal displace-

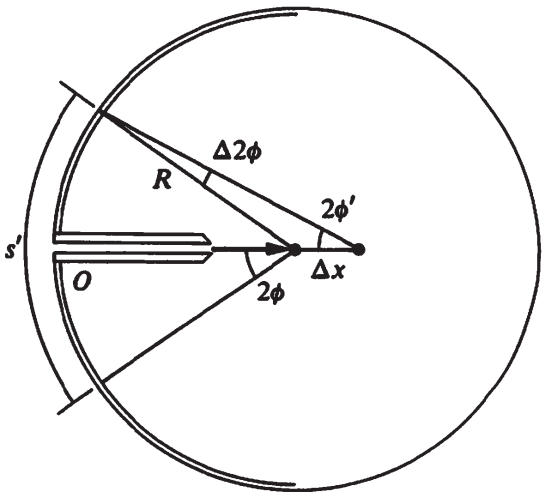

Fig. 5.10 Relations involved in the precision determination of lattice constants using symmetrical back reflection patterns.

ment, we obtain from the triangle shown in Fig. 5.10

$$\frac{\sin(\Delta 2\phi)}{\Delta x} = \frac{\sin 2\phi'}{R},$$

and hence the error in ϕ due to sample displacement is expressed by

$$\Delta\phi = \frac{\Delta x}{R} \sin\phi \cos\phi. \tag{5.14}$$

If the sample is highly opaque to x-rays, only the part of the sample facing the entrance collimator will diffract, and this produces a systematic error in the angle ϕ. To a first approximation, this effect can be considered as contained in the error due to longitudinal displacement of the sample. However, it is well to use a sample of very small diameter to minimize this error.

Combining the four systematic errors which result from film shrinkage, radius uncertainty, sample displacement, and high absorption in the sample, we obtain from Eqs. (5.12), (5.13), and (5.14)

$$\frac{\Delta d}{d} = \frac{\sin\phi}{\cos\phi}\left\{\left(\frac{\Delta s'}{s'} - \frac{\Delta R}{R}\right)\phi + \frac{\Delta x}{R}\sin\phi\cos\phi\right\}.$$

For small values of ϕ we set $\cos\phi = 1$ and $\phi = \sin\phi$. By replacing $\sin\phi$ by $\cos\theta$, we obtain

$$\frac{\Delta d}{d} = \left(\frac{\Delta s'}{s'} - \frac{\Delta R}{R} + \frac{\Delta x}{R}\right)\cos^2\theta. \tag{5.15}$$

For the four systematic errors which we have considered, the fractional error in d varies linearly with $\cos^2\theta$, and goes to zero at $\theta = 90°$. In the special case of a cubic crystal, $\Delta d/d = \Delta a/a$ for all reflections, and

$$\Delta a = aK\cos^2\theta. \tag{5.16}$$

Values of the cube axis a computed from the last two or three reflections and plotted against $\cos^2\theta$ should extrapolate linearly to the correct value of a at $\cos^2\theta = 0$.

The simplicity of the above result depends upon the fact that the four systematic errors which we have considered produce errors in d which vary approximately as $\cos^2\theta$, and hence they can all be eliminated by an extrapolation. There is another systematic error if the entrance port of Fig. 5.10 has an appreciable dimension normal to the plane of the paper. This is usually called the axial divergence error. The effect of axial divergence is to produce an error in θ which increases as θ approaches 90°, and a corresponding error in d which is independent of θ. Since the axial divergence error is not eliminated by a $\cos^2\theta$ extrapolation, it is very important to make it negligible by holding down the size of the entrance collimator.

To discuss the axial divergence error, imagine that the camera of Fig. 5.10 has a very narrow entrance slit at O. The slit has a height H and it extends from $H/2$ below the plane of the paper to $H/2$ above the paper. The sample is a cylinder of very small diameter extending from $Y/2$ below to $Y/2$ above the plane of the paper. For a primary ray passing through the entrance slit at height h above the plane of the paper and striking the sample at height y, consider the diffracted ray which arrives at the film in the plane of the paper. For this ray the true angle 2ϕ will differ from the value obtained by using the measured s' and by assuming that the primary and diffracted rays are in the plane of the paper. With suitable approximations the error $\Delta 2\phi$ is readily obtained. For high angle reflections ($2\theta \rightarrow 180°$), the fractional error in d which results from axial divergence is expressed by

$$\frac{\Delta d}{d} = \frac{h^2}{8R^2} - \left[\frac{(h-y)^2 + y^2}{4R^2}\right] \cos^2 \theta. \tag{5.17}$$

If we now include the axial divergence error in Eq. (5.15), it is evident that part of it will be eliminated by the $\cos^2 \theta$ extrapolation, but that there will remain a constant term $h^2/8R^2$. Since the constant term cannot be eliminated by an extrapolation, it is necessary to make it small enough to be negligible. For $H/R = \frac{1}{40}$, $(H/2)^2/8R^2 = 1/51{,}200$. For most of the radiation coming through the slit, $h < H/2$ and the constant term in $\Delta d/d$ will be less than 1/51,200. For either the Straumanis type camera of Fig. 5.1 or the symmetrical back reflection focusing camera of Fig. 5.3, a proper design of the entrance slit will make the axial divergence error negligible, and an extrapolation such as $\cos^2 \theta$ will eliminate the remaining systematic error. However, it is worth emphasizing again, that the experiment should always be designed so as to make all systematic errors as small as possible, with dependence on the extrapolation only for eliminating the last small remaining systematic error.

For cubic crystals an extrapolation using the last two or three reflections at 2θ approaching 180° is readily done graphically. For noncubic crystals, the systematic error can be extrapolated out by an analytical method devised by M. U. Cohen.[7] This is a least squares method which is equivalent to an extrapolation when more than one axial length is involved.

b) Diffractometer Recording

For powder patterns recorded by a counter diffractometer, the handling of the systematic errors is not as simple as it was for the powder camera. Even with a well-built diffractometer having a very accurately graduated scale, there are systematic errors such as:

1. Displacement of the sample surface from the center of the instrument.
2. Imperfect focusing resulting from a flat-faced sample.
3. Penetration of the beam, so that diffraction takes place below the sample surface.

4. A zero error in the setting of the 2θ scale.
5. With chart recording, the peak displacement which results from use of too long a time constant.
6. The axial divergence error.

For error 1, a displacement of the sample surface by the amount Δy requires a correction $\Delta d/d = (\Delta y/R)\cos^2\theta$. Error 2 can be minimized by shortening the effective length of the sample or by using a curved sample surface with an average curvature chosen for high-angle reflections. Error 3 is of importance only for samples of low absorption coefficient, and for this case the error is minimized by using as thin a sample as intensity requirements will allow. The remainder for both errors 2 and 3 has approximately the same form as for error 1, and hence all three can be lumped together:

$$(\Delta d/d)_{1,2,3} = K\cos^2\theta.$$

Error 4 gives a constant $\Delta\theta$ which is independent of θ, and for high-angle reflections it corresponds to $(\Delta d/d) = K'\cos\theta$. Error 5 produces a displacement of the peak which is analogous to the $\Delta\theta$ of error 4. Since errors 4 and 5 follow a $\cos\theta$ law rather than $\cos^2\theta$, it is desirable to minimize them. The displacement due to too long a time constant can, of course, be eliminated by using point counting. With chart recording it can also be eliminated approximately by running the same peak with several time constants and extrapolating to zero time constant. To eliminate error 4, it is necessary to determine accurately the zero of the 2θ scale. This is the position where a line from the focal line of the target through the axis of the instrument strikes the plane of the receiving slit. A modification of the method of Tournarie[8] consists of supporting a very narrow slit on the specimen holder so that the slit is closely on the axis of the instrument. With the counter recording, the receiving slit is then run through the primary beam and the operation repeated with the sample holder turned 180°. For both readings the apparatus is rotated in the same direction as used for the high-angle readings so that back lash and time constant effects are in the same direction. The average of the two readings gives the zero position of the 2θ scale. For diffractometers which allow recordings for negative values of 2θ, it is possible to record a low angle reflection from the sample, and then rotate the sample holder to pick up the same reflection on the opposite side of the 2θ zero. For all measurements, it is assumed that the sample face is symmetrical with respect to the primary and diffracted beams. Since this setting is not extremely critical for determining a peak position, the adjustment can be made with a straight edge when the receiving slit is set at $2\theta = 0$. For all precision measurements, a very slow goniometer speed should be used, thereby reducing the time constant displacement. For measurements of peak positions, only the upper part of each peak needs to be recorded and excessive times of recording are not necessary. Even though very careful adjustments

and measurements are required, it is best to try to eliminate errors 4 and 5 right in the experiment.

There is still the axial divergence error of Eq. (5.17) for which there is a constant term $\Delta d/d = h^2/8R^2$ which is not eliminated by a $\cos^2\theta$ extrapolation. Taking the Norelco diffractometer as an example, $R = 17.0$ cm and h corresponds to radiation from some point on the focal line of the x-ray tube which after diffraction arrives at a position on the receiving slit which is displaced a distance h along the length of the slit. For $h = 2.5$ mm, $h/R = \frac{1}{68}$ and $\Delta d/d = 1/37{,}000$. It would be desirable that radiation leaving any point on the focal line should not reach a position on the receiving slit more than 2.5 mm away. Although Soller slits are provided in the primary and diffracted beams for cutting down the axial divergence, they are not adequate for the restrictions needed here. The entrance and receiving slits are each about 1 cm in length. The simplest procedure is to cover them, leaving an opening of 2.5 mm length at the center of each. If it is necessary to conserve intensity, the center and ends of each could be covered so as to leave two openings of 2.5 mm length with a covered region of, say, 3 or 4 mm between them, and in addition providing a central vane mounted on the sample holder. Since most of the radiation arriving at one of the openings on the receiving slit corresponds to an h of less than 2.5 mm, the axial divergence error can be made small enough to neglect.

Even if the systematic errors can be made negligible or eliminated by a $\cos^2\theta$ extrapolation, it is necessary to obtain very accurate peak positions. For example if the highest angle reflection which can be recorded is at $2\theta = 160°$, and we desire an accuracy of $\Delta d/d = 1/50{,}000$, it is necessary to be able to read the 2θ values of the peak positions to within

$$\Delta(2\theta)° = 2\left(\frac{\Delta d}{d}\right)\frac{\sin\theta}{\cos\theta}\frac{180}{\pi} = 0.013°.$$

For high-precision measurements a correction for the index of refraction is necessary. There are two effects which result from an index of refraction: a bending of the beam at the crystal surface, and within the crystal a different wavelength $\lambda' = \lambda/\mu$, where μ is the index of refraction. When the beam enters and leaves through the same plane surface, the external 2θ is increased by the bending at the surface. When the beam enters through one plane surface, and leaves through a parallel plane surface, the external 2θ is decreased by the bending at the surface. Hence the bending effects tend to cancel. For the high-angle reflections which are of interest for precision measurements, the beam will usually enter and leave through the same surface. For this case the increase in the external 2θ approaches zero as θ approaches 90°, even for an ideally plane surface. Hence for high-angle powder pattern reflections the bending effect can be neglected, but there remains the correction for the change in wavelength as was pointed out by

A. J. C. Wilson.[9] It is the interior wavelength which must be used in the Bragg law, and hence the spacings are calculated from $\lambda' = \lambda/\mu = 2d \sin \theta$. For silver using Cu$K\alpha$ radiation, $1 - \mu = 3 \times 10^{-5}$, and hence for this case, the refraction correction amounts to 1 part in 30,000.

In spite of the fact that it is possible to present a fairly straightforward discussion of the systematic errors, in practice the problem of high-precision measurements from powder patterns is far from being in a satisfactory state. High-precision measurements by different workers often disagree by amounts which are larger than should be expected. The subject is still in the process of development.

REFERENCES

1. A. W. Hull and W. P. Davey: *Phys. Rev.* **17**, 549 (1921).
2. T. Bjurström: *Z. Physik.* **69**, 346 (1931).
3. C. W. Bunn: *Chemical Crystallography*, Clarendon Press, Oxford (1945).
4. H. Lipson: *Acta. Cryst.* **2**, 43 (1949).
5. W. Parrish and A. J. C. Wilson: *International Tables for X-Ray Crystallography*, Vol. II, p. 216, The Kynoch Press (1959).
6. J. A. Bearden: "X-Ray Wavelengths," Report NYO-10586, U.S. Atomic Energy Commission.
7. M. U. Cohen: *Rev. Scient. Inst.* **6**, 68 (1935); **7**, 155 (1936).
8. M. Tournarie: *Jour. Phys. et le Radium* **15** (1954a), Supp. No. 1, 11A and 16A.
9. A. J. C. Wilson: *Proc. Cambridge Phil. Soc.* **36**, 485 (1940).

PROBLEMS

5.1 A powder pattern of NaCl (FCC, $a = 5.63$ A) at room temperature is recorded with a diffractometer using Cu$K\alpha$ ($\lambda = 1.542$ A). The peak areas in arbitrary units A, and the multiplicity-Lorentz polarization factor (mLP) are recorded for some of the reflections.

hkl	A	mLP	$\left(\frac{\sin\theta}{\lambda}\right)^2$	f(Cl)	f(Na)
400	433	27.8	0.126		
331	58	90.0	0.149	8.30	5.65
422	718	72.5	0.189		
511–333	59	90.3	0.212	7.62	4.70
440	215	32.9	0.252		
622	390	98.4	0.346		
711–551	191	432	0.401	6.36	3.15
640	765	283	0.409		

a) Determine the values of B(Cl) and B(Na) for NaCl at room temperature; $M = B(\sin\theta/\lambda)^2$.
b) What are the root mean squares of the components of displacement $\langle u_s^2\rangle^{1/2}$ for Cl and Na?

5.2 Using monochromatic Cu$K\alpha$, $\lambda = 1.54$ A, a powder pattern diffractometer recording is made of Al (FCC, $a = 4.05$ A) with a chart speed of 30 inches per hour, and the counter turning at $\frac{1}{4}$ degree per minute. The area under the 400 peak is $A = 4.0$ in^2. For $(\sin\theta)/\lambda = 0.495$, $f_{Al}^2 = 32$, i_M(Al) $= 7.5$, and $e^{-2M} = 0.66$ for Al at room temperature. In the vicinity of the 400 peak, what is the height in inches of that part of the background due to the Compton modified scattering from the Al?

5.3 An imaginary element is orthorhombic with a ratio of atomic weight to density $A/\rho = 20.0$. The values of $1/d^2$ for the first 19 lines on a powder pattern are:

1. 0.070	2. 0.114	3. 0.184	4. 0.204
5. 0.252	6. 0.274	7. 0.280	8. 0.322
9. 0.394	10. 0.456	11. 0.484	12. 0.522
13. 0.526	14. 0.532	15. 0.592	16. 0.618
17. 0.630	18. 0.688	19. 0.736	

a) What are the three axial lengths (name them a, b, c in order of decreasing length)?
b) Indices hkl of the 19 powder pattern reflections?
c) Bravais lattice (simple, side-centered, face-centered, or body-centered orthorhombic)?
d) Number of atoms per unit cell?
e) Coordinates of the atoms?

5.4 Derive Eq. (5.17).

6

THE LAUE METHOD

The Laue method is the oldest of the x-ray diffraction methods. A collimated beam of continuous spectrum falls upon a fixed single crystal. For each set of planes *hkl*, the spacing *d*(*hkl*) and the Bragg angle *θ*(*hkl*) are fixed. A reflected beam will be produced if the correct wavelength which satisfies the Bragg law is contained in the continuous spectrum. The different reflected beams have different wavelengths and hence a Laue pattern is "colored." Since the intensity of the continuous spectrum increases with the target atomic number Z, it is preferable to use a tungsten target tube, but the unfiltered radiation from a copper target tube running at, say, 35 kv is often used for Laue patterns.

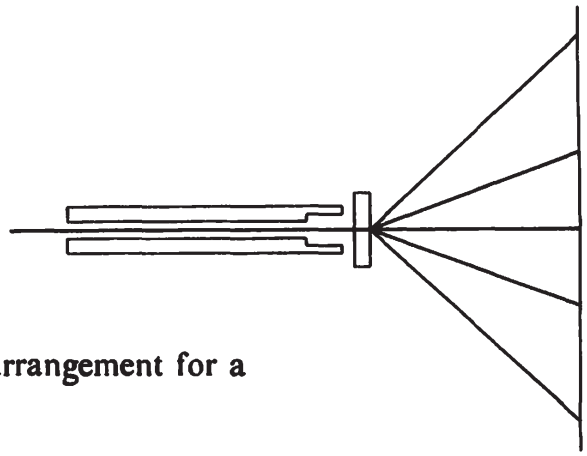

Fig. 6.1 The experimental arrangement for a transmission Laue pattern.

6.1 THE TRANSMISSION LAUE PATTERN

The experimental arrangement for a transmission Laue pattern is illustrated by Fig. 6.1. The collimated continuous spectrum passes through a thin slip of single crystal. The diffracted beams are registered on a film placed perpendicular to the primary beam at a distance of, say, 5 cm from the crystal. If the crystal is symmetrically oriented with respect to the primary beam, the Laue pattern may show a very high symmetry. Figure 6.2 shows the transmission Laue pattern of Quartz taken with the primary beam parallel to the *c*-axis. The 3-fold symmetry of the crystal is readily seen in the Laue pattern.

It is evident that the diffraction spots of Fig. 6.2 fall on sets of ellipses which pass through the central spot. This is true whether or not the crystal has a symmetrical orientation. All spots falling on an ellipse are due to

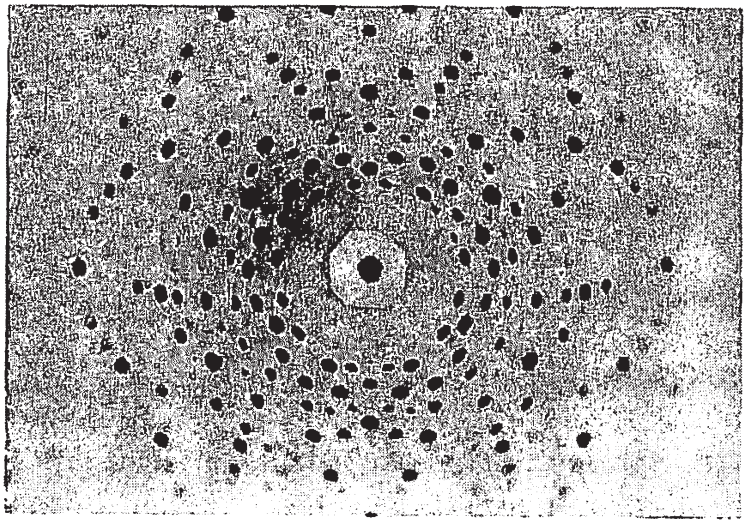

Fig. 6.2 Transmission Laue pattern of Quartz, made with the primary beam parallel to the hexagonal *c*-axis, and *D*-5.0 cm. This reproduction is half size.

planes *hkl* which belong to a particular zone *uvw*. We define a zone axis $\mathbf{A}(uvw) = u\mathbf{a}_1 + v\mathbf{a}_2 + w\mathbf{a}_3$, where *uvw* are integers. All planes *hkl* containing the direction $\mathbf{A}(uvw)$ are said to belong to the zone *uvw*. Since the planar normals must be perpendicular to the zone axis, $\mathbf{H}(hkl) \cdot \mathbf{A}(uvw) = 0$ and hence the equation for all planes *hkl* belonging to the zone *uvw* is expressed by

$$hu + kv + lw = 0. \qquad (6.1)$$

From Eq. (2.5) the direction of the diffracted beam from the planes *hkl* is given by

$$\mathbf{s} = \mathbf{s}_0 + \lambda\mathbf{H}(hkl). \qquad (6.2)$$

Suppose that the plane *hkl* belongs to the zone *uvw*. Forming the scalar product with $\mathbf{A}(uvw)$ on both sides of Eq. (6.2), we obtain

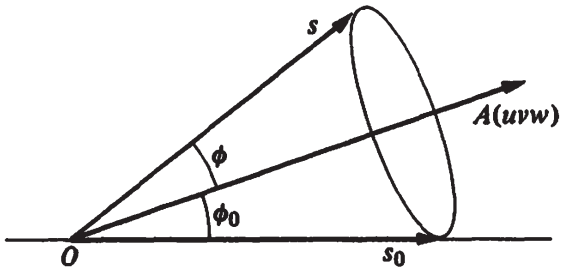

Fig. 6.3 The cone with axis $\mathbf{A}(uvw)$ whose surface contains the directions of all reflected beams *hkl* which belong to the zone *uvw*.

$$\mathbf{s} \cdot \mathbf{A}(uvw) = \mathbf{s}_0 \cdot \mathbf{A}(uvw) + \lambda\mathbf{H}(hkl) \cdot \mathbf{A}(uvw).$$

But since $\mathbf{H}(hkl) \cdot \mathbf{A}(uvw) = 0$ for all planes *hkl* belonging to the zone *uvw*, we obtain $\phi = \phi_0$, where ϕ_0 is the angle between the primary beam and the zone axis $\mathbf{A}(uvw)$, and ϕ is the angle between $\mathbf{A}(uvw)$ and the reflected beam from any plane *hkl* belonging to the zone *uvw*. As illustrated by Fig. 6.3, the reflected beams for all planes belonging to the zone *uvw* form the elements of a cone which contains the primary beam as one element and has the zone axis $\mathbf{A}(uvw)$ as the cone axis. The intersection of this cone with a film normal to the primary beam gives the ellipses observed on a transmission Laue pattern.

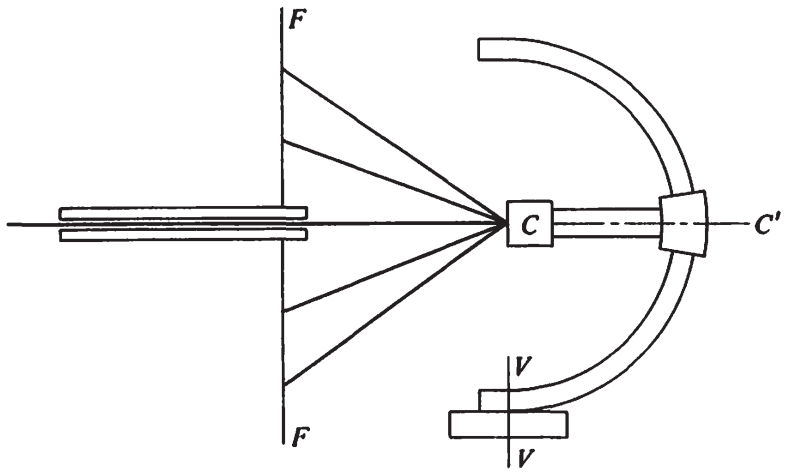

Fig. 6.4 Schematic representation of the back reflection Laue camera.

The positions of the diffraction spots give the directions of the various diffracted beams, and the corresponding planar normals **H**(*hkl*) are readily constructed. The intersections of these planar normals with the plane of the film gives the gnomonic projection of the Laue pattern. This gnomonic projection is readily interpreted as a projection of the reciprocal lattice. In the early days of structure determination, the gnomonic projection was much used to index Laue patterns, and simple structures were determined by means of transmission Laue patterns. It is not worthwhile to go into the details, since this method of structure determination has been replaced by other more powerful methods.

6.2 THE BACK REFLECTION LAUE PATTERN

Although the transmission pattern is obsolete, the back reflection Laue pattern is much used today for the orientation of single crystals, particularly for the orientation of single cubic crystals. Having grown a single crystal

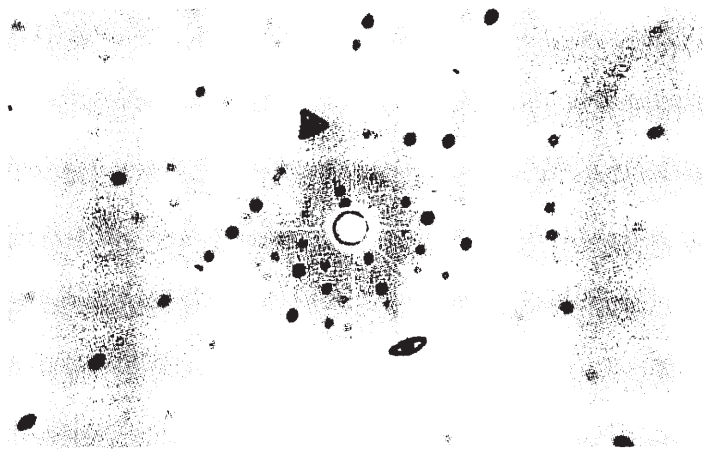

Fig. 6.5 Back reflection Laue pattern of Silicon, as seen from the sample $D = 3.0$ cm.

ingot of a metal or alloy, we may wish to determine the orientation of some principal axis or set of planes, or we may wish to orient the ingot for cutting a desired face. Figure 6.4 illustrates the back-reflection Laue camera. The collimated primary beam enters through a hole in the film and falls on the single crystal ingot placed at 3.0 cm from the film. The ingot mount is a vertical circle which is pivoted on a vertical axis *VV*. Specifying the orienta-

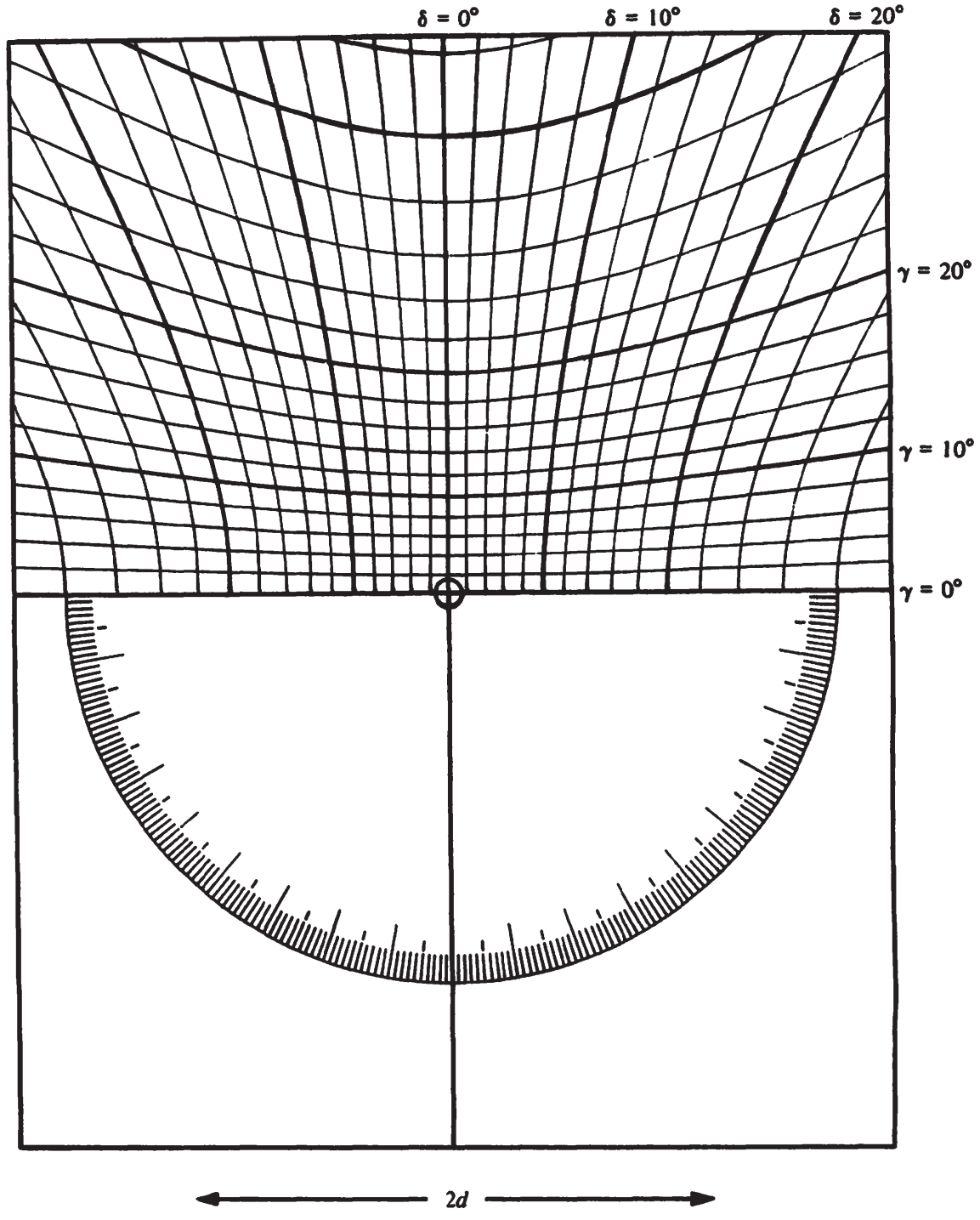

Fig. 6.6 Greninger chart for the solution of back reflection Laue patterns, reproduced in the correct size for a specimen to film distance D of 3.00 cm. Lines of constant meridian are horizontal, and lines of constant parallel are vertical; the intervals are 2°.

tion of the crystal by meridian and parallel coordinates (longitude and latitude), the meridian angle is varied by rotation about the vertical axis VV, and the parallel angle by motion of the segment along the vertical circle. A back-reflection Laue pattern of Silicon is shown by Fig. 6.5. For this type of pattern, the zone lines are hyperbolae and in general the hyperbolae do not pass through the center of the pattern.

The interpretation of the back reflection Laue pattern is greatly facilitated by the use of a Greninger[1] chart, a reproduction of which is given by Fig. 6.6. The principle of the chart is illustrated by Fig. 6.7. The film is vertical and the horizontal primary beam $\mathbf{s}_0$ falls on the single crystal C. For the diffracted beam striking the film at S, the $\mathbf{H}(hkl)$ vector normal to the diffracting planes bisects the angle between $\mathbf{s}$ and $-\mathbf{s}_0$. The intersection at point H on the film is the gnomonic projection of the planes hkl producing the spot S. We now label position S with the meridian and parallel coordinates *of point H*. If this is done for a large number of points S, we can draw curves of constant meridian and constant parallel. On the Greninger net, the North-South axis is taken horizontal, so that the horizontal curves are lines of constant meridian (longitude) and the vertical curves are lines of constant parallel (latitude). In terms of this net, the position of any diffraction spot S gives the meridian and parallel coordinates of the *corresponding planar normal H*.

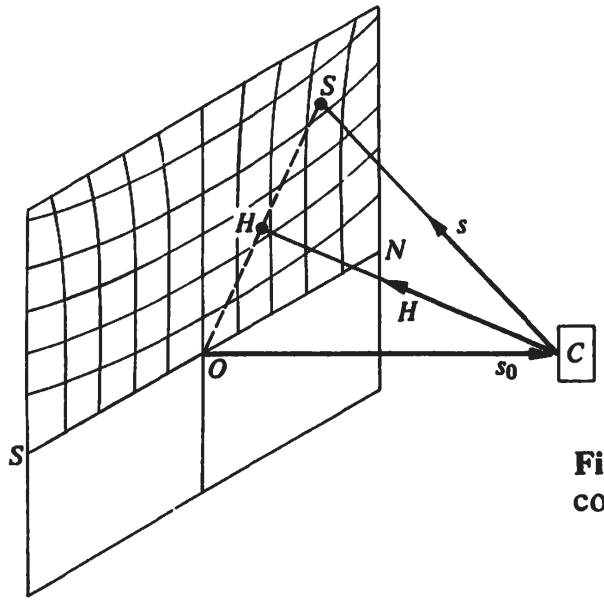

Fig. 6.7 Geometry involved in the construction of the Greninger chart.

To interpret a cubic pattern such as Fig. 6.5, we look for the three most important spots on the pattern. These will be low-index reflections, and they will be characterized by the fact that they are quite black, that there is an appreciable open space around them, and that they occur at the intersection of several prominent zone lines. On a piece of transparent paper we mark the three important spots, trace the three connecting zone lines, and indicate the center of the pattern as well as the vertical and horizontal directions. With a 9 cm × 12 cm film and the standard crystal to film distance $D = 3.0$ cm,

the pattern of a cubic crystal will always contain at least one of the three important reflections 100, 110, or 111. Since multiple orders superimpose on a Laue pattern, when we speak of the reflection 100 we mean the superposition of 100, 200, 300, 400, etc. Keeping the center of the tracing on the center of the Greninger chart, and rotating to bring two of the important reflection spots on a line of constant meridian, the difference in parallel readings gives directly the angle between the two planar normals H. Repeating for the other two pairs of diffraction spots, we obtain the three angles between the three planar normals $\mathbf{H}(hkl)$. The hkl-indices of the three principal spots are then readily obtained from Table 6.1, which gives the angles between planar normals in a cubic crystal. The angles can be read from the chart to better than 0.5° and in general two of the measured angles will suffice to index all three planes, with the third measured angle serving as a check.

Suppose that we wish to cut a 100 face. If 100 was not among the three reflections indexed, we can change the orientation of the crystal and make another pattern on which the 100 reflection appears. With the Greninger Chart we then measure the meridian and parallel coordinates of $H(100)$. In doing this we rotate the chart 90° so that the meridian and parallel coordinates of the chart correspond to the meridian and parallel scales of the Laue camera. The settings of the Laue camera are then changed to bring $H(100)$ parallel to the primary beam. A cut perpendicular to the direction of the primary beam will produce the desired 100 face. If the crystal is soft, the cut may be made with the ingot held in the goniometer of the Laue camera. To be able to handle hard crystals, it is convenient to have a graduated circle which reads rotations about the axis CC'. With the axis CC' horizontal, the $H(100)$ direction is then brought to the center of the diagram in two steps. From the circular scale on the Greninger chart we read off the angle necessary for rotation about CC' to bring $H(100)$ onto the equator of the diagram, and then the angle about axis V to bring it to the center of the diagram. The sample holder of a milling machine provides directly the rotation about the axis V, so that if a device is added to maintain the orientation about CC', the cut is readily made on the milling machine.

The procedure which has been outlined is very simple and straightforward for cubic crystals which are not so soft that the temperature factor $\exp(-2M)$ kills the high-angle reflections. To get a good Laue pattern it is generally necessary to clean and etch that part of the surface of the ingot which is being studied. Except for materials whose fluorescence radiation will be absorbed in the air, it is advisible to cover the film with a thin aluminum sheet. For crystals of lower than cubic symmetry, orientations are usually best found by making a series of Laue patterns with regular variations in the orientation of the sample. Symmetry in the pattern can usually be recognized even when the sample is still several degrees from a simple setting.

Table 6.1

ANGLES BETWEEN PLANAR NORMALS IN THE CUBIC SYSTEM*

100	100	0°	90°					
	110	45°	90°					
	111	54°44′						
	210	26°34′	63°26′	90°				
	211	35°16′	65°54′					
	221	48°11′	70°32′					
	310	18°26′	71°34′	90°				
	311	25°14′	72°27′					
	320	33°41′	56°19′	90°				
	321	36°43′	57°42′	74°30′				
110	110	0°	60°	90°				
	111	35°16′	90°					
	210	18°26′	50°46′	71°34′				
	211	30°	54°44′	73°13′	90°			
	221	19°28′	45°	76°22′	90°			
	310	26°34′	47°52′	63°26′	77°5′			
	311	31°29′	64°46′	90°				
	320	11°19′	53°58′	66°54′	78°41′			
	321	19°6′	40°54′	55°28′	67°48′	79°6′		
111	111	0°	70°32′					
	210	39°14′	75°2′					
	211	19°28′	61°52′	90°				
	221	15°48′	54°44′	78°54′				
	310	43°5′	68°35′					
	311	29°30′	58°31′	79°58′				
	320	61°17′	71°19′					
	321	22°12′	51°53′	72°1′	90°			
210	210	0°	36°52′	53°8′	66°25′	78°28′	90°	
	211	24°6′	43°5′	56°47′	79°29′	90°		
	221	26°34′	41°49′	53°24′	63°26′	72°39′	90°	
	310	8°8′	31°57′	45°	64°54′	73°34′	81°52′	
	311	19°17′	47°36′	66°8′	82°15′			
	320	7°7′	29°45′	41°55′	60°15′	68°9′	75°38′	82°53′
	321	17°1′	33°13′	53°18′	61°26′	70°13′	83°8′	90°
211	211	0°	33°33′	48°11′	60°	70°32′	80°24′	
	221	17°43′	35°16′	47°7′	65°54′	74°12′	82°12′	
	310	25°21′	49°48′	58°55′	75°2′	82°35′		
	311	10°2′	42°24′	60°30′	75°45′	90°		
	320	25°9′	37°37′	55°33′	63°5′	83°30′		
	321	10°54′	29°12′	40°12′	49°6′	56°56′		
		70°54′	77°24′	83°44′	90°			

(continued)

Table 6.1 (*continued*)

221	221	0°	27°16′	38°57′	63°37′	83°37′	90°	
	310	32°31′	42°27′	58°12′	65°4′	83°57′		
	311	25°14′	45°17′	59°50′	72°27′	84°14′		
	320	22°24′	42°18′	49°40′	68°18′	79°21′	84°42′	
	321	11°29′	27°1′	36°42′	57°41′	63°33′	74°30′	
		79°44′	84°53′					
310	310	0°	25°51′	36°52′	53°8′	72°33′	84°16′	
	311	17°33′	40°17′	55°6′	67°35′	79°1′	90°	
	320	15°15′	37°52′	52°8′	74°45′	84°58′		
	321	21°37′	32°19′	40°29′	47°28′	53°44′	59°32′	
		65°	75°19′	85°9′	90°			
311	311	0°	35°6′	50°29′	62°58′	84°47′		
	320	23°6′	41°11′	54°10′	65°17′	75°28′	85°12′	
	321	14°46′	36°19′	49°52′	61°5′	71°12′	80°44′	
320	320	0°	22°37′	46°11′	62°31′	67°23′	72°5′	90°
	321	15°30′	27°11′	35°23′	48°9′	53°37′	58°45′	63°36′
		72°45′	77°9′	85°45′	90°			
321	321	0°	21°47′	31°	38°13′	44°25′	50°	60°
		64°37′	69°4′	73°24′	81°47′	85°54′		

* From R. M. Bozorth, *Phys. Rev.* **26**, 390 (1925).

The sphere of reflection construction for the back-reflection Laue pattern is shown by Fig. 6.8. The direction of the primary beam is represented by the vector s_0/λ whose terminal point is at O, the origin of the reciprocal lattice. For each wavelength in the beam there is a sphere of radius $1/\lambda$. The largest sphere has a radius $1/\lambda_{SWL}$, where λ_{SWL} is the short wave limit of the continuous spectrum. The smallest sphere has a radius $1/\lambda_M$, where λ_M is the somewhat indefinite longest wavelength which is not drastically absorbed before reaching the film. For convenience assume that the film is a disk of radius R. The maximum value of the angle $2\phi = 180 - 2\theta$ for reflections which can be recorded on the film is given by

$$\tan 2\phi_m = R/D.$$

All reflections appearing on the Laue pattern are then represented by the reciprocal lattice points in the volume which is shown on Fig. 6.8 by the section $ABCDE$, where the sphere OAE has the radius $1/\lambda_M$ and the sphere $OBCD$ has the radius $1/\lambda_{SLW}$. This volume divided by v_b, the volume per

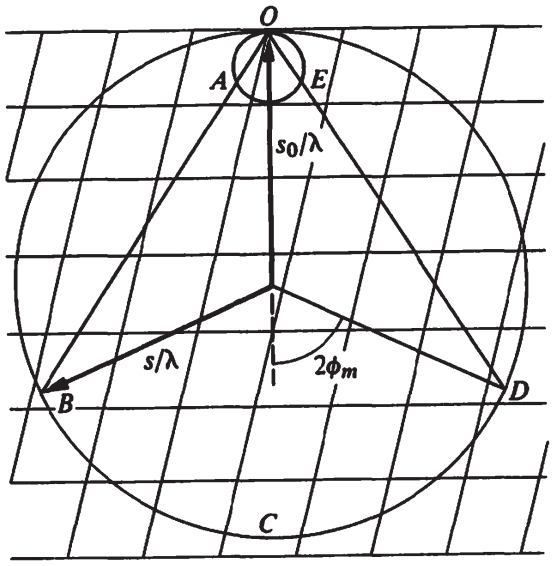

Fig. 6.8 Sphere of reflection construction for the back reflection Laue pattern.

point in reciprocal space, gives the maximum number of reflections which can appear on the Laue pattern:

$$n = \frac{4\pi}{3v_b} \sin^2 \phi_m (1 + \cos^2 \phi_m) \left(\frac{1}{\lambda^3_{SWL}} - \frac{1}{\lambda^3_{MI}} \right). \tag{6.3}$$

The number of spots which will be observed on the Laue pattern may be much smaller than this computed n since the structure factor may be small or zero for many of the reciprocal lattice points, and some of the allowed reflections will be multiple orders which superimpose as a single diffraction spot.

REFERENCES

1. A. B. GRENINGER, *Zeit. für Krist.* **A91**, 424 (1935).

PROBLEMS

6.1 The transmission Laue pattern of quartz shown by Fig. 6.2 was made with the x-ray beam parallel to c and a distance $D = 5.0$ cm. The closest spots are at $s = 17$ mm from the center of the pattern. For quartz, $a = 4.90$ A and $c = 5.39$ A. Applying the third Laue equation, compute an approximate value for the voltage on the x-ray tube.

6.2 Suppose that the transmission Laue pattern of quartz shown by Fig. 6.2 had been recorded on a disk-shaped film of radius $R = 6.0$ cm, with the tube running at 45 kv. For quartz, $a = 4.90$ A, $c = 5.39$ A. The distance $D = 5.0$ cm. By a sphere of reflection construction analogous to that of Fig. 6.8, compute an upper limit to the number of reflections which could appear on the Laue pattern.

6.3 The back reflection Laue pattern of silicon shown by Fig. 6.5 contains the 110 and 111 reflections indicated by an ellipse and a triangle. (a) What should be the changes in the meridian and parallel scales of the Laue camera to bring 110 parallel to the primary beam? (b) What are the *uvw*-indices of the zone line connecting 110 and 111?

6.4 Silicon has the diamond structure, Bravais Lattice FCC, $a = 5.43$ A, 8 atoms per cell, positions 0 0 0, $\frac{1}{4}, \frac{1}{4}, \frac{1}{4}$, etc. A back reflection Laue pattern of an arbitrarily oriented single crystal of silicon is made running the tube at 35 kv. Assume that wavelengths longer than 2.5 A are absorbed. The film is 3.0 cm from the crystal and is a disk of radius $R = 5.0$ cm.

a) For what *hkl* combinations is $F = 0$?
b) What fraction of the reciprocal lattice points give reflections?
c) What is a maximum value for the number of reflection spots on the Laue pattern?
d) Compare with Fig. 6.5.

6.5 Germanium has the diamond structure FCC, $a = 5.66$ A. A back-reflection Laue pattern is made with the tube operating at 25 kv and a crystal to film distance $D = 3.0$ cm.

a) For what classes of reflections *hkl* is $F = 0$?
b) If the $n(100)$ reflection (multiples of 100) is near the center of the pattern, what is approximately the distance from this spot to the nearest spot on the film?
c) Suppose the orientation of the crystal is such that both the $n(100)$ and $n(110)$ reflections are on the film and the midpoint of the connecting zone line is near the center of the film. By constructing the appropriate section of the reciprocal lattice, determine an approximate upper limit for the number of spots on the zone line between $n(100)$ and $n(110)$.

6.6 Derive Eq. (6.3).

THE ROTATION METHOD

For obtaining the crystal axes a_1, a_2, a_3 and assigning *hkl*-indices to the various reflections, the rotation method is the most powerful and the most used of the various diffraction methods. It uses monochromatic radiation, usually the filtered $K\alpha$ doublet. It is limited to cases where single crystals are available, but the crystal need not be large. Most rotation patterns are made with small single crystals whose size is of the order of 1 mm, but very much smaller crystals can be used when necessary. There are two main classes of rotation patterns: (a) the simple rotation pattern using a stationary film, (b) the more powerful moving film modifications such as the Weissenberg and the Precession patterns.

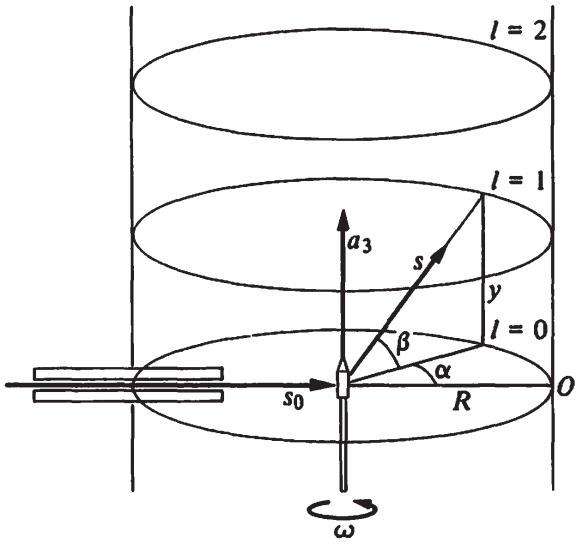

Fig. 7.1 The geometry of the simple rotation pattern in which the primary beam is perpendicular to the axis of rotation.

7.1 THE SIMPLE ROTATION PATTERN

The experimental arrangement is shown schematically by Fig. 7.1. A single crystal is mounted so that one of its axes (say a_3) is vertical and the crystal rotates continuously about this axis during the exposure. The monochromatic primary beam defined by a collimator is horizontal and perpendicular to the axis of rotation. Since $\mathbf{a}_3$ is perpendicular to $\mathbf{s}_0$, the term $\mathbf{s}_0 \cdot \mathbf{a}_3$ drops out of the third Laue equation $(\mathbf{s} - \mathbf{s}_0) \cdot \mathbf{a}_3 = l\lambda$ and we obtain

$$|\mathbf{a}_3| \sin \beta = l\lambda, \qquad \sin \beta = l\lambda/|\mathbf{a}_3|, \tag{7.1}$$

where β is a latitude angle measured above the equatorial plane. Regardless of the h and k indices, Eq. (7.1) states that all reflections with the same value

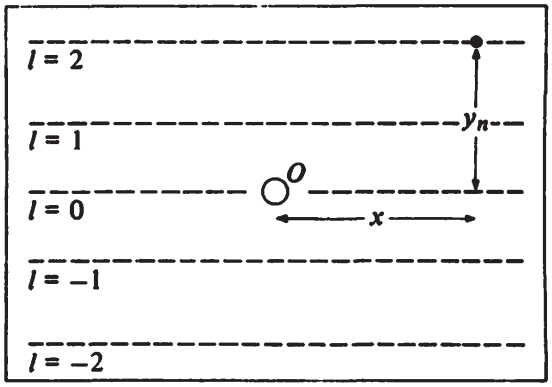

Fig. 7.2 Schematic representation of the layer lines on the rotation pattern produced by rotating about one of the crystallographic axes.

of l will make the same latitude angle β, and hence will form the elements of a cone. For each value of l ($l = 0, 1, 2, -1, -2$, etc.) there is a corresponding cone of diffracted beams. If the pattern is recorded on a cylindrical film, the intersection of the cones will be horizontal lines of diffraction spots. These lines of diffraction spots which are usually called "layer lines" are illustrated schematically by Fig. 7.2.

For a rotation about any axis $\mathbf{a}_i$, there will be a layer line pattern, and letting n denote the number of the layer line, we can rewrite Eq. (7.1) in the more general form

$$|\mathbf{a}_i| = \frac{n\lambda}{\sin \beta_n}, \tag{7.2}$$

where

$$\tan \beta_n = y_n/R. \tag{7.3}$$

From the measured distances y_n between the equator and the nth layer line, we obtain $\tan \beta_n$ from Eq. (7.3); and using the corresponding value of $\sin \beta_n$ in Eq. (7.2), we obtain directly the axial length $|\mathbf{a}_i|$. It was only necessary to have lined up the crystal for rotation about the $\mathbf{a}_i$-axis; it was not necessary to know anything about the crystal system, or to know the *hkl*-indices of any of the reflections.

Figure 7.3 shows the c-axis rotation pattern of Quartz made with filtered Cu$K\alpha$ ($\lambda = 1.542$ A) and a camera of diameter $D = 60.0$ mm. From the average of several measured distances $2y_1$ and $2y_2$, we obtain directly the length of the c-axis:

n	y_n	$\tan \beta_n$	$\sin \beta_n$	$c = n\lambda/\sin \beta_n$
1	9.0 mm	0.300	0.287	5.37 A
2	20.9 mm	0.698	0.572	5.38 A

Giving the greater weight to the second layer line measurement, we conclude that $c = 5.38$ A. The length of the a-axis could then be obtained by

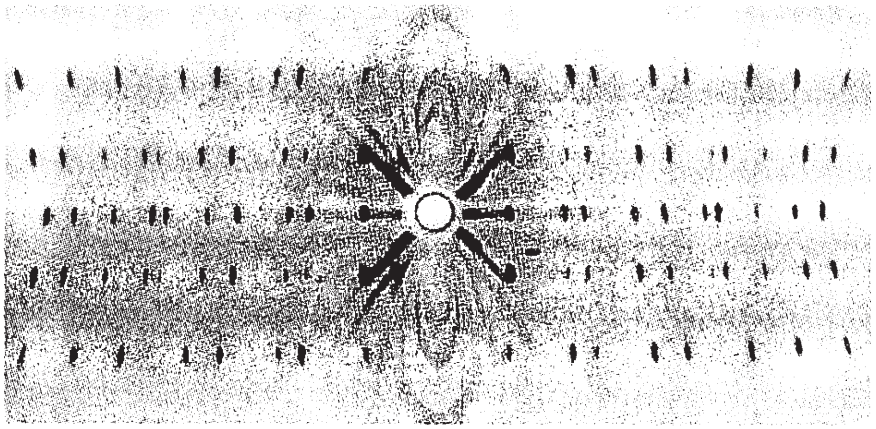

Fig. 7.3 Rotation pattern of Quartz, made by rotating about the hexagonal c-axis. Filtered Cu$K\alpha$ radiation, and camera diameter $D = 60.0$ mm. The streaks are due to the continuous spectrum. (Reduced to approximately 0.64 of original size.)

reorienting the crystal for a rotation about the a-axis, and measuring the layer line separations. However, since Fig. 7.3 is the pattern of a hexagonal crystal, we can obtain the length of the a-axis from the equator spots. For a hexagonal crystal, $1/d^2 = [4/(3a^2)](h^2 + hk + k^2)$ for $l = 0$. Accordingly, we measure distances between pairs of spots on opposite sides of the equator, compute the values of $1/d^2$, and look for a common divisor which gives simple integers. The value of this divisor is $[4/(3a^2)]$. We also know directly the value of the l-index for all the diffraction spots on Fig. 7.3; for all equator spots, $l = 0$; for all first layer line spots, $l = 1$; and so on.

If the crystal is set up for rotation about any simple crystallographic direction $u\mathbf{a}_1 + v\mathbf{a}_2 + w\mathbf{a}_3$ where uvw are integers, we will obtain a layer line pattern. By measuring the distances between layer lines, we obtain directly the distance of repetition along the direction uvw. To obtain a layer line pattern requires that we can orient the crystal for rotation about some crystallographic direction $u\mathbf{a}_1 + v\mathbf{a}_2 + w\mathbf{a}_3$. For a crystal with well-developed faces, one can often see by inspection the orientation of the principal axes. The edge formed by the intersection of two crystallographic planes $h_1k_1l_1$ and $h_2k_2l_2$ is a crystallographic direction with $u:v:w = (k_1l_2 - k_2l_1):(l_1h_2 - l_2h_1):(h_1k_2 - h_2k_1)$ and hence any edge formed by the intersection of two faces will give a layer line pattern if used as the axis of rotation. For a sample showing no faces, an orientation can be found by making oscillations of say 15° rather than complete rotations. If the axis of rotation is not too far from a simple crystallographic direction, the pattern can be recognized as a set of slanting layer lines. From the angle of slant, the necessary change in orientation is readily determined.

The sphere of reflection construction for the rotation pattern is shown by Fig. 7.4. The sphere of reflection of radius $1/\lambda$ rotates through the

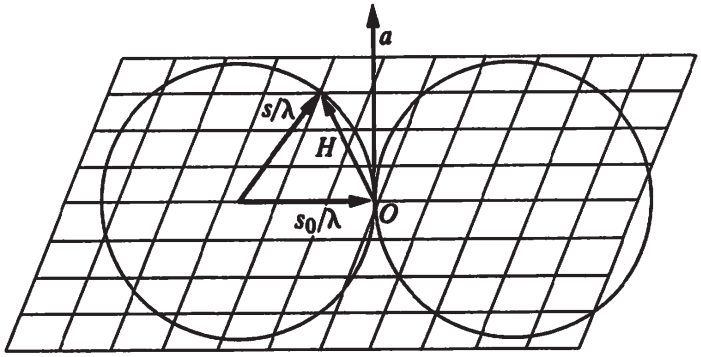

Fig. 7.4 Sphere of reflection construction for the rotation pattern. The origin of the reciprocal lattice is at O, and the rotation is about the axis a.

reciprocal lattice and sweeps out the torus whose cross section is indicated in Fig. 7.4. Only the planes *hkl* represented by the reciprocal lattice points within this torus can contribute the rotation pattern. Since the cylindrical film has a finite height, not all of the points within the torus will register on the film.

7.2 INDEXING OF ROTATION PATTERNS

On a rotation pattern made by rotating around, say, the c-axis, the value of the l index of every reflection is given immediately by the number of the layer line. However there is still the problem of assigning the h- and k-indices. Suppose that we have made three rotation patterns rotating about the a-, b-, and c-axes. From the layer line separations the lengths of the three axes are known, and from the angles through which the crystal was turned we know the angles between the axes. From these data we can compute the lengths of the three reciprocal vectors $\mathbf{b}_1\mathbf{b}_2\mathbf{b}_3$, and the angles between them. Hence we can lay out the reciprocal lattice of the crystal and write down the *hkl*-indices of each reciprocal lattice point.

In principle the indexing of a rotation pattern is simply a matter of correlating each diffraction spot with the corresponding point in the reciprocal lattice. From the position of a spot on the rotation pattern how much information do we get about the coordinates of the corresponding point in the reciprocal lattice? Represent the position of a point in the reciprocal lattice by the cylindrical coordinates H_v, H_h, and ϕ shown by Fig. 7.5. The Bragg law in vector form is $\mathbf{s} - \mathbf{s}_0 = \lambda\mathbf{H}$, and in terms of the vertical components of each of these vectors, $\mathbf{s}_v - \mathbf{s}_{0v} = \lambda\mathbf{H}_v$. But $\mathbf{s}_{0v} = 0$, and $|\mathbf{s}_v| = \sin\beta$; hence $\sin\beta = \lambda H_v$. The vertical coordinate on the film is given by

$$y = R\tan\beta = \frac{R}{\sqrt{(1/\lambda H_v)^2 - 1}}. \tag{7.4}$$

The angle α of Fig. 7.5 is given by $\alpha = x/R$ where x is the horizontal coordinate of the spot on the film. From the law of spherical right triangles $\cos 2\theta = \cos\alpha \cos\beta$ and hence

$$\cos\left(\frac{x}{R}\right) = \frac{\cos 2\theta}{\cos\beta} = \frac{1 - 2\sin^2\theta}{\sqrt{1 - \sin^2\beta}} = \frac{1 - \frac{1}{2}[(\lambda H_h)^2 + (\lambda H_v)^2]}{\sqrt{1 - (\lambda H_v)^2}}. \quad (7.5)$$

From Eq. (7.4) the vertical coordinate y of a diffraction spot gives directly the H_v coordinate of the corresponding reciprocal lattice point. Knowing H_v, Eq. (7.5) then gives directly H_h from the horizontal coordinate x of the diffraction spot.

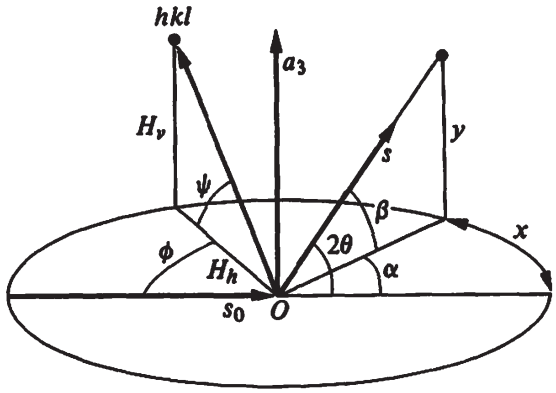

Fig. 7.5 Geometry relating the coordinates of a point in the reciprocal lattice and the position of a diffraction spot on the film.

These two operations are conveniently handled by the Bernal Chart[1] which is printed on transparent paper so that it can be placed upon the film. Equation (7.4) is represented by a set of horizontal lines at equal intervals in λH_v, and Eq. (7.5) is represented by a set of curves at equal intervals in λH_h. Placing the chart on the film, we read off directly the H_h and H_v coordinates of the reciprocal lattice points belonging to each diffraction spot.

From the position of a diffraction spot on a rotation pattern we get only two of the three cylindrical coordinates of the corresponding reciprocal lattice point. For simple structures with small unit cells where b_1, b_2, b_3 are large, the values of H_h and H_v are often enough to correlate each diffraction spot with the corresponding reciprocal lattice point. However, with complex structures there are often several reciprocal lattice points with approximately the same value of H_v and H_h, and a unique indexing of the diffraction spots is not possible.

7.3 THE WEISSENBERG PATTERN

To allow a unique indexing of each diffraction spot we need all three coordinates of the corresponding reciprocal lattice point. From a rotation pattern we obtained H_v and H_h but not the third coordinate ϕ. The great advantage of the various moving film methods is that they give all three coordinates. The Weissenberg pattern and the Precession pattern are the

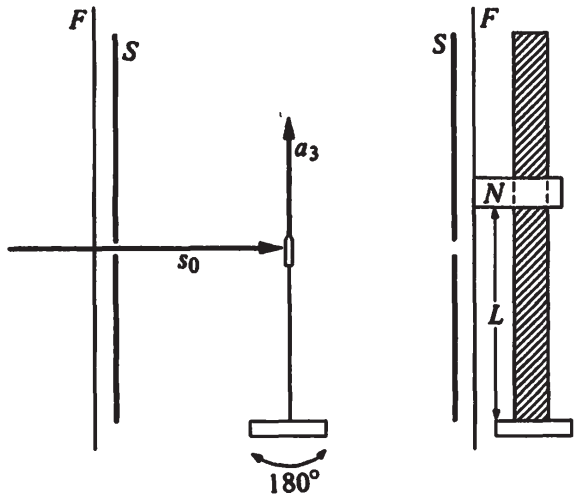

Fig. 7.6 Schematic representation of the Weissenberg camera with the sleeve set for recording equator reflections.

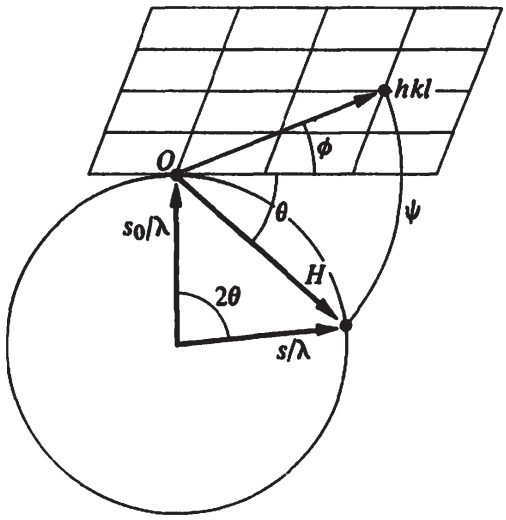

Fig. 7.7 The sphere of reflection and the zero layer of the reciprocal lattice, for the interpretation of Weissenberg equator patterns.

two most used examples of moving film patterns. The Buerger Precession camera has the great advantage that the arrangement of spots on the diffraction pattern is closely that of the corresponding points in the reciprocal lattice, and hence the indexing is not only unique but extremely straightforward. As a simple example of moving film methods, we will consider the interpretation of a Weissenberg equator pattern.

The Weissenberg camera is illustrated schematically by Fig. 7.6. For mechanical reasons the axis of rotation of a Weissenberg camera is made horizontal, but in Fig. 7.6 it is shown vertical to correspond to the rotation camera of Fig. 7.1. The crystal is mounted to rotate about some axis (say a_3) but in the Weissenberg camera it is oscillated through 180° instead of rotated. A cylindrical metal sleeve *SS* has a narrow slot around the circumference. The sleeve can be set at the right height to allow any one layer line to pass through the slot and to stop all the others. In the figure it is shown set to pass the equator reflections. With the Weissenberg Camera, we record only one layer line at a time. The cylindrical film *FF* is just outside of the sleeve. The film carriage is supported by a nut *N* which rides on a long lead screw geared to the oscillating crystal holder in such a way that as the crystal oscillates 180°, the film traverses up and down a distance *L*.

We now consider a Weissenberg equator pattern obtained by setting the sleeve as shown in Fig. 7.6 so as to pass the equator reflections and stop all the others. If the film were held stationary we would obtain the ordinary equator of a rotation pattern, but since the film moves, the spots are spread out in two dimensions on the film. Suppose that we start with the film in the extreme upper position, and with the reciprocal lattice of the crystal oriented relative to the primary beam as indicated in Fig. 7.7. The reciprocal lattice

points which are shown are all equator points whose positions are specified by $H_h = H$ and ϕ. For the point hkl to reflect, the crystal must turn through the angle $\psi = \phi + \theta$ so as to bring the point onto the sphere of reflection. During this time the film moves down, so that the reflection will occur on the film at a vertical coordinate:

$$y = \frac{L\psi}{\pi} = \frac{L}{\pi}(\phi + \theta).$$

The horizontal coordinate of the diffraction spot is given by $x = R2\theta$ and hence

$$y = \frac{L\phi}{\pi} + \frac{L}{\pi}\frac{x}{2R}. \tag{7.6}$$

Weissenberg cameras usually have the standard dimensions

$$2R = 180/\pi \text{ mm}, \qquad L = 90 \text{ mm},$$

and Eq. (7.6) takes the simple form

$$y(\text{mm}) = \frac{\phi^\circ}{2} + \frac{x(\text{mm})}{2}. \tag{7.7}$$

All reciprocal lattice points with the same ϕ-coordinate will record on the film as spots along a slanting line whose slope is $\frac{1}{2}$ and whose intercept at $x = 0$ gives $\phi^\circ/2$. Figure 7.8 shows such a line of diffraction spots together with the triangular scale which is convenient for measuring Weissenberg equator patterns. Going out from the center in both directions along the slanting edge, there is a scale graduated to read directly the λH_h-values for each spot. At the left is a millimeter scale with each mm labelled 2° to give directly the coordinate ϕ°. For a Weissenberg equator pattern it is a simple matter to read the coordinates H_h and ϕ° for reciprocal lattice points corresponding to all of the equator reflections. The equatorial layer of the

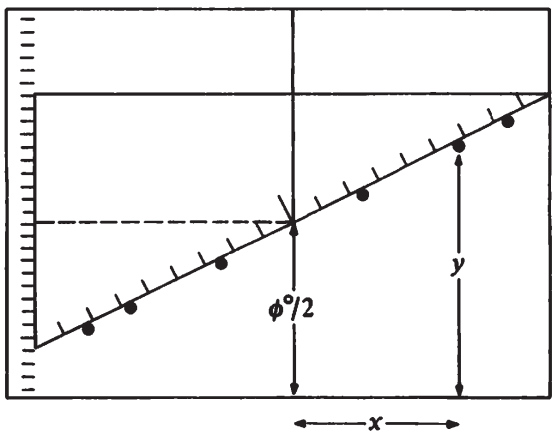

Fig. 7.8 The slanting line on a Weissenberg equator pattern formed by reflections with the same ϕ coordinate and the triangular scale for reading the two coordinates ϕ and H_h.

reciprocal lattice is then readily plotted on polar coordinate paper. For the Weissenberg equator pattern, polar coordinates in the reciprocal lattice have transformed to oblique cartesian coordinates on the film. The handling of other than equator patterns, and the short-cut methods for indexing moving film patterns have been given by M. J. Buerger.[2]

7.4 FIBER DIAGRAMS AS ROTATION PATTERNS

Figure 7.9 shows the pattern obtained by placing a bundle of Chrysotile asbestos fibers, $Mg_3Si_2O_5(OH)_4$ in a rotation camera and irradiating with Cu$K\alpha$. The fibers were aligned along the axis of the camera but the sample was not rotated during the exposure. The layer lines are clearly evident and the pattern is a typical rotation pattern. The crystal axis c is parallel to the fiber direction, and in the sample there is a completely random orientation around the fiber axis. The bundle of fibers is the equivalent of a single crystal rotated during the exposure. Using Eqs. (7.2) and (7.3), we obtain $c = 5.26$ A as the length of the crystal axis parallel to the fiber direction. Some of the reflections are spread out along the layer lines due to a peculiar type of imperfection in the structure of Chrysotile.

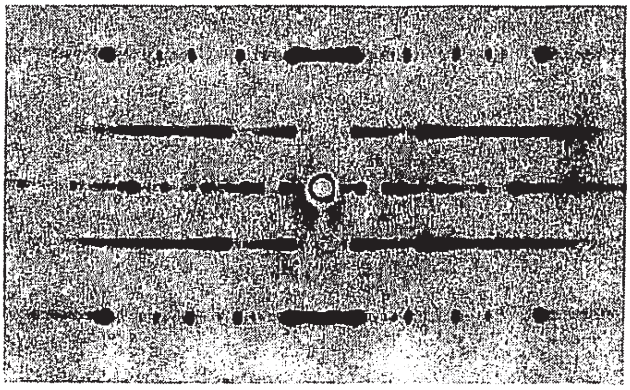

Fig. 7.9 Pattern of Chrysotile asbestos fibers $Mg_3Si_2O_5(OH)_4$, using Cu$K\alpha$ radiation. The fiber axis is perpendicular to the primary beam (vertical).

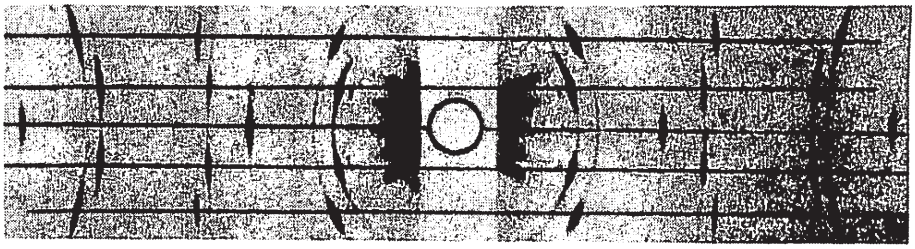

Fig. 7.10 Pattern of an etched aluminum wire using Cu$K\alpha$ radiation. The axis of the wire is perpendicular to the primary beam (vertical).

Figure 7.10 shows the pattern of an aluminum wire drawn through a die and then etched to remove the surface material. The wire was parallel to the axis of the camera but was not rotated during the exposure. The powder pattern lines are concentrated rather sharply into spots which fall on the layer lines of a typical rotation pattern. Using Eqs. (7.2) and (7.3), we obtain for the axial length $a' = 7.02$ A. Aluminum is cubic with an axial length $a = 4.05$ A. Since $7.02 = 4.05\sqrt{3}$, we conclude that the drawing process has oriented the individual grains so that the [111] directions (cube diagonals) are lined up parallel to the axis of the wire, but around this axis the orientation of the grains is random.

REFERENCES

1. J. D. BERNAL: *Proc. Roy. Soc.* **A113**, 117 (1926).
2. M. J. BUERGER: *X-Ray Crystallography*, J. Wiley and Sons, N.Y. (1942); *The Precession Method*, J. Wiley and Sons, N.Y. (1964).

PROBLEMS

7.1 A rotaton pattern is registered on a cylindrical film of radius R and length L ($L/2$ above and below the equator). The primary beam is normal to the axis of rotation.

a) Show that the volume in reciprocal space containing points which can register on the film is given by

$$V = \frac{4\pi}{\lambda^3}\left\{\frac{\sin 2\beta}{2} + \beta\right\} \quad \text{where } \tan\beta = \frac{L}{2R}.$$

b) If $2R = 180/\pi$ mm, $L = 120$ mm, and a triclinic crystal of cell volume $v_a = 100$ A^3 is rotated about the c-axis using Cu$K\alpha$ ($\lambda = 1.54$ A), what is the approximate maximum number of diffraction spots possible on one quadrant of the film?

c) Show that for the c-axis rotation of a triclinic crystal, the maximum number of diffraction spots possible on one half of the equator is given by

$$n = 2\pi v_a/(\lambda^2 c).$$

7.2 a) Prove that for the general triclinic crystal $|\mathbf{b}_1 \times \mathbf{b}_2| = |\mathbf{a}_3|/v_a$.

b) A triclinic crystal is mounted for an $\mathbf{a}_3$-axis rotation in a Weissenberg camera. From the plot of equator reciprocal lattice points: $|\mathbf{b}_1| = 0.20$ A^{-1}, $|\mathbf{b}_2| = 0.25$ A^{-1}, and $\beta_{12} = 53.1°$. With the sleeve removed to give a rotation pattern, the layer line separations give $|\mathbf{a}_3| = 6.0$ A. What is the unit cell volume v_a?

7.3 A rotation pattern is made by rotating a triclinic crystal about the c-axis, using Cu$K\alpha$ ($\lambda = 1.542$ A) and with a camera of diameter $D = 57.3$ mm. The distance from the equator to the first layer line is $y_1 = 9.3$ mm. There are 36 diffraction spots on either half of the equator (right-hand half or left-hand half). What is a minimum value for v_a the unit cell volume?

7.4 On a rotation pattern made with the primary beam normal to the axis of rotation, continuous loops often emerge from the center of the pattern due to the reflection of the continuous spectrum from some set of planes. Calling x and y the horizontal and vertical distances on a cylindrical film, show that the equation of the loop is

$$\cos\left(\frac{x}{R}\right) = \sqrt{1 + (y/R)^2} - \frac{(y/R)^2}{2\cos^2\gamma\sqrt{1 + (y/R)^2}},$$

where γ is the angle between the axis of rotaton and the planar normal H.

7.5 Tungsten is BCC with $a = 3.16$ A. The pattern of a tungsten wire is made in a cylindrical camera of diameter 57.3 mm using Cu$K\alpha$ ($\lambda = 1.542$ A). The powder lines are concentrated into intense regions which define layer lines, with the first layer line at a distance $y_1 = 1.05$ cm above the equator. What orientation of the tungsten crystals is produced by the drawing process of forming the wire?

8

THE USE OF SPACE GROUPS IN STRUCTURE DETERMINATION

The very simple structures such as those of copper, zinc, diamond, and rock salt can be obtained directly from the x-ray diffraction data without any formal use of symmetry theory. For the more complicated structures, however, there is a great deal to be gained by combining symmetry theory with the x-ray data. Formally this is known as applying space-group theory.

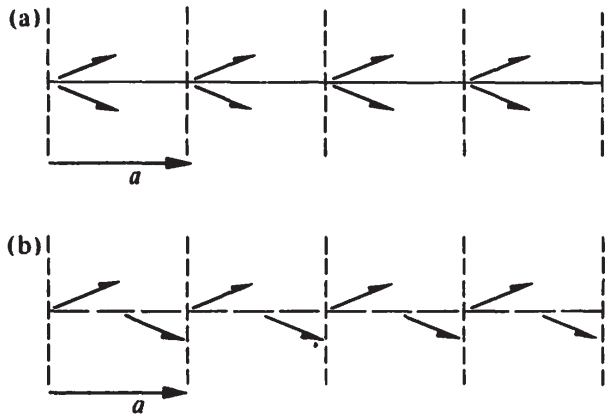

Fig. 8.1 Representation of microscopic symmetry elements. (a) Reflection plane (b) Glide plane.

A space group is the periodic three-dimensional arrangement in space of a set of consistent symmetry elements. To include all the possibilities, it is necessary to realize that in a periodic crystalline structure more than one kind of microscopic symmetry operation may correspond to a particular macroscopic symmetry operation. For example, a macroscopic reflection plane may exist in the crystal as either a reflection plane or as a glide plane. The two possibilities are represented by Figs. 8.1(a) and 8.1(b). The former shows a reflection plane with some unit of structure and its mirror image repeated by the crystal axis **a** which is parallel to the reflection plane. Figure 8.1(b) shows a glide plane. In this operation, a unit of structure reflects across the plane and glides a distance **a**/2. Repeated applications of this operation produce a pattern which repeats at distances **a**.

Similarly a macroscopic 2-fold rotation axis may exist in the crystal as a 2-fold rotation axis or as a 2-fold screw axis. Figure 8.2(a) shows a 2-fold rotation axis parallel to **b**. A unit of structure which is above the paper by

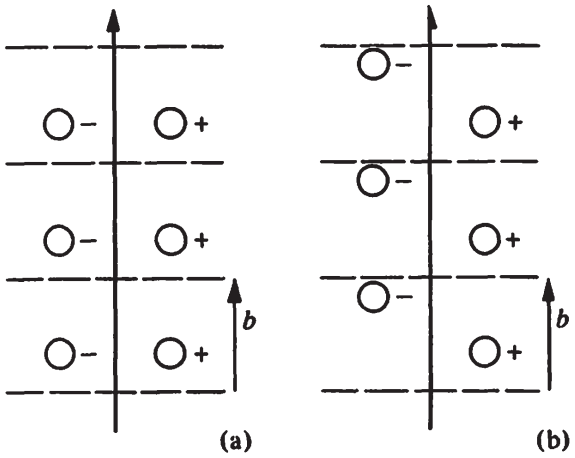

Fig. 8.2 Representation of microscopic symmetry elements. (a) 2-fold rotation axis. (b) 2-fold screw axis.

an amount (+) is rotated 180° around the axis to an equal distance below the paper. With the 2-fold screw axis illustrated by Fig. 8.2(b), a unit at the position (+) rotates 180° around the axis to the position (—) and then translates a distance **b**/2. Repeated application of this operation produces a pattern which repeats at distances **b**.

By considering all of the possible ways in which the microscopic symmetry elements and combinations of these elements can be arranged in the different Bravais lattices, we find 230 essentially different arrangements. These are the 230 space groups. All the useful information for each of the space groups is tabulated in *International Tables for X-Ray Crystallography*, Vol. 1, "Symmetry Groups."

8.1 THE SPACE GROUP Cmcm

As an illustration of space groups we will derive the properties of one space group D_{2h}^{17}-Cmcm. The first symbol D_{2h}^{17} is an old notation which is no longer used. The second symbol Cmcm is the present Hermann-Mauguin notation. This new notation has the useful feature that the symbol itself gives the spatial arrangement of the symmetry elements.

The first letter in the symbol is a capital letter which gives the type of Bravais lattice. Various capital letters may appear in the first position; P (primitive), F (face-centered), I (body-centered), A (side-centered, additional translation **b**/2 + **c**/2), C (side-centered, additional translation **a**/2 + **b**/2), etc. The next three positions correspond to the *a*-, *b*-, and *c*-axes. A figure "2" in the first of these positions would mean a 2-fold rotation axis parallel to the *a*-axis, and a letter "*m*" in the first position would mean a reflection plane perpendicular to the *a*-axis. The symbol mcm represents reflection planes perpendicular to the *a*- and *c*-axes and a glide plane perpendicular to the *b*-axis with glide of *c*/2.

The spatial arrangement of the symmetry elements is shown by Fig. 8.3. Following the convention of the International Tables, the *a*-axis is directed

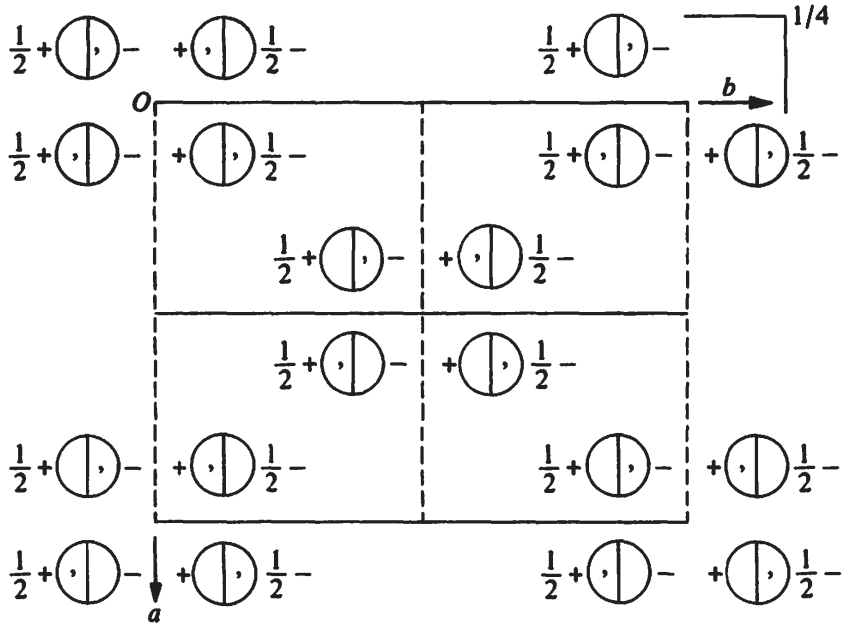

Fig. 8.3 Arrangement of symmetry elements and repeating units in the space group Cmcm.

down, the *b*-axis toward the right, and the *c*-axis up from the paper. The reflection planes perpendicular to the *a*-axis are shown by heavy lines. As soon as we have put in the repeating units of structure, it will be evident that the symmetry elements occur at intervals $a/2$ or $b/2$ or $c/2$, rather than at the repeating intervals a, b, c of the crystal lattice. The glide planes with glide $c/2$, are indicated by the rows of dots perpendicular to the *b*-axis. The reflection plane perpendicular to c is parallel to the plane of the paper. By taking this plane at a height $c/4$ above the paper, the origin O in the plane of the paper becomes a center of symmetry. The reflection planes at height $c/4$ and $3c/4$ are represented at the upper right-hand corner by the two lines labeled $\frac{1}{4}$.

We now consider how a single asymmetric unit of structure must be repeated in the space group. Let the open half circle labeled (+), which is near the upper left-hand corner, represent some unit at the position x, y, z. Because of the reflection plane at height $c/4$, there must be a mirror image of this unit at $x, y, \frac{1}{2} - z$. This second unit is shown by the comma in a half circle which is labelled $(\frac{1}{2}-)$. The reflection plane perpendicular to the *a*-axis produces the mirror image of these two units at $\bar{x}, y, z$ and $\bar{x}, y, \frac{1}{2} - z$. From the four units already produced, the glide plane perpendicular to *b* produces four more by reflecting across the plane and translating $c/2$. The symmetry elements mcm have required the eight asymmetric units which are clustered about the upper left-hand corner of the diagram. The capital *C* in the first position of the space-group symbol means that the lattice is side-centered with an additional translation $\mathbf{a}/2 + \mathbf{b}/2$. Hence the eight units

already placed are repeated identically with a translation $\mathbf{a}/2 + \mathbf{b}/2$, and these are shown near the center of the diagram. The origin is a center of symmetry, since for each unit at xyz there is another at $\bar{x}\bar{y}\bar{z}$. In addition to the elements mcm with which we started, additional symmetry elements such as centers, 2-fold rotation axes, 2-fold screw axes, and glide planes have been produced. It is not necessary to give these additional symmetry elements to specify the space group, and they are not shown on Fig. 8.3.

For the space group Cmcm, the general position is 16 fold. The coordinates of the 16 positions are expressed in terms of the coordinates xyz of the first position in the following 16-fold group of positions:

(16*h*)	x,	y,	z;	x,	$\bar{y}$,	$\bar{z}$;	$\frac{1}{2}+x$,	$\frac{1}{2}+y$,	z;	$\frac{1}{2}+x$,	$\frac{1}{2}-y$,	$\bar{z}$;
	$\bar{x}$,	$\bar{y}$,	$\bar{z}$,	$\bar{x}$,	y,	z	$\frac{1}{2}-x$,	$\frac{1}{2}-y$,	$\bar{z}$;	$\frac{1}{2}-x$,	$\frac{1}{2}+y$,	z
	x,	y,	$\frac{1}{2}-z$;	x,	$\bar{y}$,	$\frac{1}{2}+z$;	$\frac{1}{2}+x$,	$\frac{1}{2}+y$,	$\frac{1}{2}-z$;	$\frac{1}{2}+x$,	$\frac{1}{2}-y$,	$\frac{1}{2}+z$;
	$\bar{x}$,	$\bar{y}$,	$\frac{1}{2}+z$;	$\bar{x}$,	y,	$\frac{1}{2}-z$	$\frac{1}{2}-x$,	$\frac{1}{2}-y$,	$\frac{1}{2}+z$;	$\frac{1}{2}-x$,	$\frac{1}{2}+y$,	$\frac{1}{2}-z$

For a unit of structure which has the necessary symmetry to be situated on one or more of the symmetry elements, the number of required units is smaller. If the unit has the combined symmetry of a reflection plane and a center of symmetry, we could set $x = y = z = 0$ so that the first four positions in 16(*h*) coalesce into a single position on the center of symmetry at the origin. This produces the 4-fold position 4(a). We could set $x = 0$, $y = \frac{1}{2}$, $z = 0$, and coalesce to the 4-fold position 4(*b*) which is also on a symmetry center and a reflection plane. If the unit has the symmetry of two orthogonal reflection planes, we could set $x = 0$, $z = \frac{1}{4}$, and obtain the 4-fold position 4(*c*):

4(*a*)	0,	0,	0;	0,	0,	$\frac{1}{2}$;	$\frac{1}{2}$,	$\frac{1}{2}$,	0;	$\frac{1}{2}$,	$\frac{1}{2}$,	$\frac{1}{2}$;
4(*b*)	0,	$\frac{1}{2}$,	0;	0,	$\frac{1}{2}$,	$\frac{1}{2}$;	$\frac{1}{2}$,	0,	0;	$\frac{1}{2}$,	0,	$\frac{1}{2}$;
4(*c*)	0,	y,	$\frac{1}{4}$;	0,	$\bar{y}$,	$\frac{3}{4}$;	$\frac{1}{2}$,	$\frac{1}{2}+y$,	$\frac{1}{4}$;	$\frac{1}{2}$,	$\frac{1}{2}-y$,	$\frac{3}{4}$.

If the unit has the symmetry of a center of symmetry we can set $x = \frac{1}{4}$, $y = \frac{1}{4}$, $z = 0$ and obtain the 8-fold position 8(*d*) at a set of symmetry centers. If the unit has the symmetry of a 2-fold rotation axis we can set $y = 0$, $z = 0$, and obtain the 8-fold position 8(*e*) situated on 2-fold rotation axes. If the unit has the symmetry of a reflection plane, we can set $x = 0$ and

obtain the positions 8(f) or set $z = \frac{1}{4}$ and obtain the positions 8(g):

8(d) $\frac{1}{4}, \frac{1}{4}, 0;\quad \frac{1}{4}, \frac{3}{4}, 0;\quad \frac{1}{4}, \frac{1}{4}, \frac{1}{2};\quad \frac{1}{4}, \frac{3}{4}, \frac{1}{2};$
$\frac{3}{4}, \frac{3}{4}, 0;\quad \frac{3}{4}, \frac{1}{4}, 0;\quad \frac{3}{4}, \frac{3}{4}, \frac{1}{2};\quad \frac{3}{4}, \frac{1}{4}, \frac{1}{2};$

8(e) $x, 0, 0;\quad \bar{x}, 0, 0;$
$\frac{1}{2}+x, \frac{1}{2}, 0;\quad \frac{1}{2}-x, \frac{1}{2}, 0;$

$x, 0, \frac{1}{2};\quad \bar{x}, 0, \frac{1}{2};$
$\frac{1}{2}+x, \frac{1}{2}, \frac{1}{2};\quad \frac{1}{2}-x, \frac{1}{2}, \frac{1}{2};$

8(f) $0, y, z;\quad 0, \bar{y}, \bar{z};$
$\frac{1}{2}, \frac{1}{2}+y, z;\quad \frac{1}{2}, \frac{1}{2}-y, \bar{z};$

$0, y, \frac{1}{2}-z;\quad 0, \bar{y}, \frac{1}{2}+z;$
$\frac{1}{2}, \frac{1}{2}+y, \frac{1}{2}-z;\quad \frac{1}{2}, \frac{1}{2}-y, \frac{1}{2}+z;$

8(g) $x, y, \frac{1}{4};\quad \bar{x}, y, \frac{1}{4};$
$\frac{1}{2}+x, \frac{1}{2}+y, \frac{1}{4};\quad \frac{1}{2}-x, \frac{1}{2}+y, \frac{1}{4};$

$x, \bar{y}, \frac{3}{4};\quad \bar{x}, \bar{y}, \frac{3}{4};$
$\frac{1}{2}+x, \frac{1}{2}-y, \frac{3}{4};\quad \frac{1}{2}-x, \frac{1}{2}-y, \frac{3}{4}.$

We next work out the contribution to the structure factor by the 16 atoms in the general position 16(h). For each xyz there is a $\bar{x}\bar{y}\bar{z}$, and the two contributions combine to a term $2\cos 2\pi(hx + ky + lz)$. The contribution by the last 8 positions is obtained from that of the first 8 positions by multiplying by $\exp[2\pi i(h/2 + k/2)]$:

$$F/f = \{1 + \exp[2\pi i(h/2 + k/2)]\}\{2\cos 2\pi(hx + ky + lz) + 2\cos 2\pi(hx - ky - lz) + 2\cos 2\pi(hx + ky - l[\tfrac{1}{2} + z]) + 2\cos 2\pi(hx - ky + l[\tfrac{1}{2} + z])\}. \quad (8.1)$$

These terms can be combined in pairs by the relation

$$\cos(A + B) + \cos(A - B) = 2\cos A \cos B, \quad (8.2)$$

$$F/f = 4\{1 + e^{\pi i(h+k)}\}\{\cos 2\pi hx \cos 2\pi(ky + lz) + \cos 2\pi hx \cos 2\pi(ky - l[\tfrac{1}{2} + z])\}.$$

By adding and subtracting $l/4$ in the term $\cos 2\pi(ky + lz)$,

$$F/f = 4\{1 + \cos\pi(h + k)\}\cos 2\pi hx\{\cos 2\pi(ky - l/4 + lz + l/4) + \cos 2\pi(ky - l/4 - lz - l/4)\}.$$

The last two terms can be combined by Eq. (8.2) and we obtain finally

$$F/f = 16 \cos^2 \pi\left(\frac{h+k}{2}\right) \cos 2\pi hx \cos 2\pi(ky - l/4) \cos 2\pi(lz + l/4). \quad (8.3)$$

We next work out the conditions for the vanishings. By a vanishing we mean that $F/f = 0$ for certain classes of hkl-reflections regardless of the xyz-coordinates. Since $\cos^2 (h + k)\pi/2 = 0$ for $h + k =$ odd, the general reflection hkl is present only for $h + k =$ even. The term $\cos 2\pi(ky - l/4) = 0$ for $k = 0$ and $l =$ odd. Hence the special reflection $h0l$ can be present only if $l =$ even and also from the first condition only if $h =$ even. The vanishings for the space group Cmcm are as follows:

The general reflection (hkl) is present only for $h + k =$ even.
The reflection ($h0l$) is present only for $h =$ even and $l =$ even.

All of the material that we have worked out here for the space group Cmcm including the spatial arrangement of the symmetry elements, the arrangement of the asymmetric units in the general position, the tabulation of the coordinates for the general position and the various special positions, the contribution to the structure factor, and the vanishings are listed for each of the 230 space groups in the International Tables. All of this material is of very great value in a structure determination. From the systematic vanishings in the x-ray reflections, we determine the space group or the several possible space groups. When more than one space group is a possibility, we choose first the one of highest symmetry. Since this is the one which puts the greatest restrictions on the atom positions, it will be the easiest to eliminate if it is wrong. Often the number of atoms of each kind in the unit cell is less than that of the general position, so that the atoms must be in various special positions. For structures of only moderate complexity, the space-group requirements reduce the structure determination to that of finding the values of the small number of parameters associated with the special positions. A detailed treatment of the use of space-group methods in complex structure determinations can be found in Lipson and Cochran.[1]

8.2 SPACE GROUP METHODS APPLIED TO URANIUM

As an illustration of the application of space-group methods to a relatively simple case, we will consider the structure determination of Uranium from powder pattern data, as reported by Jacob and Warren.[2] A powder pattern made with Cu$K\alpha$ showed 39 lines which were carefully measured and graded in intensity as strong, medium, weak, and very weak. Simple tests showed that the pattern could not be indexed as cubic, tetragonal, or hexagonal. Since the pattern did not appear unduly complicated, it seemed likely that the structure had an orthorhombic cell.

By a procedure which is equivalent to that described in Section 5.5, and a certain amount of trial and error, three orthorhombic axes were obtained: $a = 2.86\ A$, $b = 5.88\ A$, and $c = 4.96\ A$. In terms of these axes, all the lines on the powder pattern were satisfactorily indexed. The number of atoms in the orthorhombic cell is then given by

$$n = \frac{v\rho N}{A} = \frac{2.86 \times 5.88 \times 4.96 \times 18.9 \times 0.602}{238} = 4.0.$$

From the indices of the reflections, it was seen that the general reflection hkl appeared only for $h + k =$ even, and reflections of the type $h0l$ appeared only for both h and l even. Referring to the International Tables, and assuming the highest orthorhombic symmetry, the observed vanishings indicate the space group Cmcm. Since this is the space group which we have just developed, the significance of the symbols is clear; a side-centered orthorhombic lattice with reflection planes normal to the a- and c-axes and a glide plane normal to the b-axis.

Since there are four atoms per cell, the only possibilities are the 4-fold special positions: 4(a), 4(b), or 4(c). The first two must be rejected, since for each position there is another translated from it by c/2. This would correspond to a c-axis only half the length which we are using, and only reflections with $l =$ even could have appeared. Only for a more complicated composition, where there is another group of atoms in some position other than 4(a) and 4(b), is there any significance to these two sets of positions. We are left with the position 4(c) as the only possibility:

$$4(c)\quad 0,\ y,\ \tfrac{1}{4};\qquad 0,\ \bar{y},\ \tfrac{3}{4};\qquad \tfrac{1}{2},\ \tfrac{1}{2}+y,\ \tfrac{1}{4};\qquad \tfrac{1}{2},\ \tfrac{1}{2}-y,\ \tfrac{3}{4}.$$

The structure factor for reflections with $h + k =$ even is obtained from Eq. (8.3) by replacing the 16 by 4 and setting $x = 0$ and $z = \frac{1}{4}$.

$$F/f = 4 \cos 2\pi(ky - l/4) \cos \pi l.$$

This takes the two simple forms:

$$h + k = \text{even},\quad l = \text{even}: \qquad F^2 = 16f^2 \cos^2 2\pi ky,$$
$$h + k = \text{even},\quad l = \text{odd}: \qquad F^2 = 16f^2 \sin^2 2\pi ky.$$

For determining the parameter y it is only necessary to consider the range 0.00–0.25 since a change in origin to $\frac{1}{2}$, 0, $\frac{1}{2}$ makes the range 0.25–0.50 equivalent. Since the reflections 020, 022, 220, and 024 were all very weak, $\cos^2 2\pi 2y$ is very small and $y = \frac{1}{8}$ approximately. By comparing lines which are near one another on the pattern, we can neglect the variations in the scattering factor, the Lorentz-polarization factor, the temperature factor, and the absorption for a cylindrical sample. Only the structure factor and the multiplicity m must be considered, and we can write

$$P' = Km(F/4f)^2.$$

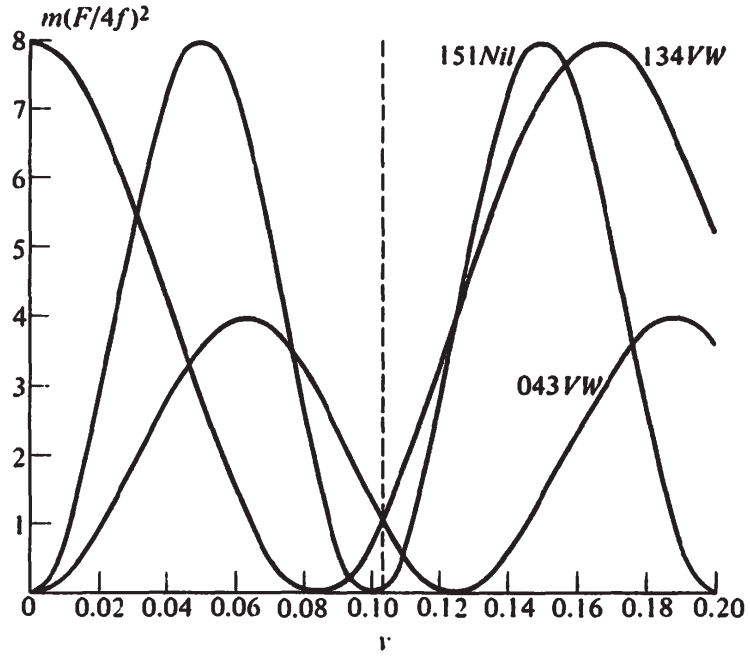

Fig. 8.4 Determination of the parameter y for Uranium by a plot of $m(F/4f)^2$ for several neighboring reflections.

For structures involving only one parameter, it is standard practice to plot a quantity proportional to P' against the parameter y for several high-order reflections. It is then a simple matter to see for what value of y the ordinates of the different curves are in the ratio of the observed intensities. Figure 8.4 shows plots of $m(F/4f)^2$ against y for the three nearby reflections 043, 151, and 134. It is evident that the curves are in the correct relation at about $y = 0.103$. Consideration of all the reflections leads to a parameter value $y = 0.105 \pm 0.005$. Hence alpha uranium has 4 atoms per orthorhombic cell, at the positions 4(*c*) of the space group Cmcm, with the parameter value $y = 0.105$. This peculiar structure can be considered as a slight distortion of the hexagonal close-packed structure.

For structures involving two or three parameters, it is often possible to find certain reflections which depend primarily on one parameter and not on the others. For example, if two parameters x and y are involved, the *h*0*l* reflections involve x but not y, and the 0*kl* reflections involve only y. Hence the parameters can be determined independently by the same procedure that was used here for a one-parameter structure.

REFERENCES

1. H. Lipson and W. Cochran: *The Determination of Crystal Structures*, G. Bell and Sons, London (1953).
2. C. W. Jacob and B. E. Warren: *J. Amer. Chem. Soc.* **59**, 2588 (1937).

PROBLEMS

8.1 Consider the monoclinic space group $P2_1/c$ which has a primitive lattice, a 2-fold screw axis parallel to b, and a glide plane perpendicular to b with glide $c/2$. Arrange to have the origin at a symmetry center. Tabulate the general and special positions, and the general vanishings.

8.2 Assume that a certain element has an orthorhombic structure with 8 atoms per unit cell. Space-group symmetry requires the atoms to be at the positions:

$$\begin{array}{llll} 0, & u, & v; & \tfrac{1}{2}, \ \tfrac{1}{2}-u, \ v; \\ 0, & -u, & -v; & \tfrac{1}{2}, \ \tfrac{1}{2}+u, \ -v; \end{array}$$

$$\begin{array}{llll} \tfrac{1}{2}, & u, & \tfrac{1}{2}+v; & 0, \ \tfrac{1}{2}-u, \ \tfrac{1}{2}+v; \\ \tfrac{1}{2}, & -u, & \tfrac{1}{2}-v; & 0, \ \tfrac{1}{2}+u, \ \tfrac{1}{2}-v. \end{array}$$

From a diffractometer recording of the powder pattern, we obtain the power per unit length P'. Values of $P'/(f^2e^{-2M}\mathrm{LP})$ in arbitrary units for 4 reflections are as follows:

hkl	$P'/(f^2e^{-2M}\mathrm{LP})$
002	0.44
004	2.42
111	7.56
113	0.84

a) Obtain a simplified expression for the structure factor F for

$$h + k = \text{even} \quad \text{and} \quad h + k = \text{odd}.$$

b) What are the vanishings (for what classes of reflections hkl does F vanish regardless of the values of u and v)?

c) Plot $F^2/64f^2$ for 002 and 004 as a function of v for the range $v = 0.000$ to $v = 0.25$. Determine two possible values of v.

d) From the 111, 113 data select the correct value of v.

e) Determine an approximate value for u. (Orthorhombic multiplicities!)

8.3 Pyrite is a cubic crystal, $a = 5.416$ A, 4 FeS_2 per unit cell. Space-group symmetry requires the atoms to be in the following positions:

$$\begin{array}{llllll} \text{Fe:} & 0\,0\,0; & 0\,\tfrac{1}{2}\,\tfrac{1}{2}; & \tfrac{1}{2}\,0\,\tfrac{1}{2}; & \tfrac{1}{2}\,\tfrac{1}{2}\,0 \\ \text{S:} & u, \ u, \ u; & \tfrac{1}{2}+u, \ \tfrac{1}{2}-u, \ \bar{u}; & & \\ & \bar{u}, \ \bar{u}, \ \bar{u}; & -\tfrac{1}{2}-u, \ -\tfrac{1}{2}+u, \ u; & & \\ & \bar{u}, \ \tfrac{1}{2}+u, \ \tfrac{1}{2}-u; & \tfrac{1}{2}-u, \ \bar{u}, \ \tfrac{1}{2}+u & & \\ & u, \ -\tfrac{1}{2}-u, \ -\tfrac{1}{2}+u; & -\tfrac{1}{2}+u, \ u, \ -\tfrac{1}{2}-u & & \end{array}$$

A diffractometer powder pattern using Co$K\alpha$ $\lambda = 1.790$ A, gives peak areas in the ratio

$$\frac{A_{200}}{A_{111}} = 4.0;$$

$(\sin\theta)/\lambda$	0.0	0.1	0.2	0.3
f(S)	16.0	13.6	10.7	8.95
f(Fe)	26.0	23.1	18.9	15.6

Neglect the temperature correction and the dispersion correction.

a) For *hkl* unmixed, derive a simplified expression for the pyrite structure factor F.

b) From the 200–111 ratio, determine the parameter u. Only the range 0.25–0.45 need be considered.

9

FOURIER SERIES METHODS IN STRUCTURE DETERMINATIONS

9.1 REPRESENTATION BY FOURIER SERIES

Since Fourier series methods play a very important role in x-ray diffraction problems, it will be worthwhile to review briefly some of the important properties of these series. Suppose that the function $y = f(x)$ shown by Fig. 9.1 is periodic in x with a period of length a. For some of the uses which we shall make, the periodic property of the function is very important, while for other uses it is only the value of the function in the interval O to a or $-a/2 + a/2$ that is of interest. We represent the function by a general Fourier series which is periodic in x with a period of length a:

$$f(x) = \sum_{n=-\infty}^{+\infty} \left\{ A_n \cos 2\pi n \frac{x}{a} + B_n \sin 2\pi n \frac{x}{a} \right\}. \tag{9.1}$$

The index n takes all integral values from $-\infty$ to $+\infty$ including zero, and for each value of n there is a cosine coefficient A_n and a sine coefficient B_n. If $f(x)$ were symmetric about $x = 0$, all of the sine coefficients would be zero.

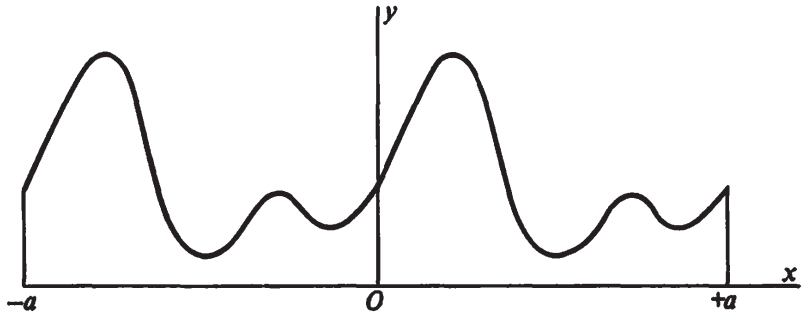

Fig. 9.1 Representation of the function $y = f(x)$ which is periodic in x with a period a.

In many cases $f(x)$ is known, for example, it might be the diffractometer tracing of a powder pattern peak. We now wish to determine the cosine and sine coefficients A_n and B_n in terms of a known function $f(x)$. To determine the cosine coefficients, we multiply both sides of Eq. (9.1) by $\cos 2\pi mx/a$,

where m is some fixed integer, and integrate over one period:

$$\int_{-a/2}^{+a/2} f(x) \cos 2\pi m \frac{x}{a}\, dx = \sum_{n=-\infty}^{+\infty} \int_{-a/2}^{+a/2} \left\{ A_n \cos 2\pi n \frac{x}{a} + B_n \sin 2\pi n \frac{x}{a} \right\} \cos 2\pi m \frac{x}{a}\, dx.$$

Since $\sin 2\pi nx/a \cos 2\pi mx/a$ is the product of an odd and an even function, its integral from $-a/2$ to $+a/2$ will be zero. Expanding the product of the cosines, we can write

$$\int_{-a/2}^{+a/2} f(x) \cos 2\pi m \frac{x}{a}\, dx = \sum_{n=-\infty}^{+\infty} \frac{A_n}{2} \int_{-a/2}^{+a/2} \left\{ \cos 2\pi(m+n) \frac{x}{a} + \cos 2\pi(m-n) \frac{x}{a} \right\} dx.$$

The integrals are zero for all terms n except the ones for which $n = -m$ or $n = +m$, and for these two terms the integral takes the value a:

$$\int_{-a/2}^{+a/2} f(x) \cos 2\pi m \frac{x}{a}\, dx = \frac{a}{2}(A_{-m} + A_m).$$

There is no loss in generality in setting $A_{-m} = A_m$, and hence the cosine coefficients for Eq. (9.1) are given by

$$A_n = \frac{1}{a} \int_{-a/2}^{+a/2} f(x) \cos 2\pi n \frac{x}{a}\, dx. \tag{9.2}$$

To determine the sine coefficients B_n we multiply both sides of Eq. (9.1) by $\sin 2\pi mx/a$ and integrate over one period. Dropping the product of the odd and even function, and expanding $\sin 2\pi nx/a \sin 2\pi mx/a$, we obtain

$$\int_{-a/2}^{+a/2} f(x) \sin 2\pi m \frac{x}{a}\, dx = \sum_{n=-\infty}^{+\infty} \frac{B_n}{2} \int_{-a/2}^{+a/2} \left\{ \cos 2\pi(n-m) \frac{x}{a} - \cos 2\pi(n+m) \frac{x}{a} \right\} dx.$$

The integrals are zero for all terms n except those for $n = m$ and $n = -m$.

$$\int_{-a/2}^{+a/2} f(x) \sin 2\pi m \frac{x}{a}\, dx = \frac{a}{2}\{B_m - B_{-m}\}.$$

There is no loss in generality in setting $B_{-m} = -B_m$, and hence the sine coefficients for Eq. (9.1) are given by

$$B_n = \frac{1}{a} \int_{-a/2}^{+a/2} f(x) \sin 2\pi n \frac{x}{a}\, dx. \tag{9.3}$$

For compactness and for carrying out derivations, it is much more convenient to write Eq. (9.1) in complex form using complex coefficients $C(n)$:

$$f(x) = \sum_{n=-\infty}^{+\infty} C(n)e^{-2\pi in(x/a)}. \tag{9.4}$$

The coefficient is made up of a real and an imaginary part, $C(n) = C_r(n) + iC_i(n)$. Expressing the exponential as $\cos 2\pi nx/a - i \sin 2\pi nx/a$, Eq. (9.4) can be written in the form

$$f(x) = \sum_{n=-\infty}^{+\infty} \left\{ C_r(n) \cos 2\pi n \frac{x}{a} + C_i(n) \sin 2\pi n \frac{x}{a} + iC_i(n) \cos 2\pi n \frac{x}{a} - iC_r(n) \sin 2\pi n \frac{x}{a} \right\}. \tag{9.5}$$

The function $f(x)$ represented by Eqs. (9.4) and (9.5) may be complex. If $f(x)$ is to represent a real function, the imaginary terms of Eq. (9.5) must vanish. Since $\cos 2\pi nx/a$ is even in n and $\sin 2\pi nx/a$ is odd in n, the imaginary term for $(+n)$ will be cancelled by the imaginary term for $(-n)$ if we require that $C_i(-n) = -C_i(n)$ and $C_r(-n) = C_r(n)$. But these are just the conditions that the complex coefficient $C(-n)$ is the complex conjugate of $C(n)$:

$$C(-n) = C^*(n). \tag{9.6}$$

Hence Eq. (9.4) represents a real function $f(x)$ if we impose the condition expressed by Eq. (9.6).

To determine the complex coefficients $C(n)$, we multiply both sides of Eq. (9.4) by $\exp [2\pi imx/a]$ and integrate over one period:

$$\int_{-a/2}^{+a/2} f(x)e^{2\pi im(x/a)}\,dx = \sum_{n=-\infty}^{+\infty} C(n) \int_{-a/2}^{+a/2} e^{2\pi i(m-n)(x/a)}\,dx = aC(m).$$

Hence the complex coefficient of Eq. (9.4) is given by

$$C(n) = \frac{1}{a} \int_{-a/2}^{+a/2} f(x)e^{2\pi in(x/a)}\,dx. \tag{9.7}$$

Equating the real and imaginary parts on either side of Eq. (9.7), we obtain the two equivalent relations:

$$\begin{aligned} C_r(n) &= \frac{1}{a} \int_{-a/2}^{+a/2} f(x) \cos 2\pi nx/a\,dx, \\ C_i(n) &= \frac{1}{a} \int_{-a/2}^{+a/2} f(x) \sin 2\pi nx/a\,dx. \end{aligned} \tag{9.8}$$

Comparing Eqs. (9.1), (9.2), and (9.3) with Eqs. (9.5) and (9.8), it is evident that $C_r(n) = A_n$ and $C_i(n) = B_n$. For purposes of derivations and

algebraic manipulations, it is usually simplest to express the Fourier series in the complex form using Eqs. (9.4) and (9.7). However, when we come to numerical evaluations, we change to the cosine and sine expressions of Eqs. (9.5) and (9.8).

9.2 FOURIER SERIES REPRESENTATION OF THE ELECTRON DENSITY

There are two methods for representing a crystalline structure:

1. by atoms, the method we have used up to now;
2. by a continuous electron density; in this representation, atoms show up as concentrations or peaks in the continuous electron density.

In the first method, where the crystal is represented by atoms, the problem of x-ray diffraction is handled in two steps. We first combine all the electrons in the atom by means of the atomic scattering factor:

$$f_n = \int 4\pi r^2 \rho_n(r) \frac{\sin kr}{kr}\, dr,$$

where f_n is the effective number of electrons concentrated at the atom center. We next combine all the atoms in the unit cell by means of a structure factor:

$$F_{hkl} = \sum_n f_n e^{2\pi i(hx_n + ky_n + lz_n)}$$

For purposes of an *hkl*-reflection, F_{hkl} is the effective number of electrons concentrated at the cell origin. It is the electrons which do the x-ray scattering, and we have covered all the electrons in the unit cell in two steps, first by using an effective concentration at the atom centers, and second by an effective concentration at the unit cell origin.

In the second method for representing a crystalline structure, we introduce a continuous electron density function $\rho(xyz)$ expressed in electrons per unit volume and including all the electrons in the cell. Since $\rho(xyz)$ is triply periodic, it can be expressed by a triple Fourier series in the distances x, y, and z parallel to the *a*-, *b*-, and *c*-axes. To obtain the general form of this series, it is instructive to develop it in three steps. For fixed values of x and y, the density is periodic in z, and hence represented by the series of Eq. (9.4). Using r as the summation index,

$$\rho(xyz) = \sum_{r=-\infty}^{+\infty} C_r(x, y) e^{-2\pi i r z/c}.$$

But for a fixed value of x, $\rho(xyz)$ is also periodic in y, and hence the coefficients $C_r(x, y)$ must be periodic in y:

$$C_r(x, y) = \sum_{q=-\infty}^{+\infty} C_{qr}(x) e^{-2\pi i q y/b}.$$

Finally since $\rho(xyz)$ is also periodic in x, the coefficient $C_{qr}(x)$ must be periodic in x:

$$C_{qr}(x) = \sum_{p=-\infty}^{+\infty} C_{pqr} e^{-2\pi i p x/a}.$$

Combining these three steps, we obtain the general representation for the triply periodic electron density

$$\rho(x, y, z) = \sum_{p} \sum_{q=-\infty}^{+\infty} \sum_{r} C_{pqr} e^{-2\pi i[p(x/a)+q(y/b)+r(z/c)]}. \tag{9.9}$$

The complex coefficients for this series are obtained by a generalization of Eq. (9.7). Multiply both sides of Eq. (9.9) by exp $[2\pi i(hx/a + ky/b + lz/c)]$, where hkl are fixed integers, and integrate over the three distances of repetition:

$$\int_0^a \int_0^b \int_0^c \rho(xyz) e^{2\pi i[h(x/a)+k(y/b)+l(z/c)]} dx\, dy\, dz$$
$$= \sum_{p} \sum_{q=-\infty}^{+\infty} \sum_{r} C_{pqr} \int_0^a \int_0^b \int_0^c e^{-2\pi i\{(p-h)(x/a)+(q-k)(y/b)+(r-l)(z/c)\}} dx\, dy\, dz. \tag{9.10}$$

Since

$$\int_0^a e^{-2\pi i(p-h)(x/a)} dx = \begin{cases} a & \text{if } p = h, \\ 0 & \text{if } p \neq h, \end{cases}$$

all the terms on the right-hand side of Eq. (9.10) are zero except the one term for which $p = h, q = k$, and $r = l$. Hence, using hkl for the summation indices of Eq. (9.9), the Fourier coefficients are given by

$$\int_0^a \int_0^b \int_0^c \rho(x, y, ze)^{2\pi i[h(x/a)+k(y/b)+l(z/c)} dx\, dy\, dz = abc\, C_{hkl}. \tag{9.11}$$

Replacing the fractional coordinates x_n, y_n, z_n of Eq. (3.10) by the present notation x_n/a, y_n/b, z_n/c, the structure factor is given by

$$F_{hkl} = \sum_{n} f_n e^{2\pi i[h(x_n/a)+k(y_n/b)+l(z_n/c)]}.$$

Following the same rules used for Eq. (1.10), the above expression for the structure factor may be replaced by one represented in terms of a continuous electron density:

$$F_{khl} = \int_0^a \int_0^b \int_0^c \rho(xyz) e^{2\pi i[h(x/a)+k(y/b)+l(z/c)]} dV. \tag{9.12}$$

To allow for axes which are not orthogonal, we can obtain dV from the proportion:

$$\frac{dV}{dx\, dy\, dz} = \frac{V}{abc}, \tag{9.13}$$

where V is the unit cell volume. Combining Eqs. (9.12) and (9.13) and comparing with (9.11), we obtain

$$VC_{hkl} = F_{hkl}.$$

The electron density expressed in electrons per unit volume is given by a triple Fourier series in which the Fourier coefficients are the well-known structure factors F_{hkl}:

$$\rho(x, y, z) = \frac{1}{V}\sum_{h}\sum_{\substack{k\\-\infty}}^{+\infty}\sum_{l} F_{hkl}e^{-2\pi i[h(x/a)+k(y/b)+l(z/c)]}. \tag{9.14}$$

Each *hkl*-reflection from a crystal corresponds to a term in the Fourier representation of the electron density, a strong *hkl*-reflection signifying a strong *hkl*-harmonic in the electron density. From this point of view, x-ray diffraction in a crystal is a Fourier analysis of the electron density in the crystal. Each coefficient in the series for $\rho(xyz)$ corresponds to a point *hkl* in the reciprocal lattice. It was pointed out by P. P. Ewald that the reciprocal lattice represents completely the electron density function, if to each point in the reciprocal lattice we attach a weighting function F_{hkl}. For crystals having a center of symmetry, $F(\bar{h}\bar{k}\bar{l}) = F(hkl)$ and Eq. (9.14) becomes

$$\rho(x, y, z) = \frac{1}{V}\sum_{h}\sum_{\substack{k\\-\infty}}^{+\infty}\sum_{l} F_{hkl}\cos 2\pi\left(h\frac{x}{a} + k\frac{y}{b} + l\frac{z}{c}\right). \tag{9.15}$$

For purposes of plotting, it is convenient to use two-dimensional sections or projections. As an example, the two-dimensional section for $z = 0$ is given by

$$\rho(x, y, 0) = \frac{1}{V}\sum_{h}\sum_{k}\left(\sum_{l} F_{hkl}\right)e^{-2\pi i[h(x/a)+k(y/b)]}. \tag{9.16}$$

Although this is a two-dimensional function, it requires the complete set of F_{hkl} coefficients. The two-dimensional projection $\rho'(xy)$ is obtained by projecting the cell contents parallel to the c-axis, onto the basal plane. If dA is an element of area in the basal plane,

$$\int \rho'(xy)\, dA = \int \rho(xyz)\, dV.$$

We can allow for axes which are not orthogonal by setting

$$dA = A_{ab}\frac{dx\, dy}{ab}, \qquad dV = \frac{V\, dx\, dy\, dz}{abc},$$

where A_{ab} is the area of the *ab*-face. From these relations,

$$\rho'(xy) = \frac{V}{cA_{ab}}\int_0^c \rho(xyz)\, dz. \tag{9.17}$$

Since

$$\int_0^c e^{-2\pi ilz/c}\,dz = \begin{cases} c & \text{if } l = 0, \\ 0 & \text{if } l \neq 0, \end{cases}$$

we obtain from Eqs. (9.14) and (9.16)

$$\rho'(xy) = \frac{1}{A_{ab}} \sum_h \sum_k F_{hk0} e^{-2\pi i[h(x/a)+k(y/b)]}. \tag{9.18}$$

This projected density requires data from only the $hk0$-reflections.

At first sight it would appear that Eq. (9.14) offers a straightforward method for structure determination, since the positions of the atoms will be given by the peaks in the electron density function $\rho(xyz)$. The trouble, of course, comes from the fact that what we measure is some sort of an integrated intensity, and this is proportional to $F_{hkl}F^*_{hkl}$. Even if all the F_{hkl} are real, what we measure is still a quantity proportional to F^2_{hkl}, and we obtain the magnitude of all the coefficients of Eq. (9.14) but not their signs. Hence Eq. (9.14) represents the electron density $\rho(xyz)$ by a Fourier series in which the magnitudes of all the coefficients can be determined from experiment, but for which the phases are unknown. Although this detracts greatly from its general usefulness, there are nevertheless many very important applications for Eq. (9.14).

a) The signs are known, and we wish to determine the electron distribution in the crystal from the measured $|F_{hkl}|$ magnitudes. Using rock salt as an example, if we choose the position of a chlorine atom as origin, all of the F_{hkl} will be real and positive.

b) The composition contains a few heavy atoms whose positions are known from space group requirements. The phase of the contribution from the heavy atoms is then known, and in general this will determine the phases for most of the F_{hkl}.

c) When isomorphous replacements are possible for some of the atoms, we can compare the intensities from one crystal with those from another crystal in which some of the atoms have been replaced. By comparing the intensities of corresponding reflections, we can obtain the phase of the contribution by the replaced atoms relative to the phase of the contribution by the remaining atoms. Under favorable conditions, such as knowing the positions of the replaced atoms, the signs of all the F_{hkl} may be determined.

d) Certain relations necessarily exist among the signs of the F_{hkl}. As a simple example $\rho(xyz)$ can never be negative and this puts certain restrictions on the signs of the F_{hkl}. Following the lead of Harker and Kasper[1] many relations have been developed for determining the signs of the F_{hkl} from relations among the intensities. This is an active field of research in which many important developments are being made. A detailed treatment of this most important field of activity can be found in Lipson and Cochran.[2]

9.3 THE PATTERSON FUNCTION

Since it is $|F_{hkl}|^2$ that is obtained from measurements of the integrated intensity, the question arises as to whether anything can be done directly with the $|F_{hkl}|^2$ values. It was shown by A. L. Patterson[3] that these values could be used to obtain another type of function, which although not as useful as the electron density function, can nevertheless be of great value in a structure determination.

It is convenient to introduce the Patterson function in terms of a one-dimensional crystal. Figure 9.2 represents the electron density $\rho(x)$ for a one-dimensional crystal having three atoms A, B, and C per unit cell. For convenience we have represented the electron density as sharply concentrated about the positions $x/a = 0.0, 0.2$, and 0.7. We now define a one-dimensional Patterson function:

$$P(X) = \int_0^a \rho(x)\rho(x + X)\, dx. \tag{9.19}$$

The Patterson function for our one-dimensional crystal is shown in the lower part of Fig. 9.2. It is evident from Eq. (9.19) that $P(X)$ differs from zero only for values of X such that in integrating across the cell there are values of x for which $\rho(x)$ and $\rho(x + X)$ both differ from zero. The first strong

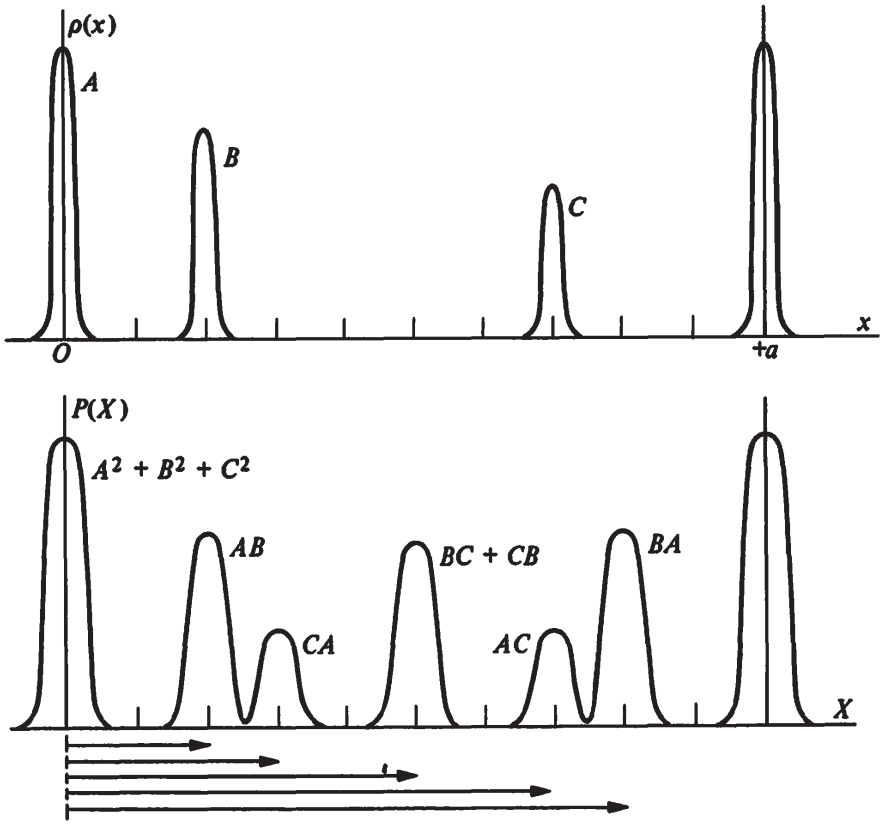

Fig. 9.2 Illustration of the Patterson function in terms of a one-dimensional crystal. (a) The electron density function $\rho(x)$. (b) The corresponding Patterson function.

peak at $X = 0$ represents the fact that all three atoms are at zero distance from themselves. The peak at $X/a = 0.2$ represents the fact that there is an atom displaced by $0.2a$ from another atom (B displaced $0.2a$ from A). The peak at $X/a = 0.3$ represents the fact that there is an atom displaced $0.3a$ from some other atom (A displaced $0.3a$ from C). The peaks on the Patterson function do not represent the positions of atoms. Each peak is simply the terminus of a vector drawn from the origin, and each vector represents the displacement of some atom relative to some other atom. The Patterson function is a correlation function giving the position of every atom relative to every other atom, but not relative to a fixed origin. Although the Patterson function does not give directly the structure, it presents very important information relating to the structure, and it will turn out that the Patterson function can be obtained without a knowledge of the phases.

We now define a general Patterson function:

$$P(XYZ) = \int_0^a \int_0^b \int_0^c \rho(xyz)\rho(x + X, y + Y, z + Z) \frac{V}{abc}\, dx\, dy\, dz. \quad (9.20)$$

Expressing $\rho(xyz)$ and $\rho(x + X, y + Y, z + Z)$ by means of Eq. (9.14), we obtain

$$P(XYZ) = \frac{1}{V^2} \int_0^a \int_0^b \int_0^c \sum_{h'} \sum_{k'} \sum_{l'} F_{h'k'l'} e^{-2\pi i[h'(x/a)+k'(y/b)+l'(z/c)]}$$

$$\times \sum_{h} \sum_{k} \sum_{l} F_{hkl} e^{-2\pi i\{[h(x+X)/a]+k[(y+Y)/b]+l[(z+Z)/c]\}} \frac{V}{abc}\, dx\, dy\, dz.$$

Rearranging,

$$P(XYZ) = \frac{1}{V} \sum_{h'} \sum_{k'} \sum_{l'} \sum_{h} \sum_{k} \sum_{l} F_{h'k'l'} F_{hkl} e^{-2\pi i[h(X/a)+k(Y/b)+l(Z/c)]}$$

$$\times \int_0^a \int_0^b \int_0^c e^{-2\pi i[(h'+h)(x/a)+(k'+k)(y/b)+(l'+l)(z/c)]} \frac{dx\, dy\, dz}{abc}.$$

Since all the integrals are zero except the one for which $h' = -h, k' = -k$, and $l' = -l$,

$$P(XYZ) = \frac{1}{V} \sum_{h} \sum_{k=-\infty}^{+\infty} \sum_{l} F_{hkl} F_{\bar{h}\bar{k}\bar{l}} e^{-2\pi i[h(X/a)+k(Y/b)+l(Z/c)]}. \quad (9.21)$$

But $F_{hkl}F_{\bar{h}\bar{k}\bar{l}} = |F_{hkl}|^2$ is directly obtainable from the measured integrated intensities, and hence the Patterson function is given by a Fourier series whose coefficients can be completely determined from experiment. However, peaks in the Patterson function do not represent the positions of atoms; the peaks are the terminal points of a set of vectors, each vector representing the displacement of some atom from some other atom. Since $F_{hkl}F_{\bar{h}\bar{k}\bar{l}}$ is the same for hkl and $\bar{h}\bar{k}\bar{l}$, Eq. (9.21) takes the symmetrical form in which it is

generally used:

$$P(XYZ) = \frac{1}{V}\sum_{h}\sum_{k=-\infty}^{+\infty}\sum_{l}|F_{hkl}|^2\cos 2\pi\left(h\frac{X}{a} + k\frac{Y}{b} + l\frac{Z}{c}\right). \qquad (9.22)$$

In addition to the same kinds of sections and projections that are used with the electron density function $\rho(xyz)$, there are special Harker-Patterson sections that make use of space group symmetry elements. Suppose that there is a reflection plane normal to the a-axis. For any atom with coordinates xyz, there will be an identical atom at the same y and z but on the opposite side of the plane. For such pairs of atoms, $Y = Z = 0$, and the appropriate Harker-Patterson section will be

$$P(X, 0, 0) = \frac{1}{V}\sum_{h}\left(\sum_{k}\sum_{l}|F_{hkl}|^2\right)\cos 2\pi h\frac{X}{a}. \qquad (9.23)$$

Except for spurious peaks, the X-values of the peaks on this plot give twice the distance of the atom from the reflection plane. As one more example, consider that there is a 2-fold screw axis parallel to the c-axis. For any atom at xyz there will be an identical atom at $z + c/2$. For such pairs of atoms $Z/c = \frac{1}{2}$ and the appropriate Harker-Patterson section will be

$$P(X, Y, c/2) = \frac{1}{V}\sum_{h}\sum_{k}\left(\sum_{l}(-1)^l|F_{hkl}|^2\right)\cos 2\pi\left(h\frac{X}{a} + k\frac{Y}{b}\right). \qquad (9.24)$$

Except for spurious peaks, the X- and Y-coordinates of peaks on this plot give twice the x- and y-coordinates of the atoms relative to the 2-fold screw axis.

Since this book is not intended to cover the problems of structure determination, the reader is referred to Lipson and Cochran for the many additional details involved in Fourier series methods.

REFERENCES

1. D. Harker and J. S. Kasper, *Jour. Chem. Phys.* **15**, 882 (1947); *Acta. Cryst.* **1**, 70 (1948).
2. H. Lipson and W. Cochran, *The Determination of Crystal Structures*, G. Bell and Sons, Ltd., London (1953).
3. A. L. Patterson, *Phys. Rev.* **46**, 372 (1934); *Zeit für Krist.* **90**, 517 (1935).

PROBLEMS

9.1 Suppose that the symmetrical function $y(x)$ is represented by a Fourier series

$$y(x) = \sum_{n=0}^{\infty} A_n \cos 2\pi n \frac{x}{a},$$

which includes terms for only the positive values of the index n. Derive expressions for the coefficients A_0 and A_n. What is the advantage to writing a Fourier series so as to include terms from $n = -\infty$ to $n = +\infty$?

9.2 In an orthorhombic crystal with axes a, b, and c, the electron density within one cell is given by

$$\rho(xyz) = \left(\frac{\alpha}{\sqrt{\pi}}\right)^3 \{N_1 e^{-\alpha^2(x^2+y^2+z^2)} + N_2 e^{-\alpha^2([x-(a/2)]^2+[y-(b/2)]^2+[z-(c/2)]^2)}\}.$$

Assume the electron densities are sharply concentrated (α^2 large) and that the appropriate integrals can be taken from $-\infty$ to $+\infty$.

a) Derive an expression for F_{hkl}.

b) If $\alpha a = 2\pi$, what are the values of F_{100} and F_{200}?

9.3 If all F_{hkl} for a crystal were to have the same positive value $F_{hkl} = A$, what would be the nature of the electron distribution $\rho(xyz)$?

9.4 Derive an expression for the partial projection $P'(XY)(-c/4 \text{ to } +c/4)$ in which the contents of the Patterson functon between $Z = -c/4$ and $Z = +c/4$ are projected parallel to the c-axis onto the basal plane. In terms of a c-axis rotation pattern, what data are needed for this partial projection? What advantages and disadvantages would this partial projection have in comparison with the full projection $P'(XY)$ or the section $P(XY0)$?

10

SCATTERING BY NONCRYSTALLINE FORMS OF MATTER

10.1 THE GENERAL SCATTERING EQUATION FOR A RANDOM ORIENTATION

We consider as our sample any form of matter in which there is a random orientation. This includes gases, liquids, amorphous solids, and crystalline powders. There can be any number of different kinds of atoms in the sample. We represent the instantaneous position of each atom m by a vector $\mathbf{r}_m$. Expressed in electron units, the intensity from the sample is given by summing the amplitude of scattering from the different atoms, and then multiplying this sum by its complex conjugate:

$$I_{eu} = \sum_m f_m e^{(2\pi i/\lambda)(\mathbf{s}-\mathbf{s}_0)\cdot\mathbf{r}_m} \sum_n f_n e^{-(2\pi i/\lambda)(\mathbf{s}-\mathbf{s}_0)\cdot\mathbf{r}_n}. \tag{10.1}$$

This is the same expression that we used for the intensity from a crystal. In that case, however, each of the sums was a geometric progression, and the sums could be evaluated. For the present case we do not assume any simple relation among the $\mathbf{r}_m$-vectors. Although the expression must be left as a double sum, it is simpler to write it in terms of the difference vector $\mathbf{r}_{mn} = \mathbf{r}_m - \mathbf{r}_n$:

$$I_{eu} = \sum_m \sum_n f_m f_n e^{(2\pi i/\lambda)(\mathbf{s}-\mathbf{s}_0)\cdot\mathbf{r}_{mn}}. \tag{10.2}$$

We are now interested in finding the average intensity when this array of atoms, considered as a rigid body, is allowed to take with equal proba-

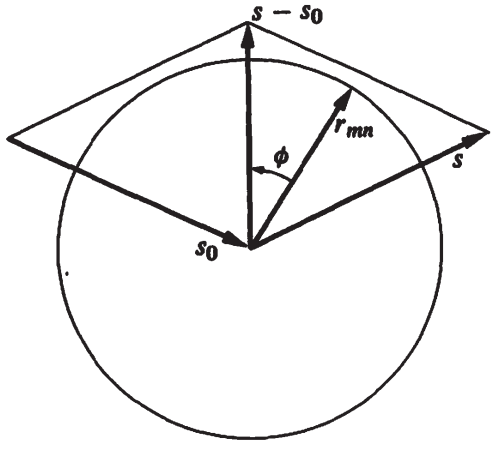

Fig. 10.1 Relations involved in letting the $\mathbf{r}_{mn}$ vector take all orientations in space.

bility all orientations in space. Since each vector $\mathbf{r}_{mn}$ takes all orientations, its terminal point takes with equal probability all positions on the sphere of Fig. 10.1. In terms of $k = (4\pi \sin\theta)/\lambda$, the average for each exponential term is given by

$$\langle e^{(2\pi i/\lambda)(\mathbf{s}-\mathbf{s}_0)\cdot\mathbf{r}_{mn}} \rangle = \frac{1}{4\pi r_{mn}^2} \int_{\phi=0}^{\pi} e^{ikr_{mn}\cos\phi} 2\pi r_{mn}^2 \sin\phi \, d\phi = \frac{\sin kr_{mn}}{kr_{mn}}.$$

Using this value for each of the terms in Eq. (10.2), we obtain a very general and important equation for the average unmodified intensity from an array of atoms which takes all orientations in space:

$$I_{eu} = \sum_m \sum_n f_m f_n \frac{\sin kr_{mn}}{kr_{mn}}. \tag{10.3}$$

Equation (10.3) is often called the Debye[1] scattering equation. It should be noticed that it involves only the magnitudes of the distances r_{mn} of each atom from every other atom.

10.2 GAS OF POLYATOMIC MOLECULES

For a polyatomic gas, Eq. (10.3) can be used to represent the unmodified intensity from each molecule. If the gas is not too dense, there will be complete incoherency between the scattering by the different molecules, and excluding the region of very small scattering angle, the intensity from the sample is N times that for a molecule. Including the Compton modified scattering, the total intensity in electron units per molecule is given by

$$I_{eu}/N = \sum_m \sum_n f_m f_n \frac{\sin kr_{mn}}{kr_{mn}} + R \sum_m i(M)_m. \tag{10.4}$$

The Breit Dirac correction factor for the modified scattering is often taken as $R^{2/3}$ when the measurements are made with a counter, on the assumption that the counter is equally efficient in recording modified and unmodified quanta.

As a simple example we can consider a carbon tetrachloride gas composed of tetrahedral molecules CCl_4. In the double sum of Eq. (10.4), we start with some atom as atom m and sum over all atoms n in the molecule including the starting atom. We then let the first atom be each of the atoms in the molecule. The unmodified intensity from one CCl_4 molecule is expressed by

$$f_C\left\{f_C + 4f_{Cl}\frac{\sin kr(C-Cl)}{kr(C-Cl)}\right\} + 4f_{Cl}\left\{f_{Cl} + f_C\frac{\sin kr(C-Cl)}{kr(C-Cl)} + 3f_{Cl}\frac{\sin kr(Cl-Cl)}{kr(Cl-Cl)}\right\}.$$

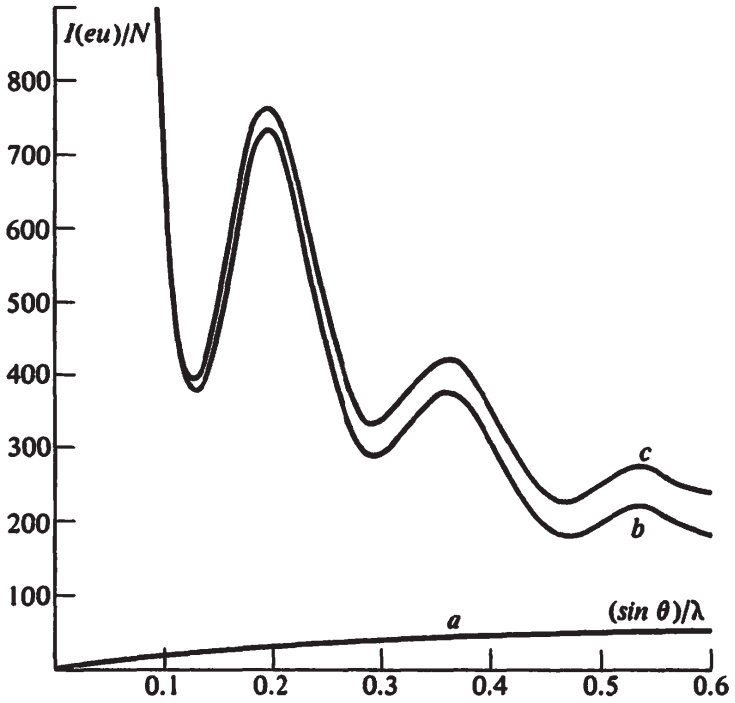

Fig. 10.2 The intensity in electron units per molecule for a CCl_4 gas in which the carbon-chlorine distance is taken as $r = 1.82$ A. (a) The modified intensity per molecule. (b) The unmodified intensity. (c) The total intensity per molecule, unmodified plus modified.

Rearranging and adding the Compton contribution, the total intensity per molecule is given by

$$I_{eu}/N = f_C^2 + 4f_{Cl}^2 + 8f_C f_{Cl} \frac{\sin kr(C - Cl)}{kr(C - Cl)} + 12f_{Cl}^2 \frac{\sin kr(Cl - Cl)}{kr(Cl - Cl)} + R\{i(M)_C + 4i(M)_{Cl}\}. \quad (10.5)$$

For a tetrahedral molecule $r(Cl - Cl) = \sqrt{\frac{8}{3}}\, r(C - Cl)$ and the intensity depends on just one unknown distance $r(C - Cl)$. Equation (10.5) can be plotted as a function of the variable $(\sin \theta)/\lambda$, assuming several values for $r(C - Cl)$. It is then a simple matter to see for what value of $r(C - Cl)$ the peaks and the dips in the scattering curve come at the same position as observed experimentally. Figure 10.2 shows the unmodified, the modified, and the total intensity per CCl_4 molecule calculated for a value $r(C - Cl) = 1.82$ A. Obviously peaks and dips in an x-ray scattering curve do not require the existence of a crystalline structure. The mere existence of certain interatomic distances which are more probable than others is enough to put peaks and dips into the scattering curve.

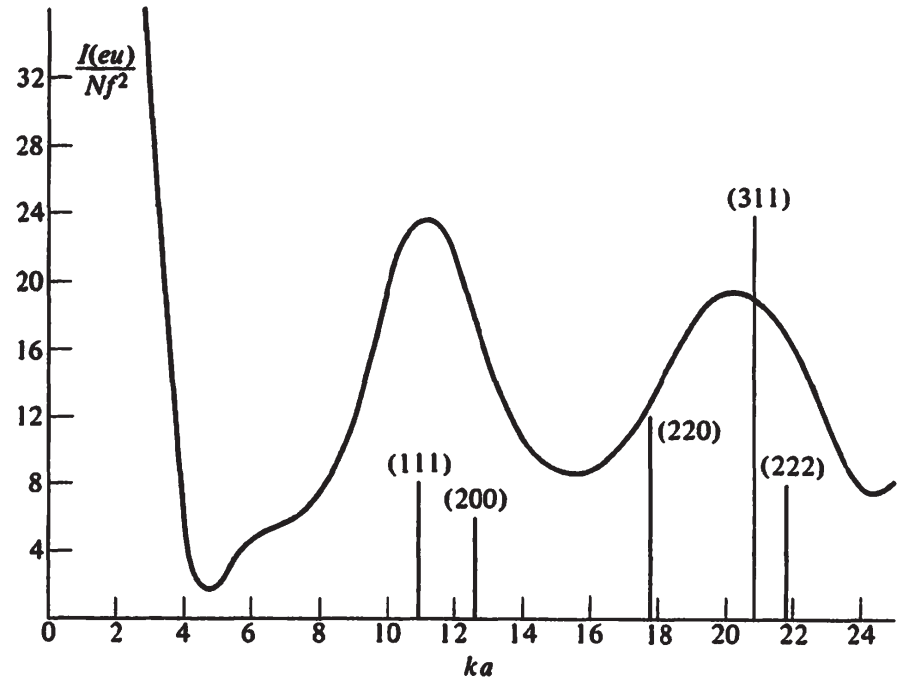

Fig. 10.3 Plot of $I(eu)/Nf^2$ for a sample of 14 atom cubes (8 corner atoms and 6 at the face centers. For comparison, the positions of the first few FCC powder pattern reflections are shown.

10.3 APPLICATION TO A CRYSTALLINE POWDER

The intensity distribution in a powder pattern can be obtained from Eq. (10.4) by treating each crystal as a molecule. However for crystallites of any appreciable size, the number of terms to be evaluated is far too large to make this approach practical. For the 14 atoms making up the usual model of a FCC metal, there are 8 atoms at the corners of a cube, and 6 atoms at the face-center positions. Calling a the edge of the cube, the unmodified intensity per crystal from this extremely small crystallite is given by

$$I_{eu}/Nf^2 = 14 + 72\frac{\sin ka/\sqrt{2}}{ka/\sqrt{2}} + \frac{30\sin ka}{ka} + \frac{48\sin ka\sqrt{1.5}}{ka\sqrt{1.5}} + \frac{24\sin ka\sqrt{2}}{ka\sqrt{2}} + \frac{8\sin ka\sqrt{3}}{ka\sqrt{3}}. \quad (10.6)$$

A plot of Eq. (10.6) in terms of the general variable ka is shown by Fig. 10.3. The positions of the first five FCC powder pattern lines are also indicated. It is interesting to notice that even for this extremely small 14-atom crystal, the features of the FCC powder pattern are beginning to appear. For materials composed of extremely small crystallites, Eq. (10.4) represents a practical approach to determining the intensity distribution in the powder pattern.

10.4 LIQUID OR AMORPHOUS SOLID WITH ONE KIND OF ATOM

A liquid has no structure with respect to a fixed origin since the atoms are continually moving about. In an amorphous solid, the atoms have permanent neighbors but there is no repeating structure, only local configurations. However, atoms have well-defined sizes and closest distances of approach, and hence both liquids and amorphous solids have definite structures relative to an origin at the center of an average atom. This type of structure is expressed by a radial distribution function $4\pi r^2\rho(r)$ such that $4\pi r^2\rho(r)\,dr$ is the average number of atom centers between distances r and $r + dr$ from the center of an average atom.

If the experimental conditions are such that we can assume that the sample takes with equal probability all orientations in space, it is relatively simple to express the intensity in terms of the radial distribution function by starting with Eq. (10.3). When this assumption cannot be made, a rigorous treatment is somewhat more involved. We consider an amorphous sample containing only one kind of atom. There are N atoms in the sample, and the instantaneous position of each atom is expressed by the vector $\mathbf{r}_m$. The intensity is given by Eq. (10.2), in which we separate the terms with $m = n$:

$$I_{eu} = \sum_m f^2 + \sum_m f^2 \sum_{n \neq m} e^{(2\pi i/\lambda)(\mathbf{s}-\mathbf{s}_0)\cdot\mathbf{r}_{nm}}.$$

We introduce a density function $\rho_m(\mathbf{r}_{nm})$ such that $\rho_m(\mathbf{r}_{nm})\,dV_n$ is the number of atom centers in the volume element dV_n at the position $\mathbf{r}_{nm}$ relative to atom m. With this density function, the sum can be replaced by an integral over the volume of the sample:

$$I_{eu} = \sum_m f^2 + \sum_m f^2 \int_S \rho_m(\mathbf{r}_{nm}) e^{(2\pi i/\lambda)(\mathbf{s}-\mathbf{s}_0)\cdot\mathbf{r}_{nm}}\,dV_n.$$

Let ρ_a be the average atom density in the sample. By adding and subtracting a term involving ρ_a, we obtain two integrals each of which is to extend only over the volume of the sample:

$$I_{eu} = \sum_m f^2 + \sum_m f^2 \int_S [\rho_m(\mathbf{r}_{nm}) - \rho_a] e^{(2\pi i/\lambda)(\mathbf{s}-\mathbf{s}_0)\cdot\mathbf{r}_{nm}}\,dV_n + \sum_m f^2 \int_S \rho_a e^{(2\pi i/\lambda)(\mathbf{s}-\mathbf{s}_0)\cdot\mathbf{r}_{nm}}\,dV_n.$$

For a fixed displacement $\mathbf{r}_{nm} = \mathbf{r}$, let $\rho(\mathbf{r}) = \langle\rho_m(\mathbf{r}_{nm})\rangle$, where the average is over all $\rho_m(\mathbf{r})$ within the sample which are at a displacement $\mathbf{r}$ from an atom. For the type of amorphous sample which we are considering, $\rho(\mathbf{r}) - \rho_a$ goes to zero for displacements $\mathbf{r}$ which are greater than a few atomic dimensions. Hence in the integral involving $\rho(\mathbf{r}) - \rho_a$, the sum over m can be replaced by N. If there is no preferred orientation in the sample, $\rho(\mathbf{r}) - \rho_a$ will have spherical symmetry and we can write $\rho(r) - \rho_a$. Using the angle ϕ

of Fig. 10.1, and the variable $k = 4\pi \sin\theta/\lambda$, the term involving $[\rho_m(\mathbf{r}_{nm}) - \rho_a]$ becomes

$$Nf^2\int_0^\infty\int_0^\pi [\rho(r) - \rho_a]e^{ikr\cos\phi}2\pi r^2 \sin\phi\, d\phi\, dr = Nf^2\int_0^\infty 4\pi r^2[\rho(r) - \rho_a]\frac{\sin kr}{kr}\, dr,$$

where the integration with respect to dr is taken from zero to infinity, since $[\rho(r) - \rho_a]$ goes to zero for very small values of r. With a little rearrangement the intensity is now given by

$$I_{eu} = Nf^2 + Nf^2\int_0^\infty 4\pi r^2[\rho(r) - \rho_a]\frac{\sin kr}{kr}\, dr + f^2\sum_m e^{-(2\pi i/\lambda)(\mathbf{s}-\mathbf{s}_0)\cdot\mathbf{r}_m}\int_S \rho_a e^{(2\pi i/\lambda)(\mathbf{s}-\mathbf{s}_0)\cdot\mathbf{r}_n}\, dV_n. \quad (10.7)$$

Let z be the component of $\mathbf{r}_m$ along the direction of $\mathbf{s} - \mathbf{s}_0$, $A(z)\, dz$ the volume of the sample between positions z and $z + dz$, and $\rho(z)A(z)\, dz$ the number of atoms in the sample between z and $z + dz$. The sum in the third term of Eq. (10.7) can then be replaced by an integral:

$$\sum_m e^{(-2\pi i/\lambda)(\mathbf{s}-\mathbf{s}_0)\cdot\mathbf{r}_m} = \int e^{-ikz}\rho(z)A(z)\, dz.$$

For an amorphous sample, there is sufficient averaging to replace $\rho(z)$ by ρ_a. With these changes, Eq. (10.7) becomes

$$I_{eu} = Nf^2 + Nf^2\int_0^\infty 4\pi r^2[\rho(r) - \rho_a]\frac{\sin kr}{kr}\, dr + f^2\rho_a^2\int e^{-ikz}A(z)\, dz\int e^{ikz}A(z)\, dz. \quad (10.8)$$

The second term in Eq. (10.8) involves only interactions between near neighbors, and the Fraunhofer approximation which has been used is adequate. However, the third term involves interactions between distant points in the sample, and for this term Fresnel diffraction is necessary. A correct treatment for the flat-faced diffractometer sample using Fresnel diffraction is given in Section 10.10.

As a simple illustration, we shall evaluate the third term of Eq. (10.8) for the special case of a spherical sample of radius R, since for a spherical sample the error in using the Fraunhofer approximation is not large. For a sphere of radius R, using the center of the sphere as origin,

$$\int e^{ikz}A(z)\, dz = \int_{-R}^{R} e^{ikz}\pi(R^2 - z^2)\, dz = \frac{4\pi}{3}R^3\Phi(kR),$$

where

$$\Phi(kR) = \frac{3}{(kR)^2}\left(\frac{\sin kR}{kR} - \cos kR\right).$$

For a spherical sample, $N = (4\pi/3)R^3\rho_a$, and Eq. (10.8) takes the form

$$I_{eu}/Nf^2 = 1 + \int_0^\infty 4\pi r^2[\rho(r) - \rho_a]\frac{\sin kr}{kr}\,dr + \frac{4\pi}{3}R^3\rho_a\Phi^2(kR). \quad (10.9)$$

We now evaluate the last term of Eq. (10.9) for the case $\theta = 3°$, $\lambda = 1$ A, $R = 1$ mm $= 10^7 A$, and $\rho_a = 0.1$ atoms per A^3. Since $kR = 2\pi \times 10^6$, $(\sin kR)/kR$ can be neglected relative to $\cos kR$, and the observable $\langle\cos^2 kR\rangle$ set equal to $\frac{1}{2}$:

$$\langle\Phi^2(kR)\rangle = \frac{9}{(kR)^4}\left\langle\left(\frac{\sin kR}{kR} - \cos kR\right)^2\right\rangle = \frac{9}{2(kR)^4}.$$

The third term of Eq. (10.9) has the value $6\pi\rho_a/Rk^4 = 1.2 \times 10^{-6}$. Since the first and second terms of Eq. (10.9) are of the order of unity, it is obvious that the third term is completely negligible. For $\theta > 3°$, the third term is even smaller. For the small spherical sample which we have considered, it is only at very small θ that the third term is not negligible, it represents a small angle scattering which is usually confined to such small angles that it is hidden by the primary beam and hence not observable.

For the flat-faced diffractometer sample which is treated in Section 10.10, the third term is completely negligible except at small angles where it can be evaluated and subtracted off. Accordingly, we drop the third term of Eq. (10.8) on the basis that it is negligible in the range of observable angles or, if not negligible, that it has been evaluated and subtracted off. In either case, I'_{eu}/N will now mean the intensity per atom due to the first two terms of Eq. (10.8):

$$I'_{eu}/N = f^2 + f^2\int_0^\infty 4\pi r^2[\rho(r) - \rho_a]\frac{\sin kr}{kr}\,dr. \quad (10.10)$$

It is convenient to introduce the abbreviation

$$i(k) = \frac{I'_{eu}/N - f^2}{f^2}. \quad (10.11)$$

As we shall see later, $i(k)$ is an experimentally observable quantity. With a little rearranging, Eq. (10.10) becomes

$$ki(k) = 4\pi\int_{r=0}^\infty r[\rho(r) - \rho_a]\sin kr\,dr. \quad (10.12)$$

Equation (10.12) can be inverted by using the inversion relations for the Fourier integral. If a function $\phi(k)$ is the Fourier transform of a function

$f(r)$, then the function $f(r)$ is given as the Fourier transform of $\phi(k)$. With constants appropriate to Eq. (10.12), the relations are expressed by

$$\phi(k) = 4\pi \int_0^\infty f(r) \sin kr \, dr,$$
$$f(r) = \frac{1}{2\pi^2} \int_0^\infty \phi(k) \sin rk \, dk. \tag{10.13}$$

Identifying $\phi(k)$ with $ki(k)$ and $f(r)$ with $r[\rho(r) - \rho_a]$, Eq. (10.12) leads to

$$r[\rho(r) - \rho_a] = \frac{1}{2\pi^2} \int_0^\infty ki(k) \sin rk \, dk.$$

With a little rearranging, we obtain the very important and much used equation:

$$4\pi r^2 \rho(r) = 4\pi r^2 \rho_a + \frac{2r}{\pi} \int_0^\infty ki(k) \sin rk \, dk. \tag{10.14}$$

Equation (10.14) was first derived by Zernicke and Prins,[2] and first applied by Debye and Menke[3] to a study of the structure of liquid mercury.

The function $ki(k)$ can be obtained from the x-ray scattering curve, and by evaluating the integral for a number of values of r, we obtain the radial distribution function $4\pi r^2 \rho(r)$. From its definition, $4\pi r^2 \rho(r)\, dr$ is the average number of atom centers between distances r and $r + dr$ from the center of an average atom. For a liquid it should be emphasized that this average is an average over the surroundings of each atom in the sample and also an average over the time of measurement. Hence it must be recognized that $4\pi r^2 \rho(r)$ represents a minimum structure in the sample. If more detailed structures exist temporarily here and there in a liquid, they will probably not be seen because $4\pi r^2 \rho(r)$ represents only a time and space average.

10.5 APPLICATION TO A SIMPLE LIQUID

The experimental problem is to determine the function $ki(k)$ in absolute units. For the patterns of liquids and amorphous solids, it is necessary to use strictly monochromatic radiation. With film recording, this requires a crystal monochromated primary beam. With counter recording, a crystal monochromator can be used in either the primary or the scattered beam. If the intensity is too low to use a crystal monochromator, satisfactory counter measurements can often be made with balanced filters. When a proportional counter is used with a pulse height analyzer, balanced filters give a rough approximation to monochromatic radiation.

The experimental intensity curve is usually obtained in arbitrary units, and the next problem is to convert to I'_{eu}/N, the intensity in electron units per

atom. In Eq. (10.10), the integral extends over only a very short distance since $[\rho(r) - \rho_a]$ approaches zero at distances of a few atomic diameters. By dividing the r-axis into small intervals with separation δ, and introducing the quantity

$$Y_i = \int_{r_i-\delta/2}^{r_i+\delta/2} 4\pi r^2[\rho(r) - \rho_a]\, dr,$$

the integral can be replaced by a sum:

$$I'_{eu}/N = f^2 + f^2 \sum_i Y_i \frac{\sin kr_i}{kr_i}. \tag{10.15}$$

It is evident that as k increases, I'_{eu}/N oscillates positive and negative about f^2, with decreasing amplitude of oscillation. To obtain I'_{eu}/N it is only necessary to divide the experimental intensity curve by the appropriate polarization factor and then multiply it by a suitable factor so that at large k, it oscillates about the f^2 curve. Since the units for the f^2 curve are known, this serves to put the experimental curve in absolute units. It is well to emphasize that at large k, I'_{eu}/N oscillates about f^2, it does not necessarily become equal to it.

For many purposes the intensity of unmodified scattering is adequately expressed by Eq. (10.10). However, for high precision work it is necessary to allow for an additional contribution from multiple scattering. The most important part of this contribution comes from diffracted radiation being diffracted again within the sample. This second-order contribution, which we shall call $I(2)$, may amount to several percent of I'_{eu}/N. Approximate methods for computing $I(2)$ are given in Section 10.11. In some cases, we obtain the unmodified scattering curve free from Compton scattering, when, for example, a sufficiently high resolution crystal monochromator is used in the diffracted beam, or the fluorescence excitation method of Warren and Mavel[4] is used. If the Compton component has not been eliminated in the experiment, we measure both the unmodified and the modified scattering. Hence at large values of k, the experimental intensity curve oscillates about $f^2 + I(2)$ if the Compton component has been eliminated, or about $f^2 + I'(2) + i(M)R$ if the Compton component has not been eliminated. The second-order contributions $I(2)$ and $I'(2)$ are, of course, different.

As a very simple illustration of the steps involved in obtaining $ki(k)$, we can consider the measurements by Tarasov and Warren[5] of the x-ray scattering curve of liquid sodium. The intensity curve which is shown by Fig. 10.4 comes from an early measurement, and it does not represent the accuracy and detail which is possible by modern methods. The measurement included both the unmodified and the modified intensity, and no allowance was made for second-order scattering. Curves c and d represent f^2 and $i(M)R$ for sodium. Curve b which is the sum of curves c and d, represents the total independent scattering per atom. Curve a represents the measured intensity curve, adjusted in ordinate scale, so that at large $(\sin\theta)/\lambda$ it is

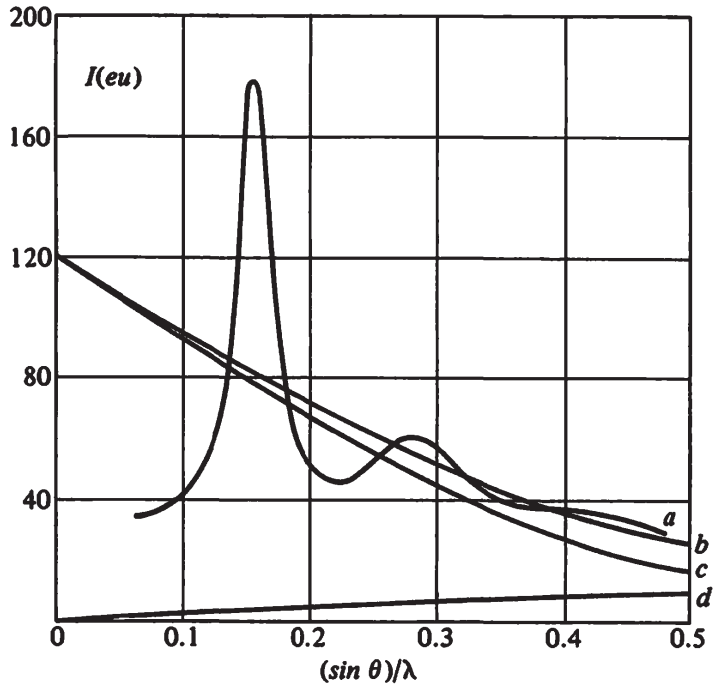

Fig. 10.4 (a) Total intensity curve for liquid sodium in electron units per atom, unmodified plus modified. (b) Total independent scattering per atom. (c) Independent unmodified scattering per atom f^2. (d) Modified scattering per atom $i(M)$.

alternately above and below curve b. Changing the abscissa scale of Fig. 10.4 from $(\sin\theta)/\lambda$ to $k = 4\pi(\sin\theta)/\lambda$, we subtract the Compton modified scattering and obtain the desired quantity $i(k)$ by the operation

$$i(k) = \frac{(a - d) - c}{c} = \frac{a - b}{c}.$$

Multiplying $(a - b)/c$ by the variable k, we obtain the curve $ki(k)$ shown by Fig. 10.5. The last peak on the intensity curve of Fig. 10.4 is very small and not very accurate. In transforming to the $ki(k)$ curve, this weak peak becomes magnified by dividing by f^2 and multiplying by k. It is shown dotted on Fig. 10.5 to indicate that it has been rounded off and is known to only very low accuracy.

The integral in Eq. (10.14) is now evaluated for a large number of values of r using a harmonic analyzer, or an electronic computer, or the Beevers and Lipson strips. The use of the strips is very simple, and for some purposes, quite adequate. The procedure for performing this operation with the strips will be outlined in Section 10.7. The average number of atoms per unit volume ρ_a is obtained from the density of the sample. The final values of $4\pi r^2\rho(r)$ are shown by Fig. 10.6.

To interpret Fig. 10.6 we recall that the origin is situated at the center of an average Na atom. Within the error of the analysis, no centers of surround-

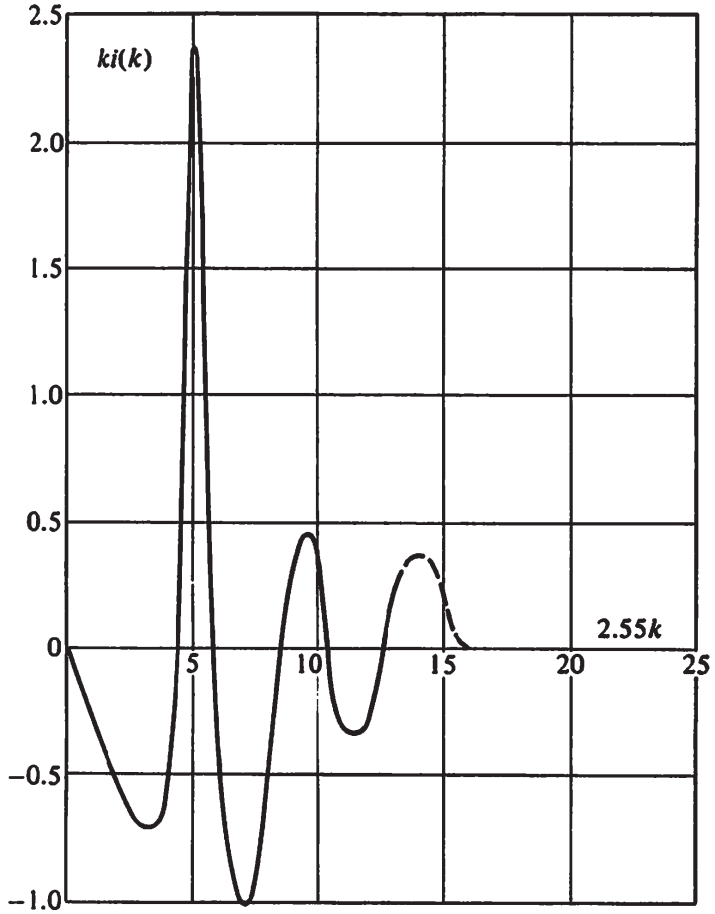

Fig. 10.5 The experimental curve $ki(k)$ for liquid sodium. The abscissa scale $2.55k$ was chosen for convenience in the use of a harmonic analyzer.

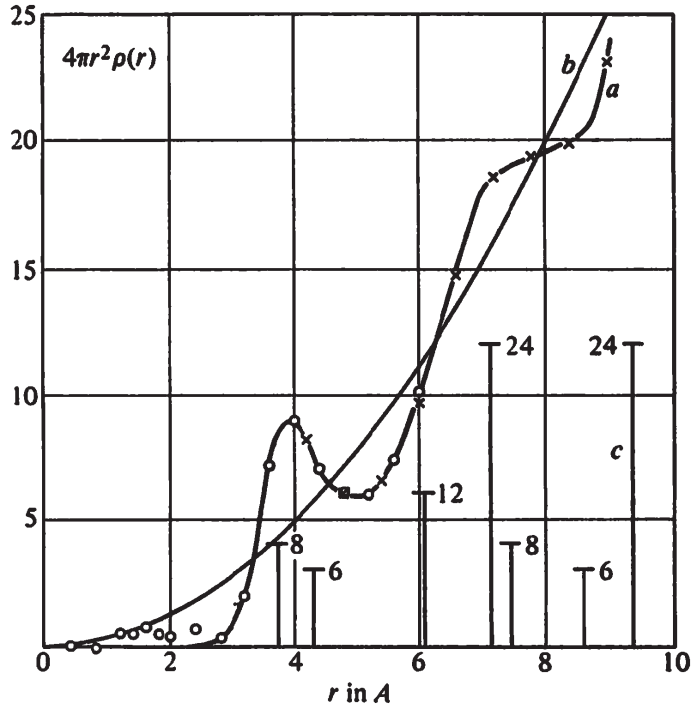

Fig. 10.6 (a) The radial distribution function $4\pi r^2\rho(r)$ for liquid sodium. (b) The average density curve $4\pi r^2\rho_a$. (c) The distribution of neighbors in crystalline sodium.

ing atoms are to be found at distances less than 3 A. At about 4 A there is a high probability for finding the centers of neighboring atoms. This concentration represents nearest neighbors, and the distance 4 A can be called the approximate atomic diameter in the liquid. Beyond 4 A there is a dip because the concentration of nearest neighbors reduces the space available for atoms at slightly larger distances. The radial distribution function alternates above and below the average density curve $4\pi r^2\rho_a$. Crystalline sodium is body centered cubic and the positions and numbers of the various neighbors are shown in Fig. 10.6. There is a marked similarity between $4\pi r^2\rho(r)$ and the distribution of neighbors in the crystalline solid. If interatomic distances are about the same in the liquid and in the solid, this similarity in distribution is to be expected, since the density of the liquid is only about 2 percent less than that of the solid. However, the marked similarity in distribution which is shown by Fig. 10.6 does not require postulating a crystalline structure for the liquid. Approximate spherical shells of first, second, and third neighbors is enough to produce the peaks and dips in $4\pi r^2\rho(r)$ shown by Fig. 10.6.

10.6 CONVERGENCE FACTOR AND TERMINATION ERRORS

The variation of I'_{eu}/N above and below f^2 is $I'_{eu}/N - f^2$, and this quantity is expressed by Eq. (10.15). It is evident that $I'_{eu}/N - f^2$ approaches zero with increasing k, due to the decrease in f^2 and the decrease in the values of $\sin kr_i/kr_i$. At a maximum value in k which we call k_m, the quantity $I'_{eu}/N - f^2$ becomes too small for measurement, and we say that the intensity curve has converged. However, to obtain $ki(k)$, we divide by f^2 and multiply by k, and hence at k_m where $I'_{eu}/N - f^2$ is no longer measureable, $ki(k)$ may still display very large peaks and dips. We accordingly apply a convergence factor $e^{-\alpha^2k^2}$ to $ki(k)$ before performing the Fourier inversion of Eq. (10.14). There are two reasons why a convergence factor is very important. Without the factor, we would be giving equal weight to the peaks and dips in $ki(k)$ at large values of k where the experimental accuracy is very low, and this can produce appreciable inaccuracies in $4\pi r^2\rho(r)$. Terminating $ki(k)$ at k_m when it has not converged will produce false termination satellites in the $4\pi r^2\rho(r)$ curve, and the magnitude of these false satellites is reduced by applying a convergence factor.

It is convenient to express the termination effect by introducing a factor $U(k)$ which has the value unity for $k < k_m$ and the value zero for $k > k_m$. From Eq. (10.14), what we desire to obtain is

$$2\pi^2 r[\rho(r) - \rho_a] = \int_0^\infty ki(k) \sin rk \, dk.$$

Because of the convergence factor $e^{-\alpha^2k^2}$ and the termination factor $U(k)$, we obtain instead

$$2\pi^2 r[\rho'(r) - \rho_a] = \int_0^\infty ki(k)e^{-\alpha^2k^2}U(k) \sin rk \, dk.$$

Introduce the abbreviations

$$F_s(k) = ki(k), \qquad G_c(k) = e^{-a^2k^2}U(k).$$

By standard Fourier transform procedure, such as is outlined on page 24 of Sneddon,[6]

$$2\pi^2 r[\rho'(r) - \rho_a] = \int_0^\infty F_s(k)G_c(k) \sin rk\, dk$$

$$= \frac{1}{2}\int_0^\infty f(\eta)[g(|r-\eta|) - g(r+\eta)]\, d\eta, \quad (10.16)$$

where

$$f(\eta) = \sqrt{2/\pi}\int_0^\infty F_s(k) \sin \eta k\, dk, \qquad F_s(k) = \sqrt{2/\pi}\int_0^\infty f(\eta) \sin k\eta\, d\eta, \quad (10.17)$$

$$g(\epsilon) = \sqrt{2/\pi}\int_0^\infty G_c(k) \cos \epsilon k\, dk, \qquad G_c(k) = \sqrt{2/\pi}\int_0^\infty g(\epsilon) \cos k\epsilon\, d\epsilon. \quad (10.18)$$

From the above definitions,

$$f(\eta) = \sqrt{2/\pi}\int_0^\infty ki(k) \sin \eta k\, dk = \sqrt{2/\pi}\, 2\pi^2\eta[\rho(\eta) - \rho_a].$$

Using this expression for $f(\eta)$, Eq. (10.16) becomes

$$2\pi^2 r[\rho'(r) - \rho_a] = \sqrt{2/\pi}\int_0^\infty \pi^2\eta\rho(\eta)[g(|r-\eta|) - g(r+\eta)]\, d\eta - Y, \quad (10.19)$$

where

$$Y = \sqrt{2/\pi}\, \pi^2\rho_a\int_0^\infty \eta[g(|r-\eta|) - g(r+\eta)]\, d\eta.$$

Making the changes in variable $\eta - r = x$ and $\eta + r = z$, we obtain

$$\int_0^\infty \eta[g(|r-\eta|) - g(r+\eta)]\, d\eta = 2r\int_0^\infty g(x)\, dx + \int_{-r}^{+r} xg(|x|)\, dx. \quad (10.20)$$

The second term is zero, since $g(|x|)$ is an even function. By letting k go to zero, Eq. (10.18) becomes

$$1 = \sqrt{2/\pi}\int_0^\infty g(\epsilon)\, d\epsilon.$$

Using this result in Eq. (10.20), we obtain $Y = 2\pi^2 r\rho_a$. Canceling Y from both sides of Eq. (10.19), we can now write

$$2\pi^2 r\rho'(r) = \sqrt{2/\pi}\int_0^\infty \pi^2\eta\rho(\eta)[g(|r-\eta|) - g(r+\eta)]\, d\eta. \quad (10.21)$$

To evaluate $g(\epsilon)$, we use the approximation

$$e^{-x^2} = A + B\cos 2.15x,$$

where $A = 0.588$ and $B = 0.412$. The approximation is good to within one percent up to $x^2 = 1.5$. Using this approximation,

$$g(\epsilon) = \sqrt{2/\pi}\int_0^{k_m} (A + B\cos 2.15\alpha k)\cos \epsilon k\, dk$$

$$= \sqrt{2/\pi}\left[A\frac{\sin \epsilon k_m}{\epsilon} + \frac{B}{2}\frac{\sin (2.15\alpha + \epsilon)k_m}{2.15\alpha + \epsilon} + \frac{B}{2}\frac{\sin (2.15\alpha - \epsilon)k_m}{2.15\alpha - \epsilon}\right].$$

We now employ this expression in Eq. (10.21) for $g(|r - \eta|)$ and drop the term $g(r + \eta)$ whose contribution, if carried along, will be found to be small compared to that from $g(|r - \eta|)$.

$$4\pi r\rho'(r) = \frac{k_m}{\pi}\int_0^{\infty} 4\pi\eta\rho(\eta)\left\{\frac{A\sin (r - \eta)k_m}{(r - \eta)k_m} + \frac{B}{2}\frac{\sin [2.15\alpha + |r - \eta|]k_m}{[2.15\alpha + |r - \eta|]k_m}\right.$$

$$\left. + \frac{B}{2}\frac{\sin [2.15\alpha - |r - \eta|]k_m}{[2.15\alpha - |r - \eta|]k_m}\right\} d\eta. \quad (10.22)$$

The significance of the terms in Eq. (10.22) is as follows: $4\pi\eta\rho(\eta)$ is the ideal function which would be obtained if there were no convergence factor and no termination, while $4\pi r\rho'(r)$ is the somewhat different quantity which we obtain from data involving termination and a convergence factor. With the abbreviations

$$x = (r - \eta)k_m, \qquad \gamma = \alpha k_m,$$

we now express the value of $4\pi r\rho'(r)$ which is due only to a narrow section $4\pi\eta\rho(\eta)\, d\eta$ in the ideal function:

$$4\pi r\rho'(r) = (4\pi\eta\rho(\eta)\, d\eta)\frac{k_m}{\pi}Q(x, \gamma), \quad (10.23)$$

where

$$Q(x, \gamma) = \frac{A\sin x}{x} + \frac{B}{2}\frac{\sin (2.15\gamma + |x|)}{2.15\gamma + |x|} + \frac{B}{2}\frac{\sin (2.15\gamma - |x|)}{2.15\gamma - |x|}.$$

Figure 10.7 shows the function $Q(x, \gamma)$ for several values of the factor γ^2. Each narrow section $4\pi\eta\rho(\eta)\, d\eta$ produces a peak in $4\pi r\rho'(r)$ at $x = 0$ and hence at $r = \eta$. In addition there is a satellite on either side at $x = \pm 7.8$ which corresponds to $r = \eta \pm 7.8/k_m$. For termination at $k_m = 4\pi$, the satellites are at 0.62 A on either side of the main peak. Termination satellites in $4\pi r\rho'(r)$ can always be recognized because they occur on either side of a main peak at separations $\Delta r = \pm 7.8/k_m$. With increasing convergence factor, the satellites are rapidly reduced, and for values such as $\gamma^2 = 1.5$, the satellites are small enough to be harmless.

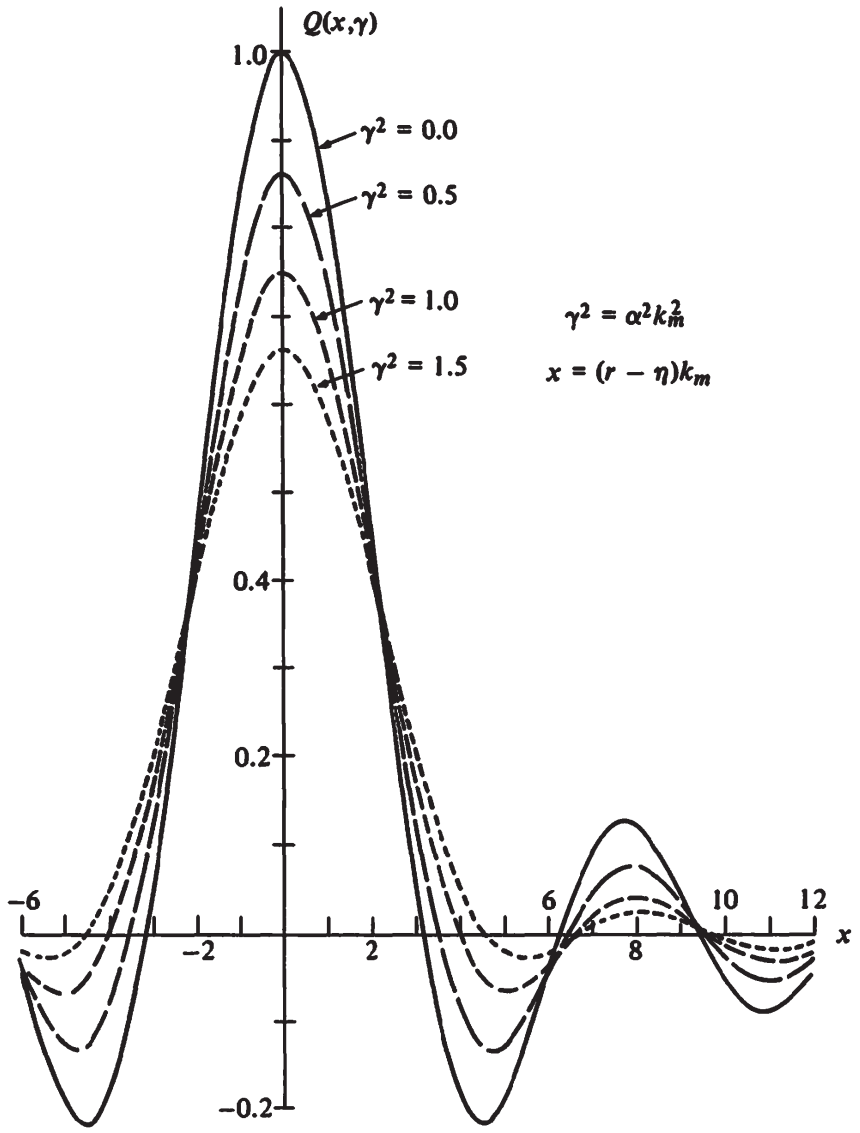

Fig. 10.7 The function $Q(x, \gamma)$ which represents the effect of termination and convergence factors on the radial distribution function. The abscissa is $x = (r - \eta)k_m$, and curves are given for several values of the convergence factor $\gamma^2 = \alpha^2 k_m^2$.

With no convergence factor ($\gamma^2 = 0.0$), the peak in $4\pi r\rho'(r)$ has a full width at half maximum of $\Delta x = 3.8$, which corresponds to $\Delta r = 3.8/k_m$. For a cut-off at $k_m = 4\pi$, this corresponds to a full width $\Delta r = 0.30$ A, and this fictitious breadth of the peak in the $4\pi r\rho'(r)$ function is due solely to the termination of experimental measurements at k_m. With a convergence factor corresponding to $\gamma^2 = 1.5$ and the same termination value $k_m = 4\pi$, the full width is $\Delta r = 0.36$ A. Hence there is not much loss in resolution by using convergence factors as high as $\gamma^2 = 1.5$, and there is the very important advantage that they weight down the inaccurate part of the $ki(k)$ curve and they minimize the termination satellites which might be mistaken for real features in the $4\pi r\rho'(r)$ curve. Sharpness in the peaks can be secured only by obtaining good data out to large values of k_m rather than by omitting a con-

vergence factor. From the curves of Fig. 10.7 it is possible to estimate what peak breadth is produced for any combination of convergence factor and termination value, and hence to see how much of the observed breadth is due to a real variation in interatomic distances.

The discussion has been in terms of $4\pi r\rho'(r)$ since this is the quantity directly affected by termination and convergence factors. It is evident that these factors produce a symmetrical broadening in $4\pi r\rho'(r)$. However, to discuss correctly the number of neighbors in any interval of distance, it is the radial distribution function $4\pi r^2\rho'(r)$ which is needed, and for this quantity the broadening will be slightly asymmetric with a slight peak displacement. It is possible to make a rough evaluation of this displacement. However, if the peak is sharp enough to justify a precision measurement of its position, the displacement due to asymmetric broadening is usually small enough to neglect. For most purposes the theory of satellites and peak broadening which has been developed here for the function $4\pi r\rho'(r)$ applies closely enough to the radial distribution function $4\pi r^2\rho'(r)$.

10.7 FOURIER INVERSION WITH THE BEEVERS-LIPSON STRIPS

Assume that we have the function $ki(k)e^{-\alpha^2k^2}$ plotted against k, and are now ready to evaluate the integral which replaces that in Eq. (10.14):

$$y(r) = \int_0^{k_m} ki(k)e^{-\alpha^2k^2} \sin rk\, dk.$$

With modern experimental methods, there is enough detail in the intensity curves which are obtainable from liquids and amorphous solids to require the evaluation of the integral by electronic computer methods, if the full available information is to be obtained. However if the experimental intensity curve is poor in detail and extent, or if a computer is not available, it is sometimes satisfactory to make a rough evaluation with the Beevers-Lipson strips.

As an illustration suppose that $k_m = 4\pi$, and we divide the range 0 to 4π into 60 intervals. We number these intervals j, and tabulate the ordinates $[ki(k)e^{-\alpha^2k^2}]_j$. The integral is then replaced by the sum

$$y(r) = \frac{4\pi}{60}\sum_{j=1}^{60}[ki(k)e^{-\alpha^2k^2}]_j \sin rk_j. \tag{10.24}$$

The second edition Beevers-Lipson strips carry the values of $A \sin 2\pi hn/120$. For each integral value of h from 1 to 30, there are strips with various values of A. Each strip is made up for a fixed value of h and A, and on it are printed the values of $A \sin 2\pi hn/120$ for integral values of n from 1 to 30. Since the quantity which is given on the strips can be written

$$A \sin\left[\left(\frac{4\pi h}{60}\right)\left(\frac{n}{4}\right)\right],$$

the terms in the summation can be represented by the numbers on the strips by making the identification

$$A = [ki(k)e^{-\alpha^2k^2}]_j, \qquad \frac{4\pi h}{60} = k_j, \qquad \frac{n}{4} = r.$$

Strips are available for integral values of h from 1 to 30. For h between 30 and 60, we use strips for $h' = 60 - h$, since

$$A \sin 2\pi hn/120 = -(-1)^n A \sin 2\pi h'n/120.$$

For even values of n, it is only necessary to use a strip which reverses the sign of A. Positive and negative amplitudes A are available in unit steps up to 100 and then in steps of 100 up to 900. To utilize the strips efficiently, all tabulated values of $[ki(k)e^{-\alpha^2k^2}]_j$ are multiplied by a factor to make the largest one about 200. The final result must, of course, be corrected for this factor. For values of A between 100 and 200 it is necessary to use two strips.

The summation represented by Eq. (10.24) is then performed by laying out the strips below one another. There is a strip for each value of h from 1 to 60, and for each h a strip with the appropriate value of A has been selected. With a desk adding machine, it is then a simple matter to sum down the columns of n. Using both sides of the strips, with appropriate changes in sign for h between 30 and 60, we obtain sums for integral values of n from 1 to 30. Since $n/4 = r$, this means that we obtain the value of $y(r)$ up to $r = 7.5\ A$ in steps of $\frac{1}{4}\ A$ in r. By a proper manipulation of strips for odd and even h, the values can be extended to $n = 60$ and hence to $r = 15\ A$. The whole procedure is very simple and it is readily performed in three or four hours. Although the values of $y(r)$ are obtained only at steps of $\frac{1}{4}\ A$ in r, this is often adequate for plotting the radial distribution function. If it is necessary to obtain $y(r)$ at some intermediate values of r, the whole process can be repeated with the range 4π divided into some number of intervals a little different from 60.

10.8 APPROXIMATE METHOD FOR SAMPLE WITH MORE THAN ONE KIND OF ATOM

We consider now an approximation method for handling an amorphous material containing more than one kind of atom. We pick some convenient unit of composition designated by uc, and let N be the number of units of composition in the sample. For a sample with a stoichiometric composition such as vitreous SiO_2, it would be obvious to use 1 silicon atom and 2 oxygen atoms as the unit of composition. For a nonstoichiometric composition such as that of a molten alloy represented by $A_{0.32}B_{0.68}$, we could use 0.32 atoms of A and 0.68 atoms of B as the unit of composition.

From Eq. (10.2), the intensity is given by

$$I_{eu} = \sum_m f_m^2 + \sum_m f_m \sum_{n \neq m} f_n e^{(2\pi i/\lambda)(s-s_0)\cdot r_{nm}}.$$

We define an average scattering factor per electron:

$$f_e = \left(\sum_{uc} f_m\right) \Big/ \sum_{uc} Z_m, \tag{10.25}$$

where the sum over *uc* means a sum over the atoms in the unit of composition. Using vitreous SiO_2 as an example, $f_e = (f_{Si} + 2f_O)/(14 + 2 \times 8)$. We next represent the scattering factor in terms of f_e by the relation

$$f_m = K_m f_e. \tag{10.26}$$

The effective electron numbers K_m defined by Eq. (10.26) will be approximately equal to the atomic numbers Z_m. For each kind of atom, the effective number K_m will vary somewhat with $(\sin\theta)/\lambda$ and the approximation which we are making involves using an average value and treating K_m as a constant for each kind of atom. With this approximation, the intensity can be written

$$I_{eu} = \sum_m f_m^2 + f_e^2 \sum_m K_m \sum_{n \neq m} K_n e^{(2\pi i/\lambda)(\mathbf{s}-\mathbf{s}_0)\cdot \mathbf{r}_{nm}}$$

Let $\rho_m(\mathbf{r}_{nm})\, dV_n$ be the number of atoms centers, each multiplied by its appropriate K_n, in the volume element dV_n at the displacement $\mathbf{r}_{nm}$ from atom m. The sum over n can then be replaced by an integral over the volume of the sample:

$$I_{eu} = \sum_m f_m^2 + f_e^2 \sum_m K_m \int \rho_m(\mathbf{r}_{nm}) e^{(2\pi i/\lambda)(\mathbf{s}-\mathbf{s}_0)\cdot \mathbf{r}_{nm}}\, dV_n.$$

We now add and subtract a term involving ρ_e, the average electron density in the sample:

$$I_{eu} = \sum_m f_m^2 + f_e^2 \sum_m K_m \int [\rho_m(\mathbf{r}_{nm}) - \rho_e] e^{(2\pi i/\lambda)(\mathbf{s}-\mathbf{s}_0)\cdot \mathbf{r}_{nm}}\, dV_n + f_e^2 \sum_m K_m \int \rho_e e^{(2\pi i/\lambda)(\mathbf{s}-\mathbf{s}_0)\cdot \mathbf{r}_{nm}}\, dV_n. \tag{10.27}$$

The third term in Eq. (10.27) represents the small angle intensity which was discussed in Section 10.4. Assuming that it is confined to such small angles that it is not observable, or if this is not the case that it has been evaluated and subtracted off, we now drop the third term and use I'_{eu} to represent the first two terms of Eq. (10.27).

We next introduce the subscript j to represent the kind of atom. Using vitreous SiO_2 as an example, $j = 1$ could mean silicon and $j = 2$ could mean oxygen. For a fixed displacement $\mathbf{r}_{nm} = \mathbf{r}$, let $\rho_j(\mathbf{r}) = \langle \rho_m(\mathbf{r}_{nm}) \rangle_v$, where the average is over all $\rho_m(\mathbf{r})$ within the sample at a displacement $\mathbf{r}$ from an atom of type j. In an amorphous sample, $\rho_j(\mathbf{r}) - \rho_e$ approaches zero for displacements $\mathbf{r}$ greater than a few atomic dimensions, and we can multiply the average by the total number of atoms of each kind:

$$I'_{eu} = N \sum_{uc} f_j^2 + f_e^2 N \sum_{uc} K_j \int [\rho_j(\mathbf{r}) - \rho_e] e^{(2\pi i/\lambda)(\mathbf{s}-\mathbf{s}_0)\cdot \mathbf{r}}\, dV.$$

For an amorphous sample without preferred orientation, $\rho_j(\mathbf{r}) - \rho_e$ will have spherical symmetry. It can be replaced by $\rho_j(r) - \rho_e$, and the integration with respect to $d\phi$ performed as in Section 10.4:

$$I'_{eu} = N\sum_{uc} f_j^2 + f_e^2 N \sum_{uc} K_j \int_0^\infty 4\pi r^2[\rho_j(r) - \rho_e]\frac{\sin kr}{kr}\,dr.$$

Introduce the abbreviation

$$i(k) = \left(I'_{eu}/N - \sum_{uc} f_j^2\right)/f_e^2. \tag{10.28}$$

The intensity function $ki(k)$ is then given in the form of a Fourier transform:

$$ki(k) = 4\pi \int_0^\infty \sum_{uc} K_j r[\rho_j(r) - \rho_e] \sin kr\,dr.$$

With the Eqs. (10.13), which were used in Section 10.4 for inverting the Fourier integral, we obtain finally

$$\sum_{uc} K_j 4\pi r^2 \rho_j(r) = 4\pi r^2 \rho_e \sum_{uc} K_j + \frac{2r}{\pi}\int_0^\infty ki(k) \sin rk\,dk. \tag{10.29}$$

In practice the integral of Eq. (10.29) will involve a convergence factor $e^{-\alpha^2 k^2}$ and termination at k_m as discussed in Section 10.6, so that a slightly broadened quantity $\rho'_j(r)$ is obtained. It is assumed that the intensity I'_{eu}/N has been corrected for second-order multiple scattering. If the measured intensity includes both the modified and the unmodified scattering, we obtain absolute units by dividing the experimental intensity curve by the polarization factor and then adjusting the scale of ordinates so that at large $(\sin\theta)/\lambda$ this curve oscillates above and below the independent scattering curve

$$\sum_{uc} [f_j^2 + i_j(M)].$$

The final curve

$$\sum_{uc} K_j 4\pi r^2 \rho_j(r)$$

represents the superposition of radial distribution functions for each kind of atom in the unit of composition. The positions of the peaks give the various interatomic distances in the sample. In some cases these distances are enough to identify the kinds of atoms represented by the peak, and in these cases the peak area can be used to get the number of neighboring atoms. As an example, consider the radial distribution function for vitreous SiO_2 where we have taken 1 silicon and 2 oxygens for the unit of composition. The first peak occurs at 1.62 *A* and from the structures of crystalline silicates, we know that this is the nearest neighbor silicon-oxygen separation. The observed peak at 1.62 *A* is the superposition of two peaks; one representing oxygens about

an average silicon, and the other representing silicons about an average oxygen. The area of this peak will be

$$A = 1K_{\mathrm{Si}}\, n_{\mathrm{O}}\, K_{\mathrm{O}} + 2K_{\mathrm{O}}\, n_{\mathrm{Si}}\, K_{\mathrm{Si}},$$

where n_{O} and n_{Si} are the numbers of nearest neighbor oxygens about a silicon and of nearest neighbor silicons about an oxygen. To satisfy the composition, $n_{\mathrm{O}} = 2n_{\mathrm{Si}}$, and hence the peak area is given by $A = 2K_{\mathrm{Si}}\, K_{\mathrm{O}} n_{\mathrm{O}}$. From the measured peak area and the known value of $K_{\mathrm{Si}}\, K_{\mathrm{O}}$, we determine n_{O} the number of nearest neighbor oxygens about a silicon.

This approximate method for handling amorphous materials with more than one kind of atom was first applied to samples of vitreous SiO_2 and B_2O_3.[7] For some samples, the different f curves really are closely proportional to one another, and the results obtained by the approximate treatment are quite reliable. In general, the f curves of the different atoms are only roughly proportional to one another, there is trouble in deciding what average values of K_m should be used, and the results of the analysis must be considered as approximate.

10.9 EXACT METHOD FOR AN AMORPHOUS SAMPLE WITH MORE THAN ONE KIND OF ATOM

Rigorous methods for handling samples with more than one kind of atom have been developed by the Norwegian school of C. Finbak. That rigorous methods exist has also been pointed out in the review article by Waser and Schomaker.[8] We pick a convenient unit of composition *uc* and let $\sum_{uc}$ be a sum over the atoms of the unit of composition. We let N be the number of units of composition in the sample, V the volume of the sample, and N/V the number of units of composition per unit volume. The sample can have any shape, and we neglect absorption since it is more convenient to put in a correction for absorption at the end.

From Eq. (10.2), the intensity is given by

$$I_{eu} = \sum_m f_m^2 + \sum_m f_m \sum_{n \neq m} f_n e^{(2\pi i/\lambda)(\mathbf{s}-\mathbf{s}_0)\cdot \mathbf{r}_{nm}}.$$

Let $\rho_m(\mathbf{r}_{nm})\, dV_n$ be the number of atoms, each multiplied by its f_n, in the volume element dV_n at the displacement $\mathbf{r}_{nm}$ from atom m. The sum over n can then be replaced by an integral over the volume of the sample:

$$I_{eu} = \sum_m f_m^2 + \sum_m f_m \int_S \rho_m(\mathbf{r}_{nm}) e^{(2\pi i/\lambda)(\mathbf{s}-\mathbf{s}_0)\cdot \mathbf{r}_{nm}}\, dV_n.$$

Designating the kind of atom by j, the average value of $\rho_n(\mathbf{r}_{nm})\, dV_n$ is expressed by

$$(N/V) \sum_{uc} f_j\, dV_n.$$

We now add and subtract a term involving this average

$$I_{eu} = \sum_m f_m^2 + \sum_m f_m \int_S \left[\rho_m(\mathbf{r}_{nm}) - \frac{N}{V} \sum_{uc} f_j \right] e^{(2\pi i/\lambda)(\mathbf{s}-\mathbf{s}_0)\cdot\mathbf{r}_{nm}} \, dV_n + \sum_m f_m \int_S \frac{N}{V} \sum_{uc} f_j e^{(2\pi i/\lambda)(\mathbf{s}-\mathbf{s}_0)\cdot\mathbf{r}_{nm}} \, dV_n. \quad (10.30)$$

The third term in Eq. (10.30) represents the small angle intensity which was discussed in Section 10.4. Assuming that it is confined to such small angles that it is not observable, or if this is not the case that it has been evaluated and subtracted off, we now drop the third term and use I'_{eu} to represent the first two terms of Eq. (10.30).

For a fixed displacement $\mathbf{r}_{nm} = \mathbf{r}$, let $\rho_j(\mathbf{r}) = \langle \rho_m(\mathbf{r}_{nm}) \rangle_j$, where the average is over all $\rho_m(\mathbf{r})$ within the sample at a displacement $\mathbf{r}$ from an atom of type j. In an amorphous sample, $\rho_j(\mathbf{r}) - (N/V) \sum_{uc} f_j$ approaches zero for displacements $\mathbf{r}$ greater than a few atomic dimensions. Hence it is only small values of $\mathbf{r}_{nm}$ which contribute in the second term of Eq. (10.30). Considering all the initial atoms m and all the nearby neighbors n, any connecting vector $\mathbf{r}_{nm}$ will be found with equal probability in all orientations. Hence we can replace the exponential by its average where $\mathbf{r}_{nm}$ takes all orientations

$$\langle e^{(2\pi i/\lambda)(\mathbf{s}-\mathbf{s}_0)\cdot\mathbf{r}_{nm}} \rangle = \frac{\sin kr_{nm}}{kr_{nm}}.$$

Using this average in Eq. (10.30) and dropping the third term, we obtain

$$I'_{eu} = \sum_m f_m^2 + \sum_m f_m \int_S \left[\rho_m(\mathbf{r}_{nm}) - \frac{N}{V} \sum_{uc} f_j \right] \frac{\sin kr_{nm}}{kr_{nm}} \, dV_n.$$

We introduced $\rho_m(\mathbf{r}_{nm})$ only to be able to justify the averaging of $\exp[(2\pi i/\lambda)(\mathbf{s} - \mathbf{s}_0) \cdot \mathbf{r}_{nm}]$. We now replace it by the original sum over n, from which it came:

$$I'_{eu} = \sum_m f_m^2 + \sum_m f_m \sum_{n \neq m} f_n \frac{\sin kr_{nm}}{kr_{nm}} - \sum_m f_m \int_S \frac{N}{V} \sum_{uc} f_j \frac{\sin kr_{nm}}{kr_{nm}} dV_n.$$

It is convenient to replace the sum over n by a sum over shells of neighbors, where the shells are designated by i. Let N_{ij} be the average number of atoms in shell i at a distance r_{ij} from an atom of type j, and let $q_m(r)$ be the fraction within the sample of the surface of a sphere of radius r which is centered on atom m. Introducing these quantities, and extending the integral to infinity since $q_m(r)$ goes to zero for large values of r, we obtain

$$I'_{eu} = N \sum_{uc} f_j^2 + N \sum_{uc} f_j \sum_i N_{ij} f_i \frac{\sin kr_{ij}}{kr_{ij}} - \frac{N}{V} \sum_{uc} f_j \sum_m f_m \int_0^\infty \frac{\sin kr}{kr} 4\pi r^2 q_m(r) \, dr.$$

Let $q(r) = \langle q_m(r) \rangle$, where the average is over all atoms m. From its definition, $q(r) = 1.0$ for $r = 0$, and $q(r)$ goes to zero for values of r greater than the sample dimensions. With a little rearranging the expression becomes

$$k\left(I'_{eu}/N - \sum_{uc} f_j^2\right) = \sum_{uc} f_j \sum_i \frac{N_{ij}}{r_{ij}} f_i \sin kr_{ij} - \frac{N}{V}\left(\sum_{uc} f_j\right)^2 4\pi \int_0^\infty rq(r) \sin kr \, dr.$$

Multiply by a convergence factor $e^{-\alpha^2 k^2}$ and a sharpening factor $1/g^2(k)$, where $g(k)$ decreases with increasing k and has the value $g(k) = 1.0$ at $k = 0$. For $g(k)$ we could use the f_e which was introduced in Section 10.8, but we could use any other suitable function which is convenient. Introducing the abbreviations

$$i(k) = \left(I'_{eu}/N - \sum_{uc} f_j^2\right) \Big/ g^2(k), \tag{10.31}$$

$$Y(k) = 4\pi \int_0^\infty rq(r) \sin kr \, dr, \tag{10.32}$$

we obtain

$$ki(k)e^{-\alpha^2 k^2} = \sum_{uc} f_j \sum_i \frac{N_{ij}}{r_{ij}} f_i \frac{e^{-\alpha^2 k^2}}{g^2(k)} \sin kr_{ij} - \frac{N}{V}\left(\sum_{uc} f_j\right)^2 \frac{e^{-\alpha^2 k^2}}{g^2(k)} Y(k).$$

We now multiply by $\sin rk$ and integrate from $k = 0$ to $k = k_m$:

$$\int_0^{k_m} ki(k)e^{-\alpha^2 k^2} \sin rk \, dk = \sum_{uc} \sum_i \frac{N_{ij}}{r_{ij}} \int_0^{k_m} \frac{f_j f_i}{g^2(k)} e^{-\alpha^2 k^2} \sin kr_{ij} \sin kr \, dk$$
$$- \frac{N}{V} \int_0^{k_m} \left(\sum_{uc} f_j\right)^2 \frac{e^{-\alpha^2 k^2}}{g^2(k)} Y(k) \sin rk \, dk. \tag{10.33}$$

The quantity $Y(k)$ is defined by Eq. (10.32), and we are now interested in showing that $Y(k)$ is negligible except at small values of k. To do this, we perform a successive series of integrations by parts, and obtain

$$Y(k) = -\frac{8\pi}{k^3}\left\{\left[\frac{dq(r)}{dr}\right]_{r=0} - \frac{2}{k^2}\left[\frac{d^3q(r)}{dr^3}\right]_{r=0} + \frac{3}{k^4}\left[\frac{d^5q(r)}{dr^5}\right]_{r=0} \cdots\right\}. \tag{10.34}$$

It is evident that $Y(k)$ decreases rapidly with increasing values of k. Hence $Y(k)$ is negligible except at small values of k, and in the last term of Eq. (10.33) we can replace all of the slowly varying quantities by their values at $k = 0$, and let the integral go to infinity. The last term of Eq. (10.33) becomes

$$\frac{N}{V}\left(\sum_{uc} Z_j\right)^2 \int_0^\infty Y(k) \sin rk \, dk.$$

From Eq. (10.32), $Y(k)$ is the Fourier transform of $rq(r)$. Using the inversion

relations of Eq. (10.13), we obtain

$$2\pi^2 rq(r) = \int_0^\infty Y(k) \sin rk \, dk,$$

and hence the last term of Eq. (10.33) has the value

$$2\pi^2 rq(r) \frac{N}{V} \left(\sum_{uc} Z_j \right)^2 = 2\pi^2 r \rho_e \sum_{uc} Z_j,$$

since $q(r) = 1.0$ for the small values of r which will be used. Incorporating this result, Eq. (10.33) becomes

$$\sum_{uc} \sum_{i} \frac{N_{ij}}{r_{ij}} \int_0^{k_m} \frac{f_j f_i}{g^2(k)} e^{-\alpha^2 k^2} \sin kr_{ij} \sin kr \, dk$$
$$= 2\pi^2 r \rho_e \sum_{uc} Z_j + \int_0^{k_m} ki(k) e^{-\alpha^2 k^2} \sin rk \, dk. \quad (10.35)$$

It is now convenient to introduce a set of pair functions $P_{ij}(r)$:

$$P_{ij}(r) = \int_0^{k_m} \frac{f_j f_i}{g^2(k)} e^{-\alpha^2 k^2} \sin kr_{ij} \sin kr \, dk. \quad (10.36)$$

Since $\sin kr_{ij} \sin kr = [\cos (r - r_{ij})k - \cos (r + r_{ij})k]/2$, the computations are simplified by using the auxiliary function

$$Q_{ij}(x) = \frac{1}{2} \int_0^{k_m} \frac{f_j f_i}{g^2(k)} e^{-\alpha^2 k^2} \cos xk \, dk. \quad (10.37)$$

The pair functions are then given by

$$P_{ij}(r) = Q_{ij}(r - r_{ij}) - Q_{ij}(r + r_{ij}), \quad (10.38)$$

where $Q_{ij}(r + r_{ij})$ is usually small enough to neglect. In terms of the pair functions, Eq. (10.35) takes the final form

$$\sum_{uc} \sum_{i} \frac{N_{ij}}{r_{ij}} P_{ij}(r) = 2\pi^2 r \rho_e \sum_{uc} Z_j + \int_0^{k_m} ki(k) e^{-\alpha^2 k^2} \sin rk \, dk. \quad (10.39)$$

Having chosen a suitable convergence coefficient α^2 and a sharpening factor $g(k)$, the right-hand side of Eq. (10.39) is evaluated and plotted as a function of r. The positions of the peaks in the function give the various interatomic distances r_{ij}. For an amorphous solid it is usually possible to identify the kinds of atoms associated with each r_{ij} by making use of known atomic sizes and interatomic distances in crystalline materials. Using the same convergence and sharpening factors, the pair functions $P_{ij}(r)$ are then evaluated for each of the r_{ij}. By trial we now find the values of N_{ij} which will bring the left-hand side of Eq. (10.39) into the best fit with the right-hand side. At the best fit, the peak areas should match, but the peaks of the right-hand side of the equation may be a little broader and lower due to a

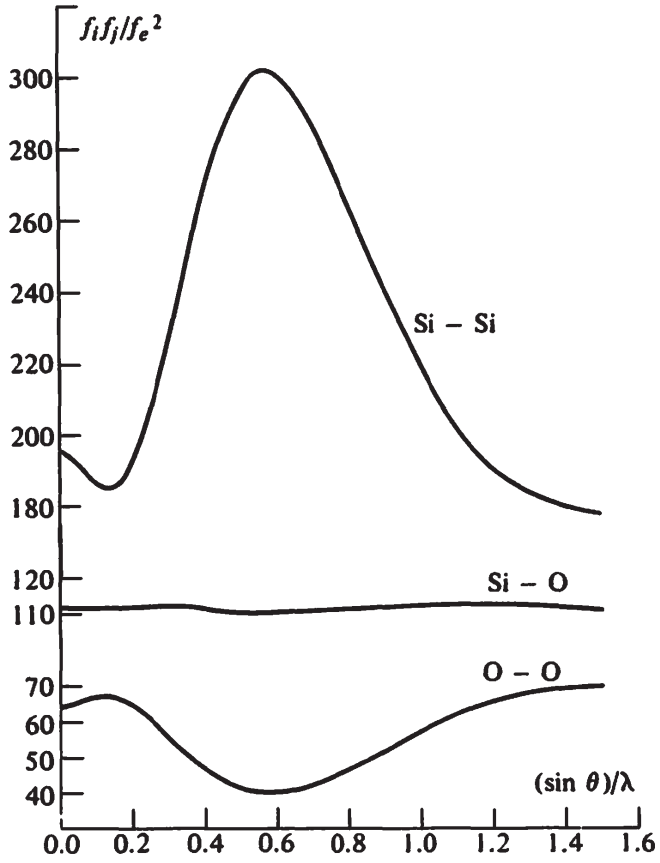

Fig. 10.8 The ratios $f_i f_j / f_e^2$ for Si–Si, Si–O, and O–O. The quantity f_e is the average f per electron defined by Eq. (10.25).

variation in each of the r_{ij} distances. An approximate evaluation of the variation in the r_{ij} distances can be obtained from the difference in the peak shapes. For an amorphous solid such as a glass, the interpretation is usually straightforward and unique for the first few peaks. For a liquid containing more than one kind of atom, such as a liquid alloy, the interpretation is not so direct, since the neighbors at any distance r from one type of atom may be of more than one kind. To reduce the ambiguity, it is often helpful to have the combination of x-ray and neutron diffraction data. The procedure has been outlined by Keating.[9]

To illustrate the appearance of pair functions, we can use vitreous SiO_2 as an example. Choosing a sharpening factor $g(k) = f_e$, and using f values from the International Tables, for the neutral atom without dispersion corrections, the quantities $f_j f_i / f_e^2$ for Si–Si, Si–O, and O–O are given in Fig. 10.8. It is evident that the method of Section 10.8, which treated $f_j f_i / f_e^2$ as a constant, is a good approximation for Si–O but a very poor one for Si–Si and O–O. Assuming termination at $k_m = 6\pi$, and using a convergence factor corresponding to $\alpha^2 k_m^2 = 1.00$, the pair functions $P_{ij}(r - r_{ij}) = Q_{ij}(x)$ are given by Fig. 10.9. The ripples outside of the main peak are the result of termination with only a moderate convergence factor. Apart from the ripples, the Si–Si curve has a pronounced negative wing just

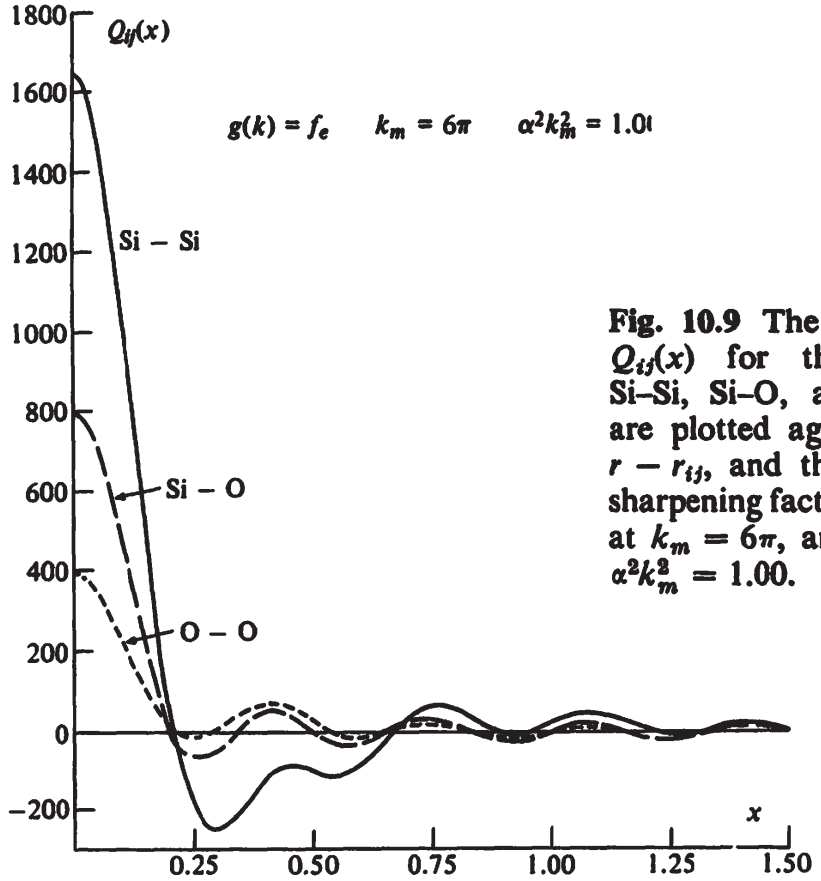

Fig. 10.9 The auxiliary pair function $Q_{ij}(x)$ for the three combinations Si–Si, Si–O, and O–O. The curves are plotted against the abscissae $x = r - r_{ij}$, and they are computed for a sharpening factor $g(k) = f_e$, termination at $k_m = 6\pi$, and a convergence factor $\alpha^2 k_m^2 = 1.00$.

outside of the main peak, and the O–O curve has a positive region just outside of the main peak. These positive or negative wings result from the shape of the $f_i f_j / f_e^2$ curves of Fig. 10.8. The ripple can be reduced by choosing a more drastic convergence factor, and if desired the positive or negative wings of a particular pair function can be reduced by choosing a different $g(k)$.

It is possible to derive a simple expression for the area under a pair function. Introducing the factor $U(k)$ where $U(k) = 1.0$ for $k < k_m$ and $U(k) = 0$ for $k > k_m$, the integral of Eq. (10.36) can be taken to infinity. Inverting by the inversion formulae of Eq. (10.13), we obtain

$$\frac{f_i f_j}{g^2(k)} e^{-\alpha^2 k^2} U(k) \sin r_{ij} k = \frac{2}{\pi} \int_0^\infty P_{ij}(r) \sin kr \, dr.$$

By now letting k be very small and replacing the slowly varying quantities by their values at $k = 0$, the relation becomes

$$(\pi/2) r_{ij} Z_i Z_j = \int_0^\infty P_{ij}(r) r \, dr.$$

Since $P_{ij}(r)$ is nearly symmetrical about $r = r_{ij}$, we can cancel r_{ij}, and obtain a simple expression for the total area under a pair function:

$$\int P_{ij}(r) \, dr = (\pi/2) Z_i Z_j. \tag{10.40}$$

In practice this simple result must be used with caution, because an appreciable part of the area may be in the positive or negative wings of the pair function.

The experimental intensity curve can be obtained in electron units per unit of composition by the condition that I'_{eu}/N oscillates above and below the unmodified independent scattering $\sum_{uc} f_j^2$. This method was discussed in Section 10.5. Another method for standardizing can be derived from Eq. (10.35). We divide both sides of the equation by r and then let r be very small:

$$\sum_{uc}\sum_{i}\frac{N_{ij}}{r_{ij}}\int_0^{k_m}\frac{f_j f_i}{g^2(k)}e^{-\alpha^2k^2}k\sin kr_{ij}\,dk = 2\pi^2\rho_e\sum_{uc}Z_j + \int_0^{k_m}k^2 i(k)e^{-\alpha^2k^2}\,dk. \tag{10.41}$$

We now wish to show that the left-hand side of Eq. (10.41) can be negligible compared to $2\pi^2\rho_e\sum_{uc}Z_j$. Suppose we use a more drastic convergence factor than would normally be used, such as $\alpha^2k^2 = 4$ at $k = k_m$. With such a convergence factor, the integral in the left-hand term can be approximated by an integration to infinity. Since we are only interested in obtaining a magnitude, we can suppose that $g(k) = f_e$, and make the approximation $f_i f_j/f_e^2 = Z_i Z_j$. The term is readily integrated and we obtain

$$\sum_{uc}\sum_{i}\frac{N_{ij}}{r_{ij}}Z_iZ_j\int_0^{\infty}e^{-\alpha^2k^2}k\sin r_{ij}k\,dk = \sum_{uc}\sum_{i}N_{ij}Z_iZ_j2\pi^3\sqrt{\pi}e^{-\pi^2r_{ij}^2}\text{A}^{-3}.$$

For a shortest interatomic distance such as $r_{ij} = 1.5$ A, $2\pi^3\sqrt{\pi}\exp[-\pi^2r_{ij}^2] = 2.5\times10^{-8}$ A^{-3}. Only the shortest interatomic distances r_{ij} can contribute, and the left-hand side of Eq. (10.41) will be of the order of 1000 times 2.5×10^{-8} A^{-3}. Since ρ_e is of the order of 1 A^{-3}, $2\pi^2\rho_e\sum_{uc}Z_j$ is of the order of 1000 A^{-3}. Hence the left-hand side of Eq. (10.41) is completely negligible compared to $2\pi^2\rho_e\sum_{uc}Z_j$. Dropping it, we obtain

$$\int_0^{k_m}k^2i(k)e^{-\alpha^2k^2}\,dk = -2\pi^2\rho_e\sum_{uc}Z_j. \tag{10.42}$$

Since the right-hand side of Eq. (10.42) is known, this expression can be used to put the intensity curve in absolute units. A corresponding expression without the convergence factor has been given by Norman.[10]

To illustrate the application of Eq. (10.42), suppose that we are recording both the unmodified and the modified scattering. The experimental intensity curve, corrected for the polarization factor, and expressed in arbitrary units, will be called I(exp). Assuming that the small angle intensity term is not observable or has been eliminated from I(exp),

$$I'_{eu}/N + \sum_{uc} i_j(M) = KI(\text{exp}), \tag{10.43}$$

and the problem is now to determine the normalizing factor K. Using the value of $i(k)$ from Eq. (10.31), and introducing I(exp) from Eq. (10.43), we

can rewrite Eq. (10.42) in the form

$$K\int_0^{k_m} \frac{k^2 e^{-a^2k^2}}{g^2(k)} I(\text{exp})\, dk = \int_0^{k_m} \frac{k^2 e^{-a^2k^2}}{g^2(k)} \sum_{uc} [f_j^2 + i_j(M)]\, dk - 2\pi^2 \rho_e \sum_{uc} Z_j. \tag{10.44}$$

The right-hand side of Eq. (10.44) can be evaluated from known quantities, and the integral on the left-hand side can be evaluated from the experimental curve $I(\text{exp})$. From Eq. (10.44), we obtain the normalizing constant K, and then from Eq. (10.43) and the known values of $\sum_{uc} i_j(M)$, we obtain I'_{eu}/N in absolute units. Since the integrands in Eq. (10.44) involve k^2, it is important to use a rather strong convergence factor.

10.10 AMORPHOUS SCATTERING FROM A FLAT-FACED DIFFRACTOMETER SAMPLE

For simplicity consider a sample containing only one kind of atom, with ρ_a atoms per unit volume. The primary beam has a cross-sectional area A_0, and it is completely intercepted by the sample, whose face is symmetrical with respect to the primary and diffracted beams. For a very small sample in which absorption can be neglected, the intensity is given by Eq. (10.8). In the first two terms only close neighbors contribute, and the Fraunhofer approximation suffices. To adapt these two terms to the flat-faced diffractometer sample, let $\rho_a(A_0/\sin\theta)\, dz$ be the number of atoms in the primary beam between depths z and $z + dz$. We include the whole sample, with proper allowance for absorption, by making the replacement

$$N \to \int_0^{\infty} e^{-(2\mu z/\sin\theta)} \frac{\rho_a A_0\, dz}{\sin\theta} = \frac{A_0\rho_a}{2\mu}.$$

The third term of Eq. (10.8) involves the interaction of widely separated

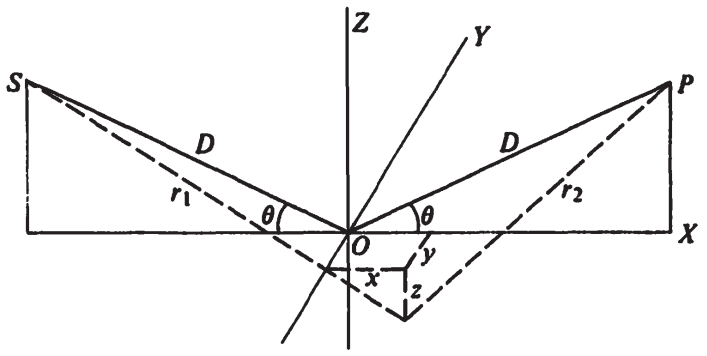

Fig. 10.10 Geometry involved in calculating $I_{eu}(SA)$ from a flat-faced diffractometer sample by Fresnel diffraction. Radiation diverges from a point source S and diffracted radiation is measured at point P. The origin O is in the face of the sample.

atoms and hence it must be treated by Fresnel diffraction. Since it is of importance only at small angles, it will be called $I_{eu}(SA)$. For the flat-faced diffractometer sample, the intensity is given by

$$I_{eu} = \frac{A_0\rho_a f^2}{2\mu} + \frac{A_0\rho_a f^2}{2\mu}\int_0^\infty 4\pi r^2[\rho(r) - \rho_a]\frac{\sin kr}{kr}\,dr + I_{eu}(SA). \quad (10.45)$$

The geometry involved in calculating $I_{eu}(SA)$ by Fresnel diffraction is shown by Fig. 10.10. Radiation diverges from a point source S, and the diffracted radiation is measured at point P. The origin O is in the face of the sample, and positioned so that the plane SOP is normal to the sample face, and the directions SO and OP make equal angles with the face of the sample. For a point at position xyz, the path lengths for the primary and diffracted beams are r_1 and r_2:

$$\begin{aligned} r_1 &= D\left[1 + 2\frac{(x\cos\theta + z\sin\theta)}{D} + \frac{x^2 + y^2 + z^2}{D^2}\right]^{1/2}, \\ r_2 &= D\left[1 + 2\frac{(-x\cos\theta + z\sin\theta)}{D} + \frac{x^2 + y^2 + z^2}{D^2}\right]^{1/2}. \end{aligned} \quad (10.46)$$

If ϵ is small, $(1 + \epsilon)^{1/2} = 1 + \epsilon/2 - \epsilon^2/8 + \cdots$. Applying this expansion to the equations (10.46), we obtain a path difference which is correct to quadratic terms:

$$r_1 + r_2 - 2D = \frac{x^2\sin^2\theta + y^2 + z^2\cos^2\theta + 2Dz\sin\theta}{D}. \quad (10.47)$$

It is interesting to notice that if the terms in x^2, y^2, z^2 are dropped from Eq. (10.47), we have the path difference for the usual Fraunhofer approximation. To obtain the amplitude at point P, we integrate over the irradiated volume of the sample, and allow for absorption by using half the linear absorption coefficient since we are considering an amplitude rather than an intensity:

$$E_{eu}(SA) = \iiint e^{(2\pi i/\lambda)\{[(x^2\sin^2\theta + y^2 + z^2\cos^2\theta)/D] + 2z\sin\theta\}} e^{-(\mu z/\sin\theta)}\rho_a f\,dx\,dy\,dz. \quad (10.48)$$

Considering first the integration with respect to dz, let

$$Z = \int_0^\infty e^{iA^2z^2} e^{az}\,dz,$$

where

$$A^2 = \frac{2\pi\cos^2\theta}{\lambda D},$$

$$a = (ik - \mu/\sin\theta).$$

With successive integrations by parts, Z is expressed by the asymptotic expansion

$$Z = -\frac{1}{a}\left[1 + i\frac{2A^2}{a^2} - 12\frac{A^4}{a^4} + \cdots\right]. \tag{10.49}$$

The ratio A^2/a^2 is largest for small values of $\sin\theta$. For rather extreme conditions, let $\sin\theta = 0.01$, $\lambda = 10^{-8}$ cm, $D = 16$ cm, and $\mu = 1000/\text{cm}$. For this case, $A^2/a^2 = -2.5 \times 10^{-7}/(1 + 0.015i)$. For larger values of $\sin\theta$, A^2/a^2 is even smaller, and hence it is evident that only the first term of Eq. (10.49) needs to be retained.

For the integration with respect to dx and dy, assume that the primary beam has a rectangular cross section with dimensions $2w$ in the xz-plane and $2v$ in the y-direction. The double integral is represented by

$$XY = \int_{-w/\sin\theta}^{w/\sin\theta}\int_{-v}^{v} e^{(2\pi i/\lambda D)(x^2\sin^2\theta + y^2)}\,dx\,dy.$$

Let

$$\epsilon = \frac{2\sin\theta x}{\sqrt{\lambda D}}, \qquad \eta = \frac{2y}{\sqrt{\lambda D}},$$

$$XY = \frac{\lambda D}{4\sin\theta}\int_{-2w/\sqrt{\lambda D}}^{2w/\sqrt{\lambda D}} e^{i(\pi/2)\epsilon^2}\,d\epsilon \int_{-2v/\sqrt{\lambda D}}^{2v/\sqrt{\lambda D}} e^{i(\pi/2)\eta^2}\,d\eta. \tag{10.50}$$

For practical diffractometer conditions $2w$ and $2v$ are both greater than 1 mm, and with reasonable values such as $\lambda = 10^{-8}$ cm and $D = 16$ cm,

$$\frac{2w}{\sqrt{\lambda D}} \quad \text{or} \quad \frac{2v}{\sqrt{\lambda D}} > \frac{0.10}{\sqrt{16 \times 10^{-8}}} = 250.$$

The integrals of Eq. (10.50) can be expressed in terms of the tabulated Fresnel integrals $C(u)$ and $S(u)$:

$$\int_0^u e^{i(\pi/2)u^2}\,du = C(u) + iS(u).$$

But for $u > 10$, $C(u) + iS(u)$ has closely converged to its limiting value $0.5 + i0.5$. Since the limits in Eq. (10.50) are greater than 250, we can use the limiting values, and hence

$$XY = \frac{\lambda D}{4\sin\theta}(1 + i)^2. \tag{10.51}$$

Combining these results, Eq. (10.48) becomes

$$E_{eu}(SA) = \frac{\rho_a f \lambda D}{4\sin\theta}(1 + i)^2\left(-\frac{1}{a}\right). \tag{10.52}$$

The intensity of the small angle term is then obtained by multiplying Eq. (10.52) by its complex conjugate:

$$I_{eu}(SA) = \frac{\rho_a^2 f^2 \lambda^2 D^2}{4(\mu^2 + k^2 \sin^2 \theta)}. \tag{10.53}$$

For the flat-faced diffractometer sample, the total intensity is given by

$$I_{eu} = \frac{A_0 \rho_a f^2}{2\mu} + \frac{A_0 \rho_a f^2}{2\mu} \int_0^\infty 4\pi r^2 [\rho(r) - \rho_a] \frac{\sin kr}{kr} dr + \frac{\rho_a^2 f^2 \lambda^2 D^2}{4(\mu^2 + k^2 \sin^2 \theta)}. \tag{10.54}$$

The first two terms are of the order of the independent scattering term $A_0 \rho_a f^2 / 2\mu$. The ratio of $I_{eu}(SA)$ to the independent scattering term is

$$\frac{\rho_2^a f^2 \lambda^2 D^2}{4(\mu^2 + k^2 \sin^2 \theta)} \Big/ \frac{A_0 \rho_a f^2}{2\mu} = \frac{\rho_a \lambda^4 D^2 \mu}{2A_0(\mu^2 \lambda^2 + 16\pi^2 \sin^4 \theta)}. \tag{10.55}$$

For an order of magnitude evaluation of the ratio, let $2\theta = 5.8°$, $\sin \theta = 0.05$, $\rho_a = 10^{23}$ atoms/cc, $A_0 = 0.2$ cm^2, $\mu = 100$/cm, $\lambda = 10^{-8}$ cm and $D = 16$ cm. For these values,

$$\frac{\rho_a \lambda^4 D^2 \mu}{2A_0(\mu^2 \lambda^2 + 16\pi^2 \sin^4 \theta)} = 0.064.$$

At $2\theta = 5.8°$, the $I_{eu}(SA)$ is about 6 percent of the independent scattering term; it is small but not negligible. With increasing θ, the ratio drops rapidly and the $I_{eu}(SA)$ becomes completely negligible. However for higher absorption coefficients such as $\mu = 1000$/cm, the $I_{eu}(SA)$ at small angles becomes comparable to the independent scattering curve. To obtain the intensity due to the first two terms of Eq. (10.54), it is necessary to evaluate $I_{eu}(SA)$ and subtract it off.

10.11 MULTIPLE SCATTERING FROM AMORPHOUS SAMPLES

So far we have considered only the single scattering process in which the intensity arriving at the point of observation is due to single scattering of the primary beam by each volume element dV_1. There is also a contribution at the point of observation due to the scattered intensity from dV_1 being scattered again by another volume element dV_2 in the sample. In addition to this double scattering process there can, of course, be a series of higher-order scattering processes. We shall consider here only the double scattering process since it represents the major part of the multiple scattering.

We consider a flat diffractometer sample whose horizontal surface is represented by OO' in Fig. 10.11. The primary beam and the direction of

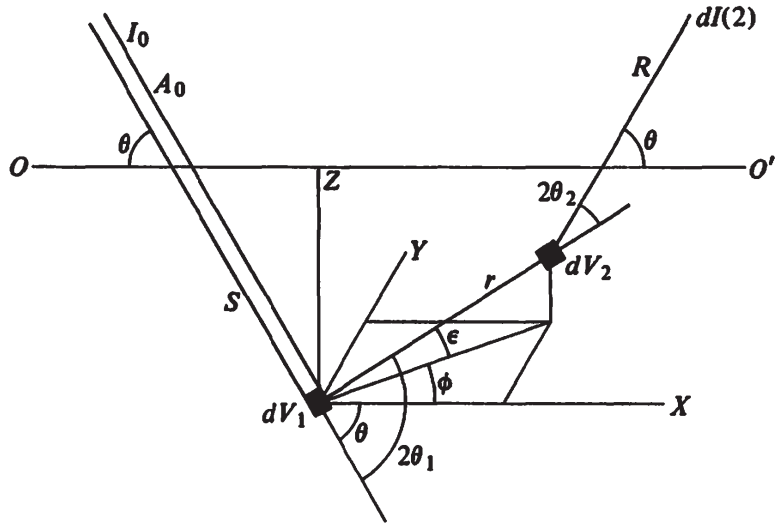

Fig. 10.11 Geometry involved in calculating the intensity of multiple scattering from a flat-faced diffractometer sample.

measurement each make an angle θ with the sample surface. Let n be the number of units of composition per unit volume, and let $J(2\theta_1)$ be the first-order intensity in electron units per unit of composition for scattering at an angle $2\theta_1$. We first neglect the effect of absorption and the polarization factor. Let dI_r be the intensity at distance r from the volume element dV_1 due to scattering of the primary beam by dV_1.

$$dI_r = I_0 \frac{e^4}{m^2c^4r^2} J(2\theta_1) n A_0 \, ds.$$

The power in the primary beam is given by $P_0 = I_0 A_0$, where I_0 is the intensity of the primary beam and A_0 is the cross sectional area. Let $dI(2)$ be the intensity at the point of observation at distance R from the sample, due to the scattering of the intensity dI_r by the volume element dV_2:

$$dI(2) = dI_r \frac{e^4}{m^2c^4R^2} J(2\theta_2) n \, dV_2.$$

In terms of a small solid angle $d\Omega$ centered on the line r, we express the second volume element by $dV_2 = r^2 \, d\Omega \, dr$, where $d\Omega = \cos \epsilon \, d\epsilon \, d\phi$. Combining the previous equations, we obtain

$$dI(2) = P_0 \left(\frac{e^4}{m^2c^4}\right)^2 \frac{n^2}{R^2} J(2\theta_1) J(2\theta_2) \cos \epsilon \, d\epsilon \, d\phi \, ds \, dr. \qquad (10.56)$$

The angle ϵ which is shown in Fig. 10.11 is the angle which the direction r makes above the horizontal plane XY. For positive values of ϵ, the path length in the sample is given by $PL = 2s + r(1 - \sin \epsilon / \sin \theta)$. In the integrations arising from Eq. (10.56), r goes from $r = 0$ to $r = s \sin \theta / \sin \epsilon$,

and assuming a thick sample, s goes from zero to infinity. Allowing now for absorption, the two integrals are readily evaluated:

$$\int_{s=0}^{\infty}\int_{r=0}^{s\sin\theta/\sin\epsilon} e^{-\mu[2s+r(1-\sin\epsilon/\sin\theta)]}\,dr\,ds = \frac{\sin\theta}{2\mu^2(\sin\theta+\sin\epsilon)}. \quad (10.57)$$

For negative values of ϵ, the integrations for both r and s are from zero to infinity. The result is again given by Eq. (10.57) if we replace $\sin\epsilon$ by its magnitude $|\sin\epsilon|$.

If an unpolarized beam is scattered first through an angle $2\theta_1$, and the scattered beam then scattered through an angle $2\theta_2$, so that the final direction makes an angle 2θ with the original primary beam, the polarization factor is given by

$$PF = [\cos^2 2\theta_1 + \cos^2 2\theta_2 + (\cos 2\theta_1 \cos 2\theta_2 - \cos 2\theta)^2]/2 \quad (10.58)$$

Introduce the abbreviations $p_1 = \cos 2\theta_1$ and $p_2 = \cos 2\theta_2$. From the spherical triangles involved in Fig. 10.11,

$$\begin{aligned} p_1 &= \cos 2\theta_1 = \cos\theta\cos\phi\cos\epsilon - \sin\theta\sin\epsilon, \\ p_2 &= \cos 2\theta_2 = \cos\theta\cos\phi\cos\epsilon + \sin\theta\sin\epsilon. \end{aligned} \quad (10.59)$$

Since the intensities of first-order scattering can equally well be represented as functions of p_1 and p_2 we shall now replace $J(2\theta_1)$ and $J(2\theta_2)$ by $J(p_1)$ and $J(p_2)$. Combining Eqs. (10.56) and (10.57), and adding the polarization factor, the intensity $I(2)$ is given by

$$I(2) = P_0\left(\frac{e^4}{m^2c^4}\right)^2\frac{n^2}{R^2}\frac{\sin\theta}{2\mu^2}\int_{\phi=-\pi}^{\pi}\int_{\epsilon=-\pi/2}^{\pi/2}\frac{J(p_1)J(p_2)(PF)\cos\epsilon\,d\epsilon\,d\phi}{\sin\theta+|\sin\epsilon|} \quad (10.60)$$

In changing from a value ϵ to a value $-\epsilon$, there is no change in the integrand of Eq. (10.60) except that p_1 and p_2 are interchanged. Hence we can limit the integration with respect to $d\epsilon$ to the range from $\epsilon = 0$ to $\epsilon = \pi/2$ and multiply the expression by 2. There is no change in the integrand of Eq. (10.60) on replacing ϕ by $-\phi$, and we can again multiply by 2 and restrict the integration to the range $\phi = 0$ to $\phi = \pi$.

$$I(2) = P_0\left(\frac{e^4}{m^2c^4}\right)^2\frac{n^2}{R^2}\frac{2\sin\theta}{\mu^2}\int_{\phi=0}^{\pi}\int_{\epsilon=0}^{\pi/2}\frac{J(p_1)J(p_2)(PF)\cos\epsilon\,d\epsilon\,d\phi}{\sin\theta+\sin\epsilon}. \quad (10.61)$$

On changing from an angle ϕ to the angle $\pi - \phi$, $\cos\phi$ is replaced by $-\cos\phi$. From Eq. (10.59), it follows that p_1 changes to $-p_2$ and p_2 changes to $-p_1$. There is no change in the polarization factor (PF) and hence by adding $J(-p_1)J(-p_2)$ in the integrand, the integration over ϕ can be reduced

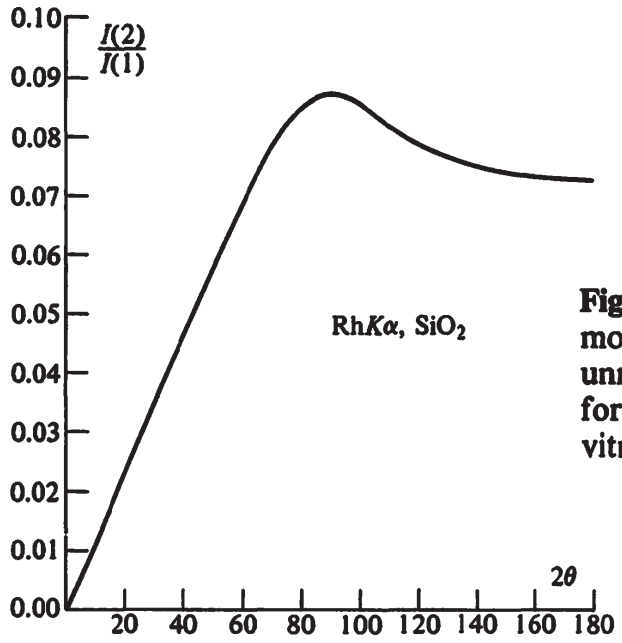

Fig. 10.12 Ratio of the intensity of unmodified double scattering to that of unmodified independent single scattering for a flat-faced diffractometer sample of vitreous SiO_2 using Rh$K\alpha$ radiation.

to the range $\phi = 0$ to $\phi = \pi/2$:

$$I(2) = P_0\left(\frac{e^4}{m^2c^4}\right)^2\frac{n^2}{R^2}\frac{2\sin\theta}{\mu^2}\int_0^{\pi/2}\int_0^{\pi/2}\frac{[J(p_1)J(p_2) + J(-p_1)J(-p_2)]}{\sin\theta + \sin\epsilon} \times (PF)\cos\epsilon\, d\epsilon\, d\phi. \quad (10.62)$$

The ratio n/μ is conveniently expressed by $n/\mu = N/\sum_i A_i\mu_i(m)$, where N is the Avogadro number, the sum is over the unit of composition, and A_i and $\mu_i(m)$ are the atomic weights and mass absorption coefficients of the atoms.

For an unpolarized primary beam, the corresponding first-order intensity $I(1)$ is given by

$$I(1) = P_0\left(\frac{e^4}{m^2c^4}\right)\frac{1}{R^2}\left(\frac{1 + \cos^2 2\theta}{2}\right)J(2\theta)\frac{n}{2\mu}. \quad (10.63)$$

Dividing Eq. (10.62) by Eq. (10.63), we obtain the ratio

$$\frac{I(2)}{I(1)} = \left(\frac{e^4}{m^2c^4}\right)\frac{8N\sin\theta}{(1 + \cos^2 2\theta)J(2\theta)\sum_i A_i\mu_i(m)} \times \int_0^{\pi/2}\int_0^{\pi/2}\frac{[J(p_1)J(p_2) + J(-p_1)J(-p_2)]}{\sin\theta + \sin\epsilon}(PF)\cos\epsilon\, d\epsilon\, d\phi. \quad (10.64)$$

Since the integraions in Eq. (10.64) result in an averaging of $J(p_1)J(p_2)$ over a range of angles, it is a good enough approximation for amorphous samples to express $J(p)$ in terms of the independent scattering curve. If the Compton modified scattering has been eliminated and we are interested only in the $I(2)$ which arises from unmodified scattering, we can express $J(p)$ in terms of $\sum_i f_i^2$. To obtain the ratio of $I(2)$ to the intensity of the unmodified independent single scattering, we also express the $J(2\theta)$ in Eq. (10.64) in

terms of $\sum_i f_i^2$. The integrations involved in Eq. (10.64) are readily programmed for computer calculation. Tabulated correction factors have been given by Warren and Mozzi.[11]

To illustrate the magnitude of the second-order multiple scattering, Fig. 10.12 gives the ratio $I(2)/I(1)$ for vitreous SiO_2 using Rh$K\alpha$ radiation. Both $I(1)$ and $I(2)$ include only the unmodified scattering, and $I(1)$ represents the independent first-order intensity. For this case the multiple scattering is of the order of 8 percent of the single scattering over the range of high angles. Except for samples with very high absorption coefficients, the correction for multiple scattering is too large to be neglected.

REFERENCES

1. P. DEBYE, *Ann. Physik*, **46**, 809 (1915).
2. F. ZERNICKE and J. A. PRINS, *Zeit Physik*, **41**, 184 (1927).
3. P. DEBYE and H. MENKE, *Physikal. Zeit.*, **31**, 797 (1930).
4. B. E. WARREN and G. MAVEL, *Rev. Scient. Inst.*, **36**, 196, (1965).
5. L. P. TARASOV and B. E. WARREN, *Jour. Chem. Phys.*, **4**, 236 (1936).
6. I. N. SNEDDON, *Fourier Transforms*, McGraw-Hill Book Co., Inc., New York (1951).
7. B. E. WARREN, H. KRUTTER, and O. MORNINGSTAR, *J. Amer. Cer. Soc.*, **19**, 202 (1936).
8. J. WASER and V. SCHOMAKER, *Rev. Mod. Phys.*, **25**, 680 (1953).
9. D. T. KEATING, *Jour. Appl. Phys.*, **34**, 923 (1963).
10. N. NORMAN, *Acta. Cryst.*, **10**, 370 (1957).
11. B. E. WARREN and R. L. MOZZI, *Acta. Cryst.*, **21**, 459 (1966).

PROBLEMS

10.1 The benzene molecule C_6H_6 has six carbons at the corners of a hexagon with C—C = 1.39 A. Approximate the scattering from H as completely Compton modified.

a) Express the total intensity (unmodified plus modified) in electron units per molecule $I(eu)/N$ for a sample of benzene vapor.

b) Make a plot of $I(eu)/N$ vs. $(\sin\theta)/\lambda$ covering the range $(\sin\theta)/\lambda$ 0.0–0.6.

c) If the pattern is recorded with Cu$K\alpha$ (λ = 1.542 A), at approximately what scattering angle 2θ will the first peak occur?

10.2 The phosphorus molecule P_4 is assumed to have a tetrahedral structure with a P—P distance 2.20 A. For an x-ray pattern of P_4 vapor, plot the total intensity (unmodified plus modified) in electron units per molecule, covering the range $(\sin\theta)/\lambda$ 0.0–0.5. If the pattern is made with Cu$K\alpha$ (λ = 1.542 A), at approximately what scattering angle 2θ will the first peak occur?

10.3 Consider an oversimplified model of a simple monatomic liquid. Each atom has n nearest neighbors at a distance d, and a uniform density ρ_a of neighboring atomic centers starting at a distance R such that $(4\pi/3)R^3\rho_a = n + 1$. Let N be the number of atoms in the sample.

a) Deduce an expression for $I(eu)/Nf^2$ in terms of n, kd, and $\Phi(kR)$.

b) Let $n = 10$, $d = 4$ A and $R = 5$ A. Plot $I(eu)/Nf^2$ vs. k for the range $k = 0 - 4$.

c) What is the significance of negative values if they appear on a plot such as that of $I(eu)/Nf^2$?

10.4 Suppose that one of the diffraction peaks at $k = k_1$ is measured a little too high so that we introduce an excess intensity $I_E(eu)$ such that $\int I_E(eu)\,dk = E$. Assuming that this excess contribution E is concentrated sharply at $k = k_1$, what is the effect on the radial distribution function $4\pi r^2\rho(r)$ of Eq. (10.14)?

10.5 The intensity of small angle scattering from a small sample taking all orientations, can be expressed by

$$I_{SA}(eu) = \rho_e^2 V \int_{R=0}^{\infty} \langle q(R)\rangle 4\pi R^2 \frac{\sin kR}{kR}\,dR.$$

By a series of integrations by parts show that

$$I_{SA}(eu) = \frac{8\pi\rho_e^2 V}{k^4}\left\{-\left[\frac{d\langle q(R)\rangle}{dR}\right]_{R=0} + \frac{2}{k^2}\left[\frac{d^3\langle q(R)\rangle}{dR^3}\right]_{R=0} + \cdots\right\}.$$

10.6 Let the sample have a volume V and surface area S. Consider a very thin surface layer of thickness R. The volume inside of this surface layer is $V - SR$, and throughout this volume $q(R) = 1$. In the surface layer, $q(R)$ varies.

a) For small R show that $\langle q(R)\rangle$ can be approximated by $\langle q(R)\rangle = 1 - SR/4V$.

b) Combine this result with the answer to Problem 10.5, where the third derivative can be neglected except at very small values of k. Show that with increasing k, the small angle intensity can be approximated by $I_{SA}(eu) = 2\pi\rho_e^2 S/k^4$.

10.7 From Problem 10.5, show that the integral of kI_{SA} over the receiving surface is given by

$$\int kI_{SA}\,dA = I_0 \frac{e^4}{m^2c^4}\pi\rho_e^2\lambda^2 V.$$

10.8 Reformulate Eq. (10.35) to allow for an imaginary part of the atomic scattering factor $f_m \rightarrow f_m + i\Delta f_m''$. It is necessary to remember that for every term ij there is a term ji with the same $r_{ij} = r_{ji}$.

10.9 Suppose that there is a small variation in the distance r_{ij} so that by introducing a distribution function $G(r_{ij})$, the left-hand side of Eq. (10.39) becomes

$$\sum_{uc}\sum_{i}\frac{N_{ij}}{\langle r_{ij}\rangle}\int G(r_{ij})P_{ij}(r)\,dr_{ij}.$$

Develop a general method for determining the distribution function $G(r_{ij})$ from the experimental peak represented by the right-hand side of Eq. (10.39) and the $P_{ij}(r)$ defined by Eq. (10.36).

11

THE EFFECT OF TEMPERATURE VIBRATION ON X-RAY DIFFRACTION

11.1 INTRODUCTION

The development of the theory of the effect of temperature vibration on the diffraction of x-rays in crystals is associated primarily with the names of Debye,[1] Waller,[2] Faxen,[3] Laval,[4] and James.[5] The whole subject was brought together for the first time in an easily readable form in the book by James.[5] Although some of the important newer developments will be included, the treatment which we shall develop in this chapter rests heavily on the excellent presentation by James, and reference should be made to his Chapter 5 for many of the details which will not be included here.

The most familiar effect of temperature vibration is the reduction of the intensities of the crystalline reflections by the well-known Debye temperature factor $\exp[-2M]$. Except for the fact that it gives a method for obtaining the mean square amplitudes of vibration of the atoms $\langle u_s^2 \rangle$, the reduction in intensity is a nuisance, since it weakens the reflections which we desire to measure, and we must make adequate corrections for it in crystal structure determinations where quantitative values of the structure factor are necessary. In addition to reducing the intensities of the crystalline reflections, temperature vibrations produce a diffuse intensity. It was first shown by Laval[4] that the frequency spectrum of the elastic waves which constitute the thermal vibrations, could be obtained from quantitative measurements of this temperature diffuse scattering. This pioneer work of Laval opened up a whole new field involving the x-ray study of the elastic spectrum of crystals. In this chapter, we shall be interested in the diffuse intensity as a means for studying the elastic spectrum, as well as in the more familiar reduction in the intensities of the crystalline reflections.

In Section 3.4 we considered the effect on the intensities of the small displacements of the atoms due to thermal vibrations. For a crystal containing only one kind of atom, the intensities were reduced by a factor $\exp[-2M]$. For the general crystal containing more than one kind of atom, the effect was to replace each f_n in the structure factor by $f_n \exp[-M_n]$.

The factors M_n were expressed by

$$M_n = 8\pi^2\langle u_s^2\rangle_n(\sin^2\theta)/\lambda^2, \tag{11.1}$$

where $\langle u_s^2\rangle_n$ is the mean square component of displacement of atom n normal to the reflecting planes. For simple structures, values of the factor $\exp[-2M]$ can be obtained directly from the measured integrated intensities, and the corresponding values of the root mean square components of displacement $\langle u_s^2\rangle^{1/2}$ turn out to be of the order of 0.2 A at room temperature. Since the nearest neighbor distance in these simple structures is of the order of 3 A, the displacements at room temperature are of the order of 5 percent of the nearest neighbor distance.

Obviously, the vibrations of the different atoms cannot be independent of one another, there must be a coupling between the displacements of the different atoms. This coupling is best expressed by representing the thermal vibrations in the crystal in terms of a set of traveling elastic waves. The elastic waves propagate in a large number of different directions, and in each direction there are waves with a wide variety of wavelengths. At any instant, the displacement of a particular atom is the sum of the displacements due to each of the elastic waves. Since the system of elastic waves which constitute the thermal energy of a crystal is fundamental in expressing the instantaneous displacements of the atoms, it is worthwhile to first consider the propagation of elastic waves in a cubic crystal.

11.2 LONG WAVELENGTH ELASTIC WAVES IN A CUBIC CRYSTAL

For a cubic crystal the normal and shearing stresses (σ and τ) are represented in terms of the normal and shearing strains (ϵ and γ) by means of three elastic moduli c_{11}, c_{12}, and c_{44}:

$$\begin{aligned}
\sigma_x &= c_{11}\epsilon_x + c_{12}\epsilon_y + c_{12}\epsilon_z,\\
\sigma_y &= c_{12}\epsilon_x + c_{11}\epsilon_y + c_{12}\epsilon_z,\\
\sigma_z &= c_{12}\epsilon_x + c_{12}\epsilon_y + c_{11}\epsilon_z,\\
\tau_{yz} &= c_{44}\gamma_{yz},\\
\tau_{zx} &= c_{44}\gamma_{zx},\\
\tau_{xy} &= c_{44}\gamma_{xy},
\end{aligned} \tag{11.2}$$

Examples of elastic moduli for a few cubic crystals are given in Table 11.1. Crystals in which the atoms are at symmetry centers and the forces are central, satisfy the Cauchy relation $c_{44} = c_{12}$; examples are NaCl and KCl. Crystals in which $2c_{44} = (c_{11} - c_{12})$, satisfy the Isotropy condition; W satisfies the condition very closely and Al approximately.

Table 11.1

ELASTIC MODULI FOR SEVERAL CUBIC CRYSTALS AT ROOM TEMPERATURE IN UNITS OF 10^{12} dynes/cm^2

	c_{11}	c_{12}	c_{44}	$2c_{44}/(c_{11}-c_{12})$
NaCl	0.486	0.127	0.128	0.71
KCl	0.40	0.062	0.062	0.36
Na	0.055	0.042	0.049	7.5
W	5.01	1.98	1.51	1.0
Al	1.08	0.62	0.28	1.2
Cu	1.684	1.214	0.754	3.2

Following the treatment of deLaunay,[6] we let uvw be the components of displacement at position xyz. The strains are then expressed as

$$\epsilon_x = \frac{\partial u}{\partial x}, \qquad \gamma_{yz} = \frac{\partial v}{\partial z} + \frac{\partial w}{\partial y},$$

$$\epsilon_y = \frac{\partial v}{\partial y}, \qquad \gamma_{zx} = \frac{\partial w}{\partial x} + \frac{\partial u}{\partial z},$$

$$\epsilon_z = \frac{\partial w}{\partial z}, \qquad \gamma_{xy} = \frac{\partial u}{\partial y} + \frac{\partial v}{\partial x}.$$

With this representation, Eqs. (11.2) become

$$\begin{aligned}
\sigma_x &= c_{11}\frac{\partial u}{\partial x} + c_{12}\left(\frac{\partial v}{\partial y} + \frac{\partial w}{\partial z}\right),\\
\sigma_y &= c_{11}\frac{\partial v}{\partial y} + c_{12}\left(\frac{\partial u}{\partial x} + \frac{\partial w}{\partial z}\right),\\
\sigma_z &= c_{11}\frac{\partial w}{\partial z} + c_{12}\left(\frac{\partial u}{\partial x} + \frac{\partial v}{\partial y}\right),\\
\tau_{yz} &= c_{44}\left(\frac{\partial v}{\partial z} + \frac{\partial w}{\partial y}\right),\\
\tau_{zx} &= c_{44}\left(\frac{\partial w}{\partial x} + \frac{\partial u}{\partial z}\right),\\
\tau_{xy} &= c_{44}\left(\frac{\partial u}{\partial y} + \frac{\partial v}{\partial x}\right).
\end{aligned} \tag{11.3}$$

For a small volume element $dx\,dy\,dz$, we now set the resultant force equal to the mass times the acceleration. For X components of force, this

condition is expressed by

$$\frac{\partial \sigma_x}{\partial x}\,dx\,dy\,dz + \frac{\partial \tau_{xy}}{\partial y}\,dy\,dx\,dz + \frac{\partial \tau_{zx}}{\partial z}\,dz\,dx\,dy = \rho\,dx\,dy\,dz\,\frac{\partial^2 u}{\partial t^2},$$

where ρ is the density. Simplifying, and writing similar equations for the other components, we obtain

$$\begin{aligned}
\frac{\partial \sigma_x}{\partial x} + \frac{\partial \tau_{xy}}{\partial y} + \frac{\partial \tau_{zx}}{\partial z} &= \rho \frac{\partial^2 u}{\partial t^2}, \\
\frac{\partial \sigma_y}{\partial y} + \frac{\partial \tau_{xy}}{\partial x} + \frac{\partial \tau_{yz}}{\partial z} &= \rho \frac{\partial^2 v}{\partial t^2}, \\
\frac{\partial \sigma_z}{\partial z} + \frac{\partial \tau_{zy}}{\partial y} + \frac{\partial \tau_{zx}}{\partial x} &= \rho \frac{\partial^2 w}{\partial t^2}.
\end{aligned} \tag{11.4}$$

By substituting Eqs. (11.3) into Eqs. (11.4), we can eliminate the stresses:

$$\begin{aligned}
c_{11}\frac{\partial^2 u}{\partial x^2} + c_{12}\left(\frac{\partial^2 v}{\partial x\,\partial y} + \frac{\partial^2 w}{\partial x\,\partial z}\right) + c_{44}\left(\frac{\partial^2 u}{\partial y^2} + \frac{\partial^2 v}{\partial x\,\partial y} + \frac{\partial^2 w}{\partial x\,\partial z} + \frac{\partial^2 u}{\partial z^2}\right) &= \rho \frac{\partial^2 u}{\partial t^2}, \\
c_{11}\frac{\partial^2 v}{\partial y^2} + c_{12}\left(\frac{\partial^2 u}{\partial x\,\partial y} + \frac{\partial^2 w}{\partial y\,\partial z}\right) + c_{44}\left(\frac{\partial^2 v}{\partial x^2} + \frac{\partial^2 v}{\partial z^2} + \frac{\partial^2 u}{\partial x\,\partial y} + \frac{\partial^2 w}{\partial y\,\partial z}\right) &= \rho \frac{\partial^2 v}{\partial t^2}, \\
c_{11}\frac{\partial^2 w}{\partial z^2} + c_{12}\left(\frac{\partial^2 u}{\partial x\,\partial z} + \frac{\partial^2 v}{\partial y\,\partial z}\right) + c_{44}\left(\frac{\partial^2 w}{\partial x^2} + \frac{\partial^2 w}{\partial y^2} + \frac{\partial^2 u}{\partial x\,\partial z} + \frac{\partial^2 v}{\partial y\,\partial z}\right) &= \rho \frac{\partial^2 w}{\partial t^2}.
\end{aligned} \tag{11.5}$$

We now look for a solution to Eqs. (11.5) in terms of a traveling plane wave whose propagation direction **g** has direction cosines lmn, and whose vibration direction **e** has direction cosines ABC. If a is the amplitude of the wave, V the velocity, and Λ the wavelength, the components of displacement are expressed by

$$\begin{aligned}
u &= Aa \exp\,[(2\pi i/\Lambda)(Vt - lx - my - nz)], \\
v &= Ba \exp\,[(2\pi i/\Lambda)(Vt - lx - my - nz)], \\
w &= Ca \exp\,[(2\pi i/\Lambda)(Vt - lx - my - nz)].
\end{aligned} \tag{11.6}$$

By substituting the values of uvw expressed by Eqs. (11.6) into the Eqs. (11.5), we obtain the three conditions which determine the velocities and vibration directions of the possible elastic waves:

$$\begin{aligned}
\{c_{11}l^2 + c_{44}(m^2 + n^2) - \rho v^2\}A + (c_{12} + c_{44})lmB + (c_{12} + c_{44})lnC &= 0, \\
(c_{12} + c_{44})lmA + \{c_{11}m^2 + c_{44}(n^2 + l^2) - \rho v^2\}B + (c_{12} + c_{44})mnC &= 0, \\
(c_{12} + c_{44})nlA + (c_{12} + c_{44})mnB + \{c_{11}n^2 + c_{44}(l^2 + m^2) - \rho v^2\}C &= 0.
\end{aligned} \tag{11.7}$$

For any specified propagation direction, the values of *lmn* are fixed, and Eqs. (11.7) can be considered as a set of homogeneous equations in the variables *ABC*. For a solution other than $A = B = C = 0$, the determinant of the coefficients must vanish, and this condition leads to a cubic equation in the variable ρv^2. There are three independent waves for each direction *lmn*, and the velocities and vibration directions *ABC* can be obtained from Eqs. (11.7). For the three simple directions [100], [110], and [111], the velocities and vibration directions can be obtained directly from Eqs. (11.7) without needing to solve a cubic equation.

For waves propagating in the [100] direction, $l = 1$, $m = 0$, $n = 0$, and Eqs. (11.7) become

$$(c_{11} - \rho v^2)A = 0,$$
$$(c_{44} - \rho v^2)B = 0,$$
$$(c_{44} - \rho v^2)C = 0.$$

The three solutions of these equations are

$$\begin{aligned} v_1^2 &= c_{11}/\rho, \quad & A_1 &= 1, \quad & B_1 &= 0, \quad & C_1 &= 0, \\ v_2^2 &= c_{44}/\rho, \quad & A_2 &= 0, \quad & B_2^2 + C_2^2 &= 1, \\ v_3^2 &= c_{44}/\rho, \quad & A_3 &= 0, \quad & B_3^2 + C_3^2 &= 1. \end{aligned} \tag{11.8}$$

The first solution represents a pure longitudinal wave. The second and third represent pure transverse waves, but this is a degenerate case and the vibration directions can be in any direction normal to the propagation direction. To have three independent waves it is convenient to choose $A_2 = 0$, $B_2 = 1$, $C_2 = 0$ and $A_3 = 0$, $B_3 = 0$, $C_3 = 1$ for the vibration directions of the transverse waves.

For waves propagating in the [110] direction, we set $l = 1/\sqrt{2}$, $m = 1/\sqrt{2}$, $n = 0$. Inserting these values in Eqs. (11.7) we get three equations, and to put these in the form of products we use the sum of the first and second, the difference of the first and second, and the third equation.

$$(c_{11} + c_{12} + 2c_{44} - 2\rho v^2)(A + B) = 0,$$
$$(c_{11} - c_{12} - 2\rho v^2)(A - B) = 0,$$
$$(c_{44} - \rho v^2)C = 0.$$

The three solutions are

$$\begin{aligned} 2\rho v_1^2 &= c_{11} + c_{12} + 2c_{44}, \quad & A_1 &= 1/\sqrt{2}, \quad & B_1 &= 1/\sqrt{2}, \quad & C_1 &= 0, \\ 2\rho v_2^2 &= c_{11} - c_{12}, \quad & A_2 &= 1/\sqrt{2}, \quad & B_2 &= -1/\sqrt{2}, \quad & C_2 &= 0, \\ \rho v_3^2 &= c_{44}, \quad & A_3 &= 0, \quad & B_3 &= 0, \quad & C_3 &= 1. \end{aligned} \tag{11.9}$$

In this case there are three different velocities, the first represents a pure longitudinal wave and the other two represent pure transverse waves.

For waves propagating in the [111] direction, we set $l = m = n = 1/\sqrt{3}$ in Eqs. (11.7). With the resulting three equations, we take first the sum of the three, then the first minus the second, and finally the first plus the second minus twice the third:

$$(c_{11} + 2c_{12} + 4c_{44} - 3\rho v^2)(A + B + C) = 0,$$
$$(c_{11} - c_{12} + c_{44} - 3\rho v^2)(A - B) = 0,$$
$$(c_{11} - c_{12} + c_{44} - 3\rho v^2)(A + B - 2C) = 0.$$

The solutions are

$$3\rho v_1^2 = c_{11} + 2c_{12} + 4c_{44}, \quad A_1 = 1/\sqrt{3}, \quad B_1 = 1/\sqrt{3}, \quad C_1 = 1/\sqrt{3},$$
$$3\rho v_2^2 = c_{11} - c_{12} + c_{44}, \quad A_2 + B_2 + C_2 = 0, \tag{11.10}$$
$$3\rho v_3^2 = c_{11} - c_{12} + c_{44}, \quad A_3 + B_3 + C_3 = 0.$$

The first solution is that for a pure longitudinal wave and the other two represent pure transverse waves. This is again a degenerate case, to have independent transverse waves we can choose any two mutually perpendicular transverse directions such as $A_2 = 1/\sqrt{2}$, $B_2 = -1/\sqrt{2}$, $C_2 = 0$ and $A_3 = 1/\sqrt{6}$, $B_3 = 1/\sqrt{6}$, $C_3 = -2/\sqrt{6}$.

For directions other than the three simple directions [100], [110], and [111], the three waves are independent, but in general they are no longer pure longitudinal and pure transverse. However, the vibration direction is seldom off more than a few degrees. The velocities which have been derived in this section apply only to elastic waves of such long wavelength that the lattice nature of the crystal can be neglected. However, in the interpretation of the temperature diffuse scattering, we shall be very much interested in these long wavelength limits for the velocities, and in the vibration directions for the simple propagation directions. We now consider the restrictions which are placed on the kinds of possible elastic waves by the lattice nature of the sample and its finite size.

11.3 RESTRICTIONS DUE TO THE LATTICE NATURE AND FINITE SIZE OF THE SAMPLE

In a periodic lattice, there is no need to consider elastic waves of wavelength less than a certain minimum value because these are equivalent to waves of a longer wavelength. To illustrate the point consider the transverse waves in a one-dimensional crystal with repetition distance a as shown by Fig. 11.1. Waves of wavelength $\Lambda = 4a$ and $\Lambda = 2a$ are properly represented, but

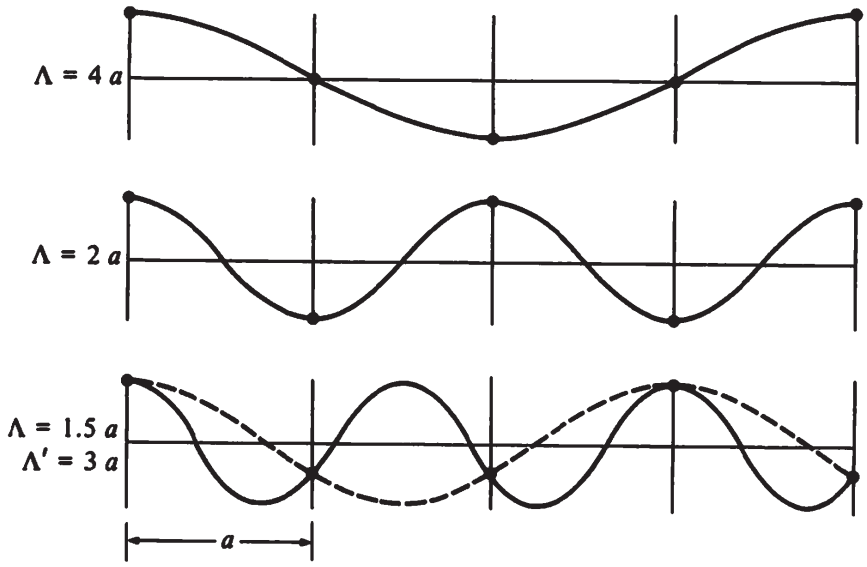

Fig. 11.1 Representation of elastic waves in a one-dimensional crystal. The wave with $\Lambda = 1.5\,a$ is equivalent to a wave with $\Lambda = 3\,a$, illustrating the point that it is not necessary to consider any wave with $\Lambda < 2\,a$, since it is included among the waves with $\Lambda > 2\,a$.

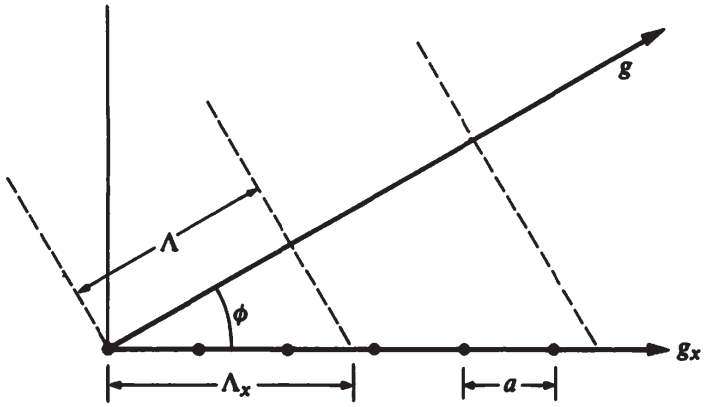

Fig. 11.2 Illustration of an elastic wave with wave vector **g** in a simple cubic crystal with repetition length a.

the wave of wavelength $\Lambda = 1.5\,a$ is seen to be equivalent to a wave with $\Lambda' = 3\,a$. Any wave of wavelength $\Lambda < 2\,a$ need not be discussed, because it is completely equivalent to a wave with $\Lambda' > 2\,a$.

To extend the argument to a simple cubic crystal with one atom per cell, we consider the elastic wave represented in Fig. 11.2 by the vector **g** whose direction gives the direction of propagation and whose length is determined by $|\mathbf{g}| = 1/\Lambda$. In the x-direction the crystal repeats at intervals a, and along this direction the elastic wave repeats at intervals Λ_x. But we have just seen that for each dimension $\Lambda_x > 2\,a$. Since $\Lambda_x = \Lambda/\cos\phi = 1/g_x$ and for a cubic crystal $1/|\mathbf{a}| = |\mathbf{b}|$, where **b** is a reciprocal vector, the restric-

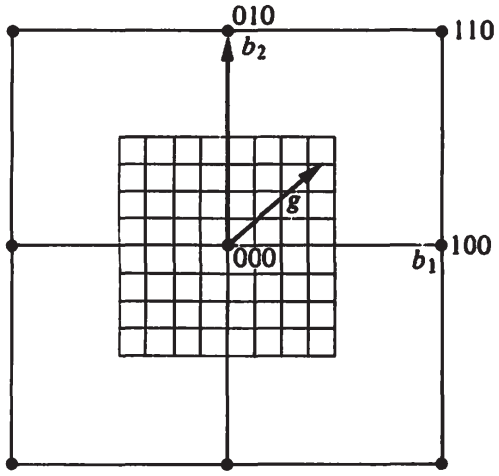

Fig. 11.3 The first Brillouin zone for a simple cubic crystal. All possible wave vectors g must terminate within this zone. The zone is divided by a grid with intervals b/N_1, b/N_2, and b/N_3.

tion is expressed by $g_x < |\mathbf{b}|/2$. The same conditions apply to all three dimensions, and hence for a one atom simple cubic crystal, the only possible elastic waves are those whose components satisfy the following conditions:

$$\begin{aligned} -|\mathbf{b}_1|/2 < g_x < |\mathbf{b}_1|/2, \\ -|\mathbf{b}_2|/2 < g_y < |\mathbf{b}_2|/2, \\ -|\mathbf{b}_3|/2 < g_z < |\mathbf{b}_3|/2. \end{aligned} \tag{11.11}$$

The first Brillouin zone is constructed by drawing vectors from the origin to the various active reciprocal lattice points which surround it. The volume about the origin, which is enclosed by planes which bisect each of these vectors, is called the first Brillouin zone. For the one atom simple cubic case, the first Brillouin zone is the cube shown by Fig. 11.3. Equations (11.11) are just the conditions which restrict all the possible g vectors to the first Brillouin zone. For the body-centered cubic case (2 atoms per cubic cell) the first Brillouin zone is a dodecahedron whose faces are the planes bisecting the 12 vectors to 110 type points in the reciprocal lattice. For the face-centered cubic case (4 atoms per cubic cell) the first Brillouin zone is a 14-faced figure made up of 8 faces which are bisectors of vectors to 111 type points and 6 faces bisecting vectors to 200 type points. For all three cases (simple, body-centered, or face-centered cubic), the restrictions of Eqs. (11.11) are generalized by stating that the g vectors are confined to the first Brillouin zone.

That all g vectors must be confined to the first Brillouin zone is the restriction arising from the lattice nature of the crystal. There is also a limit to the possible g vectors due to the finite size of the crystal. For a crystal containing N atoms, the number of g vectors is N, and the terminal points of these vectors are distributed uniformly throughout the first Brillouin zone. Since a rigorous general proof of this important fact is difficult, it is customary to content oneself with a simple argument which makes the result plausible. Assume that the crystal is a rectangular block of

dimensions N_1a_1, N_2a_2, and N_3a_3. Depending on whether or not there are constraints, the surface of the crystal will represent displacement or stress nodes, and this places restrictions on the possible $\mathbf{g}$ vectors. Instead of considering boundary conditions, we can imagine that our rectangular block forms part of an infinite lattice in which the wave system repeats identically in blocks N_1a_1, N_2a_2, N_3a_3. Because of this repetition, the Λ_x of Fig. 11.2 must satisfy the condition $p\Lambda_x = N_1a_1$, where p is an integer. Applying the same reasoning to all three dimensions we obtain the three conditions

$$\begin{aligned} g_x &= p\,|\mathbf{b}_1|/N_1, \\ g_y &= q\,|\mathbf{b}_2|/N_2, \\ g_z &= r\,|\mathbf{b}_3|/N_3. \end{aligned} \tag{11.12}$$

The effect of these conditions is to subdivide the first Brillouin zone of Fig. 11.3 by a grid with grid intervals b_1/N_1, b_2/N_2, and b_3/N_3. The only allowed $\mathbf{g}$ vectors are those which terminate on the points of this grid. Since Eqs. (11.11) limit the values of p, q, and r to integers between $\pm N_1/2$, $\pm N_2/2$, and $\pm N_3/2$, the total number of grid points is $N_1N_2N_3 = N$, where N is the number of atoms in the crystal. For each wave vector $\mathbf{g}$, there are three independent waves, and the total number of waves is $3N$. Instead of specifying the three components of displacement of N atoms, we specify the amplitudes of the $3N$ independent elastic waves. These $3N$ waves become the normal coordinates of the system.

11.4 INTENSITY FROM A CUBIC CRYSTAL WITH ONE ATOM PER CELL

We represent the position of each atom in the crystal by $\mathbf{r}_n = n_1\mathbf{a}_1 + n_2\mathbf{a}_2 + n_3\mathbf{a}_3$. Due to the elastic wave of wave vector $\mathbf{g}$ and vibration direction $\mathbf{e}_j$ ($j = 1, 2, 3$) the displacement of atom n can be expressed by

$$\mathbf{u}_n(gj) = a_{gj}\mathbf{e}_{gj} \cos\{\omega_{gj}t - 2\pi\mathbf{g}\cdot\mathbf{r}_n - \delta_{gj}\},$$

where a_{gj} is the amplitude of the wave, $\mathbf{e}_{gj}$ is a unit vector giving the vibration direction, ω_{gj} is the circular frequency, and δ_{gj} is an arbitrary phase factor which allows for the fact that there are no phase relations among the thermal waves. The resultant displacement of atom n due to all the waves is expressed by

$$\mathbf{u}_n = \sum_{gj} a_{gj}\mathbf{e}_{gj} \cos\{\omega_{gj}t - 2\pi\mathbf{g}\cdot\mathbf{r}_n - \delta_{gj}\}. \tag{11.13}$$

With the abbreviations $k = 2\pi/\lambda$ and $\mathbf{S} = \mathbf{s} - \mathbf{s}_0$, the intensity in electron units is given by

$$I_{eu} = f^2 \sum_m \sum_n e^{ik\mathbf{S}\cdot(\mathbf{r}_m - \mathbf{r}_n)}.$$

Due to the thermal vibrations, the atoms have small displacements, $\mathbf{r}_m \to \mathbf{r}_m + \mathbf{u}_m$ and the instantaneous value of the intensity becomes

$$I_{eu} = f^2 \sum_m \sum_n e^{ik\mathbf{S}\cdot(\mathbf{r}_m - \mathbf{r}_n)} e^{ik\mathbf{S}\cdot(\mathbf{u}_m - \mathbf{u}_n)}.$$

With the abbreviation

$$p_{mn} = k\mathbf{S} \cdot (\mathbf{u}_m - \mathbf{u}_n), \tag{11.14}$$

the time average of the intensity is expressed by

$$I_{eu} = f^2 \sum_m \sum_n e^{ik\mathbf{S}\cdot(\mathbf{r}_m - \mathbf{r}_n)} \langle e^{ip_{mn}} \rangle.$$

As shown in the derivation of Eq. (3.20), if p_{mn} is small with equal probability of being positive or negative, or if it follows a Gaussian probability:

$$\langle e^{ip_{mn}} \rangle = e^{-\langle p_{mn}^2 \rangle / 2}. \tag{11.15}$$

Allowing for thermal vibrations, the average intensity is given by

$$I_{eu} = f^2 \sum_m \sum_n e^{ik\mathbf{S}\cdot(\mathbf{r}_m - \mathbf{r}_n)} e^{-\langle p_{mn}^2 \rangle / 2}. \tag{11.16}$$

We now express $\langle p_{mn}^2 \rangle$ by means of Eqs. (11.14) and (11.13):

$$\langle p_{mn}^2 \rangle = \left\langle \left[\sum_{gj} k\mathbf{S} \cdot \mathbf{e}_{gj} a_{gj} \{ \cos(\omega_{gj} t - 2\pi \mathbf{g} \cdot \mathbf{r}_m - \delta_{gj}) - \cos(\omega_{gj} t - 2\pi \mathbf{g} \cdot \mathbf{r}_n - \delta_{gj}) \} \right]^2 \right\rangle.$$

The cross product terms involve waves gj and $g'j'$, and since the phases of two different waves δ_{gj} and $\delta_{g'j'}$ are completely independent, the averages of all the cross product terms will vanish:

$$\langle p_{mn}^2 \rangle = \sum_{gj} (k\mathbf{S} \cdot \mathbf{e}_{gj})^2 \times \langle a_{gj}^2 \{ \cos(\omega_{gj} t - 2\pi \mathbf{g} \cdot \mathbf{r}_m - \delta_{gj}) - \cos(\omega_{gj} t - 2\pi \mathbf{g} \cdot \mathbf{r}_n - \delta_{gj}) \}^2 \rangle.$$

Using the relation $2 \cos A \cos B = \cos(A - B) + \cos(A + B)$, it follows that

$$\begin{aligned} \langle (\cos x_1 - \cos x_2)^2 \rangle &= \langle \cos^2 x_1 \rangle + \langle \cos^2 x_2 \rangle - 2\langle \cos x_1 \cos x_2 \rangle \\ &= 1 - \langle \cos(x_1 - x_2) \rangle - \langle \cos(x_1 + x_2) \rangle. \end{aligned}$$

With this simplification, our expression for $\langle p_{mn}^2 \rangle$ becomes

$$\langle p_{mn}^2 \rangle = \sum_{gj} (k\mathbf{S} \cdot \mathbf{e}_{gj})^2 \langle a_{gj}^2 \rangle \times [1 - \langle \cos 2\pi \mathbf{g} \cdot (\mathbf{r}_m - \mathbf{r}_n) \rangle - \langle \cos\{2\omega_{gj} t - 2\pi \mathbf{g} \cdot (\mathbf{r}_m - \mathbf{r}_n) - 2\delta_{gj}\} \rangle].$$

Since the average of the last term is zero,

$$\tfrac{1}{2} \langle p_{mn}^2 \rangle = \tfrac{1}{2} \sum_{gj} (k\mathbf{S} \cdot \mathbf{e}_{gj})^2 \langle a_{gj}^2 \rangle [1 - \langle \cos 2\pi \mathbf{g} \cdot (\mathbf{r}_m - \mathbf{r}_n) \rangle]. \tag{11.17}$$

The amplitude squared for each wave gj is written with an average $\langle a_{gj}^2 \rangle$, since the elastic waves due to thermal vibrations are completely random, starting and stopping and changing in amplitude, so that only an average square can be discussed. The first term in Eq. (11.17) has a simple significance. Let u_s be the component of u parallel to the diffraction vector $\mathbf{S} = \mathbf{s} - \mathbf{s}_0$, and hence the component of u normal to the reflecting planes:

$$\langle u_s^2 \rangle = \left\langle \left(\sum_{gj} u_{gjs} \right)^2 \right\rangle = \sum_{gj} \langle u_{gj}^2 \rangle \cos^2 (S, e_{gj}) = \sum_{gj} \tfrac{1}{2} \langle a_{gj}^2 \rangle \cos^2 (S, e_{gj}).$$

Since u_{gj} varies sinusoidally between $\pm a_{gj}$, the $\frac{1}{2}$ comes from the average of $\sin^2 \omega t$. With this relation

$$\tfrac{1}{2} \sum_{gj} (k\mathbf{S} \cdot \mathbf{e}_{gj})^2 \langle a_{gj}^2 \rangle = \left(\frac{4\pi \sin \theta}{\lambda} \right)^2 \cos^2 (S, e_{gj}) \langle a_{gj}^2 \rangle / 2 = \left(\frac{4\pi \sin \theta}{\lambda} \right)^2 \langle u_s^2 \rangle.$$

In Section 3.4 we introduced the abbreviation

$$2M = \left(\frac{4\pi \sin \theta}{\lambda} \right)^2 \langle u_s^2 \rangle, \tag{11.18}$$

and hence the first term in Eq. (11.17) has the simple significance

$$\tfrac{1}{2} \sum_{gj} (k\mathbf{S} \cdot \mathbf{e}_{gj})^2 \langle a_{gj}^2 \rangle = 2M. \tag{11.19}$$

We now wish to express the mean square amplitude of a wave in terms of its thermal energy. The kinetic energy of the crystal is given by

$$E_{\text{kin}} = \tfrac{1}{2} \sum_n m \dot{u}_n^2.$$

But from Eq. (11.13),

$$\dot{u}_n = -\sum_{gj} a_{gj} \omega_{gj} \sin (\omega_{gj} t - 2\pi \mathbf{g} \cdot \mathbf{r}_n - \delta_{gj}).$$

The mean square average is

$$\langle \dot{u}_n^2 \rangle = \tfrac{1}{2} \sum_{gj} \langle a_{gj}^2 \rangle \omega_{gj}^2$$

and the mean kinetic energy is given by

$$\langle E_{\text{kin}} \rangle = \tfrac{1}{4} Nm \sum_{gj} \langle a_{gj}^2 \rangle \omega_{gj}^2.$$

The mean total energy is twice the mean kinetic energy. If $\langle E_{gj} \rangle$ is the average energy associated with the wave gj, then

$$\langle E_{\text{total}} \rangle = \tfrac{1}{2} Nm \sum_{gj} \omega_{gj}^2 \langle a_{gj}^2 \rangle = \sum_{gj} \langle E_{gj} \rangle,$$

and the average energy per wave is given by

$$\langle E_{gj}\rangle = \tfrac{1}{2}Nm\omega_{gj}^2\langle a_{gj}^2\rangle. \tag{11.20}$$

Treating each elastic wave as a harmonic oscillator, the energy per wave is given by the quantum theory of the harmonic oscillator:

$$\langle E_{gj}\rangle = \left\{\frac{1}{\exp\left[\hbar\omega_{gj}/kT\right]-1}+\frac{1}{2}\right\}\hbar\omega_{gj}, \tag{11.21}$$

where $\hbar = h/2\pi$. For T large we can expand the exponential, and keeping terms through the quadratic, we obtain

$$\langle E_{gj}\rangle \to kT.$$

In general the mean square amplitude of each wave is expressed in terms of the mean energy of the wave by the relation

$$\langle a_{gi}^2\rangle = \frac{2\langle E_{gj}\rangle}{Nm\omega_{gj}^2}, \tag{11.22}$$

and for high temperature, the mean square amplitude can be approximated by

$$\langle a_{gj}^2\rangle = \frac{2kT}{Nm\omega_{gj}^2}. \tag{11.23}$$

We now abbreviate Eq. (11.17) by writing

$$\tfrac{1}{2}\langle p_{mn}^2\rangle = \sum_{gj} G_{gj}[1-\cos 2\pi\mathbf{g}\cdot(\mathbf{r}_m-\mathbf{r}_n)], \tag{11.24}$$

where

$$G_{gj} = \tfrac{1}{2}(k\mathbf{S}\cdot\mathbf{e}_{gj})^2\langle a_{gj}^2\rangle \tag{11.25}$$

and

$$\sum_{gj} G_{gj} = 2M.$$

The diffracted intensity is obtained by inserting Eq. (11.24) in Eq. (11.16):

$$I_{eu} = f^2e^{-2M}\sum_m\sum_n e^{(2\pi i/\lambda)\mathbf{S}\cdot(\mathbf{r}_m-\mathbf{r}_n)}e^{\sum G_{gj}\cos 2\pi\mathbf{g}\cdot(\mathbf{r}_m-\mathbf{r}_n)}. \tag{11.26}$$

Treating $\sum_{gj} G_{gj}\cos 2\pi\mathbf{g}\cdot(\mathbf{r}_m-\mathbf{r}_n)$ as a small quantity and making the expansion $\exp[x] = 1 + x + x^2/2 + \ldots$, we obtain the intensity as a sum of terms:

$$\begin{aligned} I_{eu} = {} & f^2e^{-2M}\sum_m\sum_n e^{(2\pi i/\lambda)\mathbf{S}\cdot(\mathbf{r}_m-\mathbf{r}_n)} \\ & + f^2e^{-2M}\sum_m\sum_n e^{(2\pi i/\lambda)\mathbf{S}\cdot(\mathbf{r}_m-\mathbf{r}_n)}\sum_{gj} G_{gj}\cos 2\pi\mathbf{g}\cdot(\mathbf{r}_m-\mathbf{r}_n) \\ & + f^2e^{-2M}\sum_m\sum_n e^{(2\pi i/\lambda)\mathbf{S}\cdot(\mathbf{r}_m-\mathbf{r}_n)}\left[\sum_{gj} G_{gj}\cos 2\pi\mathbf{g}\cdot(\mathbf{r}_m-\mathbf{r}_n)\right]^2\Big/2. \end{aligned} \tag{11.27}$$

The zero-order term in Eq. (11.27) is the ordinary sharp crystalline reflection reduced by the temperature factor exp $[-2M]$. The first-order term is called the first-order temperature diffuse scattering (first-order TDS). The second-order term is called the second-order TDS. We now abbreviate Eq. (11.27) by writing

$$I(S/\lambda) = f^2 e^{-2M} I_0(S/\lambda) + I_1(S/\lambda) + I_2(S/\lambda), \tag{11.28}$$

where

$$I_0(S/\lambda) = \sum_m \sum_n e^{(2\pi i/\lambda)\mathbf{S}\cdot(\mathbf{r}_m - \mathbf{r}_n)}. \tag{11.29}$$

11.5 THE FIRST-ORDER TEMPERATURE DIFFUSE SCATTERING

The first-order temperature diffuse scattering is given by Eq. (11.27):

$$I_1(S/\lambda) = f^2 e^{-2M} \sum_m \sum_n \sum_{gj} e^{(2\pi i/\lambda)\mathbf{S}\cdot(\mathbf{r}_m - \mathbf{r}_n)} G_{gj} \cos 2\pi \mathbf{g}\cdot(\mathbf{r}_m - \mathbf{r}_n).$$

By means of the identity

$$2\cos 2\pi \mathbf{g}\cdot(\mathbf{r}_m - \mathbf{r}_n) = e^{2\pi i \mathbf{g}\cdot(\mathbf{r}_m - \mathbf{r}_n)} + e^{-2\pi i \mathbf{g}\cdot(\mathbf{r}_m - \mathbf{r}_n)}$$

the first-order TDS can be expressed by

$$I_1(S/\lambda) = \tfrac{1}{2} f^2 e^{-2M} \sum_{gj} G_{gj} \sum_m \sum_n \{e^{2\pi i(\mathbf{S}/\lambda + \mathbf{g})\cdot(\mathbf{r}_m - \mathbf{r}_n)} + e^{2\pi i(\mathbf{S}/\lambda - \mathbf{g})\cdot(\mathbf{r}_m - \mathbf{r}_n)}\}.$$

Comparing this with Eq. (11.29) we can write

$$I_1(S/\lambda) = \tfrac{1}{2} f^2 e^{-2M} \sum_{gj} G_{gj}\{I_0(\mathbf{S}/\lambda + \mathbf{g}) + I_0(\mathbf{S}/\lambda - \mathbf{g})\}. \tag{11.30}$$

The crystalline reflection $I_0(S/\lambda)$ has sharp maxima when the terminal point of the diffraction vector is in the vicinity of a reciprocal lattice point, that is to say, when $\mathbf{S}/\lambda = \mathbf{H}_{hkl}$. In the vicinity of the *hkl*-point in reciprocal space,

$$I_0(S/\lambda) = \frac{\sin^2 \pi N_1 h_1}{(\pi h_1)^2} \frac{\sin^2 \pi N_2 h_2}{(\pi h_2)^2} \frac{\sin^2 \pi N_3 h_3}{(\pi h_3)^2}, \tag{11.31}$$

where $\mathbf{S}/\lambda = \mathbf{H}_{hkl} + h_1\mathbf{b}_1 + h_2\mathbf{b}_2 + h_3\mathbf{b}_3$. The functions $I_0(\mathbf{S}/\lambda \pm \mathbf{g})$ will have sharp maxima at positions $\mathbf{S}/\lambda$ in reciprocal space such that

$$\mathbf{S}/\lambda \pm \mathbf{g} = \mathbf{H}_{hkl}.$$

In terms of the variables $h_1 h_2 h_3$ defined by

$$\mathbf{S}/\lambda \pm \mathbf{g} = \mathbf{H}_{hkl} + h_1\mathbf{b}_1 + h_2\mathbf{b}_2 + h_3\mathbf{b}_3, \tag{11.32}$$

the function $I_0(\mathbf{S}/\lambda \pm \mathbf{g})$ is given by the right-hand side of Eq. (11.31).

Since N is very large, the sum over g of Eq. (11.30) can be replaced by an integration over the first Brillouin zone of Fig. (11.3). The density of points is N/b^3. From Eq. (11.32), a volume element for the terminal points of the g vectors is expressed by $dv_g = b^3\, dh_1\, dh_2\, dh_3$. Expressed as an integral,

Eq. (11.30) becomes

$$I_1(S/\lambda) = \tfrac{1}{2}f^2e^{-2M}\sum_j \int G_{gj}\{I_0(\mathbf{S}/\lambda + \mathbf{g}) + I_0(\mathbf{S}/\lambda - \mathbf{g})\}\frac{N}{b^3}\,b^3\,dh_1\,dh_2\,dh_3. \tag{11.33}$$

For a fixed position of measurement in reciprocal space $\mathbf{S}/\lambda$, the only **g**-vectors which contribute to Eq. (11.33) are those for which $I_0(\mathbf{S}/\lambda \pm \mathbf{g})$ is in the vicinity of a maximum. Since G_{gj} is a slowly varying function, we can take it outside of the integral and use the value corresponding to the **g**-vector which makes $I_0(\mathbf{S}/\lambda \pm \mathbf{g})$ a maximum. In the following equations it will be understood that **g** refers to the vector connecting the point of measurement $\mathbf{S}/\lambda$ with the nearest active reciprocal lattice point. The integrals in Eq. (11.33) are readily evaluated

$$\int_{-\infty}^{+\infty}\!\!\int\!\!\int \frac{\sin^2 \pi N_1h_1}{(\pi h_1)^2}\frac{\sin^2 \pi N_2h_2}{(\pi h_2)^2}\frac{\sin^2 \pi N_3h_3}{(\pi h_3)^2}\,dh_1\,dh_2\,dh_3 = N_1N_2N_3 = N,$$

and we obtain

$$I_1(S/\lambda) = \tfrac{1}{2}f^2e^{-2M}\sum_j G_{gj}(N + N)N = f^2e^{-2M}N^2\sum_j G_{gj}. \tag{11.34}$$

From Eqs. (11.25) and (11.22),

$$G_{gj} = \frac{(k\mathbf{S}\cdot\mathbf{e}_{gj})^2\langle E_{gj}\rangle}{Nm\omega_{gj}^2} = \frac{4\pi^2\,|\mathbf{S}/\lambda|^2\cos^2(S, e_{gj})\langle E_{gj}\rangle}{Nm\omega_{gj}^2}.$$

Using this value in Eq. (11.34), we obtain a general expression for the first-order TDS in a crystal with one atom per unit cell:

$$I_1(S/\lambda) = f^2e^{-2M}\frac{4\pi^2N}{m}\,|\mathbf{S}/\lambda|^2\sum_j\langle E_{gj}\rangle\frac{\cos^2(S, e_{gj})}{\omega_{gj}^2}. \tag{11.35}$$

If V_{gj} is the velocity of the gj-wave, $\omega_{gj} = 2\pi\,|\mathbf{g}|\,V_{gj}$, and for temperatures high enough to set $\langle E_{gj}\rangle = kT$, the first-order TDS takes the simpler form

$$I_1(S/\lambda) = f^2e^{-2M}\frac{NkT}{m}\frac{|\mathbf{S}/\lambda|^2}{|\mathbf{g}|^2}\sum_j\frac{\cos^2(S, e_{gj})}{V_{gj}^2}. \tag{11.36}$$

In making a measurement of the diffuse intensity at a position $\mathbf{S}/\lambda$ in reciprocal space, we measure not only the first-order TDS but also the second-order and third-order TDS, as well as the Compton modified scattering. The Compton modified can be computed and subtracted from the measured values, and the third-order TDS is usually negligible. However, the second-order TDS is in general not small enough to neglect, and hence before we can apply Eqs. (11.35) and (11.36), it is necessary to evaluate the second-order TDS.

11.6 THE SECOND-ORDER TEMPERATURE DIFFUSE SCATTERING

From Eqs. (11.27) and (11.28) the second-order TDS is expressed in electron units by

$$I_2(S/\lambda) = \frac{f^2 e^{-2M}}{2} \sum_m \sum_n \sum_{gj} \sum_{g'j'} e^{(2\pi i/\lambda)\mathbf{S}\cdot(\mathbf{r}_m - \mathbf{r}_n)} G_{gj} G_{g'j'} \cos 2\pi \mathbf{g} \cdot (\mathbf{r}_m - \mathbf{r}_n) \times \cos 2\pi \mathbf{g}' \cdot (\mathbf{r}_m - \mathbf{r}_n).$$

Using the relation $2 \cos A \cos B = \cos (A + B) + \cos (A - B)$, and expressing $\cos (A \pm B)$ in the complex exponential form, we obtain

$$I_2(S/\lambda) = \frac{f^2 e^{-2M}}{8} \sum_m \sum_n \sum_{gj} \sum_{g'j'} G_{gj} G_{g'j'} \Big\{ e^{2\pi i[(\mathbf{S}/\lambda)+\mathbf{g}+\mathbf{g}']\cdot(\mathbf{r}_m - \mathbf{r}_n)} + e^{2\pi i[(\mathbf{S}/\lambda)-\mathbf{g}-\mathbf{g}']\cdot(\mathbf{r}_m - \mathbf{r}_n)} + e^{2\pi i[(\mathbf{S}/\lambda)+\mathbf{g}-\mathbf{g}']\cdot(\mathbf{r}_m - \mathbf{r}_n)} + e^{2\pi i[(\mathbf{S}/\lambda)-\mathbf{g}+\mathbf{g}']\cdot(\mathbf{r}_m - \mathbf{r}_n)} \Big\}. \quad (11.37)$$

From Eq. (11.29),

$$\sum_m \sum_n e^{2\pi i[(\mathbf{S}/\lambda)\pm\mathbf{g}\pm\mathbf{g}']\cdot(\mathbf{r}_m - \mathbf{r}_n)} = I_0[(\mathbf{S}/\lambda) \pm \mathbf{g} \pm \mathbf{g}']. \quad (11.38)$$

Since each of the four terms in Eq. (11.37) makes the same contribution in the integrations which follow, we can use one term and then multiply by four:

$$I_2(S/\lambda) = \frac{f^2 e^{-2M}}{2} \sum_{gj} \sum_{g'j'} G_{gj} G_{g'j'} I_0[(\mathbf{S}/\lambda) + \mathbf{g} - \mathbf{g}']. \quad (11.39)$$

The function $I_0[(\mathbf{S}/\lambda) + \mathbf{g} - \mathbf{g}']$ is essentially zero except for vectors $\mathbf{g}$ and $\mathbf{g}'$ such that $\mathbf{S}/\lambda + \mathbf{g} - \mathbf{g}'$ falls closely on an active reciprocal lattice point. The relation is shown by Fig. 11.4. We approximate the first Brillouin zone by a sphere of radius g_m, such that the volume of the sphere is equal to that of the zone. Spheres are centered on the active reciprocal lattice point *hkl*, and on the tip of the $\mathbf{S}/\lambda$ vector (the position in reciprocal space where the intensity is being measured). The vectors $\mathbf{g}$ and $\mathbf{g}'$ are confined to these

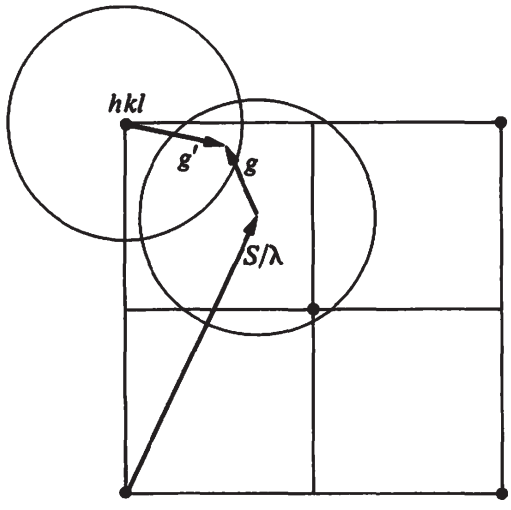

Fig. 11.4 The relations involved in computing the contribution to the second-order TDS at the position $\mathbf{S}/\lambda$ which is due to the active reciprocal lattice point *hkl*.

two spheres, and for vectors $\mathbf{g}'$ starting from the point *hkl*, it is only for those pairs which meet at a point within the overlap region of the two spheres that $I_0(\mathbf{S}/\lambda + \mathbf{g} - \mathbf{g}')$ will differ from zero. We now hold $\mathbf{S}/\lambda + \mathbf{g}$ constant and let $\mathbf{g}'$ vary. Following the procedures of the previous section, we replace the sum over $\mathbf{g}'$ by an integral in the zone. In addition we sum over all *hkl*-reciprocal lattice points whose spheres have an overlap region with the sphere centered on $\mathbf{S}/\lambda$:

$$I_2(S/\lambda) = \frac{f^2 e^{-2M}}{2} \sum_{hkl} \sum_{gj} G_{gj} \sum_{j'} \int G_{g'j'} I_0(\mathbf{S}/\lambda + \mathbf{g} - \mathbf{g}') \frac{N}{b^3} b^3 \, dh_1 \, dh_2 \, dh_3.$$

The integral is evaluated as in the previous section, and the slowly varying $G_{g'j'}$ is taken out of the integral and replaced by the value $[G_{g'j'}]$ for which $\mathbf{S}/\lambda + \mathbf{g} - \mathbf{g}' = \mathbf{H}_{hkl}$:

$$I_2(S/\lambda) = \frac{f^2 e^{-2M}}{2} \sum_{hkl} \sum_{gj} G_{gj} \sum_{j'} [G_{g'j'}].$$

From Eqs. (11.22) and (11.25), and making the substitution $\omega_{gj} = 2\pi\nu_{gj}$,

$$G_{gj} = \left|\frac{\mathbf{S}}{\lambda}\right|^2 \frac{E_{gj}}{Nm\nu_{gj}^2} \cos^2(S, e_{gj}).$$

The sum over $\mathbf{g}$ can be replaced by an integral over the overlap region, where v_0 is the volume per atom:

$$\sum_{gj} \left\{ G_{gj} \sum_{j'} [G_{g'j'}] \right\} \to \sum_{j} \int G_{gj} \sum_{j'} [G_{g'j'}] \frac{N}{v_{BZ}} \, dv = N v_0 \sum_{j} \int G_{gj} \sum_{j'} [G_{g'j'}] \, dv.$$

With these changes, the second-order TDS at the position $\mathbf{S}/\lambda$ is given by

$$I_2(S/\lambda) = \frac{f^2 e^{-2M} N v_0}{2m^2} \left|\frac{\mathbf{S}}{\lambda}\right|^4 \sum_{hkl} \int \sum_{j} \sum_{j'} \frac{E_{gj} \cos^2(S, e_{sj})}{\nu_{gj}^2} \frac{E_{g'j'} \cos^2(S, e_{g'j'})}{\nu_{g'j'}^2} dv. \tag{11.40}$$

To evaluate rigorously the integral in Eq. (11.40), we would need to know the frequencies and vibration directions for all the elastic waves. In general, it is the frequencies that we are trying to obtain from experiment, and hence we would need to know the complete answer, to rigorously evaluate the second-order TDS correction term. To obtain a workable expression for the correction, it is necessary to make approximations. The first calculation of the second-order TDS correction was made by Olmer[7] with approximations which allow a very simple evaluation. Although the Olmer approximations are probably a little too drastic for an accurate calculation of the correction, we will consider this case because of its simplicity.

We assume the temperature to be high enough for equipartition, so that all $E_{gj} = E_{g'j'} = kT$. We assume all waves to be pure longitudinal and pure

transverse, with the same mean velocity V_m. The mean velocity is an average for long wavelength waves, averaged over the three principal directions [100], [110], and [111]:

$$\frac{1}{V_m^2} = \frac{1}{3}\left(\left\langle \frac{1}{V_l^2} \right\rangle + \left\langle \frac{2}{V_t^2} \right\rangle\right). \tag{11.41}$$

In using a long wavelength mean velocity V_m, we are neglecting dispersion (the variation of velocity with wavelength). With these approximations, $v = V_m g$ and $\sum_j \cos^2(S, e_{gj}) = 1$. Equation (11.40) takes the simpler form

$$I_2(S/\lambda) = \frac{f^2 e^{-2M} N V_0}{2m^2} \left|\frac{\mathbf{S}}{\lambda}\right|^4 \frac{(kT)^2}{V_m^4} \sum_{hkl} \Phi_{hkl}, \tag{11.42}$$

where Φ_{hkl} represents the overlap integral

$$\Phi_{hkl} = \int \frac{dv}{(g)^2(g')^2}. \tag{11.43}$$

A simple evaluation of the overlap integral of Eq. (11.43) has been given by Borie.[8] Let g_m be the radius of the spheres, and y the center-to-center distance as illustrated by Fig. 11.5. Since the overlap region has rotational symmetry around the horizontal axis, and reflection plane symmetry across the vertical plane, we can write

$$\Phi = \iint \frac{2\pi g^2 \sin\phi \, d\phi \, dg}{g^2(g^2 + y^2 - 2yg\cos\phi)}.$$

We integrate from $\phi = 0$ to $\phi = \arccos y/2g$ and multiply by 2:

$$\Phi = \frac{2\pi}{y} \int \ln\left(\frac{g}{y-g}\right)^2 \frac{dg}{g}. \tag{11.44}$$

We consider first the case $0 < y < g_m$, and divide the integration with

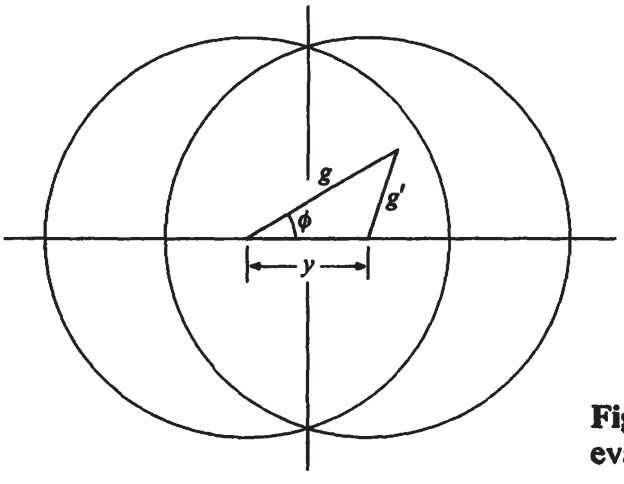

Fig. 11.5 The geometry involved in the evaluation of the overlap integral.

respect to dg into the intervals $y/2$ to y and y to g_m:

$$\Phi = -\frac{4\pi}{y}\int_{y/2}^{y} \ln\left(\frac{y}{g} - 1\right)\frac{dg}{g} - \frac{4\pi}{y}\int_{y}^{g_m} \ln\left(1 - \frac{y}{g}\right)\frac{dg}{g}.$$

In the first integral make the change in variable $(y/g - 1) = u$, and in the second integral make the expansion $\ln(1 - y/g) = -[y/g + (y/g)^2/2 + (y/g)^3/3 + \cdots]$

$$\Phi = -\frac{4\pi}{y}\left(-\frac{\pi^2}{12}\right) - \frac{4\pi}{y}\left\{\frac{y}{g_m} + \frac{1}{4}\left(\frac{y}{g_m}\right)^2 + \frac{1}{9}\left(\frac{y}{g_m}\right)^3 + \cdots - \frac{\pi^2}{6}\right\},$$

$$\Phi = \frac{\pi^3}{y} - \frac{4\pi}{g_m}\left\{1 + \frac{1}{4}\left(\frac{y}{g_m}\right) + \frac{1}{9}\left(\frac{y}{g_m}\right)^2 + \cdots\right\}. \tag{11.45}$$

For the case $g_m < y < 2g_m$, the integration with respect to ϕ is the same as before. The integration with respect to dg is from $y/2$ to g_m, and this is written as the difference of the integrals $y/2$ to y and g_m to y:

$$\Phi = -\frac{4\pi}{y}\int_{y/2}^{y} \ln\left(\frac{y}{g} - 1\right)\frac{dg}{g} + \frac{4\pi}{y}\int_{g_m}^{y} \ln\left(\frac{y}{g} - 1\right)\frac{dg}{g},$$

$$\Phi = -\frac{4\pi}{y}\left(-\frac{\pi^2}{12}\right) + \frac{4\pi}{y}\int_{1}^{y/g_m} \ln(u - 1)\frac{du}{u},$$

$$\Phi = -\frac{\pi^3}{3y} + \frac{4\pi}{y}\left\{[\ln(y/g_m)]^2/2 + \frac{g_m}{y}\left[1 + \frac{1}{4}\frac{g_m}{y} + \frac{1}{9}\left(\frac{g_m}{y}\right)^2 + \cdots\right]\right\}. \tag{11.46}$$

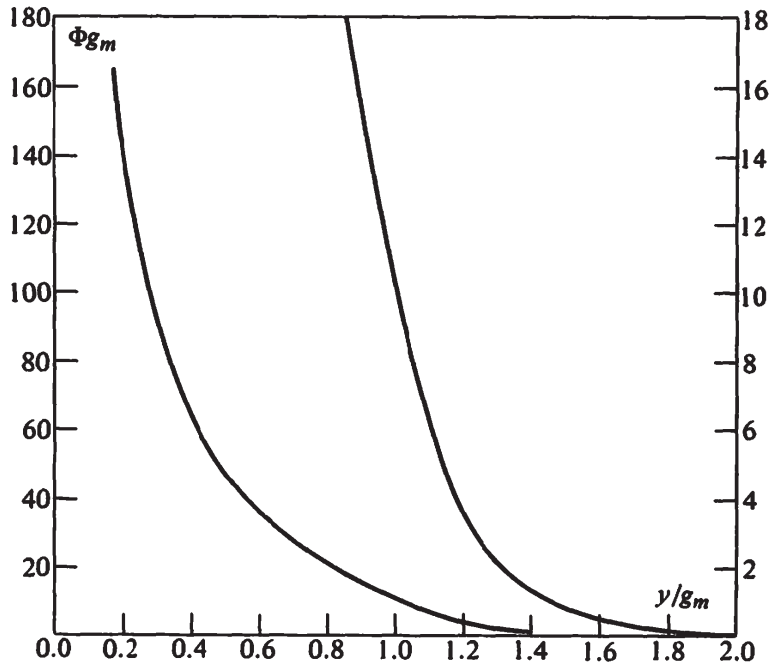

Fig. 11.6 Computed values of Φg_m as a function of the general variable y/g_m from Eqs. (11.45) and (11.46).

From Eqs. (11.45) and (11.46), the quantity Φg_m can be plotted as a function of the general variable y/g_m for the range $y/g_m = 0$ to $y/g_m = 2$. The curve is shown by Fig. 11.6. Using Eq. (11.42) and the values from Fig. 11.6, we can obtain approximate values for the second-order TDS at any desired position in reciprocal space. These approximate values are good enough if the second-order TDS is small relative to the first-order or if we are not interested in high accuracy. When highly accurate values of the first-order TDS are desired, the second-order correction term must be evaluated more accurately. A better approximation for the second-order scattering, which has been developed by Walker,[9] uses separate average velocities for the longitudinal and transverse waves and makes an approximate allowance for dispersion of the waves.

11.7 THE MEASUREMENT OF TEMPERATURE DIFFUSE SCATTERING

Measurements of the temperature diffuse scattering are made with a single crystal, using either ionization chamber or counter recording. Strictly monochromatic radiation is necessary and this can be obtained with balanced filters or preferably by the use of a crystal monochromator. It is not necessary to have precisely defined directions in measuring diffuse intensities, and accordingly curved focusing crystals are used to conserve intensity at the expense of a tolerable loss of resolution. The monochromating crystal can be put between the tube and the sample or between the sample and the counter. At first sight it would seem to be preferable to put the crystal between the sample and the counter and attempt to make the reflection conditions sharp enough to exclude the troublesome Compton modified scattering. However, the difference in wavelength between the modified and the unmodified is very small, and since the modified scattering extends over a range of wavelengths, it would require such a high degree of collimation to exclude the modified scattering that this procedure is usually impractical for intensity reasons. It is better to include all of the modified scattering than an unknown fraction of it, and in general the curved focusing crystal is placed between the tube and the sample as illustrated by Fig. 11.7. In general, the monochromating crystal reflects not only the desired $K\alpha$ wavelength, but also $\lambda/2$ from the continuous spectrum. The $\lambda/2$ component can, of course, always be eliminated by using a monochromator such as silicon 111, since $F(222) = 0$. For Cu$K\alpha$ radiation a bent LiF crystal is very convenient, and for this case the $\lambda/2$ component is eliminated by using a proportional counter set to discriminate against $\lambda/2$ or by using balanced filters accurately matched at $\lambda/2$.

Since LiF bends so easily if it is given an anneal at, say, 450°C before bending, the crystal is often prepared with a double curvature. The advantage

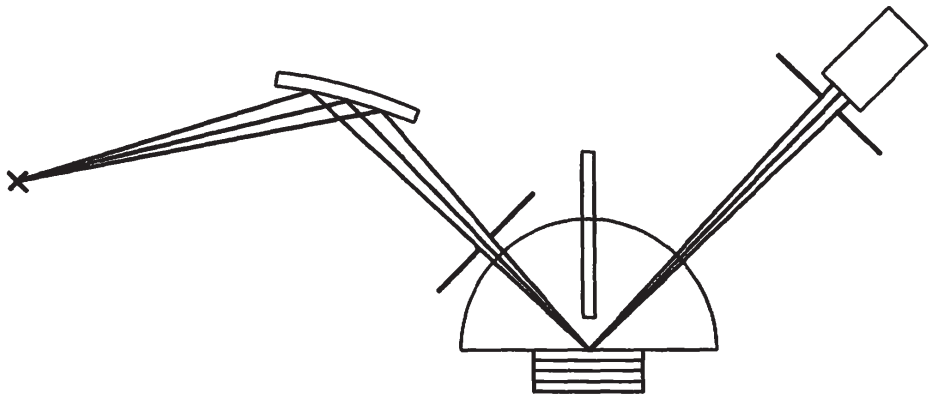

Fig. 11.7 Schematic arrangement for measuring the temperature diffuse scattering. The primary beam has been monochromated by a bent focusing crystal.

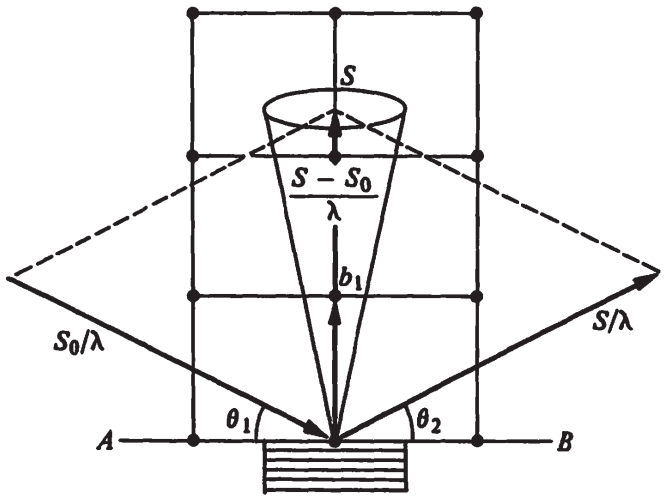

Fig. 11.8 Illustration of the method for bringing the diffraction vector $(\mathbf{s} - \mathbf{s}_0)/\lambda$ to various positions in reciprocal space, while maintaining the symmetrical condition $\theta_1 = \theta_2$.

is that still more intensity is provided, and in addition the conditions can be so adjusted that although an extended region on the face of the sample is illuminated, all scattered radiation reaching the counter corresponds to the same position in reciprocal space. The geometry involved in maintaining this condition has been given by Warren.[10] To minimize air scattering by the primary beam, it is advantageous to have the sample in a thin-walled container which can be evacuated or flushed with He or H_2. The baffle shown in Fig. 11.7 prevents the counter from receiving radiation from that part of the window struck by the primary beam.

The measurements can be made at desired positions in reciprocal space by the scheme illustrated by Fig. 11.8. Suppose the crystal has been cut to a 100 face. The primary beam is represented by the vector $\mathbf{S}_0/\lambda$ and the direction in which we measure scattered radiation by the vector $\mathbf{S}/\lambda$. It is

convenient terminology to say that we are measuring the intensity at the position S in reciprocal space, this position being at the terminal point of the diffraction vector $(\mathbf{S} - \mathbf{S}_0)/\lambda$. Keeping θ_1 equal to θ_2 but varying their magnitude, the diffraction vector is always parallel to $\mathbf{b}_1$. We measure the intensity at the position h_100 in reciprocal space, where h_1 can be varied continuously by changing θ_1 and θ_2. To reach positions other than h_100, we could let θ_2 be different from θ_1. However, a better way is to keep $\theta_1 = \theta_2$ and rotate the crystal about the axis AB. This is equivalent to moving the terminal point of the diffraction vector up or down in the reciprocal lattice normal to the plane of the paper. For any fixed position about the AB-axis, the crystal can be rotated about an axis normal to the 100 face. This corresponds to moving the diffraction vector around the cone of Fig. 11.8. The length of the diffraction vector is varied by changing θ_1 and θ_2, the cone angle is varied by rotation about the axis AB, and the position on the cone by rotation of the crystal around the normal to the 100 face. It is thus possible to make the terminal point of the diffraction vector cover an appreciable volume in reciprocal space, while still maintaining the symmetrical diffraction conditions ($\theta_1 = \theta_2$) for which the absorption factor is angular independent.

Figure 11.9 shows a type of goniometer which is useful for obtaining the motions required by Fig. 11.8. Rotation about the axis VV varies the angle θ_1, motion of the slide on the goniometer arc corresponds to rotation about the axis AB of Fig. 11.8, and rotation about the axis XX corresponds to motion of the $(\mathbf{s} - \mathbf{s}_0)/\lambda$ vector around the surface of the cone. To avoid working with cone angles of more than, say, 30°, it is advisible to have several crystals cut to different faces.

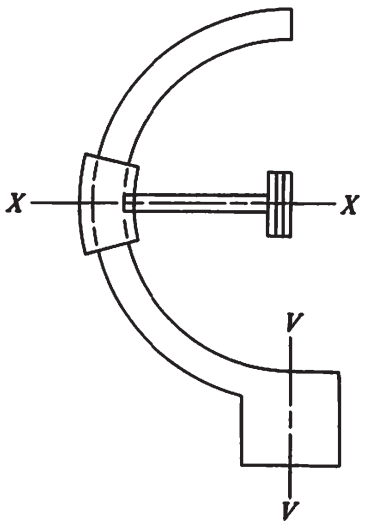

Fig. 11.9 Type of goniometer which is used for obtaining the motions represented by Fig. 11.8.

To make full use of diffuse intensities, it is necessary to have quantitative measurements such as intensities expressed in electron units per atom $I(eua)$. For the flat-faced sample, with the primary and diffracted beams making equal angles with the sample face, the measured intensity from the sample I_s is given by

$$I_s = \frac{I_0 e^4}{m^2 c^4 R^2}\left(\frac{1 + \cos^2 2\theta_M \cos^2 2\theta}{1 + \cos^2 2\theta_M}\right) I(eua) \int_0^\infty e^{-(2\mu z/\sin\theta)} \frac{M A_0\, dz}{\sin\theta},$$

where θ_M is the Bragg angle for the monochromating crystal, μ is the linear absorption coefficient in the sample, M is the number of atoms per unit volume, and A_0 is the cross sectional area of the primary beam. For a fixed

opening of the receiving slit, the counting rate (CR) is proportional to the diffuse intensity $(\mathrm{CR})_s = KI_s$.

$$(\mathrm{CR})_s = \frac{KI_0e^4}{m^2c^4R^2}\left(\frac{1 + \cos^2 2\theta_M \cos^2 2\theta}{1 + \cos^2 2\theta_M}\right) I(eua)\,\frac{MA_0}{2\mu}$$

It is convenient to express $M/2\mu$ in terms of the Avogadro number L, the atomic weight A, and the mass absorption coefficient μ_m:

$$\frac{M}{2\mu} = \frac{L\rho}{2\mu_m \rho A} = \frac{L}{2\mu_m A}.$$

Lumping together all the quantities which are independent of the particular sample, the counting rate is expressed by

$$(\mathrm{CR})_s = \frac{KI_0e^4A_0L}{m^2c^4R^2 2}\left(\frac{1 + \cos^2 2\theta_M \cos^2 2\theta}{1 + \cos^2 2\theta_M}\right)\frac{I(eua)}{\mu_m A}. \qquad (11.47)$$

We now replace the sample by a block of some amorphous standard such as quenched paraffin $C_{29}H_{60}$, which has not been at high enough temperature to crystallize, or polystyrene CH, or lucite $C_5H_8O_2$. For these amorphous materials, the intensity at high angles approaches the sum of the independent unmodified and modified scattering by the individual atoms. Suppose that we are using lucite as the standard. Let M' be the number of $C_5H_8O_2$ per unit volume, and μ' the linear absorption coefficient in lucite. For high-angle scattering, the counting rate from the lucite sample is given by

$$(\mathrm{CR})_L = \frac{KI_0e^4}{m^2c^4R^2}\left(\frac{1 + \cos^2 2\theta_M \cos^2 2\theta}{1 + \cos^2 2\theta_M}\right)\frac{M'A_0}{2\mu'}\sum [f^2 + i(M)],$$

where

$$\sum [f^2 + i(M)] = 5[f^2 + i(M)]_C + 8 + 2[f^2 + i(M)]_O$$

represents the independent unmodified plus modified scattering in electron units per $C_5H_8O_2$. Since

$$\frac{M'}{2\mu'} = \left(\frac{\rho L}{\sum A}\right)\Big/\left(\frac{2\rho \sum \mu_m A}{\sum A}\right) = \frac{L}{2\{5(A\mu_m)_C + 8(A\mu_m)_H + 2(A\mu_m)_O\}},$$

the counting rate from the lucite can be put in the convenient form

$$(\mathrm{CR})_L = \left[\frac{KI_0e^4A_0L}{m^2c^4R^2 2}\right]\left(\frac{1 + \cos^2 2\theta_M \cos^2 2\theta}{1 + \cos^2 2\theta_M}\right) \times \frac{\{5[f^2 + i(M)]_C + 8 + 2[f^2 + i(M)]_O\}}{\{5(A\mu_m)_C + 8(A\mu_m)_H + 2(A\mu_m)_O\}}. \qquad (11.48)$$

By measuring $(\mathrm{CR})_L$ at several high-angle positions, a good average value is obtained for the constant $[KI_0e^4A_0L/m^2c^4R^2 2]$. This constant is then used in Eq. (11.47) to obtain $I(eua)$ from the measured counting rate $(\mathrm{CR})_s$ from

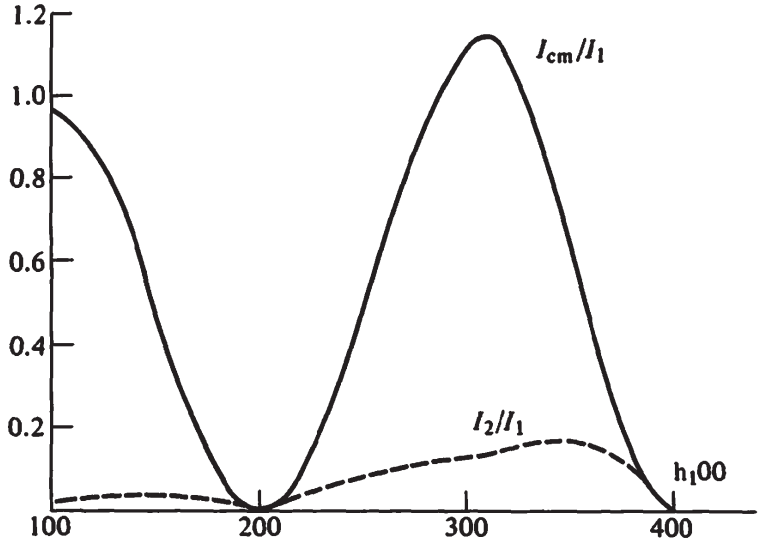

Fig. 11.10 Illustration of the magnitudes of the Compton scattering and the second-order TDS relative to the first-order TDS for positions along the h_100 line in a copper crystal at $T = 300°K$. The values must be considered as very rough, since they were obtained by an approximate treatment.

the sample. For precise work it is necessary to include a multiple scattering contribution from the lucite. This correction term has been treated in Section 10.11, and it may amount to several percent.

Assuming that other sources of diffuse radiation such as fluorescence and air scattering have been eliminated in the experiment, the values of $I(eua)$ comprise the Compton modified, the first-order TDS, and the second-order TDS. Higher-order terms in the TDS can usually be neglected:

$$I(eua) = i(M) + I_1(S/\lambda)/N + I_2(S/\lambda)/N. \tag{11.49}$$

The Compton modified scattering is taken from the tables and the second-order TDS per atom from Eq. (11.42) or from the more accurate calculation by the method of Walker. The result is the value in absolute units of the quantity $I_1(S/\lambda)/N$ expressed by Eqs. (11.35) or (11.36). It would be desirable to have the correction terms of Eq. (11.49) small relative to the first-order TDS, but unfortunately this is not always the case. As an illustration, Fig. 11.10 shows approximate computed values of the ratios $I(\mathrm{CM})/I_1$ and I_2/I_1 for measurements along the line h_100 in reciprocal space for a copper crystal at $T = 300°K$. In the computation of I_1 from Eq. (11.36) an approximate allowance is made for dispersion by setting

$$V = V_\infty \left(\sin \frac{\pi}{2} \frac{g}{g_m}\right) \Big/ \left(\frac{\pi}{2} \frac{g}{g_m}\right),$$

where V_∞ is the long wavelength velocity computed from the elastic constants. The value of I_2 was computed by the approximate method and it is probably too small by at least a factor of 2.

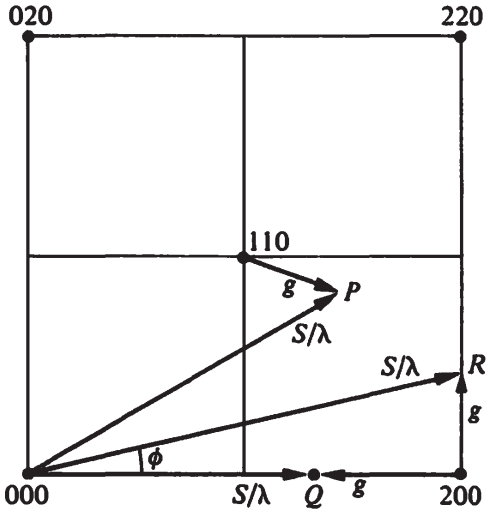

Fig. 11.11 The significance of a measurement of first-order TDS at various positions in reciprocal space. At the general position P there is a contribution from three modes. At the position Q there is a contribution only from [100] longitudinal waves. At position R there is a contribution from longitudinal and transverse [100] waves.

11.8 INTERPRETATION OF TEMPERATURE DIFFUSE SCATTERING MEASUREMENTS

Having measured the total diffuse intensity in absolute units, and corrected for the Compton modified and second-order TDS, we now have the first-order TDS is electron units per atom. For purposes of illustration, assume the temperature high enough for equipartition, so that Eq. (11.36) may be used:

$$I(S/\lambda)/N = f^2 e^{-2M} \frac{kT}{m} \frac{|\mathbf{S}/\lambda|^2}{|\mathbf{g}|^2} \sum_j \frac{\cos^2(S, e_{gj})}{V_{gj}^2}. \tag{11.50}$$

Figure 11.11 represents the reciprocal lattice of a BCC crystal. Suppose the intensity has been measured at the position P. The vector $\mathbf{g}$ is drawn from the nearest active reciprocal lattice point to the position of measurement P. The measured intensity is due only to elastic waves with the wave vector $\mathbf{g}$, and hence only to waves propagating in the direction of $\mathbf{g}$ with wavelength $\Lambda = 1/|\mathbf{g}|$. There are always three independent waves, and even in the general case, one is approximately a longitudinal wave (vibration direction $\mathbf{e}$ parallel to $\mathbf{g}$), and the other two are approximately transverse waves (vibration direction $\mathbf{e}$ perpendicular to $\mathbf{g}$). Since $f^2 e^{-2M} kT/m$ is known, and $|\mathbf{S}/\lambda|^2/|\mathbf{g}|^2$ is given by the position of measurement, what we obtain from Eq. (11.50) is a sum of the three inverse velocities squared, each weighted by the cosine squared of the angle between the diffraction vector and the corresponding vibration direction:

$$\frac{\cos^2(S, e_l)}{V_l^2} + \frac{\cos^2(S, e_{t1})}{V_{t1}^2} + \frac{\cos^2(S, e_{t2})}{V_{t2}^2}.$$

In general, the three velocities are different, and from the measured intensity we get a combination of three unknowns, but not the value of any one of the velocities.

To break down the sum and obtain the velocities of the individual modes, it is necessary to make the measurements in certain strategic regions of reciprocal space. Suppose the intensity is measured at the point Q of Fig. 11.11. The vector $\mathbf{g}$ from the nearest active point 200 gives the direction and inverse wavelength of the waves contributing to the intensity at Q. As we have seen from Eq. (11.8), the waves propagating in the [100] direction of a cubic crystal are pure longitudinal and pure transverse, and hence $\cos^2(S, e)$ is unity for the longitudinal wave and zero for the two transverse waves. The measured intensity at Q gives directly the value of $V_l(100)$ for the wavelength $\Lambda = 1/|\mathbf{g}|$. By measuring at different positions Q along the line from the origin through the point 200, we obtain the velocity of longitudinal waves propagating in the [100] direction as a function of the wavelength $\Lambda = 1/|\mathbf{g}|$. To obtain the velocity of transverse waves propagating in the [100] direction, we make measurements at a position such as point R of Fig. 11.11. The waves contributing to the intensity at R are those propagating in the direction of the corresponding vector $\mathbf{g}$. From the measured intensity we obtain

$$\frac{\sin^2\phi}{V_l^2(100)} + \frac{\cos^2\phi}{V_t^2(100)}.$$

Since ϕ is known from the position of measurement, and values of $V_l(100)$ are known from the measurements at positions such as Q, we obtain values of $V_t(100)$ as a function of $\Lambda = 1/|\mathbf{g}|$.

Measurements along a line from the origin through the 110 point give directly the longitudinal velocities $V_l(110)$. Measurements along a line connecting 110 and 020, or along a line connecting 200 and 211, after correction for the contribution by the longitudinal waves, give the two transverse velocities $V_{t1}(110)$ and $V_{t2}(110)$. Similar choices give the velocities of longitudinal and transverse waves propagating in the [111] direction. In a cubic crystal, for directions other than [100], [110], and [111], the elastic waves are no longer pure longitudinal and pure transverse, and it becomes more difficult to obtain the separate velocities.

Beta brass CuZn has a CsCl structure when in the ordered form, and in the disordered form it can be approximated as a BCC element of $Z = 29.5$. The measurements by Cole and Warren[11] of the diffuse intensity from a single crystal of β brass at $T = 295°\text{K}$ are shown by the contour plot of Fig. 11.12. The contours represent the total diffuse intensity, temperature diffuse scattering plus Compton modified, for a series of h_1h_20 positions in reciprocal space. As plotted, the values are in arbitrary units with each contour line representing a doubling of the intensity. The temperature diffuse scattering rises to peak values at the active reciprocal lattice points, but the distribution is far from spherically symmetrical about each point. In Fig. 11.12 there are

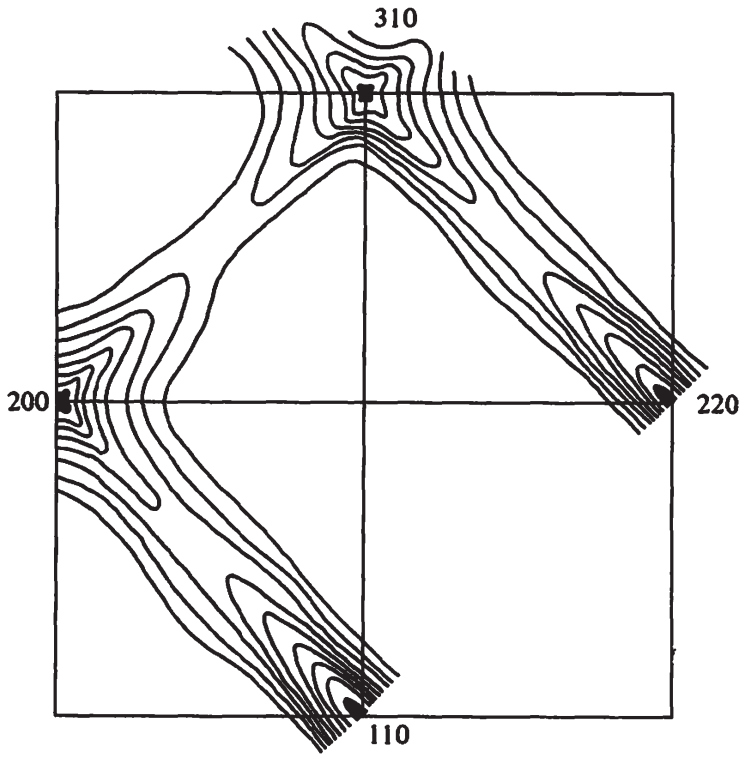

Fig. 11.12 Measured diffuse intensity (TDS plus Compton) for a single crystal of beta brass CuZn at $T = 295°K$. The measurements are at positions h_1h_20 in reciprocal space with successive contours representing a doubling of the intensity. The shape of the contours is largely due to the first-order TDS.

strong ridges of TDS running in the [110] and [1$\bar{1}$0] directions. These are largely due to the transverse waves in the [110] direction whose long wavelength velocity is given by $V_t^2 = (c_{11} - c_{12})/2\rho$. In beta brass, c_{12} is almost as large as c_{11}, and the resulting unusually small velocities for transverse waves in the [110] direction produce the strong ridges of diffuse intensity shown by Fig. 11.12.

Values of the corrected first-order TDS, for β CuZn at 295°K, were used to get the velocities in the three simple directions. From measurements along the line connecting 200 and 220, values of $V_t(100)$ are obtained as a function of $1/\Lambda$. The values of the velocity and the corresponding frequency $\nu = (1/\Lambda)V$ are shown by Fig. 11.13. The measured values cover a range from $(1/\Lambda)_{max}$ equal to the radius of the Brillouin zone, down to values about $\frac{1}{20}$ as large, these lower values being limited by approach to an *hkl*-point with consequent picking up of the strong crystalline reflection. The long wavelength velocity computed from the elastic constants is indicated. The x-ray values approach this limiting value reasonably well. The possibility of determining the elastic constants from the x-ray values of the long wavelength velocities has been developed by Wooster.[12]

The velocity curve of Fig. 11.13 shows a decrease in velocity with decreasing wavelength. This effect is known as the dispersion of the elastic

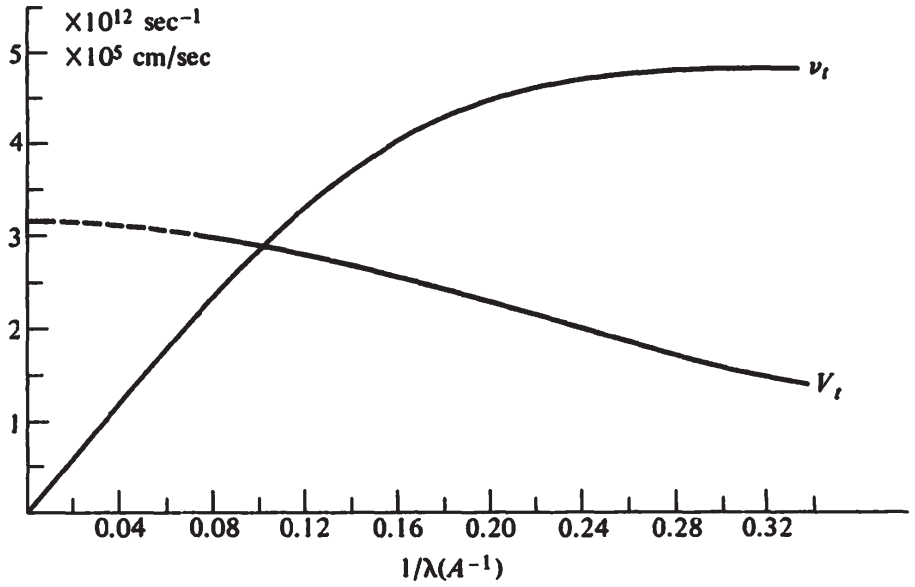

Fig. 11.13 Velocity and frequency for transverse [100] waves in beta brass, obtained from data such as represented by Fig. 11.12. The long wavelength velocity calculated from the elastic constants is shown by the heavy dash on the axis of ordinates.

waves. The dispersion effect is well known in the classical problem of masses m spaced along a line at distances d and connected by linear restoring forces such as springs. For this analogy to a one-dimensional crystal, it was shown by Baden-Powell[13] in 1841 that the velocity of a wave of wavelength Λ is given by

$$V = V_\infty \frac{\sin \pi d/\Lambda}{\pi d/\Lambda}, \tag{11.51}$$

where V_∞ is the velocity for waves of long wavelength. Since the shortest wavelength is $\Lambda_{\min} = 2d$, it follows from Eq. (11.51) that the velocity at $\Lambda_{\min}$ is given by $V(\Lambda_{\min}) = V_\infty 2/\pi$. The dispersion of the elastic waves found from the x-ray temperature scattering is comparable to that predicted by the simple Baden-Powell formula. It is only in the high-frequency range 10^{11} to 10^{13} that the dispersion becomes evident. By the various electromechanical methods, it is difficult to generate frequencies which even approach 10^{11}. Elastic waves in the high-frequency range, where dispersion effects can be studied, are fortunately provided by nature in the form of the elastic waves due to temperature vibration.

Frequency curves for the longitudinal and transverse waves in the three simple directions do not represent a good sampling for all directions. Although they can be used to construct approximate frequency distribution curves $N(\nu)$ vs. ν, where $N(\nu)\,d\nu$ is the number of waves with frequencies between ν and $\nu + d\nu$, the poor sampling produces false peaks in the curve. To obtain reliable frequency distribution curves, it is necessary to include waves for a

large variety of directions. To attempt to obtain dispersion curves for a large number of directions by making the corresponding x-ray measurements involves too much work to be practical. A more reasonable procedure is to use the Born[14] theory which expresses the frequencies in terms of a set of interatomic force constants, and then determine these force constants from the x-ray results for the three simple directions.

11.9 DETERMINATION OF THE INTERATOMIC FORCE CONSTANTS FROM TEMPERATURE SCATTERING

The Born-von Karman theory of lattice vibrations, as generalized by Born and his colleagues (Born),[14] assumes that the atomic vibrations are harmonic and that the restoring forces acting between atoms can be described as general Hooke's law forces that are functions only of the nuclear coordinates. The force on atom l is then proportional to the relative displacements of all the other atoms. The components of force along the three orthogonal axes x, y, and z can be written

$$\begin{aligned}
F(l)_x &= \sum_{n\neq l}\{D(nl)_{xx}(u_{nx}-u_{lx}) + D(nl)_{xy}(u_{ny}-u_{ly}) + D(nl)_{xz}(u_{nz}-u_{lz})\},\\
F(l)_y &= \sum_{n\neq l}\{D(nl)_{yx}(u_{nx}-u_{lx}) + D(nl)_{yy}(u_{ny}-u_{ly}) + D(nl)_{yz}(u_{nz}-u_{lz})\},\\
F(l)_z &= \sum_{n\neq l}\{D(nl)_{zx}(u_{nx}-u_{lx}) + D(nl)_{zy}(u_{ny}-u_{ly}) + D(nl)_{zz}(u_{nz}-u_{lz})\},
\end{aligned} \tag{11.52}$$

where u_{nk} represents the kth component of the displacement of atom n, and where the sum extends over all atoms except atom l.

The quantities $D(nl)_{ij}$, the interatomic force constants acting between atom n and atom l, determine the force on atom l in the i-direction when atom n is given a unit relative displacement in the j-direction. The number of these force constants that are unique and significant depends on the symmetry of the lattice and the range of the interatomic forces.

The form of Eq. (11.52) can be simplified by introducing additional constants, $D(ll)_{ij}$, defined by the relation

$$D(ll)_{ij} = -\sum_{n\neq l} D(nl)_{ij}, \tag{11.53}$$

where $i, j = x, y$, and z. These may be considered as constants determining the force on atom l in the i-direction when atom l itself is displaced in the j direction. Using these, Eq. (11.52) becomes

$$F(l)_i = \sum_{n}\{D(nl)_{ix}u_{nx} + D(nl)_{iy}u_{ny} + D(nl)_{iz}u_{nz}\}, \tag{11.54}$$

where $i = x, y$, and z, and where the sum now extends over all atoms.

Equating the force on an atom to the product of its mass and its acceleration, we obtain the equations of motion with $i = x, y$, and z:

$$m_l \frac{d^2 u_{li}}{dt^2} = \sum_n \{D(nl)_{ix} u_{nx} + D(nl)_{iy} u_{ny} + D(nl)_{iz} u_{nz}\}, \qquad (11.55)$$

We restrict ourselves to considering only lattices with one atom per primitive unit cell. All atoms l are then equivalent, and the force constants $D(nl)_{ij}$ must depend only on the vector separation $\mathbf{r}_n - \mathbf{r}_l$. The displacement of any atom is given by the sum of its displacements due to each of the $3N$ independent traveling elastic waves in the crystal. The displacement of atom n due to a traveling elastic wave of wave vector $\mathbf{g}$ and polarization p ($p = 1, 2, 3$) can be written in the form

$$\mathbf{u}_n = a\mathbf{e} \cos \{\omega t - 2\pi \mathbf{g} \cdot \mathbf{r}_n - \delta\}, \qquad (11.56)$$

where a is the amplitude of the wave, $\mathbf{e}$ is a unit vector (with direction cosines A, B, and C) along the direction of vibration, ω is the circular frequency of the wave, and δ is a random phase factor that prevents coherence between the different elastic waves. Since the waves are independent, the displacement due to each such elastic wave must satisfy the equations of motion, Eq. (11.55). Substituting Eq. (11.56) into Eq. (11.55), we obtain for $i = x$

$$-m\omega^2 A \cos \{\omega t - 2\pi \mathbf{g} \cdot \mathbf{r}_l - \delta\} = \sum_n \{D(nl)_{xx} A + D(nl)_{xy} B + D(nl)_{xz} C\} \times \cos \{\omega t - 2\pi \mathbf{g} \cdot \mathbf{r}_n - \delta\}.$$

To simplify, we use the relation

$$\cos \{\omega t - 2\pi \mathbf{g} \cdot \mathbf{r}_n - \delta\} = \cos \{\omega t - 2\pi \mathbf{g} \cdot \mathbf{r}_l - \delta\} \cos 2\pi \mathbf{g} \cdot (\mathbf{r}_n - \mathbf{r}_l) + \sin \{\omega t - 2\pi \mathbf{g} \cdot \mathbf{r}_l - \delta\} \sin 2\pi \mathbf{g} \cdot (\mathbf{r}_n - \mathbf{r}_l).$$

The structures which we are considering are centrosymmetrical, such that for every neighbor at $\mathbf{r}_n - \mathbf{r}_l$ there is a neighbor at $\mathbf{r}_{n'} - \mathbf{r}_l = -(\mathbf{r}_n - \mathbf{r}_l)$; hence

$$\sum_n D(nl)_{ij} \sin 2\pi \mathbf{g} \cdot (\mathbf{r}_n - \mathbf{r}_l) = 0.$$

With these simplifications, we obtain the conditions which must be satisfied by the frequencies and directions of vibration of the possible elastic waves of wave vector $\mathbf{g}$:

$$\begin{aligned}
-m\omega^2 A &= \sum_n \{D(nl)_{xx} A + D(nl)_{xy} B + D(nl)_{xz} C\} \cos 2\pi \mathbf{g} \cdot (\mathbf{r}_n - \mathbf{r}_l), \\
-m\omega^2 B &= \sum_n \{D(nl)_{yx} A + D(nl)_{yy} B + D(nl)_{yz} C\} \cos 2\pi \mathbf{g} \cdot (\mathbf{r}_n - \mathbf{r}_l), \\
-m\omega^2 C &= \sum_n \{D(nl)_{zx} A + D(nl)_{zy} B + D(nl)_{zz} C\} \cos 2\pi \mathbf{g} \cdot (\mathbf{r}_n - \mathbf{r}_l).
\end{aligned} \qquad (11.57)$$

We now define a new set of coefficients

$$D_{ij}(\mathbf{g}) = -\frac{1}{m}\sum_{n} D(nl)_{ij} \cos 2\pi \mathbf{g}\cdot(\mathbf{r}_n - \mathbf{r}_l), \tag{11.58}$$

where $i, j = x, y$, and z. With these coefficients, Eq. (11.57) becomes

$$\begin{aligned} &[D_{xx}(\mathbf{g}) - \omega^2]A + D_{xy}(\mathbf{g})B + D_{xz}(\mathbf{g})C = 0,\\ &D_{yx}(\mathbf{g})A + [D_{yy}(\mathbf{g}) - \omega^2]B + D_{yz}(\mathbf{g})C = 0,\\ &D_{zx}(\mathbf{g})A + D_{zy}(\mathbf{g})B + [D_{zz}(\mathbf{g}) - \omega^2]C = 0. \end{aligned} \tag{11.59}$$

Since Eqs. (11.59) can be considered as a set of homogeneous equations in the variables A, B, C, for a solution other than the trivial solution

$$A = B = C = 0,$$

the determinant of the coefficients must vanish:

$$\begin{vmatrix} D_{xx}(\mathbf{g}) - \omega^2 & D_{xy}(\mathbf{g}) & D_{xz}(\mathbf{g}) \\ D_{yx}(\mathbf{g}) & D_{yy}(\mathbf{g}) - \omega^2 & D_{yz}(\mathbf{g}) \\ D_{zx}(\mathbf{g}) & D_{zy}(\mathbf{g}) & D_{zz}(\mathbf{g}) - \omega^2 \end{vmatrix} = 0. \tag{11.60}$$

Equation (11.60), the so-called secular equation, is a cubic equation in ω^2, with coefficients that are functions of the wave vector $\mathbf{g}$; its solutions give the frequencies of the three modes of vibration of elastic waves with this wave vector. By then substituting these frequencies into Eq. (11.59), one can determine ratios of the direction cosines (A, B, and C) and hence the vibration directions of the three waves with wave vector $\mathbf{g}$.

As an example, we shall develop the theory in detail for a monatomic face-centered cubic element such as Al or Cu. We orient the orthogonal axes x, y, and z parallel respectively to the lattice vectors $\mathbf{a}_1$, $\mathbf{a}_2$, and $\mathbf{a}_3$. Let

$$\begin{aligned} \mathbf{r}_n - \mathbf{r}_l &= \tfrac{1}{2}(n_1\mathbf{a}_1 + n_2\mathbf{a}_2 + n_3\mathbf{a}_3),\\ \mathbf{g} &= g_x\mathbf{b}_1 + g_y\mathbf{b}_2 + g_z\mathbf{b}_3, \end{aligned} \tag{11.61}$$

where the $\mathbf{a}_i$ and $\mathbf{b}_i$ are respectively the real lattice and reciprocal lattice vectors, n_1, n_2, and n_3 are integers ($n_1 + n_2 + n_3 =$ even), and g_x, g_y, and g_z are the three components of the wave vector $\mathbf{g}$ in units of the reciprocal vector length $|\mathbf{b}|$. Incorporating Eqs. (11.58) and (11.61), we obtain

$$D_{ij}(\mathbf{g}) = -\frac{1}{m}\sum_{n_1 n_2 n_3} D(n_1 n_2 n_3)_{ij} \cos \pi(n_1 g_x + n_2 g_y + n_3 g_z), \tag{11.62}$$

where $i, j = x, y$, and z, and where the index nl has become the n_1, n_2, n_3 defined by Eq. (11.61). The sum over n_1, n_2, n_3 extends over any atom l and all its neighbors.

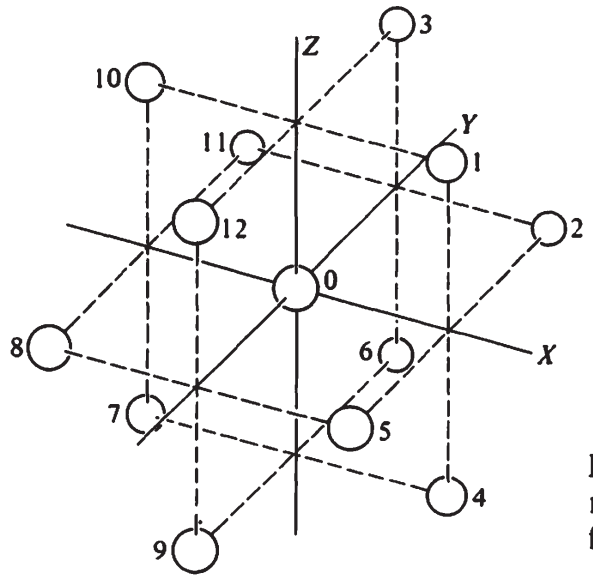

Fig. 11.14 Representation of the 12 nearest neighbors about any atom in a face-centered cubic metal.

Consider now the restrictions that the symmetry of a face-centered cubic element such as Al or Cu imposes on the interatomic force constants. Figure 11.14 shows the twelve nearest neighbors of any atom l. For simplicity we denote the atoms by numbers 0 through 12, rather than by the index triplet $n_1n_2n_3$.

Atoms 1 and 0 are in a reflection plane which is perpendicular to the Y axis. For atom 1, a displacement which lies within the reflection plane (u_{1x} or u_{1z}) cannot produce a y-component of force on atom 0, such as expressed by Eq. (11.52), since by symmetry, a reversal of the displacement could not produce a reversal of the force. This requires that $D(1)_{yx} = D(1)_{yz} = 0$. Similarly the displacement u_{1y} of atom 1 which is perpendicular to the reflection plane cannot produce on atom 0 a component of force which is in the reflection plane, since by symmetry a reversal of the displacement could not produce a reversal of the force. From Eq. (11.52), this requires that $D(1)_{xy} = D(1)_{zy} = 0$. Applying the same reasoning to atoms 4, 7, and 10 we obtain the vanishings:

$$D(1)_{yx} = D(1)_{yz} = D(4)_{yx} = D(4)_{yz} = D(7)_{yx} = D(7)_{yz} = D(10)_{yx} = D(10)_{yz} = 0,$$

$$D(1)_{xy} = D(1)_{zy} = D(4)_{xy} = D(4)_{zy} = D(7)_{xy} = D(7)_{zy} = D(10)_{xy} = D(10)_{zy} = 0.$$

The y-axis is an axis of 4-fold rotational symmetry and the force on atom 0 due to displacements of atoms, 1, 4, 7, and 10 must show this same rotational symmetry. For example, the force on atom 0 in the $+z$-direction due to a displacement of atom 1 in the $+x$-direction must be equal to the force on atom 0 in the $+x$-direction due to an equal displacement of atom 4 in the $-z$-direction. To satisfy the 4-fold rotational symmetry, the following

relations must exist between the coefficients of Eq. (11.52):

$$\begin{aligned}
D(1)_{xx} &= \quad D(4)_{zz} = D(7)_{xx} = \quad D(10)_{zz},\\
D(1)_{zz} &= \quad D(4)_{xx} = D(7)_{zz} = \quad D(10)_{xx},\\
D(1)_{xz} &= -D(4)_{xz} = D(7)_{xz} = -D(10)_{xz},\\
D(1)_{zx} &= -D(4)_{zx} = D(7)_{zx} = -D(10)_{zx},\\
D(1)_{yy} &= \quad D(4)_{yy} = D(7)_{yy} = \quad D(10)_{yy},
\end{aligned}$$

Atoms 0 and 1 lie in a reflection plane which is perpendicular to the $[\bar{1}01]$ lattice direction. Since the force components on atom 0, due to displacements of atom 1, must show this symmetry, it follows that

$$D(1)_{xx} = D(1)_{zz}, \qquad D(1)_{xz} = D(1)_{zx}.$$

Consider next the reflection plane through atom 0 perpendicular to the $[0\bar{1}1]$ direction. Atoms 2, 5, 8, and 11 are mirror images of atoms 1, 4, 7, and 10. The forces on atom 0 due to displacements of these two sets of atoms must show this same reflection symmetry. From Fig. 11.14, it is seen that this requires only a simple interchange of axes with yz of one set becoming zy of the mirror set. For example,

$$\begin{aligned}
D(2)_{xy} &= D(1)_{xz}; \qquad D(5)_{yy} = D(4)_{zz};\\
D(8)_{zy} &= D(7)_{yz}; \qquad D(11)_{xx} = D(10)_{xx}.
\end{aligned}$$

Finally, there is a reflection plane through atom 0 perpendicular to the $[\bar{1}10]$ direction, and atoms 3, 6, 9, and 12 are mirror images of atoms 1, 4, 7, and 10. To satisfy this symmetry requires only an interchange of axes with xy of one set becoming yx of the mirror set. For example,

$$\begin{aligned}
D(3)_{xz} &= D(1)_{yz}; \qquad D(6)_{xx} = D(4)_{yy};\\
D(9)_{xy} &= D(7)_{yx}; \qquad D(12)_{zz} = D(10)_{zz}.
\end{aligned}$$

As a result of symmetry restrictions in a face-centered cubic structure, the Hooke's law restoring forces between an atom and its twelve nearest neighbors can be specified by only three coefficients:

$$\begin{aligned}
D(1)_{xx} &= D(101)_{xx} = \alpha_1,\\
D(1)_{yy} &= D(101)_{yy} = \beta_1,\\
D(1)_{zx} &= D(101)_{zx} = \gamma_1,
\end{aligned}$$

where we have reintroduced the triple index $n_1n_2n_3$ defined by Eq. (11.61).

One can apply the same symmetry considerations to the force constants for more distant atoms. In this manner the Hooke's law restoring forces between an atom and its six second neighbors can be expressed by the two

Table 11.2

INTERATOMIC FORCE CONSTANTS FOR A FACE-CENTERED CUBIC ELEMENT SUCH AS ALUMINUM,

$D(n_1n_2n_3)_{ij} = D(\bar{n}_1\bar{n}_2\bar{n}_3)_{ij}$

$n_1n_2n_3$	D_{xx}	D_{xy}	D_{xz}	D_{yx}	D_{yy}	D_{yz}	D_{zx}	D_{zy}	D_{zz}
101	α_1	0	γ_1	0	β_1	0	γ_1	0	α_1
110	α_1	γ_1	0	γ_1	α_1	0	0	0	β_1
011	β_1	0	0	0	α_1	γ_1	0	γ_1	α_1
$10\bar{1}$	α_1	0	$-\gamma_1$	0	β_1	0	$-\gamma_1$	0	α_1
$1\bar{1}0$	α_1	$-\gamma_1$	0	$-\gamma_1$	α_1	0	0	0	β_1
$01\bar{1}$	β_1	0	0	0	α_1	$-\gamma_1$	0	$-\gamma_1$	α_1
200	α_2	0	0	0	β_2	0	0	0	β_2
020	β_2	0	0	0	α_2	0	0	0	β_2
002	β_2	0	0	0	β_2	0	0	0	α_2
211	α_3	δ_3	δ_3	δ_3	β_3	γ_3	δ_3	γ_3	β_3
121	β_3	δ_3	γ_3	δ_3	α_3	δ_3	γ_3	δ_3	β_3
112	β_3	γ_3	δ_3	γ_3	β_3	δ_3	δ_3	δ_3	α_3
$\bar{2}11$	α_3	$-\delta_3$	$-\delta_3$	$-\delta_3$	β_3	γ_3	$-\delta_3$	γ_3	β_3
$\bar{1}21$	β_3	$-\delta_3$	$-\gamma_3$	$-\delta_3$	α_3	δ_3	$-\gamma_3$	δ_3	β_3
$\bar{1}12$	β_3	$-\gamma_3$	$-\delta_3$	$-\gamma_3$	β_3	δ_3	$-\delta_3$	δ_3	α_3
$2\bar{1}1$	α_3	$-\delta_3$	δ_3	$-\delta_3$	β_3	$-\gamma_3$	δ_3	$-\gamma_3$	β_3
$1\bar{2}1$	β_3	$-\delta_3$	γ_3	$-\delta_3$	α_3	$-\delta_3$	γ_3	$-\delta_3$	β_3
$1\bar{1}2$	β_3	$-\gamma_3$	δ_3	$-\gamma_3$	β_3	$-\delta_3$	δ_3	$-\delta_3$	α_3
$21\bar{1}$	α_3	δ_3	$-\delta_3$	δ_3	β_3	$-\gamma_3$	$-\delta_3$	$-\gamma_3$	β_3
$12\bar{1}$	β_3	δ_3	$-\gamma_3$	δ_3	α_3	$-\delta_3$	$-\gamma_3$	$-\delta_3$	β_3
$11\bar{2}$	β_3	γ_3	$-\delta_3$	γ_3	β_3	$-\delta_3$	$-\delta_3$	$-\delta_3$	α_3

second neighbor coefficients:

$$D(200)_{xx} = \alpha_2, \qquad D(200)_{yy} = \beta_2,$$

while the Hooke's law forces between an atom and its 24 third neighbors can be expressed by four third neighbor coefficients:

$$D(211)_{xx} = \alpha_3, \qquad D(211)_{yy} = \beta_3,$$

$$D(211)_{yz} = \gamma_3, \qquad D(211)_{xy} = \delta_3.$$

The first, second, and third neighbor force constants are given in Table 11.2. Interactions with all atoms beyond the third neighbors will be assumed to be negligible.

If the Hooke's law forces between atoms in a crystal are central, in the sense that they depend only on the distance between atoms and act along a line joining their centers, the number of unique force constants is reduced still more. Simple geometrical arguments show that for this special case,

$$\alpha_1 = \gamma_1, \qquad \beta_1 = \beta_2 = 0, \qquad \alpha_3 = 2\delta_3 = 4\beta_3 = 4\gamma_3. \tag{11.63}$$

The quantities $D_{ij}(\mathbf{g})$ can now be calculated from Eq. (11.62) by using Eq. (11.53) and the values of Table 11.2. We obtain the following expressions:

$$D_{ii}(\mathbf{g}) = \frac{4}{m}\left\{\begin{aligned}&\alpha_1[2 - \cos \pi g_i(\cos \pi g_j + \cos \pi g_k)]\\ &+ \beta_1[1 - \cos \pi g_j \cos \pi g_k]\\ &+ \alpha_2 \sin^2 \pi g_i + \beta_2[\sin^2 \pi g_j + \sin^2 \pi g_k]\\ &+ 2\alpha_3[1 - \cos 2\pi g_i \cos \pi g_j \cos \pi g_k]\\ &+ 2\beta_3[2 - \cos \pi g_i(\cos 2\pi g_j \cos \pi g_k + \cos \pi g_j \cos 2\pi g_k)]\end{aligned}\right\},$$

(11.64)

$$D_{ij}(\mathbf{g}) = \frac{4}{m}\left\{\begin{aligned}&(\gamma_1 + 2\gamma_3 \cos 2\pi g_k) \sin \pi g_i \sin \pi g_j\\ &+ 2\delta_3 \cos \pi g_k(\sin 2\pi g_i \sin \pi g_j + \sin \pi g_i \sin 2\pi g_j)\end{aligned}\right\},$$

where $i, j, k = x, y$, and z, with $i \neq j \neq k$.

Substitution of these quantities into the secular equation, Eq. (11.60), now gives an explicit expression for the frequencies of the three modes of vibration of an elastic wave in terms of its wave vector components g_x, g_y, and g_z, and the various force constants. This is a cubic equation in ω^2, and its solution for an arbitrary elastic wave can be complicated. However, when the wave vector $\mathbf{g}$ is parallel to a direction of high symmetry, the solutions become quite simple.

For waves propagating in the [100] direction, $g_y = g_z = 0$, and the first Brillouin zone limits g_x to $-1 \leq g_x \leq 1$. From Eq. (11.64), $D_{ij}(\mathbf{g}) = 0$ for all $i \neq j$. The determinant in Eq. (11.60) is just the product of its diagonal terms, so that each of these must equal zero. Using Eq. (11.64), the frequencies for the three modes are given by

$$\omega_1^2 = D_{xx}(\mathbf{g}) = \frac{16}{m}(\alpha_1 + 2\beta_3) \sin^2 \frac{\pi}{2} g_x + \frac{4}{m}(\alpha_2 + 4\alpha_3) \sin^2 \pi g_x,$$

$$\omega_2^2 = D_{yy}(\mathbf{g}) = \frac{8}{m}(\alpha_1 + \beta_1 + 2\alpha_3 + 2\beta_3) \sin^2 \frac{\pi}{2} g_x + \frac{4}{m}(\beta_2 + 4\beta_3) \sin^2 \pi g_x,$$

$$\omega_3^2 = \omega_2^2. \tag{11.65}$$

From Eq. (11.59) the wave with frequency ω_1 is characterized by $A = 1$, $B = C = 0$, which represents a pure longitudinal wave. The waves with frequency $\omega_2 = \omega_3$ are characterized by $A = 0$, which represents pure transverse waves. There are no restrictions on the orientation of the vibration directions of these transverse waves except that they must be in a plane perpendicular to $\mathbf{g}$.

For waves propagating in the [111] direction, $g_x = g_y = g_z$, and the first Brillouin zone limits g_x to $-\frac{1}{2} \leq g_x \leq \frac{1}{2}$. From Eq. (11.64), all $D_{ij}(\mathbf{g})$ equal $D_{xy}(\mathbf{g})$ and all $D_{ii}(\mathbf{g})$ equal $D_{xx}(\mathbf{g})$. With a little manipulation Eq. (11.60)

becomes

$$\{D_{xx}(\mathbf{g}) + 2D_{xy}(\mathbf{g}) - \omega^2\}\{D_{xx}(\mathbf{g}) - D_{xy}(\mathbf{g}) - \omega^2\}^2 = 0,$$

from which

$$\begin{aligned}
\omega_1^2 &= D_{xx}(\mathbf{g}) + 2D_{xy}(\mathbf{g}) \\
&= \frac{4}{m}\left\{\begin{aligned}&(2\alpha_1 + \beta_1 + \alpha_2 + 2\beta_2 + 2\alpha_3 + 4\beta_3 + 2\gamma_1 - 4\gamma_3)\sin^2 \pi g_x \\ &+ (\alpha_3 + 2\beta_3 + 2\gamma_3 + 4\delta_3)\sin^2 2\pi g_x\end{aligned}\right\}, \\
\omega_2^2 &= \omega_3^2 = D_{xx}(\mathbf{g}) - D_{xy}(\mathbf{g}) \\
&= \frac{4}{m}\left\{\begin{aligned}&(2\alpha_1 + \beta_1 + \alpha_2 + 2\beta_2 + 2\alpha_3 + 4\beta_3 - \gamma_1 + 2\gamma_3)\sin^2 \pi g_x \\ &+ (\alpha_3 + 2\beta_3 - \gamma_3 - 2\delta_3)\sin^2 2\pi g_x\end{aligned}\right\}.
\end{aligned} \tag{11.66}$$

From Eq. (11.59), the wave with frequency ω_1 is characterized by $A = B = C$, which represents a pure longitudinal wave. The waves with frequency $\omega_2 = \omega_3$ are characterized by $A + B + C = 0$, which represents a pure transverse wave. Again there are no restrictions on the orientation of the vibrations of these transverse waves in the plane perpendicular to $\mathbf{g}$.

For waves propagating in the [110] direction, $g_z = 0$, $g_x = g_y$, and the first Brillouin zone limits g_x to $-\frac{3}{4} \leq g_x \leq \frac{3}{4}$. From Eq. (11.64), $D_{xz}(\mathbf{g}) = D_{yz}(\mathbf{g}) = D_{zx}(\mathbf{g}) = D_{zy}(\mathbf{g}) = 0$; $D_{xy}(\mathbf{g}) = D_{yx}(\mathbf{g})$ and $D_{xx}(\mathbf{g}) = D_{yy}(\mathbf{g})$. With a little manipulation, Eq. (11.60) becomes

$$\{D_{xx}(\mathbf{g}) + D_{xy}(\mathbf{g}) - \omega^2\}\{D_{xx}(\mathbf{g}) - D_{xy}(\mathbf{g}) - \omega^2\}\{D_{zz}(\mathbf{g}) - \omega^2\} = 0.$$

For this case there are three distinct solutions:

$$\omega_1^2 = D_{xx}(\mathbf{g}) + D_{xy}(\mathbf{g}) = \frac{4}{m}\left\{\begin{aligned}&(2\alpha_1 + 2\beta_1 + 2\alpha_3 + 2\beta_3 - 4\delta_3)\sin^2 \frac{\pi}{2} g_x \\ &+ (\alpha_1 + \alpha_2 + \beta_2 + 2\beta_3 + \gamma_1 + 2\gamma_3)\sin^2 \pi g_x \\ &+ (2\alpha_3 + 2\beta_3 + 4\delta_3)\sin^2 \frac{3\pi}{2} g_x\end{aligned}\right\},$$

$$\omega_2^2 = D_{xx}(\mathbf{g}) - D_{xy}(\mathbf{g}) = \frac{4}{m}\left\{\begin{aligned}&(2\alpha_1 + 2\beta_1 + 2\alpha_3 + 2\beta_3 + 4\delta_3)\sin^2 \frac{\pi}{2} g_x \\ &+ (\alpha_1 + \alpha_2 + \beta_2 + 2\beta_3 - \gamma_1 - 2\gamma_3)\sin^2 \pi g_x \\ &+ (2\alpha_3 + 2\beta_3 - 4\delta_3)\sin^2 \frac{3\pi}{2} g_x\end{aligned}\right\},$$

$$\omega_3^2 = D_{zz}(\mathbf{g}) = \frac{4}{m}\left\{\begin{aligned}&(4\alpha_1 + 4\beta_3)\sin^2 \frac{\pi}{2} g_x \\ &+ (\beta_1 + 2\beta_2 + 2\alpha_3)\sin^2 \pi g_x \\ &+ 4\beta_3 \sin^2 \frac{3\pi}{2} g_x\end{aligned}\right\}. \tag{11.67}$$

From Eq. (11.59), the wave with the frequency ω_1 is characterized by $C = 0$ and $B = A$, which represents a pure longitudinal wave. The wave with frequency ω_2 is characterized by $C = A + B = 0$, which represents a pure transverse wave with the direction of vibration in the xy-plane. The wave with frequency ω_3 is characterized by $C = 1$ and $A = B = 0$, which represents a pure transverse wave with the direction of vibration parallel to the z-axis.

The dispersion relations (the dependence of ω on $\mathbf{g}$), for waves propagating along the three directions of high symmetry for this lattice, all have the same simple form:

$$m\omega^2 = \sum_{n=1} A_n \sin^2 n\frac{\pi}{2} g_x$$

$$= \sum_{n=0} B_n \cos n\pi g_x, \tag{11.68}$$

where the A_n (or the B_n) are linear combinations of the interatomic force constants. Foreman and Lomer[15] have pointed out that the elastic waves propagating along these three directions correspond physically to vibrations of complete planes of atoms with respect to one another. Then by analogy with the mathematically equivalent problem of the vibrations of a linear chain, the quantities B_n can be thought of as the harmonic force constants per atom acting between nth neighbor planes. It follows also that the dispersion relations for waves along these three directions can always be written in the form of Eq. (11.68) regardless of the range of the interatomic forces, since an increase in the range of the forces will only alter the number of nonzero B_n coefficients. From the form of Eqs. (11.65), (11.66), and (11.67), it is evident that at the maximum value of g_x, the ω-versus-g_x curves should have zero slope for waves in the [100] and [111] directions, and a nonzero slope for waves in the [110] direction.

Elastic waves with angular frequency ω and wave vector $\mathbf{g}$ travel with a phase velocity $V = \omega/2\pi|\mathbf{g}|$. The phase velocities of waves propagating along the three symmetry directions of this structure obey the relation

$$V^2 = \frac{1}{m}\sum_{n=1} A_n \frac{\sin^2 n(\pi/2)g_x}{4\pi^2|\mathbf{g}|^2}.$$

In the limit of very long wavelength, this takes the form

$$V^2(g \to 0) = \frac{1}{4a\rho}\sum_{n=1} n^2 A_n \frac{g_x^2}{g_x^2 + g_y^2 + g_z^2},$$

where $\rho = 4m/a^3$ is the density. These velocities must equal the corresponding velocities determined by the elasticity theory of Section 11.2. A comparison of the two gives a set of relations between the elastic constants and the interatomic force constants. If interactions beyond third neighbors

are neglected, we obtain

$$\begin{aligned} aC_{11} &= 4\alpha_1 + 4\alpha_2 + 16\alpha_3 + 8\beta_3, \\ aC_{44} &= 2\alpha_1 + 2\beta_1 + 4\beta_2 + 4\alpha_3 + 20\beta_3, \\ a(C_{12} + C_{44}) &= 4\gamma_1 + 8\gamma_3 + 32\delta_3. \end{aligned} \tag{11.69}$$

The Born–von Karman theory gives explicit expressions for the elastic constants and the dispersion of the elastic waves in terms of the various interatomic force constants. By matching Eqs. (11.65), (11.66), and (11.67) to the ω-versus-g_x curves for waves in the three simple directions, obtained from measurements of the temperature diffuse scattering of x-rays, and in addition making use of the relations to the elastic constants expressed by Eq. (11.69), we obtain numerical values for the nine interatomic force constants. For both face-centered cubic and body-centered cubic monatomic elements, the measured dispersion curves for waves along the three simple directions are sufficient if we limit ourselves to interactions between first, second, and third neighbors only. In terms of the Born–von Karman theory, the measurement of the temperature diffuse scattering of x-rays is used solely to determine the interatomic force constants. Once the constants are known, the theory can be used to calculate the frequencies and polarizations for elastic waves of any wave vector. Thus by programming a digital computer to solve these equations for a uniform, reasonably dense distribution of wave vectors throughout the first Brillouin zone, one can determine an approximate distribution $N(\nu)$ of the frequencies of the elastic waves.

A study of lattice vibrations in aluminum by Walker[9] illustrates the use of this approach. Single crystal x-ray diffuse scattering measurements at room temperature yielded experimental dispersion curves for the elastic waves propagating along the three primary symmetry directions of this face-centered cubic crystal. By fitting these dispersion curves to the Born–von Karman theory, and also using the measured elastic constants, the nine general first, second, and third neighbor force constants of Table 11.3 were obtained. For central forces, the necessary relations between the interatomic

Table 11.3
INTERATOMIC FORCE CONSTANTS FOR ALUMINUM IN UNITS, 10^3 dynes/cm

$\alpha_1 = D(101)_{xx} =$	8.45	$\alpha_3 = D(211)_{xx} =$	0.27
$\beta_1 = D(101)_{yy} =$	−0.93	$\beta_3 = D(211)_{yy} =$	−0.31
$\gamma_1 = D(101)_{xz} =$	10.67	$\gamma_3 = D(211)_{yz} =$	0.10
$\alpha_2 = D(200)_{xx} =$	2.14	$\delta_3 = D(211)_{xy} =$	−0.19
$\beta_2 = D(200)_{yy} =$	0.40		

force constants are given by Eq. (11.63). The relations are not satisfied, and hence the forces are not true central forces. However, there is an approximate agreement, and it is not too bad as a first approximation to consider the forces in aluminum as central forces.

Using the force constants of Table 11.3, the secular equation was then solved by a digital computer for the 2791 wave vectors distributed on a cubic net throughout the volume element of the first Brillouin zone that is irreducible under symmetry operations, a sampling that is equivalent to over 108,000 wave vectors distributed throughout the entire first Brillouin zone. The resulting solutions gave the approximate frequency spectrum shown by the histogram of Fig. 11.15. Below approximately 0.7×10^{13} cps, this spectrum derives primarily from transverse-like modes, while above this frequency the longitudinal-like modes are predominant. The various discontinuities in slope arise from critical points (van Hove,[16] Phillips[17]) in the Brillouin zone, where the gradient of the frequency of a given branch vanishes. For comparison, a Debye spectrum that gives the measured specific heat of aluminum at this temperature would have a cut-off frequency of 0.796×10^{13} cps.

Since the required measurements of the intensity of temperature diffuse scattering are not simple, and considerable work is involved, there have been relatively few complete determinations of the frequency spectrum from x-ray measurements. Examples of other determinations of frequency distributions are given by the study of α iron by Curien[18] and of copper by Jacobsen.[19]

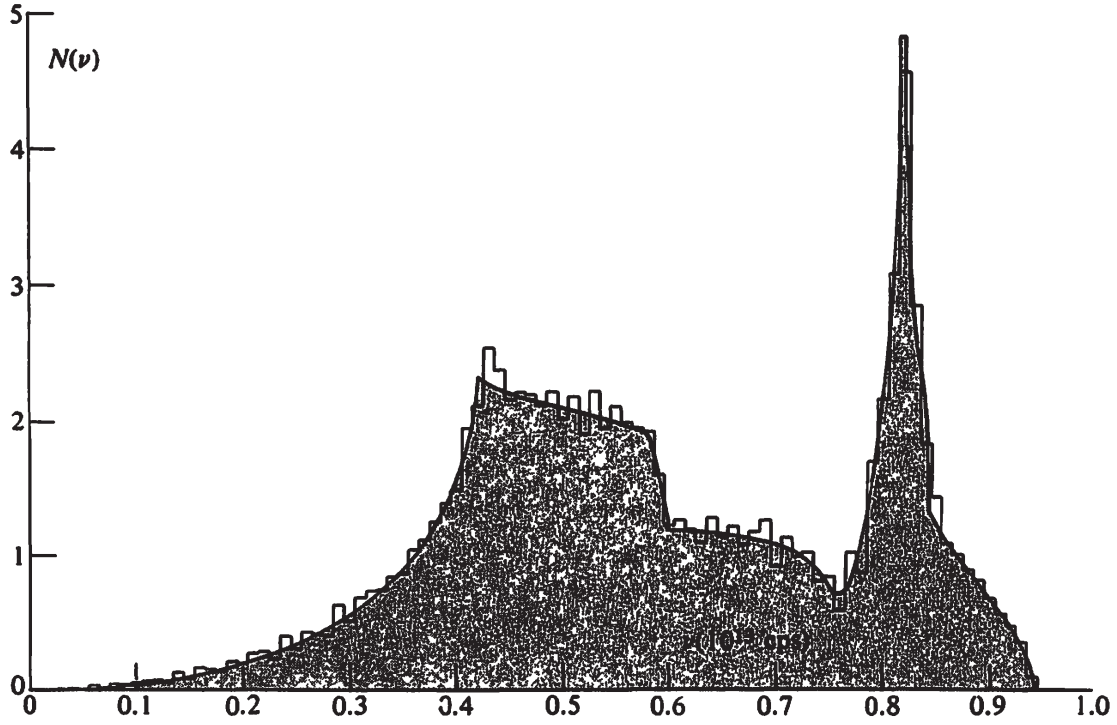

Fig. 11.15 Frequency distribution for elastic waves in aluminum from x-ray measurements at room temperature (C. B. Walker).

11.10 EVALUATION OF $2M$

In this section we shall consider first a cubic crystal containing only one kind of atom. From Eqs. (11.19), (11.21), and (11.22), the value of $2M$ is expressed by

$$2M = \frac{h}{4\pi^2 Nm} \sum_{gj} \frac{(k\mathbf{S} \cdot \mathbf{e}_{gj})^2}{\nu_{gj}} \left\{ \frac{1}{e^{(h\nu_{gj}/kT)} - 1} + \frac{1}{2} \right\}. \tag{11.70}$$

Since $2M$ involves a sum over all of the elastic waves, it is possible to make certain approximations which amount to an averaging before the summation. Following the method of Debye as presented by James,[5] we assume that all waves can be considered as pure longitudinal and pure transverse. The velocities of all longitudinal waves are replaced by an average longitudinal velocity, and the velocities of all transverse waves by an average transverse velocity. Each average velocity is considered to be a constant independent of the wavelength of the elastic wave. From the diffuse scattering studies in the previous section, we have seen that there is an appreciable variation in velocity with wavelength. This effect, which we call dispersion, is allowed for indirectly in the present treatment by expressing the result in terms of a Debye characteristic temperature Θ which itself includes a dispersion effect.

To facilitate the summation in Eq. (11.70), the Brillouin zone is replaced by a sphere of radius g_m, whose volume is equal to that of the Brillouin zone $(\frac{4}{3})\pi g_m^3 = v(\text{BZ})$. The density of points in the sphere is $N/v(\text{BZ})$, and the summation over g is replaced by an integration throughout the sphere. Using a hollow sphere of radii g and $g + dg$, the element of volume is $4\pi g^2\, dg$. For each type of wave, longitudinal and transverse, the vibration direction $\mathbf{e}_{gj}$ takes with equal probability all orientations relative to $\mathbf{S}$, and for all waves whose vectors $\mathbf{g}$ terminate in the hollow sphere, we can use the average $\langle (k\mathbf{S} \cdot \mathbf{e}_{gj})^2 \rangle = k^2 |\mathbf{S}|^2 \langle \cos^2 (S, e) \rangle = (4\pi \sin \theta/\lambda)^2/3$. With these approximations and simplifications, Eq. (11.70) becomes

$$2M = \frac{h}{4\pi^2 Nm3} \left(\frac{4\pi \sin \theta}{\lambda} \right)^2 \sum_j \int_0^{g_m} \frac{1}{\nu_{gj}} \left\{ \frac{1}{e^{(h\nu_{gj}/kT)} - 1} + \frac{1}{2} \right\} \frac{N}{v(\text{BZ})} 4\pi g^2\, dg \tag{11.71}$$

The sum over j represents one longitudinal and two transverse waves. In terms of a constant velocity V_j for each kind of wave, $\nu_j = V_j g$ so that $g^2\, dg = (\nu_j^2/V_j^3)\, d\nu_j$. The volume of the Brillouin zone can be written in terms of the maximum frequency and the corresponding velocity, $(4\pi/3)g_m^3 = (4\pi/3)\nu_{mj}^3/V_j^3$. With these relations, the integral of Eq. (11.71) is expressed in terms of the variable ν:

$$2M = \frac{4h}{m} \left(\frac{\sin \theta}{\lambda} \right)^2 \sum_j \frac{1}{\nu_{mj}^3} \int_0^{\nu_{mj}} \left\{ \frac{1}{e^{(h\nu/kT)} - 1} + \frac{1}{2} \right\} \nu\, d\nu. \tag{11.72}$$

Let

$$\epsilon = \frac{h\nu}{kT}, \qquad x_j = \frac{h\nu_{mj}}{kT}.$$

Using the function $\Phi(x)$ introduced by Debye,

$$\Phi(x) = \frac{1}{x}\int_0^x \frac{\epsilon\, d\epsilon}{e^\epsilon - 1}. \tag{11.73}$$

Equation (11.72) becomes

$$2M = \frac{4kT}{m}\left(\frac{\sin\theta}{\lambda}\right)^2 \sum_j \frac{1}{\nu_{mj}^2}\left\{\Phi(x_j) + \frac{x_j}{4}\right\}. \tag{11.74}$$

In the Debye theory of specific heats, a characteristic temperature Θ is defined by $h\nu_m = k\Theta$. Our model requires separate characteristic temperatures and coefficients x_j for the longitudinal and the transverse waves:

$$h\nu_{ml} = k\Theta_l, \qquad h\nu_{mt} = k\Theta_t, \qquad x_l = \Theta_l/T, \qquad x_t = \Theta_t/T.$$

In terms of the characteristic temperatures, $2M$ is given by

$$2M = \frac{4h^2T}{mk}\left(\frac{\sin\theta}{\lambda}\right)^2\left\{\frac{1}{\Theta_l^2}\left[\Phi(x_l) + \frac{x_l}{4}\right] + \frac{2}{\Theta_t^2}\left[\Phi(x_t) + \frac{x_t}{4}\right]\right\}.$$

By expanding the exponential in Eq. (11.73), it is readily shown that

$$\left[\Phi(x) + \frac{x}{4}\right] = 1 + \frac{x^2}{36} - \frac{x^4}{3600} + \cdots. \tag{11.75}$$

For $x \langle 2$, corresponding to $T \rangle \Theta/2$, $[\Phi(x) + x/4]$ is closely the same for the longitudinal and transverse waves. We next introduce an average Θ_M for use in the $2M$ factor, defined by

$$\frac{3}{\Theta_M^2} = \frac{1}{\Theta_l^2} + \frac{2}{\Theta_t^2}. \tag{11.76}$$

With this average characteristic temperature Θ_M, and the average ratio $x = \Theta_M/T$, we obtain finally

$$2M = \frac{12h^2T}{mk\Theta_M^2}\left[\Phi(x) + \frac{x}{4}\right]\left(\frac{\sin\theta}{\lambda}\right)^2. \tag{11.77}$$

The average involved in Eq. (11.76) is a little different from that in the Debye theory of specific heats, so that the Θ_M of Eq. (11.77) is not quite the same as the Θ_D of the specific heat theory. The difference, however, is not great,*

* A striking exception is germanium where Θ_M is about 20 percent lower than Θ_D (B. Batterman and D. Chipman, *Phys. Rev.* **127**, 690, 1962).

and to a first approximation we can use for Θ_M the tabulated Debye temperature Θ_D.

Equation (11.77) is particularly useful for the cubic metals, most of which have tabulated values of Θ_D. For temperatures equal to or greater than Θ_D but not high enough for anharmonicity and variation in Θ_D to be important, the quantity $2M$ is closely a linear function of T and $(\sin\theta/\lambda)^2$. As an example, let us evaluate $2M$ for copper at $T = 300°\text{K}$. From the tables $\Theta_D = 315°$, $m = 63.6/6.02 \times 10^{23} = 10.55 \times 10^{-23}$ gm, $x = \frac{315}{300} = 1.05$, and $[\Phi(x) + x/4] = 1.03$. Using these values,

$$2M = \frac{12 \times (6.62 \times 10^{-27})^2 \times 300 \times 1.03 \times 10^{16}}{10.55 \times 10^{-23} \times 1.38 \times 10^{-16}(315)^2}\left(\frac{\sin\theta}{\lambda_A}\right)^2 = 1.13\left(\frac{\sin\theta}{\lambda_A}\right)^2.$$

For Co$K\alpha$ radiation $\lambda = 1.79$ A and reflections near $\theta = 90°$, $2M = 0.35$ and $\exp[-2M] = 0.70$. For this example, the effect of thermal vibrations is to reduce the integrated intensities of the high-angle crystalline reflections to 70 percent of the value which would otherwise have been obtained. For the cubic metals for which Θ_D values are available, the measured reductions in the integrated intensities are reasonably well predicted by Eq. (11.77).

It is also possible to obtain a value for $2M$ from the three elastic constants. By making the approximation of central forces, and considering only nearest and next nearest neighbor interactions, only two interatomic force constants are involved, and these can be computed from the elastic constants. Using these two interatomic force constants in the equations of the Born theory, it is possible to compute the frequencies of a large enough number of waves to allow a good evaluation of $2M$ from Eq. (11.70). A reliable value can be expected since it is known that this method for obtaining a frequency distribution curve leads to a specific heat curve which is an improvement over that of the simple Debye model. In this procedure there is no neglect of dispersion because this factor is automatically included in the frequencies computed from the Born theory equations. Where good elastic constants can be obtained, and a computer is available, this would seem to be a possible procedure for computing $2M$ which is relatively free from doubtful approximations.

For a cubic crystal containing only one kind of atom such as FCC copper or BCC α iron, Eq. (11.77) predicts that $2M$ should be isotropic, depending only on $(\sin\theta/\lambda)^2$ and not on the individual hkl-values. If the crystal contains more than one kind of atom, the $2M$ for any atom type should be isotropic if the surroundings of the atom have cubic symmetry. A general expression for $2M$ was given by Eq. (3.21):

$$2M = 16\pi^2\langle u_s^2\rangle \frac{\sin^2\theta}{\lambda^2},$$

where $\langle u_s^2\rangle$ is the mean square of the component of displacement along the

$\mathbf{s} - \mathbf{s}_0$ direction. In terms of displacement components along the x-, y-, z-axes,

$$u_s = u_x \cos(s, x) + u_y \cos(s, y) + u_z \cos(s, z).$$

In forming the square and taking the average, we make the approximation that u_x, u_y, u_z are independent:

$$\langle u_s^2 \rangle = \langle u_x^2 \rangle \cos^2(s, x) + \langle u_y^2 \rangle \cos^2(s, y) + \langle u_z^2 \rangle \cos^2(s, z). \qquad (11.78)$$

Since $\langle u_x^2 \rangle = \langle u_y^2 \rangle = \langle u_z^2 \rangle$ and $\cos^2(s, x) + \cos^2(s, y) + \cos^2(s, z) = 1$, it follows from Eq. (11.78) that $\langle u_s^2 \rangle$ is independent of the orientation of the component u_s, and accordingly $2M$ is isotropic for an atom whose surroundings have cubic symmetry.

For an atom whose surroundings have hexagonal symmetry, $\langle u_s^2 \rangle$ is given by Eq. (11.78) in terms of mean square components along the orthogonal axes x, y, z. Let the projection of $\mathbf{s} - \mathbf{s}_0$ on the xy-plane have the direction r. From the law of spherical right triangles,

$$\cos^2(s, x) = \cos^2(s, r) \cos^2(r, x), \qquad \cos^2(s, y) = \cos^2(s, r) \cos^2(r, y),$$

and Eq. (11.78) becomes

$$\langle u_s^2 \rangle = \{\langle u_x^2 \rangle \cos^2(r, x) + \langle u_y^2 \rangle \cos^2(r, y)\} \cos^2(s, r) + \langle u_z^2 \rangle \cos^2(s, z).$$

If r is parallel to the $\mathbf{a}_1$ axis, $\cos^2(r, x) = 1$ and $\cos^2(r, y) = 0$. For the equivalent case where r is parallel to the $\mathbf{a}_2$-axis, $\cos^2(r, x) = \frac{1}{4}$ and $\cos^2(r, y) = \frac{3}{4}$. Since $\langle u_s^2 \rangle$ must be the same in either case, it follows that $\langle u_y^2 \rangle = \langle u_x^2 \rangle$, and hence $\{\langle u_x^2 \rangle \cos^2(r, x) + \langle u_y^2 \rangle \cos^2(r, y)\} = \langle u_r^2 \rangle$ is independent of the direction of r in the xy-plane. In terms of the angle between the z-axis and the planar normal $\mathbf{s} - \mathbf{s}_0$.

$$\langle u_s^2 \rangle = \langle u_r^2 \rangle \sin^2(s, z) + \langle u_z^2 \rangle \cos^2(s, z), \qquad (11.79)$$

where $\langle u_z^2 \rangle$ and $\langle u_r^2 \rangle$ are the mean square components parallel and perpendicular to the z-axis. Equation (11.79) is applicable to either hexagonal or tetragonal surroundings. In general, $\langle u_r^2 \rangle$ and $\langle u_z^2 \rangle$ are different, and hence $2M$ depends upon the angle between the z-axis and the planar normal, as well as upon $(\sin \theta/\lambda)^2$.

Cubic structures of the NaCl, CsCl, and ZnS type involve two different kinds of atoms. For such structures there are two Debye factors M_A and M_B. Intuitively, one feels that it should be possible to calculate these two quantities from basic crystallographic data, but as yet no satisfying procedure has been evolved, and the two different Debye factors are obtained only by x-ray measurements. It is really surprising that except for the simplest of cubic structures, we are not yet in a position to compute $2M$-values, and that corrections for temperature vibration must be made from experimentally determined $2M$-values.

11.11 TEMPERATURE DIFFUSE SCATTERING FOR CUBIC POWDER PATTERNS

Allowing for thermal vibrations, the intensity from a crystal containing only one kind of atom is given by Eqs. (11.14) and (11.16):

$$I = I_e f^2 \sum_m \sum_n e^{ik\mathbf{S}\cdot(\mathbf{r}_m - \mathbf{r}_n)} e^{-(k^2S^2/2)\langle(u_{sm}-u_{sn})^2\rangle},$$

where u_{sm} is the component along S of the displacement of atom m. Separating the N terms for which $n = m$,

$$I = I_e N f^2 + I_e f^2 \sum_m \sum_{m \neq n} e^{ik\mathbf{S}\cdot(\mathbf{r}_m - \mathbf{r}_n)} e^{-(k^2S^2/2)(\langle u_{sm}^2\rangle - 2\langle u_{sm}u_{sn}\rangle + \langle u_{sn}^2\rangle)}.$$

The early Debye theory was based on the approximation that the atoms vibrate independently, so that $\langle u_{sm}u_{sn}\rangle = 0$ for all pairs $n \neq m$. In terms of the Debye factor defined by Eq. (11.1),

$$(k^2S^2/2)\langle u_{sm}^2\rangle = (k^2S^2/2)\langle u_{sn}^2\rangle = M.$$

With these simplifications,

$$I = I_e N f^2 + I_e f^2 e^{-2M} \sum_m \sum_{n \neq m} e^{ik\mathbf{S}\cdot(\mathbf{r}_m - \mathbf{r}_n)}.$$

Adding and subtracting the N terms which are needed to complete the double sum, we obtain the classical intensity expression for the approximation of independent vibration of the atoms:

$$I = I_e N f^2 (1 - e^{2M}) + I_e f^2 e^{-2M} \sum_m \sum_n e^{ik\mathbf{S}\cdot(\mathbf{r}_m - \mathbf{r}_n)}. \tag{11.80}$$

The second term of Eq. (11.80) represents the ordinary crystalline reflection reduced by the Debye factor $\exp[-2M]$. The first term is the temperature diffuse scattering on the basis of the early approximation involving independent vibration of the atoms. Since $2M = 16\pi^2\langle u_s^2\rangle (\sin\theta/\lambda)^2$, the diffuse intensity is zero at $\sin\theta/\lambda = 0$, it increases with increasing $\sin\theta/\lambda$, and at high values of $\sin\theta/\lambda$ it approaches the limiting value $I_e N f^2$. In this early picture, the diffuse background was a slanting straight line in the vicinity of a Bragg reflection. There was a clear cut separation between the crystalline peak and the flat background, and it was quite correct to say that there was no broadening of the Bragg peak, only a reduction in area by the factor $\exp[-2M]$. In the modern theory, this is no longer true; the temperature diffuse scattering comes to a peak at the position of the Bragg reflection, and there is no longer a clear cut separation between a Bragg reflection reduced by $\exp[-2M]$ and the diffuse intensity. If the two components are considered together, with no attempt to separate them, there is actually an increase in the peak width resulting from the temperature vibration. It is well to keep in mind that the separation of a reduced crystalline peak from the diffuse intensity is somewhat artificial in the immediate vicinity

of the peak and that the idea of a clear cut separation is an inheritance from a former oversimplified theory. Outside of the immediate vicinity of a Bragg peak, there is only the diffuse intensity and hence no trouble in separating the two components.

Following a treatment by Warren,[20] it is possible to compute a temperature diffuse scattering curve for cubic powder patterns which is a much better approximation than the diffuse term of Eq. (11.80). For crystals containing one kind of atom and for temperatures high enough to assume equipartition, the first-order TDS contribution is given by Eq. (11.36):

$$I_1(S/\lambda) = I_e f^2 e^{-2M} \frac{NkT}{m} \frac{|\mathbf{S}/\lambda|^2}{|\mathbf{g}|^2} \sum_j \frac{\cos^2(S, e_{gj})}{V_{gj}^2}.$$

We assume that all elastic waves have the same average velocity V, and hence $\sum_j \cos^2(S, e_{gj}) = 1$. We set $|\mathbf{S}/\lambda|^2 = 4(\sin\theta/\lambda)^2$ and replace the Brillouin zone by a sphere of equal volume $(\frac{4}{3})\pi g_m^3$. Since $V = \nu_m/g_m$ and $h\nu_m = k\Theta$, we can write $V = k\Theta/hg_m$. With these changes, the first-order TDS at the position $\mathbf{S}/\lambda$ in reciprocal space is expressed by

$$I_1(S/\lambda) = I_e f^2 e^{-2M} \frac{4Nh^2T}{mk\Theta^2} \left(\frac{\sin\theta}{\lambda}\right)^2 \frac{g_m^2}{g^2}.$$

If we introduce $2M$ from Eq. (11.77) with the approximation $[\Phi(x) + x/4] = 1$, we can express $I_1(S/\lambda)$ in terms of $2M$:

$$I_1(S/\lambda) = I_e N f^2 e^{-2M} 2M g_m^2/3g^2. \tag{11.81}$$

This is the intensity corresponding to a point P in the hkl Brillouin zone of Fig. 11.16. The distance of point P from the origin is denoted by R, where $R = |\mathbf{S}/\lambda| = 2\sin\theta/\lambda$, and the distance of the point hkl is represented by R_{hkl}. For a fixed value of $\sin\theta/\lambda$, the intensity on a powder pattern is given by averaging Eq. (11.81) over all points P on the surface of the sphere of constant radius $R = 2\sin\theta/\lambda$. To obtain this average we integrate $1/g^2$ over the surface of that part of the sphere which is within the Brillouin zone, we

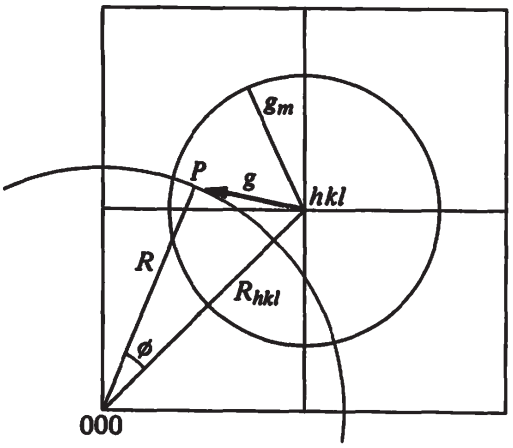

Fig. 11.16 Illustration of the averaging of $1/g^2$ over that part of the surface of a sphere of radius R which is contained within the Brillouin zone which is centered on the hkl point.

then add the contribution from all zones which are traversed by the sphere, and finally we divide by the sphere area $4\pi R^2$. The sum over the Brillouin zones can be expressed in terms of a multiplicity $j(hkl)$ and a sum over non-equivalent hkl:

$$I_1\left(\frac{\sin\theta}{\lambda}\right) = I_e N f^2 e^{-2M} 2M \frac{g_m^2}{3} \frac{1}{4\pi R^2} \sum_{hkl} j(hkl) \int \frac{dA}{g^2}.$$

Since $g^2 = R_{hkl}^2 + R^2 - 2R_{hkl}R\cos\phi$ and $dA = 2\pi R^2 \sin\phi\, d\phi$,

$$I_1\left(\frac{\sin\theta}{\lambda}\right) = I_e N f^2 e^{-2M} 2M \frac{g_m^2}{3} \frac{1}{4\pi R^2} \sum_{hkl} j(hkl) \int_0^{\phi_0} \frac{2\pi R^2 \sin\phi\, d\phi}{R^2 + R_{hkl}^2 - 2RR_{hkl}\cos\phi},$$

where ϕ_0 is determined by $g_m^2 = R^2 + R_{hkl}^2 - 2RR_{hkl}\cos\phi_0$. The integral is readily evaluated and the expression reduced to

$$I_1\left(\frac{\sin\theta}{\lambda}\right) = I_e N f^2 e^{-2M} 2M \frac{g_m^2}{6} \sum_{hkl} \frac{j(hkl)}{RR_{hkl}} \ln\left[\frac{g_m}{|R - R_{hkl}|}\right].$$

To obtain a general expression for cubic powder patterns, it is convenient to introduce the general notation $x = (2a/\lambda)\sin\theta$ and $x_{hkl} = (2a/\lambda)\sin\theta_{hkl}$:

$$I_1\left(\frac{\sin\theta}{\lambda}\right) = I_e N f^2 e^{-2M} 2M \frac{(ag_m)^2}{6x} \sum_{hkl} \frac{j(hkl)}{x_{hkl}} \ln\left[\frac{ag_m}{|x - x_{hkl}|}\right]. \quad (11.82)$$

For cubic crystals, the volume of the Brillouin zone is the reciprocal of the volume per atom $(\frac{4}{3})\pi g_m^3 = 1/v_0$. Since $v_0 = a^3/n$, where n is the number of atoms per unit cell, $ag_m = (3/2\pi)^{1/3}$ for BCC crystals and $ag_m = (3/\pi)^{1/3}$ for the FCC case.

For temperatures high enough to assume equipartition, the contribution by first-order TDS for a FCC element is expressed by

$$\frac{I\left(\frac{\sin\theta}{\lambda}\right)}{I_e N f^2 e^{-2M} 2M} = Q_1 = \frac{(3/\pi)^{2/3}}{6x} \sum_{hkl} \frac{j(hkl)}{x_{hkl}} \ln\left[\frac{(3/\pi)^{1/3}}{|x - x_{hkl}|}\right]. \quad (11.83)$$

In plotting Eq. (11.83) against the general variable $x = 2a\sin\theta/\lambda$, each zone with unmixed indices hkl contributes over the range $|x - x_{hkl}| < (3/\pi)^{1/3}$. For the 000 zone where $\mathbf{S}/\lambda = \mathbf{g}$, the contribution is given by $(3/\pi)^{2/3}/3x^2$. A plot of Eq. (11.83) is shown on Fig. 11.17. The first-order TDS rises to rather sharp peaks at the position of each of the hkl-reflections. Between the peaks there are dips such that $Q_1 = I_1/(I_e N^2 e^{-2M} 2M)$ has an average value of approximately unity when averaged over $\sin\theta/\lambda$. Curves for the first-order TDS at three different temperatures for both the FCC and the BCC cases have been given by Herbstein and Averbach.[21]

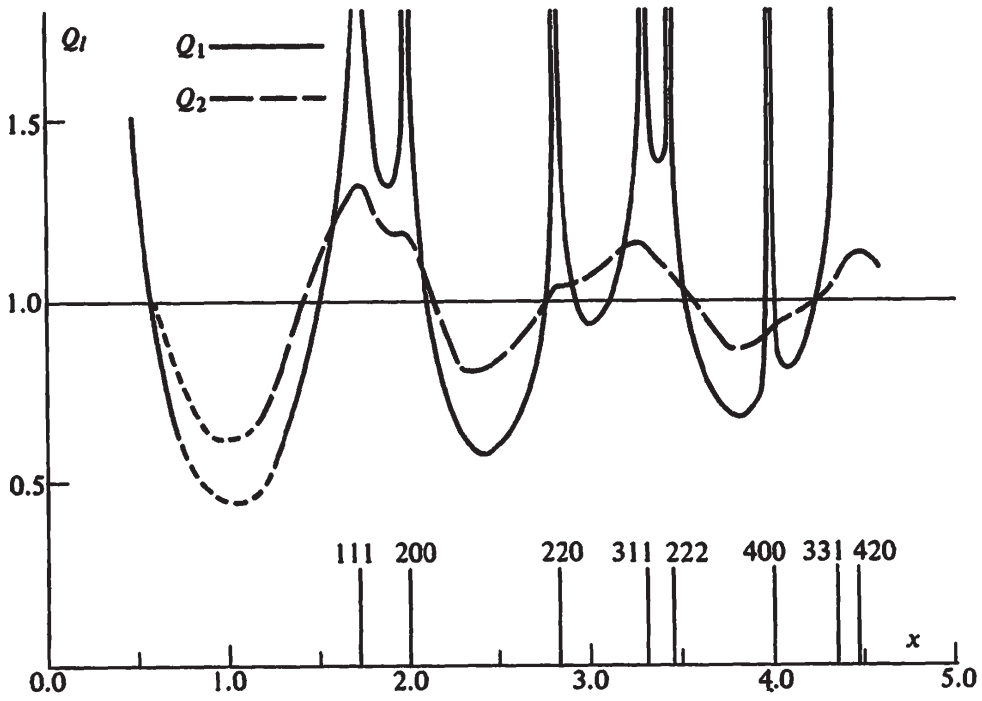

Fig. 11.17 The first-order and second-order TDS for the powder pattern of a FCC element, as a function of $x = (2a/\lambda)\sin\theta$. $Q_1 = I_1/I_e N f^2 e^{-2M} 2M$ and $Q_2 = I_2/I_e N f^2 e^{-2M}(2M)^2/2$. The first-order TDS peaks rather sharply at the positions of the various Bragg reflections.

The second-order and higher-order TDS contributions to cubic powder patterns are readily evaluated by making several simplifying approximations. From Eq. (11.26),

$$I = I_e f^2 e^{-2M} \sum_m \sum_n e^{(2\pi i/\lambda)\cdot \mathbf{S}(\mathbf{r}_m - \mathbf{r}_n)} e^{Y_{mn}},$$

where

$$Y_{mn} = \sum_{gj} G_{gj} \cos 2\pi \mathbf{g} \cdot (\mathbf{r}_m - \mathbf{r}_n). \tag{11.84}$$

By expanding the exponential $e^Y = 1 + Y + Y^2/2 + \cdots Y^l/l!$, we express the lth-order TDS by the equation

$$I_l = I_e f^2 e^{-2M} \sum_m \sum_n e^{(2\pi i/\lambda)\mathbf{S}\cdot(\mathbf{r}_m - \mathbf{r}_n)} Y_{mn}^l / l!. \tag{11.85}$$

Assuming the temperature to be high enough for equipartition, using a spherical Brillouin zone of radius g_m, and replacing all wave velocities by an average velocity $V = k\Theta/hg_m$, Eq. (11.84) becomes

$$Y_{mn} = \sum_g \frac{4h^2 T}{Nmk\Theta^2} \left(\frac{\sin\theta}{\lambda}\right)^2 \frac{g_m^2}{g^2} \cos 2\pi \mathbf{g} \cdot \mathbf{r}_{mn}.$$

Introducing $2M$ from Eq. (11.77) with the approximation $[\Phi(x) + x/4] = 1$, we obtain the simple form

$$Y_{mn} = \frac{2M}{3N} g_m^2 \sum_g \frac{\cos 2\pi \mathbf{g} \cdot \mathbf{r}_{mn}}{g^2}.$$

The summation over g is replaced by an integration in the Brillouin zone using a density of points $N/(4\pi g_m^3/3)$:

$$Y_{mn} = \frac{2Mg_m^2}{3N} \int_0^{g_m} \int_0^{\pi} \frac{\cos 2\pi g r_{mn} \cos\phi}{g^2} \frac{N}{(4\pi g_m^3/3)} 2\pi g^2 \sin\phi \, d\phi \, dg.$$

The integrations are readily performed and we obtain

$$Y_{mn} = 2M\left[\frac{\mathrm{Si}(z_{mn})}{z_{mn}}\right], \tag{11.86}$$

where

$$\mathrm{Si}(z) = \int_0^z \frac{\sin u}{u} du \quad \text{and} \quad z_{mn} = 2\pi g_m r_{mn}.$$

The position of measurement is $\mathbf{S}/\lambda = \mathbf{H}_{hkl} + \mathbf{q}$, where $\mathbf{q}$ is the vector from the nearest active reciprocal lattice point. Combining Eqs. (11.85) and (11.86), we express the lth-order TDS at a position $\mathbf{q}$ in reciprocal space:

$$I_l(\mathbf{q}) = I_e f^2 e^{-2M} \frac{(2M)^l}{l!} \sum_m \sum_n e^{2\pi i \mathbf{q}\cdot\mathbf{r}_{mn}} \left[\frac{\mathrm{Si}(z_{mn})}{z_{mn}}\right]^l. \tag{11.87}$$

Because of the cubic symmetry involved in the summation over n, and the averaging which will follow in obtaining a powder pattern intensity from Eq. (11.87), we make the approximation of replacing $\exp[2\pi i \mathbf{q}\cdot\mathbf{r}_{mn}]$ by its average when $\mathbf{q}$ takes all orientations:

$$\langle e^{2\pi i \mathbf{q}\cdot\mathbf{r}_{mn}} \rangle = \frac{1}{2} \int_0^{\pi} e^{2\pi i q r_{mn} \cos\phi} \sin\phi \, d\phi = \frac{\sin 2\pi q r_{mn}}{2\pi q r_{mn}}.$$

In terms of the magnitude $q = |\mathbf{q}|$, the average intensity is given by

$$I_l(q) = I_e f^2 e^{-2M} \frac{(2M)^l}{l!} \sum_m \sum_n \frac{\sin 2\pi q r_{mn}}{2\pi q r_{mn}} \left[\frac{\mathrm{Si}(z_{mn})}{z_{mn}}\right]^l. \tag{11.88}$$

To obtain the lth-order powder pattern intensity at a fixed value of $\sin\theta/\lambda$, we average $I_l(q)$ over the surface of the sphere of radius R shown by Fig. 11.16:

$$I_l\left(\frac{\sin\theta}{\lambda}\right) = \frac{1}{4\pi R^2} \sum_{hkl} j(hkl) \int I_l(q) \, dA. \tag{11.89}$$

Since $q^2 = R^2 + R_{hkl}^2 - 2RR_{hkl}\cos\phi$ and $q\,dq = R_{hkl} R \sin\phi \, d\phi$, the element of area can be expressed in the form

$$dA = 2\pi R^2 \sin\phi \, d\phi = (2\pi R/R_{hkl}) q \, dq.$$

The integral over q is between the limits $q = |R - R_{hkl}|$ and $q = g_m$:

$$\int \frac{\sin 2\pi q r_{mn}}{2\pi q r_{mn}} dA = \frac{R}{2\pi r_{mn}^2 R_{hkl}} \{\cos 2\pi |R - R_{hkl}| r_{mn} - \cos 2\pi g_m r_{mn}\}.$$

For $l = 2$ or greater, there is a rapid convergence in the sum over n of Eq. (11.88) due to r_{mn} in the denominator and $[\mathrm{Si}(z_{mn})/z_{mn}]^l$. The sum over n is replaced by a sum over shells i with multiplication by C_i, the number of neighbors in shell i. The sum over m is then replaced by multiplication by N, Introducing the abbreviation

$$I_l'\left(\frac{\sin\theta}{\lambda}\right) = Q_l = \frac{I_l(\sin\theta/\lambda)}{I_e N f^2 e^{-2M}(2M)^l/l!}, \tag{11.90}$$

we can write

$$I_l'\left(\frac{\sin\theta}{\lambda}\right) = \frac{1}{2R}\sum_{hkl}\frac{j(hkl)}{R_{hkl}}\sum_{i=0}^{\infty} C_i\left\{\frac{\cos 2\pi\,|R - R_{hkl}|\,r_i - \cos 2\pi g_m r_i}{(2\pi r_i)^2}\right\}\left[\frac{\mathrm{Si}(z_i)}{z_i}\right]^l.$$

Introduce the more convenient notation $x = aR = (2a/\lambda)\sin\theta$ and $x_{hkl} = (2a/\lambda)\sin\theta_{hkl}$, where a is the edge of the cubic cell. For the $i = 0$ term, where $C_i = 1$, $r_i = 0$, and $[\mathrm{Si}(z_i)/z_i] = 1$, a simpler expression can be used. The lth-order TDS is given by

$$I_l'\left(\frac{\sin\theta}{\lambda}\right) = Q_l = \frac{1}{2x}\sum_{hkl}\frac{j(hkl)}{x_{hkl}}\Phi_l(|x - x_{hkl}|), \tag{11.91}$$

where

$$\Phi_l(|x - x_{hkl}|) = \frac{(ag_m)^2 - |x - x_{hkl}|^2}{2} + \frac{1}{4\pi^2}\sum_{i=1}^{\infty}\frac{C_i}{(r_i/a)^2}\left[\frac{\mathrm{Si}(z_i)}{z_i}\right]^l$$

$$\times\{\cos 2\pi\,|x - x_{hkl}|\,r_i/a - \cos 2\pi a g_m r_i/a\} \tag{11.92}$$

and $z_i = 2\pi a g_m r_i/a$.

Let us now consider a FCC element where $ag_m = (3/\pi)^{1/3}$. Using Eq. (11.92), we evaluate $\Phi_l(|x - x_{hkl}|)$ over the range $|x - x_{hkl}| = 0$ to $|x - x_{hkl}| = ag_m$. For $l = 2$, it is good enough to sum discretely over the first eight shells of neighbors and aproximate the small remainder by an integral. For $l > 2$, the convergence is quite rapid, and summation over the first few neighbor shells is sufficient. Figure 11.18 shows Φ_l for $l = 2$, 3, and infinity. It is evident that $\Phi_2(|x - x_{hkl}|)$ would be fairly well approximated by the straight line $0.670\,(0.984 - |x - x_{hkl}|)$. Using the values of $\Phi_2(|x - x_{hkl}|)$ from Fig. 11.18, we evaluate $I_2'(\sin\theta/\lambda) = Q_2$ from Eq (11.91). The curve is shown on Fig. 11.17. It is in good agreement with the curve originally obtained by Borie[22] using a different method.

The total TDS for a FCC powder pattern is given by

$$I\left(\frac{\sin\theta}{\lambda}\right) = I_e N f^2 e^{-2M}\left\{(2M)Q_1 + \frac{(2M)^2}{2!}Q_2 + \frac{(2M)^3}{3!}Q_3 + \cdots\right\}. \tag{11.93}$$

Since Fig. 11.18 shows no great difference in Φ_l for l values 2 or greater, it is evident that Q_3, Q_4, etc., will be a little flatter than Q_2 but not very different. To a good enough approximation we can set $Q_l = Q_2$ for all $l > 2$ and Eq.

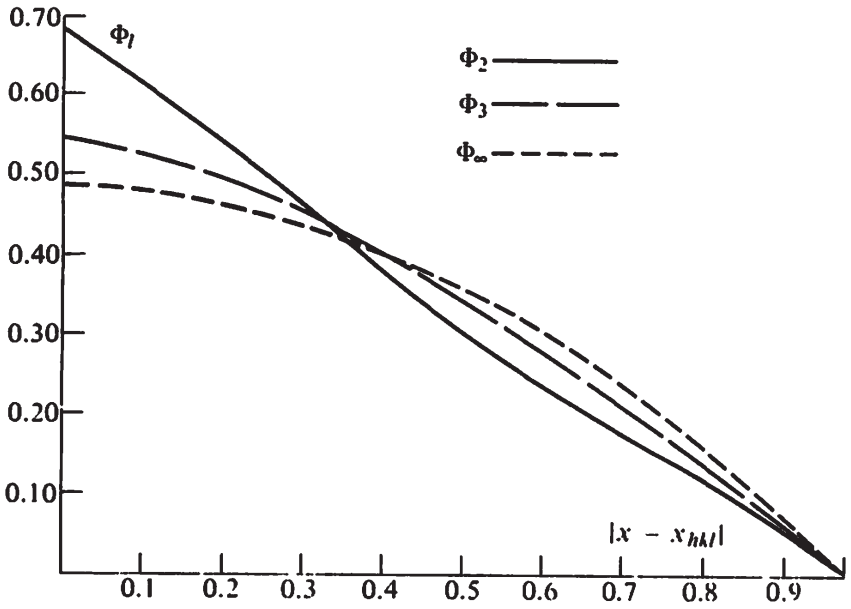

Fig. 11.18 The factors Φ_i which are used in Eq. (11.91) to compute the higher-order TDS contributions for a FCC powder pattern.

(11.103) becomes

$$I\left(\frac{\sin\theta}{\lambda}\right) = I_e N f^2\{e^{-2M}2M(Q_1 - Q_2) + (1 - e^{-2M})Q_2\}. \quad (11.94)$$

Borie has suggested that for many purposes it is a good enough approximation to set $Q_2 = (1 + Q_1)/2$, so that only the Q_1 function and $2M$ would be needed to obtain the TDS for a powder pattern. For small values of $2M$ such as $2M < 0.4$, Eq. (11.94) is well approximated by $I_e N f^2(1 - e^{-2M})Q_1$.

There still remains the question of how much TDS is included in the usual evaluation of the peak area of a crystalline reflection. We have just seen that for the powder patterns of cubic elements, the first-order TDS gives relatively sharp peaks at the positions of the crystalline reflections. Suppose that the background line for the *hkl*-peak joins the experimental intensity curve at $2\theta = 2\theta_{hkl} - \phi/2$ and $2\theta = 2\theta_{hkl} + \phi/2$, so that ϕ in radians is the total length of the background line on a 2θ scale. The peak area above this line includes a contribution from the first-order TDS as well as the integrated intensity of the crystalline reflection. Let $P'(\text{TDS})$ and $P'(hkl)$ be the power per unit length of diffraction circle contributed by first-order TDS and by the *hkl* integrated intensity. Let σ be the ratio of the two contributions:

$$\sigma = \frac{P'(\text{TDS})}{P'(hkl)}. \quad (11.95)$$

As an illustration, we now derive an expression for σ for the powder pattern of a FCC element. In the vicinity of an *hkl* peak, that part of the

first-order TDS which is above the background line from $2\theta_{hkl} - \phi/2$ to $2\theta_{hkl} + \phi/2$ is obtained from Eq. (11.83):

$$I = I_e N f^2 e^{-2M} 2M \frac{(3/\pi)^{2/3} j(hkl)}{6 x_{hkl} x} \left\{ \ln \left[\frac{(3/\pi)^{1/3}}{|x - x_{hkl}|} \right] - \ln \left[\frac{(3/\pi)^{1/3}}{|x - x_{hkl}|_{\phi/4}} \right] \right\},$$

where $|x - x_{hkl}|_{\phi/4}$ is the value of $|x - x_{hkl}|$ at $\theta = \theta_{hkl} \pm \phi/4$. The power per unit length of diffraction circle contributed by first-order TDS is

$$P'(\text{TDS}) = \int_{\theta=\theta_{hkl}-\phi/4}^{\theta=\theta_{hkl}+\phi/4} IR2 \, d\theta.$$

Since $|x - x_{hkl}|$ is always small, we can make the approximation

$$|x - x_{hkl}| = (2a/\lambda)(\sin\theta - \sin\theta_{hkl}) = (2a/\lambda)\cos\theta_{hkl}\epsilon,$$

where $\theta = \theta_{hkl} + \epsilon$. Similarly $|x - x_{hkl}|_{\phi/4} = (2a/\lambda)\cos\theta_{hkl}(\phi/4)$. In the integration, we replace the x in the denominator by its average value $x_{hkl} = (2a/\lambda)\sin\theta_{hkl}$:

$$\int_{\theta=\theta_{hkl}-\phi/4}^{\theta=\theta_{hkl}+\phi/4} \ln \left\{ \frac{|x - x_{hkl}|\ \phi/4}{|x - x_{hkl}|} \right\} d\theta = 2\int_{\epsilon=0}^{\epsilon=\phi/4} \{\ln(\phi/4) - \ln\epsilon\}\, d\epsilon = \phi/2.$$

Combining the last three equations, the TDS contribution is expressed by

$$P'(\text{TDS}) = \frac{I_e N f^2 e^{-2M} 2M (3/\pi)^{2/3} j(hkl) 2R(\phi/2)}{6(2a/\lambda)^2 \sin^2\theta_{hkl}}. \tag{11.96}$$

The power per unit length of diffraction circle for a crystalline reflection is given by Eq. (4.21). For a FCC element, $VF^2/v_a^2 = 4Nf^2/a^3$ and hence

$$P'(hkl) = \frac{I_e N f^2 e^{-2M} R\lambda^3 j(hkl)}{4\pi a^3 \sin^2\theta_{hkl} \cos\theta_{hkl}}. \tag{11.97}$$

Using the values expressed by Eqs. (11.96) and (11.97), we obtain finally the ratio σ:

$$\sigma = \frac{P'(\text{TDS})}{P'(hkl)} = (\pi/3)^{1/3} M (a/\lambda)\phi \cos\theta_{hkl}. \tag{11.98}$$

To illustrate the magnitude of σ, consider the (511, 333) reflection from copper at room temperature using Mo$K\alpha$ ($\lambda = 0.711$ A). For this case $M = 0.29$, $(a/\lambda) = 5.1$ and $\cos\theta_{hkl} = 0.86$. On a diffractometer tracing the background line covered a range $\phi = 2.0° = 0.035$ radian. Using these values in Eq. (11.98), we obtain $\sigma = 0.044$. Equation (11.98) was first derived by Chipman and Paskin.[23] It is probably a good enough approximation to include only the effect of the first-order TDS, since the higher-order

contributions do not peak up as sharply in the vicinity of an *hkl*-reflection. Corresponding equations for the TDS correction in making integrated intensity measurements with single crystals have been given by Nilsson.[24]

11.12 EXISTENCE OF AN INVERSION TEMPERATURE FOR THE DIFFUSE SCATTERING

For a monoatomic single crystal at a temperature high enough for equipartition, the intensity of first-order diffuse scattering is given by Eq. (11.36), and for measurements at a fixed position in reciprocal space the first-order TDS can be put in the simple form

$$I(1) = KTe^{-2M}. \tag{11.99}$$

In this range of temperature $2M$ is proportional to T, and hence Eq. (11.99) predicts that $I(1)$ should increase with T, reach a maximum at the so-called inversion temperature, and then decrease. However, the second; third; and higher-order TDS contributions are not negligible, and when these are considered along with the first-order scattering, it is not obvious whether there really should be an inversion temperature for the total diffuse scattering.

For the approximation of independent vibrations of the atoms, Eq. (11.80) predicts a diffuse intensity with increases monotonically with temperature:

$$I(\text{TDS})/Nf^2 = 1 - e^{-2M} = e^{-2M}[2M + (2M)^2/2 + (2M)^3/6 + \cdots]. \tag{11.100}$$

The total TDS expressed as the sum of the contributions by the different orders can be put in a form analogous to Eq. (11.100) by means of coefficients A_n for the different orders:

$$I(\text{TDS})/Nf^2 = e^{-2M}[A_1 2M + A_2(2M)^2/2 + A_3(2M)^3/6 + \cdots]. \tag{11.101}$$

If A_1 is much larger than the other A_n, it is evident that there will be an inversion temperature, while if the A_n are all roughly equal as in Eq. (11.100), there will be only a monotonic increase in $I(\text{TDS})/Nf^2$. Since A_1 expresses the magnitude of the first-order contribution, the relation of A_1 to the other A_n values will depend upon the position in the Brillouin zone where the measurement is made.

To have a quantitative example, we consider the simple case of a FCC crystal (4 atoms per cell) with all elastic waves having the same average velocity and $T > \Theta$. We consider the diffuse intensity along the line $h_1\,00$ in reciprocal space at the positions $(h + q)\mathbf{b}_1$, where h is an even integer. Using the approximation methods for the different orders of TDS that have been developed in this chapter, the coefficients A_n are computed for the

Table 11.4
VALUES OF THE COEFFICIENTS A_n OF EQ. (11.101)

q	A_1	A_2	A_3	A_4
0.1	33.3	7.91	2.38	1.00
0.6	0.93	1.07	1.02	1.00

position $q = 0.1$ close to the center of the Brillouin zone, and for the position $q = 0.6$ about halfway out to the boundary. The values of A_n are given in Table 11.4.

Since $2M$ is proportional to T in the range of interest, the plots of Eq. (11.101) which are shown by Fig. 11.19 can be considered as illustrating the variation of intensity with temperature. Close to the center of the Brillouin zone, the contribution by the first-order TDS is much stronger than that of the higher orders, and hence the curve for $q = 0.1$ shows an inversion effect. Moving out from the center of the Brillouin zone, the contribution by the first-order scattering decreases rapidly, the A_n coefficients of Eq. (11.101) become nearly equal, and we find the monotonic increase in intensity with temperature which is illustrated by the curve for $q = 0.6$.

For a single crystal of copper the inversion could be demonstrated by making measurements close to the 600 position and varying the temperature

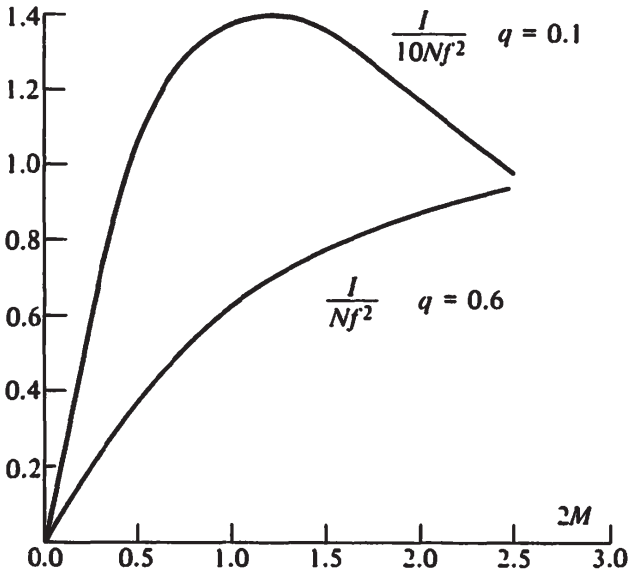

Fig. 11.19 The temperature diffuse scattering $I(\text{TDS})/Nf^2$ for a FCC element at positions on the $h_1 00$ line of reciprocal space which are displaced by qb_1 from an $h00$ reciprocal lattice point. For $q = 0.1$, we are close to a reciprocal lattice point and there is an inversion.

between room temperature and 500°C. For a single crystal of lead, the inversion has been demonstrated by Cartz.[25] It is only in a very small fraction of the volume of the Brillouin zone that the intensity can show a decrease with rise in temperature; in the remainder of the zone it increases, and summed over the whole zone there is a net increase in intensity with rise in temperature.

REFERENCES

1. P. DEBYE, *Verh. d. Deutsch. Phys. Ges.*, **15**, 678, 738, 857 (1913). *Ann der Physik*, **43**, 49 (1914).
2. I. WALLER, *Zeit f Physik*, **17**, 398 (1923).
3. H. FAXEN, *Ann d. Physik*, **54**, 615 (1918). *Zeit f Physik*, **17**, 266 (1923).
4. J. LAVAL, *C. R. Acad. Sci, Paris*, **207**, 169 (1938); **208**, 1512 (1939); *Bull. Soc. franc Miner*, **62**, 137 (1939).
5. R. W. JAMES, *Optical Principles of the Diffraction of X-rays*, G. Bell and Sons, London, 1948.
6. J. DELAUNAY, *J. Chem. Phys*, **21**, 1975 (1953).
7. P. OLMER, *Bull. Soc. franc Miner*, **71**, 145 (1948).
8. B. BORIE, *Acta Cryst.*, **14**, 566 (1961).
9. C. B. WALKER, *Phys. Rev.*, **103**, 547 (1956).
10. B. E. WARREN, *J. Appl. Phys.*, **25**, 814 (1954).
11. H. COLE and B. E. WARREN, *J. Appl. Phys.*, **23**, 335 (1952).
12. W A. WOOSTER, *Diffuse X-Ray Reflections from Crystals*, Oxford, Clarendon Press (1962).
13. BADEN-POWELL in L. Brillouin, *Wave Propagation in Periodic Structures*, p. 4, Dover Publications, Inc. (1953).
14. M. BORN and G. H. BEGBIE, *Proc. Roy. Soc.*, **A188**, 179 (1946). M. BORN and K. HUANG, *Dynamical Theory of Crystal Lattices*, Oxford University Press, London, 1954.
15. A. J. E. FOREMAN and W. M. LOMER, *Proc. Phys. Soc.*, **B70**, 1143 (1957).
16. L. VAN HOVE, *Phys. Rev.*, **89**, 1189 (1953).
17. J. C. PHILLIPS, *Phys. Rev.*, **104**, 1263 (1956).
18. H. CURIEN, *Acta Cryst.*, **5**, 393 (1952).
19. E. H. JACOBSEN, *Phys. Rev.*, **97**, 654 (1955).
20. B. E. WARREN, *Acta Cryst.*, **6**, 803 (1953).
21. F. H. HERBSTEIN and B. L. AVERBACH, *Acta Cryst.*, **8**, 843 (1955).
22. B. BORIE, *Acta Cryst.*, **14**, 566 (1961).
23. D. R. CHIPMAN and A. PASKIN, *J. Appl. Phys.*, **30**, 1998 (1959).
24. N. NILSON, *Arkiv Fysik*, **12**, 247 (1957).
25. L. CARTZ, *Proc. Phys. Soc.*, **68**, 951 (1955).

PROBLEMS

11.1 Introduce the isotropy condition $c_{11} - c_{12} = 2c_{44}$ into Eqs. (11.7), and solve for the three velocities. Show that the velocities are isotropic and the waves pure longitudinal and pure transverse.

11.2 To compute the velocities of elastic waves in a cubic crystal for other than the simple directions, we set equal to zero the determinant of the coefficients in Eqs. (11.7). This gives a cubic equation from which the three velocities can be obtained. For copper, use the values $\rho = 8.94$ gm/cc, $c_{11} = 1.684 \times 10^{12}$ dynes/cm^2, $c_{12} = 1.214 \times 10^{12}$ dynes/cm^2, $c_{44} = 0.754 \times 10^{12}$ dynes/cm^2.

a) Compute the velocities of the three waves propagating in the [321] direction in copper.

b) For each of the three waves, compute the angle between the vibration direction and the [321] direction. How closely are the waves pure longitudinal and pure transverse?

11.3 Silver is FCC, $a = 4.09$ A. A diffractometer tracing of the powder pattern of silver at 27°C is made using Mo$K\alpha$ radiation. Let f be the atomic scattering factor, and (LP) the Lorentz-polarization factor. Numbers proportional to the peak areas divided by f^2(LP) are as follows:

hkl	331	422	531
A/f^2(LP)	3.15	2.83	4.45

a) From these data determine $2B$ for silver at 27°C. The quantity $2B$ is defined by $2M = 2B\,(\sin\theta/\lambda)^2$.

b) From the Debye temperature for silver $\Theta = 210°$, calculate $2B$ for silver at 27°C.

c) By what fraction is the integrated intensity of the (531) reflection reduced by the temperature factor at 27°C?

d) What is the root mean square component of displacement $\langle u_s^2\rangle^{1/2}$ in silver at 27°C?

e) What is the ratio of $\langle u_s^2\rangle^{1/2}$ at 27°C to the nearest neighbor distance in silver?

11.4 Show that even at zero degrees absolute, the value of $2M$ for a cubic element cannot be less than about one quarter of its value at $T = \Theta$.

11.5 Fluorite, CaF_2, is FCC, $a = 5.46$ A, with positions Ca 000 and F $\frac{1}{4}\frac{1}{4}\frac{1}{4}$, $\bar{\frac{1}{4}}\bar{\frac{1}{4}}\bar{\frac{1}{4}}$. Assume that the temperature factors are proportional to the absolute temperature in the range 20°C to 300°C and that at 20°C they have the values B(Ca) = 0.50 A^2 and B(F) = 0.60 A^2. For the 200 reflection using Mo$K\alpha$ radiation $\lambda = 0.711$ A, we include a dispersion correction for calcium but neglect it for fluorine:

$$f_0(\text{Ca}) = 14.90, \qquad \Delta f'(\text{Ca}) = 0.20, \qquad \Delta f''(\text{Ca}) = 0.20, \qquad f_0(\text{F}) = 7.25,$$

where

$$f = f_0 + \Delta f' + i\,\Delta f''.$$

a) Compute values of $(F/4)^2_{200}$ for 20°C and for 300°C.

b) For this reflection, what is the effect on the integrated intensity of raising the temperature?

11.6 The fourth-order TDS contribution for a FCC powder pattern is given by

$$I_4\left(\frac{\sin\theta}{\lambda}\right) = I_e N f^2 e^{2M} \frac{(2M)^4}{4!}\,\Phi_4.$$

Compute and plot a curve for Φ_4 as a function of $x = (2a/\lambda)\sin\theta$, similar to the curve Φ_2 of Fig. 11.18.

11.7 To make an approximate allowance for dispersion in a FCC element, assume that

$$V_\lambda = V_\infty \sin\frac{\pi g}{2 b}\Big/\left(\frac{\pi g}{2 b}\right),$$

where V_∞ is the velocity computed from the elastic constants and $b = 1/a$. Let $I_1(h_1, 0, 0)$ be the intensity in *eu* of first-order TDS at the position $(h_1, 0, 0)$. Compute and plot I_1/Nf^2 vs. h_1 for copper at temperatures 300°K, 77°K, and 0°K. Consider only the positions $h_1 = 3.00$, 3.25, 3.50, and 3.75.

11.8 Start with Eqs. (11.14) and (11.17) and make several approximations. Assume that the temperature is high enough for equipartition, that all elastic waves have the same velocity, that the Brillouin zone can be replaced by an equal sphere, and that the sum over the waves can be replaced by an integration in the sphere.

a) In terms of the tabulated function

$$\mathrm{Si}(x) = \int_0^x \frac{\sin u}{u}\,du,$$

show that to a good approximation

$$\langle (u_{ms} - u_{ns})^2 \rangle = 2\langle u_s^2 \rangle \left[1 - \frac{\mathrm{Si}(Z_{mm})}{Z_{mm}}\right],$$

where $Z_{mm} = 2\pi g_m r_{mn}$.

b) Compute the value of $\langle (u_{ms} - u_{ns})^2 \rangle / \langle u_s^2 \rangle$ for the first five sets of neighbors in a FCC element. What value does this quotient approach for distant neighbors?

12

X-RAY STUDIES OF ORDER-DISORDER

12.1 INTRODUCTION

The study of order-disorder changes in binary alloys by x-ray diffraction methods has been actively pursued during recent years. The review articles by Nix and Shockley,[1] Lipson,[2] Guttman,[3] and Gerold[4] and the chapters in Guinier's[5] book cover many of the historical, theoretical, and experimental aspects. We shall introduce the subject by means of the three classical examples: βCuZn, Cu_3Au, and CuAu.

The β brass phase of the copper-zinc system extends over a small range of composition near the equiatomic composition CuZn. If brought to equilibrium at low temperature, the atoms take up the ordered structure shown by Fig. 12.1(a). The copper atoms take one set of positions such as the cube corners, and the zinc atoms take the cube center positions. Using correct crystal structure terminology, we say that ordered βCuZn has a CsCl type structure. At somewhat higher temperatures, the distribution is no longer perfect, but a majority of copper atoms on one set of positions and zinc atoms on the other set serves to specify which are the correct positions for

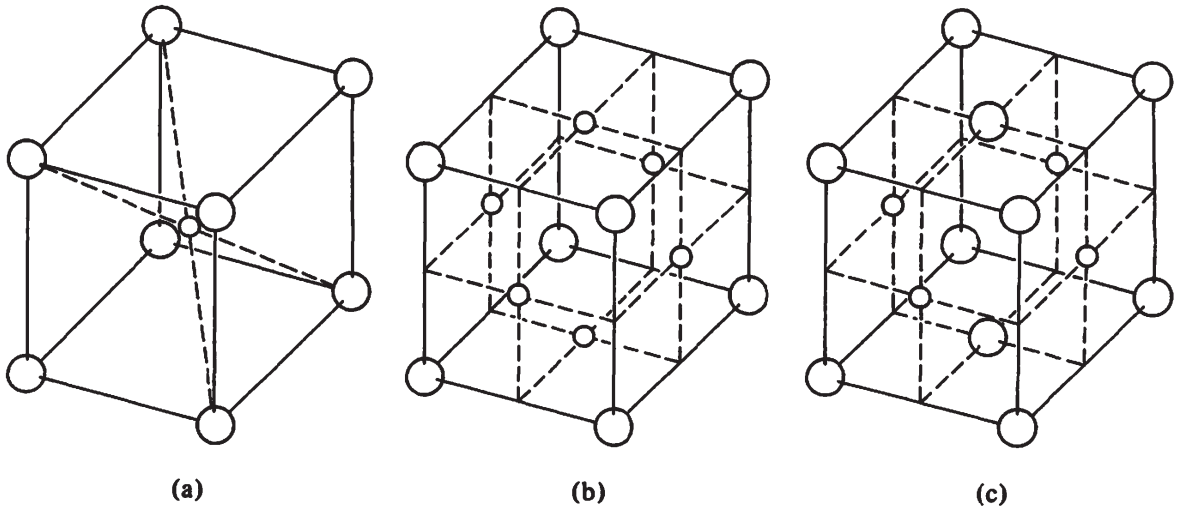

Fig. 12.1 Ordered structures (a) CuZn, (b) Cu_3Au, (c) CuAu.

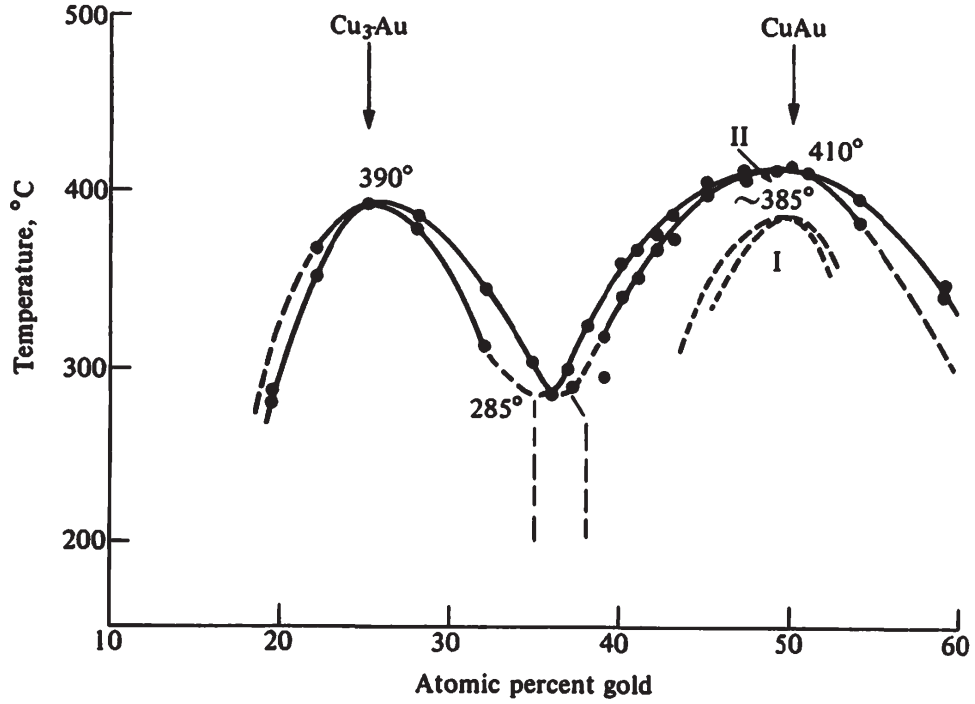

Fig. 12.2 Part of the equilibrium diagram for the Cu–Au system from *Constitution of Binary Alloys*, Hansen and Anderko, by permission of McGraw-Hill Book Company.

each type of atom. We say that long-range order still exists, but that it is only a partial long-range order. Depending on the exact composition, there is a critical temperature of around $T_c = 460°C$. Above this temperature, long-range order ceases to exist. The atom positions are still those of Fig. 12.1(a), but the corner and center positions are now occupied indiscriminately by copper and zinc atoms. Statistically, the atoms are arranged on a body-centered cubic lattice. Although the long-range order vanishes above T_c, there is still a short-range order. This means that the kind of atom at a certain position affects the probability of finding copper and zinc atoms at the various close-neighbor positions, but is not able to influence the occupancy of the more distant positions.

Figure 12.2 shows part of the equilibrium diagram for the copper-gold system. Around the composition Cu_3Au, there is an ordered structure which is shown by Fig. 12.1(b). The gold atoms occupy one set of positions such as the cube corners, and the copper atoms occupy the face-center positions. With increasing temperature, part of the positions become incorrectly occupied, and at a critical temperature $T_c = 390°C$, long-range order vanishes. Above T_c there is only a short-range order, and the occupancy of a certain position merely affects the occupancy of the near-neighbor positions. In the vicinity of the composition CuAu, there is a CuAu I ordered structure which is shown by Fig. 12.1(c). The structure is tetragonal, and the layers of

atoms perpendicular to the tetragonal axis are alternately all gold or all copper. Between 385°C and 410°C there is a more complex orthorhombic ordered form called CuAuII. Above $T_c = 410$°C long-range order vanishes, only short-range order exists and the material is statistically face-centered cubic.

12.2 LONG-RANGE ORDER IN BINARY COMPOSITIONS

We consider a binary composition, and call the two kinds of atoms A and B. In the ordered structure there are two kinds of positions which are designated as α- and β-sites. For the ideal stoichiometric composition and perfect long-range order, the α-sites are all occupied by A-atoms and the β-sites by B-atoms. The composition of the sample is represented by the atom fractions x_A and x_B, where $x_A + x_B = 1$. If N is the number of atoms in the sample, $N_A = x_A N$ and $N_B = x_B N$. Let y_α and y_β be the fractions of α-sites and β-sites, where $y_\alpha + y_\beta = 1$. These are simple fractions determined by the type of ordered structure. The number of each kind of site is given by $N_\alpha = y_\alpha N$ and $N_\beta = y_\beta N$.

Nix and Shockley[1] introduced four very useful parameters:

r_α = fraction of α-sites occupied by the right atom (A),

w_α = fraction of α-sites occupied by the wrong atom (B),

r_β = fraction of β-sites occupied by the right atom (B),

w_β = fraction of β-sites occupied by the wrong atom (A).

Two relations between the parameters are immediately obvious:

$$r_\alpha + w_\alpha = 1, \qquad r_\beta + w_\beta = 1.$$

There are also the conditions that the fraction of the sites occupied by A-atoms must equal the fraction of A-atoms, and the fraction of the sites occupied by B-atoms must equal the fraction of B-atoms. These two equivalent conditions are expressed by:

$$y_\alpha r_\alpha + y_\beta w_\beta = x_A, \qquad y_\beta r_\beta + y_\alpha w_\alpha = x_B. \tag{12.1}$$

Hence the four parameters r_α, w_α, r_β, w_β represent only one independent variable.

It is convenient to generalize the Bragg and Williams long-range order parameter S to make it convenient for nonstoichiometric compositions. We define a long-range order parameter S which is linearly proportional to $(r_\alpha + r_\beta)$, with $S = 0$ for a completely random arrangement, and $S = 1$ if the composition is stoichiometric and $r_\alpha = r_\beta = 1$. Expressing the linear dependence by $S = a + b(r_\alpha + r_\beta)$, the first condition gives $0 = a + b(x_A + x_B) = a + b$, and the second condition gives $1 = a + 2b$. Eliminating the constants a and b, the long-range order parameter is expressed in

the simple form:

$$S = r_\alpha + r_\beta - 1 = r_\alpha - w_\beta = r_\beta - w_\alpha. \tag{12.2}$$

By combining with Eqs. (12.1), we obtain expressions which are convenient for interpreting the measured values of S:

$$S = (r_\alpha - x_A)/y_\beta = (r_\beta - x_B)/y_\alpha. \tag{12.3}$$

The parameter S can reach its maximum value of unity only for a stoichiometric composition, for a nonstoichiometric composition even the best distribution of the available atoms gives a parameter value which is less than unity. With this definition for S, the structure factors for the super-structure reflections turn out to be proportional to S even for nonstoichiometric compositions, and hence a general parameter S^2 is obtained from experiment.

The structure factor involves a sum over all the atomic positions in the unit cell. This can be divided into a sum over the α-positions and a sum over the β-positions using the average scattering factor for each kind of site:

$$F = \sum_\alpha (r_\alpha f_A + w_\alpha f_B) e^{2\pi i(hx_n + ky_n + lz_n)} + \sum_\beta (r_\beta f_B + w_\beta f_A) e^{2\pi i(hx_n + ky_n + lz_n)}. \tag{12.4}$$

For the case of partial long-range order, we now apply Eq. (12.4) to the three kinds of ordered structures shown by Fig. 12.1, but without assuming stoichiometric compositions. Simplification of the expressions is made by using Eqs. (12.1) and (12.2):

a) βCuZn type of ordered structure:

$$\beta = 000;\ \alpha = \tfrac{1}{2}\,\tfrac{1}{2}\,\tfrac{1}{2};\ y_\alpha = \tfrac{1}{2};\ y_\beta = \tfrac{1}{2};$$

$$F = (r_\alpha f_A + w_\alpha f_B) e^{\pi i(h+k+l)} + (r_\beta f_B + w_\beta f_A), \quad h + k + l = \text{even}; \tag{12.5}$$

$$F = (r_\alpha f_A + w_\alpha f_B) + (r_\beta f_B + w_\beta f_A) = 2(x_B f_B + x_A f_A) \text{ Fundamental}, \quad h + k + l = \text{odd};$$

$$F = (r_\beta f_B + w_\beta f_A) - (r_\alpha f_A + w_\alpha f_B) = S(f_B - f_A) \text{ Superstructure}.$$

b) Cu_3Au type of ordered structure:

$$\beta = 000;\ \alpha = \tfrac{1}{2}\,\tfrac{1}{2}0,\ 0\,\tfrac{1}{2}\,\tfrac{1}{2},\ \tfrac{1}{2}\,0\,\tfrac{1}{2};\ y_\alpha = \tfrac{3}{4};\ y_\beta = \tfrac{1}{4};$$

$$F = (r_\alpha f_A + w_\alpha f_B)[e^{\pi i(h+k)} + e^{\pi i(k+l)} + e^{\pi i(l+h)}] + (r_\beta f_B + w_\beta f_A); \quad hkl \text{ unmixed}; \tag{12.6}$$

$$F = 3(r_\alpha f_A + w_\alpha f_B) + (r_\beta f_B + w_\beta f_A) = 4(x_B f_B + x_A f_A) \text{ Fundamental}, \quad hkl \text{ mixed};$$

$$F = (r_\beta f_B + w_\beta f_A) - (r_\alpha f_A + w_\alpha f_B) = S(f_B - f_A) \text{ Superstructure}.$$

c) CuAu I type of ordered structure:

$$\beta = 000, \tfrac{1}{2}\tfrac{1}{2}0; \alpha = \tfrac{1}{2}0\tfrac{1}{2}; 0\tfrac{1}{2}\tfrac{1}{2}; y_\alpha = \tfrac{1}{2}; y_\beta = \tfrac{1}{2};$$

$$F = (r_\alpha f_A + w_\alpha f_B)[e^{\pi i(h+l)} + e^{\pi i(k+l)}] + (r_\beta f_B + w_\beta f_A)[1 + e^{\pi i(h+k)}], \quad (12.7)$$

hkl unmixed;

$$F = 2[(r_\alpha f_A + w_\alpha f_B) + (r_\beta f_B + w_\beta f_A)] = 4(x_B f_B + x_A f_A)$$ Fundamental, $h + k =$ even, $k + l =$ odd;

$$F = 2[(r_\beta f_B + w_\beta f_A) - (r_\alpha f_A + w_\alpha f_B)] = 2S(f_B - f_A)$$ Superstructure.

Reflections which are independent of the degree of order are called fundamental reflections, and reflections which vanish if the order vanishes are called superstructure reflections. The existence of superstructure reflections is the evidence for ordering, and it is from the integrated intensities of the superstructure reflections that we measure the long-range order parameter S. Figure 12.3 shows diffractometer tracings for ordered and disordered Cu_3Au. The upper pattern was made with a sample quenched from 600°C. The material is in a disordered state and the pattern shows only the fundamental reflections (111), (200), and (220). For the lower tracing the sample had been annealed at various temperatures from T_c down to 280°C, and the long-range order is nearly perfect. In this case the pattern contains the same fundamental

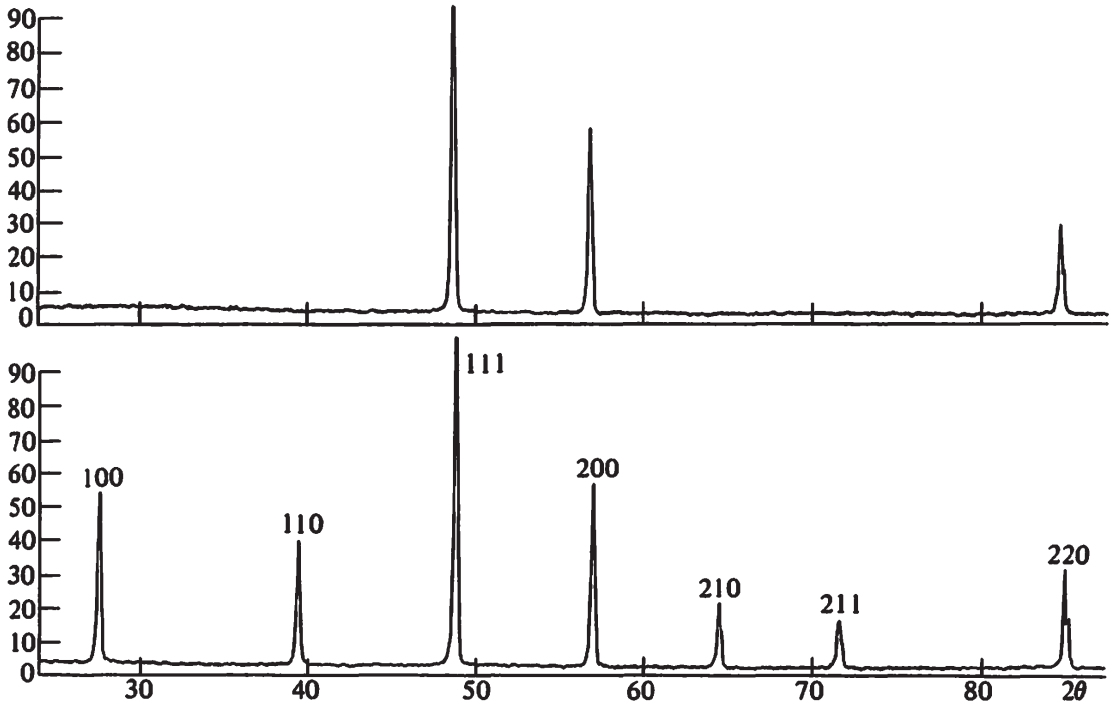

Fig. 12.3 Diffractometer tracings of powder samples of Cu_3Au using Cu$K\alpha$ radiation. Upper pattern: disordered form obtained by quenching from 600°C. Lower pattern: ordered form obtained by annealing 20 days at 365°C and 40 days at 280°C.

reflections as above and, in addition, the complete set of superstructure reflections.

In principle it is a simple matter to determine the long-range order parameter S by comparing the integrated intensity of a superstructure reflection with that of a fundamental reflection. As is so often the case, however, the practical application requires careful procedures which either eliminate or correct for several effects which can produce appreciable errors. The low-order fundamental reflections are much stronger than the superstructure reflections, and their measured values tend to be too small due to extinction; hence we prefer to use the weaker high-order fundamentals. In general the two different atoms have different Debye factors exp $[-M_A]$ and exp $[-M_B]$, and since the difference becomes particularly important for high-order superstructure reflections, we prefer to use only the low orders of the superstructure reflections. With powder pattern recordings, it is usually only the low-order superstructure reflections, which can be measured.

As an illustration, we shall consider the determination of S from a diffractometer recording of the powder pattern of a sample having a Cu_3Au type of ordered structure. For an ideal diffractometer sample, there is no angular dependence in the absorption correction, but for a sample with a high-absorption coefficient and a rough surface, there is a surface roughness effect which makes the low-angle reflections weaker than they should be. We shall assume that the sample has been prepared with a sufficiently smooth surface to make the surface roughness effect negligible. To allow for the dispersion correction, we can consider that f includes the real part of the correction so that $f = f_0 + \Delta f'$, and we abbreviate the imaginary part by writing $\Delta = \Delta f''$.

In terms of a constant K, multiplicity m, and Lorentz-polarization factor (LP), the area of a fundamental peak is represented by

$$A_F = Km(\mathrm{LP})FF^*,$$

where

$$\begin{aligned} FF^* &= 16[x_A(f_A + i\Delta_A)e^{-M_A} + x_B(f_B + i\Delta_B)e^{-M_B}] \\ &\quad \times [x_A(f_A - i\Delta_A)e^{-M_A} + x_B(f_B - i\Delta_B)e^{-M_B}] \\ &= 16[(x_A f_A e^{-M_A} + x_B f_B e^{-M_B})^2 + (x_A\Delta_A e^{-M} + x_B\Delta_B e^{-M_B})^2]. \end{aligned}$$

In terms of an average Debye factor M, we can write

$$M_A = M + \epsilon, \qquad M_B = M - \epsilon,$$

and since ϵ is small, we can make the approximation $\exp[\epsilon] = 1 + \epsilon$, and drop terms in ϵ^2:

$$\begin{aligned} FF^* = 16e^{-2M}\{&(x_A f_A + x_B f_B)^2 + (x_A\Delta_A + x_B\Delta_B)^2 \\ &+ [x_B^2(f_B^2 + \Delta_B^2) - x_A^2(f_A^2 + \Delta_A^2)]2\epsilon\}. \end{aligned}$$

With the abbreviation

$$p = \frac{x_B^2(f_B^2 + \Delta_B^2) - x_A^2(f_A^2 + \Delta_A^2)}{(x_A f_A + x_B f_B)^2 + (x_A \Delta_A + x_B \Delta_B)^2}$$

and the approximation $1 + 2p\epsilon = \exp[2p\epsilon]$,

$$FF^* = 16[(x_A f_A + x_B f_B)^2 + (x_A \Delta_A + x_B \Delta_B)^2] e^{-2(M - p\epsilon)}.$$

Writing $M = B(\sin\theta/\lambda)^2$, $\epsilon = b(\sin\theta/\lambda)^2$, we obtain finally

$$\ln\left\{\frac{A_F}{m(\mathrm{LP})16[(x_A f_A + x_B f_B)^2 + (x_A \Delta_A + x_B \Delta_B)^2]}\right\} = \ln K - 2(B - pb)\left(\frac{\sin\theta}{\lambda}\right)^2. \quad (12.8)$$

For a superstructure reflection, the area is given by

$$A_S = Km(\mathrm{LP})FF^*,$$

where

$$\begin{aligned} FF^* &= S^2[(f_B + i\Delta_B)e^{-M_B} - (f_A + i\Delta_A)e^{-M_A}] \\ &\quad \times [(f_B - i\Delta_B)e^{-M_B} - (f_A - i\Delta_A)e^{-M_A}] \\ &= S^2[(f_B e^{-M_B} - f_A e^{-M_A})^2 + (\Delta_B e^{-M_B} - \Delta_A e^{-M_A})^2]. \end{aligned}$$

As before, let $M_A = M + \epsilon$, $M_B = M - \epsilon$:

$$FF^* = S^2 e^{-2M}[(f_B - f_A)^2 + (\Delta_B - \Delta_A)^2 + (f_B^2 + \Delta_B^2 - f_A^2 - \Delta_A^2)2\epsilon].$$

Introduce the abbreviation

$$g = \frac{(f_B^2 + \Delta_B^2) - (f_A^2 + \Delta_A^2)}{(f_B - f_A)^2 + (\Delta_B - \Delta_A)^2}.$$

The quantity g will not be small, but since we shall be working only with low-order superstructure reflections where ϵ is very small, we can make the approximation $1 + 2g\epsilon = \exp[2g\epsilon]$:

$$FF^* = S^2[(f_B - f_A)^2 + (\Delta_B - \Delta_A)^2] e^{-2(M - g\epsilon)}.$$

Changing to $M = B(\sin\theta/\lambda)^2$, $\epsilon = b(\sin\theta/\lambda)^2$, we obtain finally

$$\ln\left\{\frac{A_S}{m(\mathrm{LP})[(f_B - f_A)^2 + (\Delta_B - \Delta_A)^2]}\right\} = \ln K + \ln S^2 - 2(B - gb)\left(\frac{\sin\theta}{\lambda}\right)^2. \quad (12.9)$$

In both Eqs. (12.8) and (12.9), the left-hand side is known for each measured reflection, and this quantity can be plotted against $(\sin\theta/\lambda)^2$. Since p is very small and nearly constant, the plot of Eq. (12.8) should be closely

linear, and hence to obtain an intercept on the axis of ordinates there is no need to use the low-order fundamentals which may be in error because of extinction. In Eq. (12.9) the quantity g is not small and the approximations which were made are rather rough so that the plot of Eq. (12.9) cannot be expected to be strictly linear. However, if at least three low-order superstructure reflections are measureable, a plot can be made from which the intercept on the axis of ordinates can be obtained. From the difference in the intercepts of the plots of Eqs. (12.8) and (12.9), we obtain directly $\ln S^2$. The initial slopes of the two curves give $2(B - pb)$ and $2(B - gb)$, and from these we obtain the two temperature factors:

$$\begin{aligned} B_A &= [(g + 1)(B - pb) - (1 + p)(B - gb)]/(g - p), \\ B_B &= [(g - 1)(B - pb) + (1 - p)(B - gb)]/(g - p). \end{aligned} \tag{12.10}$$

Under some conditions it may be desirable to bring the sample to a state of perfect order and then use combinations of the superstructure and fundamental reflections to measure the temperature factors for the two atoms. Assuming that the factors are proportional to the absolute temperature, and neglecting any dependence on the state of order, we can then obtain S from high-order reflections where extinction can be assumed to be negligible. Another procedure by which we determine the three quantities S, B_A, and B_B has been developed by Chipman.[6] The determination of S is very greatly simplified by making the approximation $M_A = M_B$. Although many of the

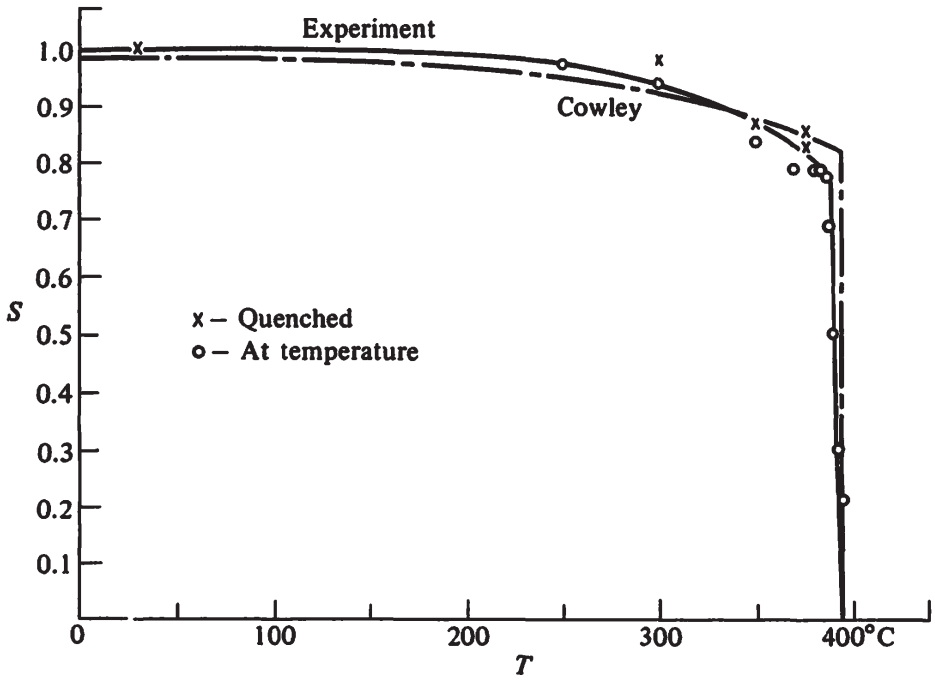

Fig. 12.4 Measurements by Keating of the long-range order parameter S from a sample of Cu_3Au filings. The dashed curve represents the variation predicted by the Cowley theory.

determinations of S have been made with the use of this approximation, the available data indicate that, in general, it is not safe to assume that $M_A = M_B$. Equations (12.8) and (12.9) apply directly to powder pattern determinations of long-range order in Cu_3Au type structures. Corresponding equations for other types of ordering or for measurements from single crystals are readily developed.

Figure 12.4 shows Keatings' measurement[7] of the long-range order parameter S for the stoichiometric composition Cu_3Au. Measurements of the (210) and (222) reflections were made on filings, either held at temperature, or annealed to equilibrium and quenched to room temperature. The measurements indicate that for Cu_3Au the order starts with $S = 1.0$ at low temperature, and that it decreases continuously with rising temperature to a value of $S = 0.8$ at a critical temperature $T_c = 390°C$, where it drops discontinuously to zero. The measured points along the supposedly discontinuous drop are presumably the result of nonuniformity in temperature in the briquet. Included is also a plot of Cowley's theoretical expression[8] for order in a Cu_3Au type structure:

$$\ln\left\{\frac{(\frac{1}{3}+S^2)(3+S^2)}{(1-S^2)^2}\right\} = \tfrac{16}{3}S^2\left(\frac{T_c}{T}\right). \tag{12.11}$$

Figure 12.5 shows Chipman's measurement[9] of long-range order in βCuZn. Since Cu and Zn are neighboring elements, $(f_{Zn} - f_{Cu})^2$ is very small. From a powder pattern the intensities of the superstructure reflections would

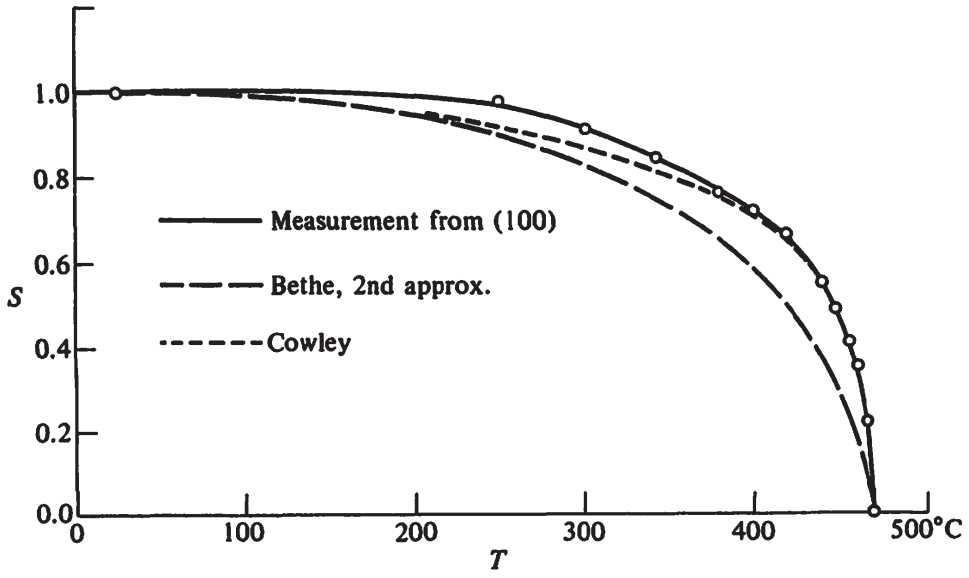

Fig. 12.5 Measurements by Chipman of the long-range order parameter S for βCuZn. The measurements were made on a single crystal cut to a 100 face and held at temperature. Included are the variations predicted by the Bethe theory and the Cowley theory.

be too small for accurate measurement even with a wavelength chosen to accentuate the difference in scattering factors. However, by using a single crystal of βCuZn cut to a 100 face, there was ample intensity for a measurement of the 100 superstructure reflection. The single crystal was held at temperature for each of the measurements, and the values were normalized by setting $S = 1.0$ for $T = 0°C$. The measurements indicate that in the βCuZn type structure, the long-range order decreases continuously to zero at T_c, apparently with an infinite slope at T_c. Included is also a plot of Cowley's theoretical expression for order in a βCuZn type structure:

$$\ln\left\{\frac{1+S^2}{1-S^2}\right\} = 2S^2\left(\frac{T_c}{T}\right). \tag{12.12}$$

When a material such as βCuZn changes from the ordered to the disordered state, there is not only a continuous decrease in the intensity of the superstructure reflections but also a change in the cell dimensions. For a disordered material, the cell volume is generally greater than for an ordered material, and this change gives another x-ray method for observing a change in order. Keating's measurement of the change in the 2θ positions of the 222 reflection from a single crystal of βCuZn held at various temperatures is shown by Fig. 12.6. The general decrease in 2θ with increase in temperature is, of course, the result of thermal expansion in the sample. The upper dashed line is an extrapolated position for the reflection from an ordered cell; the lower dashed line is the extrapolated position for the reflection from a disordered cell. There is a continuous transition from one line to the other in the

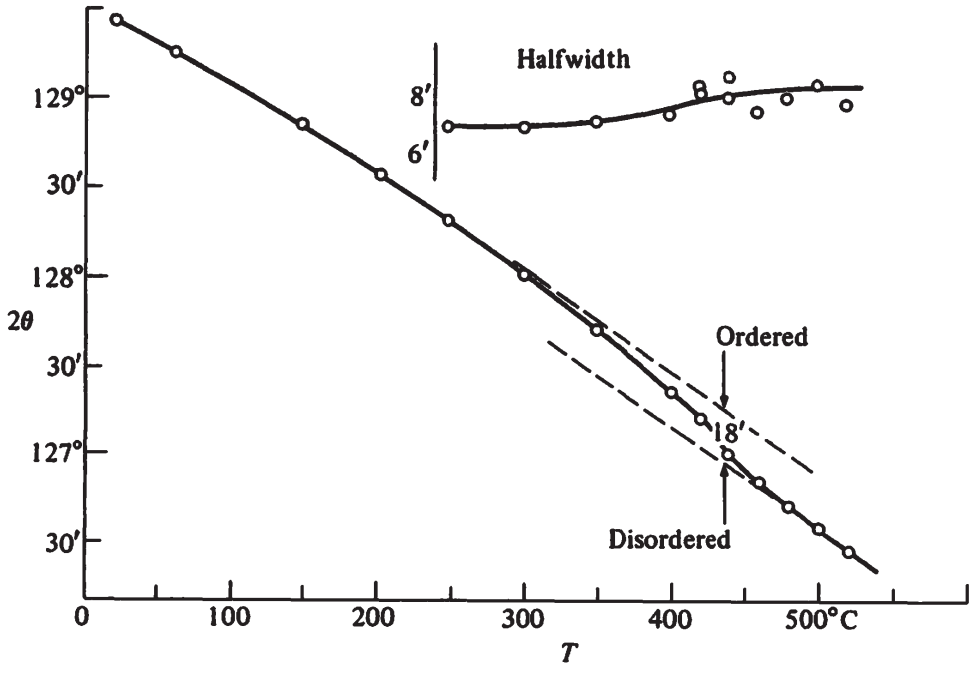

Fig. 12.6 Change with temperature of the position and width of the 222 reflection for βCuZn using Cu$K\alpha_1$ radiation.

temperature interval in which Fig. 12.5 shows the disappearance of long-range order. Since the half maximum width of the 222 peak is about 7′, and the separation between the two limiting lines is 18′, it is clear that the change is one of decreasing order in a single phase, rather than a change in the relative amounts of completely ordered and completely disordered phases.

12.3 ANTIPHASE DOMAINS

When a crystal orders, it is likely that the ordering starts at a large number of positions throughout the crystal. At each position it is pure chance which will be chosen as α-sites and β-sites, and hence there can be neighboring regions in which there has been an opposite choice. This condition is illustrated schematically by Fig. 12.7. In the right-hand half of the crystal the choice of sites is opposite to that in the left-hand half. Such regions are called antiphase domains, and the boundary between the two regions is called an antiphase domain boundary.

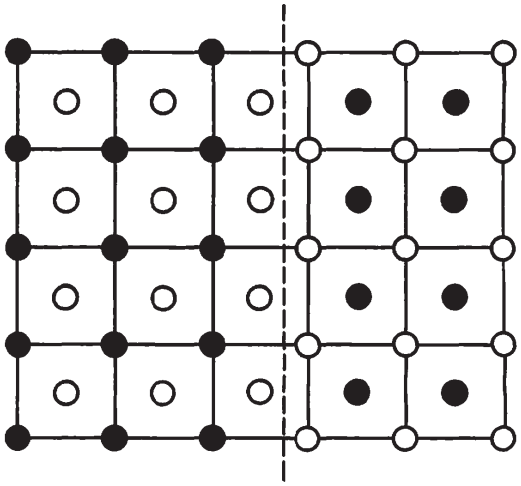

Fig. 12.7 Illustration of two antiphase domains and an antiphase domain boundary.

In a βCuZn type structure, antiphase domain boundaries produce a large number of like nearest neighbors. Presumably this is an unstable situation, and hence antiphase domains are not likely to persist in the βCuZn structure. In the Cu_3Au type structure, the situation is quite different. As seen from Fig. 12.1(b), atomic layers parallel to the cube faces are alternately either all copper or half copper and half gold. Considering a plane perpendicular to the $\mathbf{a}_1$-axis, suppose that the material on one side of the plane is given a displacement $(\mathbf{a}_2 + \mathbf{a}_3)/2$ relative to the material on the other side. Two antiphase domains have been formed, but the numbers of like and unlike nearest neighbors remain unchanged. Such antiphase domains produced by half diagonal slip on planes perpendicular to the cube axes introduce only a small instability and hence can be expected to persist in the Cu_3Au type structure.

In a crystal containing antiphase boundaries there could be perfect order within any one domain but zero order over the crystal as a whole, if we use

the same designation of α- and β-sites throughout the crystal. For a superstructure reflection, the diffracted amplitudes from the different antiphase domains can be opposite in phase, and the question arises as to whether the intensities of superstructure reflections will be reduced by the presence of antiphase boundaries. The answer is that antiphase domains in a sample influence the intensity and the peak shape but not the integrated intensity.

a) Integrated Intensity Independent of Antiphase Domains

We now wish to show that the integrated intensity is independent of the existence of antiphase domains. As a simple example we consider a crystal of Cu_3Au of dimensions $2N_1a_1$, N_2a_2, and N_3a_3. The crystal is divided into halves by an antiphase domain boundary which is normal to the $\mathbf{a}_1$-axis. Each half of the crystal is perfectly ordered, but in the right-hand half, the Au atoms are shifted by $(\mathbf{a}_2 + \mathbf{a}_3)/2$ from the positions corresponding to the left-hand half. In terms of the correct positions in the left-hand half, the long-range order for the whole crystal is given formally by

$$S = r_\beta - w_\beta = (1 - 0)/2 - (0 + \tfrac{1}{3})/2 = \tfrac{1}{3},$$

although $S = 1$ for each half individually.

In terms of the continuous variables $h_1h_2h_3$, we express the diffraction vector by $(\mathbf{s} - \mathbf{s}_0)/\lambda = h_1\mathbf{b}_1 + h_2\mathbf{b}_2 + h_3\mathbf{b}_3$. For the left-hand half of the crystal, the structure factor is given by

$$F = f(\text{Au}) + f(\text{Cu})[e^{\pi i(h_1+h_2)} + e^{\pi i(h_2+h_3)} + e^{\pi i(h_3+h_1)}],$$

and for the right-hand half, it can be written as $F\exp[\pi i(h_2 + h_3)]$. The amplitude in electron units from the whole crystal is then given by

$$A_{eu} = F\left\{\sum_{m_1=0}^{N_1-1} e^{2\pi i h_1 m_1} + e^{\pi i(h_2+h_3)} \sum_{m_1=N_1}^{2N_1-1} e^{2\pi i h_1 m_1}\right\} \sum_{m_2=0}^{N_2-1} e^{2\pi i h_2 m_2} \sum_{m_3=0}^{N_3-1} e^{2\pi i h_3 m_3}.$$

Evaluating the sums and multiplying by the complex conjugate, we obtain an expression for the intensity

$$I = I_e FF^* \frac{\sin^2 \pi h_1 N_1}{\sin^2 \pi h_1} \frac{\sin^2 \pi h_2 N_2}{\sin^2 \pi h_2} \frac{\sin^2 \pi h_3 N_3}{\sin^2 \pi h_3} \times [1 + e^{\pi i(h_2+h_3+2N_1h_1)}][1 + e^{-\pi i(h_2+h_3+2N_1h_1)}].$$

Assuming that N_1, N_2, and N_3 are not small, the intensity is closely confined to integral values of $h_1h_2h_3$, and it is convenient to make the replacements

$$h_1 = h + h_1', \qquad h_2 = k + h_2', \qquad h_3 = l + h_3',$$

where $h_1'h_2'h_3'$ will be small in the region of nonvanishing intensity. In the antiphase factor $\exp[\pi i(h_2 + h_3)]$ and the structure factor F, we can replace $h_1h_2h_3$ by the integral values hkl, since these are slowly varying quantities.

With these changes, the intensity is given by

$$I = I_e FF^* \frac{\sin^2 \pi h_1' N_1}{(\pi h_1')^2} \frac{\sin^2 \pi h_2' N_2}{(\pi h_2')^2} \frac{\sin^2 \pi h_3' N_3}{(\pi h_3')^2} 2[1 + (-1)^{k+l} \cos 2\pi h_1' N_1].$$

There are now two cases to consider:

$k + l =$ even,

$$I = I_e FF^* \frac{\sin^2 \pi h_1' 2N_1}{(\pi h_1')^2} \frac{\sin^2 \pi h_2' N_2}{(\pi h_2')^2} \frac{\sin^2 \pi h_3' N_3}{(\pi h_3')^2}; \tag{12.13}$$

$k + l =$ odd,

$$I = I_e FF^* 4 \sin^2 \pi h_1' N_1 \frac{\sin^2 \pi h_1' N_1}{(\pi h_1')^2} \frac{\sin^2 \pi h_2' N_2}{(\pi h_2')^2} \frac{\sin^2 \pi h_3' N_3}{(\pi h_3')^2}. \tag{12.14}$$

In Chapter 4 it was shown that the integrated intensity of an *hkl*-reflection is always proportional to an integral of $I(h_1' h_2' h_3')$ throughout the volume of reciprocal space surrounding the point *hkl*:

$$P = K \iiint I(h_1' h_2' h_3')\, dh_1'\, dh_2'\, dh_3'.$$

For $k + l =$ even, the intensity which is given by Eq. (12.13) is exactly the same as that for a crystal without antiphase domains, and the integration leads to

$$P = K I_e FF^* 2N_1 N_2 N_3. \tag{12.15}$$

For $k + l =$ odd, the intensity expressed by Eq. (12.14) is zero for $h_1' = 0$. This means that exactly at the *hkl* point in reciprocal space, the intensity is zero for a superstructure reflection with $k + l =$ odd. To obtain the integrated intensity for this case, we let $\sin^2 \pi h_1' N_1 = 1 - \cos^2 \pi h_1' N_1$, and note that

$$\int_{-\infty}^{+\infty} 4 \sin^2 \pi h_1' N_1 \frac{\sin^2 \pi h_1' N_1}{(\pi h_1')^2}\, dh_1'$$

$$= \int_{-\infty}^{+\infty} \left[\frac{4 \sin^2 \pi h_1' N_1}{(\pi h_1')^2} - \frac{\sin^2 \pi h_1' 2N_1}{(\pi h_1')^2} \right] dh_1' = 4N_1 - 2N_1 = 2N_1.$$

The integrated intensity is again given by Eq. (12.15). For this type of reflection, the effect of the antiphase domains is to make the intensity zero at the center of the reflection where $h_1' = 0$, but the integrated intensity is the same as though no antiphase domain boundary existed.

For the sake of clarity, the treatment has been restricted to a simple case, but for the general case in which the crystal may contain a complex system of antiphase boundaries, the result is the same. Antiphase boundaries broaden a superstructure reflection but have no effect on the integrated intensity of the peak. Long-range order parameters can be determined from

the integrated intensities of the superstructure reflections independent of whether or not antiphase domains exist in the sample. There is, however, a practical restriction on this general result. The antiphase domains must not be so small that the superstructure peaks broaden to such an extent that some of the peak area is lost in the long tails of the reflection.

b) Effect of Antiphase Domains on the Reflection Shape in Reciprocal Space

In the ordered Cu_3Au type structure, antiphase domains are generally present unless the material has been given long anneals in the proper range of temperature. The existence of the domains is evidenced by a broadening of the superstructure reflections even when there is no appreciable broadening of the fundamentals. Not only can the broadening be very pronounced, but in addition there is a curious *hkl*-dependence. The problem was first treated by Wilson,[10] who showed that a domain structure, formed by half diagonal glides on planes perpendicular to the cube axes, gave a reasonably good explanation of the *hkl*-dependence of the superstructure broadenings. The half diagonal glides are ones involving displacements $(\mathbf{a}_2 + \mathbf{a}_3)/2$ across planes perpendicular to $\mathbf{a}_1$, displacements $(\mathbf{a}_3 + \mathbf{a}_1)/2$ across planes perpendicular to $\mathbf{a}_2$, and displacements $(\mathbf{a}_1 + \mathbf{a}_2)/2$ across planes perpendicular to $\mathbf{a}_3$. These are displacements parallel to atomic planes which are all copper. Since they do not decrease the nearest neighbor order, they can produce an antiphase domain array which is rather stable. It is of interest to develop the diffraction theory for this type of structure, since the problem illustrates several very useful procedures for treating diffraction in imperfect structures.

We assume that the three mutually perpendicular sets of antiphase boundaries are completely independent of one another. Along one of the cube axis directions, let γ be the probability of crossing a domain boundary in a distance a, where a is the edge of the cubic cell. Defined in this way, a/γ is the average distance between antiphase boundaries. The structure factor for the cell $m_1m_2m_3$ is expressed by $F(m_1m_2m_3) = F \exp[i\phi(m_1m_2m_3)]$, where

$$F = f_\beta + f_\alpha\{e^{\pi i(h+k)} + e^{\pi i(k+l)} + e^{\pi i(l+h)}\}.$$

Corresponding to the four displacements: O, $(\mathbf{a}_1 + \mathbf{a}_2)/2$, $(\mathbf{a}_2 + \mathbf{a}_3)/2$, and $(\mathbf{a}_3 + \mathbf{a}_1)/2$, the phase $\phi(m_1m_2m_3)$ can have the four values: O, $\pi(h + k)$, $\pi(k + l)$, and $\pi(l + h)$. The intensity from the crystal is given in the usual way by summing the amplitude from all cells in the crystal, and then multiplying by the complex conjugate:

$$I_{eu} = F \sum_{m_1m_2m_3} e^{i\phi(m_1m_2m_3)} e^{(2\pi i/\lambda)(\mathbf{s}-\mathbf{s}_0)\cdot(m_1\mathbf{a}_1+m_2\mathbf{a}_2+m_3\mathbf{a}_3)} \times F^* \sum_{m_1'm_2'm_3'} e^{-i\phi(m_1'm_2'm_3')} e^{-(2\pi i/\lambda)(\mathbf{s}-\mathbf{s}_0)\cdot(m_1'\mathbf{a}_1+m_2'\mathbf{a}_2+m_3'\mathbf{a}_3)}.$$

We express the diffraction vector in terms of reciprocal space coordinates:

$$(\mathbf{s} - \mathbf{s}_0)/\lambda = (h + h_1)\mathbf{b}_1 + (k + h_2)\mathbf{b}_2 + (l + h_3)\mathbf{b}_3.$$

The vector $h_1\mathbf{b}_1 + h_2\mathbf{b}_2 + h_3\mathbf{b}_3$ represents the departure of the tip of the diffraction vector from the reciprocal lattice point *hkl*. In terms of the continuous variables $h_1h_2h_3$, the intensity is given by

$$I_{eu}(h_1h_2h_3) = FF^* \sum_{m_1m_2m_3} \sum_{m_1m_2'm_3} e^{i[\phi(m_1m_2m_3) - \phi(m_1m_2'm_3)]} e^{2\pi i[(m_1 - m_1')h_1 + (m_2 - m_2')h_2 + (m_3 - m_3')h_3]} \tag{12.16}$$

Introduce the abbreviations $m_1 - m_1' = n_1$, $m_2 - m_2' = n_2$, $m_3 - m_3' = n_3$, and $\phi(m_1m_2m_3) - \phi(m_1'm_2'm_3') = \phi(n_1n_2n_3)(m_1m_2m_3)$. The double sum of Eq. (12.16) is now changed to a single sum. We pick out all terms with the same value of $n_1n_2n_3$, introduce an average phase factor for these terms, multiply by the number of the terms $N(n_1n_2n_3)$, and then sum over all values of $n_1n_2n_3$:

$$I_{eu}(h_1h_2h_3) = F^2 \sum_{n_1} \sum_{n_2} \sum_{n_3} N(n_1n_2n_3) \langle e^{i\phi(n_1n_2n_3)} \rangle e^{2\pi i(n_1h_1 + n_2h_2 + n_3h_3)}. \tag{12.17}$$

The change in phase between a cell called 000 and its $n_1n_2n_3$ neighbor can be expressed as the sum of the phase changes along a path made up of three orthogonal steps:

$$\phi(n_1n_2n_3) = \phi(n_100 - 000) + \phi(n_1n_20 - n_100) + \phi(n_1n_2n_3 - n_1n_20).$$

But the three sets of mutually perpendicular antiphase boundaries are independent of one another, and hence the phases ϕ for the three steps are completely independent. For quantities which are independent, the average of a product is the product of the averages:

$$\langle e^{i\phi(n_1n_2n_3)} \rangle = \langle e^{i\phi(n_1)} \rangle \langle e^{i\phi(n_2)} \rangle \langle e^{i\phi(n_3)} \rangle. \tag{12.18}$$

The difference in phase $\phi(n_1)$ between a cell called *O* and its n_1th neighbor along the direction of the $\mathbf{a}_1$ axis can be represented as the sum of the phase changes between each consecutive pair of cells:

$$\phi(n_1) = \phi(1 - 0) + \phi(2 - 1) + \phi(3 - 2) + \cdots + \phi(n - [n - 1]).$$

We assume that the probability of an antiphase boundary between any two neighboring cells is the same for all such pairs of cells. For each pair the probability is independent of the other pairs, so that the average of the product is the product of the averages:

$$\langle e^{i\phi(n_1)} \rangle = \langle e^{i\phi(1-0)} \rangle \langle e^{i\phi(2-1)} \rangle \langle e^{i\phi(3-2)} \rangle \cdots = \langle e^{i\phi(1)} \rangle^{|n_1|}, \tag{12.19}$$

where $\langle \exp [i\phi(1)] \rangle$ is the average phase factor for pairs of neighboring cells.

For problems involving independent probabilities, Méring[11] showed that relations such as Eq. (12.19) are extremely useful. Along the $\mathbf{a}_1$-direction, the only phase changes between neighboring cells are $\phi(1) = 0$ with probability $1 - \gamma$, and $\phi(1) = \pi(k + l)$ with probability γ. The average phase factor for neighboring pairs is

$$\langle e^{i\phi(1)} \rangle = (1 - \gamma)1 + \gamma e^{i\pi(k+l)} = 1 - 2\gamma \sin^2 \frac{\pi}{2}(k + l).$$

For the sum over n_1, the phase factor takes two values:

$$k + l = \text{even}, \qquad \langle e^{i\phi(n_1)} \rangle = \langle e^{i\phi(1)} \rangle^{|n_1|} = 1,$$

$$k + l = \text{odd}, \qquad \langle e^{i\phi(n_1)} \rangle = \langle e^{i\phi(1)} \rangle^{|n_1|} = (1 - 2\gamma)^{|n_1|}.$$

The same reasoning applies to the other two sums:

Sum over n_2:

$$l + h = \text{even}, \qquad \langle e^{i\phi(n_2)} \rangle = 1,$$

$$l + h = \text{odd}, \qquad \langle e^{i\phi(n_2)} \rangle = (1 - 2\gamma)^{|n_2|};$$

Sum over n_3:

$$h + k = \text{even}, \qquad \langle e^{i\phi(n_3)} \rangle = 1,$$

$$h + k = \text{odd}, \qquad \langle e^{i\phi(n_3)} \rangle = (1 - 2\gamma)^{|n_3|}.$$

In the case of a fundamental reflection, the sums $(h + k)$, $(k + l)$, and $(l + h)$ are each even and there is no effect of antiphase domains. With superstructure reflections, two indices are of the same parity, and the other one is different. We shall adopt the convention that all superstructure reflections will be written with h and k having the same parity, so that $h + k =$ even, $k + l =$ odd, and $l + h =$ odd. Combining these results with Eqs. (12.17) and (12.18), we can write

$$I_{eu}(h_1h_2h_3) = F^2 \sum_{n_1} \sum_{n_2} \sum_{n_3} N(n_1n_2n_3)(1 - 2\gamma)^{|n_1|}(1 - 2\gamma)^{|n_2|} e^{2\pi i(n_1h_1 + n_2h_2 + n_3h_3)}. \quad (12.20)$$

The factor $N(n_1n_2n_3)$ is the number of cells having a $n_1n_2n_3$ neighbor within the crystal. For very small $n_1n_2n_3$, $N(n_1n_2n_3) = N_1N_2N_3$. Because of the factors $(1 - 2\gamma)^{|n_1|}$ and $(1 - 2\gamma)^{|n_2|}$, only small values of $|n_1|$ and $|n_2|$ contribute in Eq. (12.20). We can replace $N(n_1n_2n_3)$ by its value for very small $|n_1|$ and $|n_2|$, and use the approximation $N(n_1n_2n_3) = N_1N_2(N_3 - |n_3|)$. With this simplification, Eq. (12.20) becomes the product of three independent sums:

$$I_{eu}(h_1h_2h_3) = F^2N_1 \sum_{n_1} (1 - 2\gamma)^{|n_1|} e^{2\pi i n_1h_1} N_2 \sum_{n_2} (1 - 2\gamma)^{|n_2|} e^{2\pi i n_2h_2} \sum_{n_3} (N_3 - |n_3|) e^{2\pi i n_3h_3}.$$

The sum over n_3 is equivalent to the product of sums over m_3 and m_3':

$$\sum_{n_3=-N_3}^{+N_3} (N_3 - |n_3|)e^{2\pi i n_3 h_3} = \sum_{m_3=0}^{N_3-1} e^{2\pi i m_3 h_3} \sum_{m_3'=0}^{N_3-1} e^{-2\pi i m_3' h_3} = \frac{\sin^2 \pi N_3 h_3}{\sin^2 \pi h_3}.$$

The sums over n_1 and n_2 are of the form

$$\sum_{n=-\infty}^{+\infty} (1-2\gamma)^{|n|} e^{2\pi i n h} = 1 + \sum_{n=1}^{\infty} [(1-2\gamma)e^{2\pi i h}]^n + \sum_{n=1}^{\infty} [(1-2\gamma)e^{-2\pi i h}]^n$$

$$= 1 + \frac{(1-2\gamma)e^{2\pi i h}}{1-(1-2\gamma)e^{2\pi i h}} + \frac{(1-2\gamma)e^{-2\pi i h}}{1-(1-2\gamma)e^{-2\pi i h}} = \frac{\gamma(1-\gamma)}{\gamma^2 + (1-2\gamma)\sin^2 \pi h}.$$

Since the intensity is concentrated in the vicinity of the point hkl, we are interested only in small values of $h_1 h_2 h_3$. Making the additional approximation that γ is small, we express the intensity distribution in terms of the variables $h_1 h_2 h_3$ for an hkl-superstructure reflection in which h and k are the indices of equal parity:

$$I_{eu}(h_1 h_2 h_3) = F^2 \frac{N_1 \gamma}{\gamma^2 + (\pi h_1)^2} \frac{N_2 \gamma}{\gamma^2 + (\pi h_2)^2} \frac{\sin^2 \pi N_3 h_3}{(\pi h_3)^2}. \qquad (12.21)$$

This peculiar intensity distribution was first obtained by Wilson.[12] At each superstructure point, the intensity distribution has approximately the shape of a thin disk, the plane of the disk being that of the $h_1 h_2$-plane. The thickness of the disk is determined by the crystal dimension $N_3 a_3$, and the radius of the disk increases with the probability γ of antiphase boundaries. In the small region of reciprocal space shown by Fig. 12.8, the fundamental reflections are represented by small spheres, and the superstructure reflections by properly oriented disks. Using single crystals of Cu_3Au, annealed for short times below the critical temperature, superstructure reflections having approximately the predicted disk shapes, have been observed by Edmunds, Hinde, and Lipson[13] and in more detail by Edmunds and Hinde.[14]

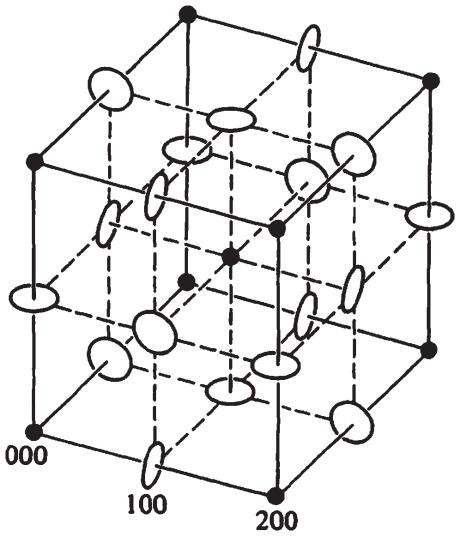

Fig. 12.8 Representation in reciprocal space of the shapes of the reflections for a sample of Cu_3Au in which there are antiphase boundaries normal to the three axes. The fundamental reflections are sharp spheres, and the superstructure reflections are disk-shaped.

c) Effect of Antiphasing on Powder Pattern Integral Breadths

The peculiar shapes in reciprocal space which are represented by Eq. (12.21) produce an equally curious system of antiphase broadening of the powder pattern reflections. Although it is possible to obtain expressions for integral breadths starting out from Eq. (12.21), it is more instructive to follow a general procedure which was developed by Wilson.[10] In Chapter 4 we obtained an integrated intensity by first summing over all the cells in the crystal and then carrying out an integration in reciprocal space. In Wilson's method the order is reversed, we first carry out the integration in reciprocal space, and then afterwards the summation over the cells in the crystal. The mathematics is considerably simplified by considering an $H00$ reflection from a crystal with orthorhombic axes. For any reflection hkl in terms of cubic axes, it is always possible to choose orthorhombic axes for which the reflection becomes $H00$. Actually the final result which we obtain is quite general and independent of the original formulation in terms of orthorhombic axes.

We consider a reflection of the type $H00$ from a crystal with orthorhombic axes $\mathbf{A}_1\mathbf{A}_2\mathbf{A}_3$, reciprocal axes $\mathbf{B}_1\mathbf{B}_2\mathbf{B}_3$, and indices HKL. In terms of the orthorhombic axes, the position of the cell $n_1n_2n_3$ is expressed by $\mathbf{R}_n = n_1\mathbf{A}_1 + n_2\mathbf{A}_2 + n_3\mathbf{A}_3$. Allowing for the fact that the structure factor may vary from cell to cell, the intensity from the crystal is given by

$$I = I_e \sum_n \sum_{n'} F_n F_{n'}^* e^{(2\pi i/\lambda)(\mathbf{s}-\mathbf{s}_0)\cdot(\mathbf{R}_{n'}-\mathbf{R}_n)} .$$

Representing the diffraction vector by $(\mathbf{s} - \mathbf{s}_0)/\lambda = h_1\mathbf{B}_1 + h_2\mathbf{B}_2 + h_3\mathbf{B}_3$, where $h_1h_2h_3$ are continuous variables, the intensity can be put in the form

$$I = I_e \sum_n \sum_{n'} F_n F_{n'}^* e^{2\pi i[(n_1'-n_1)h_1+(n_2'-n_2)h_2+(n_3'-n_3)h_3} . \tag{12.22}$$

As shown in Chapter 4, the integrated intensity of an HKL reflection is proportional to an integral in reciprocal space about the HKL point:

$$P = K \iiint I(h_1h_2h_3)\, dh_1\, dh_2\, dh_3 = \int P(2\theta)\, d(2\theta), \tag{12.23}$$

where $P(2\theta)$ represents the distribution with respect to 2θ of the diffracted power in a powder pattern reflection. For an $H00$ reflection the intensity is nonvanishing only for very small values of h_2 and h_3, and hence we can make the approximation

$$\frac{|\mathbf{s} - \mathbf{s}_0|}{\lambda} = \frac{2\sin\theta}{\lambda} = |h_1\mathbf{B}_1 + h_2\mathbf{B}_2 + h_3\mathbf{B}_3| \to h_1 |\mathbf{B}_1| .$$

From the approximate relation $2\sin\theta/\lambda = |\mathbf{B}_1|\, h_1$, we obtain $d(2\theta) = (\lambda\, |\mathbf{B}_1|/\cos\theta)\, dh_1$. Using this expression for $d(2\theta)$ in Eq. (12.23), we can drop

the integration with respect to dh_1 on both sides of the equation, and obtain the powder pattern profile $P(2\theta)$:

$$P(2\theta) = \frac{K \cos\theta}{\lambda\,|\mathbf{B}_1|} \iint I(h_1h_2h_3)\, dh_2\, dh_3.$$

We now introduce the intensity $I(h_1h_2h_3)$ from Eq. (12.22) and carry out the two integrations from $-\frac{1}{2}$ to $+\frac{1}{2}$ so as to include everything in $P(2\theta)$ which belongs to the $H00$ reflection:

$$P(2\theta) = \frac{KI_e \cos\theta}{\lambda\,|\mathbf{B}_1|} \sum_n \sum_{n'} F_n F^*_{n'} e^{2\pi i(n_1' - n_1)h_1} \frac{\sin \pi(n_2' - n_2)}{\pi(n_2' - n_2)} \frac{\sin \pi(n_3' - n_3)}{\pi(n_3' - n_3)}.$$

Since quotients of the form $\sin \pi(n_2' - n_2)/\pi(n_2' - n_2)$ are equal to unity for $n_2' = n_2$ but otherwise are zero, all terms in $P(2\theta)$ are zero except those with $n_2' = n_2$ and $n_3' = n_3$:

$$P(2\theta) = \frac{KI_e \cos\theta}{\lambda\,|\mathbf{B}_1|} \sum_{n_1} \sum_{n_1'} \sum_{n_2} \sum_{n_3} F_{n_1n_2n_3} F^*_{n_1'n_2n_3} e^{2\pi i(n_1' - n_1)h_1}.$$

When h_1 takes the integral value H, $\exp[2\pi i(n_1' - n_1)h_1] = 1$. For this value of h_1, $P(2\theta)$ is close to its maximum value $P_m(2\theta)$:

$$P_m(2\theta) = \frac{KI_e \cos\theta}{\lambda\,|\mathbf{B}_1|} \sum_{n_1} \sum_{n_1'} \sum_{n_2} \sum_{n_3} F_{n_1n_2n_3} F^*_{n_1'n_2n_3}.$$

Let $\langle FF^*_m \rangle$ be an average of all products $F_{n_1n_2n_3} F^*_{n_1'n_2n_3}$ with $n_1' - n_1 = m$, and let N_m be the number of such terms. The four-fold summation can then be reduced to a single sum over m:

$$P_m(2\theta) = \frac{KI_e \cos\theta}{\lambda\,|\mathbf{B}_1|} \sum_m N_m \langle FF^*_m \rangle.$$

In terms of a distance $t = m\,|\mathbf{A}_1|$, the sum can be replaced by an integral:

$$P_m(2\theta) = \frac{KI_e \cos\theta}{\lambda} \int N_t \langle FF^*_t \rangle\, dt. \tag{12.24}$$

To obtain the total power P in the reflection, we go back to Eq. (12.23). Inserting $I(h_1h_2h_3)$ from Eq. (12.22) and carrying out the integration with respect to dh_1 from $H - \frac{1}{2}$ to $H + \frac{1}{2}$ and the integrations with respect to dh_2 and dh_3 from $-\frac{1}{2}$ to $+\frac{1}{2}$, we obtain

$$P = KI_e \sum_n \sum_{n'} F_n F^*_{n'} \frac{\sin \pi(n_1' - n_1)}{\pi(n_1' - n_1)} \frac{\sin \pi(n_2' - n_2)}{\pi(n_2' - n_2)} \frac{\sin \pi(n_3' - n_3)}{\pi(n_3' - n_3)}.$$

In this case all terms drop out except those with $n_1' = n_1$, $n_2' = n_2$, and $n_3' = n_3$.

If N is the total number of cells in the crystal, we can write

$$P = \int P(2\theta)\, d(2\theta) = KI_e \sum_{n_1} \sum_{n_2} \sum_{n_3} F_{n_1 n_2 n_3} F^*_{n_1 n_2 n_3} = KI_e NFF^*. \qquad (12.25)$$

The integral breadth of a powder pattern reflection is defined by

$$\beta(2\theta) = \frac{\int P(2\theta)\, d(2\theta)}{P_m(2\theta)}.$$

Using the values from Eqs. (12.24) and (12.25), we obtain a very general expression for the integral breadth

$$\beta(2\theta) = \frac{\lambda NFF^*}{\cos\theta \int N_t \langle FF_t^* \rangle\, dt}. \qquad (12.26)$$

For a crystal in which there is no antiphasing, $\langle FF_t^* \rangle = FF^*$ and the expression gives the integral breadth due to particle size broadening only. If the crystals are large and the broadening is due primarily to antiphasing, $\langle FF_t^* \rangle$ decreases so rapidly with increasing t that N_t can be replaced by N since $N_t = N$ for $t = 0$.

We now change to cubic axes $\mathbf{a}_1\mathbf{a}_2\mathbf{a}_3$ and cubic indices hkl. Considering a superstructure reflection with $h + k =$ even, the results of the previous section give

$$\langle FF^*_{n_1 n_2 n_3} \rangle = FF^* \langle e^{i\phi(n_1 n_2 n_3)} \rangle = FF^* (1 - 2\gamma)^{|n_1|} (1 - 2\gamma)^{|n_2|}.$$

From its definition, the distance t is a distance in the crystal parallel to the direction $h\mathbf{b}_1 + k\mathbf{b}_2 + l\mathbf{b}_3$, and hence the distances $n_1 a_1$ and $n_2 a_2$ can be expressed as components of t:

$$n_1 a_1 = th/\sqrt{h^2 + k^2 + l^2},$$
$$n_2 a_2 = tk/\sqrt{h^2 + k^2 + l^2}.$$

From these expressions, we can write

$$|n_1| + |n_2| = \frac{|t|\,(|h| + |k|)}{a\sqrt{h^2 + k^2 + l^2}} = \alpha\,|t|,$$

where $\alpha = (|h| + |k|)/a\sqrt{h^2 + k^2 + l^2}$.

Incorporating these results in Eq. (12.26), we obtain

$$\beta(2\theta) = \frac{\lambda}{\cos\theta \int_{-\infty}^{+\infty} (1 - 2\gamma)^{\alpha|t|}\, dt} = -\frac{\lambda\alpha}{2\cos\theta} \ln(1 - 2\gamma).$$

The antiphasing probability is usually small enough to make the approximation $\ln(1 - 2\gamma) = -2\gamma$, and we arrive at a final expression which is similar to that first obtained by Wilson[12] for the integral breadth due to the

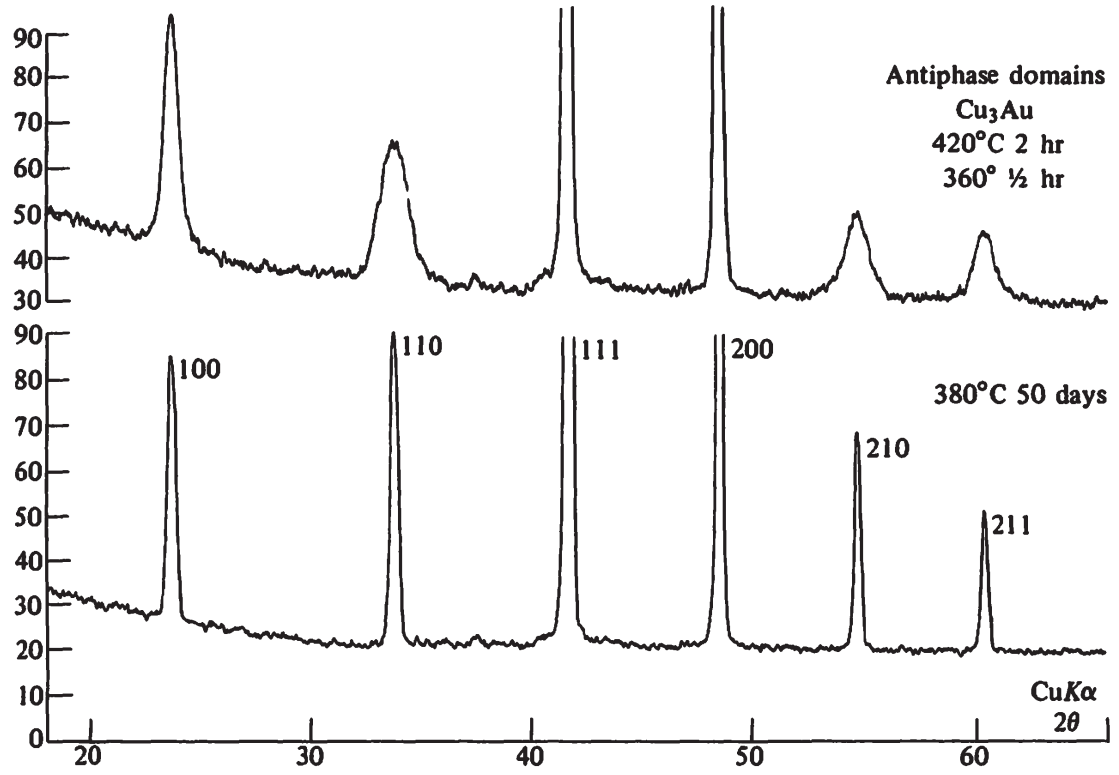

Fig. 12.9 Illustration of the broadening of superstructure reflections resulting from antiphase domains in a sample of Cu_3Au. Upper pattern: disordered sample annealed ½ hour at 360°C, producing long-range order with antiphase boundaries. Lower pattern: long-range ordered sample, annealed 50 days at 380°C to eliminate antiphase boundaries.

half diagonal glide type of antiphasing:

$$\beta(2\theta) = \frac{\lambda\gamma(|h| + |k|)}{a\cos\theta\sqrt{h^2 + k^2 + l^2}}. \tag{12.27}$$

The peculiar *hkl* dependence of the broadening results from the ratio $(|h| + |k|)/\sqrt{h^2 + k^2 + l^2}$, and the values of this quantity for the first four superstructure reflections are as follows:

hkl	001	110	201	112
$(\|h\| + \|k\|)/\sqrt{h^2 + k^2 + l^2}$	0.00	1.41	0.89	0.82

A diffractometer tracing of a sample of Cu_3Au which has been ordered for ½ hour at 360°C is shown by Fig. 12.9. There is qualitative agreement between the breadths of the superstructure reflections and the values of $(|h| + |k|)/\sqrt{h^2 + k^2 + l^2}$, in that 001 is the narrowest and 110 the broadest. Although the major part of the broadening can be attributed to the kind of antiphasing which we have considered, it is evident that there is an additional small contribution of another kind which can produce a broadening of 001.

Table 12.1
EFFECTIVE PARTICLE SIZES IN Cu_3Au

hkl	$\frac{\sqrt{h^2 + k^2 + l^2}}{(\|h\| + k\|)}$	*L*(eff) comp	*L* measured
001	∞	∞	200 A
110	0.707	82 A	100 A
201	1.108	128 A	120 A
112	1.225	142 A	142 A

For broadening due to particle size only, it is customary to define an effective particle size L by the relation $L = \lambda/\beta(2\theta)\cos\theta$. The broadening due to antiphasing can be expressed in terms of effective sizes L(eff), but it must be emphasized that this is purely formal, since the values will vary from one reflection to another:

$$L(\text{eff}) = \frac{a}{\gamma}\frac{\sqrt{h^2 + k^2 + l^2}}{|h| + |k|}. \tag{12.28}$$

An early set of measurements by Jones and Sykes[15] was interpreted in terms of effective sizes. The values are listed in Table 12.1, together with values computed from Eq. (12.28) using $a/\gamma = 116$ A.

There is qualitative agreement, but again it is evident that there is another source of broadening in addition to that due to the half diagonal glide type of antiphasing which has been considered.

12.4 SHORT-RANGE ORDER DIFFUSE INTENSITY

We now consider a binary solid solution in which long-range order is absent. This condition can be obtained by holding the sample at a temperature above T_c, or in some cases by quenching from above T_c. The atom positions are designated by the index m and represented by the vectors $\mathbf{R}_m$. The composition need not be stoichiometric, and we express the number of atoms of either kind by $N_A = x_A N$ and $N_B = x_B N$. The intensity from the sample is written in the usual way:

$$I_{eu} = \sum_m f_m e^{(2\pi i/\lambda)(\mathbf{s}-\mathbf{s}_0)\cdot\mathbf{R}_m} \sum_{m'} f_{m'} e^{-(2\pi i/\lambda)(\mathbf{s}-\mathbf{s}_0)\cdot\mathbf{R}_{m'}}$$
$$= \sum_m \sum_{m'} f_m f_{m'} e^{(2\pi i/\lambda)(\mathbf{s}-\mathbf{s}_0)\cdot(\mathbf{R}_m - \mathbf{R}_{m'})}.$$

We have specified that long-range order does not exist, and hence for two positions m and m' which are not close neighbors, the occupancy of either

one is completely independent of the other. For such pairs of positions,

$$\langle f_m f_{m'} \rangle = \langle f_m \rangle \langle f_{m'} \rangle = (x_A f_A + x_B f_B)^2.$$

Adding and subtracting a term involving $(x_A f_A + x_B f_B)^2$, the intensity is expressed by

$$I_{eu} = \sum_m \sum_{m'} \{f_m f_{m'} - (x_A f_A + x_B f_B)^2\} e^{(2\pi i/\lambda)(\mathbf{s}-\mathbf{s}_0)\cdot(\mathbf{R}_m - \mathbf{R}_{m'})} + \sum_m \sum_{m'} (x_A f_A + x_B f_B)^2 e^{(2\pi i/\lambda)(\mathbf{s}-\mathbf{s}_0)\cdot(\mathbf{R}_m - \mathbf{R}_{m'})}. \quad (12.29)$$

The second term of Eq. (12.29) represents the sharp crystalline reflections which we call the fundamentals. The first term is a diffuse intensity, since $\{\langle f_m f_{m'} \rangle - (x_A f_A + x_B f_B)^2\}$ is zero except for positions m and m' which are close neighbors and hence only small values of $\mathbf{R}_m - \mathbf{R}_{m'}$ contribute. The angular distribution of this diffuse intensity depends upon the short-range order in the specimen (SRO) and we shall designate it by

$$I_{eu}(\text{SRO}) = \sum_m \sum_{m'} \{f_m f_{m'} - (x_A f_A + x_B f_B)^2\} e^{(2\pi i/\lambda)(\mathbf{s}-\mathbf{s}_0)\cdot \mathbf{r}_{mm'}}. \quad (12.30)$$

Most of the studies of short-range order have been made on the βCuZn and Cu_3Au type structures for which it is always possible to choose axes so as to have one atom per unit cell. In these structures for every neighbor at displacement $\mathbf{r}$, there is another neighbor at $-\mathbf{r}$, and the exponential term in Eq. (12.30) can be reduced to a cosine. In the hexagonal close-packed and the diamond type structures, it is not possible to choose axes corresponding to less than two atoms per cell. We designate the two positions by 1 and 2. For any neighbor at a displacement $\mathbf{r}$ from position 2, there is a neighbor at $-\mathbf{r}$ from position 1. Assuming the same ordering about positions 1 and 2, the exponential again reduces to a cosine.

For the sake of simplicity we shall now develop the theory in terms of the βCuZn and Cu_3Au type structure, but the final equations apply equally well to some other kinds of structures in which each atom has the same number of neighbors. Let $\langle f_m f_{m'} \rangle_n$ be the average for all pairs of atoms at a fixed displacement $\mathbf{r}_n$, and let N_n be the number of atoms in the sample having a neighbor at $\mathbf{r}_n$. The double sum in Eq. (12.30) can then be reduced to a single sum over n:

$$I_{eu}(\text{SRO}) = \sum_n N_n [\langle f_m f_{m'} \rangle_n - (x_A f_A + x_B f_B)^2] \cos \frac{2\pi}{\lambda} (\mathbf{s} - \mathbf{s}_0) \cdot \mathbf{r}_n. \quad (12.31)$$

Since the term in square brackets vanishes except for small values of $|\mathbf{r}_n|$, we can set $N_n = N$, where N is the number of atoms in the sample. Introduce the two probabilities:

$p_A(n)$ = probability of finding an A atom as a $\mathbf{r}_n$ neighbor of a B atom,
$p_B(n)$ = probability of finding a B atom as a $\mathbf{r}_n$ neighbor of an A atom.

For the AB pairs which are $\mathbf{r}_n$ neighbors, there is equal probability for finding B as the $\mathbf{r}_n$ neighbor of an A, or A as the $\mathbf{r}_n$ neighbor of a B. This gives the connecting relation $x_A p_B(n) = x_B p_A(n)$. The average in Eq. (12.31) is now expressed in terms of these probabilities:

$$\begin{aligned}\langle f_m f_{m'}\rangle_n &= x_A f_A\{p_B(n) f_B + [1 - p_B(n)] f_A\} \\ &\quad + x_B f_B\{p_A(n) f_A + [1 - p_A(n)] f_B\} \\ &= x_A f_A^2 + x_B f_B^2 - x_B p_A(n)(f_B - f_A)^2\end{aligned}$$

and the term in square brackets becomes

$$[\langle f_m f_{m'}\rangle_n - (x_A f_A + x_B f_B)^2] = x_A x_B (f_B - f_A)^2 [1 - p_A(n)/x_A].$$

A convenient set of short-range order parameters $\alpha(n)$ were introduced by Cowley[16]:

$$\alpha(n) = 1 - p_A(n)/x_A = 1 - p_B(n)/x_B. \tag{12.32}$$

When there is a preference for unlike neighbors, $p_A(n) > x_A$ and $\alpha(n)$ is negative; when the preference is for like neighbors, $\alpha(n)$ is positive, and for complete randomness, $\alpha(n) = 0$. Incorporating the above results in Eq. (12.31), we express the diffuse intensity in terms of the short-range order parameters:

$$I_{eu}(\text{SRO}) = N x_A x_B (f_B - f_A)^2 \sum_n \alpha(n) \cos \frac{2\pi}{\lambda} (\mathbf{s} - \mathbf{s}) \cdot \mathbf{r}_n. \tag{12.33}$$

Equation (12.33) is quite general for structures in which the smallest unit cell contains either one or two atoms. In either case N is the total number of atoms in the sample, and the summation over n covers all of the neighbors of any one atom (including itself).

For a sample in which there is no short-range order and the atoms are distributed at random, $p_A(n) = x_A$ and $\alpha(n) = 0$ for all $r_n \neq 0$. For this case Eq. (12.33) is reduced to the single term $\mathbf{r}_n = 0$ for which $p_A(0) = 0$ and $\alpha(0) = 1$:

$$I_{eu}(\text{Random}) = N x_A x_B (f_B - f_A)^2. \tag{12.34}$$

This is a diffuse scattering which decreases monotonically with increasing scattering angle. The expression was first derived by von Laue, and hence it is often called the Laue monotonic scattering. Experiment shows that binary alloys tend to show short-range order, and it can be expected that the simple Laue monotonic scattering will be seldom observed on x-ray patterns.

a) Short-Range Order from Powder Patterns

For recording the short-range order diffuse scattering, we consider first a powder pattern. To handle the average of $\cos\{(2\pi/\lambda)(\mathbf{s} - \mathbf{s}_0) \cdot \mathbf{r}_n\}$ in Eq. (12.33), we write $(2\pi/\lambda)(\mathbf{s} - \mathbf{s}_0) \cdot \mathbf{r}_n = k r_n \cos\phi$, where $k = 4\pi \sin\theta/\lambda$ and

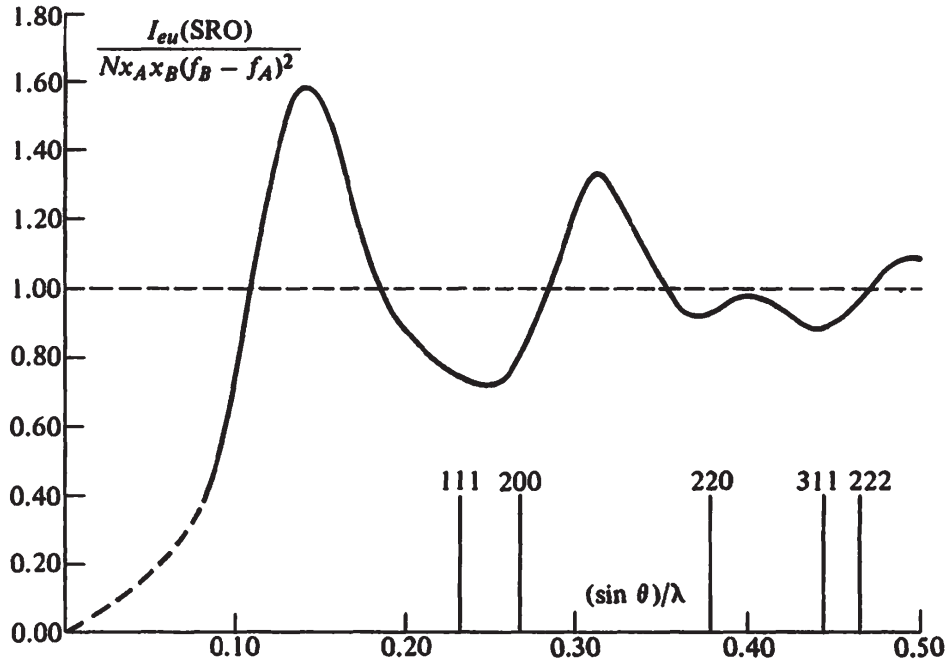

Fig. 12.10 Computed ratio of the short-range order intensity to the Laue monotonic for a powder sample of Cu_3Au. Computed from the first five Cowley parameters for Cu_3Au at $T = 405°C$; $\alpha_1 = -0.152$, $\alpha_2 = 0.186$, $\alpha_3 = 0.009$, $\alpha_4 = 0.095$, and $\alpha_5 = -0.053$.

ϕ is the angle between $(\mathbf{s} - \mathbf{s}_0)$ and $\mathbf{r}_n$. Since each vector $\mathbf{r}_n$ takes with equal probability all orientations, the average is given by

$$\left\langle \cos \frac{2\pi}{\lambda} (\mathbf{s} - \mathbf{s}_0) \cdot \mathbf{r} \right\rangle = \frac{1}{4\pi r^2} \int_0^{\pi} \cos (kr \cos \phi) 2\pi r^2 \sin \phi \, d\phi = \frac{\sin kr}{kr}.$$

It is convenient to designate the neighbors in terms of shells i, where c_i is the number of neighbors in shell i, and r_i is the radius of shell i. For powder pattern recording Eq. (12.33) is changed to a sum over shells i:

$$I_{eu}(\text{SRO}) = Nx_Ax_B(f_B - f_A)^2 \sum_{i=0}^{\infty} c_i\alpha_i \frac{\sin kr_i}{kr_i}. \tag{12.35}$$

The ratio $I_{eu}(\text{SRO})/Nx_Ax_B(f_B - f_A)^2$ is the short-range order intensity relative to the Laue monotonic scattering. In general, the $c_i\alpha_i$ converge fairly rapidly with increasing i, and the relative intensity can be written in the form of a series which converges particularly well for the large values of k:

$$\frac{I_{eu}(\text{SRO})}{Nx_Ax_B(f_B - f_A)^2} = 1 + c_1\alpha_1 \frac{\sin kr_1}{kr_1} + c_2\alpha_2 \frac{\sin kr_2}{kr_2} + c_3\alpha_3 \frac{\sin kr_3}{kr_3} + \cdots \tag{12.36}$$

Figure 12.10 illustrates the relative short-range order intensity represented by Eq. (12.36). The curve is computed from Cowley's first five parameters[16]

for Cu_3Au at 405°C:

$$\alpha_1 = -0.152, \quad \alpha_2 = 0.186, \quad \alpha_3 = 0.009,$$
$$\alpha_4 = 0.095, \quad \alpha_5 = -0.053.$$

The first two peaks occur roughly in the positions where the superstructure reflections 100, 110 and 210, 211 would appear if long-range order were present.

As seen from Eq. (12.36), the intensity per atom $I_{eu}(\text{SRO})/N$ averages to $x_A x_B (f_B - f_A)^2$ at large values of k. This gives a method for obtaining the intensity in absolute units. Neglecting for the present what is called the size effect, and assuming that all fluorescence has been eliminated, the total diffuse intensity includes the short-range order diffuse intensity, the Compton modified scattering, and the temperature diffuse scattering. At large k the total intensity per atom in electron units has an average value:

$$I_{eu}/N = x_A x_B (f_B - f_A)^2 + \{x_A i_A(M) + x_B i_B(M)\} + I(\text{TDS})/N. \quad (12.37)$$

Approximating the TDS by an expression such as Eq. (11.104), we plot the right-hand side of Eq. (12.37), and adjust the ordinate scale of the measured diffuse intensity divided by the polarization factor so that it oscillates above and below at large values of k. This establishes the measured intensity curve in electron units per atom, and by then subtracting the Compton modified and the TDS, we have $I_{eu}(\text{SRO})/N$ in absolute units.

An approximate evaluation of the order parameters can be made in terms of Eq. (12.36). Since the c_i and r_i are all known, measurements of the relative intensity for several values of k can be treated by a set of linear equations in the α_i. A more complicated but probably more reliable method for obtaining the α_i involves a Fourier inversion of the intensity data. Let

$$\frac{I_{eu}(\text{SRO})}{N x_A x_B (f_B - f_A)^2} - 1 = j(k).$$

Equation (12.35) is represented by a summation starting with $i = 1$:

$$j(k) = \sum_{i=1}^{\infty} c_i \alpha_i \frac{\sin kr_i}{kr_i}.$$

Introduce a function $g(r)$ which differs from zero only in the vicinity of the positions $r = r_i$ where it shows positive or negative peaks with areas

$$\int_{r<r_i}^{r>r_i} g(r)\, dr = c_i \alpha_i.$$

With this function, the sum over i can be replaced by an integral

$$kj(k) = \int_0^{\infty} \frac{g(r)}{r} \sin kr\, dr.$$

Using the inversion formulae of Eq. (10.13), we obtain finally

$$g(r) = \frac{2r}{\pi} \int_0^\infty kj(k) \sin rk \, dk. \tag{12.38}$$

The values of $c_i\alpha_i$ are then obtained from the areas under the peaks of the $g(r)$ curve. The Fourier inversion method has the disadvantage that it requires good intensity data out to large values of $\sin\theta/\lambda$, but it contains a self-consistency check in that peaks in the $g(r)$ curve have no significance if they do not occur at the known r_i positions.

b) Short-Range Order from Single Crystals

Short-range order determinations should always be made from single crystals if they are available. The short-range order diffuse scattering is better concentrated, and the always troublesome TDS occurs most strongly in the regions of reciprocal space where the short-range order intensity is a minimum. We now develop the theory for the βCuZn or Cu_3Au type structures with BCC or FCC lattices. For either kind of structure the vector $\mathbf{r}_n$ can be expressed by

$$\mathbf{r}_n = l\mathbf{a}_1/2 + m\mathbf{a}_2/2 + n\mathbf{a}_3/2,$$

where $\mathbf{a}_1\mathbf{a}_2\mathbf{a}_3$ are the usual cubic axes, and the lmn are integers restricted to the values:

$l + m + n$ = even for the FCC Cu_3Au type structure,

lmn unmixed for the BCC βCuZn type structure.

We represent the diffraction vector by

$$(\mathbf{s} - \mathbf{s}_0)/\lambda = h_1\mathbf{b}_1 + h_2\mathbf{b}_2 + h_3\mathbf{b}_3,$$

where $h_1h_2h_3$ are continuous variables, and the $\mathbf{b}_i$ are vectors reciprocal to the cubic $\mathbf{a}_i$. The summation over n of Eq. (12.33) is now replaced by a summation over the three indices lmn:

$$\frac{I_{eu}(\text{SRO})}{Nx_Ax_B(f_B - f_A)^2} = I'(h_1h_2h_3) = \sum_l \sum_m \sum_n \alpha(lmn) \cos \pi(lh_1 + mh_2 + nh_3).$$

For the cubic structures under consideration, there are neighbors represented by $\pm l$, $\pm m$, and $\pm n$, all with the same value of $\alpha(lmn)$. Hence when $\cos \pi(lh_1 + mh_2 + nh_3)$ is broken up into products of cosines and sines, all terms involving sines cancel out, and we obtain the simpler expression:

$$I'(h_1h_2h_3) = \sum_l \sum_m \sum_n \alpha(lmn) \cos \pi lh_1 \cos \pi mh_2 \cos \pi nh_3. \tag{12.39}$$

The form of Eq. (12.39) is extremely interesting and important. The reduced intensity $I'(h_1h_2h_3)$ is periodic in reciprocal space with periods $\Delta h_1 = 2$, $\Delta h_2 = 2$, and $\Delta h_3 = 2$ in the directions of the $\mathbf{b}_1$-, $\mathbf{b}_2$-, and $\mathbf{b}_3$-axes.

Equation (12.39) expresses $I'(h_1h_2h_3)$ as a three-dimensional Fourier series in which the Fourier coefficients are the short-range order parameters $\alpha(lmn)$. If values for $I'(h_1h_2h_3)$ are available throughout one repeating volume, the short-range order coefficients are obtained by the usual procedure for evaluating Fourier coefficients. Letting $l'm'n'$ be fixed integers, we multiply both sides of Eq. (12.39) by $\cos \pi l'h_1 \cos \pi m'h_2 \cos \pi n'h_3$ and integrate over one repeating volume:

$$\int_0^2\int\int I'(h_1h_2h_3) \cos \pi l'h_1 \cos \pi m'h_2 \cos \pi n'h_3 \, dh_1 \, dh_2 \, dh_3$$

$$= \sum_{lmn} \alpha(lmn) \int_0^2\int\int \cos \pi lh_1 \cos \pi l'h_1 \cos \pi mh_2 \cos \pi m'h_2 \times \cos \pi nh_3 \cos \pi n'h_3 \, dh_1 \, dh_2 \, dh_3.$$

The integrals on the right-hand side of the equation are zero except for $l = \pm l'$, $m = \pm m'$, and $n = \pm n'$, and hence

$$\alpha(lmn) = \tfrac{1}{8} \int_0^2\int\int I'(h_1h_2h_3) \cos \pi lh_1 \cos \pi mh_2 \cos \pi nh_3 \, dh_1 \, dh_2 \, dh_3. \tag{12.40}$$

There is considerable symmetry within a repeating volume in reciprocal space such as the cube $2b_1 \times 2b_2 \times 2b_3$ shown by Fig. 12.11. Since $\cos \pi lh_1$ and $\cos \pi mh_2$ are symmetrical about integral values of h_1 and h_2, there is reflection symmetry across the plane through 100 and 120 and across the plane through 010 and 210 of Fig. 12.11. The intensity distribution in the

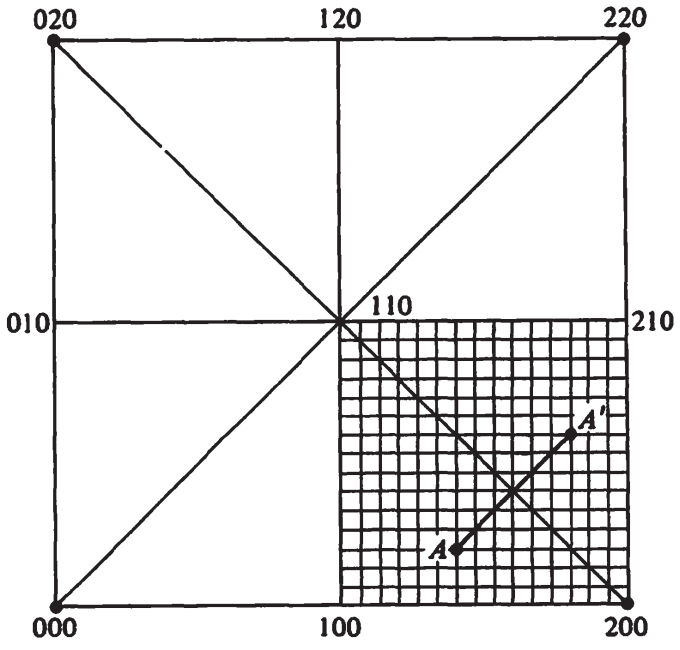

Fig. 12.11 Illustration of the repeating volume in reciprocal space for the short-range order diffuse intensity in the βCuZn and Cu_3Au type structures.

repeating volume is completely expressed by the distribution in one octant. There is additional symmetry across certain diagonal planes. In terms of coordinates h_1 and h_2 for point A, the coordinates of point A' are $h_1' = 2 - h_2$ and $h_2' = 2 - h_1$. The reduced intensity at A' is expressed by

$$I'(A') = \sum_{lmn} \alpha(lmn) \cos \pi l(2 - h_2) \cos \pi m(2 - h_1) \cos \pi n h_3.$$

Since $\alpha(mln) = \alpha(lmn)$,

$$I'(A') = \sum_{lmn} \alpha(mln) \cos \pi l h_2 \cos \pi m h_1 \cos \pi n h_3 = I'(A).$$

There is reflection symmetry across diagonal planes such as the ones through 020 and 200 and through 000 and 220 shown by Fig. 12.11. There are also additional symmetry operations which depend upon the particular structure under consideration. Evidently, the intensity distribution in only a fraction of one octant is enough to reproduce the whole repeating volume. However, it is preferable to make intensity measurements through more than the minimum volume, so as to have a self-consistency check, and also to facilitate correction for the size effect which will be discussed later. Since all the troublesome corrections increase with $\sin \theta/\lambda$, it is preferable to make the measurements as close as possible to the origin of reciprocal space. Measurements are to be preferred in the octant with front face 100, 200, 210, 110 shown by Fig. 12.11, or if necessary, in the next octant to the right with front face 200, 300, 310, 210.

Suppose that by symmetry operations our values of the reduced intensity $I'(h_1h_2h_3)$ cover the repeating volume $2b_1 \times 2b_2 \times 2b_3$ of Fig. 12.11. We divide the volume into $30 \times 30 \times 30$ intervals, so that the octant which is shown is divided into $15 \times 15 \times 15$ intervals. Setting $h_1 = 1 + h_1'$, then $\cos \pi l(1 + h_1') = (-1)^l \cos \pi l h_1'$ and Eq. (12.40) becomes

$$\alpha(lmn) = \tfrac{1}{8}(-1)^l \int_0^2\int\int I'(h_1'h_2h_3) \cos \pi l h_1' \cos \pi m h_2 \cos \pi n h_3 \, dh_1' \, dh_2 \, dh_3.$$

We replace the integral by a sum, perform the sum over just the octant, and then multiply the result by 8:

$$\alpha(lmn) = \left(\frac{2}{30}\right)^2 (-1)^l \sum_0^1 \sum \sum I'(h_1'h_2h_3) \cos \pi l h_1' \cos \pi m h_2 \cos \pi n h_3.$$

The second edition Lipson and Beevers cosine strips give the values of $A \cos 2\pi hn/120$ in unit steps for h and n. If we use only alternate positions on the n = even side of the strips and number these $n' = n/4$, the values given by the strips will be $A \cos \pi n'h/15$. In the summations which are to be performed, h_1', h_2, and h_3 take the values: $0, \frac{1}{15}, \frac{2}{15}, \ldots, \frac{15}{15}$. Hence the

values on the strips cos $\pi n'h/15$ can represent cos $\pi lh_1'$ or cos πmh_2 or cos πnh_3, where n' represents l or m or n, and h takes unit values from 0 to 15. The summation can be formulated in the following way:

$$\alpha(lmn) = \left(\frac{2}{30}\right)^2(-1)^l \sum_{h_1'}\left\{\sum_{h_2}\left[\sum_{h_3} I'(h_1'h_2h_3)\cos \pi nh_3\right]\cos \pi mh_2\right\}\cos \pi lh_1'. \tag{12.41}$$

For each interval $h_1'h_2$ of Fig. 12.11 there is a column of values of $I'(h_1'h_2h_3)$. The sum over h_3 shown in square brackets in Eq. (12.41) is evaluated by using strips with h values from 0 to 15, and amplitudes $A = I'(h_1'h_2h_3)$, except that half values of the amplitudes are used for the two ends $h_3 = \frac{0}{15}$ and $h_3 = \frac{15}{15}$. Sums are recorded only for $n' = 0$, 1, and 2. It is not necessary to carry out this summation for all of the 16 × 16 $h_1'h_2$ positions shown on Fig. 12.11. There is reflection symmetry across the plane 110–200 for either the βCuZn or the Cu_3Au structures. For the sum over h_3, there is reflection symmetry across the plane 100–210 for the βCuZn structure, and reflection with change of sign if n is odd for the Cu_3Au structure. The summation is carried out for only a quarter of the $h_1'h_2$ positions and the others generated by symmetry operations. At this stage we have the square bracket sums of Eq. (12.41) for $n = 0$, and 1 and 2 for the 16 × 16 $h_1'h_2$ positions of Fig. 12.11. For each value of h_1' and $n = 0$, 1, 2, we next use the strips to perform the sum over h_2, using half values for $h_2 = \frac{0}{15}$ and $h_2 = \frac{15}{15}$ and recording the sums for only $m = 0$, 1, 2, and 3. Finally, we perform the sum over h_1' for the 12nm combinations and record only for $l = 0$, 1, 2, 3, 4. The 60 $\alpha(lmn)$-values thus obtained are ample for all of the desired short-range order parameters. For the two types of structures considered, the available lmn combinations for different neighbors are as follows:

	Cu_3Au	βCuZn
1st neighbor	110, 101, 011	111
2nd neighbor	200, 020, 002	200, 020, 022
3rd neighbor	211, 121, 112	220, 202, 022
4th neighbor	220, 202, 022	311, 131
5th neighbor	310, 130, 301, 031	222
6th neighbor	222	400
7th neighbor	321, 231, 312, 132	331
8th neighbor	400	420

As an example of the short-range order diffuse intensity from a single crystal, Fig. 12.12 shows Cowley's measurements[16] of $I'(h_1h_2h_3)$ in the h_1h_20 plane of reciprocal space for a single crystal of Cu_3Au held at 405°C. The intensity concentrates at each of the positions where there would have been

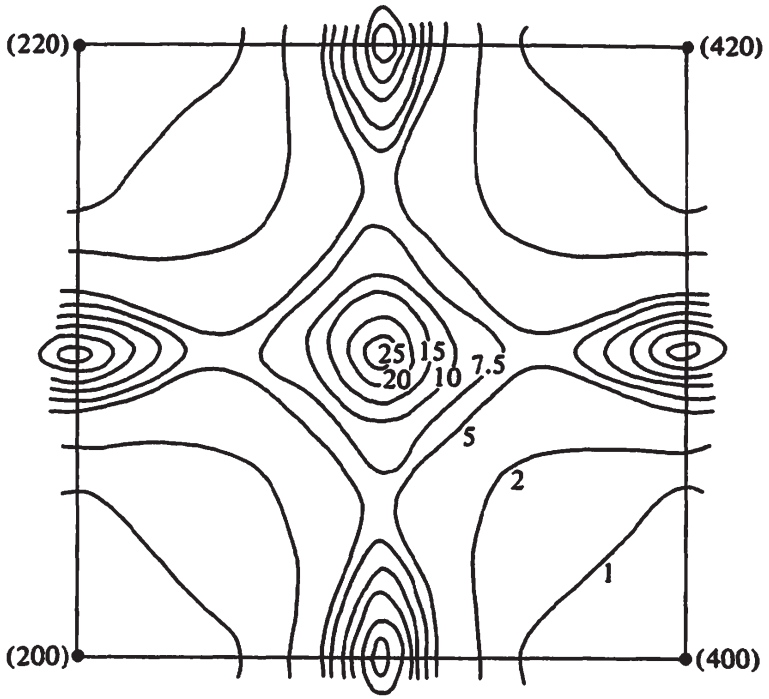

Fig. 12.12 Cowley's measurement of the short-range order diffuse intensity in the h_1h_20 plane of reciprocal space for a single crystal of Cu_3Au held at 405°C.

superstructure reflections if long-range order had been present. The concentrations are somewhat disk shaped, and it is of interest to note that the orientation of the disks in reciprocal space is exactly that of the disks resulting from antiphase domains which are shown by Fig. 12.8. Cowley's short-range order values for Cu_3Au held at three temperature are given by Table 12.2. For each set of neighbors, the table gives the number of neighbors, the *lmn*-coordinates, the value of $\alpha(lmn)$ for perfect order, and the measured values of $\alpha(lmn)$ for temperatures of 405°C, 460°C, and 550°C. As seen from the table, α_1 is negative, indicating a preference for unlike nearest neighbors.

Table 12.2
MEASURED VALUES OF SHORT-RANGE ORDER PARAMETERS FOR Cu_3Au

i	c_i	*lmn*	Perfect order, $\alpha(lmn)$	405°C, $\alpha(lmn)$	460°C, $\alpha(lmn)$	550°C, $\alpha(lmn)$
1	12	110	−0.333	−0.152	−0.148	−0.131
2	6	200	1.00	0.186	0.172	0.105
3	24	211	−0.333	0.009	0.019	0.026
4	12	220	1.00	0.095	0.068	0.045
5	24	310	−0.333	−0.053	−0.049	−0.032
6	8	222	1.00	0.025	0.007	−0.009
7	48	321	−0.333	−0.016	−0.008	−0.003
8	6	400	1.00	0.048	0.042	0.019

Since $\alpha_i = 1 - p_A(i)/x_A$, the number of Cu atoms which are ith neighbors of an Au atom is given by $n_A(i) = c_i p_A(i) = c_i x_A(1 - \alpha_i)$. For nearest neighbors at 405°C, $n_A(1) = 12 \times 0.75 \times 1.152 = 10.4$. At 405°C, there are on the average 10.4 Cu atoms as first neighbors of an Au atom. This is about halfway between the numbers 9 and 12 corresponding to complete randomness or to perfect order. For second neighbors $n_A(2) = 6 \times 0.75 \times 0.814 = 3.67$, which is closer to $n_A(2) = 4.50$ for complete randomness than to $n_A(2) = 0$ for perfect order. The short-range order for first and second neighbors decreases with rising temperature but not rapidly. At first sight the values for third neighbors in Table 12.2 seem to be completely wrong; not only are the signs opposite to the sign for perfect order, but also the values increase with rising temperature. However, we must remember that a third neighbor of, say, a Au has 12 first neighbors, of which 2 are Cu rich by being first neighbors of the Au, and only 1 is Au rich by being a second neighbor of the Au. As long as the short-range order is low, there could be a small tendency for the third neighbor of the Au atom to be Au rich. A more recent measurement of the short-range order parameters in Cu_3Au, with several improvements in technique and interpretation, has been made by Moss.[17] The new-order parameters are a little larger, but otherwise follow the same trend as the Cowley values.

Most binary solid solutions give a negative value for α_1 indicating a preference for unlike nearest neighbors. A positive value for α_1 would be interpreted as a preference for like nearest neighbors. But like nearest neighbors should produce a preference for like second and third neighbors. This condition is not possible unless the sample is made up of small regions with compositions differing from the average composition, some of the small regions being A rich and the others B rich. This condition in the sample has been given the name of clustering.

Our treatment of the short-range order diffuse intensity is incomplete, in that so far we have made no allowance for the effect of temperature vibration on what we have called the SRO diffuse intensity, and we have made no allowance for the effect of a difference in size of the atoms. We consider first the effect of temperature vibration.

12.5 EFFECT OF TEMPERATURE VIBRATION ON SHORT-RANGE ORDER INTENSITIES

The effect of temperature vibration on the short-range order diffuse intensity has been treated by Walker and Keating.[18] We shall develop here a somewhat simplified treatment by making some additional approximations. To allow for thermal vibrations we replace $\mathbf{R}_m$ by $\mathbf{R}_m + \mathbf{u}_m$, and Eq. (12.30) becomes

$$I_{eu}(\text{SRO}) = \sum_m \sum_{m'} \{f_m f_{m'} - (x_A f_A + x_B f_B)^2\} e^{(2\pi i/\lambda)(\mathbf{s}-\mathbf{s}_0)\cdot(\mathbf{R}_m - \mathbf{R}_{m'})} \times e^{(2\pi i/\lambda)(\mathbf{s}-\mathbf{s}_0)\cdot(\mathbf{u}_m - \mathbf{u}_{m'})}. \quad (12.42)$$

With the abbreviations $k = 2\pi/\lambda$ and $\mathbf{S} = \mathbf{s} - \mathbf{s}_0$, we can write

$$e^{(2\pi i/\lambda)(\mathbf{s}-\mathbf{s}_0)\cdot(\mathbf{u}_m-\mathbf{u}_{m'})} = e^{ik\mathbf{S}\cdot(\mathbf{u}_m-\mathbf{u}_{m'})} = e^{ip_{mm'}}.$$

Following Eq. (11.15), the time average is given by

$$\langle e^{ip_{mm'}}\rangle = e^{-\langle p^2_{mm'}\rangle/2},$$

and Eq. (12.42) becomes

$$I_{eu}(\text{SRO}) = \sum_m \sum_{m'} \{f_m f_{m'} - (x_A f_A + x_B f_B)^2\} e^{(2\pi i/\lambda)(\mathbf{s}-\mathbf{s}_0)\cdot(\mathbf{R}_m-\mathbf{R}_{m'})} e^{-\langle p^2_{mm'}\rangle/2}. \tag{12.43}$$

We now make the approximation that the temperature displacements are the same for the two kinds of atoms, so that from Eqs. (11.24) and (11.25),

$$\langle p^2_{mm'}\rangle/2 = 2M - \tfrac{1}{2}\sum_{gj} (k\mathbf{S}\cdot\mathbf{e}_{gj})^2 \langle a^2_{gj}\rangle \cos 2\pi\mathbf{g}\cdot(\mathbf{R}_m - \mathbf{R}_{m'}).$$

Next, we make the approximation that the temperature is high enough for equipartition so that $\langle a^2_{gj}\rangle$ is expressed by Eq. (11.23), and also that we can replace all wave velocities by an average velocity V. Since $\omega_{gj} = 2\pi V g$ and $V = \nu_m/g_m$, by introducing the definition $h\nu_m = k\Theta$, we obtain $\nu_{gj} = 2\pi k\Theta g/h g_m$. Writing $(kS)^2 = (4\pi \sin\theta/\lambda)^2$ and $\sum_j \cos^2(S, e_{gj}) = 1$, our expression for $\langle p^2_{mm'}\rangle/2$ becomes

$$\langle p^2_{mm'}\rangle/2 = 2M - \frac{12h^2T}{mk\Theta^2}\left(\frac{\sin\theta}{\lambda}\right)^2 \sum_g \frac{g_m^2}{3Ng^2} \cos 2\pi\mathbf{g}\cdot(\mathbf{R}_m - \mathbf{R}_{m'}).$$

With the approximation $\{\Phi(x) + x/4\} = 1$, the factor before the summation over g is equal to $2M$. We replace the summation by an integration, using a density of points $N/(4\pi/3)g_m^3$ and an element of volume $2\pi g^2 \sin\phi\, d\phi\, dg$:

$$\langle p^2_{mm'}\rangle/2 = 2M\left\{1 - \int_{g=0}^{g_m}\int_{\phi=0}^{\pi} \frac{\cos(2\pi g r_{mm'}\cos\phi)}{2g_m} \sin\phi\, d\phi\, dg\right\}. \tag{12.44}$$

The integrations are readily performed:

$$\int_{g=0}^{g_m}\int_{\phi=0}^{\pi} \frac{\cos(2\pi g r_{mm'}\cos\phi)}{2g_m} \sin\phi\, d\phi\, dg = \int_{g=0}^{g_m} \frac{\sin 2\pi g r_{mm'}\, dg}{g_m 2\pi g r_{mm'}}$$

$$= \frac{\text{Si}(2\pi g_m r_{mm'})}{2\pi g_m r_{mm'}},$$

where $\text{Si}(x)$ is the tabulated function

$$\text{Si}(x) = \int_0^x \frac{\sin u}{u}\, du.$$

With the abbreviation

$$\phi(r_{mm'}) = 1 - \frac{\text{Si}(2\pi g_m r_{mm'})}{2\pi g_m r_{mm'}},$$

Eq. (12.44) takes the simple form

$$\langle p^2_{mm'}\rangle/2 = 2M\phi(r_{mm'}),$$

and Eq. (12.43) can be written

$$I_{eu}(\text{SRO}) = \sum_m \sum_{m'} \{f_m f_{m'} - (x_A f_A + x_B f_B)^2\} e^{-2M\phi(r_{mm'})} e^{(2\pi i/\lambda)(\mathbf{s}-\mathbf{s}_0)\cdot \mathbf{r}_{mm'}}. \tag{12.45}$$

Making the same averages that were used to get from Eq. (12.30) to Eq. (12.33), the short range order diffuse intensity is expressed in terms of a sum over the $\mathbf{r}_n$ neighbors of any one atomic site:

$$I_{eu}(\text{SRO}) = Nx_A x_B (f_B - f_A)^2 \sum_n \alpha(n) e^{-2M\phi(r_n)} \cos \frac{2\pi}{\lambda} (\mathbf{s} - \mathbf{s}) \cdot \mathbf{r}_n, \tag{12.46}$$

where

$$\phi(r_n) = 1 - \frac{\text{Si}(2\pi g_m r_n)}{2\pi g_m r_n}. \tag{12.47}$$

In deriving Eq. (12.46) we have made the rather drastic approximation that the two kinds of atoms can be considered to have the same values of $2M$. Walker and Keating have suggested introducing the two quantities $2M_A\phi(r_n)$ and $2M_B\phi(r_n)$, where $2M_A$ and $2M_B$ could be determined experimentally from the sample when in the state of long-range order. Our derivation provides no sound justification for doing this, but intuitively one feels that it is probably fully as good an approximation as that of assuming that $M_A = M_B$. In terms of separate values for M_A and M_B,

$$I_{eu}(\text{SRO}) = Nx_A x_B \sum_n \{f_B e^{-M_B\phi(r_n)} - f_A e^{-M_A\phi(r_n)}\}^2 \alpha(n) \cos \frac{2\pi}{\lambda} (\mathbf{s} - \mathbf{s}_0) \cdot \mathbf{r}_n. \tag{12.48}$$

We now consider the determination of the short-range order parameters from measurements with single crystals. For the approximation that the same $2M$ can be used for both kinds of atoms, Eq. (12.39) is replaced by

$$I'(h_1h_2h_3) = \sum_l \sum_m \sum_n \alpha(lmn) e^{-2M\phi(lmn)} \cos \pi l h_1 \cos \pi m h_2 \cos \pi n h_3. \tag{12.49}$$

If, on the other hand, we use separate temperature factors M_A and M_B, the intensity is given by the more complicated expression

$$\frac{I_{eu}(\text{SRO})}{Nx_A x_B} = \sum_l \sum_m \sum_n \{f_B e^{-M_B\phi(lmn)} - f_A e^{-M_A\phi(lmn)}\}^2 \times \alpha(lmn) \cos \pi l h_1 \cos \pi m h_2 \cos \pi n h_3. \tag{12.50}$$

It is important to notice that the temperature factor $2M\phi(lmn)$, which has been introduced in the expression for the short-range order intensity,

is quite different from the familiar Debye factor $2M$ which determines the decrease in the crystalline reflections. The value of $2M\phi(lmn)$ is different for each set of neighbors; nearest, next nearest, and so forth. In particular, for $r_n = 0$, it follows from Eq. (12.47) that $\phi(0) = 0$, and hence there is no temperature decrease for the $l = m = n = 0$ term in Eq. (12.49). It is this constant term which determines the area under a peak, the other terms merely distribute the intensity. The temperature factor in Eq. (12.49) lowers and broadens the peak but does not decrease the area. For the short-range order peaks there is no separate temperature diffuse scattering to be considered, the formulation of Eq. (12.49) is such that it includes everything. Since

$$2M = 2B(\sin\theta/\lambda)^2 = 2B(b/2)^2(h_1^2 + h_2^2 + h_3^2), \tag{12.51}$$

it is evident that with the inclusion of a temperature factor, the reduced intensity $I'(h_1h_2h_3)$ is no longer strictly periodic in reciprocal space. With the exception of the $(l = m = n = 0)$-term, there is an exponential decrease in the amplitude of the other terms which varies as the square of the distance from the origin of reciprocal space.

Since the reduced intensity is no longer strictly periodic in reciprocal space, the evaluation of the short-range order parameters requires some approximations. The simplest treatment would be that for a single $2M$, the case which is represented by Eq. (12.49). The variable $2M$ could be replaced by the constant value appropriate to the center of the octant containing the $I'(h_1h_2h_3)$-values being analyzed. The Fourier analysis then proceeds by the methods developed in the previous section. For each lmn we obtain values of the combination $\alpha(lmn)\exp[-2M\phi(lmn)]$. The value of $2M$ can be obtained from the fundamentals, and $\phi(lmn)$ is readily evaluated from Eq. (12.47). The correction for the temperature factor is easily made and we obtain the order parameter $\alpha(lmn)$.

It is instructive to make a rough evaluation of the temperature factor assuming a single value of $2M$. For measurements in the vicinity of the 300 position in a sample of Cu_3Au held at 405°C, we can use the value $2M = 0.39$ obtained from measurements on the fundamental reflections. The temperature factor for the nearest-neighbor order parameter $\alpha(110)$ is found to be $\exp[-2M\phi(110)] = 0.79$. With no correction for the temperature effect, we would obtain a value of $\alpha(110)$ which is 21 percent too small if the measurement is made in the vicinity of the 300 position. If, however, the measurements were made near the 100 position, $2M = 0.39/9 = 0.043$; and $\exp[-2M\phi(110)] = 0.97$. The recent measurements by Moss[17] included the diffuse peaks for Cu_3Au at 100 and 300. The difference between the two was much less than would be expected from the two numbers 0.79 and 0.97, and it seemed necessary to conclude that one must allow for two different values of $2M$ with $2M$(Cu) about twice that of $2M$(Au). Curiously enough this is the ratio of $2M$(Cu) to $2M$(Au) which Chipman[6] had found from measurements on ordered Cu_3Au.

The very meager experimental data which are at present available suggest that an accurate temperature correction for I(SRO) must allow for separate values of $2M_A$ and $2M_B$. But in general these are unknown, or at the best extremely difficult to obtain for the disordered state. At the present time, the only safe procedure seems to require making the measurements close to the origin of reciprocal space at positions such as 100, where the importance of the temperature correction will be so small that in general it can be neglected.

12.6 SIZE EFFECT IN DISORDERED BINARY COMPOSITIONS

In a disordered binary solid solution, if the two kinds of atoms A and B have a difference in size, there will be static displacements from the exact lattice positions. For close neighbors there can be three different distances depending on whether it is an AA-, AB-, or BB-pair. Between two atoms which are not close neighbors, there will be a variation in distance resulting from variations in the composition of the region between them. The variation in close neighbor distances depends upon the kind of atoms making up the pair. This effect produces a modulation in the diffuse intensity, and the theory of this modulation has been given by Warren, Averbach, and Roberts.[19] The variation in the remote neighbor distances does not depend upon the kind of atoms making up the pair. The displacements which are produced act in the same way as the displacements due to temperature vibration, decreasing the intensities of the crystalline peaks and producing a diffuse intensity. This effect was first treated by Huang.[20] A unified treatment which combines both effects has been given by Borie,[21] and reference should be made to his papers for the complete theory. Since the derivations are rather involved, we shall restrict ourselves here to the effect of variations in close-neighbor distances.

For close neighbors (such as first and second), there can be three different distances depending upon whether it is an AA-, AB-, or BB-pair. Denoting the kind of neighbor by i where $i = 1$ for first neighbors, and letting r_i be the average ith neighbor distance as computed from the lattice constant, we represent the three distances by

$$r^i_{AA} = r_i(1 + \epsilon^i_{AA}), \qquad r^i_{AB} = r_i(1 + \epsilon^i_{AB}), \qquad r^i_{BB} = r_i(1 + \epsilon^i_{BB}). \quad (12.52)$$

With the abbreviation $\mathbf{k} = (2\pi/\lambda)(\mathbf{s} - \mathbf{s}_0)$, the intensity in electron units is expressed by

$$I_{eu} = \sum_m \sum_n f_m f_n e^{i\mathbf{k}\cdot(\mathbf{R}_m - \mathbf{R}_n)}.$$

In terms of the distances expressed by Eq. (12.52) and the short-range order probabilities which were introduced in Section 12.4, the intensity is given by

$$I_{eu} = \sum_m \sum_n \{x_A f_A[(1 - p^i_B) f_A e^{i\mathbf{k}\cdot(\mathbf{R}_m - \mathbf{R}_n)(1+\epsilon^i_{AA})} + p^i_B f_B e^{i\mathbf{k}\cdot(\mathbf{R}_m - \mathbf{R}_n)(1+\epsilon^i_{AB})}]$$
$$+ x_B f_B[p^i_A f_A e^{i\mathbf{k}\cdot(\mathbf{R}_m - \mathbf{R}_n)(1+\epsilon^i_{AB})} + (1 - p^i_A) f_B e^{i\mathbf{k}\cdot(\mathbf{R}_m - \mathbf{R}_n)(1+\epsilon^i_{BB})}]\}. \quad (12.53)$$

Since the quantity ϵ in Eq. (12.52) is small, we can make an expansion and keep only the linear term

$$e^{i\mathbf{k}\cdot(\mathbf{R}_m-\mathbf{R}_n)(1+\epsilon)} = e^{i\mathbf{k}\cdot(\mathbf{R}_m-\mathbf{R}_n)}[1 + i\mathbf{k}\cdot(R_m - R_n)\epsilon].$$

Using this expression in Eq. (12.53) and adding and subtracting a term involving $(x_A f_A + x_B f_B)^2$, we express the intensity in the form

$$\begin{aligned} I_{eu} = &\sum_m \sum_n \{x_A(1 - p_B^i)f_A^2 + 2x_B p_A^i f_A f_B + x_B(1 - p_A^i)f_B^2\}e^{i\mathbf{k}\cdot(\mathbf{R}_m-\mathbf{R}_n)} \\ &+ \sum_m \sum_n \{x_A(1 - p_B^i)\epsilon_{AA}^i f_A^2 + 2x_B p_A^i \epsilon_{AB}^i f_A f_B + x_B(1 - p_A^i)\epsilon_{BB}^i f_B^2\} \\ &\times i\mathbf{k}\cdot(\mathbf{R}_m - \mathbf{R}_n)e^{i\mathbf{k}\cdot(\mathbf{R}_m-\mathbf{R}_n)} - \sum_m \sum_n (x_A f_A + x_B f_B)^2 e^{i\mathbf{k}\cdot(\mathbf{R}_m-\mathbf{R}_n)} \\ &+ \sum_m \sum_n (x_A f_A + x_B f_B)^2 e^{i\mathbf{k}\cdot(\mathbf{R}_m-\mathbf{R}_n)}. \end{aligned} \tag{12.54}$$

The first and third terms in Eq. (12.54) can be combined as was done in Section 12.4. The fourth term represents the fundamental reflections, and by omitting this term we obtain the diffuse intensity $I_{eu}(\mathrm{D})$:

$$\begin{aligned} I_{eu}(\mathrm{D}) = &Nx_A x_B(f_B - f_A)^2 \sum_i \alpha(i)e^{i\mathbf{k}\cdot(\mathbf{R}_m-\mathbf{R}_n)} \\ &+ \sum_m \sum_n \{x_A(1 - p_B^i)\epsilon_{AA}^i f_A^2 + 2x_B p_A^i \epsilon_{AB}^i f_A f_B + x_B(1 - p_A^i)\epsilon_{BB}^i f_B^2\} \\ &\times i\mathbf{k}\cdot(\mathbf{R}_m - \mathbf{R}_n)e^{i\mathbf{k}\cdot(\mathbf{R}_m-\mathbf{R}_n)}. \end{aligned} \tag{12.55}$$

Since the average of the ith neighbor distances must equal r_i, we have the additional relation

$$\begin{aligned} x_A(1 - p_B^i)r_i(1 + \epsilon_{AA}^i) + (x_A p_B^i + x_B p_A^i)r_i(1 + \epsilon_{AB}^i) \\ + x_B(1 - p_A^i)r_i(1 + \epsilon_{BB}^i) = r_i, \end{aligned}$$

and this reduces to

$$2x_B p_A^i \epsilon_{AB}^i = -(x_A - x_B p_A^i)\epsilon_{AA}^i - (x_B - x_B p_A^i)\epsilon_{BB}^i. \tag{12.56}$$

We now use this expression in the second term of Eq. (12.55), and since only close neighbors are involved we use the abbreviation $\mathbf{r}_i = \mathbf{R}_m - \mathbf{R}_n$:

$$\begin{aligned} I_{eu}(\mathrm{D}) = &Nx_A x_B(f_B - f_A)^2 \sum_i \alpha(i)e^{i\mathbf{k}\cdot\mathbf{r}_i} + Nx_A x_B(f_B - f_A) \\ &\times \sum_i \left\{-\left(\frac{x_A}{x_B} + \alpha_i\right)\epsilon_{AA}^i f_A + \left(\frac{x_B}{x_A} + \alpha_i\right)\epsilon_{BB}^i f_B\right\} i\mathbf{k}\cdot\mathbf{r}_i e^{i\mathbf{k}\cdot\mathbf{r}_i}. \end{aligned}$$

It is convenient to introduce the ratio $\eta = f_B/f_A$. This ratio has a small θ dependence, and it is an approximation to treat it as a constant. We also

introduce a size effect coefficient $\beta(i)$ which is defined by

$$\beta(i) = \left(\frac{1}{\eta - 1}\right)\left\{-\left(\frac{x_A}{x_B} + \alpha_i\right)\epsilon^i_{AA} + \left(\frac{x_B}{x_A} + \alpha_i\right)\eta\epsilon^i_{BB}\right\}. \tag{12.57}$$

The diffuse intensity is then expressed in the compact form

$$I_{eu}(\mathrm{D}) = Nx_Ax_B(f_B - f_A)^2 \sum_i \alpha(i)e^{i\mathbf{k}\cdot\mathbf{r}_i} + Nx_Ax_B(f_B - f_A)^2 \sum_i \beta(i)i\mathbf{k}\cdot\mathbf{r}_i e^{i\mathbf{k}\cdot\mathbf{r}_i} \tag{12.58}$$

The first term is the usual short-range order diffuse intensity involving the short-range order coefficients, and the second term is a modulation which involves the size-effect coefficients.

Although it is often possible to see the size effect modulations on powder patterns, it is preferable to use a single crystal if quantitative measurements are desired. For cubic structures such as Cu_3Au or βCuZn, it is convenient to represent the vectors to near neighbors by means of the integers lmn:

$$\mathbf{r}_i = l\mathbf{a}_1/2 + m\mathbf{a}_2/2 + n\mathbf{a}_3/2. \tag{12.59}$$

In terms of the reciprocal vectors and the continuous variables $h_1h_2h_3$, the vector $\mathbf{k}$ is expressed by

$$\mathbf{k} = 2\pi(h_1\mathbf{b}_1 + h_2\mathbf{b}_2 + h_3\mathbf{b}_3).$$

The product $\mathbf{k}\cdot\mathbf{r}_i$ is then given by

$$\mathbf{k}\cdot\mathbf{r}_i = \pi(lh_1 + mh_2 + nh_3).$$

Using this result, the size effect term in Eq. (12.58) is expressed by

$$I_{eu}(\mathrm{SE}) = Nx_Ax_B(f_B - f_A)^2 \sum_{lmn} \beta(lmn)i\pi(lh_1 + mh_2 + nh_3)e^{i\pi(lh_1+mh_2+nh_3)}.$$

In the structures being considered, for every neighbor lmn there is a neighbor $\bar{l}\bar{m}\bar{n}$, and the expression reduces to

$$I_{eu}(\mathrm{SE}) = -Nx_Ax_B(f_B - f_A)^2 \sum_{lmn} \beta(lmn)\pi(lh_1 + mh_2 + nh_3) \times \sin\pi(lh_1 + mh_2 + nh_3). \tag{12.60}$$

As an illustration we now consider the size effect modulation along the line h_100 in reciprocal space for a single crystal of disordered Cu_3Au in which we assume that all size effect coefficients can be neglected except those for nearest neighbors $\beta(1)$. For the 12 nearest neighbors, the lmn values are given by $(\pm1\ \pm1\ 0)$, $(\pm1\ 0\ \pm1)$, and $(0\ \pm1\ \pm1)$; and for only 8 of them does lh_1 differ from zero. Restricted to nearest neighbor effects only, the size effect modulation along h_100 is expressed by

$$I_{eu}(h_100) = -Nx_Ax_B(f_B - f_A)^2 8\beta(1)\pi h_1 \sin\pi h_1. \tag{12.61}$$

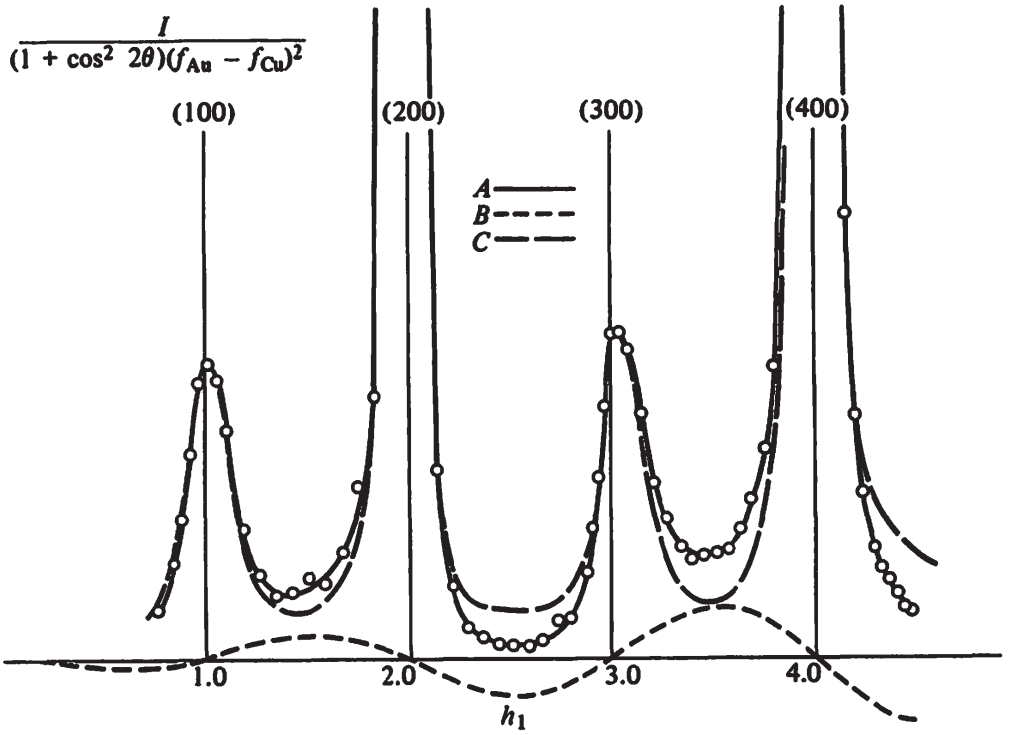

Fig. 12.13 Measurements by Roberts of the intensity along the line h_100 of reciprocal space for a crystal of Cu_3Au quenched from 500°C. (A) The measured intensity. (B) The size effect modulation predicted by Eq. (12.61). (C) Curve *A* minus curve *B*, giving the diffuse intensity if there were no size effect modulation.

Letting *A* represent Cu and *B* represent Au, we can expect ϵ^1_{AA} to be negative and ϵ^1_{BB} to be positive, so that from Eq. (12.57), $\beta(1)$ should be positive. From Eq. (12.61), $I_{eu}(h_100)$ should oscillate sinusoidally with negative maxima at $h_1 = 0.5, 2.5$, and positive maxima at $h_1 = 1.5, 3.5$.

Figure 12.13 shows the measurements by Roberts[19] along the line h_100 for a crystal of Cu_3Au quenched from 500°C. The lower curve shows the size effect modulation which is predicted by Eq. (12.61). It is the addition of this modulating term to the other diffuse intensities which causes the measured diffuse intensity to be high between 100 and 200, low between 200 and 300, and high between 300 and 400. The size effect modulation which is seen in Fig. 12.13 is surprisingly large, and it is the experimental evidence for the fact that there is an effective difference in size of the Cu and Au atoms in the disordered alloy. From the magnitude of the $\beta(1)$ coefficient which is obtained from Fig. 12.13, it can be concluded that the effective difference in size of the Cu and Au atoms in the alloy is something less than half of what it would be if the atoms maintained the same size as in the elemental form.

In addition to the near-neighbor size effect modulation which we have developed here, Huang[20] showed that there is also a general variation in distances between atoms which results from differences in the size of the

atoms. This has the effect of reducing the integrated intensities of the fundamental reflections by a pseudo-temperature factor exp $[-2M']$ and producing a corresponding diffuse intensity. Even when strictly monochromatic radiation is used, the diffuse intensity from a disordered crystal may contain five components:

1) Compton modified scattering,
2) Temperature diffuse scattering,
3) Short-range order diffuse scattering,
4) Size effect modulation,
5) Huang diffuse scattering.

A satisfactory separation of these different components is often very difficult.

12.7 EXPERIMENTAL MEASUREMENTS OF SHORT-RANGE ORDER INTENSITY

The experimental measurement of short-range order intensity follows closely the procedures described in Section 11.7 for the measurement of temperature diffuse scattering. A crystal monochromated primary beam falls upon a single crystal mounted in a goniometer, such as illustrated by Fig. 11.9. The diffuse intensity is recorded with a counter. Measurements are made at enough positions in reciprocal space, so that by symmetry operations one repeating unit is covered. The intensity is standardized in electron units per atom by comparison with the high-angle scattering from an amorphous material such as Lucite, as previously described. Short-range order intensities can also be standardized by the condition that $\alpha(000) = 1$. However, it is probably better to standardize in the usual way, and use this condition as a self consistency check.

Most measurements of short-range order intensity require holding the sample at elevated temperatures. Under these conditions, the temperature diffuse scattering can be rather intense and the correction for TDS becomes the major problem in the measurement. Various methods have been used for making the correction, none of them completely satisfactory. One procedure is to get the crystal in the long-range ordered form at a temperature which is high, but not so high as to reduce the long-range order parameter below, say, $S = 0.95$. Under these conditions there will be Compton modified scattering, a small short-range order intensity about the superstructure points, and temperature diffuse scattering which comes to a peak at both the superstructure and the fundamental points. The Compton modified scattering is readily subtracted. The short-range order and temperature scattering which center on the superstructure points are then eliminated in the vicinity of the superstructure points. The TDS which centers on the

fundamental points is now extrapolated over the repeating volume by using the known variation with distance from the center of a Brillouin zone. From these values, the temperature scattering at the desired temperature is then obtained by assuming proportionality to Te^{-2M}.

A still cruder procedure is to work directly with the measurements at the desired temperature. Having standardized them in absolute units by comparison with the scattering from, say, Lucite, the Compton modified contribution is subtracted. In the vicinity of the fundamental points the intensity is largely TDS, and this is removed. The peak which centers at the superstructure point is the desired short-range order intensity. From its shape in the vicinity of the point, the peak is extrapolated out to a low background in the rest of the repeating volume using the fact that $\alpha(100) = 1$ as a guide in the extrapolation.

The short-range order intensity is proportional to $(f_B - f_A)^2$. It is only when there is sufficient difference in the atomic numbers to make the SRO intensity greater than the temperature scattering, that the corrections can be handled well enough to make possible a determination of the short-range order parameters. Assuming that air scattering and fluorescence radiation have been eliminated in the experiment, there remain the short-range order, the Compton modified, the size effect, and the temperature diffuse scattering intensities. The short-range order intensity decreases while the other three increase as we go out from the origin of reciprocal space. It is only by making the measurements as close as possible to the origin of reciprocal space, that the magnitude of the corrections can be kept small enough, so that the low accuracy in the corrections is not serious.

REFERENCES

1. F. C. Nix and W. Shockley, *Rev. Mod. Phys.* **10** 1, (1938).
2. H. Lipson, *Prog. Metal Phys.* **2**, 1 (1950).
3. L. Guttman, *Solid State Phys.* **3**, 145 (1956).
4. V. Gerold, *Erg. d. Exakten Naturu.* **33**, 105 (1961).
5. A. Guinier, *Theore et Technique de la Radiocrystallographie*, Dunod, Paris (1956).
6. D. R. Chipman, *J. Appl. Phys.* **27**, 739 (1956).
7. D. T. Keating and B. E. Warren, *J. Appl. Phys.* **22**, 286 (1951).
8. J. M. Cowley, *Phys. Rev.* **77**, 667 (1950).
9. D. Chipman and B. E. Warren, *J. Appl. Phys.* **21**, 696 (1950).
10. A. J. C. Wilson, *Proc. Roy. Soc.* **A181**, 360 (1943).
11. J. Mering, *Acta Cryst.* **2**, 371 (1949).

12. A. J. C. WILSON, *X-Ray Optics*, Methuen Co. London (1949), p. 96.
13. I. G. EDMUNDS, R. M. HINDE, and H. LIPSON, *Nature* **160**, 304 (1947).
14. I. G. EDMUNDS and R. M. HINDE, *Proc. Phys. Soc.* **B65**, 716 (1952).
15. C. SYKES and F. W. JONES, *Proc. Roy. Soc.* **A157**, 213 (1936); F. W. JONES and C. SYKES, *Proc. Roy. Soc.* **A166**, 376 (1938).
16. J. M. COWLEY, *J. Appl. Phys.* **21**, 24 (1950).
17. S. C. Moss, *J. Appl. Phys.* **35**, 3547 (1964).
18. C. B. WALKER and D. T. KEATING, *Acta Cryst.* **14**, 1170 (1961).
19. B. E. WARREN, B. L. AVERBACH, and B. W. ROBERTS, *J. Appl. Phys.* **22**, 1493 (1951).
20. K. HUANG, *Proc. Roy. Soc.* **A190**, 102 (1947).
21. B. BORIE, *Acta Cryst.* **10**, 89 (1957); **12**, 280 (1959); **14**, 472 (1961).

PROBLEMS

12.1 In the zinc blende type structure, α positions are at 000, $\frac{1}{2}\frac{1}{2}0$, $\frac{1}{2}0\frac{1}{2}$, $0\frac{1}{2}\frac{1}{2}$, and β positions at $\frac{1}{4}\frac{1}{4}\frac{1}{4}$, $\frac{3}{4}\frac{3}{4}\frac{1}{4}$, $\frac{3}{4}\frac{1}{4}\frac{3}{4}$, $\frac{1}{4}\frac{3}{4}\frac{3}{4}$. Assume a nonstoichiometric composition x_A, x_B and a partial long-range order S.

a) In terms of f_A, f_B, x_A, x_B, and S, deduce expressions for F^2 for $h + k + l =$ odd, $h + k + l = 2(2n + 1)$, $h + k + l = 4n$.

b) If $x_A = 0.60$, $x_B = 0.40$, what is the maximum possible value of S? If $x_A = 0.60$, $x_B = 0.40$, and $S = 0.70$, what fraction of the α-positions are correctly occupied?

12.2 For a powder pattern, the power in electron units per unit length of diffraction line is given by Eq. (4.21):

$$P'(eu) = \frac{R\lambda^3 N_c F^2 m}{8\pi v_a \sin\theta \sin 2\theta},$$

where N_c is the number of unit cells in the sample. For the whole diffraction line the power is $P(eu) = P'(eu)2\pi R \sin 2\theta$. For each line there are m contributing points in the reciprocal lattice, and the power per point is $P(eu)/m$. The total diffracted power in all of the powder lines from the sample is $P_T(eu) = \sum P(eu)/m$, where the summation is over all the effective reciprocal lattice points. If K is the fraction of reciprocal lattice points which reflect, K/v_b is the density of effective points in reciprocal space. The summation can be approximated by an integral in reciprocal space involving the point density.

a) For the powder pattern of a simple substance with only one expression for F. show that the total diffracted power in the powder lines can be approximated by

$$P_T(eu) = 2\pi R^2 N_c K \int_0^{\pi} F^2 \sin 2\theta \, d(2\theta).$$

b) A powder sample contains N atoms: $N/4$ Au and $3N/4$ Cu. Consider the sample in three different states.

A. Mechanical mixture of crystals of Au and crystals of Cu. (Lines with *hkl* unmixed)

B. Alloy Cu_3Au in perfect long-range order. (Fundamental and superstructure lines)

C. Alloy Cu_3Au in complete disorder. (Fundamental lines and the Laue diffuse scattering)

Demonstrate the approximate conservation of total diffracted power for a powder pattern by showing that the total power in all directions is approximately the same for cases *A*, *B*, and *C*.

12.3 Make the approximation that the same value of $2M$ can be used for both atoms in a binary cubic crystal. If the diffracted power is measured for a superstructure reflection and a fundamental reflection at two temperatures T_1 and T_2, show that the long-range order at T_2 is given in terms of that at T_1 by

$$S_2 = S_1\left[\left(\frac{P_2}{P_1}\right)_{SS}\left(\frac{P_1}{P_2}\right)_F^{\gamma}\right]^{1/2},$$

where

$$\gamma = (h^2 + k^2 + l^2)_{SS}/(h^2 + k^2 + l^2)_F.$$

12.4 In a ternary solid solution there are N atoms: $N_A = x_A N$, $N_B = x_B N$, $N_C = x_C N$. Suppose that the atoms are distributed completely at random on a FCC lattice. Deduce an expression for the diffuse intensity in electron units.

12.5 A sample of copper contains N atoms. Suppose that one tenth of the atoms are picked out at random and thrown away without disturbing the remaining atoms. We now have $0.9N$ atoms of copper and $0.1N$ vacancies.

a) Give an expression for the diffuse intensity in electron units.

b) What fraction of the original total diffracted power is now represented by the powder pattern lines? What fraction of the original total diffracted power is represented by the diffuse intensity? See Problem 12.2(a).

c) For copper at $\sin\theta/\lambda = 0.10$, $f(\text{Cu}) = 27.2$ and $i(\text{M}) = 2.0$. What is the ratio of the vacancy diffuse scattering to the Compton modified scattering at $\theta/\lambda = 0.05$?

12.6 A tetragonal crystal containing N unit cells has axes $a_1 = a_2 = 2A$, $a_3 = 3A$, and contains one AB molecule per unit cell. Normally the atoms are at the positions: A, 00ϵ; B, $00\bar{\epsilon}$; where ϵ is a fractional coordinate $\epsilon = z/a_3 = \frac{1}{6}$. Suppose the crystal is in a disordered form, so that completely at random the molecules may be reversed; B at 00ϵ and A at $00\bar{\epsilon}$. There will be a diffuse intensity $I_D(eu)$, let

$$I' = I_D(eu)/N(f_A - f_B)^2.$$

a) Deduce an expression for I' in terms of $h_1h_2h_3$.

b) Give an expression for I' in terms of $(\sin\theta)/\lambda$ for a powder pattern; the sample contains M crystals with competely random orientation.

c) At approximately what value of $(\sin\theta)/\lambda$ will the first peak in the powder pattern diffuse intensity occur?

12.7 For a single crystal of disordered Cu_3Au, measurements of the corrected diffuse intensity due to short-range order

$$I'(h_1h_2h_3) = I(eu)/Nx_Ax_B(f_B - f_A)^2$$

are made in the h_1h_20 plane of reciprocal space, so that values of $I'(h_1h_20)$ are available in the range $h_1 = 0 - 2$ and $h_2 = 0 - 2$.

a) From a Fourier analysis using these measurements, what information can be obtained concerning the short-range order coefficients $\alpha(lmn)$?

b) Can the coefficients for the first few neighbor types be obtained by assuming $\alpha(lmn) = 0$ beyond sixth neighbors?

12.8 Consider a beta brass type alloy $AB(x_A = x_B = 0.5)$, atoms at 000, $\frac{1}{2}\frac{1}{2}\frac{1}{2}$, with short-range order only. There are similar short-range order peaks at each of the superstructure positions. Assume that the reduced intensity at each position has spherical symmetry, $I = A\exp[-a^2(p_1^2 + p_2^2 + p_3^2)]$ and that it approaches zero so rapidly that integrals can be taken between plus and minus infinity. To cover one repeating volume, it is sufficient to include everything belonging to the peaks at $h_1h_2h_3 = 100, 010, 001$, and 111:

$$\alpha(lmn) = \frac{A}{8}\int_{-\infty}^{+\infty}\iiint\{e^{-a^2[(h_1-1)^2+h_2^2+h_3^2]} + e^{a^2[h_1^2+(h_2-1)^2+h_3^2]}$$

$$+ e^{-a^2[h_1^2+h_2^2+(h_3-1)^2]} + e^{-a^2[(h_1-1)^2+(h_2-1)^2+(h_3-1)^2]}\}$$

$$\times \cos \pi l h_1 \cos \pi m h_2 \cos \pi n h_3\, dh_1\, dh_2\, dh_3.$$

Let $a^2 = 3\pi^2/4 \ln 4$, $A = 2(a/\sqrt{\pi})^3$.

a) Verify that $\alpha(000) = 1$.

b) Obtain the short-range order parameters α_1 and α_2 for nearest and next nearest neghbors.

12.9 Consider a beta brass type alloy AB with $x_A = 0.60$, $x_B = 0.40$. Assume that the α-positions are all occupied by A atoms and the β-positions are occupied at random by the B atoms and excess A atoms. There will be superstructure reflections and also a diffuse intensity. Obtain an expression for the diffuse intensity in terms of N, x_A, x_B, f_A, f_B. (As a check, this must vanish for $x_A = x_B$.)

12.10 Figure 12.13 gives the reduced short-range order intensity $I'(h_100)$ in arbitrary units for Cu_3Au. Including contributions up to 5th neighbors, show that for the the peak at $h_1 = 3$,

$$\int_{2.5}^{3.5} I'(h_100)\, dh_1 = 1 + 4\alpha_1 + 4\alpha_2 + 4\alpha_4 + 8\alpha_5$$

$$- \frac{2}{\pi}(8\alpha_1 + 16\alpha_3 + 8\alpha_5) + \frac{2}{3\pi} \times 8\alpha_5.$$

From the measured area of this peak, the Cowley coefficients for 405°C, and the amplitude of the size effect curve at $h = 3.5$, determine an approximate value for β_1, the nearest-neighbor size effect coefficient.

12.11 Consider a crystal of Cu_3Au having short-range order. There are short-range order diffuse peaks at each of the superstructure positions. To allow for the peaks being disk-shaped, represent the reduced intensity at, say, the 110 peak by

$$I = Ae^{-[a^2(h_1-1)^2+a^2(h_2-1)^2+b^2h_3^2]}.$$

Assume the intensity approaches zero so rapidly that integrations can be carried out between plus and minus infinity. To cover one repeating volume, it is sufficient to include everything belonging to peaks at 100, 010, 001, 110, 101, and 011. The intensity at each position is given by the above expression with suitable orientation of the axes.

a) Deduce an expression for $\alpha(lmn)$ in terms of l, m, n, A, a, b. Eliminate A by the condition $\alpha(000) = 1$.

b) Determine the values of a and b from Cowley's measured $\alpha_1 = -0.152$, $\alpha_2 = +0.186$.

c) If $u(a)$ and $u(b)$ are the distances from the center of a peak to the point where I has fallen to half its maximum value, what is the ratio $u(a)/u(b)$? Are the short-range order peaks disk-shaped or egg-shaped?

12.12 A binary solid solution AB with composition x_A and x_B crystallizes in a diamond structure with partial short-range order. Set up the equations for the reduced short-range order diffuse intensity $I'_{eu}(h_1h_2h_3)$ for a single crystal. Set up the equations for determining α_1 from the measured intensity.

12.13 A binary solid solution AB with composition x_A and x_B crystallizes in the hexagonal close-packed structure (2 atoms per cell) with partial short-range order. Set up the equations for the reduced short-range order diffuse intensity $I'_{eu}(h_1h_2h_3)$ for a single crystal. Set up the equations for determining α_1 from the measured intensity.

13

DIFFRACTION BY IMPERFECT CRYSTALS

13.1 PARTICLE SIZE BROADENING

In this chapter we shall consider the effect on the diffraction pattern of various crystal imperfections such as small crystallite size, strains, and faulting. Since it is the simplest kind of imperfection, we start with the consideration of the effect of small crystallite size. From Eq. (3.6), the intensity from a single small parallelopipedon crystal is given by

$$I = I_e F^2 \frac{\sin^2(\pi/\lambda)(\mathbf{s} - \mathbf{s}_0) \cdot N_1\mathbf{a}_1}{\sin^2(\pi/\lambda)(\mathbf{s} - \mathbf{s}_0) \cdot \mathbf{a}_1} \frac{\sin^2(\pi/\lambda)(\mathbf{s} - \mathbf{s}_0) \cdot N_2\mathbf{a}_2}{\sin^2(\pi/\lambda)(\mathbf{s} - \mathbf{s}_0) \cdot \mathbf{a}_2} \times \frac{\sin^2(\pi/\lambda)(\mathbf{s} - \mathbf{s}_0) \cdot N_3\mathbf{a}_3}{\sin^2(\pi/\lambda)(\mathbf{s} - \mathbf{s}_0) \cdot \mathbf{a}_3}, \quad (13.1)$$

where N_1, N_2, N_3 are the numbers of unit cells along the $\mathbf{a}_1$, $\mathbf{a}_2$, $\mathbf{a}_3$ directions. In general the N_1, N_2, N_3 are such large numbers, that each of the three quotients differs from zero only if the three Laue equations are closely satisfied, and hence the powder pattern reflections are sharp. For very small crystals where N_1, N_2, N_3 are small, the three quotients broaden, and the smaller the crystals the broader the powder pattern reflections. The peak breadth can be expressed in terms of the crystallite size, and hence a measurement of the peak breadth gives a simple method for determining crystallite sizes in the size range up to about 1000 A.

a) The Scherrer Equation

The first treatment of particle size broadening was due to Scherrer.[1] Although the derivation is of restricted generality, the Scherrer equation has had considerable application, and it is of interest to reproduce the derivation. We assume a powder sample of small cubic crystals, all of the same size with $N_1 = N_2 = N_3 = N$. The crystals are assumed to be free from strains and faulting, so that the peak broadening is due only to the small crystallite size. For convenience we now replace the powder sample by a single crystal which takes all orientations. Let the unit vectors s and $\mathbf{s}_0$ represent the exact Bragg law directions for the reflection *hkl*, so that

$$\mathbf{s} - \mathbf{s}_0 = \lambda(h\mathbf{b}_1 + k\mathbf{b}_2 + l\mathbf{b}_3).$$

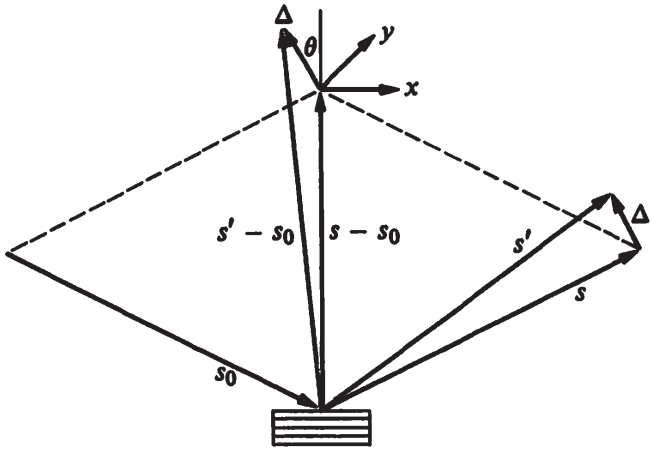

Fig. 13.1 Geometrical relations involved in the derivation of the Scherrer equation.

We now consider slightly different directions $\mathbf{s}'$ and $\mathbf{s}_0'$ for the diffracted and primary beams, and relate them to $\mathbf{s} - \mathbf{s}_0$ by the small difference vector $\Delta\mathbf{s}$.

$$\mathbf{s}' - \mathbf{s}_0' = \mathbf{s} - \mathbf{s}_0 + \Delta\mathbf{s}. \tag{13.2}$$

Expressing Eq. (13.1) in terms of the general directions $(\mathbf{s}' - \mathbf{s}_0')$, we obtain

$$I = I_e F^2 \frac{\sin^2(\pi/\lambda)\,\Delta\mathbf{s}\cdot N_1\mathbf{a}_1}{\sin^2(\pi/\lambda)\,\Delta\mathbf{s}\cdot\mathbf{a}_1} \frac{\sin^2(\pi/\lambda)\,\Delta\mathbf{s}\cdot N_2\mathbf{a}_2}{\sin^2(\pi/\lambda)\,\Delta\mathbf{s}\cdot\mathbf{a}_2} \frac{\sin^2(\pi/\lambda)\,\Delta\mathbf{s}\cdot N_3\mathbf{a}_3}{\sin^2(\pi/\lambda)\,\Delta\mathbf{s}\cdot\mathbf{a}_3}.$$

We now approximate each of the three quotients by a Gaussian function which has the same maximum ordinate and the same area:

$$\frac{\sin^2 Nx}{\sin^2 x} \to N^2 e^{-(Nx)^2/\pi}.$$

With this approximation, the intensity expression becomes

$$I = I_e F^2 N^6 e^{-(\pi/\lambda^2)N^2\{(\Delta\mathbf{s}\cdot\mathbf{a}_1)^2+(\Delta\mathbf{s}\cdot\mathbf{a}_2)^2+(\Delta\mathbf{s}\cdot\mathbf{a}_3)^2\}}.$$

Since the axes $\mathbf{a}_1$, $\mathbf{a}_2$, $\mathbf{a}_3$ are equal and orthogonal, the expression reduces to

$$I = I_e F^2 N^6 e^{-(\pi/\lambda^2)(Na)^2(\Delta s)^2}.$$

The exact Bragg law directions $\mathbf{s}$ and $\mathbf{s}_0$ are shown by Fig. 13.1. We are interested in the intensity for a direction $\mathbf{s}' = s + \Delta$ which makes a fixed angle with the Bragg law direction $\mathbf{s}$. Maintaining $\mathbf{s}'$ at a fixed angle from $\mathbf{s}$, we now wish to find the total contribution to the intensity when the crystal is rocked through the whole region where there is any contribution. Instead of rocking the crystal, it is simpler to hold the crystal fixed and rock the $\mathbf{s}' - \mathbf{s}_0$ vector by adding the small vectors $\mathbf{x}$ and $\mathbf{y}$ which are in a plane normal to $\mathbf{s} - \mathbf{s}_0$. The difference vector $\Delta\mathbf{s}$ which was introduced in Eq. (13.2), becomes $\Delta\mathbf{s} = \mathbf{x} + \mathbf{y} + \Delta$, and the magnitude squared is given by

$$(\Delta s)^2 = (x - \Delta\sin\theta)^2 + y^2 + (\Delta\cos\theta)^2.$$

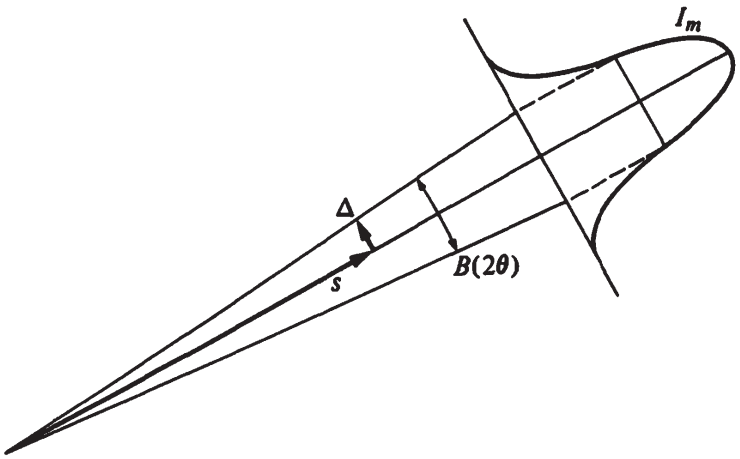

Fig. 13.2 The breadth $B(2\theta)$ representing the angle in radians on a 2θ scale which subtends the half maximum intensity breadth of a powder pattern peak.

The intensity $I(\Delta)$ at a fixed departure Δ is proportional to the sum over all values of x and y, and since the contribution differs from zero only for small values of x and y, the integrals can be carried out from $-\infty$ to $+\infty$:

$$I(\Delta) = KI_eF^2N^6e^{-\pi(Na/\lambda)^2\Delta^2\cos^2\theta}\int_{-\infty}^{+\infty} e^{-\pi(Na/\lambda)^2(x-\Delta\sin\theta)^2}dx\int_{-\infty}^{+\infty} e^{-\pi(Na/\lambda)^2y^2}dy.$$

By making the replacement $x' = x - \Delta\sin\theta$, $dx' = dx$, the two integrals are independent of Δ, and the values of the integrals can be combined in the new constant K':

$$I(\Delta) = K'e^{-\pi(Na/\lambda)^2\Delta^2\cos^2\theta}.$$

When $\Delta = 0$ we are at the center of the peak and $I(\Delta) = I_m$, where I_m is the peak maximum:

$$I(\Delta) = I_me^{-\pi(Na/\lambda)^2\Delta^2\cos^2\theta}.$$

Referring to Fig. 13.2, when $I(\Delta) = I_m/2$, the angle defined by Δ is half the angle $B(2\theta)$ which subtends the half maximum intensity width of the peak

$$\tfrac{1}{2} = e^{-\pi(Na/\lambda)^2(B/2)^2\cos^2\theta}.$$

The value of $B(2\theta)$ is then given by

$$B(2\theta) = \frac{2[(\ln 2)/\pi]^{1/2}\lambda}{Na\cos\theta}.$$

Letting $L = Na$ represent the cube edge dimension of the crystals, we obtain the Scherrer equation

$$B(2\theta) = \frac{0.94\lambda}{L\cos\theta}. \tag{13.3}$$

In the Scherrer equation, $B(2\theta)$ is the full width in radians subtended by the half maximum intensity width of the powder pattern peak. In making the Gaussian approximation if we had matched the peak maxima and the half

maximum peak widths, the numerical constant would have been 0.89 instead of 0.94. The constant in the Scherrer equation is close to unity, but the exact numerical value has little significance. Although the Scherrer equation was derived for a sample of cubic crystals, it is often applied to the peak breadths of noncubic materials. It is not a bad approximation, if for each *hkl*-reflection the value of L is interpreted as an average crystal dimension perpendicular to the reflecting planes.

For a given crystal dimension L, the peak breadth increases as $1/\cos\theta$, and hence particle-size broadening becomes most pronounced at large values of θ. As an order of magnitude example, suppose $\lambda = 1.54$ A, $L = 200$ A, and $2\theta = 160°$. The peak breadth due to small particle size is then $B(2\theta) = 0.042$ radians $= 2.4°$. In general there is an additional instrumental broadening arising from effects such as slit widths, wavelength widths of the $K\alpha_1$ and $K\alpha_2$ lines, or the superposition of the peaks due to $K\alpha_1$ and $K\alpha_2$ when the peaks are not resolved. The correction for instrumental broadening is very important, and methods for making the correction will be discussed later.

b) The Method of Stokes and Wilson

A more general treatment of the particle size broadening problem has been given by Stokes and Wilson.[2] Since it illustrates several interesting and useful variations in the treatment of diffraction problems, we will now consider this method. In Chapter 4, where we evaluated the integrated intensity of a reflection, we first summed over all the unit cells of the crystal to obtain an intensity and then carried out an integration of the intensity in reciprocal space. It is sometimes of considerable advantage to reverse the order, carrying out first the integration in reciprocal space, and then later carrying out the summation in crystal space. We have already used this method in Section 12.3(c), where we considered the effect of antiphasing on powder pattern integral breadths, and we now apply it to the problem of particle size broadening.

For simplicity, we consider a 00*l*-reflection for an orthorhombic crystal. The result is independent of this simplifying assumption, and we use it only because the mathematics is considerably simplified. The position of the unit cell $n_1n_2n_3$ is given by $\mathbf{R}_n = n_1\mathbf{a}_1 + n_2\mathbf{a}_2 + n_3\mathbf{a}_3$. Expressing the diffraction vector by $(\mathbf{s} - \mathbf{s}_0)/\lambda = h_1\mathbf{b}_1 + h_2\mathbf{b}_2 + h_3\mathbf{b}_3$, where h_1, h_2, h_3 are continuous variables, the intensity from one crystal is expressed by

$$I(h_1h_2h_3) = I_eF^2 \sum_n \sum_{n'} e^{2\pi i\{(n_1'-n_1)h_1+(n_2'-n_2)h_2+(n_3'-n_3)h_3\}}. \qquad (13.4)$$

As shown in Chapter 4, the integrated intensity of a reflection is proportional to an integral of $I(h_1h_2h_3)$ in reciprocal space. It is also given by an integral of $P(2\theta)$, where $P(2\theta)$ is the distribution with respect to 2θ of the power in a

powder pattern peak:

$$P = \int P(2\theta)\, d(2\theta) = K \iiint I(h_1h_2h_3)\, dh_1\, dh_2\, dh_3. \tag{13.5}$$

For a 00*l*-reflection, the intensity is nonvanishing only for very small values of h_1 and h_2, and hence we can make the approximation

$$\left|\frac{\mathbf{s} - \mathbf{s}_0}{\lambda}\right| = \frac{2 \sin\theta}{\lambda} = |h_1\mathbf{b}_1 + h_2\mathbf{b}_2 + h_3\mathbf{b}_3| \to h_3\,|\mathbf{b}_3|.$$

From the approximate relation $2 \sin\theta/\lambda = |\mathbf{b}_3|\, h_3$, we obtain $d(2\theta) = (\lambda\,|\mathbf{b}_3|/\cos\theta)\, dh_3$. Using this expression for $d(2\theta)$ in Eq. (13.5), we can drop the integration with respect to dh_3 on both sides of the equation, and obtain the powder pattern profile:

$$P(2\theta) = \frac{K \cos\theta}{\lambda\,|\mathbf{b}_3|} \int\int I(h_1h_2h_3)\, dh_1\, dh_2.$$

We now introduce the expression for $I(h_1h_2h_3)$ from Eq. (13.4), and carry out the two integrations from $-\frac{1}{2}$ to $+\frac{1}{2}$ to include everything belonging to the 00*l*-reflection:

$$P(2\theta) = \frac{KI_eF^2 \cos\theta}{\lambda\,|\mathbf{b}_3|} \sum_{n_1'n_2'n_3'} \sum_{n_1n_2n_3} \frac{\sin\pi(n_1' - n_1)}{\pi(n_1' - n_1)} \frac{\sin\pi(n_2' - n_2)}{\pi(n_2' - n_2)}\, e^{2\pi i(n_3' - n_3)h_3}.$$

Since quotients of the form $\sin\pi(n_1' - n_1)/\pi(n_1' - n_1)$ are equal to unity for $n_1' = n_1$ but otherwise are zero, all terms in $P(2\theta)$ are zero except those with $n_1' = n_1$ and $n_2' = n_2$:

$$P(2\theta) = \frac{KI_eF^2 \cos\theta}{\lambda\,|\mathbf{b}_3|} \sum_{n_1} \sum_{n_2} \sum_{n_3} \sum_{n_3'} e^{2\pi i(n_3' - n_3)h_3}.$$

Letting $N_3(n_1n_2)$ represent the number of cells in the row (n_1n_2), the sum over n_3 and n_3' can be expressed as

$$\sum_{0}^{N_3-1} e^{2\pi i n_3' h_3} \sum_{0}^{N_3-1} e^{-2\pi i n_3 h_3} = \frac{\sin^2 \pi N_3 h_3}{\sin^2 \pi h_3}.$$

At the peak maximum where $h_3 = l$, the quotient takes a maximum value $N_3^2(n_1n_2)$. The maximum in the peak profile $P_m(2\theta)$ is then given by

$$P_m(2\theta) = \frac{KI_eF^2 \cos\theta}{\lambda\,|\mathbf{b}_3|} \sum_{n_1} \sum_{n_2} N_3^2(n_1n_2). \tag{13.6}$$

If in Eq. (13.5) we carry out the integrations for dh_1, dh_2 from $-\frac{1}{2}$ to $+\frac{1}{2}$ and for dh_3 from $l - \frac{1}{2}$ to $l + \frac{1}{2}$, we obtain the total power or peak area

$$\int P(2\theta)\, d(2\theta) = KI_eF^2N, \tag{13.7}$$

where N is the total number of cells in a crystal.

The integral breadth of a reflection is defined as the ratio of the peak area to the peak maximum. In general, integral breadths are not favored by the experimenter, since they involve the difficulty of evaluating the area in the tails of the reflection. However, it often happens that it is possible to derive a general expression for an integral breadth when this is not possible for the more useful half maximum intensity breadth. The present derivation is such a case, and we now express the integral breadth $\beta(2\theta)$ by means of Eqs. (13.6) and (13.7):

$$\beta(2\theta) = \frac{\int P(2\theta)\, d(2\theta)}{P_m(2\theta)} = \frac{\lambda N}{a_3 \cos\theta \sum_{n_1} \sum_{n_2} N_3^2(n_1 n_2)}.$$

Let $T(n_1 n_2) = a_3 N_3(n_1 n_2)$ be the crystal dimension in the a_3-direction for the column of cells $n_1 n_2$. The double sum can be replaced by an integral in crystal space in terms of the orthogonal axes x, y, z:

$$\sum_{n_1} \sum_{n_2} N_3^2(n_1 n_2) = \iint \frac{T^2(x, y)}{a_3^2} \frac{dx\, dy}{a_1 a_2}.$$

If V is the volume of the crystal, then $N = V/a_1 a_2 a_3$, and the integral breadth can be expressed by

$$\beta(2\theta) = \frac{\lambda V}{\cos\theta \iint T^2(xy)\, dx\, dy}.$$

Since $T = \int dz$, the integral breadth reduces to the simple form

$$\beta(2\theta) = \frac{\lambda V}{\cos\theta \int T\, dV} = \frac{\lambda}{L \cos\theta} \tag{13.8}$$

The effective particle dimension L is a volume average of the crystal dimension in the a_3-direction and hence normal to the reflecting planes

$$L = \frac{1}{V} \int T\, dV. \tag{13.9}$$

If A is the projected cross-sectional area of the crystal parallel to the reflecting planes, then

$$V = A\langle T \rangle, \qquad \iint T^2\, dx\, dy = A\langle T^2 \rangle,$$

and the effective dimension L can also be expressed by the ratio

$$L = \langle T^2 \rangle / \langle T \rangle. \tag{13.10}$$

The results expressed by Eqs. (13.8), (13.9), and (13.10) are quite general and independent of the initial assumption of a 00l-reflection. They are also independent of the distribution in size and shape of the crystals making up

the powder sample. The effective dimension L which is obtained is a volume average, over the whole sample, of the crystal dimension normal to the reflecting planes.

13.2 CORRECTIONS FOR INSTRUMENTAL BROADENING

In addition to the broadening due to small particle size, there is always extraneous broadening due to causes such as slit widths, sample size, penetration in the sample, imperfect focusing, unresolved α_1 and α_2 peaks, or the wavelength widths of α_1 and α_2 in cases where the peaks are resolved. All of these extraneous sources of broadening are grouped together under the name "instrumental broadening." To correct for the instrumental broadening in the pattern of the sample, it is convenient to run a standard peak using a powder sample in which the particle size is large enough to eliminate all particle-size broadening. The standard peak is run under instrumental conditions which are identical to those of the sample, so that the broadening of the standard is exactly the instrumental broadening in the pattern of the sample.

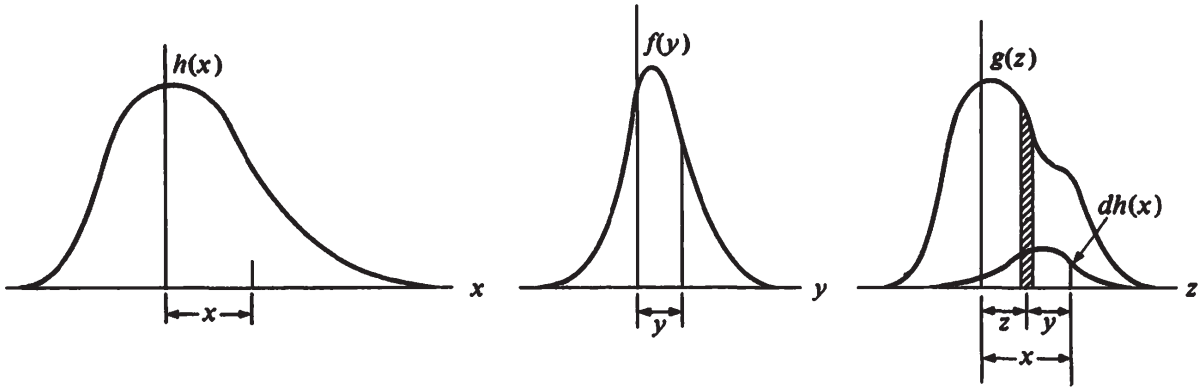

Fig. 13.3 The three curves which are involved in the correction for instrumental broadening. $f(y)$ is the desired curve which would be obtained if there were no instrumental broadening. $g(z)$ is the curve representing instrumental broadening which is obtained from the standard. $h(x)$ is the curve from the sample, containing both the desired broadening and the instrumental broadening.

The principle of the correction can be discussed in terms of the three curves of Fig. 13.3. The curve $f(y)$ represents the broadening due to particle size only; this is the function which we wish to obtain. If there were no particle-size broadening, $f(y)$ would be sharply concentrated at $y = 0$. The curve is drawn asymmetric to allow for the fact that there may be a peak displacement accompanying the small particle size. The curve $g(z)$ represents the effect of instrumental broadening only; this is the peak obtained from the standard. The curve $h(x)$ is the diffraction peak from the sample, and it contains both the particle-size and the instrumental broadening. The peaks

$g(z)$ and $h(x)$ are both experimentally observable curves, such as the diffractometer tracings from the standard and the sample. The origins for $g(z)$ and $h(x)$ are chosen for convenience, but at the same value of 2θ.

The relation between the three curves is obtained by considering the cross-hatched area $g(z)\,dz$ on the curve for instrumental broadening only. If in addition there is particle-size broadening, the area $g(z)\,dz$ is spread out by the function $f(y)$, and at a displacement y the ordinate is the contribution $dh(x)$ at the position $x = z + y$ on the $h(x)$-curve. Since the ordinates in the two curves are proportional to the peak areas,

$$\frac{dh(x)}{f(y)} = \frac{g(z)\,dz}{A},$$

where A is the area of the $f(y)$-curve. With the replacement $y = x - z$, the ordinate of the $h(x)$ curve is given by

$$h(x) = \frac{1}{A}\int g(z)f(x - z)\,dz. \tag{13.11}$$

Equation (13.11) indicates that the profile for the sample is a convolution of the functions representing particle-size broadening and instrumental broadening. We measure the curves $h(x)$ and $g(z)$, and wish to obtain the particle-size broadening curve $f(y)$. This is not convenient, since $f(y)$ is buried inside of the convolution integral. By assuming shapes for the three curves, it is possible to use Eq. (13.11) to obtain relations between the half maximum breadths of the curves:

Gaussian shape:	$u = U\exp[-a^2v^2]$,	$B^2(h) = B^2(g) + B^2(f)$,
Cauchy shape:	$u = U/(1 + a^2v^2)$,	$B(h) = B(g) + B(f)$.

However, the curves are never pure Gaussian or pure Cauchy, and they vary from sample to sample, so that it is very unsafe to make any use of relations involving assumed shapes for the curves.

a) The Stokes Correction

A rigorous method for solving Eq. (13.11) to obtain $f(y)$ from the measured $h(x)$ and $g(z)$ was presented by Stokes.[3] The three functions $f(y)$, $g(z)$, and $h(x)$ are expressed as Fourier series in an interval $-a/2$ to $+a/2$. Since $h(x)$ is the broadest of the three curves, the interval is chosen large enough to include everything in the $h(x)$-curve. Using the complex form which was introduced in Eq. (9.4),

$$f(y) = \sum_n F(n)e^{-2\pi i n y/a}, \tag{13.12a}$$

$$g(z) = \sum_{n'} G(n')e^{-2\pi i n' z/a}, \tag{13.12b}$$

$$h(x) = \sum_{n''} H(n'')e^{-2\pi i n'' x/a}. \tag{13.12c}$$

Introducing these expressions in Eq. (13.11),

$$h(x) = \frac{1}{A}\int \sum_{n'} G(n')e^{-2\pi i n'z/a} \sum_{n} F(n)e^{-2\pi i n(x-z)/a}\, dz.$$

The integral can be confined to the limits $-a/2$ to $+a/2$ because $g(z)$ is nonvanishing only in this interval. Combining the terms involving z, we express $h(x)$ in the form

$$h(x) = \frac{1}{A}\sum_{n'}\sum_{n} G(n')F(n)e^{-2\pi i n x/a}\int_{-a/2}^{+a/2} e^{-2\pi i(n'-n)z/a}\, dz.$$

Since

$$\int_{-a/2}^{+a/2} e^{-2\pi i(n'-n)z/a}\, dz = \begin{cases} a, & n' = n, \\ 0, & n' \neq n, \end{cases}$$

the expression reduces to

$$h(x) = \frac{a}{A}\sum_{n} G(n)F(n)e^{-2\pi i n x/a}.$$

Comparing with Eq. (13.12c), and equating coefficients, we obtain

$$\frac{a}{A}G(n)F(n) = H(n).$$

In general, we are interested only in the shapes of the curves, and the multiplicative factor a/A can be dropped. The Fourier coefficient of the $f(y)$-curve is then given by the simple relation

$$F(n) = H(n)/G(n). \tag{13.13}$$

By means of Eq. (13.13), we have an exact and completely general solution of Eq. (13.11). From the experimental curves $h(x)$ and $g(z)$, we obtain the Fourier coefficients $H(n)$ and $G(n)$. The quotient gives the Fourier coefficients $F(n)$, and from these the particle-size broadening function $f(y)$ is readily synthesized. Although we have carried through the derivation, Eq. (13.13) expresses a well-known mathematical theorem which states that if a function such as $h(x)$ is given by the convolution of two functions $g(z)$ and $f(y)$, then the Fourier transform of $h(x)$ is equal to the product of the Fourier transforms of $g(z)$ and $f(y)$.

In general Eq. (13.13) is not as simple as it appears, because all three coefficients may be complex involving real and imaginary parts:

$$F_r(n) + iF_i(n) = \frac{H_r(n) + iH_i(n)}{G_r(n) + iG_i(n)}.$$

Multiplying the right-hand side above and below by $G_r(n) - iG_i(n)$, and then equating the real and imaginary parts on either side of the equation, we

obtain

$$F_r(n) = \frac{H_r(n)G_r(n) + H_i(n)G_i(n)}{G_r^2(n) + G_i^2(n)},$$
$$F_i(n) = \frac{H_i(n)G_r(n) - H_r(n)G_i(n)}{G_r^2(n) + G_i^2(n)}. \tag{13.14}$$

From the two experimental curves $h(x)$ and $g(z)$ it is necessary to determine both the cosine and the sine coefficients. These are then combined as indicated by Eq. (13.14) to give the coefficients $F_r(n)$ and $F_i(n)$ from which the broadening function $f(y)$ is synthesized:

$$f(y) = \sum_n \{F_r(n) \cos 2\pi ny/a + F_i(n) \sin 2\pi ny/a\}.$$

This is the Stokes method for the correction for instrumental broadening. Although it is completely general and rigorous, the amount of work involved would be prohibitive for routine application if it were not for the fact that all of the operations can be programmed for computer calculation.

b) The Rachinger Correction

It is evident that the work involved in the Stokes correction would be greatly reduced if the three functions were symmetrical. In many cases the peak asymmetry is largely due to the unresolved $\alpha_1\alpha_2$ peaks, so that by correcting $h(x)$ and $g(z)$ for the contribution by α_2 to obtain that part of $h(x)$ and $g(z)$ due to α_1 alone, essentially symmetrical peaks will be obtained. A simple method for doing this was introduced into diffraction calculations by Rachinger,[4] and the procedure is usually called the Rachinger correction. Essentially the same procedure had been proposed earlier by DuMond,[5] but for a different purpose, and hence it had remained unknown in the x-ray diffraction field.

The Rachinger correction assumes that the intensity of α_2 is one half that of α_1, so that for a diffraction peak the contribution by α_2 has the same shape as that by α_1, except that it is of half the height and shifted toward large angles by $\Delta(2\theta) = 2 \tan\theta\, \Delta\lambda/\lambda$, where $\Delta\lambda = \lambda(\alpha_2) - \lambda(\alpha_1)$. The principle of the Rachinger correction is illustrated by Fig. 13.4. The figure on the left represents the contributions by α_1 and α_2 alone, the curves are identical except that α_2 is half the height of α_1, and it is displaced on the recording by an amount Δ which corresponds to the wavelength difference. The figure on the right shows the two curves superposed as they are in the experimental recording. Starting on the left-hand side (small-angle side) at a position where the intensity can be considered to be zero, we lay off intervals with separation Δ/m. The integer m can be 1 or 2 or 3, the choice being determined by the need to have an adequate number of points on the experimental curve. The intervals on Fig. 13.4 correspond to $m = 2$. If I_i

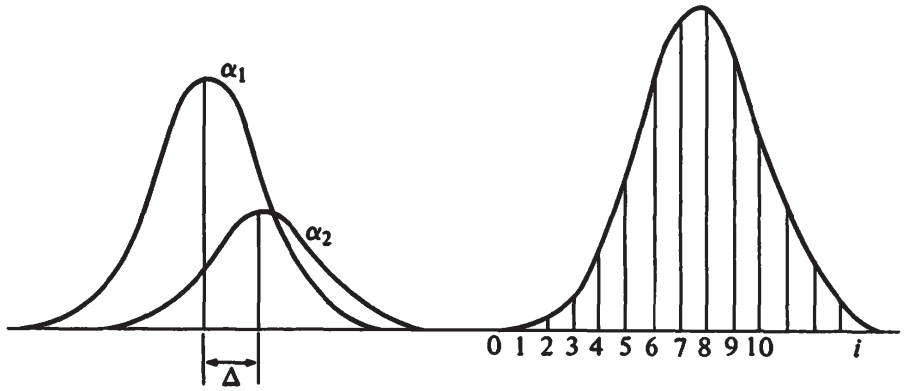

Fig. 13.4 Curves illustrating the principle of the Rachinger correction. On the left, the contributions by α_1 and α_2 are shown separately. On the right, they are combined as in an experimental recording.

is the ordinate at position i and $I_i(\alpha_1)$ is the part due to α_1 alone, it follows that

$$I_i(\alpha_1) = I_i - \tfrac{1}{2}I_{i-m}(\alpha_1).$$

For the two cases $m = 1$ and $m = 2$, the ordinates due to α_1 alone are given by the following set of equations:

$m = 1$	$m = 2$
$I_0(\alpha_1) = 0$	$I_0(\alpha_1) = 0$
$I_1(\alpha_1) = I_1$	$I_1(\alpha_1) = I_1$
$I_2(\alpha_1) = I_2 - \tfrac{1}{2}I_1(\alpha_1)$	$I_2(\alpha_1) = I_2$
$I_3(\alpha_1) = I_3 - \tfrac{1}{2}I_2(\alpha_1)$	$I_3(\alpha_1) = I_3 - \tfrac{1}{2}I_1(\alpha_1)$
$I_4(\alpha_1) = I_4 - \tfrac{1}{2}I_3(\alpha_1)$	$I_4(\alpha_1) = I_4 - \tfrac{1}{2}I_2(\alpha_1)$

Starting at the left-hand end of the curve, the values of $I_i(\alpha_1)$ are readily evaluated. The accuracy is satisfactory from the left-hand end to about half way down on the right-hand side. For the lower half of the right-hand side, a small difference between nearly equal quantities is involved, so that the accuracy is low, and it may be necessary to smooth out the fluctuations in the calculated values.

The Rachinger correction is very easy to apply, and if it results in symmetrical curves, the resulting simplification in the Stokes correction makes it well worthwhile. Since the diffraction conditions should always be carefully arranged to keep the instrumental broadening as small as possible, the standard curve $g(z)$ will often have α_1 and α_2 nearly enough resolved to separate the α_1 peak by inspection. If symmetrical peaks are obtained for $g(z)$ and $h(x)$ as a result of the Rachinger correction, we choose origins at the center of the $g(z)$- and $h(x)$-curves even though these may not be at the same value of 2θ. The Stokes correction will now involve cosine coefficients

only. The final $f(y)$-curve, which in this case will be symmetrical, is then displaced from $y = 0$ by the separation between the origins of $h(x)$ and $g(z)$. When only symmetrical curves are involved, the Stokes correction is simple enough to be carried out with the Beevers and Lipson strips if a computer is not available.

13.3 POWDER PATTERN POWER THEOREM

Problems involving diffraction in powder samples of imperfect crystals are often simplified by the use of the powder pattern power theorem. Some of the ideas which are involved have already been used in Chapter 4, but it is worthwhile to now develop them as a general theorem. If the diffraction vector is represented in terms of the continuous variables h_1, h_2, h_3 by the relation

$$(\mathbf{s} - \mathbf{s}_0)/\lambda = h_1\mathbf{b}_1 + h_2\mathbf{b}_2 + h_3\mathbf{b}_3$$

and this expression is used in Eq. (13.1), the intensity in electron units from a single parallelopipedon crystal takes the form

$$I_{eu}(h_1h_2h_3) = F^2 \frac{\sin^2 \pi N_1 h_1}{\sin^2 \pi h_1} \frac{\sin^2 \pi N_2 h_2}{\sin^2 \pi h_2} \frac{\sin^2 \pi N_3 h_3}{\sin^2 \pi h_3}.$$

The quantity $I_{eu}(h_1h_2h_3)$ is an example of what we shall call an "interference function," the intensity in electron units from one crystal, expressed in terms of the coordinates in reciprocal space of the diffraction vector.

We first imagine a sample of crystals in which the interference function is zero everywhere in reciprocal space except close to the position $(h_1'h_2'h_3')$. Let $90 - \theta$ be the angle between $-\mathbf{s}_0$ and $h_1'\mathbf{b}_1 + h_2'\mathbf{b}_2 + h_3'\mathbf{b}_3$ when $(\mathbf{s} - \mathbf{s}_0)/\lambda = h_1'\mathbf{b}_1 + h_2'\mathbf{b}_2 + h_3'\mathbf{b}_3$. If there are M crystals in the sample, the number of crystals dM, whose vectors $h_1'\mathbf{b}_1 + h_2'\mathbf{b}_2 + h_3'\mathbf{b}_3$ make angles between $90 - (\theta + \alpha)$ and $90 - (\theta + \alpha + d\alpha)$ with the direction $-\mathbf{s}_0$, is given by

$$\frac{dM}{M} = \frac{2\pi r^2 \sin [90 - (\theta + \alpha)]\, d\alpha}{4\pi r^2},$$

and since we are interested only in small values of α,

$$dM = (M/2) \cos \theta \, d\alpha.$$

Figure 13.5 illustrates one crystal in the sample whose $h_1'\mathbf{b}_1 + h_2'\mathbf{b}_2 + h_3'\mathbf{b}_3$ vector is related to the primary direction $\mathbf{s}_0/\lambda$ and the diffraction direction $\mathbf{s}/\lambda$ so as to exactly satisfy the relation $(\mathbf{s} - \mathbf{s}_0)/\lambda = h_1'\mathbf{b}_1 + h_2'\mathbf{b}_2 + h_3'\mathbf{b}_3$. By means of small angles β perpendicular to the paper and γ in the plane of the paper, we represent a slightly different direction $\mathbf{s}'/\lambda$ for the diffracted beam. On a receiving surface which is normal to $\mathbf{s}/\lambda$ and at a distance R from the sample, we produce a small area $dA = R^2 \, d\beta \, d\gamma$ by means of small changes

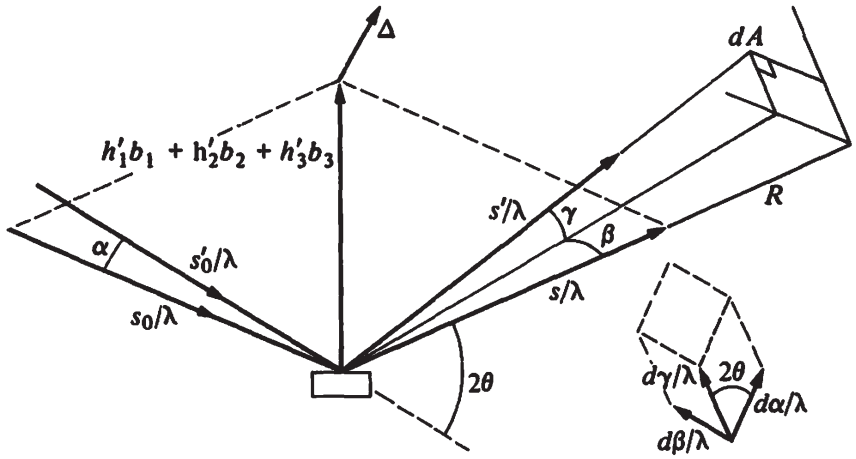

Fig. 13.5 Relations involved in the derivation of the powder pattern power theorem.

$d\beta$ and $d\gamma$. We are interested in the contribution from crystals whose $h'_1\mathbf{b}_1 + h'_2\mathbf{b}_2 + h'_3\mathbf{b}_3$ direction makes angles between $90 - (\theta + \alpha)$ and $90 - (\theta + \alpha + d\alpha)$ with the primary beam direction $\mathbf{s}_0/\lambda$. It is simplest to keep the $h'_1\mathbf{b}_1 + h'_2\mathbf{b}_2 + h'_3\mathbf{b}_3$ vector fixed, and let the primary beam change to the direction $\mathbf{s}'_0/\lambda$ which makes an angle $90 - (\theta + \alpha)$ with $h'_1\mathbf{b}_1 + h'_2\mathbf{b}_2 + h'_3\mathbf{b}_3$. The total power arriving at the receiving surface is then given by integrating the intensity from one crystal over the area of the receiving surface, and then integrating over the number of crystals in each range of orientation with respect to the primary beam:

$$P = I_e \iiint I_{eu}(h_1h_2h_3)R^2\, d\beta\, d\gamma (M/2) \cos\theta\, d\alpha. \tag{13.15}$$

The interference function $I_{eu}(h_1h_2h_3)$ refers to the position in reciprocal space

$$h_1\mathbf{b}_1 + h_2\mathbf{b}_2 + h_3\mathbf{b}_3 = h'_1\mathbf{b}_1 + h'_2\mathbf{b}_2 + h'_3\mathbf{b}_3 + \boldsymbol{\Delta},$$

where

$$\boldsymbol{\Delta} = \mathbf{s}'/\lambda - \mathbf{s}/\lambda - (\mathbf{s}'_0/\lambda - \mathbf{s}_0/\lambda).$$

Changes $d\alpha\, d\beta\, d\gamma$ cause changes in the tip of the $\boldsymbol{\Delta}$-vector of amounts $d\boldsymbol{\alpha}/\lambda$ normal to $\mathbf{s}'_0/\lambda$ and $d\boldsymbol{\beta}/\lambda$ and $d\boldsymbol{\gamma}/\lambda$ normal to $\mathbf{s}/\lambda$. The three small vector changes are shown separately in Fig. 13.5 with $d\boldsymbol{\alpha}/\lambda$ and $d\boldsymbol{\gamma}/\lambda$ in the plane of the paper, and $d\boldsymbol{\beta}/\lambda$ perpendicular to the paper. The variation $d\alpha\, d\beta\, d\gamma$ causes the tip of the $\boldsymbol{\Delta}$-vector to sweep through a small volume in reciprocal space:

$$dV(RS) = d\alpha/\lambda\, d\gamma/\lambda \sin 2\theta\, d\beta/\lambda = (\sin 2\theta/\lambda^3)\, d\alpha\, d\beta\, d\gamma. \tag{13.16}$$

From Eq. (13.16), the product $d\alpha\, d\beta\, d\gamma$ can be expressed in terms of a volume element $dV(RS)$, and Eq. (13.15) becomes a volume integral in reciprocal space:

$$P = \frac{I_e R^2 M \lambda^3}{4} \iiint \frac{I_{eu}(h_1h_2h_3)}{\sin\theta}\, dV(RS). \tag{13.17}$$

The derivation has been carried through with the restriction that the interference function differs from zero only in the immediate vicinity of $h_1'h_2'h_3'$. If $I_{eu}(h_1h_2h_3)$ differs from zero over an extended region, the result applies to each small volume element in the region, and Eq. (13.17) becomes a completely general theorem. For a powder sample, the power on the receiving surface due to any region in reciprocal space is obtained from Eq. (13.17) by integrating $I_{eu}(h_1h_2h_3)/\sin\theta$ over the desired volume in reciprocal space. Since it is a powder sample, the power expressed by Eq. (13.17) is the total power in a hollow cone whose axis is the direction of the primary beam.

It is often convenient to express the volume element in terms of the variables $h_1h_2h_3$:

$$dV(RS) = \mathbf{b}_1\, dh_1 \cdot \mathbf{b}_2\, dh_2 \times \mathbf{b}_3\, dh_3 = v_b\, dh_1\, dh_2\, dh_3 = (1/v_a)\, dh_1\, dh_2\, dh_3.$$

Equation (13.17) then takes the form

$$P = \frac{I_e R^2 M \lambda^3}{4v_a} \iiint \frac{I_{eu}(h_1h_2h_3)}{\sin\theta}\, dh_1\, dh_2\, dh_3. \tag{13.18}$$

The powder pattern power theorem is represented by either Eq. (13.17) or Eq. (13.18). For imperfect structures, it is usually simplest to express an interference function in terms of the variables $h_1h_2h_3$ in reciprocal space, and the observable quantity P is then obtained from $I_{eu}(h_1h_2h_3)$ by means of the theorem.

13.4 SMALL COHERENT DOMAINS AND STRAINS

We next consider a powder sample in which there is both particle size and strain broadening. As an example, cold work in a metal could produce dislocation arrays, such as small angle boundaries which subdivide the original grains into small coherent domains. We assume that there is enough disorientation from one domain to the next, so that the domains scatter incoherently with respect to one another, and hence the domains act as very small crystals. The dislocations, which produce the subdivision into domains, can also produce both tensile and compressive strains within the domains. Except that we are neglecting the effects of faulting, this is a simple model for a cold-worked polygrained metal.

We consider the 00*l*-reflection from a crystal having orthorhombic axes. It has been shown by Stokes and Wilson[6] and by Warren[7] that a general treatment of the problem leads to exactly the same results as those obtained by considering a 00*l*-reflection in terms of orthorhombic axes. We shall use this representation because it simplifies greatly the mathematical derivations. For one domain, the position of the origin of the unit cell $m_1m_2m_3$ is expressed by

$$\mathbf{R}_m = m_1\mathbf{a}_1 + m_2\mathbf{a}_2 + m_3\mathbf{a}_3 + \boldsymbol{\delta}(m_1m_2m_3).$$

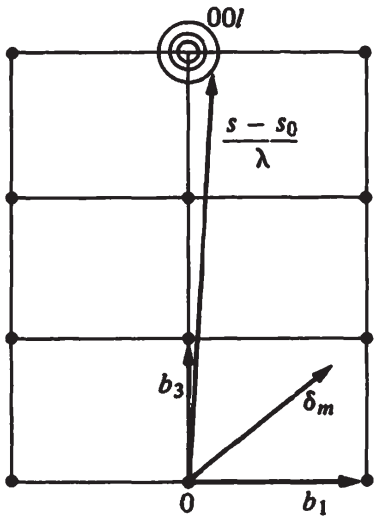

Fig. 13.6 Representation of reciprocal space for a 00*l* reflection with orthorhombic axes.

The displacement $\boldsymbol{\delta}(m_1m_2m_3)$ allows for distortions within the domain, and in general the displacement will be different for each unit cell $m_1m_2m_3$. Assuming that the strains are continuous, we can neglect any distortion within the unit cell, and use the same structure factor F for all cells. The intensity is then given by the double sum

$$I = I_e F^2 \sum_m \sum_{m'} e^{(2\pi i/\lambda)(\mathbf{s}-\mathbf{s}_0)\cdot(\mathbf{R}_{m'}-\mathbf{R}_m)}.$$

With the usual representation of the diffraction vector in terms of the continuous variables h_1, h_2, h_3:

$$(\mathbf{s} - \mathbf{s}_0)/\lambda = h_1\mathbf{b}_1 + h_2\mathbf{b}_2 + h_3\mathbf{b}_3,$$

the intensity expression becomes

$$I = I_e F^2 \sum_m \sum_{m'} e^{2\pi i\{(m_1'-m_1)h_1+(m_2'-m_2)h_2+(m_3'-m_3)h_3+[(\mathbf{s}-\mathbf{s}_0)/\lambda]\cdot(\boldsymbol{\delta}_{m'}-\boldsymbol{\delta}_m)\}}. \quad (13.19)$$

It is convenient to represent the displacement $\boldsymbol{\delta}_m$ in terms of its components along the three orthogonal axes:

$$\boldsymbol{\delta}_m = X_m\mathbf{a}_1 + Y_m\mathbf{a}_2 + Z_m\mathbf{a}_3.$$

Equation (13.19) involves the scalar product of the two vectors $(\mathbf{s} - \mathbf{s}_0)/\lambda$ and $\boldsymbol{\delta}_m$ which are shown by Fig. 13.6. For obtaining the scalar product, it is a good enough approximation to replace $(\mathbf{s} - \mathbf{s}_0)/\lambda$ by its average value $l\mathbf{b}_3$, and hence

$$\left(\frac{\mathbf{s} - \mathbf{s}_0}{\lambda}\right) \cdot \boldsymbol{\delta}_m = l\mathbf{b}_3 \cdot (X_m\mathbf{a}_1 + Y_m\mathbf{a}_2 + Z_m\mathbf{a}_3) = lZ_m.$$

Using this result in Eq. (13.19), we obtain an expression for the interference function

$$I_{eu}(h_1h_2h_3) = F^2 \sum_m \sum_{m'} e^{2\pi i[(m_1'-m_1)h_1+(m_2'-m_2)h_2+(m_3'-m_3)h_3+l(Z_{m'}-Z_m)]}. \quad (13.20)$$

As might be expected, it is only the component of the displacement perpendicular to the reflecting planes which appears in the interference function.

The total power in a reflection is obtained from the powder pattern power theorem as expressed by Eq. (13.18). Since the total power can also be expressed in terms of the power distribution $P(2\theta)$, we can write

$$\int P(2\theta)\, d(2\theta) = \frac{I_e M R^2 \lambda^3 p(hkl)}{4 v_a} \iiint \frac{I_{eu}(h_1 h_2 h_3)}{\sin\theta}\, dh_1\, dh_2\, dh_3. \quad (13.21)$$

By adding a multiplicity factor $p(hkl)$ in Eq. (13.21), the integration of the interference function is reduced to one equivalent region in reciprocal space. For a $00l$-reflection, the intensity is nonvanishing only for small values of h_1 and h_2, and the length of the diffraction vector can be approximated by its vertical component, as illustrated by Fig. 13.6:

$$\left|\frac{\mathbf{s} - \mathbf{s}_0}{\lambda}\right| = \frac{2\sin\theta}{\lambda} = |h_1\mathbf{b}_1 + h_2\mathbf{b}_2 + h_3\mathbf{b}_3| \to h_3\,|\mathbf{b}_3|.$$

With this approximation, $2\sin\theta/\lambda = h_3\,|\mathbf{b}_3|$ and

$$dh_3 = \frac{\cos\theta\, d(2\theta)}{\lambda\,|\mathbf{b}_3|}.$$

Introducing this expression for dh_3 in the right-hand side of Eq. (13.21), we can drop the integration with respect to $d(2\theta)$ on both sides of the equation and obtain the power distribution

$$P(2\theta) = \frac{I_e M R^2 \lambda^2 p(hkl)\cos\theta}{4 v_a\,|\mathbf{b}_3|\sin\theta} \iint I_{eu}(h_1 h_2 h_3)\, dh_1\, dh_2.$$

What we measure, however, is the power per unit length of the intersection of the diffraction cone with a receiving surface at distance R from the sample:

$$P'(2\theta) = \frac{P(2\theta)}{2\pi R \sin 2\theta}.$$

With the abbreviation

$$K = \frac{I_e R \lambda^2 p(hkl)}{16\pi v_a\,|\mathbf{b}_3|}$$

and the value of the interference function from Eq. (13.20), the experimentally observable $P'(2\theta)$ is given by

$$P'(2\theta) = \frac{KMF^2}{\sin^2\theta} \iint \sum_m \sum_{m'} e^{2\pi i[(m_1'-m_1)h_1 + (m_2'-m_2)h_2 + (m_3'-m_3)h_3 + l(Z_{m'}-Z_m)]}\, dh_1\, dh_2.$$

To include everything belonging to the reflection $00l$, we carry out the integration over h_1 and h_2 from $-\frac{1}{2}$ to $+\frac{1}{2}$. Since

$$\int_{-1/2}^{+1/2} e^{2\pi i(m_1'-m_1)h_1}\, dh_1 = \frac{\sin\pi(m_1' - m_1)}{\pi(m_1' - m_1)},$$

the expression for $P'(2\theta)$ becomes

$$P'(2\theta) = \frac{KMF^2}{\sin^2\theta} \sum_m \sum_{m'} \frac{\sin \pi(m_1' - m_1)}{\pi(m_1' - m_1)} \frac{\sin \pi(m_2' - m_2)}{\pi(m_2' - m_2)} e^{2\pi i[(m_3' - m_3)h_3 + l(Z_{m'} - Z_m)]}.$$

The sine quotients are equal to unity for $m_1' = m_1$ and $m_2' = m_2$; otherwise they are zero. Hence $P'(2\theta)$ can be reduced to the simple form:

$$P'(2\theta) = \frac{KMF^2}{\sin^2\theta} \sum_{m_1} \sum_{m_2} \sum_{m_3} \sum_{m_3'} [e^{2\pi i l[Z(m_3') - Z(m_3)]} e^{2\pi i(m_3' - m_3)h_3}]_{m_1 m_2}. \quad (13.22)$$

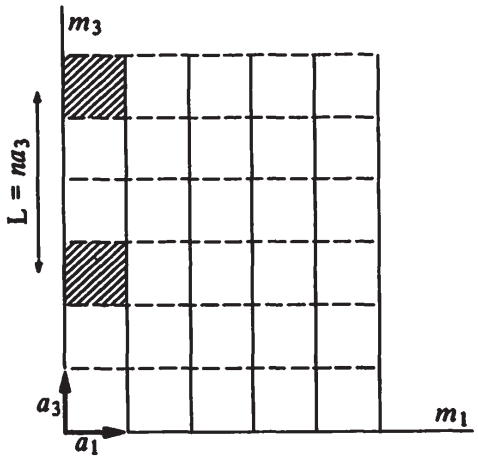

Fig. 13.7 Representation of the crystal in terms of columns of cells along the a_3 direction.

In Eq. (13.22) there are contributions only from pairs of cells for which $m_1' = m_1$ and $m_2' = m_2$. It was pointed out by Bertaut[8] that it is useful to think of the domain in terms of columns of unit cells along the $\mathbf{a}_3$-direction and hence perpendicular to the reflecting planes $00l$. The columns are illustrated schematically by Fig. 13.7. For a fixed $m_1 m_2$, the sums over m_3 and m_3' give the contribution from all pairs of cells in a column $m_1 m_2$. The sums over m_1 and m_2 then give the contribution from all the columns making up the domain. Introduce the abbreviations

$$n = m_3' - m_3, \qquad Z_n = Z(m_3') - Z(m_3).$$

For a fixed value of n, let N_n (sample) be the number of cells in the whole sample having an nth neighbor in the same column, and let $\langle \exp [2\pi i l Z_n] \rangle$ be an average over all such pairs of nth neighbors in the same column for the whole sample. The four-fold sum in Eq. (13.22), and the factor M which represents a sum over all the domains in the sample, can then be replaced by a single sum over all values of n:

$$P'(2\theta) = \frac{KF^2}{\sin^2\theta} \sum_{n=-\infty}^{+\infty} N_n(\text{sample}) \langle e^{2\pi i l Z_n} \rangle e^{2\pi i n h_3}.$$

We now introduce the quantities

N = number of cells in the sample,

$N(\text{col})$ = number of columns in the sample,

$N/N(\text{col}) = N_3$ = average number of cells per column,

$N_n(\text{sample})/N(\text{col}) = N_n$ = average number of n pairs per column.

In terms of these quantities, $P'(2\theta)$ becomes

$$P'(2\theta) = \frac{KNF^2}{\sin^2\theta} \sum_{n=-\infty}^{+\infty} \frac{N_n}{N_3} \langle e^{2\pi i l Z_n} \rangle_n e^{2\pi i n h_3}.$$

Expanding the exponentials into their real and imaginary parts, we can write

$$P'(2\theta) = \frac{KNF^2}{\sin^2\theta} \sum_{n=-\infty}^{+\infty} \frac{N_n}{N_3} \{\langle \cos 2\pi l Z_n \rangle \cos 2\pi n h_3 - \langle \sin 2\pi l Z_n \rangle \sin 2\pi n h_3$$

$$+ i(\langle \cos 2\pi l Z_n \rangle \sin 2\pi n h_3 + \langle \sin 2\pi l Z_n \rangle \cos 2\pi n h_3)\}.$$

Every pair of cells m_3' and m_3 enters into the summation twice, once as $n = m_3' - m_3$ and again as $-n = m_3 - m_3'$. Since $Z_n = Z(m_3') - Z(m_3)$ and $Z_{-n} = Z(m_3) - Z(m_3')$, it follows that $Z_{-n} = -Z_n$ and hence the imaginary terms cancel out.

Introducing the two coefficients

$$A_n = \frac{N_n}{N_3} \langle \cos 2\pi l Z_n \rangle, \qquad B_n = -\frac{N_n}{N_3} \langle \sin 2\pi l Z_n \rangle, \tag{13.23}$$

we express $P'(2\theta)$ as a Fourier series:

$$P'(2\theta) = \frac{KNF^2}{\sin^2\theta} \sum_{n=-\infty}^{+\infty} \{A_n \cos 2\pi n h_3 + B_n \sin 2\pi n h_3\}. \tag{13.24}$$

The Fourier series is expressed in terms of the variable

$$h_3 = \frac{2 \sin\theta}{\lambda |\mathbf{b}_3|} = \frac{2 |\mathbf{a}_3| \sin\theta}{\lambda}, \tag{13.25}$$

and the harmonic number n corresponds to the separation $L = na_3$ of Fig. 13.7, between a pair of cells in a column perpendicular to the $00l$-planes. By plotting the experimental quantity $P'(2\theta) \sin^2\theta/F^2$ against $h_3 = 2a_3 \sin\theta/\lambda$ in the range between $h_3 = l - \frac{1}{2}$ and $h_3 = l + \frac{1}{2}$, we can determine a set of uncorrected Fourier coefficients A_n and B_n. Running the corresponding peak from a standard sample, and making the Stokes correction, we obtain a set of corrected Fourier coefficients A_n and B_n but in arbitrary units. For $n = 0$, it is evident that $N_n = N_3$ and $Z_n = 0$, and hence from Eq. (13.23) it follows that $A_0 = 1$. In principle this gives a method for normalizing the coefficients

A_n and B_n in terms of $A_0 = 1$. However we shall see later that there are experimental difficulties in obtaining the A_0-coefficient, and hence this method of normalizing must be used with caution.

The cosine coefficient is the product of the two quantities N_n/N_3 and $\langle \cos 2\pi l Z_n \rangle$. Since N_n/N_3 depends only on the column lengths, it is a size coefficient and we represent it by $A_n^S = N_n/N_3$. The other quantity $\langle \cos 2\pi l Z_n \rangle$ depends on the distortion in the domain, and it is represented by $A_n^D = \langle \cos 2\pi l Z_n \rangle$. The cosine coefficient, which we determine from experiment, is the product of a size coefficient and a distortion coefficient:

$$A_n = A_n^S A_n^D.$$

A method for separating the size and distortion components was proposed by Warren and Averbach.[9] Suppose that we have measured several orders of $00l$ such as 001, 002, 003, and that we have the corresponding cosine coefficients $A_n(l) = A_n^S A_n^D(l)$. The size coefficient $A_n^S = N_n/N_3$ is independent of the order l. The distortion coefficient $A_n^D(l) = \langle \cos 2\pi l Z_n \rangle$ depends upon the order l, and it approaches the value unity as l goes to zero. From this difference in the dependence on l, it is possible to separate the two coefficients. For small values of l and n, so that the product lZ_n is small, the cosine can be expanded $\langle \cos 2\pi l Z_n \rangle \to 1 - 2\pi^2 l^2 \langle Z_n^2 \rangle$, and the logarithm can be written

$$\ln \langle \cos 2\pi l Z_n \rangle = \ln (1 - 2\pi^2 l^2 \langle Z_n^2 \rangle) = -2\pi^2 l^2 \langle Z_n^2 \rangle.$$

For small values of l and n, the logarithm of the measured Fourier coefficient is given by

$$\ln A_n(l) = \ln A_n^S - 2\pi^2 l^2 \langle Z_n^2 \rangle. \tag{13.26}$$

For a fixed value of n, we plot the values of $\ln A_n(l)$ against l^2 as indicated by Fig. 13.8. The intercepts at $l = 0$ give the values of the size coefficients A_n^S, and the slopes give $-2\pi^2 \langle Z_n^2 \rangle$. The distance $L = na_3$ represented on

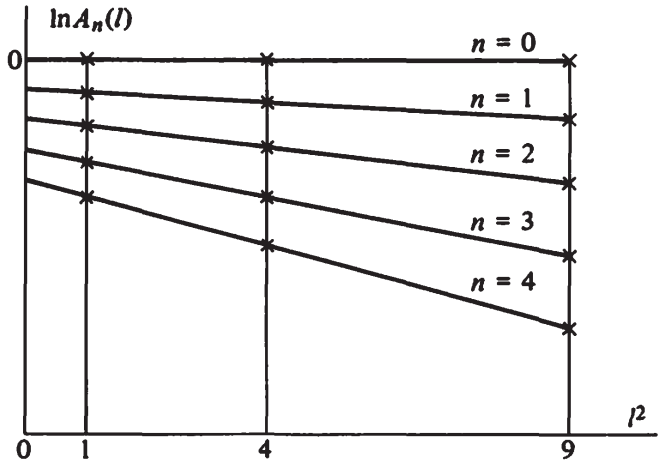

Fig. 13.8 The logarithmic plot which is used to separate particle size and distortion effects when multiple orders $00l$ are available.

Fig. 13.7, is the undistorted distance between the cells m_3' and m_3. Due to distortion this distance is changed by $\Delta L = a_3 Z_n$. The ratio $\Delta L/L = \epsilon_L$ is a component of strain along the a_3-direction, averaged over the length L. Hence $Z_n/n = \epsilon_L$, and the value of the slope can be written as $-2\pi^2 n^2 \langle \epsilon_L^2 \rangle$. From the initial slopes of the lines of Fig. 13.8, we obtain mean square values of an average component of strain.

Since Eq. (13.26) is exact only for small values of l and n, it is only in the small l region that the lines are necessarily straight, but this is just the region where they are required to be straight in order to make a linear extrapolation to $l = 0$. Although this method of separation makes no assumption about the nature of the strains except that $\langle Z_n^2 \rangle$ is not too large, it is interesting to consider the case of a hypothetical Gaussian strain distribution such as

$$p(Z_n) = \frac{a}{\sqrt{\pi}} e^{-a^2 Z_n^2}.$$

In terms of such a distribution,

$$\langle Z_n^2 \rangle = \frac{a}{\sqrt{\pi}} \int_{-\infty}^{+\infty} Z_n^2 e^{-a^2 Z_n^2} \, dZ_n = \frac{1}{2a^2},$$

$$\langle \cos 2\pi l Z_n \rangle = \frac{a}{\sqrt{\pi}} \int_{-\infty}^{+\infty} \cos (2\pi l Z_n) e^{-a^2 Z_n^2} \, dZ_n = e^{-\pi^2 l^2 / a^2} = e^{-2\pi^2 l^2 \langle Z_n^2 \rangle}.$$

For this case, Eq. (13.26) would be exact for all values of l and n, and the lines of Fig. 13.8 would remain straight for any value of n and out to indefinitely large values of l. Since considerable misunderstanding of this point has appeared in the literature, numerical examples to clarify the question have been given in a review article by Warren.[10]

Suppose that we have the A_n^S coefficients for different values of n, obtained from the intercepts on the plot of $\ln A_n(l)$. We can then make a plot of A_n^S vs. n as illustrated by Fig. 13.9. To interpret the values of A_n^S,

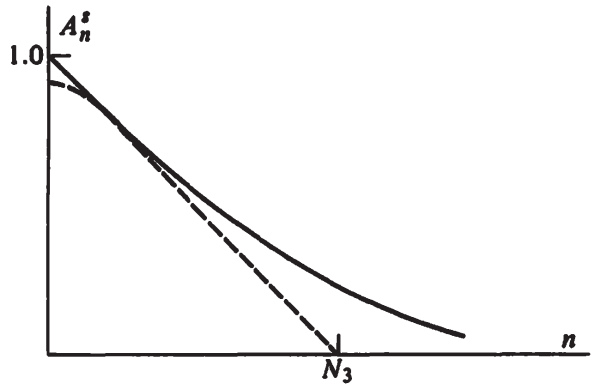

Fig. 13.9 Plot of the size coefficient A_n^s against the variable n. The intercept of the initial slope on the axis of abscissae is the mean column length number N_3.

we follow a treatment first given by Bertaut.[11] In terms of columns of cells, let $p(i)$ be the fraction of the columns of length i cells. The values of N_n can then be expressed in terms of $p(i)$:

$$N_0 = \sum_{i=0}^{\infty} ip(i) = N_3,$$

$$N_1 = \sum_{i=1}^{\infty} (i-1)p(i),$$

$$N_2 = \sum_{i=2}^{\infty} (i-2)p(i),$$

$$N_n = \sum_{i=|n|}^{\infty} (i-|n|)p(i).$$

The size coefficient A_n^S is given in terms of $p(i)$ by the expression

$$A_n^s = \frac{N_n}{N_3} = \frac{1}{N_3} \sum_{i=|n|}^{\infty} (i-|n|)p(i). \tag{13.27}$$

By introducing a continuous $p(i)$, such that $p(i)\,di$ is the fraction of columns having lengths between i and $i+di$ cells, the sum can be replaced by an integral:

$$A_n^s = \frac{1}{N_3} \int_{i=|n|}^{\infty} (i-|n|)p(i)\,di. \tag{13.28}$$

The experimental A_n^s-coefficients vary smoothly with n as illustrated by Fig. 13.9, and it is meaningful to discuss the slope of the A_n^s-curve. It will be shown later that in practice the Fourier coefficients are determined by a generalized procedure. The method depends upon the fact that A_n^s can be considered as a continuous quantity, and the values of A_n^s which are obtained do not correspond to the integral values of n which appear in Eq. (13.27). To determine the derivative of A_n^s it is helpful to rewrite Eq. (13.28) in the form

$$A_n^s = \frac{1}{N_3} \left\{ \int_{i=|n|}^{\infty} ip(i)\,di - |n| \int_{|n|}^{\infty} p(i)\,di \right\}.$$

Since the variable appears in the lower limit of the integral, we make use of the theorem

$$y = \int_{\epsilon}^{\infty} f(x)\,dx, \qquad \frac{dy}{d\epsilon} = -f(\epsilon),$$

and obtain for the derivative

$$\frac{dA_n^s}{dn} = \frac{1}{N_3} \left\{ -|n|\,p(|n|) - \int_{i=|n|}^{\infty} p(i)\,di + |n|\,p(|n|) \right\} = -\frac{1}{N_3} \int_{i=|n|}^{\infty} p(i)\,di. \tag{13.29}$$

For the initial slope, n approaches zero, and

$$\left(\frac{dA_n^s}{dn}\right)_{n\to 0} = -\frac{1}{N_3}\int_{i=0}^{\infty} p(i)\,di = -\frac{1}{N_3}. \tag{13.30}$$

The initial slope of the A_n^s-vs.-n curve is given by $-1/N_3$, and as shown by Fig. 13.9, N_3 is just the intercept of the initial slope on the axis of abscissae. Since $N_3 a_3$ is an average column length perpendicular to the 00l-planes, the initial slope of the A_n^s-curve gives an average domain dimension normal to the 00l-planes. This result is independent of the size and shape distribution of the domains.

By differentiating Eq. (13.29), we obtain the second derivative of A_n^s:

$$\frac{d^2A_n^s}{dn^2} = \frac{p(|n|)}{N_3}. \tag{13.31}$$

It is evident that the second derivative of the A_n^s-curve gives directly a column length distribution. In practice this possibility of obtaining a distribution is of rather limited importance, because the second derivative of an experimental quantity such as A_n^s is of low accuracy, and furthermore the method of separating the size and distortion coefficients is limited to small values of n. However, there is one aspect of Eq. (13.31) which is of very great importance. Since $p(|n|)$ is a column length distribution, it can never be negative, and hence the second derivative $d^2A_n^s/dn^2$ can never be negative. This means that the plot of A_n^s, which is shown by Fig. 13.9, can be concave upward but can never be concave downward.

Sometimes an experimental A_n^s-curve is obtained which has a small "hook" or concave downward part near $n = 0$, as illustrated by the dashed line of Fig. 13.9. This is often called the "hook effect" and since it is in principle impossible, it is an indication that something is wrong in the data. The trouble is usually the result of too small an A_0-coefficient. In general, there is overlapping of the long tails of neighboring reflections, so that one is likely to take the background level too high, and thereby obtain peak areas which are too small. This results in values of A_0 which are too small relative to the other A_n, since A_0 is proportional to the peak area. In evaluating the Fourier coefficients for a peak, it is very important to allow for overlapping tails and not estimate the background level too high. Using crystal monochromated radiation and diffractometer recording, it is possible to determine an upper limit for the correct background level by running the pattern of an annealed sample under identical experimental conditions. When the A_n^s-curve shows a hook at small n, the initial slope has no significance. An approximate correction, which is better than no correction at all, is to use the slope at small n values, disregarding the A_0 point.

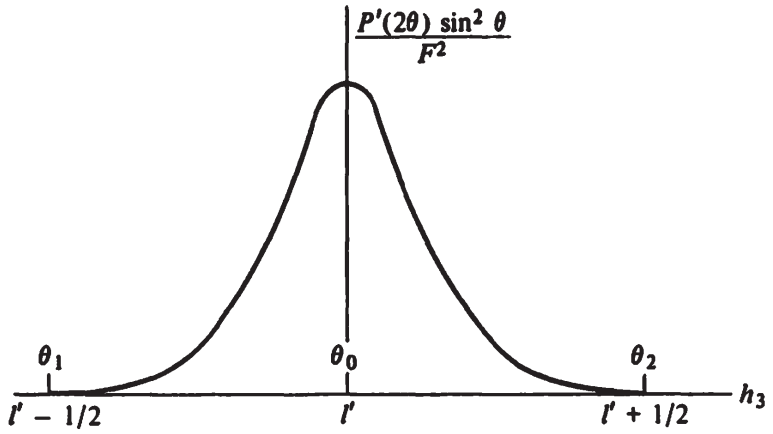

Fig. 13.10 The corrected experimental curve represented in terms of the fictitious quantities h_3' and l'.

The theory which has been developed in this section has been based upon a $00l$-reflection for a crystal with orthorhombic axes. The results are, however, quite general and applicable to any powder pattern reflection. To generalize the results, and make the determination of the Fourier coefficients more efficient, we introduce a set of fictitious quantities a_3', b_3', l', h_3', n'. The experimental peak of Fig. 13.10 is represented in terms of the new variable

$$h_3' = 2a_3' \sin\theta/\lambda.$$

At the peak origin where $\theta = \theta_0$, we set $h_3' = l'$. We then select an interval $h_3' = l' - \frac{1}{2}$ to $h_3' = l' + \frac{1}{2}$ which is large enough to include all observable variation in the peak. In terms of the measured θ_1, θ_0, and θ_2,

$$l' - 1/2 = (2a_3'/\lambda)\sin\theta_1,$$
$$l' = (2a_3'/\lambda)\sin\theta_0,$$
$$l' + 1/2 = (2a_3'/\lambda)\sin\theta_2.$$

From these equations we obtain

$$1/2 = (2a_3'/\lambda)(\sin\theta_2 - \sin\theta_0), \tag{13.32}$$

and this determines the value of the fictitious a_3'. The Fourier coefficients are then evaluated for the interval $l' - \frac{1}{2}$ to $l' + \frac{1}{2}$ and designated by the harmonic numbers n'. Since $L = n'a_3'$ is a real distance along the columns of cells perpendicular to the reflecting planes, we multiply all n' by the value of a_3' obtained from Eq. (13.32) and represent the coefficients by A_L. Since a_3'/l' is the real planar spacing d, and Z_n'/n' is the component of strain ϵ_L, the distortion coefficient $\langle\cos 2\pi l' Z_n'\rangle$ can be written $\langle\cos 2\pi\epsilon_L L/d\rangle$ and Eq. (13.26) becomes

$$\ln A_L(1/d) = \ln A_L^S - 2\pi^2\langle\epsilon_L^2\rangle L^2/d^2. \tag{13.33}$$

Using multiple orders, the extrapolation is made by plotting $\ln A_L(1/d)$ against $(1/d)^2$. For each of the peaks, the Fourier interval is chosen for convenience, but the final results are the real quantities involved in Eq. (13.33). The values of A_L^s are then plotted against L as indicated by Fig. 13.11. The intercept of the initial slope on the L-axis gives directly the average column length $\langle D \rangle$ perpendicular to the set of planes under consideration.

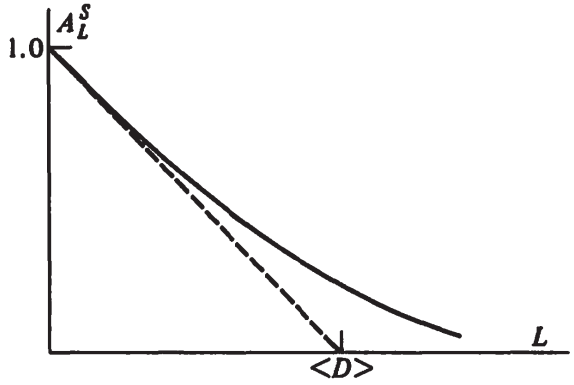

Fig. 13.11 Plot of the particle size coefficient against L, where $L = n'a_3'$ is a real distance along the columns of cells.

For cubic crystals, $d = a/h_0$, where $h_0^2 = h^2 + k^2 + l^2$, and Eq. (13.33) is conveniently expressed in the form

$$\ln A_L(h_0) = \ln A_L^S - 2\pi^2\langle \epsilon_L^2 \rangle L^2 h_0^2/a^2. \tag{13.34}$$

If a set of multiple orders are available such as 110, 220, 330 or 111, 222, 333, we plot $\ln A_L(h_0)$ against h_0^2 and determine the size coefficient A_L^S from the intercept at $h_0^2 = 0$. To make an extrapolation to $h_0^2 = 0$, it is desirable to have measurements for the first three orders. However, for a cubic crystal, the third order of any simple reflection is always buried under another reflection at the same position and of higher multiplicity. This is readily seen by considering the first four cubic reflections:

100	110	111	200
200	220	222	400
300, 221	330, 411	333, 511	600, 442

Except where there is drastic preferred orientation, it is not possible to obtain the third order for cubic materials, and the extrapolation is usually made using only the first two orders.

If there is no average expansion or contraction of the lattice as a result of cold work, the peaks are broadened but not shifted in position. However, when there is an overall expansion or contraction, there is a peak shift in addition to the peak broadening. If the Stokes correction is made using the same origin for the broadened and the standard peaks, the expansion will be

included as part of an asymmetric strain. On the other hand, if we choose separate origins for $g(z)$ and $h(x)$ at the approximate center of each peak, we obtain a smaller mean square strain. In this case the average expansion is obtained separately from the difference in peak position, and the mean square strain is relative to the new average lattice parameter. Both procedures are correct but they give different quantities. In general, the second procedure is used, since the calculations are considerably simplified, and either result can be obtained approximately from the other.

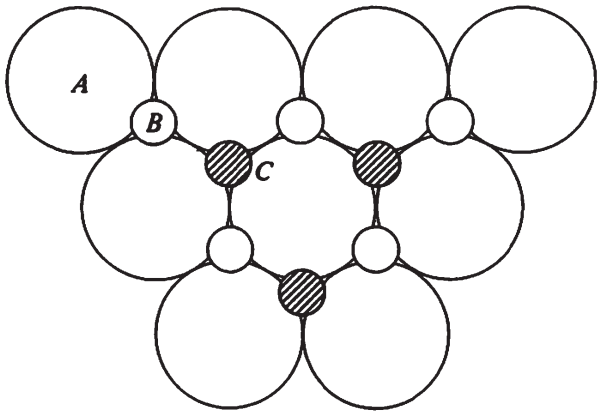

Fig. 13.12 Representation of the 111 layers in the structure of a FCC element. For the correct FCC sequence, a layer in position *A* is followed by a layer in position *B* and this is followed by a layer in position *C*.

13.5 EFFECTS OF DEFORMATION AND TWIN FAULTING IN FCC METALS

In many metals, faulting is one of the important results of cold work. It is convenient to introduce the subject in terms of faulting on the 111-planes of a face-centered cubic metal. In Fig. 13.12 the large circles marked *A* represent one of the 111 layers of a FCC metal. The structure is formed by placing successive layers of atoms upon the one already shown. It is evident that the next layer could be at either of the positions *B* or *C*, and that for each successive layer there is such a two-fold possibility. If the layers are placed in the sequence *ABCABC* we have the face-centered cubic (FCC) metal structure, while sequences such as *ABABAB* produce the hexagonal close-packed (HCP) structure.

The correct FCC sequence *ABCABC* is shown by Fig. 13.13(a). The deformation fault which is represented by Fig. 13.13(b) is produced by shifting everything above the dashed line, so that the first layer which should be in position *A* is moved to position *B*. A deformation fault is a jog in the sequence, with the same *ABC* sequence maintained in the parts above and below the fault. In building up a FCC crystal layer by layer as in a growth process, it is evident that each new layer should be different from the two previous ones in order to follow the FCC sequence. In Fig. 13.13(c), which

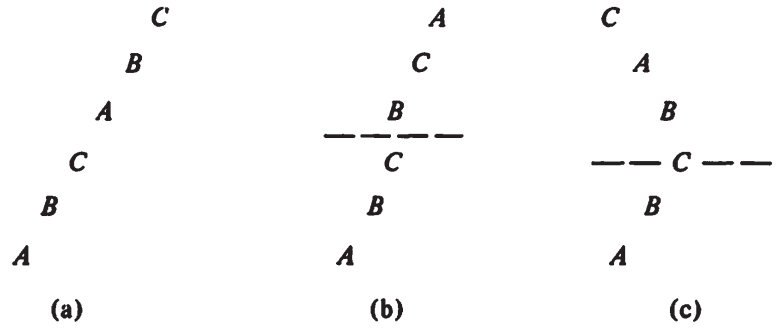

Fig. 13.13 Sequences of 111 layers expressed in terms of the *A*, *B*, *C* positions of Fig. 13.12. (a) The correct FCC sequence *ABCABC*. (b) A deformation fault. (c) A growth or twin fault.

represents a growth fault, suppose that for some reason the layer after *ABC* takes the position *B* instead of the correct position *A*. The next layer has positions *B* and *C* preceding it, so it takes position *A*. The following layer is preceded by *A* and *B*, so it takes position *C*. The result of a growth fault is therefore to reverse the sequence *ABCABC* into *CBACBA*. Since the upper part of Fig. 13.13(c) is the twin of the lower part, a growth fault is also a twin fault in the FCC structures.

We shall consider the effects of deformation and twin faulting in FCC metals. In treating this problem we shall make the simplifying assumption that in each crystal the faulting takes place on only one of the sets of {111} planes. In terms of this set of 111 planes, we assume that each of the layers is perfect, but that here and there in the sequence there is a fault which extends across the crystal. Since each of the layers is perfect, it is convenient to change to a set of hexagonal axes $A_1A_2A_3$, where A_1 and A_2 are in the plane of the layer, and A_3 is perpendicular to the 111-layers. In terms of the hexagonal axes $A_1A_2A_3$ and their corresponding reciprocal axes $B_1B_2B_3$, we introduce the indices $H_0K_0L_0$, where the subscript zero has been added to distinguish the index L_0 from the letter L which has already been used as a length. The two sets of axes are shown by Fig. 13.14, and the transformation

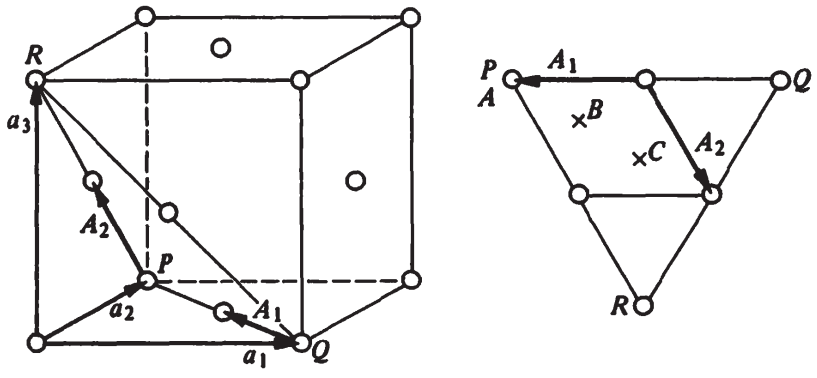

Fig. 13.14 Relation between the cubic axes $a_1a_2a_3$ and the hexagonal axes $A_1A_2A_3$ for a FCC element.

equations are as follows:

$$\begin{aligned} \mathbf{A}_1 &= -\mathbf{a}_1/2 + \mathbf{a}_2/2 + 0, & H_0 &= -h/2 + k/2 + 0, \\ \mathbf{A}_2 &= 0 - \mathbf{a}_2/2 + \mathbf{a}_3/2, & K_0 &= 0 - k/2 + l/2, \\ \mathbf{A}_3 &= \mathbf{a}_1 + \mathbf{a}_2 + \mathbf{a}_3, & L_0 &= h + k + l. \end{aligned} \tag{13.35}$$

The hexagonal axes $A_1A_2A_3$ define a 3-atom unit cell containing 3 layers with 1 atom per layer, so that $A_3/3$ is the perpendicular distance between successive layers.

In terms of the hexagonal axes, the position of the atom m_1m_2 in the layer m_3 can be expressed by

$$\mathbf{R}_{m_1m_2m_3} = m_1\mathbf{A}_1 + m_2\mathbf{A}_2 + m_3\mathbf{A}_3/3 + \boldsymbol{\delta}(m_3). \tag{13.36}$$

The displacement $\boldsymbol{\delta}(m_3)$ is in the plane of the layer, and hence in the plane of $\mathbf{A}_1$ and $\mathbf{A}_2$. The intensity from one crystal is given by the usual double sum:

$$I = I_e \sum_m f_m e^{(2\pi i/\lambda)(\mathbf{s}-\mathbf{s}_0)\cdot\mathbf{R}_m} \sum_{m'} f_{m'} e^{-(2\pi i/\lambda)(\mathbf{s}-\mathbf{s}_0)\cdot\mathbf{R}_{m'}}.$$

Incorporating Eq. (13.36) in the intensity expression, the sums over $m_1m_2m_1'm_2'$ can be carried out immediately since they are independent of $\boldsymbol{\delta}(m_3)$. For simplicity we approximate the layers as parallelograms of dimensions N_1A_1 and N_2A_2. With the abbreviation

$$\psi^2 = I_e f^2 \frac{\sin^2(\pi/\lambda)(\mathbf{s}-\mathbf{s}_0)\cdot N_1\mathbf{A}_1}{\sin^2(\pi/\lambda)(\mathbf{s}-\mathbf{s}_0)\cdot\mathbf{A}_1} \frac{\sin^2(\pi/\lambda)(\mathbf{s}-\mathbf{s}_0)\cdot N_2\mathbf{A}_2}{\sin^2(\pi/\lambda)(\mathbf{s}-\mathbf{s}_0)\cdot\mathbf{A}_2}, \tag{13.37}$$

the intensity reduces to

$$I = \psi^2 \sum_{m_3} \sum_{m_3}' e^{2\pi i[(\mathbf{s}-\mathbf{s}_0)/\lambda]\cdot[(m_3-m_3')\mathbf{A}_3/3+\boldsymbol{\delta}(m_3)-\boldsymbol{\delta}(m_3')]}.$$

We represent the diffraction vector in terms of the reciprocal vectors $\mathbf{B}_1\mathbf{B}_2\mathbf{B}_3$ and the continuous variables $h_1h_2h_3$:

$$(\mathbf{s}-\mathbf{s}_0)/\lambda = h_1\mathbf{B}_1 + h_2\mathbf{B}_2 + h_3\mathbf{B}_3.$$

Introducing the abbreviations

$$\begin{aligned} m &= m_3 - m_3', & \boldsymbol{\delta}(m) &= \boldsymbol{\delta}(m_3) - \boldsymbol{\delta}(m_3'), \\ \phi(m) &= 2\pi(h_1\mathbf{B}_1 + h_2\mathbf{B}_2 + h_3\mathbf{B}_3)\cdot\boldsymbol{\delta}(m), \end{aligned} \tag{13.38}$$

the intensity expression becomes

$$I = \psi^2 \sum_{m_3} \sum_{m_3}' e^{i\phi(m)} e^{2\pi i m h_3/3}.$$

By letting $\langle \exp[i\phi(m)] \rangle$ be an average for all mth neighbor pairs, and letting N_m be the number of layers having an mth neighbor, we reduce the double sum

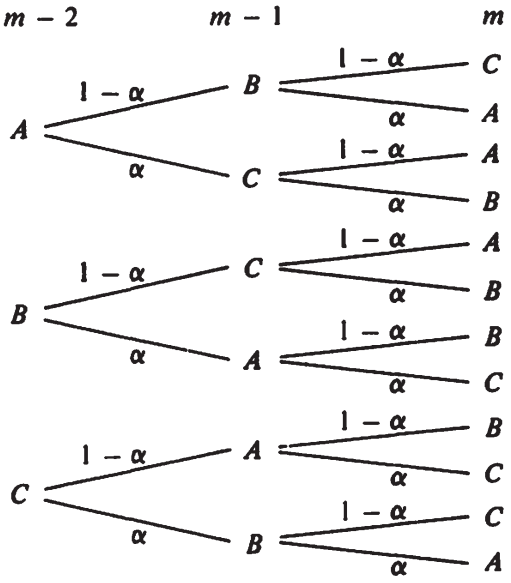

Fig. 13.15 All of the possible sequences in three layers $m-2$, $m-1$ and m for the 111 layers of a FCC element in which ABC is taken as the correct sequence. A deformation fault is indicated by α wherever the ABC sequence is not followed.

to a single sum over values of m:

$$I = \psi^2 \sum_{m=-\infty}^{+\infty} N_m \langle e^{i\phi(m)} \rangle e^{2\pi i m h_3/3}. \tag{13.39}$$

The original treatment of the problem of deformation faulting and twin faulting in FCC metals was due to M. S. Paterson,[12] who used a method involving difference equations. A later treatment by Warren and Warekois,[13] which was restricted to deformation faulting, made use of a relation introduced by Mering.[14] This relation is very convenient for deformation faulting, but it is not applicable to the problem of twin faulting. Since we are interested in the effects of both deformation and twin faulting, we shall follow the method of difference equations.

We consider first the problem of deformation faulting, and define α as the probability of finding a deformation fault between any two layers. The average number of layers between faults is $1/\alpha$ and we assume that the probability of a fault between any two layers is independent of the faulting between other layers. For a FCC crystal in which ABC represents the correct sequence, Fig. 13.15 illustrates all of the possible sequences in three successive layers $m-2$, $m-1$ and m. The probability of each succession is labelled $1-\alpha$ or α, depending on whether it follows the correct sequence or represents a deformation fault. From the figure, we obtain an expression for the probability of finding an A-position in the mth layer, in terms of the probabilities of A-, B-, or C-positions in the $m-2$ layer:

$$P_m^A = P_{m-2}^A 2\alpha(1-\alpha) + P_{m-2}^B (1-\alpha)^2 + P_{m-2}^C \alpha^2. \tag{a}$$

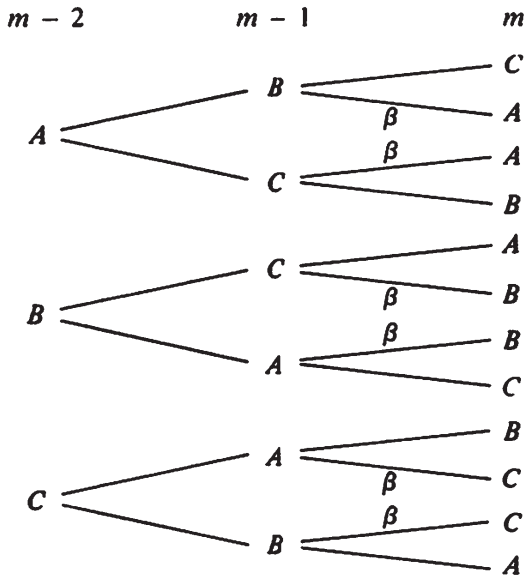

Fig. 13.16 All of the possible sequences in three layers $m-2$, $m-1$, and m for the layers of a FCC element. A growth fault is indicated by β wherever the mth layer is not different from both the $m-1$ and $m-2$ layers.

Similarly, the probability of finding an A-position in the $m-1$ layer is given by

$$P^A_{m-1} = P^B_{m-2}\alpha + P^C_{m-2}(1-\alpha). \tag{b}$$

Since the $m-2$ layer is certain to be either A or B or C:

$$P^A_{m-2} + P^B_{m-2} + P^C_{m-2} = 1. \tag{c}$$

Adding equations (a) and (b), we obtain

$$P^A_m + P^A_{m-1} - P^A_{m-2}2\alpha(1-\alpha) = (1-\alpha+\alpha^2)(P^B_{m-2} + P^C_{m-2}).$$

Eliminating $P^B_{m-2} + P^C_{m-2}$ by means of equation (c), we can write a relation involving only the P^A:

$$P^A_m + P^A_{m-1} + P^A_{m-2}(1-3\alpha+3\alpha^2) = 1-\alpha+\alpha^2. \tag{13.40}$$

Equation (13.40) is the difference equation for deformation faulting in FCC metals.

We next consider the problem of twin faulting, and let β represent the probability of a twin fault between any two layers. Regardless of how the FCC sequence is designated, each successive layer should be different from the two preceding layers, and places where the layer is not different from the two preceding layers are designated as twin faults. All of the possible sequences in three successive layers, $m-2$, $m-1$, and m, are shown by Fig. 13.16. Steps from $m-1$ to m, which do not result in an m-position which is different from both $m-2$ and $m-1$, are labelled β. From the sequences of Fig. 13.16, it is evident that P^A_{m-2} represents the combined probability of A followed by B and A followed by C in the $m-2$ and $m-1$ layers. Similarly,

$P^B_{m-2} + P^C_{m-2} - P^A_{m-1}$ is the combined probability of B followed by C and C followed by B in the $m-2$ and $m-1$ layers. Using these facts, we obtain a simple expression for P^A_m:

$$P^A_m = P^A_{m-2}\beta + (P^B_{m-2} + P^C_{m-2} - P^A_{m-1})(1 - \beta).$$

Since the $m-2$ layer is sure to be A or B or C,

$$P^A_{m-2} + P^B_{m-2} + P^C_{m-2} = 1.$$

From these two equations, we eliminate $P^B_{m-2} + P^C_{m-2}$ and obtain a difference equation for twin faulting

$$P^A_m + (1 - \beta)P^A_{m-1} + (1 - 2\beta)P^A_{m-2} = 1 - \beta. \tag{13.41}$$

For a crystal in which there is no faulting, $(P^A_m + P^A_{m-1} + P^A_{m-2} - 1)$ should be equal to zero, since P^A is sure to be unity in one of the layers and zero in the other two. The departure of this quantity from zero, due to deformation faulting and twin faulting, is readily obtained from Eqs. (13.40) and (13.41):

$$(P^A_m + P^A_{m-1} + P^A_{m-2} - 1)_\alpha = \alpha(1 - \alpha)(3P^A_{m-2} - 1),$$
$$(P^A_m + P^A_{m-1} + P^A_{m-2} - 1)_\beta = \beta(P^A_{m-1} + 2P^A_{m-2} - 1).$$

Assuming that α and β are each so small that neither one has any appreciable effect on the other, the contributions are additive, and hence for a sample containing both deformation and twin faulting,

$$P^A_m + P^A_{m-1} + P^A_{m-2} - 1 = \alpha(1 - \alpha)(3P^A_{m-2} - 1) + \beta(P^A_{m-1} + 2P^A_{m-2} - 1).$$

Approximating $\alpha(1 - \alpha)$ by α, we obtain a simple difference equation for combined deformation and twin faulting:

$$P^A_m + (1 - \beta)P^A_{m-1} + (1 - 3\alpha - 2\beta)P^A_{m-2} = 1 - \alpha - \beta. \tag{13.42}$$

Considering first the case that m is positive, we try a solution of the form

$$P^A_m = a + bx^m, \tag{13.43}$$

where a, b, and x are independent of m. Substituting the trial solution in Eq. (13.42), we obtain

$$(1 - \alpha - \beta)(3a - 1) + bx^{m-2}[x^2 + (1 - \beta)x + 1 - 3\alpha - 2\beta] = 0.$$

Since the expression must vanish independently of m, α, and β, each of the two terms must vanish. For the first term, $(1 - \alpha - \beta)(3a - 1) = 0$, and hence $a = \frac{1}{3}$. From the second term,

$$x^2 + (1 - \beta)x + 1 - 3\alpha - 2\beta = 0.$$

This is a quadratic equation in x, with the two solutions:

$$x = [-(1 - \beta) \pm is]/2,$$

where

$$s = (3 - 12\alpha - 6\beta)^{1/2} \tag{13.44}$$

is obtained by neglecting quadratic terms. Using both solutions, since they will be needed to satisfy the boundary conditions, Eq. (13.43) becomes

$$P_m^A = \frac{1}{3} + b_1\left[\frac{-(1-\beta)+is}{2}\right]^m + b_2\left[\frac{-(1-\beta)-is}{2}\right]^m. \tag{13.45}$$

It is convenient to introduce the more general notation P_m^0, P_m^+, and P_m^- representing the probabilities that the mth layer is the same as the zero layer, or one step ahead in the sequence, or one step behind in the sequence. The expression for P_m^A given by Eq. (13.45) can be used for any of the three probabilities P_m^0, P_m^+ and P_m^- by determining the coefficients b_1 and b_2 so as to satisfy the particular boundary conditions. For P_m^0 we have the two conditions; $P_0^0 = 1$ since the zero layer is sure to be the same as the zero layer, and $P_1^0 = 0$ since the first layer cannot be the same as the zero layer. Letting P_m^0 be represented by Eq. (13.45), the two boundary conditions lead to

$$P_0^0 = 1 = \tfrac{1}{3} + b_1 + b_2,$$

$$P_1^0 = 0 = \frac{1}{3} + b_1\left[\frac{-(1-\beta)+is}{2}\right] + b_2\left[\frac{-(1-\beta)-is}{2}\right].$$

Solving the two equations, we find

$$b_1 = \frac{1}{3}\left(1 - \frac{\beta}{is}\right), \qquad b_2 = \frac{1}{3}\left(1 + \frac{\beta}{is}\right),$$

and P_m^0 is expressed by

$$P_m^0 = \frac{1}{3}\left\{1 + \left(1 - \frac{\beta}{is}\right)\left[\frac{-(1-\beta)+is}{2}\right]^m + \left(1 + \frac{\beta}{is}\right)\left[\frac{-(1-\beta)-is}{2}\right]^m\right\}. \tag{13.46}$$

Since Eq. (13.46) involves complex quantities raised to the mth power, it is convenient to introduce the abbreviation

$$\frac{(1-\beta) \pm is}{2} = Ze^{\pm i\gamma} = Z(\cos\gamma \pm i\sin\gamma).$$

Equating real and imaginary parts on either side of the equation, and using s from Eq. (13.44), we evaluate Z and $\tan\gamma$. Correct to first order in α and β, the expressions are

$$Z = (1 - 3\alpha - 2\beta)^{1/2} = 1 - 1.5\alpha - \beta, \tag{13.47}$$

$$\tan\gamma = \sqrt{3}(1 - 2\alpha).$$

Letting γ_0 be the value of γ when $\alpha = 0$, it follows that $\tan\gamma_0 = \sqrt{3}$ and

$\gamma_0 = \pi/3$. To obtain a more convenient expression for γ, we write

$$\tan(\gamma - \gamma_0) = \frac{\tan\gamma - \tan\gamma_0}{1 + \tan\gamma\tan\gamma_0} = \frac{\sqrt{3}(1-2\alpha) - \sqrt{3}}{1 + 3(1-2\alpha)} = \frac{-\sqrt{3}\alpha}{2 - 3\alpha}.$$

For values of α which are small, $\gamma - \gamma_0 = -\sqrt{3}\alpha/2$ and hence

$$\gamma = \gamma_0 + (\gamma - \gamma_0) = \frac{\pi}{3} - \frac{\sqrt{3}\alpha}{2}. \tag{13.48}$$

Using the abbreviation for $[(1-\beta) \pm is]/2$, Eq. (13.46) reduces to

$$P_m^0 = \tfrac{1}{3}\{1 + 2(-1)^m Z^m[\cos m\gamma + (\beta/s)\sin m\gamma]\}. \tag{13.49}$$

In a powder sample, for every crystal with the sequence *ABC*, there will be another with the same orientation of 111-planes but with the sequence *CBA*, since the second is obtained from the first by rotation of 180° about the normal to the 111-planes. No matter how the sequence is designated, if we average over the powder sample $P_m^+ = P_m^-$, and since $P_m^0 + P_m^+ + P_m^- = 1$, we can write

$$P_m^+ = P_m^- = (1 - P_m^0)/2. \tag{13.50}$$

For the triangle of Fig. 13.14, the A_3-axis is directed up from the plane of the paper. If the position of the layer represented by the circles is called *A*, the layer below would be at position *C*, and the layer above would be at position *B* to correspond to an *ABC* sequence up from the plane of the paper. For such a sequence, the displacements $\boldsymbol{\delta}_m$ and phases ϕ_m of Eq. (13.38) are

$$\begin{aligned} \boldsymbol{\delta}_m^0 &= 0, & \phi_m^0 &= 0, \\ \boldsymbol{\delta}_m^+ &= (-\mathbf{A}_1 + \mathbf{A}_2)/3, & \phi_m^+ &= -2\pi(h_1 - h_2)/3, \\ \boldsymbol{\delta}_m^- &= (\mathbf{A}_1 - \mathbf{A}_2)/3, & \phi_m^- &= 2\pi(h_1 - h_2)/3. \end{aligned} \tag{13.51}$$

The average phase factor of Eq. (13.39) is expressed by

$$\langle\exp[i\phi(m)]\rangle = P_m^0 \exp[i\phi_m^0] + P_m^+ \exp[i\phi_m^+] + P_m^- \exp[i\phi_m^-].$$

Incorporating Eqs. (13.50) and (13.51), and recognizing from Eq. (13.37) that ψ^2 will differ appreciably from zero only if h_1 and h_2 are close to the integer values H_0 and K_0, the phase factor is obtained in a form which allows for both sequences:

$$\langle\exp[i\phi(m)]\rangle = P_m^0 + (1 - P_m^0)\cos 2\pi(H_0 - K_0)/3. \tag{13.52}$$

In using Eq. (13.52), there are two cases to consider:

a) $H_0 - K_0 = 3M$, $\langle\exp[i\phi(m)]\rangle = 1$, Independent of faulting,

b) $H_0 - K_0 = 3M \pm 1$, $\langle\exp[i\phi(m)]\rangle = (-1 + 3P_m^0)/2$.

It is more convenient to express the two conditions in terms of the third

index L_0. From Eq. (13.35),

$$L_0 = 3k - 2(H_0 - K_0)$$

and hence if $H_0 - K_0 = 3M \pm 1$, it follows that $L_0 = 3M' \pm 1$.

We now consider the case $L_0 = 3M' \pm 1$, where faulting plays a role. Using the value of P_m^0 from Eq. (13.49), the average phase factor is given by

$$\langle \exp [i\phi(m)] \rangle = (-1)^m Z^m [\cos m\gamma + (\beta/s) \sin m\gamma].$$

This result has been obtained by considering that m is positive. To treat the case for m negative, we replace Eq. (13.43) by an appropriate trial solution $P_m^{\prime 1} = a + bx^{-m}$. Proceeding in the same way, we obtain the same expression for $\langle \exp [i\phi(m)] \rangle$ except that Z^m is replaced by Z^{-m} and $\sin m\gamma$ is replaced by $-\sin m\gamma$. Hence for m either positive or negative, the result can be expressed in the general form

$$\langle \exp [i\phi(m)] \rangle = (-1)^m Z^{|m|} \left(\cos m\gamma + \frac{\beta}{s} \sin |m| \gamma\right).$$

We now introduce this expression in Eq. (13.39). Making the expansion $\exp [2\pi i m h_3/3] = \cos 2\pi m h_3/3 + i \sin 2\pi m h_3/3$, the terms involving $\sin 2\pi m h_3/3$ will cancel in pairs since all other quantities are even in m, and the intensity reduces to

$$I = \psi^2 \sum_{m=-\infty}^{+\infty} N_m Z^{|m|} [\cos m\gamma + (\beta/s) \sin |m| \gamma] \cos 2\pi m \left(\frac{h_3}{3} + \frac{1}{2}\right). \quad (13.53)$$

With the relations for

$$\cos mA \cos mB \quad \text{and} \quad \sin |m| A \cos mB = \sin |m| A \cos |m| B,$$

we break Eq. (13.53) into four terms. Introducing the value of γ from Eq. (13.48) and replacing β/s by $\beta/\sqrt{3}$, the expression becomes

$$I = \frac{\psi^2}{2} \sum_{m=-\infty}^{+\infty} N_m Z^{|m|} \left\{ \cos 2\pi m \left(\frac{h_3 - 1}{3} - \frac{\sqrt{3}\alpha}{4\pi}\right) + \frac{\beta}{\sqrt{3}} \sin 2\pi |m| \right.$$
$$\times \left(\frac{h_3 - 1}{3} - \frac{\sqrt{3}\alpha}{4\pi}\right) + \cos 2\pi m \left(\frac{h_3 + 1}{3} + \frac{\sqrt{3}\alpha}{4\pi}\right)$$
$$\left. - \frac{\beta}{\sqrt{3}} \sin 2\pi |m| \left(\frac{h_3 + 1}{3} + \frac{\sqrt{3}\alpha}{4\pi}\right) \right\}. \quad (13.54)$$

For any value of h_3 which produces a peak in the upper cosine series, the lower cosine series will show a peak for $-h_3$. The reflection represented by the lower expression is the twin of that represented by the upper expression. In each of the two expressions there is a peak shift due to $\sqrt{3}\alpha/4\pi$ and an asymmetry due to the sine terms. On a powder pattern, either reflection and

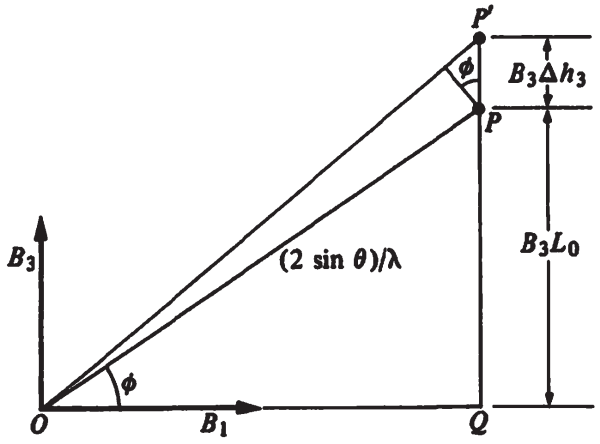

Fig. 13.17 The reciprocal lattice in terms of the hexagonal axes B_1B_1 and B_3. The reciprocal lattice point $H_0K_0L_0$ is represented by P.

its twin occur at the same position with the same peak shift and asymmetry, and hence we can use twice the value of either expression if proper signs are ensured. The upper expression peaks near $h_3 = L_0$ where $L_0 = 3N + 1$, and the lower expression peaks near $h_3 = L_0$ where $L_0 = 3N - 1$. Letting the sign $(\pm)$ be determined by $L_0 = 3N \pm 1$, for purposes of a powder pattern, Eq. (13.54) is equivalent to

$$I = \psi^2 \sum_{m=-\infty}^{+\infty} N_m Z^{|m|} \left\{ \cos 2\pi m \left(\frac{h_3 - L_0}{3} - (\pm) \frac{\sqrt{3}\alpha}{4\pi} \right) \right.$$

$$\left. \pm \frac{\beta}{\sqrt{3}} \sin 2\pi |m| \left(\frac{h_3 - L_0}{3} - (\pm) \frac{\sqrt{3}\alpha}{4\pi} \right) \right\}. \quad (13.55)$$

Equation (13.55) represents the intensity as a function of the position $h_1h_2h_3$ in reciprocal space, but what we observe experimentally is the distribution of power with respect to 2θ in a powder pattern peak. The necessary relations for converting to an observable quantity are shown by Fig. 13.17, where the reciprocal lattice point $H_0K_0L_0$ is represented by P. Equation (13.55) expresses the spreading out of the intensity about point P. Due to faulting there is a decrease in the Fourier coefficients $N_mZ^{|m|}$, and this spreads the intensity up and down along the line PQ. There is also a spreading of the intensity perpendicular to the line PQ, which is determined by the h_1h_2 dependency of ψ^2. A general treatment which allows for spreading in all directions from P has been given by Warren.[15] To simplify the mathematics, we shall restrict ourselves here to the case where the layer dimensions N_1A_1 and N_2A_2 are so large that the intensity is closely confined to the vertical line PQ. Due to faulting, the intensity spreads up and down from point P along the line PQ, but we assume that any lateral spreading is very small.

The distance from the origin to point P is given by $2 \sin \theta/\lambda$. For the position P', which is displaced from P by $B_3\Delta h_3$, there is a change in 2θ which

is expressed by

$$B_3 \Delta h_3 \sin \phi = \Delta\left(\frac{2 \sin \theta}{\lambda}\right) = \frac{\cos \theta}{\lambda} \Delta(2\theta). \tag{13.56}$$

To obtain the distribution of power with respect to 2θ, we now use the powder pattern power theorem from Eq. (13.18). Expressing dh_3 by means of Eq. (13.56) we can write

$$P = \int P_{2\theta}\, d(2\theta) = \frac{MR^2\lambda^3}{4v_a} \iiint \frac{I(h_1h_2h_3)}{\sin \theta}\, dh_1\, dh_2 \frac{\cos \theta\, d(2\theta)}{\lambda B_3 |\sin \phi|}.$$

By dropping the integration with respect to $d(2\theta)$ on either side of the equation, we have an expression for $P_{2\theta}$. What is observed experimentally is the power distribution per unit length of diffraction circle:

$$P'_{2\theta} = \frac{P_{2\theta}}{2\pi R \sin 2\theta},$$

and this quantity is given by

$$P'_{2\theta} = \frac{MR\lambda^2}{16\pi v_a B_3 \sin^2 \theta\, |\sin \phi|} \iint I(h_1h_2h_3)\, dh_1\, dh_2. \tag{13.57}$$

As seen from Eq. (13.55), the only h_1h_2 dependence of $I(h_1h_2h_3)$ is contained in ψ^2, and the integral is readily evaluated:

$$\iint \psi^2\, dh_1\, dh_2 = I_e f^2 \iint \frac{\sin^2 \pi N_1 h_1}{(\pi h_1)^2} \frac{\sin^2 \pi N_2 h_2}{(\pi h_2)^2}\, dh_1\, dh_2 = I_e f^2 N_1 N_2.$$

Letting N_3 be the average number of layers in a crystal, and N_0 the number of atoms in the sample, $N_0 = MN_1N_2N_3$. The volume of the 3-atom unit cell was v_a, and if we now let v_0 be the volume per atom, $v_0 = v_a/3$. We introduce the abbreviation

$$G = \frac{N_0 R\lambda^2 I_e f^2}{16\pi v_0 \sin^2 \theta}, \tag{13.58}$$

where G is a factor which varies slowly with θ because of the dependence on f^2, I_e, and $\sin^2 \theta$. With this abbreviation, Eq. (13.57) becomes

$$P'_{2\theta} = \frac{G}{3B_3 |\sin \phi|} \sum_{m=-\infty}^{+\infty} \frac{N_m}{N_3} Z^{|m|} \left\{ \cos 2\pi m \left[\frac{h_3 - L_0}{3} - (\pm) \frac{\sqrt{3}\alpha}{4\pi} \right] \right.$$
$$\left. + (\pm) \frac{\beta}{\sqrt{3}} \sin 2\pi |m| \left[\frac{h_3 - L_0}{3} - (\pm) \frac{\sqrt{3}\alpha}{4\pi} \right] \right\}. \tag{13.59}$$

To combine the broadened and unbroadened components of a powder pattern line, and also to use the Fourier coefficients conveniently, we now consider the reflection $H_0K_0L_0$ as a reflection $00l'$ in terms of orthorhombic

axes a_3', b_3'. The b_3'-axis is directed along the line OP of Fig. 13.17, and in terms of the new continuous variable h_3', the diffraction vector is expressed by $2 \sin \theta/\lambda = h_3' b_3'$. From the geometry of Fig. 13.17, we can write

$$\Delta(2 \sin \theta/\lambda) = (h_3 - L_0)B_3 \sin \phi = (h_3' - l')b_3',$$

and from this we obtain

$$\left[\frac{h_3 - L_0}{3} - (\pm)\frac{\sqrt{3}\alpha}{4\pi}\right] = \frac{b_3'}{3B_3 \sin \phi}\left[h_3' - l' - (\pm)\frac{\sqrt{3}\alpha 3B_3 \sin \phi}{4\pi b_3'}\right].$$

Introducing the abbreviations

$$q = \frac{b_3'}{3B_3 \sin \phi}, \qquad \epsilon = (\pm)\frac{3\sqrt{3}\alpha B_3 \sin \phi}{4\pi b_3'}, \tag{13.60}$$

we express Eq. (13.59) in terms of the new variable $h_3' - l'$:

$$P_{2\theta}' = \frac{G}{3B_3 |\sin \phi|} \sum_{m=-\infty}^{+\infty} \frac{N_m}{N_3} Z^{|m|} \times \left\{\cos 2\pi m q(h_3' - l' - \epsilon) + (\pm)\frac{\beta}{\sqrt{3}} \sin 2\pi |m| q(h_3' - l' - \epsilon)\right\}. \tag{13.61}$$

To conveniently combine the contributions by the different components of a powder pattern line, we now make an approximation which depends upon the fact that in Eq. (13.61), the coefficient $N_m Z^{|m|}/N_3$ decreases slowly and continuously with increasing m. In the expression

$$y = \sum_m A(m) \cos 2\pi m q x,$$

suppose that the coefficients $A(m)$ decrease slowly and continuously with increasing m. We replace the sum by an integral, and then introduce the new quantity $n = mq$:

$$y = \int A(m) \cos 2\pi m q x \, dm = \frac{1}{|q|} \int A(n/q) \cos 2\pi n x \, dn.$$

The second integral is now converted back to a sum over integral values of n, and we obtain

$$\sum_m A(m) \cos 2\pi m q x = \frac{1}{|q|} \sum_n A(n/q) \cos 2\pi n x, \tag{13.61a}$$

where $A(n/q)$ means $A(m)$ with $m = n/q$. By similar reasoning we obtain

$$\sum_m B(m) \sin 2\pi |m| q x = \frac{1}{q} \sum_n B(n/q) \sin 2\pi |n| x. \tag{13.61b}$$

Using these approximations, Eq. (13.61) becomes

$$P'_{2\theta} = \frac{G}{b'_3} \sum_{n=-\infty}^{+\infty} \frac{N(n/q)}{N_3} Z^{|n/q|} \times \left\{\cos 2\pi n(h'_3 - l' - \epsilon) + (\pm)\frac{\beta}{\sqrt{3}} \frac{L_0}{|L_0|} \sin 2\pi |n| (h'_3 - l' - \epsilon)\right\}. \quad (13.62)$$

Equation (13.62) gives the contribution by one of the $H_0K_0L_0$ components which make up a powder pattern reflection. Some of the components are broadened by faulting, and others are unbroadened by faulting. We shall designate by b (broadened) the component $L_0 = 3N \pm 1$ which are broadened by faulting, and by u (unbroadened) the components $L_0 = 3N$ which are not broadened by faulting. The contribution by a broadened component is given by Eq. (13.62) and that by an unbroadened component by Eq. (13.62) with $Z = 1$, $\epsilon = 0$ and $\beta = 0$. The total contribution to a powder pattern reflection $P'_{2\theta}(h_0)$, where $h_0 = (h^2 + k^2 + l^2)^{1/2}$, is then given by a sum over the broadened and unbroadened components:

$$P'_{2\theta}(h_0) = \frac{G}{b'_3} \sum_{n=-\infty}^{+\infty} \left\{ \sum_b \frac{N(n/q)}{N_3} Z^{|n/q|} \cos 2\pi n(h'_3 - l' - \epsilon) + \sum_u \frac{N(n/q)}{N_3} \cos 2\pi n(h'_3 - l') + \frac{\beta}{\sqrt{3}} \sum_b \frac{N(n/q)}{N_3} Z^{|n/q|}(\pm) \frac{L_0}{|L_0|} \sin 2\pi |n| (h'_3 - l' - \epsilon) \right\}.$$

We make the approximation that the two cosine terms can be replaced by a single cosine term having an average coefficient and an average displacement. Since the coefficient of the sine terms is small and proportional to β, it is a good enough approximation to use the same displacement for the sine terms as for the cosine terms. Letting $(u + b)$ represent the total number of components, unbroadened plus broadened, the expression reduces to the simple form:

$$P'_{2\theta}(h_0) = \frac{G(u + b)}{b'_3} \sum_{n=-\infty}^{+\infty} \times \{A_n \cos 2\pi n(h'_3 - l' - \delta) + B_n \sin 2\pi |n| (h'_3 - l' - \delta)\}, \quad (13.63)$$

where

$$A_n = \left(\frac{1}{u + b}\right)\left\{\sum_b \frac{N(n/q)}{N_3} Z^{|n/q|} + \sum_u \frac{N(n/q)}{N_3}\right\}, \quad (13.64)$$

$$B_n = \left(\frac{1}{u + b}\right)\frac{\beta}{\sqrt{3}} \sum_b \frac{N(n/q)}{N_3} Z^{|n/q|}(\pm) \frac{L_0}{|L_0|}, \quad (13.65)$$

$$\delta = \left(\frac{1}{u + b}\right) \sum_b \epsilon = \left(\frac{1}{u + b}\right) \frac{3\sqrt{3}\alpha B_3}{4\pi b'_3} \sum_b (\pm) \sin \phi. \quad (13.66)$$

Three important effects are contained in Eq. (13.63). With increasing n, there is a decrease in the cosine coefficients A_n, and this results in a peak broadening. The sine coefficients B_n are proportional to β, and they produce a peak asymmetry. The constant δ, which is proportional to α, produces a shift in the peak position. There is also a small shift in the peak position due to the asymmetry term. However, if the peak position is measured near the top of the peak, the effect of asymmetry is usually small, and we can consider only the effect of δ on the position of the cosine peak.

a) Determination of α from the Peak Shift

We develop first a method for determining α from the measured peak shift. Since the coefficients A_n are all positive, it follows from Eq. (13.63) that the cosine peak occurs at a position h_3' such that $h_3' - l' - \delta = 0$. The change in h_3' due to faulting is $\Delta h_3' = \delta$, and since

$$\Delta(2 \sin \theta/\lambda) = b_3' \Delta h_3',$$

the peak displacement $\Delta(2\theta)$ is given by

$$\Delta(2\theta) = \lambda b_3' \delta / \cos \theta.$$

Introducing δ from Eq. (13.66), and multiplying by $180/\pi$ to convert to degrees, we obtain

$$\Delta(2\theta)^0 = \frac{135\sqrt{3}\lambda B_3 \alpha}{\pi^2 (u + b) \cos \theta} \sum_b (\pm) \sin \phi.$$

From Fig. 13.17 we can write $\sin \phi = B_3 L_0 d$, where d is the planar spacing of the reflection. In terms of the cubic cell dimensions a, and the abbreviation $h_0^2 = h^2 + k^2 + l^2$, we make the substitutions $B_3^2 = 1/A_3^2 = 1/3a^2$ and $d^2 = a^2/h_0^2$. Replacing λ by $2d \sin \theta$, the peak displacement is expressed in the compact form

$$\Delta(2\theta)^0 = \frac{90\sqrt{3}\alpha \tan \theta}{\pi^2 h_0^2 (u + b)} \sum_b (\pm) L_0. \tag{13.67}$$

From a measured peak displacement $\Delta(2\theta)^0$, we obtain directly the deformation fault probability α, since all the other quantities in Eq. (13.67) are readily evaluated.

We now illustrate the calculation of the peak displacement for the four powder pattern reflections 111, 200, 222, and 400. In Table 13.1, we list all the hkl-components for each of the four reflections. The value of L_0 for each component is obtained from Eq. (13.35), and the value of $(\pm)$ is determined by $L_0 = 3M \pm 1$. Components for which $L_0 = 3M$ are not included in the sum over b, and hence for these components $(\pm)$ is recorded as zero.

Table 13.1
COMPONENTS OF THE REFLECTIONS 111, 200, 222, AND 400

hkl	L_0	$(\pm)$	hkl	L_0	$(\pm)$	hkl	L_0	$(\pm)$	hkl	L_0	$(\pm)$
111	3	0	200	2	−	222	6	0	400	4	+
11$\bar{1}$	1	+	020	2	−	22$\bar{2}$	2	−	040	4	+
1$\bar{1}$1	1	+	002	2	−	2$\bar{2}$2	2	−	004	4	+
$\bar{1}$11	1	+	$\bar{2}$00	$\bar{2}$	+	$\bar{2}$22	2	−	$\bar{4}$00	$\bar{4}$	−
1$\bar{1}\bar{1}$	$\bar{1}$	−	0$\bar{2}$0	$\bar{2}$	+	2$\bar{2}\bar{2}$	$\bar{2}$	+	0$\bar{4}$0	$\bar{4}$	−
$\bar{1}$1$\bar{1}$	$\bar{1}$	−	00$\bar{2}$	$\bar{2}$	+	$\bar{2}$2$\bar{2}$	$\bar{2}$	+	00$\bar{4}$	$\bar{4}$	−
$\bar{1}\bar{1}$1	$\bar{1}$	−				$\bar{2}\bar{2}$2	$\bar{2}$	+			
$\bar{1}\bar{1}\bar{1}$	$\bar{3}$	0				$\bar{2}\bar{2}\bar{2}$	$\bar{6}$	0			

From the quantities in Table 13.1, values of $\sum_b(\pm)L_0/h_0^2(u+b)$ are calculated for the reflections 111, 200, 222, and 400. These values together with those for 220 and 311 are listed in Table 13.2. Using the tabulated values, the peak shifts are obtained from Eq. (13.67):

$$(111)\quad \frac{1}{h_0^2(u+b)}\sum_b(\pm)L_0 = \frac{6}{3\times 8} = +1/4$$

$$\Delta(2\theta)^\circ = \frac{90\sqrt{3}\alpha\tan\theta_{111}}{\pi^2}(+1/4)$$

$$(200)\quad \frac{1}{h_0^2(u+b)}\sum_b(\pm)L_0 = \frac{-12}{4\times 6} = -1/2$$

$$\Delta(2\theta)^\circ = \frac{90\sqrt{3}\alpha\tan\theta_{200}}{\pi^2}(-1/2)$$

$$(222)\quad \frac{1}{h_0^2(u+b)}\sum_b(\pm)L_0 = \frac{-12}{12\times 8} = -1/8$$

$$\Delta(2\theta)^\circ = \frac{90\sqrt{3}\alpha\tan\theta_{222}}{\pi^2}(-1/8)$$

$$(400)\quad \frac{1}{h_0^2(u+b)}\sum_b(\pm)L_0 = \frac{+24}{16\times 6} = +1/4$$

$$\Delta(2\theta)^\circ = \frac{90\sqrt{3}\alpha\tan\theta_{400}}{\pi^2}(+1/4)$$

As a result of deformation faulting, the reflection 111 shifts toward larger 2θ, while 200 moves toward smaller values of 2θ. For the reflections 222 and 400, which are second orders of 111 and 200, the effect is just the reverse; 222 moves toward smaller 2θ and 400 toward larger 2θ. The peak displacement due to faulting is usually very small, and since there can be other

sources of displacement such as incorrect positioning of the sample in the diffractometer, or changes in the cell dimensions, it is in general not advisable to try to measure the displacement for a single peak. Instead we choose a pair of close reflections with opposite displacements such as 111–200 or 222–400. By recording both peaks on the same diffractometer run, and doing it once for the cold worked sample and again for an annealed sample, the change in peak separation which we obtain is largely independent of the effects of positioning errors and lattice changes. For the pairs 111–200 and 222–400, the changes in peak separation which are due to deformation faulting are given by

$$\begin{aligned}\Delta(2\theta_{200} - 2\theta_{111})^\circ &= \frac{-90\sqrt{3}\alpha}{\pi^2}\left(\frac{\tan\theta_{200}}{2} + \frac{\tan\theta_{111}}{4}\right),\\ \Delta(2\theta_{400} - 2\theta_{222})^\circ &= \frac{+90\sqrt{3}\alpha}{\pi^2}\left(\frac{\tan\theta_{400}}{4} + \frac{\tan\theta_{222}}{8}\right).\end{aligned} \tag{13.68}$$

It is important that the measurements be made in terms of the peak position. A measurement in terms of the centroids of the peaks would be incorrect, since it would include the additional effect of the peak asymmetries which arise from twin faulting.

As an illustration of the peak shifts produced by deformation faulting, we reproduce an early set of measurements by Warren and Warekois[16] on 70–30 α brass filings using Co$K\alpha$ radiation. Figure 13.18 shows the measured

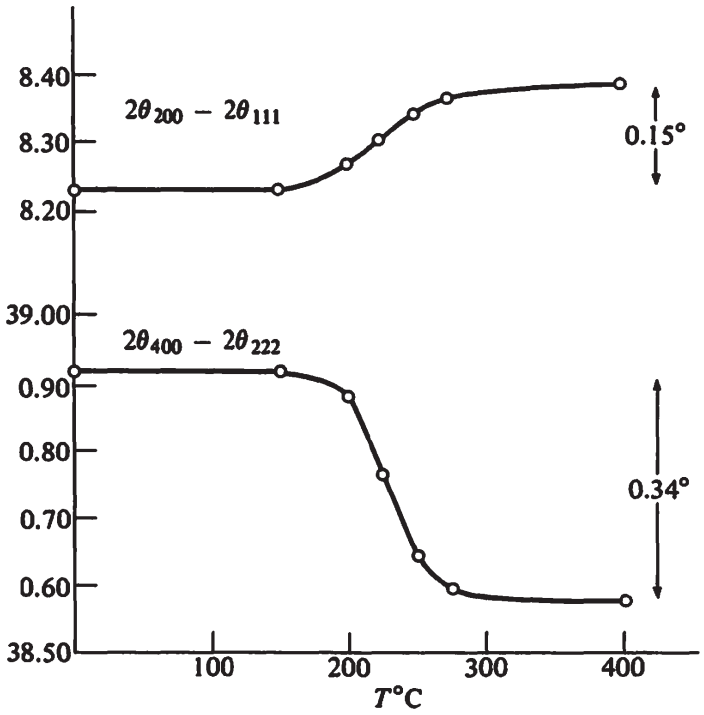

Fig. 13.18 Peak separations (111)–(200) and (222)–(400) for cold-worked 70–30α brass filings given subsequent 1 hour anneals at the various temperatures indicated. Radiation Co$K\alpha$.

separations $2\theta(200) - 2\theta(111)$ and $2\theta(400) - 2\theta(222)$ for the filings as freshly made and after 1 hour anneals at various temperatures. The separations at the right side of the figure are those for the normal material, while those at the left side correspond to the sample in a cold-worked state. As a result of the deformation faulting which is produced by cold work, there is a decrease in the $2\theta(200) - 2\theta(111)$ separation and an increase in the $2\theta(400) - 2\theta(222)$ separation, as predicted by Eq. (13.68). The change for $2\theta(200) - 2\theta(111)$ is smaller than for $2\theta(400) - 2\theta(222)$, but it is usually more accurate, since the 400 reflection may be so broad that it is difficult to locate the peak. Using the appropriate constants for 70—30 α brass and Co$K\alpha$ radiation, Eq. (13.68) reduces to

$$\Delta(2\theta_{200} - 2\theta_{111})^\circ = -6.2\alpha.$$

with the measured value shown by Fig. 13.18, we obtain $\alpha = -0.15/(-6.2) = 0.024$. Since $1/\alpha = 42$, this corresponds to a stacking fault on the average once every 42 layers in the stacking of 111-layers. For the FCC case, the deformation fault probability is obtained directly from changes in peak separations, independent of other effects which can contribute to the peak broadening.

b) Effects of Faulting on the Peak Broadening

We now return to Eq. (13.63) to consider the information which is available in the peak broadening. Allowing for the θ dependence of G, we represent the experimental quantity $P'_{20}(h_0) \sin^2\theta/f^2(1 + \cos^2 2\theta)$ as a function of $h'_3 - l' - \delta = 2(a'_3/\lambda)(\sin\theta - \sin\theta_0)$. With a representation similar to that of Fig. 13.10, we determine the Fourier coefficients A_n. Although obtained in arbitrary units, they are standardized by the condition that A_n must approach unity as n approaches zero. Assuming that two or more multiple orders are available, we use the method of logarithmic plots which is represented by Eq. (13.26) to separate the particle size and the strain coefficients. The particle size coefficient A_n^S which is obtained in this way is the quantity represented by Eq. (13.64), and it involves both the size of the coherently diffracting domains and also a contribution which is due to faulting.

We shall be interested only in coefficients A_n^S for which n is small, and hence we can make approximations which are appropriate for small values of n. Since α and β are small, we can write $Z = 1 - 1.5\alpha - \beta$. We then make the approximation

$$Z^{|n/q|} = (1 - 1.5\alpha - \beta)^{|n/q|} = 1 - |n/q|\,(1.5\alpha + \beta).$$

For small values of m, $N_m/N_3 = (N_3 - |m|)/N_3 = 1 - |m|/N_3$, and hence for the case of small n, we can make the approximation

$$\frac{N(n/q)}{N_3} = 1 - \frac{|n/q|}{N_3}.$$

Using these approximations in Eq. (13.64), the size coefficient is given by

$$A_n^S = \left(\frac{1}{u+b}\right)\left\{\sum_b \left(1 - \frac{|n/q|}{N_3}\right)\left[1 - |n/q|(1.5\alpha + \beta)\right] + \sum_u \left(1 - \frac{|n/q|}{N_3}\right)\right\}.$$

Neglecting the product of small quantities, this reduces to

$$A_n^S = 1 - \left(\frac{1}{u+b}\right)\left\{\sum_b \left[\frac{|n/q|}{N_3} + |n/q|\,(1.5\alpha + \beta)\right] + \sum_u \frac{|n/q|}{N_3}\right\}.$$

From Eq. (13.60),

$$\frac{1}{|q|} = \frac{3B_3\,|\sin\phi|}{b_3'} = \frac{|\sin\phi|}{b_3' d(111)},$$

and with this substitution,

$$A_n^S = 1 - \left(\frac{1}{u+b}\right)\frac{|n|}{b_3'}\left\{\sum_b \left[\frac{|\sin\phi|}{N_3 d(111)} + \frac{|\sin\phi|}{d(111)}(1.5\alpha + \beta)\right] + \sum_u \frac{|\sin\phi|}{N_3 d(111)}\right\}.$$

In terms of crystals made up of N_3-layers of the 111-type where the layers are assumed to be large, $N_3 d(111)$ is the thickness of the crystal in a direction normal to the layers, and $N_3 d(111)/|\sin\phi|$ is the crystal dimension in a direction normal to the reflecting planes. It is convenient to abbreviate this crystal dimension by $D(\phi) = N_3 d(111)/|\sin\phi|$. With the additional substitution

$$\frac{|\sin\phi|}{d(111)} = \frac{|L_0|\,B_3 d}{d(111)} = \frac{|L_0|}{ah_0},$$

the coefficient can be written

$$A_n^S = 1 - \left(\frac{1}{u+b}\right)\frac{|n|}{b_3'}\left\{\sum_{u+b} \frac{1}{D(\phi)} + \sum_b \frac{(1.5\alpha + \beta)\,|L_0|}{ah_0}\right\}.$$

Defining an average crystal dimension D by

$$\frac{1}{D} = \left(\frac{1}{u+b}\right)\sum_{u+b} \frac{1}{D(\phi)}$$

and making the replacement

$$|n|/b_3' = |n|\,a_3' = L,$$

we express the Fourier coefficient in terms of a length L perpendicular to the reflecting planes:

$$A_L^S = 1 - L\left\{\frac{1}{D} + \frac{(1.5\alpha + \beta)}{ah_0(u+b)}\sum_b |L_0|\right\}. \tag{13.69}$$

In general the Fourier coefficients have been determined in terms of fictitious quantities, and converted to the real variable L by the relation $L = n'a_3'$. The values of A_L^S are then plotted against L. When only particle

Table 13.2
CONSTANTS FOR POWDER PATTERNS OF FAULTED FCC METALS

hkl	$\sum_b \frac{(\pm)L_0}{h_0^2(u+b)}$	$\sum_b \frac{\lvert L_0\rvert}{h_0(u+b)}$	$\sum_b (\pm)\frac{L_0}{\lvert L_0\rvert}$
111	$\frac{1}{4}$	$\sqrt{3}/4$	6
200	$-\frac{1}{2}$	1	−6
220	$\frac{1}{4}$	$1/\sqrt{2}$	6
311	$-\frac{1}{11}$	$\frac{3}{2}\sqrt{11}$	0
222	$-\frac{1}{8}$	$\sqrt{3}/4$	−6
400	$\frac{1}{4}$	1	6

size broadening was involved, the intercept of the initial slope on the axis of abscissae gave the average crystal dimension $\langle D\rangle$, as indicated by Fig. 13.11. In the present case we call the intercept D(eff), since it involves both a true particle dimension D, and also a contribution from faulting which acts like a particle size effect. Differentiating Eq. (13.69), we obtain an expression for the intercept D(eff):

$$-\frac{dA_L^S}{dL} = \frac{1}{D(\text{eff})} = \frac{1}{D} + \frac{(1.5\alpha+\beta)}{ah_0(u+b)}\sum_b |L_0|. \tag{13.70}$$

Values of $\sum_b |L_0|/h_0(u+b)$ for FCC powder pattern reflections are given in Table 13.2.

To illustrate the behavior of the faulting term, we now use the constants in Table 13.2 to evaluate Eq. (13.70) for the first two powder pattern reflections 111 and 200:

$$-\left(\frac{dA_L^S}{dL}\right)_{111} = \frac{1}{D(\text{eff. }111)} = \frac{1}{D} + \frac{(1.5\alpha+\beta)}{a}\frac{\sqrt{3}}{2},$$

$$-\left(\frac{dA_L^S}{dL}\right)_{200} = \frac{1}{D(\text{eff. }200)} = \frac{1}{D} + \frac{(1.5\alpha+\beta)}{a}.$$

The contribution to $1/D$(eff) which is due to faulting is evidently $4/\sqrt{3} = 2.3$ times as great for 200 as it is for 111. In cases where the true domain sizes D are so large that $1/D$ can be neglected, the D(eff) ratio will be

$$\frac{D(\text{eff. }111)}{D(\text{eff. }200)} = 4/\sqrt{3} = 2.3.$$

Ratios which are close to this value are often obtained from samples of filings of FCC metals, and it is only by recognizing the effects of faulting that the

numerical ratio can be understood. From the value of D(eff) for any reflection, we obtain only a combination of the domain size D and a faulting probability term $(1.5\alpha + \beta)$. The two quantities can be separated by making use of the *hkl*-dependence of D(eff). From a combination of the numerical values of D(eff, 111) and D(eff, 200), values of D and $(1.5\alpha + \beta)$ are readily determined. From the Fourier coefficients derived from peak broadening, only the combination $(1.5\alpha + \beta)$, and not the individual values of α and β, can be obtained. Fortunately the deformation fault probability α can be determined independently by the peak shift method which has already been developed. We next consider the possibility of obtaining an independent value of β from the peak asymmetry.

c) Twin Fault Probability from the Peak Asymmetry

The twin fault probability β appears in the Fourier sine coefficients of Eqs. (13.63) and (13.65), and it would appear that β could be obtained in a straightforward way by determining the sine coefficients B_n of Eq. (13.63). The method was first used by Wagner,[17] who determined β for several FCC metals by measuring the sine coefficients for the 200-reflection. In principle, β can be obtained in a very simple way by finding the limit of B_n as n approaches zero:

$$(B_n)_{n\to 0} = \frac{\beta}{\sqrt{3}(u+b)} \sum_b (\pm) \frac{L_0}{|L_0|}.$$

However, there are serious difficulties in the experimental evaluation of the sine coefficients. Since the values of B_n are very small, they are extremely sensitive to the exact origin which is chosen, because even a symmetrical peak produces sine coefficients if the origin is displaced slightly from the peak center. Furthermore there is serious overlapping of peaks such as 111 and 200, and a determination of the sine coefficients requires guessing the best separation of the overlapping tails.

A rather simple determination of β can be obtained from the 200 reflection by measuring the value of the ordinate on either side of the peak at two positions which are equidistant from the peak center. To allow for the θ dependency in G, we write $G = G'/\Phi(\theta)$, where

$$\Phi(\theta) = \frac{\sin^2\theta}{f^2(1+\cos^2 2\theta)}.$$

Incorporating the angular factor, and introducing the abbreviation $z = (h_3' - l' - \delta)$, Eq. (13.63) becomes

$$P_{2\theta}'\Phi(\theta) = \frac{G'(u+b)}{b_3'} \sum_n \{A_n \cos 2\pi n z + B_n \sin 2\pi |n| z\}. \quad (13.71)$$

Since $1/D$, α, and β are small, we can make the approximation

$$\frac{N(n/q)}{N_3} Z^{|n/q|} = \left(1 - \frac{1}{b_3' D}\right)^{|n|} \left[1 - \frac{|L_0|}{b_3' a h_0}(1.5\alpha + \beta)\right]^{|n|} = Q^{|n|}, \quad (13.72)$$

where

$$Q = 1 - \frac{1}{b_3'}\left[\frac{1}{D} + \frac{|L_0|}{a h_0}(1.5\alpha + \beta)\right].$$

For the reflection 200, the values of $|L_0|$ and $(\pm)L_0/|L_0|$ are the same for all the broadened components, and the sum over b can be replaced by multiplication by b. Using these results, the sine coefficient of Eq. (13.65) can be approximated by

$$B_n = \frac{b\beta}{\sqrt{3}(u + b)}(\pm)\frac{L_0}{|L_0|} Q^{|n|}.$$

Letting $[P_{2\theta}' \Phi(\theta)]_S$ represent the contribution from the sine terms in Eq. (13.71),

$$[P_{2\theta}' \Phi(\theta)]_S = \frac{G' b\beta}{\sqrt{3}\, b_3'}(\pm)\frac{L_0}{|L_0|} \sum_{n=-\infty}^{+\infty} Q^{|n|} \sin 2\pi |n| z.$$

By expressing $\sin 2\pi |n| z$ in exponential form, the sum is readily evaluated:

$$\sum_{n=-\infty}^{+\infty} Q^{|n|} \sin 2\pi |n| z = \frac{1}{c \tan \pi z}, \quad (13.73)$$

where

$$c = 1 + \left(\frac{1 - Q}{2\sqrt{Q} \sin \pi z}\right)^2.$$

We choose equidistant positions $2\theta_2$ and $2\theta_1$ on the high-angle and low-angle sides of the peak center at $2\theta_0$. The difference between the values of $P_{2\theta}' \Phi(\theta)$ at positions 2 and 1 will be due only to the sine terms, since the contribution from the cosine terms will cancel:

$$[P_{2\theta}' \Phi(\theta)]_2 - [P_{2\theta}' \Phi(\theta)]_1 = \frac{G' b\beta}{\sqrt{3}\, b_3'}(\pm)\frac{L_0}{|L_0|}\left[\frac{1}{c_2 \tan \pi z_2} - \frac{1}{c_1 \tan \pi z_1}\right].$$

Since $z = (h_3' - l' - \delta)$, we obtain from the geometry of Fig. 13.17,

$$z b_3' = \frac{2}{\lambda}(\sin \theta - \sin \theta_0) = \frac{2 \cos \theta_0}{\lambda}(\theta - \theta_0).$$

Let x be an abscissa distance on the recording, measured from the peak center, so that $x = p(\theta - \theta_0)$ and

$$z = \frac{2 \cos \theta_0 x}{\lambda b_3' p}.$$

For the two positions $2\theta_2$ and $2\theta_1$, it follows that $z_1 = -z_2$ and $c_1 = c_2$. If y is an ordinate distance on the corrected plot of $P'_{2\theta}\Phi(\theta)$,

$$P'_{2\theta}\Phi(\theta) = ky$$

and hence

$$k(y_2 - y_1) = \frac{G'b\beta}{\sqrt{3}\, b'_3}(\pm)\frac{L_0}{|L_0|}\frac{2}{c_2 \tan \pi z_2}. \tag{13.74}$$

The constants k and G' of Eq. (13.74) can be evaluated from the peak area. On integrating Eq. (13.71), the contribution by the sine terms drops out and we have

$$\int_{-1/2}^{+1/2} P'_{2\theta}\Phi(\theta)\, dz = \frac{G'(u+b)}{b'_3}\sum_n A_n \frac{\sin \pi n}{\pi n} = \frac{G'(u+b)A_0}{b'_3} = \frac{G'(u+b)}{b'_3}.$$

In terms of distances x and y on the corrected plot

$$\int_{-1/2}^{+1/2} P'_{2\theta}\Phi(\theta)\, dz = \int ky \frac{2\cos\theta_0\, dx}{\lambda b'_3 p} = \frac{k2\cos\theta_0}{\lambda b'_3 p} A,$$

where A is the peak area on the plot. Equating the two expressions,

$$G'(u+b) = \frac{k2\cos\theta_0 A}{\lambda p}.$$

Using this expression for G', and making the replacement

$$\tan \pi z_2 = \pi z_2 = \frac{\pi 2\cos\theta_0}{\lambda b'_3 p} x_2,$$

Eq. (13.74) becomes

$$y_2 - y_1 = \frac{2Ab\beta}{\sqrt{3}\,\pi(u+b)}(\pm)\frac{L_0}{|L_0|}\frac{1}{c_2 x_2}.$$

For the 200-reflection where $(u+b)/b = 1$ and $(\pm)L_0/|L_0| = -1$, the equation reduces to

$$y_1 - y_2 = \frac{2A\beta}{\sqrt{3}\pi}\frac{1}{c_2 x_2}. \tag{13.75}$$

It only remains to evaluate the coefficient c_2. From Eq. (13.72), it follows that $1 - Q$ can be expressed in terms of the D(eff. 200)-value of Eq. (13.70) which is obtained from the initial slope of the plot of the Fourier coefficients:

$$1 - Q = \frac{1}{b'_3}\left[\frac{1}{D} + \frac{|L_0|}{ah_0}(1.5\alpha + \beta)\right] = \frac{1}{b'_3 D(\text{eff. } 200)}.$$

Using this expression in Eq. (13.73), and making the approximations $\sqrt{Q} = 1$

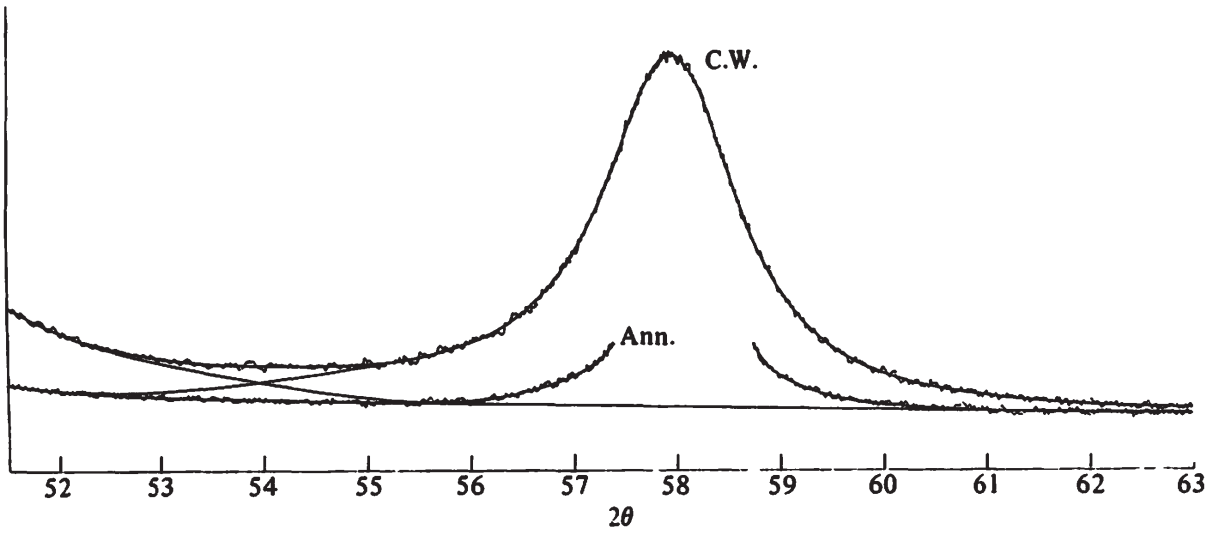

Fig. 13.19 Diffractometer recordings of the (200) peak of 70–30α brass for a cold-worked and an annealed sample. The cold-worked sample was filings made under liquid nitrogen. Radiation Co$K\alpha$. The pattern of the annealed sample serves to determine the background level between (111) and (200) where there is overlapping of the tails.

and $\sin \pi z_2 = \pi z_2 = 2\pi(\sin \theta_2 - \sin \theta_0)/\lambda b_3$, we obtain a simple expression for c_2:

$$c_2 = 1 + \left[\frac{\lambda}{4\pi D(\text{eff. } 200)(\sin \theta_2 - \sin \theta_0)}\right]^2.$$

Combining with Eq. (13.75), we obtain a final expression for β:

$$\beta = \frac{\sqrt{3}\,\pi x_2(y_1 - y_2)}{2A}\left\{1 + \left[\frac{\lambda}{4\pi D(\text{eff. } 200)(\sin \theta_2 - \sin \theta_0)}\right]^2\right\}. \quad (13.76)$$

To illustrate the use of Eq. (13.76), we consider a sample of 70–30α brass, cold worked by making filings under liquid nitrogen. Figure 13.19 shows diffractometer recordings at room temperature with Co$K\alpha$ radiation for the cold-worked sample and for a similar annealed sample. Since there is overlapping of the tails between the 111 and 200 peaks, the pattern of the annealed sample is necessary for determining the background level of the cold-worked sample. The tails of the two peaks are readily resolved to an accuracy which is good enough for the kind of analysis which is being used. The ordinates above background for the 200 peak are now multiplied by $\Phi(\theta)$ and the corrected values are shown by Fig. 13.20. The peak center, measured near the top of the peak, is at $2\theta_0 = 57.98°$. We choose equidistant positions $2\theta_2 = 59.50°$ and $2\theta_1 = 56.45°$ as indicated. The choice in positions is a compromise. We wish $2\theta_1$ to be so large that there will be no contribution from the tail of 111, but on the other hand the two positions should be well removed from $2\theta_0$ so that the difference in ordinates will not depend critically

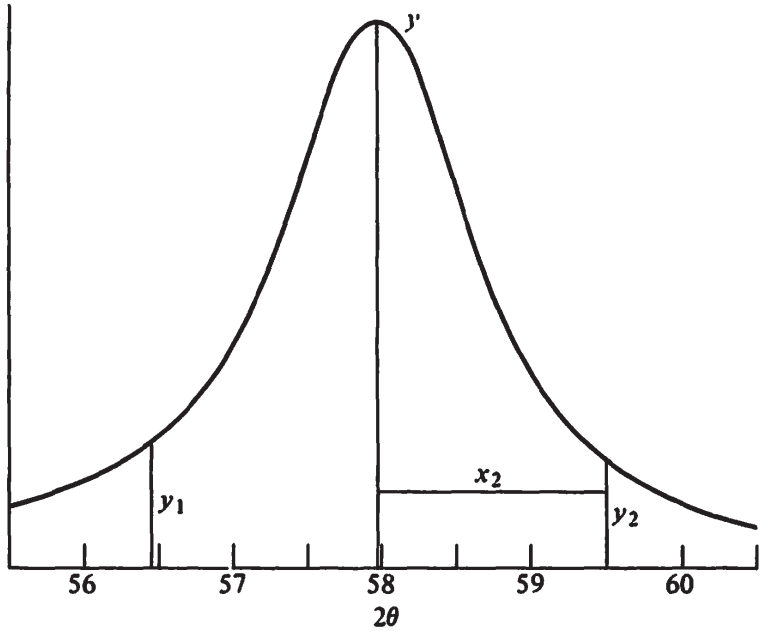

Fig. 13.20 The corrected ordinates $P'(2\theta)\,\Phi(2\theta)$ for the (200) peak of cold-worked 70–30α brass obtained from Fig. 13.19. The twin fault probability β is obtained from the asymmetry of this peak.

on the center position. The measured values are $y_1 = 4.20$ cm, $y_2 = 3.56$ cm, $x_2 = 7.8$ cm, $A = 212$ cm^2, and $\sin\theta_2 - \sin\theta_0 = 0.0117$. From Wagner's[17] measurement on 70–30 brass filed under liquid nitrogen, D(eff. 200) = 38 A. Using these values in Eq. (13.76), we obtain

$$\beta = \frac{\sqrt{3}\,\pi \times 7.8(4.20 - 3.56)}{2 \times 212}\left\{1 + \left(\frac{1.790}{4\pi \times 38 \times 0.0117}\right)^2\right\} = 0.07.$$

The value of β depends critically on the difference in ordinates $(y_1 - y_2)$ and since this difference is always very small, it is not possible to obtain an accurate value of β from the peak asymmetry. The above value $\beta = 0.07$ is probably uncertain by at least $\pm 20\%$. There is an additional ambiguity due to the fact that the value of β which is obtained is based on the assumption that all of the corrected peak asymmetry is due to twin faulting. It was shown by Warren[18] that double deformation faulting produces a peak asymmetry which is completely similar to that resulting from twin faulting, and hence it is uncertain how much of the value of β which is obtained represents twin faulting and how much represents double deformation faulting.

13.6 EFFECTS OF DEFORMATION AND TWIN FAULTING IN HCP METALS

Both growth faults and deformation faults are possible on the 002 planes of a HCP structure. The effect of growth faults has been treated by Wilson,[19] in a paper which was probably the first systematic treatment of the effect of

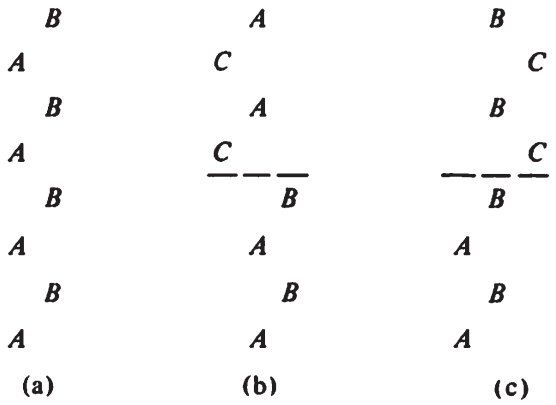

Fig. 13.21 Sequences in the stacking of 002 layers in the HCP structure. (a) The normal *ABAB* sequence. (b) A deformation fault. (c) A growth fault.

stacking faults in a metal. The effect of deformation faulting in HCP metals has been given by Christian.[20] The two kinds of fault are illustrated by Fig. 13.21. The normal sequence is represented by *ABAB*, but it could just as well be designated by *BCBC* or *CACA*. For the correct HCP sequence, each layer should be the same as the layer two steps below. In the deformation fault represented by (b), everything above the dashed line is shifted so that the layer which should be *A* becomes instead *C*. A growth fault is represented by (c), and here we think of the crystal as being built up layer by layer. The first layer above the dashed line should be *A*, but we suppose that for some reason it takes the position *C*. The next layer takes the position *B* so as to be the same as the layer two steps down. As before, let α be the probability of a deformation fault and β the probability of a growth fault.

We consider first the effect of deformation faulting alone. Figure 13.22(a) illustrates all the possibilities in the $m-2$ and $m-1$ layers which lead to

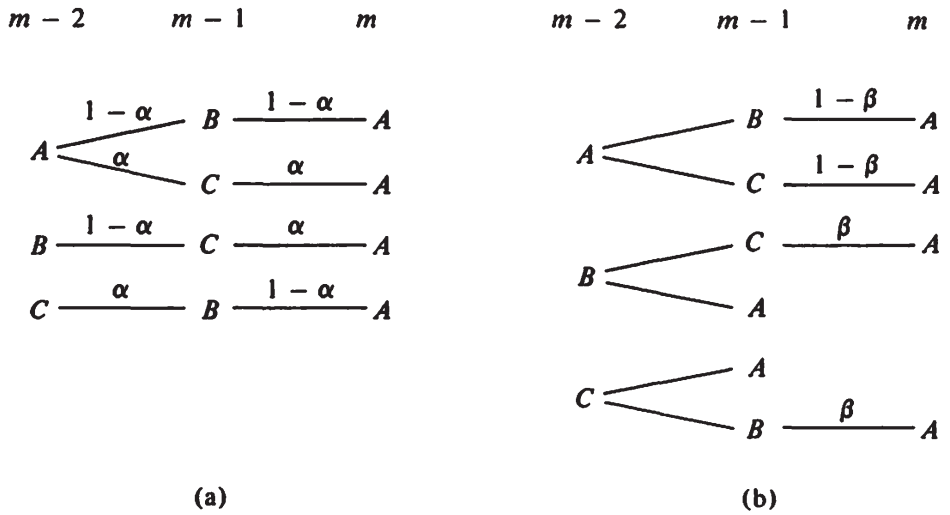

Fig. 13.22 Sequences in the three layers $m-2$, $m-1$ and m which lead to an *A* position in the *m*th layer for a HCP structure. (a) In terms of deformation faulting. (*b*) In terms of growth faulting.

an A-position in the mth layer. In the two sequences ABA and ACA, regardless of whether A should be followed by B or by C, one sequence will involve the probability $(1 - \alpha)^2$ and the other α^2. The probability of the sequence BCA will be $(1 - \alpha)\alpha$ or $\alpha(1 - \alpha)$ depending on whether or not B should be followed by C. Similarly the probability of the sequence CBA will be either $\alpha(1 - \alpha)$ or $(1 - \alpha)\alpha$. Allowing for all possibilities, the mth layer is given by

$$P_m^A = P_{m-2}^A[(1 - \alpha)^2 + \alpha^2] + [P_{m-2}^B + P_{m-2}^C]\alpha(1 - \alpha).$$

With the additional relation $P_{m-2}^A + P_{m-2}^B + P_{m-2}^C = 1$, and dropping quadratic terms, we obtain

$$P_m^A - P_{m-2}^A = \alpha(1 - 3P_{m-2}^A). \tag{13.77}$$

We consider next the effect of growth faulting alone. The sequences leading to an A-position in the mth layer are shown by Fig. 13.22(b). The sequences ABA and ACA are labeled $1 - \beta$, since they are in the correct order. The sequences BCA and CBA are labeled β since they make the mth layer different from the $m - 2$ layer. The probability of finding an A-position in an average mth layer is given by

$$P_m^A = P_{m-2}^A(1 - \beta) + (P_{m-2}^B + P_{m-2}^C - P_{m-1}^A)\beta.$$

With the relation $P_{m-2}^A + P_{m-2}^B + P_{m-2}^C = 1$, we obtain

$$P_m^A - P_{m-2}^A = \beta(1 - P_{m-1}^A - 2P_{m-2}^A). \tag{13.78}$$

If there is no faulting, $P_m^A - P_{m-2}^A = 0$. Assuming that α and β are each so small that neither one has any appreciable effect on the other, the contributions to $P_m^A - P_{m-2}^A$ from Eqs. (13.77) and (13.78) are additive:

$$P_m^A - P_{m-2}^A = \alpha(1 - 3P_{m-2}^A) + \beta(1 - P_{m-1}^A - 2P_{m-2}^A).$$

Rearranging, we obtain a difference equation for combined deformation and twin faulting, which to first order is equivalent to that of Gevers:[21]

$$P_m^A + \beta P_{m-1}^A - (1 - 3\alpha - 2\beta)P_{m-2}^A = \alpha + \beta. \tag{13.79}$$

Considering first the case that m is positive, we try a solution of the form $P_m^A = a + bx^m$, where a, b, and x are independent of m. Inserting this in Eq. (13.79) we find $a = \frac{1}{3}$ and $x^2 + \beta x - (1 - 3\alpha - 2\beta) = 0$. With the abbreviation $s = (1 - 3\alpha - 2\beta)^{1/2}$, the two solutions to the quadratic equation are given by $x = -\beta/2 \pm s$. To be able to satisfy the boundary conditions, we must use both solutions:

$$P_m^A = \tfrac{1}{3} + b_1(-\beta/2 + s)^m + b_2(-\beta/2 - s)^m. \tag{13.80}$$

Let P_m^0 be the probability that the mth layer is the same as the origin layer,

and let P_m^+ and P_m^- be the probabilities that the mth layer is displaced from the origin layer by displacements $\boldsymbol{\delta}^+ = (-\mathbf{A}_1 + \mathbf{A}_2)/3$ and $\boldsymbol{\delta}^- = (\mathbf{A}_1 - \mathbf{A}_2)/3$. Since the origin layer can be called A, Eq. (13.80) gives the value of P_m^0. The coefficients b_1 and b_2 are determined by the two boundary conditions:

$$P_0^0 = 1, \qquad 1 = \tfrac{1}{3} + b_1 + b_2,$$

$$P_1^0 = 0, \qquad 0 = \tfrac{1}{3} + b_1(-\beta/2 + s) + b_2(-\beta/2 - s).$$

With approximations which are appropriate for small values of α and β, and replacing m by $|m|$ since $P_{-m}^0 = P_m^0$, we obtain an expression for P_m^0 which is correct for either positive or negative values of m:

$$P_m^0 = \frac{1}{3} + \frac{1}{6}\left(1 - \frac{3\alpha}{2}\right)\left(1 - \frac{3\alpha}{2} - \frac{3\beta}{2}\right)^{|m|} + \frac{1}{6}\left(3 + \frac{3\alpha}{2}\right)\left(1 - \frac{3\alpha}{2} - \frac{\beta}{2}\right)^{|m|}(-1)^m. \quad (13.81)$$

We use ordinary hexagonal axes $\mathbf{A}_1\mathbf{A}_2\mathbf{A}_3$ where $|\mathbf{A}_3|$ is twice the layer spacing, and reciprocal vectors $\mathbf{B}_1\mathbf{B}_2\mathbf{B}_3$ which are reciprocal to the $\mathbf{A}_1\mathbf{A}_2\mathbf{A}_3$. The indices HKL_0 are the corresponding hexagonal indices. The intensity is given by a summation over layers similar to that used for Eq. (13.39):

$$I = \psi^2 \sum_{m=-\infty}^{+\infty} N_m \langle \exp [i\phi_m] \rangle \exp [2\pi i m h_3/2], \quad (13.82)$$

where ψ^2 is given by Eq. (13.37), N_m is the number of layers having an mth neighbor, and $\phi_m = 2\pi(h_1\mathbf{B}_1 + h_2\mathbf{B}_2 + h_3\mathbf{B}_3) \cdot \boldsymbol{\delta}_m$. For a HCP structure $P_m^+ = P_m^- = (1 - P_m^0)/2$, and the average over the three values of $\boldsymbol{\delta}_m$ becomes

$$\langle \exp [i\phi_m] \rangle = P_m^0 + \{e^{-2\pi i(h_1 - h_2)/3} + e^{2\pi i(h_1 - h_2)/3}\}(1 - P_m^0)/2.$$

Since ψ^2 differs significantly from zero only if h_1 and h_2 have approximately the integral values H and K, we can write

$$\langle \exp [i\phi_m] \rangle = P_m^0 + (1 - P_m^0) \cos 2\pi(H - K)/3.$$

If $H - K = 3N$, then $\langle \exp [i\phi_m] \rangle = 1$, and the reflection is independent of stacking faults.

If $H - K = 3N \pm 1$, then $\langle \exp [i\phi_m] \rangle = (-1 + 3P_m^0)/2$ and Eq. (13.82) becomes

$$I = \frac{\psi^2}{4} \sum_{m=-\infty}^{+\infty} N_m \left\{ \left(1 - \frac{3\alpha}{2}\right)\left(1 - \frac{3\alpha}{2} - \frac{3\beta}{2}\right)^{|m|} + (-1)^m \left(3 + \frac{3\alpha}{2}\right)\left(1 - \frac{3\alpha}{2} - \frac{\beta}{2}\right)^{|m|} \right\} \cos \pi m h_3.$$

The equation is conveniently written as the sum of two terms:

$$I = \frac{\psi^2}{4}\left(1 - \frac{3\alpha}{2}\right)\sum_{m=-\infty}^{+\infty} N_m\left(1 - \frac{3\alpha}{2} - \frac{3\beta}{2}\right)^{|m|} \cos 2\pi m\left(\frac{h_3 - L_0 + L_0}{2}\right)$$
$$+ \frac{\psi^2}{4}\left(3 + \frac{3\alpha}{2}\right)\sum_{m=-\infty}^{+\infty} N_m\left(1 - \frac{3\alpha}{2} - \frac{\beta}{2}\right)^{|m|} \cos 2\pi m\left(\frac{h_3 - L_0 + L_0 + 1}{2}\right). \tag{13.83}$$

The first term in Eq. (13.83) gives a peak at $h_3 = L_0$ if L_0 is even, and the second term gives a peak at $h_3 = L_0$ if L_0 is odd. Deformation faults decrease slightly the intensity for peaks with L_0 even, and increase the intensity for peaks with L_0 odd. The broadening due to deformation faults is the same for L_0 even or odd, but the broadening due to growth faults is only one-third as large for L_0 odd as for L_0 even. There are no peak displacements and no peak asymmetries as a result of either deformation or growth faults.

We now convert to the observable power distribution in a powder pattern reflection, using the powder pattern power theorem, and following the same procedure that was used for the FCC case in starting from Eq. (13.55). If N_3 is the average number of layers in a crystal, and if N_3 is large and α and β small, we can make an approximation which is valid for small values of m:

$$N_m\left(1 - \frac{3\alpha}{2} - \frac{3\beta}{2}\right)^{|m|} = N_3\left(1 - \frac{|m|}{N_3}\right)\left(1 - \frac{3\alpha}{2} - \frac{3\beta}{2}\right)^{|m|}$$
$$= N_3\left[1 - |m|\left(\frac{1}{N_3} + \frac{3\alpha}{2} + \frac{3\beta}{2}\right)\right].$$

Considering each reflection as $00l'$ in terms of orthorhombic axes a_3' and b_3', we express the powder pattern peak shapes $P_{2\theta}'$ for $H - K = 3N \pm 1$ by two Fourier series in which the Fourier coefficients are correctly expressed only for small values of n:

L_0 even:

$$P_{2\theta}' = \frac{G}{4b_3'}\left(1 - \frac{3\alpha}{2}\right)\sum_n \left\{1 - \frac{|n|}{b_3'}\left[\frac{1}{D} + \frac{|L_0|\,d}{c^2}(3\alpha + 3\beta)\right]\right\} \cos 2\pi n(h_3' - l'), \tag{13.84}$$

L_0 odd:

$$P_{2\theta}' = \frac{G}{4b_3'}\left(3 + \frac{3\alpha}{2}\right)\sum_n \left\{1 - \frac{|n|}{b_3'}\left[\frac{1}{D} + \frac{|L_0|\,d}{c^2}(3\alpha + \beta)\right]\right\} \cos 2\pi n(h_3' - l'),$$

where d is the spacing for the HKL_0-reflection, $c = A_3$, and D is the average crystal dimension in a direction normal to the reflecting planes. The peak shape is expressed in terms of the variable $(h_3' - l') = 2a_3'(\sin\theta - \sin\theta_0)/\lambda$, and the fictitious axis a_3' is chosen to correspond to the $\sin\theta$ interval within

which the peak is expressed as a Fourier series. If in addition to faults, there are also distortions, we will assume that it is a good enough approximation to merely add a symmetrical distortion coefficient to Eqs. (13.84). Either equation can then be expressed in the form

$$P'_{2\theta} = KG \sum_n A_n^S A_n^D \cos 2\pi n(h'_3 - l').$$

The size coefficients A_n^S include the effects of domain size and faulting, and it is convenient to express them in terms of a length $L = na'_3 = n/b'_3$. If distortions are negligible, or have been corrected by the use of multiple orders, we can obtain the size coefficients. Normalizing by the condition $A_L^S = 1.0$ for $L = 0$, we then make plots of A_L^S against L. From the initial slopes of these plots, we determine three different combinations of D, α, and β:

$$\begin{aligned}
&H - K = 3N: && -\left(\frac{dA_L^S}{dL}\right)_0 = \frac{1}{D},\\
&H - K = 3N \pm 1, \quad L_0 = \text{even}: && -\left(\frac{dA_L^S}{dL}\right)_0 = \frac{1}{D} + \frac{|L_0|\,d}{c^2}(3\alpha + 3\beta),\\
&H - K = 3N \pm 1, \quad L_0 = \text{odd}: && -\left(\frac{dA_L^S}{dL}\right)_0 = \frac{1}{D} + \frac{|L_0|\,d}{c^2}(3\alpha + \beta).
\end{aligned} \tag{13.85}$$

For cases where $1/D$ is negligibly small, or if it can be assumed constant for planes which are nearly parallel, the different dependence of $(-dA_L^S/dL)_0$ on D, α, and β allows all three of these quantities to be determined from suitable combinations of reflections.

Stacking faults are sometimes found in a HCP metal such as cobalt with no appreciable distortion and large coherent domains. For this case the reflections with $H - K = 3N$ will be sharp, but those with $H - K = 3N \pm 1$ will be broadened by faulting. Neglecting instrumental broadening or making a rough correction, it is then possible to obtain values for α and β directly from the peak breadths. We will consider the full breadth at half the maximum intensity, since this is an easier quantity to measure than the integral breadth. In the intensity expressions of Eq. (13.83), N_m can be replaced by N_3 and taken outside of the summation, since we are restricting ourselves to the case that true particle size broadening is negligible compared to that due to faulting. The peak ordinate is then proportional to

$$Y = \sum_{m=-\infty}^{+\infty} x^{|m|} \cos \pi m(h_3 - L) = \frac{1 - x^2}{1 + x^2 - 2x \cos \pi(h_3 - L_0)},$$

where for

$$\begin{aligned}
L_0 \text{ even}: &\quad x = 1 - (3\alpha + 3\beta)/2,\\
L_0 \text{ odd}: &\quad x = 1 - (3\alpha + \beta)/2.
\end{aligned}$$

For $h_3 - L_0 = 0$, there is a maximum value $Y_m = (1 + x)/(1 - x)$. If $B(h_3)$ is the full width at half maximum in terms of the variable h_3, we have

$$\frac{(1+x)}{2(1-x)} = \frac{1-x^2}{1+x^2-2x\cos[\pi B(h_3)/2]},$$

from which to a good approximation $B(h_3) = (1 - x)2/\pi$.

On the powder pattern let $B^0_{2\theta}$ be the full width at half maximum intensity expressed in degrees 2θ. From Fig. 13.17, we have the relations

$$B^0_{2\theta} = \frac{180\lambda B_3 |\sin\phi| B(h_3)}{\pi\cos\theta},$$

$$|\sin\phi| = |L_0| B_3 d,$$

and $B^0_{2\theta}$ is given by

$$B^0_{2\theta} = (360/\pi^2)\tan\theta\,|L_0|\,(d/c)^2 2(1-x),$$

where d is the HKL_0-spacing, and $c = A_3 = 2d_{002}$. For reflections of the type $H - K = 3N \pm 1$, equations which are useful for a direct determination of α and β from the measured full breadth at half maximum intensity are given by

$$\begin{aligned} L_0 \text{ even:} \quad & B^0_{2\theta} = (360/\pi^2)\tan\theta\,|L_0|\,(d/c)^2(3\alpha + 3\beta), \\ L_0 \text{ odd:} \quad & B^0_{2\theta} = (360/\pi^2)\tan\theta\,|L_0|\,(d/c)^2(3\alpha + \beta). \end{aligned} \tag{13.86}$$

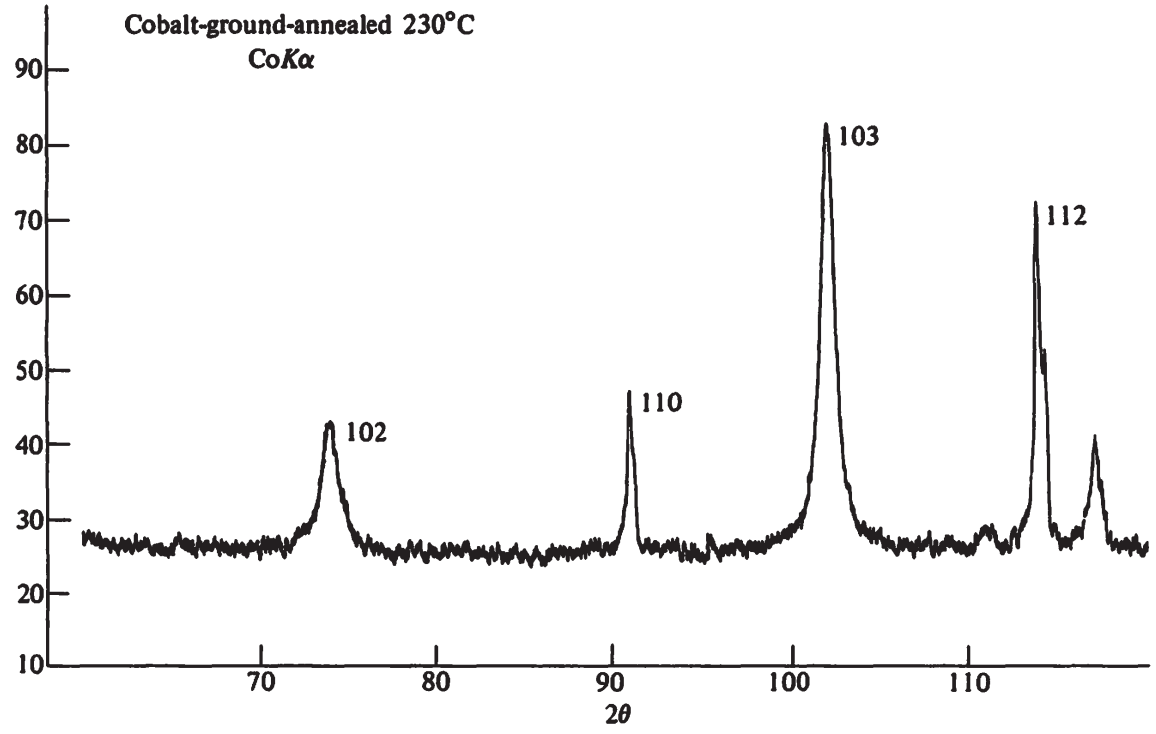

Fig. 13.23 Diffractometer recording for HCP cobalt, cold worked by grinding, and then annealed at 230°C for 2 hours. Radiation Co$K\alpha$. The broadening of 102 and 103 is due to both deformation and growth faulting.

Broadening by faulting in a HCP metal is illustrated by the diffractometer tracing of Fig. 13.23. The sample is cobalt powder, cold-worked by grinding, and then annealed at 230°C for 2 hours. The reflections 110 and 112 are sharp since they are independent of faulting. The broadening of 102 and 103 is due to both deformation and growth faulting.

13.7 EFFECT OF DEFORMATION AND TWIN FAULTS IN BCC METALS

In BCC metals, deformation faults and twin faults are possible on the 211-planes. The effect of faulting on the diffraction pattern has been treated by Hirsch and Otte[22] and by Guentert and Warren.[23] The study of faults on the 211-planes of a BCC structure, with cubic axes $\mathbf{a}_1\mathbf{a}_2\mathbf{a}_3$ and indices hkl is greatly facilitated by using orthorhombic axes $\mathbf{A}_1\mathbf{A}_2\mathbf{A}_3$ and orthorhombic indices HKL_0. The transformation is given by

$$\begin{aligned} \mathbf{A}_1 &= \mathbf{a}_1 - \mathbf{a}_2, & H &= h - k, \\ \mathbf{A}_2 &= \mathbf{a}_1/2 + \mathbf{a}_2/2 + \mathbf{a}_3/2, & K &= h/2 + k/2 + l/2, \\ \mathbf{A}_3 &= -\mathbf{a}_1 - \mathbf{a}_2 + 2\mathbf{a}_3, & L_0 &= -h - k + 2l. \end{aligned} \tag{13.87}$$

The equations define $\mathbf{A}_1$ and $\mathbf{A}_2$ as orthogonal axes in the cubic $\bar{1}\bar{1}2$-plane, with $\mathbf{A}_2$ in the cubic [111]-direction, and $\mathbf{A}_3$ perpendicular to the $\bar{1}\bar{1}2$-plane. The new cell can be considered as being built up of six $\bar{1}\bar{1}2$ layers, each of which contributes one atom to the cell. The positions of the six atoms can be designated as $AB'CA'BC'$ as shown by Fig. 13.24. The number within each

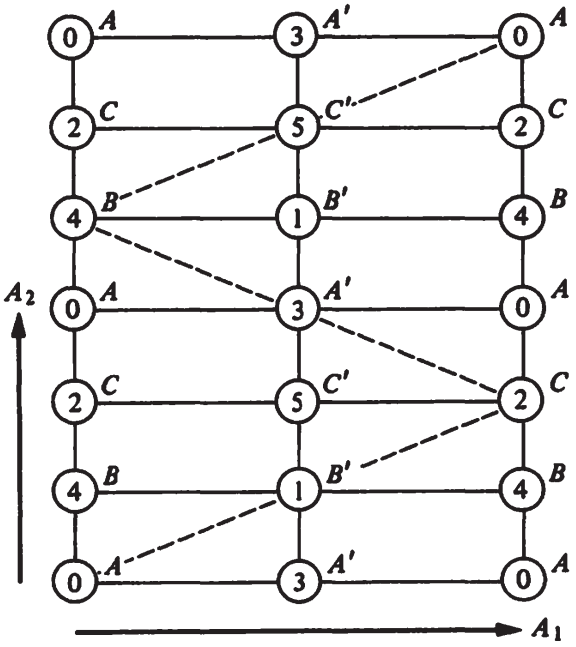

Fig. 13.24 Representation of the structure of a BCC element in terms of orthorhombic axes $\mathbf{A}_1\mathbf{A}_2\mathbf{A}_3$. The structure is shown as a stacking of cubic $\bar{1}\bar{1}2$ layers. The figure within each circle gives the number of the layer. The dashed line follows the correct BCC sequence $AB'CA'BC'A$.

circle gives the number of the layer. A deformation fault above layer 2 would give the sequence $AB'CB'CA'B$ in which everything above layer 2 has been shifted by $-2\mathbf{A}_3/3$ or $+\mathbf{A}_3/3$. A twin on layer 2 would be represented by the sequence $AB'CB'AC'$. At a deformation fault two layers are directly over second neighboring layers, and at a twin fault one layer is directly over a second neighbor layer. A slight expansion of the spacing would be required if the atoms were considered to be hard spheres, but to simplify the presentation we shall neglect this expansion. We let α and β be the probabilities for deformation faults and twin faults.

The intensity per crystal is given by a summation over layers similar to that of Eq. (13.39):

$$I = \psi^2 \sum_{m=-\infty}^{+\infty} N_m \langle \exp [i\phi_m] \rangle \exp [2\pi i m h_3/6], \tag{13.88}$$

where N_m is the number of layers having an mth neighbor, $\phi_m = 2\pi(h_1\mathbf{B}_1 + h_2\mathbf{B}_2 + h_3\mathbf{B}_3) \cdot \boldsymbol{\delta}_m$, and ψ^2 is given by Eq. 13.37.

Referring to Fig. 13.24, it is evident that the primed positions are displaced from the unprimed positions by $\mathbf{A}_1/2$. In the stacking of layers, an unprimed position can only be followed by a primed position, for example A in the zero layer can be followed only by B' or C' in the first layer. For considering sequences, it is a considerable simplification to first disregard the difference between primed and unprimed positions, since the additional displacement $\mathbf{A}_1/2$ is conveniently put in later. With this simplification, the correct sequence is expressed by $ABCABC$, exactly the same as for the FCC case.

For deformation faulting only, the sequences leading to an A-position in the mth layer are represented by Fig. 13.15, and from Eq. (13.40) we have

$$P_m^A + P_{m-1}^A + P_{m-2}^A - 1 = \alpha(1 - \alpha)(3P_{m-2}^A - 1).$$

For twin faulting only, the sequences are represented by Fig. 13.16, and from Eq. (13.41),

$$P_m^A + P_{m-1}^A + P_{m-2}^A - 1 = \beta(P_{m-1}^A + 2P_{m-2}^A - 1).$$

Assuming that α and β are each so small that neither one has any appreciable effect on the other, the two contributions to $P_M^A + P_{M-1}^A + P_{M-2}^A - 1$ are additive. Neglecting quadratic terms, we obtain a difference equation for combined deformation and twin faulting which is identical to Eq. (13.42):

$$P_m^A + (1 - \beta)P_{m-1}^A + (1 - 3\alpha - 2\beta)P_{m-2}^A = 1 - \alpha - \beta.$$

Considering first that m is positive, we try a solution $P_m^A = a + bx^m$, as was done with Eq. (13.42). Following the same steps, and using the same notation, we obtain the result expressed by Eq. (13.49):

$$P_m^0 = \tfrac{1}{3}\{1 + 2(-1)^m Z^m[\cos m\gamma + (\beta/s) \sin m\gamma]\}.$$

For the case that m is negative, we try a solution $P_m^A = a + bx^{-m}$. With the same notation we find

$$P_m^0 = \tfrac{1}{3}\{1 + 2(-1)^m Z^{-m}[\cos m\gamma - (\beta/s)\sin m\gamma]\}.$$

Hence for m either positive or negative, we can write a general expression for P_m^0:

$$P_m^0 = \tfrac{1}{3}\{1 + 2(-1)^m Z^{|m|}[\cos m\gamma + (\beta/s)\sin |m|\,\gamma]\}. \qquad (13.89)$$

In writing expressions for the displacements δ_m, we now allow for the difference between primed and unprimed positions by adding a term $mA_1/2$, since if m is odd, the zero and the mth layer must be different (one primed and the other unprimed). The probabilities, displacements, and phases are as follows:

$$\begin{aligned}
P_m^0: &\quad \delta_m^0 = mA_1/2, &&\quad \phi_m = 2\pi m h_1/2,\\
P_m^+: &\quad \delta_m^+ = mA_1/2 + A_2/3, &&\quad \phi_m = 2\pi(mh_1/2 + h_2/3),\\
P_m^-: &\quad \delta_m^- = mA_1/2 - A_2/3, &&\quad \phi_m = 2\pi(mh_1/2 - h_2/3).
\end{aligned}$$

The average phase factor is expressed by

$$\langle \exp[i\phi_m]\rangle = \exp[\pi i m h_1]\{P_m^0 + P_m^+ \exp[2\pi i h_2/3] + P_m^- \exp[-2\pi i h_2/3]\}.$$

For a powder pattern $P_m^+ = P_m^- = (1 - P_m^0)/2$. Since ψ^2 differs from zero only if h_1 and h_2 are close to the integral values H and K, the expression simplifies to

$$\langle \exp[i\phi_m]\rangle = \exp[\pi i m H]\{P_m^0 + (1 - P_m^0)\cos 2\pi K/3\}. \qquad (13.90)$$

There are two cases to consider. If $K = 3N$, then $\langle \exp[i\phi_m]\rangle = \exp[\pi i m H]$, independent of stacking faults. If $K = 3N \pm 1$, then

$$\langle \exp[i\phi_m]\rangle = \exp[\pi i m H](-1 + 3P_m^0)/2.$$

From Eq. (13.87), it follows that $K - L_0 = 3M$, since for all BCC reflections $h + k + l =$ even. Hence $K = 3N$ is equivalent to $L_0 = 3N$, and $K = 3N \pm 1$ is equivalent to $L_0 = 3N \pm 1$.

We now consider reflections of the type $L_0 = 3N \pm 1$ where

$$\langle \exp[i\phi_m]\rangle = \exp[\pi i m H](-1 + 3P_m^0)/2.$$

Introducing Eq. (13.89), we obtain

$$\langle \exp[i\phi_m]\rangle = \exp[\pi i m H](-1)^m Z^{|m|}[\cos m\gamma + (\beta/\sqrt{3})\sin |m|\,\gamma].$$

Using this expression in Eq. (13.88), the intensity is given by

$$I = \psi^2 \sum_{m=-\infty}^{+\infty} N_m Z^{|m|}[\cos m\gamma + (\beta/\sqrt{3})\sin |m|\,\gamma] \exp\left[2\pi i m\left(\frac{h_3}{6} + \frac{H}{2} + \frac{1}{2}\right)\right].$$

All the factors preceding the exponential are even in m, and hence the

exponential can be replaced by a cosine term:

$$I = \psi^2 \sum_{m=-\infty}^{+\infty} N_m Z^{|m|}[\cos m\gamma + (\beta/\sqrt{3}) \sin |m|\,\gamma] \cos 2\pi m\left(\frac{h_3}{6} + \frac{H}{2} + \frac{1}{2}\right). \tag{13.91}$$

From Eq. (13.48), $\gamma = \pi/3 - \sqrt{3}\alpha/2$. With this value for γ, and the usual relations for $\cos A \cos B$ and $\cos A \sin B$, we split Eq. (13.91) into two terms:

$$\begin{aligned} I = \frac{\psi^2}{2} \sum_m N_m Z^{|m|} \Bigg\{ & \cos 2\pi m\left(\frac{h_3}{6} + \frac{H}{2} + \frac{1}{3} + \frac{\sqrt{3}\alpha}{4\pi}\right) \\ & - \frac{\beta}{\sqrt{3}} \sin 2\pi |m| \left(\frac{h_3}{6} + \frac{H}{2} + \frac{1}{3} + \frac{\sqrt{3}\alpha}{4\pi}\right)\Bigg\} + \frac{\psi^2}{2} \sum_m N_m Z^{|m|} \\ & \times \left\{\cos 2\pi m\left(\frac{h_3}{6} + \frac{H}{2} - \frac{1}{3} - \frac{\sqrt{3}\alpha}{4\pi}\right) + \frac{\beta}{\sqrt{3}} \sin 2\pi |m| \left(\frac{h_3}{6} + \frac{H}{2} - \frac{1}{3} - \frac{\sqrt{3}\alpha}{4\pi}\right)\right\}. \end{aligned} \tag{13.92}$$

In the variables for the upper and lower terms, we add and subtract $L_0/6$, and use the relation $H = L_0 + 2(h - l)$ from Eq. (13.87). For the upper term, the variable becomes $(h_3 - L_0)/6 + Q + \sqrt{3}\alpha/4\pi$, where $Q = [4L_0 + 6(h - l) + 2]/6$. If $L_0 = 3N + 1$, Q is an integer, and the variable reduces to $(h_3 - L_0)/6 + \sqrt{3}\alpha/4\pi$. Hence the upper term will give a peak in the vicinity of $h_3 = L_0$ if $L_0 = 3N + 1$. Similarly the lower term will give a peak in the vicinity of $h_3 = L_0$ if $L_0 = 3N - 1$. If one of the terms gives a reflection HKL_0, the other will give the twin reflection HKL_0. On the 2θ-scale of a powder pattern, either reflection and its twin have the same peak displacement and peak asymmetry. Hence it is possible to replace the two terms of Eq. (13.92) by twice the value of either one of them, if proper signs are ensured. The upper term peaks near $h_3 = L_0$, where $L_0 = 3N + 1$, and the lower term near $h_3 = L_0$, where $L_0 = 3N - 1$. Hence letting the choice in sign ($\pm$) be fixed by $L_0 = 3N \pm 1$, for purposes of a powder pattern Eq. (13.92) can be condensed to

$$\begin{aligned} I = \psi^2 \sum_m N_m Z^{|m|} \Bigg\{ & \cos 2\pi m\left(\frac{h_3 - L_0}{6} \pm \frac{\sqrt{3}\alpha}{4\pi}\right) \\ & - (\pm)\frac{\beta}{\sqrt{3}} \sin 2\pi |m| \left(\frac{h_3 - L_0}{6} \pm \frac{\sqrt{3}\alpha}{4\pi}\right)\Bigg\}. \end{aligned}$$

With the same notation, and using the powder pattern power theorem in the same way that it was used for the FCC case, we express the contribution

of the reflection HKL_0 to the observable $P'_{2\theta}$ for a powder pattern:

$$P'_{2\theta} = \frac{G}{6B_3|\sin\phi|}\sum_m \frac{N_m}{N_3} Z^{|m|} \times \left\{\cos 2\pi m\left(\frac{h_3 - L_0}{6} \pm \frac{\sqrt{3}\alpha}{4\pi}\right) - (\pm)\frac{\beta}{\sqrt{3}}\sin 2\pi|m|\left(\frac{h_3 - L_0}{6} \pm \frac{\sqrt{3}\alpha}{4\pi}\right)\right\}.$$

For purposes of a Fourier analysis, it is convenient to treat each reflection as a $00l'$ in terms of a new set of orthorhombic axes $\mathbf{a}'_1\mathbf{a}'_2\mathbf{a}'_3$ and corresponding reciprocal axes $\mathbf{b}'_1\mathbf{b}'_2\mathbf{b}'_3$. The connecting relations are obtained from Fig. 13.17:

$$\frac{2\sin\theta}{\lambda} = h'_3 b'_3, \qquad (h_3 - L_0)B_3\sin\phi = (h'_3 - l')b'_3.$$

With the abbreviations

$$q = \frac{b'_3}{6B_3\sin\phi}, \qquad \epsilon = \frac{\sqrt{3}\alpha}{4\pi q}, \tag{13.93}$$

and the relations of Eqs. (13.61a) and (13.61b), the contribution of the reflection HKL_0 is represented by

$$P'_{2\theta} = \frac{G}{b'_3}\sum_n \frac{N(n/q)}{N_3} Z^{|n/q|} \times \left\{\cos 2\pi n(h'_3 - l' \pm \epsilon) - (\pm)\frac{L_0}{|L_0|}\frac{\beta}{\sqrt{3}}\sin 2\pi|n|(h'_3 - l' \pm \epsilon)\right\}. \tag{13.94}$$

Each powder pattern reflection contains contributions from several components, some of which are broadened by faulting and others are unbroadened by faulting. Designate by b the components broadened by faulting, and by u the components unbroadened. The broadened components of type $L_0 = 3N \pm 1$ are represented by Eq. (13.94), and the unbroadened components of type $L_0 = 3N$ are represented by Eq. (13.94) with $Z = 1$, $\epsilon = 0$, and $\beta = 0$. The total powder pattern reflection $P'_{2\theta}(h_0)$ is then given by a sum over the u and b components:

$$P'_{2\theta}(h_0) = \frac{G}{b'_3}\sum_n \left\{\sum_u \frac{N(n/q)}{N_3}\cos 2\pi n(h'_3 - l') + \sum_b \frac{N(n/q)}{N_3} Z^{|n/q|} \times \left[\cos 2\pi n(h'_3 - l' \pm \epsilon)\right] - \frac{\beta}{\sqrt{3}}\sum_b \frac{N(n/q)}{N_3} Z^{|n/q|}(\pm) \times \left[\frac{L_0}{|L_0|}\sin 2\pi|n|(h'_3 - l' \pm \epsilon)\right]\right\}.$$

We replace the two cosine terms with a single cosine term having an average coefficient and an average displacement. Since the sine term coefficients are

proportional to β, the displacement of the sine terms is a second-order effect which can be neglected. For the powder pattern reflection $h_0^2 = h^2 + k^2 + l^2$, the observable $P'_{2\theta}(h_0)$ can be expressed in the simple form

$$P'_{2\theta}(h_0) = \frac{G(u+b)}{b'_3} \sum_n \{A_n \cos 2\pi n(h'_3 - l' + \delta) + B_n \sin 2\pi |n| (h'_3 - l')\}, \tag{13.95}$$

where

$$A_n = \left(\frac{1}{u+b}\right)\left\{\sum_u \frac{N(n/q)}{N_3} + \sum_b \frac{N(n/q)}{N_3} Z^{|n/q|}\right\},$$

$$\delta = \left(\frac{1}{u+b}\right)\sum_b (\pm)\epsilon,$$

$$B_n = \frac{-\beta}{\sqrt{3}\,(u+b)} \sum_b \frac{N(n/q)}{N_3} Z^{|n/q|}(\pm)\frac{L_0}{|L_0|}. \tag{13.96}$$

The peak displacement δ is given by Eq. (13.96). Using Eq. (13.93) and the relation $\sin\phi = L_0 B_3 d$ from Fig. 13.17, the displacement can be expressed as

$$\delta = \frac{\sqrt{3}\alpha}{4\pi b'_3 a(u+b)h_0} \sum_b (\pm)L_0. \tag{13.97}$$

The broadened reflections are of the type $L_0 = 3N \pm 1$ and the choice in sign $(\pm)$ of Eq. (13.97) is that of $L_0 = 3N \pm 1$. Since

$$L_0 = -h - k + 2l = 3l - (h + k + l)$$

if a given set of indices $h_1k_1l_1$ are interchanged in all ways in position but not in sign, $(h + k + l)$ remains constant and for this group the choice $(\pm)$ remains the same. Since each of the three integers $h_1k_1l_1$ occurs equally often in the three positions of hkl but is weighted by $+2$ in position l and by -1 in positions h and k, for this group of reflections $\sum (\pm)L_0 = 0$. All broadened reflections are made up of such groups, and hence $\sum_b (\pm)L_0 = 0$. Although deformation faults in a BCC metal produce peak shifts in some of the individual components HKL_0, when an average is taken over all the components, the net shift is zero for all powder pattern reflections. For BCC metals there is no possibility of determining α directly from measured peak shifts of powder pattern reflections. In general no peak shift is observed experimentally, but it is not excluded that there might be a small shift due to the change in spacing at a fault, an effect which we neglected in setting up the theory.

There is an asymmetry in $P'_{2\theta}(h_0)$ due to the sine terms in Eq. (13.95). Proceeding in the same way as was done for the FCC case, corresponding equations can be developed, and the asymmetry comes out proportional to β. However, for the BCC case, the asymmetry term is smaller, relative to the

Table 13.3
CONSTANTS FOR POWDER PATTERNS OF FAULTED BCC METALS

hkl	$\frac{\sum_b \lvert L_0\rvert}{(u+b)h_0}$	$\sum_b (\pm)\frac{L_0}{\lvert L_0\rvert}$	Rel. D_F
110	$2/3\sqrt{2}$	+2	2.83
200	$\frac{4}{3}$	−2	1.00
211	$2/\sqrt{6}$	+6	1.63
220	$2/3\sqrt{2}$	−2	
310	$4/\sqrt{10}$	0	
222	$2/\sqrt{3}$	+2	
321	$5/2\sqrt{14}$	0	
400	$\frac{4}{3}$	+2	

peak from the cosine terms, than it was for the FCC case. In principle, the twin fault probability β can be determined from a measured peak asymmetry, but in practice it is doubtful if the effect would ever be large enough to make the result significant.

There still remains an effect of faulting in the peak breadth. Proceeding in the same way as in the FCC case, let $n/(|q|\,N_3) = n/(b_3'D)$, where $1/D = \langle|\sin\phi|/N_3 d_{211}\rangle$ is an averaged reciprocal domain dimension in a direction normal to the reflecting planes. With the additional relation $|q| = b_3' a h_0/|L_0|$, and with appropriate approximations for n small, the cosine coefficients are expressed in terms of a length $L = na_3' = n/b_3'$:

$$A_L = 1 - L\left[\frac{1}{D} + \frac{(1.5\alpha+\beta)}{a(u+b)h_0}\sum_b |L_0|\right].$$

By the use of multiple orders and the usual logarithmic plots, we can correct for the effects of strains, and obtain particle size coefficients A_L^S. From the initial slope of the curve relating A_L^S to L, we obtain an effective particle size D_{eff} which is made up of the effect of the true domain size D and the effect of faulting:

$$-\left(\frac{dA_L^S}{dL}\right)_0 = \frac{1}{D_{\text{eff}}} = \frac{1}{D} + \frac{(1.5\alpha+\beta)}{a(u+b)h_0}\sum_b |L_0|. \tag{13.98}$$

Values of $(\sum_b |L_0|)/h_0(u+b)$ are given in Table 13.3.

Although Eq. (13.98) involves both the domain size D and the faulting probability $(1.5\alpha + \beta)$, the two can be partially separated by using the strong hkl-dependence of the faulting term. If D is large enough to make $1/D$ negligible in Eq. (13.98), we obtain directly $(1.5\alpha + \beta)$. Otherwise, if D can be assumed roughly constant for two reflections such as (110) and (200),

measured values of D_{eff} for (110) and (200) allow a direct determination of $(1.5\alpha + \beta)$ and D. Introducing D_F as a fictitious particle size due to faulting, Eq. (13.98) can be expressed as

$$\frac{1}{D_{eff}} = \frac{1}{D} + \frac{1}{D_F},$$

where

$$\frac{1}{D_F} = \frac{(1.5\alpha + \beta)}{a(u + b)h_0} \sum_b |L_0|.$$

Relative values of D_F (normalized to $D_F(200) = 1$) are given in Table 13.3. The ratio $D_{eff}(110)/D_{eff}(200)$ is a useful parameter for the importance of faulting. If the particle size broadening is due completely to faulting, the ratio has a maximum value of 2.83. If faulting is of no importance, and the domain size broadening is isotropic, the ratio should approach unity. For all BCC metals so far measured, the ratio is found to fall in the range 1.00–2.83.

From powder patterns of BCC metals, it is not possible to determine a deformation fault probability α from peak shifts. Twin faulting produces a peak asymmetry, but the effect is probably too small to allow obtaining a meaningful value of β. From the slopes of the Fourier coefficient plots, it is possible to obtain a domain size D and the combination $(1.5\alpha + \beta)$. If we exclude the possibility of measuring a peak asymmetry, it is not possible to obtain separate values of α and β. For measuring faulting parameters from powder patterns, the BCC metals present a more difficult problem than do the FCC and HCP metals.

13.8 GENERAL REMARKS

In this chapter, we have considered a few of the more important kinds of imperfections in crystals. This has required rather long and wearisome manipulations, but a result is not of practical use unless it is carried far enough to express the desired quantity in terms of experimentally observable aspects of the diffraction pattern. In cases where faulting is not involved, and the only imperfections are those of small crystal size and strains, a more elegant treatment in terms of Fourier transforms and convolution operations is possible. For the details and procedures, reference should be made to Chapter 10 of Guinier.[24]

No attempt has been made to include the many experimental x-ray studies of cold-worked metals. A partial resumé of studies prior to 1959, which involved primarily faulting, has been given in a previous review article.[10] Subsequent x-ray studies of cold-worked metals are too numerous to attempt to list and discuss them here.

REFERENCES

1. P. SCHERRER, *Nachr. Göttinger Gesell.*, 98 (1918); *Zsigmondy's Kolloidchemie*, 3rd Ed., p. 394.
2. A. R. STOKES and A. J. C. WILSON, *Proc. Camb. Phil. Soc.*, **38**, 313 (1942).
3. A. R. STOKES, *Proc. Phys. Soc. London*, **61**, 382 (1948).
4. W. A. RACHINGER, *Jour. Sci. Inst.*, **25**, 254 (1948).
5. J. W. M. DUMOND, *Rev. Mod. Phys.*, **5**, 30 (1933).
6. A. R. STOKES and A. J. C. WILSON, *Proc. Camb. Phil. Soc.*, **40**, 197 (1944).
7. B. E. WARREN, *Acta Cryst.*, **8**, 483 (1955).
8. F. BERTAUT, *C. R. Acad. Sci. Paris*, **228**, 187 (1949).
9. B. E. WARREN and B. L. AVERBACH, *Jour. Appl. Phys.*, **21**, 595 (1950); **23**, 497 (1952).
10. B. E. WARREN, *Prog. in Metal Phys.* Vol. VIII, 147 (1959).
11. F. BERTAUT, *C. R. Acad. Sci. Paris*, **228**, 492 (1949).
12. M. S. PATERSON, *J. Appl. Phys.*, **23**, 805 (1952).
13. B. E. WARREN and E. P. WAREKOIS, *Acta Met.*, **3**, 473 (1955).
14. J. MERING, *Acta Cryst.*, **2**, 371 (1949).
15. B. E. WARREN, *J. Appl. Phys.*, **32**, 2428 (1961).
16. B. E. WARREN and E. P. WAREKOIS, *J. Appl. Phys.*, **24**, 951 (1953).
17. C. N. J. WAGNER, *Acta Met.*, **5**, 427, 477 (1957).
18. B. E. WARREN, *J. Appl. Phys.*, **34**, 1973 (1963).
19. A. J. C. WILSON, *Proc. Roy. Soc.*, **A180**, 277 (1942).
20. J. W. CHRISTIAN, *Acta Cryst.*, **7**, 415 (1954).
21. R. GEVERS, *Acta Cryst.*, **7**, 337 (1954).
22. P. B. HIRSCH and H. M. OTTE, *Acta Cryst.*, **10**, 447 (1957).
23. O. J. GUENTERT and B. E. WARREN, *J. Appl. Phys.*, **29**, 40 (1958).
24. A. GUINIER, *Théorie et Technique de la Radio-Cristallographie*, Dunod, Paris (1956).

PROBLEMS

13.1 For a powder pattern peak, let $f(y)$, $g(z)$, and $h(x)$ represent the profiles due to particle size only, instrumental effects only, and the measured peak containing both effects. They are related by Eq. (13.11).

a) Suppose that $g(z)$ and $f(y)$ have Gaussian shapes: $g(z) = \exp[-a^2z^2]$ and $f(y) = \exp[-b^2y^2]$. Show that the half maximum breadths are related by

$$B^2(h) = B^2(g) + B^2(f).$$

b) Suppose that $g(z)$ and $f(y)$ have Cauchy shapes: $g(z) = 1/(1 + a^2z^2)$ and $f(y) = 1/(1 + b^2y^2)$. Show that the half maximum breadths are related by

$$B(h) = B(g) + B(f),$$

$$\int_{-\infty}^{+\infty} \frac{dz}{(1 + a^2z^2)(1 + b^2[x - z]^2)} = \frac{\pi(a + b)}{(a + b)^2 + a^2b^2x^2}.$$

13.2 Using the powder pattern power theorem of Eq. (13.18), derive Eq. (4.11) which expresses the power per unit length of diffraction circle from a powder sample containing a volume V of material.

13.3 Consider the powder pattern of a FCC material such as alpha brass. Assume that deformation faults occur at random on one set of 111 planes, with probability α. In addition to the shift parallel to the planes, assume that wherever a fault occurs the spacing increases from $(A_3/3)$ to $(A_3/3)(1 + \epsilon)$. Use the Mering relation which involves the idea that the displacement of the mth layer relative to the zero layer is the sum of all the intermediate displacements:

$$\delta_m = \delta(0, 1) + \delta(1, 2) + \cdots + \delta(m - 1, m).$$

Assuming independent faulting,

$$\langle \exp [i\phi(m)] \rangle = \langle \exp [i\phi(0, 1)] \rangle \langle \exp [i\phi(1, 2)] \rangle \cdots \langle \exp [i\phi(m - 1, m)] \rangle.$$

For m positive, $\langle \exp [i\phi(m)] \rangle = \langle \exp [i\phi(0, 1)] \rangle^m$. Assuming that both α and ϵ are small, obtain an expression for $\langle \Delta(2\theta)° \rangle$, the peak shift in degrees for a powder pattern reflection hkl.

13.4 Replace a hexagonal close-packed structure by one in which the 002-planes follow a completely random sequence. An A-layer has equal probability of being followed by a B or a C. The equations which have been derived for small faulting probabilities are obviously not applicable. However, the average occupancy of successive layers is readily obtained. For example, starting with an A atom in the zero layer, we have

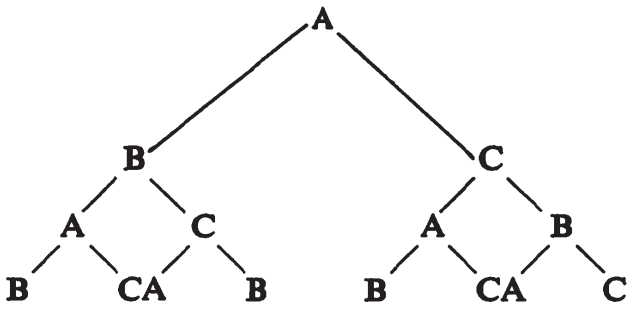

Assume that the crystals are large enough to neglect any particle-size broadening. Develop the theory for obtaining the powder pattern of this material.

13.5 For the powder pattern of a BCC metal, develop the theory for obtaining the twin fault probability β from the measured asymmetry of a reflection. Follow the same method that was used for the FCC case.

14

PERFECT CRYSTAL THEORY

14.1 INTRODUCTION

If the primary beam falls on a crystal at the correct Bragg law angle θ, there will be the usual reflected beam. But as illustrated by Fig. 14.1, the reflected beam also makes the correct angle θ with the planes, and hence there will be a second reflected beam which will have the direction of the original primary beam. The theory of x-ray diffraction which has been developed in the previous chapters has completely neglected this second reflected beam, and this kind of approximate treatment is usually called the kinematical theory. The more rigorous treatment, which makes proper allowance for the reflection of the reflected beam, is called the dynamical theory. Since the magnitude of the second reflected beam from a single layer is very small, the effect is of importance only when it can build up over a large number of layers in a perfect crystal. It is for this reason that the kinematical theory which we have been using is a good first approximation, when applied to highly imperfect crystals consisting of very small mosaic blocks. For the highly perfect type of crystal however, it is very necessary to use the more rigorous dynamical theory, and grossly incorrect results would be obtained by using the kinematical approximation.

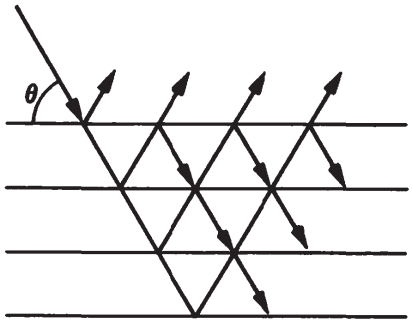

Fig. 14.1 Illustration of the reflection of the reflected beam.

The first dynamical theory of x-ray diffraction in crystals was given by Darwin[1] in 1914, in two classical papers which are usually called Darwin I and II. A completely different and in many ways more elegant kind of treatment was presented independently by Ewald[2] in 1916–1917, and it is from the terminology in these papers that the name dynamical theory has come into use. In 1931, the Ewald treatment of the problem was reformulated by von Laue[3] as a problem involving the solution of the Maxwell equations for a

medium with a periodic complex dielectric constant. Excellent introductions to the different forms of the dynamical theory are to be found in the books by James[4] and Zachariasen[5]. Important extensions and summaries are contained in articles by Hirsch,[6] Kato,[7] Borrmann,[8] Kohra,[9] and Authier.[10] A complete and up-to-date summary of the Ewald-von Laue formulation of the dynamical theory is to be found in the excellent review article by Batterman and Cole.[11]

For the fine details of perfect crystal theory it is necessary to use the Ewald-von Laue dynamical treatment. However, this chapter is not intended for the specialists in perfect crystal theory, but rather for the general x-ray diffraction worker who is interested only in a simple introduction to perfect crystal theory, and to the important differences between the kinematical and the dynamical theories. For this reason we shall follow the Darwin treatment, since the Darwin method of formulating the problem is closely related to the kinematical theory which has been used in the previous chapters, and hence it provides the simplest introduction to the dynamical theory. With the recent extension by Borie,[12] the Darwin treatment is now able to handle most of the interesting aspects of perfect crystal theory in a way which is readily understandable. Since the Ewald-von Laue formulation is so completely covered in the review article by Batterman and Cole, there seems to be no need for repeating it here. For this way of handling the problem, reference to the article is recommended.

14.2 THE DARWIN TREATMENT FOR BRAGG REFLECTION

We consider first the reflection from a single layer of atoms, all of the same kind, with M atoms per unit area. The XY-plane of Fig. 14.2 is the plane of atoms, the primary beam originates at point S, and we measure the scattered radiation at point P. The origin O is chosen so that the path length $SO + OP$ is a minimum and the rays SO and OP make equal angles θ with the plane. We let E_O be the amplitude of the primary beam at O, and consider first the

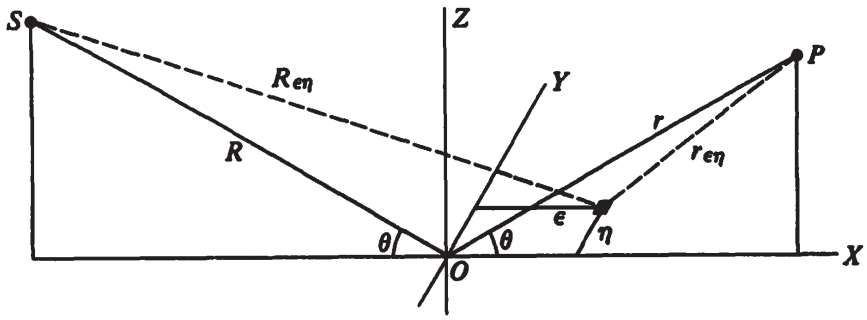

Fig. 14.2 Representation of x-rays from a point source S falling on a single layer of atoms in the XY-plane. Scattered radiation is observed at the point P. For the origin O, the path length $R + r$ is a minimum.

case for a polarized beam with E_O parallel to Y. For a position in the plane at $\epsilon\eta$, the total path length is $R_{\epsilon\eta} + r_{\epsilon\eta}$. The instantaneous value of the electric field at point P, due to radiation scattered from the atoms in the element of area $d\epsilon\, d\eta$, is given by

$$dE_P = -E_O \frac{e^2}{mc^2 r_{\epsilon\eta}} f(2\theta) e^{(2\pi i/\lambda)[ct-(R_{\epsilon\eta}+r_{\epsilon\eta})]} M\, d\epsilon\, d\eta. \tag{14.1}$$

The phase has been expressed in terms of an origin at the source, $f(2\theta)$ is the usual scattering factor for scattering through an angle 2θ, and the minus sign allows for the 180° jump in phase in the scattering process. Very often we neglect to write this minus sign since it always drops out in the squaring of the amplitude to obtain an intensity. This time we shall include it, because it will turn out to be important in connection with the index of refraction:

We now express $R_{\epsilon\eta} + r_{\epsilon\eta}$ in terms of ϵ and η:

$$R_{\epsilon\eta}^2 = (R\cos\theta + \epsilon)^2 + \eta^2 + (R\sin\theta)^2 = R^2 + 2R\epsilon\cos\theta + \epsilon^2 + \eta^2$$

from which

$$R_{\epsilon\eta} = R\left[1 + \frac{2\epsilon\cos\theta}{R} + \frac{\epsilon^2+\eta^2}{R^2}\right]^{1/2}.$$

Since ϵ and η are very small compared to R, we expand the square root and keep terms through the quadratic:

$$R_{\epsilon\eta} = R + \epsilon\cos\theta + \frac{\epsilon^2\sin^2\theta + \eta^2}{2R}.$$

In the same way we find

$$r_{\epsilon\eta} = r - \epsilon\cos\theta + \frac{\epsilon^2\sin^2\theta + \eta^2}{2r}.$$

The sum is then given correctly to quadratic terms by

$$R_{\epsilon\eta} + r_{\epsilon\eta} = R + r + \frac{\epsilon^2\sin^2\theta + \eta^2}{2\rho},$$

where $\rho = Rr/(R + r)$.

The electric field at P is now given by summing the contributions from all atoms in the plane, and since the phases vary slowly, we replace the sum by an integral. It will turn out that only atoms close to O contribute to the integral, and hence we replace the $r_{\epsilon\eta}$ in the denominator by the average value r, and use a constant value of $f(2\theta)$:

$$E_P = -E_O \frac{e^2}{mc^2 r} M f(2\theta) e^{(2\pi i/\lambda)[ct-(R+r)]} \iint e^{-(2\pi i/\lambda)[(\epsilon^2\sin^2\theta+\eta^2)/2\rho]} d\epsilon\, d\eta. \tag{14.2}$$

With the abbreviations

$$u = \left(\frac{2\sin^2\theta}{\lambda\rho}\right)^{1/2}\epsilon, \qquad v = \left(\frac{2}{\lambda\rho}\right)^{1/2}\eta,$$

the double integral can be put in the form

$$\iint = \frac{\lambda\rho}{2\sin\theta}\int e^{-i(\pi/2)u^2}\,du\int e^{-i(\pi/2)v^2}\,dv.$$

These are expressible in terms of the familiar Fresnel integrals:

$$\int_0^v e^{-i(\pi/2)v^2}\,dv = \int_0^v \cos\frac{\pi}{2}v^2\,dv - i\int_0^v \sin\frac{\pi}{2}v^2\,dv = C(v) - iS(v).$$

Both $C(v)$ and $S(v)$ approach very rapidly the value $\frac{1}{2}$, so that the integral from $-v$ to $+v$ can be equated to $(1 - i)$. The double integral becomes

$$\iint = \frac{\lambda\rho}{2\sin\theta}(1 - i)^2 = \frac{\lambda\rho}{\sin\theta}(-i) = \frac{\lambda\rho}{\sin\theta}\,e^{-i(\pi/2)}.$$

Introducing this result in Eq. (14.2), putting in the value of ρ, and cancelling r above and below, we obtain

$$E_P = -E_O\frac{e^2}{mc^2}Mf(2\theta)e^{(2\pi i/\lambda)[ct-(R+r)]}\frac{\lambda R}{(R + r)\sin\theta}\,e^{-i(\pi/2)}. \quad (14.3)$$

By now restricting ourselves to distances r which are small compared to R, such as $R = 10$ cms and $r < 0.1$ mm, we can set $R/(R + r) = 1$.

$$E_P = -E_O\frac{e^2}{mc^2}\frac{M\lambda f(2\theta)}{\sin\theta}\,e^{(2\pi i/\lambda)[ct-(R+r)]}e^{-i(\pi/2)}. \quad (14.4)$$

For all atoms other than ones right at O, the path length is longer than the minimum distance $R + r$ and the weighted average of the contributions corresponds to an effective increase in path length of $\lambda/4$. This is the significance of the factor $\exp[-i\pi/2]$ in Eq. (14.4). In terms of the path of minimum distance $R + r$, there is a 90° phase change in the reflected beam. This shift will play a very important role when we consider crystal diffraction, because a beam which has been reflected twice has suffered two shifts of 90°, and the second reflected beam is 180° out of phase with the primary beam. It should also be noticed from Eq. (14.4) that the amplitude of the reflected beam is independent of r, and hence in the range of small values to which we have restricted r, the reflected beam can be considered as a plane wave. However, Eq. (14.4) does not apply to a value of r which is indefinitely small, because in setting up the integral we assumed that the point P was far enough away to replace all $r_{\epsilon\eta}$ in the denominator by r, and also that for all atoms contributing to E_P, we could use an average $f(2\theta)$. As a rough lower limit, r must be greater than 100λ.

For convenience we introduce the abbreviation

$$q = \left(\frac{e^2}{mc^2}\right)\frac{M\lambda f(2\theta)}{\sin\theta}. \quad (14.5)$$

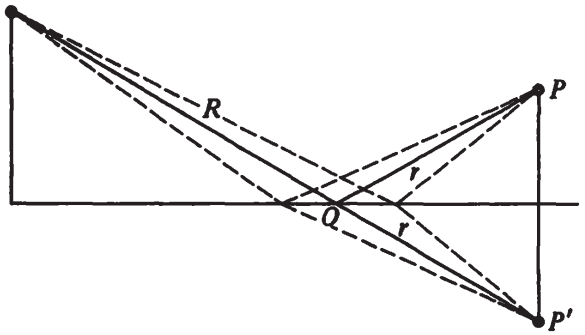

Fig. 14.3 For the scattering by the atoms in a plane, the path lengths are the same for a point P and its mirror image P'.

This is just the negative of the expression which is often used for q, but we are purposely defining it in this way so that q will be a positive quantity. From Eq. (14.4), we now obtain a convenient expression for the instantaneous value of the electric field in the radiation scattered from a single layer:

$$E_{P'} = E_O(iq)e^{(2\pi i/\lambda)[ct-(R+r)]}. \tag{14.6}$$

In Fig. 14.3 let P' be the mirror image of point P. For radiation scattered by the various atoms in the plane, the path lengths to P' are the same as to P, and hence the electric field at P' due to scattering will be given by Eq. (14.6) except that we replace q by q_0, where

$$q_0 = \left(\frac{e^2}{mc^2}\right)\frac{M\lambda f(0)}{\sin\theta}. \tag{14.7}$$

At P' we have a combination of the primary wave and the scattered wave:

$$E_{P'} = E_O(1 + iq_0)e^{(2\pi i/\lambda)[ct-(R+r)]} = E_O e^{(2\pi i/\lambda)[ct-(R+r)]}e^{iq_0}. \tag{14.8}$$

Continuing to neglect absorption, we can say that after passing through s layers, the field in the combined wave will be

$$E_{P'} = E_O e^{(2\pi i/\lambda)[ct-(R+r)]}e^{isq_0}.$$

If we now consider a crystal with layer spacing d, and let r be a distance along the beam within the crystal, the number of layers is given by $s = r\sin\theta/d$. Using this expression for s, the electric field can be written

$$E_{P'} = E_O e^{2\pi i[\nu t-(R/\lambda)-(r/\lambda)(1-q_0\lambda\sin\theta)/(2\pi d)]}. \tag{14.9}$$

For a wave of frequency ν, which travels a distance R through empty space where the wavelength is λ, and a distance r in a medium where the wavelength is λ', the electric field is expressed by

$$E_{P'} = E_O e^{2\pi i[\nu t-(R/\lambda)-(r/\lambda')]}. \tag{14.10}$$

The index of refraction in the medium is $n = \lambda/\lambda'$. Comparing Eqs. (14.9) and (14.10), we obtain

$$n = \frac{\lambda}{\lambda'} = 1 - \frac{q_0\lambda\sin\theta}{2\pi d}.$$

Introducing the value of q_0, replacing $f(0)$ by Z, the atomic number of the atom, and letting $M/d = N$, where N is the number of atoms per unit volume, the index of refraction is expressed by

$$n = 1 - \left(\frac{e^2}{mc^2}\right)\frac{N\lambda^2 Z}{2\pi}. \tag{14.11}$$

Equation (14.11) is identical to the expression which is usually derived from electron theory for the index of refraction in matter for x-rays. It predicts an index which is less than unity, in agreement with the experimentally measured values. It is worth noting that the very important negative sign in Eq. (14.11) results from the negative sign which we included in Eq. (14.1). In expressions for the intensity of a diffracted beam, the negative sign in Eq. (14.1) always drops out in the process of squaring the amplitude to obtain an intensity. But in the index of refraction, we have a phenomenon which can be considered as an interference between the amplitudes of scattered radiation and the primary beam itself, and here the negative sign plays an important role. Wholly apart from the fact that it follows directly from the Maxwell equations, the experimental verification for the correctness of the negative sign in Eq. (14.1) is found in the fact that the index of refraction is less than unity.

Following Darwin, we now allow for a small absorption of the beam, in passing through a layer of atoms, by multiplying Eq. (14.8) by the factor $(1 - h)$, where h is very small. Since both h and q_0 are very small, we can drop the second-order term and write the product as $(1 - h)(1 + iq_0) = 1 - h + iq_0$. Allowing for both absorption and scattering, the electric field in the beam which has passed through a layer of atoms is expressed by

$$E_{P'} = (1 - h + iq_0)E_O e^{(2\pi i/\lambda)[ct-(R+r)]}. \tag{14.12}$$

We now consider diffraction in the crystal represented by Fig. 14.4. The atomic planes have a spacing d, and they are designated by the index r. Let T_r represent in amplitude and phase the total transmitted wave just above the rth layer, and let S_r be the amplitude and phase in the reflected wave at the

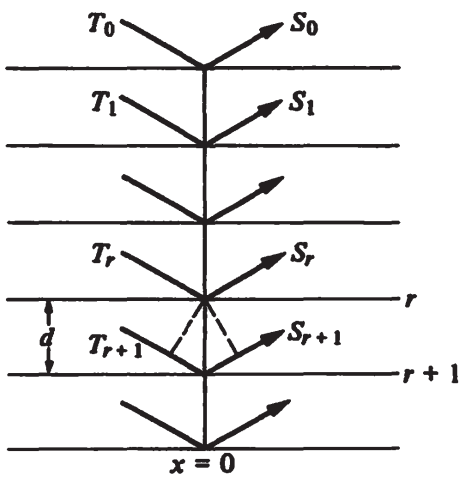

Fig. 14.4 Diffraction from a set of atomic planes. T_r and S_r represent the amplitude and phase of the transmitted and reflected beams just above the rth plane at the horizontal coordinate $x = 0$.

same position. All quantities T_r and S_r refer to the horizontal coordinate $x = 0$. The relation between the reflected and transmitted waves is now expressed by the two Darwin difference equations.

The wave S_r is made up of two components: a reflection of T_r which is given by Eq. (14.6), and a transmission of S_{r+1} which is given by Eq. (14.12). However, since S_{r+1} means the amplitude and phase just above the $(r + 1)$-layer, we must move ahead on the S_{r+1} beam by an amount $d \sin \theta$ to be on the wave front for which S_r represents the phase. This is accomplished by adding a factor exp $[-i\phi]$, where the phase angle ϕ is given by

$$\phi = 2\pi \frac{d \sin \theta}{\lambda} . \tag{14.13}$$

In this way we obtain the first of the two difference equations:

$$S_r = T_r(iq) + (1 - h + iq_0)S_{r+1}e^{-i\phi}. \tag{14.14}$$

The wave T_{r+1} is also made up of two components: a transmission of T_r given by Eq. (14.12) and a reflection of S_{r+1} given by Eq. (14.6). To the component due to the transmission of T_r, we must add a factor exp $[-i\phi]$ to move ahead to the wave front where T_{r+1} represents the phase. For the contribution due to the reflection of S_{r+1}, we must move ahead on S_{r+1} by a distance $d \sin \theta$ to be on a wave front which passes through the plane r at $x = 0$, and on the reflected contribution to T_{r+1} which arises at this point we must move ahead a distance $d \sin \theta$ to be on the wave front for which T_{r+1} represents the phase. In this case the phase factor exp $[-i\phi]$ comes in twice. The second of the two difference equations is then expressed by

$$T_{r+1} = (1 - h + iq_0)T_r e^{-i\phi} + iqS_{r+1}e^{-i2\phi}. \tag{14.15}$$

The two difference equations have been written as though Eqs. (14.6) and (14.12) could be applied indefinitely close to the plane r. This is obviously wrong, since it is only at distances greater than, say, 100λ that the scattered waves combine to the values which have been used. However, the additions which we are considering become important only when they build up over many hundreds of layers, and we are expressing the change at each layer in terms of what that change will contribute at a more distant point.

We now wish to eliminate S_r and S_{r+1} from Eqs. (14.14) and (14.15) to obtain a difference equation involving only the T_r. From Eq. (14.15) we obtain

$$S_{r+1} = \frac{T_{r+1} - (1 - h + iq_0)T_r e^{-i\phi}}{iqe^{-i2\phi}}, \tag{14.16}$$

and since this must apply for any value of r, we can also write

$$S_r = \frac{T_r - (1 - h + iq_0)T_{r-1}e^{-i\phi}}{iqe^{-i2\phi}}. \tag{14.17}$$

Using these values of S_r and S_{r+1}, Eq. (14.14) becomes

$$(1 - h + iq_0)e^{-i\phi}[T_{r-1} + T_{r+1}] = T_r[1 + q^2e^{-i2\phi} + (1 - h + iq_0)^2e^{-i2\phi}]. \tag{14.18}$$

We are interested in diffraction in a thick crystal, and for this case it is reasonable to try a solution of the form

$$T_r = T_0x^r. \tag{14.19}$$

where x must be independent of r, and $|x| < 1$. Inserting the trial solution in Eq. (14.18), we obtain

$$(1 - h + iq_0)e^{-i\phi}[x^{-1} + x] = 1 + q^2e^{-i2\phi} + (1 - h + iq_0)^2e^{-i2\phi}. \tag{14.20}$$

This is a quadratic equation in x, whose solution will be deferred until later, but we keep in mind that the root to be used is the one for which $|x| < 1$.

By putting the trial solution $T_r = T_0x^r$ in Eqs. (14.16) and (14.17), it follows that $S_{r+1} = S_rx$. Using this relation in Eq. (14.14), we obtain an expression for S_r:

$$S_r = \frac{iqT_0x^r}{1 - x(1 - h + iq_0)e^{-i\phi}},$$

and by setting $r = 0$, we express the ratio of the reflected and primary waves at the surface of the crystal:

$$\frac{S_0}{T_0} = \frac{iq}{1 - x(1 - h + iq_0)e^{-i\phi}}. \tag{14.21}$$

It is convenient to define an angle θ_0 by the relation

$$\frac{2\pi d \sin\theta_0}{\lambda} = m\pi + q_0. \tag{14.22}$$

Equation (14.22) is identical to the usual form of the Bragg law corrected for refraction for the case of symmetrical reflection:

$$m\lambda = 2d \sin\theta_0\left[1 - \frac{(1 - n)}{\sin^2\theta}\right],$$

and hence θ_0 is the exact Bragg law angle with index of refraction correction included. Since we are only interested in angles θ which are close to the exact Bragg law angle θ_0, it is convenient to represent θ in a form which is analogous to Eq. (14.22), by introducing a small difference v:

$$\frac{2\pi d \sin\theta}{\lambda} = m\pi + q_0 + v. \tag{14.23}$$

The difference v is expressed by

$$v = 2\pi(d/\lambda)(\sin\theta - \sin\theta_0) = 2\pi(d/\lambda)\cos\theta(\theta - \theta_0). \tag{14.24}$$

Combining Eqs. (14.13) and (14.23), we can write

$$e^{-i\phi} = e^{-i(m\pi+q_0+v)} = (-1)^m(1 - iq_0 - iv). \tag{14.25}$$

Inserting this expression for exp $[-i\phi]$ in Eq. (14.21) and dropping second-order quantities,

$$\frac{S_0}{T_0} = \frac{iq}{1 - x(1 - h + iq_0)(-1)^m(1 - iq_0 - iv)}$$

$$= \frac{iq}{1 - x(-1)^m(1 - h - iv)}. \tag{14.26}$$

We now go back to Eq. (14.20), introduce exp $[-i\phi]$ from Eq. (14.25), and by appropriate dropping of higher orders, obtain

$$(-1)^m(1 - h - iv)[x^{-1} + x] = 1 + q^2 + (1 - h - iv)^2. \tag{14.27}$$

To solve the quadratic equation, we try a solution which is physically reasonable:

$$x = (-1)^m(1 - \eta), \tag{14.28}$$

where η is a small quantity, and we choose the solution for which the real part of η is positive, in order that $|x| < 1$. Keeping terms only to the quadratic in η:

$$x^{-1} + x = (-1)^m\left[\frac{1}{1-\eta} + 1 - \eta\right]$$

$$= (-1)^m(1 + \eta + \eta^2 + \cdots + 1 - \eta) = (-1)^m(2 + \eta^2).$$

Combining with Eq. (14.27), we find $(1 - h - iv)\eta^2 = q^2 + (h + iv)^2$, from which

$$\eta = \pm[q^2 + (h + iv)^2]^{1/2}. \tag{14.29}$$

Inserting the results of Eqs. (14.28) and (14.29) in Eq. (14.26), and dropping higher orders in small quantities, we obtain

$$\frac{S_0}{T_0} = \frac{iq}{h + iv \pm [q^2 + (h + iv)^2]^{1/2}}. \tag{14.30}$$

Equation (14.30) expresses the ratio of the reflected and primary waves in terms of the variable v which was defined by Eq. (14.24). Since it is more convenient to have the ratio in terms of an angular variable $\epsilon = \theta - \theta_0$, we introduce the three parameters:

$$\epsilon = \theta - \theta_0 = \frac{v\lambda}{2\pi d\cos\theta}, \qquad s = \frac{q\lambda}{2\pi d\cos\theta}, \qquad b = \frac{h\lambda}{2\pi d\cos\theta}. \tag{14.31}$$

The ratio is then given by

$$\frac{S_0}{T_0} = \frac{is}{b + i\epsilon \pm [s^2 + (b + i\epsilon)^2]^{1/2}}. \tag{14.32}$$

14.3 BRAGG REFLECTION FOR A THICK CRYSTAL WITH NEGLIGIBLE ABSORPTION

We consider first the case of Bragg reflection in a thick crystal whose absorption is so small relative to the reflecting power that it can be neglected. Setting $b = 0$, we write

$$\frac{S_0}{T_0} = \frac{is}{i\epsilon \pm (s^2 - \epsilon^2)^{1/2}}. \tag{14.33}$$

This is a convenient representation for $\epsilon^2 < s^2$, but for $\epsilon^2 > s^2$ it is better to write $(s^2 - \epsilon^2)^{1/2} = i(\epsilon^2 - s^2)^{1/2}$ and express the ratio by

$$\frac{S_0}{T_0} = \frac{s}{\epsilon \pm (\epsilon^2 - s^2)^{1/2}}. \tag{14.34}$$

The ambiguity in sign is most simply determined from the condition that the denominator cannot go to zero for large values of ϵ, and hence in Eq. (14.34) we use the negative sign for ϵ negative and the positive sign for ϵ positive. The intensity ratio is given by $I/I_0 = (S_0/T_0)(S_0/T_0)^*$ and the values appropriate to the three angular ranges are as follows:

$$\epsilon < -s \quad \frac{I}{I_0} = \left[\frac{s}{\epsilon - (\epsilon^2 - s^2)^{1/2}}\right]\left[\frac{s}{\epsilon - (\epsilon^2 - s^2)^{1/2}}\right] = \frac{s^2}{[\epsilon - (\epsilon^2 - s^2)^{1/2}]^2},$$

$$-s < \epsilon < +s \quad \frac{I}{I_0} = \left[\frac{is}{i\epsilon \pm (s^2 - \epsilon^2)^{1/2}}\right]\left[\frac{-is}{-i\epsilon \pm (s^2 - \epsilon^2)^{1/2}}\right]$$

$$= \frac{s^2}{\epsilon^2 + s^2 - \epsilon^2} = 1, \tag{14.35}$$

$$\epsilon > +s \quad \frac{I}{I_0} = \left[\frac{s}{\epsilon + (\epsilon^2 - s^2)^{1/2}}\right]\left[\frac{s}{\epsilon + (\epsilon^2 - s^2)^{1/2}}\right] = \frac{s^2}{[\epsilon + (\epsilon^2 - s^2)^{1/2}]^2}.$$

The angular range $-s < \epsilon < +s$ is usually called the middle region, and in this range of angle the reflection is perfect, the intensity of the reflected beam being equal to that of the primary beam. A plot of I/I_0 as a function of $\epsilon = \theta - \theta_0$ is shown by Fig. 14.5. It should be noted that the reflection is symmetrical about the angle θ_0. This angle was defined by Eq. (14.22), and it represents a Bragg law θ_0 corrected for the effect of refraction.

We are now interested in evaluating the integrated intensity. A primary beam of intensity I_0 and cross-sectional area A_0 falls upon the extended face crystal represented by Fig. 14.6. The crystal rotates at constant angular velocity ω through the Bragg law position, and the total diffracted energy is measured in a chamber whose opening is so wide that the whole diffracted beam is included. If I is the intensity in the diffracted beam, the diffracted energy E is given by an integration of I over time and over the area of the

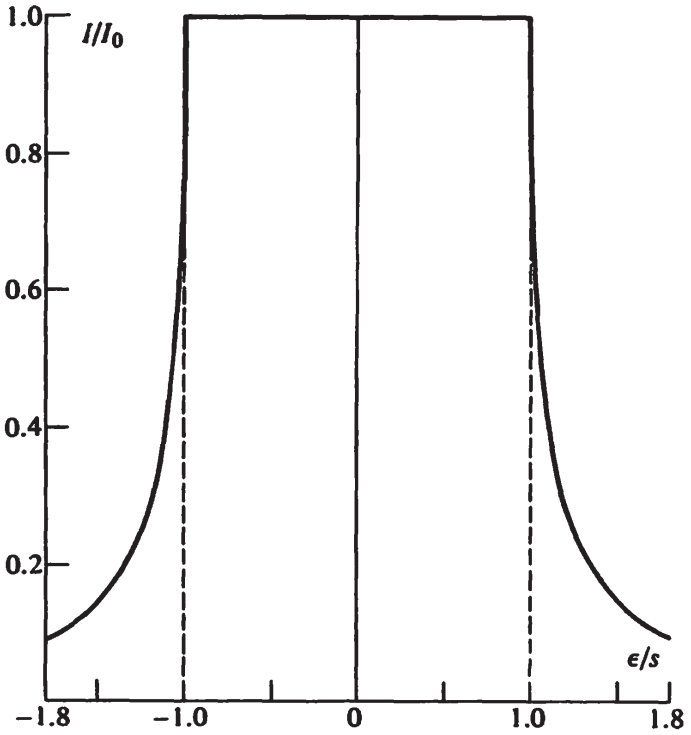

Fig. 14.5 Plot of I/I_0 as a function of ϵ/s for symmetrical Bragg reflection from a thick crystal with negligible absorption. The reflection is symmetrical about the corrected angle θ_0. In the middle region between $\epsilon/s = -1.0$ and $\epsilon/s = +1.0$, there is a perfect reflection.

receiving surface:

$$E = \iint I \, dA \, dt.$$

Since the power in the diffracted beam is given by $P = \int I \, dA$, and an element of time can be represented by $dt = d\epsilon/\omega$, the diffracted energy can also be expressed by

$$E = \frac{1}{\omega} \int P \, d\epsilon.$$

We can consider that the measurement is made close to the crystal, where the cross-sectional areas of the diffracted and primary beams are equal, so that

$$\frac{P}{P_0} = \frac{IA}{I_0 A_0} = \frac{I}{I_0},$$

and this allows us to represent the diffracted energy by

$$E = \frac{P_0}{\omega} \int \frac{I}{I_0} \, d\epsilon.$$

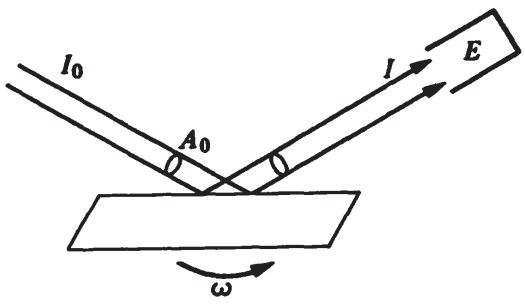

Fig. 14.6 Primary beam of intensity I_0 and cross sectional area A_0 falling on a crystal which rotates at velocity ω through the Bragg law position. The total diffracted energy is E.

Using the intensity ratios from Eq. (14.35), the integrated reflection $E\omega/P_0$ is given by

$$\frac{E\omega}{P_0} = \int_{\epsilon=-\infty}^{-s} \frac{s^2\, d\epsilon}{[\epsilon - (\epsilon^2 - s^2)^{1/2}]^2} + \int_{-s}^{+s} (1)\, d\epsilon + \int_{\epsilon=s}^{\infty} \frac{s^2\, d\epsilon}{[\epsilon + (\epsilon^2 - s^2)^{1/2}]^2}.$$

The first and third integrals are readily evaluated with the substitutions $\epsilon = -s \cosh x$ and $\epsilon = s \cosh x$. The result is

$$\frac{E\omega}{P_0} = \frac{s}{3} + 2s + \frac{s}{3} = \frac{8s}{3}.$$

From Eqs. (14.31) and (14.5),

$$s = \frac{q\lambda}{2\pi d \cos\theta} = \left(\frac{e^2}{mc^2}\right)\frac{N\lambda^2 f}{\pi \sin 2\theta},$$

where $N = M/d$ is the number of atoms per unit volume. Combining the last two equations, we obtain

$$\frac{E\omega}{P_0} = \frac{8}{3\pi}\left(\frac{e^2}{mc^2}\right)\frac{N\lambda^2 f}{\sin 2\theta}. \tag{14.36}$$

This result corresponds to our original assumption that the primary beam was polarized with E_0 perpendicular to the plane of the primary and reflected beams. If the beam had been polarized with E_0 in the plane of the primary and reflected beams, an additional factor $\cos 2\theta$ would have appeared in Eqs. (14.1) and (14.5). In Eq. (14.36) there would be an additional factor of $(+\cos 2\theta)$ if $\cos 2\theta$ is positive, and $(-\cos 2\theta)$ if $\cos 2\theta$ is negative. Either case is represented by adding the factor $|\cos 2\theta|$ to Eq. (14.36). Since an unpolarized primary beam is equivalent to two polarized beams, each of half the intensity, and with mutually perpendicular directions of polarization, the result for an unpolarized beam is obtained by adding the factor $(1 + |\cos 2\theta|)/2$ to Eq. (14.36). To generalize the result we now let N be the number of unit cells per unit volume, and replace f by the structure factor per unit cell F. For an unpolarized primary beam, and a perfect crystal in which absorption can be neglected, the integrated reflection is given by

$$\frac{E\omega}{P_0} = 8/3\pi\left(\frac{e^2}{mc^2}\right)\frac{N\lambda^2|F|}{\sin 2\theta}\left(\frac{1 + |\cos 2\theta|}{2}\right). \tag{14.37}$$

For comparison, we repeat from Eq. (4.7), the corresponding expression for the integrated reflection for an ideally imperfect crystal:

$$\frac{E\omega}{P_0} = \frac{1}{2\mu}\left(\frac{e^2}{mc^2}\right)^2 \frac{N^2\lambda^3 F^2}{\sin 2\theta}\left(\frac{1 + \cos^2 2\theta}{2}\right). \tag{14.38}$$

To have a comparison of these two extreme cases, we use as an example the 200-reflection from NaCl, measured with Mo$K\alpha$:
Ideally perfect:

$$\frac{E\omega}{P_0} = \frac{8}{3\pi}\frac{(2.82 \times 10^{-13})}{0.250}(5.58 \times 10^{21})(0.711 \times 10^{-8})^2 \times 87.5 \times 0.984 = 23 \times 10^{-6},$$

Ideally imperfect:

$$\frac{E\omega}{P_0} = \frac{(2.82 \times 10^{-13})^2}{2 \times 17.7 \times 0.250}(5.58 \times 10^{21})^2(0.711 \times 10^{-8})^3(87.5)^2 \times 0.969 = 744 \times 10^{-6}.$$

The experimentally measured values fall between these two extremes, the values depending upon the state of imperfection in the crystal. For a sample of rather imperfect rock salt, whose face has been ground on emery paper to increase the degree of imperfection, a measured value for the 200-reflection is usually obtained which is about two thirds of that for the ideally imperfect case. In general, the integrated reflection is appreciably larger for the ideally imperfect crystal than for one which is ideally perfect.

Since F is the amplitude per unit cell, it would appear that an integrated intensity must involve F^2, and hence it looks wrong that $|F|$ appears in the first power in Eq. (14.37). However for a perfect crystal, the intensity ratio is unity throughout the middle region, and this value is wholly independent of the structure factor. The integrated reflection involves a unit intensity ratio over an effective angular width of $8s/3$, and s is proportional to $|F|$. It is for this reason that $|F|$ occurs in the first power, the integrated reflection is given by a unit intensity ratio extending over a width which is proportional to $|F|$. A large value of $|F|$ results in a large integrated reflection by increasing the width of the reflection. Unfortunately the old problem of determining the phase of F for use in electron density plots is not helped by measurements on perfect crystals, because it is only the magnitude $|F|$ which is obtained from the value of the integrated reflection.

Equation (14.35) predicts that the intensity of the reflected beam should equal the intensity of the primary beam in the middle region. To the experimenter, who is accustomed to placing a crystal in the strong beam from an x-ray tube and obtaining a reflected beam which is weaker by several orders of magnitude, this prediction appears at first sight to be completely wrong. However, Eq. (14.35) applies only to a monochromatic primary beam which is parallel to within a few seconds of arc. In the usual beam coming from an x-ray tube, only a very small fraction of the intensity is closely monochromatic and parallel to within a few seconds of arc, and hence the prediction of perfect reflecting power has no significance for the usual experimental arrangement.

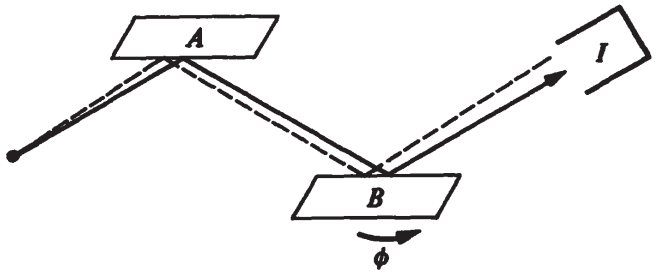

Fig. 14.7 Double crystal spectrometer arrangement with two perfect crystals in the parallel position. At the parallel setting, any wavelength reflected by *A* falls on *B* at the correct angle for reflection.

The assumed conditions are, however, very closely satisfied in a double crystal spectrometer experiment with two perfect crystals set in the parallel position as indicated by Fig. 14.7. Here we do find that the reflected beam from crystal *B* is nearly as strong as the beam between crystals *A* and *B*.

When a perfect crystal is set in the reflecting position, there is an attenuation of the primary beam. From the amplitude ratio which was given by Eq. (14.19), we can write the intensity ratio in the middle region as $I_r/I_0 = x^{2r}$. In the middle region where the effect is greatest,

$$x = -(-1)^m[1 - (q^2 - v^2)^{1/2}] = (-1)^m e^{-(q^2-v^2)^{1/2}}.$$

In terms of a distance s along the primary beam, $r = s \sin\theta/d$, and the intensity ratio is given by

$$I_r/I_0 = e^{-(2\sin\theta/d)(q^2-v^2)^{1/2}s} = e^{-\tau s}.$$

The coefficient

$$\tau = \frac{2\sin\theta}{d}(q^2 - v^2)^{1/2}$$

can be called an attenuation coefficient which represents a decrease in the intensity of the primary beam resulting from the reflection of the reflected beam. If we take an average over the middle region $-q < v < q$, $\langle(q^2 - v^2)^{1/2}\rangle = q\pi/4$, and introduce the value of q, we obtain an average attenuation coefficient for the middle region:

$$\langle\tau\rangle = \frac{\pi}{2}\left(\frac{e^2}{mc^2}\right)N\lambda|F|. \tag{14.39}$$

For a numerical example, we can consider the 200-reflection in a perfect NaCl crystal using Mo$K\alpha$ radiation:

$$\langle\tau\rangle = \frac{\pi}{2}(2.82 \times 10^{-13})(5.6 \times 10^{21})(0.71 \times 10^{-8})(80) = 1380/\text{cm}.$$

It is interesting to compare the value $\langle\tau\rangle = 1380/\text{cm}$ with the value of the ordinary linear absorption coefficient $\mu = 18/\text{cm}$ for Mo$K\alpha$ in NaCl. For the 200-reflection in a perfect NaCl crystal using Mo$K\alpha$ radiation, it is evident that ordinary absorption is almost negligible in comparison with attenuation when the crystal is in the reflecting position.

14.4 WIDTH OF A BRAGG REFLECTION

To illustrate the width of a perfect reflection, we shall use the first-order reflection from the planes parallel to the cleavage face of calcite. In terms of the rhombohedral axes, these are the 211-planes, with spacing $d(211) = 3.035\,A$ and a structure factor $F(211) = f_{Ca} + f_C + f_O$ per $CaCO_3$. For Cu$K\alpha$ radiation, $\lambda = 1.542\,A$, and with no allowance for thermal vibration, $F(211) = 26.2$ per $CaCO_3$. The number of $CaCO_3$ per cm^3 is $N = 1.64 \times 10^{22}$. For an unpolarized primary beam, we obtain from Eqs. (14.5) and (14.31):

$$s = \left(\frac{e^2}{mc^2}\right)\frac{N\lambda^2|F|}{\pi \sin 2\theta}\left(\frac{1 + |\cos 2\theta|}{2}\right), \tag{14.40}$$

$$s = \frac{(2.82 \times 10^{-13})(1.64 \times 10^{22})(1.54 \times 10^{-8})^2(26.2)(0.936)}{\pi \times 0.491}$$

$$= 17.4 \times 10^{-6}\ \text{rad} = 3.59''.$$

There is perfect reflection over a width $2s$, and allowing for the two wings, the full width at half maximum intensity is given by

$$\Delta\theta = 2.12s = 2.12 \times 3.59 = 7.61''.$$

A simple way to measure the width of perfect crystal reflection is to use the double crystal spectrometer in the parallel position as shown by Fig. 14.7. It is important to note that when used in the parallel position, the double crystal spectrometer has no dispersion. For example, if both α_1 and α_2 are being reflected from crystal A, the two reflected beams fall on crystal B at the correct angles to be simultaneously reflected. Hence as we rotate crystal B, the angular width of the I_B-vs.-ϕ curve is independent of wavelength variations in the $\alpha_1\alpha_2$ doublet, and is dependent only on the reflecting power widths of the two crystals. For any wavelength, there is a small range in the direction of the beam reflected from crystal A, and each of these directions is reflected over a small angular range as crystal B is turned. What we measure is the curve I_B-vs.-ϕ, and this is usually called the rocking curve. The width of the rocking curve is determined by a combination of the reflecting power widths of both crystals, and it is correctly obtained as a convolution of the two reflecting power curves. Assuming Darwin shapes, the convolution operation leads to a rocking curve width which is 1.32 times the half maximum width of the single Darwin curve. For calcite in first order

with Cu$K\alpha$ radiation, we should therefore expect a rocking curve width:

$$\Delta\phi = 7.61 \times 1.32 = 10.0''.$$

The measured values, of course, depend upon the perfection of the calcite crystals which are used, and many crystals give values well above 10.0″, but the best of the crystals give values ranging down to just about the predicted width $\Delta\phi = 10.0''$. In spite of the fact that we have slightly oversimplified by neglecting absorption in the crystal, the breadth of perfect crystal reflection predicted by the Darwin theory is satisfactorily verified by the double crystal spectrometer rocking curves.

Suppose that the double crystal spectrometer of Fig. 14.7 is changed so that the Cu$K\alpha$ beam is reflected from the two calcite crystals in second order rather than in first order. For this case, the width of the rocking curve I_B-vs.-ϕ is reduced to something like $\Delta\phi = 5''$, roughly half of the first order width $\Delta\phi = 10''$. To x-ray diffraction workers who are long accustomed to finding second-order reflections wider than the corresponding first-order reflection, this is a very surprising result. It is, however, exactly what would be expected from Eq. (14.40). For the second-order reflection, $|F|$ is smaller than in first order and sin 2θ is larger, so that s for second order is only about half the value for first order.

In a rough qualitative way, we can understand the width of perfect crystal reflection as a particle-size effect which can be expressed by the Scherrer equation of Chapter 13. No matter how thick the crystal may be, the attenuation coefficient τ limits the diffraction process to a layer of effective thickness z(eff). To reach a depth z, the primary beam travels a distance $z/\sin\theta$ in the crystal, and the decrease by attenuation is exp $[-\tau z/\sin\theta]$. For an effective depth z, we can set $\tau z/\sin\theta = 1$, and from this we obtain $z(\text{eff}) = \sin\theta/\tau$. Using the value $\langle\tau\rangle = 1380/\text{cm}$, which was computed from Eq. (14.39) for a 200-reflection from NaCl with Mo$K\alpha$ radiation, we find an effective thickness

$$z(\text{eff}) = 0.126/1380 = 9100 \times 10^{-8}\,\text{cm} = 9100\,A.$$

Treating z(eff) as the particle size L in the Scherrer equation, we obtain

$$\Delta(2\theta) = \frac{0.94\lambda}{L\cos\theta} = \frac{0.94 \times 0.71}{9100 \times 0.99} = 74 \times 10^{-6}\,\text{rad} = 15''$$

and correspondingly $\Delta\theta = 7.5''$. A correct value for the full width at half maximum intensity for 200 NaCl with Mo$K\alpha$ radiation can be computed from Eq. (14.40); $\Delta\theta = 2s(1.06) = 3.5''$. The two values 3.5″ and 7.5″ are close enough to illustrate the point that the width of perfect reflection can be thought of as a particle size effect with the effective particle size determined by the attenuation of the beam.

14.5 EXTINCTION

If we measure the integrated intensity from an ideally perfect crystal and interpret the measurements by the equation for an ideally perfect crystal, there is satisfactory agreement. At the other extreme, if we measure the integrated intensity from an ideally imperfect crystal, and interpret by the equation for an ideally imperfect crystal, there is again satisfactory agreement. Since most crystals are rather imperfect, and can often be made still more imperfect by grinding or dipping in liquid nitrogen, it is customary to interpret integrated intensity measurements by the ideally imperfect crystal formula. Usually the crystal is imperfect but not ideally imperfect, and hence the measured integrated intensity is somewhat less than the value predicted by the ideally imperfect formula. We describe the situation by saying that there is extinction in the crystal, the term extinction meaning that the integrated intensity is less than predicted by the ideally imperfect crystal equation.

An ideally imperfect crystal is usually defined as one comprised of very small mosaic blocks, the different blocks having appreciable variations in orientation, and the blocks being so small that the integrated intensity from each block is correctly given by Eq. (4.6) which was derived for a very small crystal. An ideally imperfect crystal is illustrated schematically by Fig. 14.8. The concept is of course highly oversimplified, since imperfection in a crystal may be the result of dislocations and inhomogeneous strains, without any clear cut subdivision into mosaic blocks. Darwin clearly recognized that the concept was oversimplified. Nevertheless it has persisted, largely because it is much more amenable to mathematical treatment than a more general and more nearly correct picture of an imperfect crystal. In terms of this concept of an imperfect crystal, Darwin introduced two kinds of extinction.

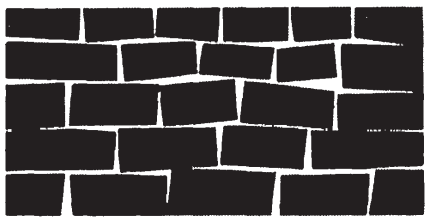

Fig. 14.8 Schematic illustration of an ideally imperfect crystal made up of small disoriented mosaic blocks.

Primary extinction is said to be present if the integrated intensity from each of the mosaic blocks is less than predicted by Eq. (4.6). The deficiency in integrated intensity is due to the fact that the mosaic blocks are too large to neglect attenuation, and the simple kinematical theory for a very small crystal is not applicable. Primary extinction becomes negligibly small when the mosaic blocks are very small, or if the structure factor $|F|$ is very small.

Even if the mosaic blocks of Fig. 14.8 are all so small that there is no primary extinction, there may not be enough disorientation of the blocks.

In this case, the primary beam which is reflected from an interior block, may have already passed through several other blocks at the correct orientation to diffract, so that the intensity of the beam is reduced by more than the ordinary absorption. When the contribution by the interior blocks is less than assumed in Eq. (14.38), due to loss of intensity by reflection in previous blocks, we say that secondary extinction is present. Secondary extinction becomes negligible small when the disorientation of the blocks becomes sufficiently large or if the reflection is very weak.

Rough treatment of a mosaic crystal, such as grinding the crystal on emery paper, tends to reduce the size of the mosaic blocks and to increase their disorientation, so that both primary and secondary extinction are reduced. In a random powder sample we can consider that secondary extinction is negligible, but there may still be primary extinction unless the individual crystals are extremely small. Various methods have been proposed for correcting for extinction, but for the most part they are based on the over-simplified concept of a clear-cut separation into primary and secondary extinction. A satisfactory and practical method for extinction correction has been given by W. H. Zachariasen[13] in a recent treatment which combines both types of extinction.

An interesting experiment by White[14] showed that the integrated intensity from a perfect crystal could be changed reversibly from the ideally perfect value to the ideally imperfect value by elastic bending of the crystal. A highly monochromatic beam was obtained by reflection from two calcite crystals in the antiparallel position. This primary beam then fell on a slab of polished and etched quartz which could be bent elastically either concave or convex. The counter opening was so wide, that all diffracted radiation entered the counter, regardless of whether the bending was concave or convex. By rotating the quartz crystal through the reflecting position, a measurement of the integrated intensity was obtained, and this was compared with the power P_0 in the beam falling on the quartz crystal. Measurements of the integrated reflection for 202 Quartz using Mo$K\alpha$-radiation, as a function of $1/R$, where R is the radius of bending, are shown by Fig. 14.9. With increasing curvature, the measured integrated reflection increased from the value for an ideally perfect crystal to that for an ideally imperfect crystal. The values could be changed reversibly from one extreme to the other, and they were independent of whether the bending was concave or convex. This interesting experiment can be considered to be an example of varying reversibly the extinction in a perfect crystal.

In discussing the difference between perfect and imperfect crystals, it is always very important to keep clearly in mind whether one is talking about intensity or integrated intensity, and when talking about intensity whether or not the primary beam is highly parallel. If a highly parallel beam falls on a perfect crystal at the correct angle, there is nearly perfect reflection, and

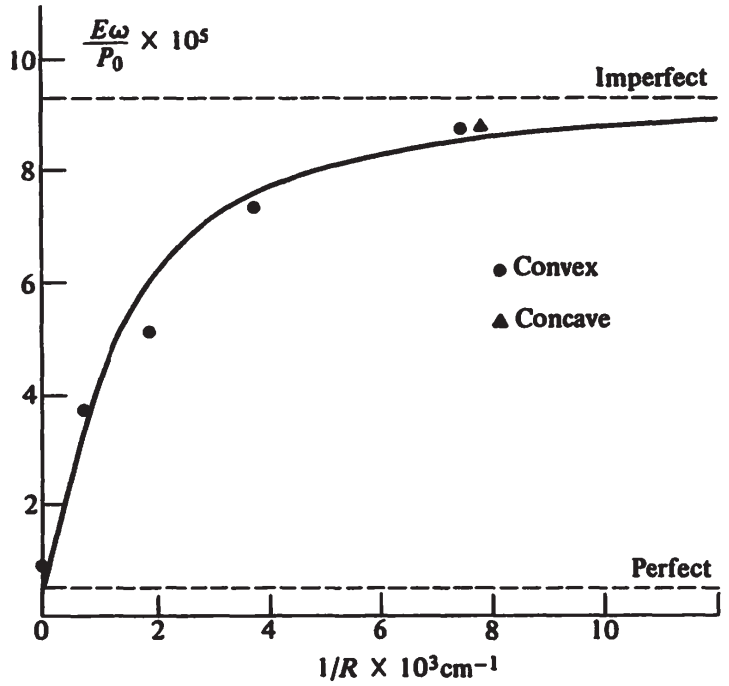

Fig. 14.9 The integrated reflection $E\omega/P_0$ for the 202 reflection from a slab of Quartz as a function of $1/R$ where R is the radius of bending, Mo$K\alpha$ radiation. The values were reversible, and extended all the way from the ideally perfect to the ideally imperfect case.

the intensity of the reflected beam will in general be considerably greater than that of the reflected beam from an ideally imperfect crystal. If the primary beam is not highly parallel, only a small fraction of it can be reflected from a stationary perfect crystal, and in general the reflected power will be greater from an imperfect crystal. Independent of whether or not the primary beam is highly parallel, the integrated intensity will in general be greater for the ideally imperfect crystal.

14.6 BRAGG REFLECTION WHEN THE REFLECTING POWER IS SMALL

A general expression for the ratio S_0/T_0 was given by Eq. (14.32). If the reflecting power is very small compared to the absorption, we can drop s^2 in the denominator, and write

$$\frac{S_0}{T_0} = \frac{is}{2(b + i\epsilon)}.$$

The intensity ratio is then given by

$$\frac{I}{I_0} = \left[\frac{is}{2(b + i\epsilon)}\right]\left[\frac{-is}{2(b - i\epsilon)}\right] = \frac{s^2}{4(b^2 + \epsilon^2)}.$$

With the same reasoning that was used to obtain Eq. (14.36), we can readily evaluate the integrated reflection

$$\frac{E\omega}{P_0} = \int \frac{I}{I_0}\, d\epsilon = \int_{-\infty}^{+\infty} \frac{s^2}{4(b^2 + \epsilon^2)}\, d\epsilon = \frac{\pi}{4}\frac{s^2}{b}. \tag{14.41}$$

In going from half way between one pair of planes to half way between the next pair of planes, we go a distance $d/\sin\theta$ along the beam. From the way in which it was introduced in Eq. (14.12), $(1 - h)^2$ is the corresponding decrease in intensity due to absorption, and hence

$$(1 - h)^2 = e^{-\mu d/\sin\theta}, \tag{14.42}$$

from which, $h = \mu d/2 \sin\theta$. Using this result in Eq. (14.31),

$$b = \frac{h\lambda}{2\pi d \cos\theta} = \frac{\mu\lambda}{2\pi \sin 2\theta}. \tag{14.43}$$

The value of s is given by Eq. (14.31). Generalizing by replacing f by the structure factor F, and letting N be the number of unit cells per unit volume, we write

$$s = \frac{q\lambda}{2\pi d \cos\theta} = \left(\frac{e^2}{mc^2}\right)\frac{N\lambda^2 F}{\pi \sin 2\theta}. \tag{14.44}$$

Using the values of b and s in Eq. (14.41), we obtain

$$\frac{E\omega}{P_0} = \frac{1}{2\mu}\left(\frac{e^2}{mc^2}\right)^2 \frac{N^2\lambda^3 F^2}{\sin 2\theta}.$$

This expression corresponds to our original assumption that the primary beam was polarized with E_0 perpendicular to the plane of the primary and reflected beams. For polarization with E_0 parallel to the plane of the primary and reflected rays, there is an additional factor of $\cos^2 2\theta$. An unpolarized beam can be considered as two polarized beams, each of half the intensity, and polarized in mutually perpendicular directions, so that for an unpolarized primary beam, the integrated reflection is given by

$$\frac{E\omega}{P_0} = \frac{1}{2\mu}\left(\frac{e^2}{mc^2}\right)^2 \frac{N^2\lambda^3 F^2}{\sin 2\theta}\left(\frac{1 + \cos^2 2\theta}{2}\right). \tag{14.45}$$

This is identical to Eq. (14.38), which expressed the usual kinematical result for the integrated intensity from an ideally imperfect crystal. For reflections with very small structure factor $|F|$, the integrated reflection from a perfect crystal approaches that for an ideally imperfect crystal. Intuitively this is just what should be expected, because with decreasing $|F|$, the attenuation approaches zero, and the difference between the kinematical and the

dynamical theories vanishes. This result is the basis for the well known rule that for reflections with very small $|F|$, a measurement of the integrated reflection will be independent of any extinction errors.

The result suggests a possible method for reducing extinction errors in measuring the integrated reflection when $|F|$ is not small and the crystal is not ideally imperfect. Suppose that a suitable x-ray source is available with wavelength such that the reflection will occur at a value of 2θ which is in the vicinity of 90°. Using a polarized primary beam with E_0 in the plane of the primary and reflected beams, F is replaced by $F\cos 2\theta$. If 2θ is close enough to 90°, $F\cos 2\theta$ can be so small that extinction corrections become negligible. From the measurement of the integrated intensity, we obtain $(F\cos 2\theta)^2$ and from this we get F^2. Obviously the method is not simple enough to be used in a routine way, but in principle it is applicable to either single crystals or powders, and it is independent of any arbitrary concept of primary and secondary extinction.

14.7 BRAGG REFLECTION WITH ABSORPTION

We now consider the general case of a Bragg reflection, with proper allowance for absorption in the crystal. Darwin made partial allowance for absorption by introducing the factor $(1 - h)$ to allow for the decrease in the amplitude of the beam in passing through one layer of atoms. In a very important contribution by Prins,[15] it was pointed out that there is also an effect of absorption in the scattering process, and that this additional absorption effect contributes an imaginary part to q. It is this effect which produces the imaginary part $\Delta f''$ in the usual representation of the scattering factor $f = f_0 + \Delta f' + i\,\Delta f''$. In the Prins formulation, allowance for absorption was made by introducing a complex index of refraction.

For a wave passing through a medium with index of refraction n and wavelength λ' in the medium, the electric field is given by the usual expression for a traveling wave:

$$\epsilon = E_0 e^{2\pi i(\nu t - x/\lambda')}.$$

If λ is the wavelength in empty space, $n = \lambda/\lambda'$ and the electric field can also be expressed by

$$\epsilon = E_0 e^{2\pi i(\nu t - nx/\lambda)}. \tag{14.46}$$

For x-rays we usually write $n = 1 - \delta$, but if we now formally add an imaginary part, δ is replaced by $\delta + i\beta$, and $n = 1 - \delta - i\beta$. With this complex index, Eq. (14.46) becomes

$$\epsilon = E_0 e^{2\pi i[\nu t - (x/\lambda)(1-\delta)]} e^{-(2\pi\beta x/\lambda)}. \tag{14.47}$$

The imaginary quantity β produces an exponential decrease in the amplitude. In the intensity, this exponential decrease would be squared, and hence β

can be expressed in terms of the linear absorption coefficient by the relation

$$4\pi\beta/\lambda = \mu. \tag{14.48}$$

In writing Eq. (14.12), we introduced a factor $(1 - h + iq_0)$, where h allowed for absorption and q_0 allowed for scattering. If we now replace q_0 by $(q_0' + iq_0'')$, where q_0'' represents the imaginary part of q_0, it is no longer necessary to write $(1 - h + iq_0)$. Instead we write $(1 + iq_0) = (1 + iq_0' - q_0'')$ and h has been replaced by q_0''. From Eq. (14.42), $h = \mu d/2 \sin\theta$ and hence the value of q_0'' is determined by the linear absorption coefficient $q_0'' = \mu d/2 \sin\theta$. Similarly, we replace q by a real and imaginary part $q = q' + iq''$. It is then possible to determine q'' from the value of q_0'' by a consideration of the values of polarization, scattering angle, and temperature factor for the particular reflection.

We shall develop here a simplified version of the Prins treatment. This is possible merely because we now have tabulated values of $\Delta f''$ the imaginary part of the scattering factor. To work directly with the angular variable $\epsilon = \theta - \theta_0$, we use the parameters introduced in Eqs. (14.31):

$$s = \frac{q\lambda}{2\pi d \cos\theta}, \qquad b = \frac{h\lambda}{2\pi d \cos\theta}.$$

We start with the ratio S_0/T_0 given by Eq. (14.32):

$$\frac{S_0}{T_0} = \frac{is}{b + i\epsilon \pm [s^2 + (b + i\epsilon)^2]^{1/2}}.$$

Since $f = f_0 + \Delta f' + i\,\Delta f''$, it is evident that q is complex, and hence s is also complex. To allow for this, we write $s = s_r(1 + i\sigma)$, where s_r is the real part of s, and σ is the ratio of the imaginary and real parts of s, so that $\sigma = \Delta f''/(f_0 + \Delta f')$. Introducing the new parameters

$$\eta = \epsilon/s_r, \qquad g = b/s_r, \tag{14.49}$$

the ratio S_0/T_0 is expressed by

$$\frac{S_0}{T_0} = \frac{i(1 + i\sigma)}{g + i\eta \pm [(1 + i\sigma)^2 + (g + i\eta)^2]^{1/2}}. \tag{14.50}$$

To put this in a form which will be convenient for subsequent calculations, we introduce the abbreviation

$$(1 + i\sigma)^2 + (g + i\eta)^2 = Ze^{i\gamma}, \tag{14.51}$$

where Z is a positive real quantity. Equating real and imaginary parts in Eq. (14.51),

$$1 + g^2 - \sigma^2 - \eta^2 = Z\cos\gamma,$$
$$2(\sigma + g\eta) = Z\sin\gamma,$$

and from these two relations, we obtain

$$Z^2 = (1 + g^2 - \sigma^2 - \eta^2)^2 + 4(\sigma + g\eta)^2,$$

$$\tan\gamma = \frac{\sin\gamma}{\cos\gamma} = \frac{2(\sigma + g\eta)}{1 + g^2 - \sigma^2 - \eta^2}. \tag{14.52}$$

Combining Eqs. (14.50) and (14.51),

$$\frac{S_0}{T_0} = \frac{i(1 + i\sigma)}{g + i\eta \pm Z^{1/2}e^{i\gamma/2}}.$$

The intensity ratio is then given by $(S_0/T_0)(S_0/T_0)^*$:

$$\frac{I}{I_0} = \frac{1 + \sigma^2}{g^2 + \eta^2 + Z \pm 2Z^{1/2}(g\cos\gamma/2 + \eta\sin\gamma/2)}. \tag{14.53}$$

In using Eq. (14.53) for numerical evaluation, the choice in sign can be fixed by the condition that I/I_0 cannot be greater than unity, but in obtaining γ from Eq. (14.52) it is important to consider the signs of both $\sin\gamma$ and $\cos\gamma$ to be sure that the correct quadrant has been chosen. To allow for the two states of polarization, we introduce a factor P, where $P = 1$ or $P = |\cos 2\theta|$ depending on whether E_0 is perpendicular or parallel to the plane of the primary and reflected beams. Representing the real part of f by $f' = f_0 + \Delta f'$, and with the addition of a temperature factor $\exp[-M]$, the real part of s is given by

$$s_r = \left(\frac{e^2}{mc^2}\right)\frac{\lambda^2 NPf'e^{-M}}{\pi\sin 2\theta}, \tag{14.54}$$

where N is the number of atoms per cm^3. The parameter g is then expressed by

$$g = \frac{\mu}{2(e^2/mc^2)\lambda NPf'e^{-M}}, \tag{14.55}$$

where μ is the linear absorption coefficient.

As an illustration, we now apply Eq. (14.53) to the 200- and 400-reflections from NaCl at room temperature, using Cu$K\alpha$ radiation. Since the imaginary part of the scattering factor $\Delta f''$ is given in the International Tables only to the first decimal place, it is appropriate to make approximations such as using an average temperature factor M for both atoms. Letting N be the number of NaCl per cm^3, and replacing f' by $f'(\text{Na}) + f'(\text{Cl})$, Eq. (14.55) reduces to

$$g = \frac{0.852}{[f'(\text{Na}) + f'(\text{Cl})]Pe^{-M}}.$$

Table 14.1

CONSTANTS FOR NaCl WITH Cu$K\alpha$ RADIATION

	P	e^{-M}	$f'(\text{Na}) + f'(\text{Cl})$	g	σ
200 $\perp$	1.000	0.954	22.2	0.040	0.039
200 $\parallel$	0.851	0.954	22.2	0.047	0.039
400 $\perp$	1.000	0.824	15.0	0.068	0.060
400 $\parallel$	0.403	0.824	15.0	0.170	0.060

The parameter σ is obtained from

$$\sigma = \frac{\Delta f''(\text{Na}) + \Delta f''(\text{Cl})}{f'(\text{Na}) + f'(\text{Cl})}.$$

For the four reflections to be considered, the appropriate numerical values are listed in Table 14.1. From the value of $\Delta f''(\text{Na}) + \Delta f''(\text{Cl}) = 0.9$, which is obtained from the International Tables, σ for 200 is computed to be 0.040. But since the value is uncertain by at least 5 percent, and in principle σ must be less than g, we have replaced 0.040 by the value 0.039 which appears in Table 14.1.

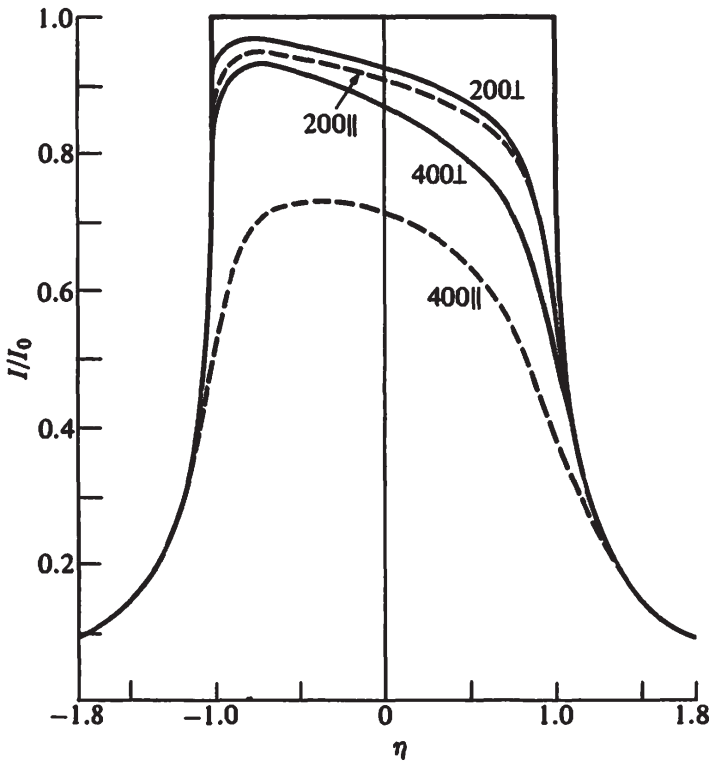

Fig. 14.10 Effect of absorption on the intensity ratio I/I_0 for the 200 and 400 reflections from NaCl using Cu$K\alpha$ radiation as evaluated from Eq. (14.53).

With the constants of Table 14.1, Eq. (14.53) has been evaluated for the four reflections indicated. The values of I/I_0 as a function of η are shown by Fig. 14.10. The curves are quite similar to those obtained originally by Renninger.[16] The region between $\eta = -1.0$ and $\eta = +1.0$ is the region of perfect reflection when the absorption is negligible. For the two states of polarization, this width is the same in terms of the variable η, but it is not the same in terms of the angular variable ϵ. In addition to cutting down the intensity of reflection, the effect of absorption is also to make the reflection asymmetric.

14.8 THE SYMMETRICAL LAUE CASE AND THE BORRMANN EFFECT

The diffraction geometry which is illustrated by Fig. 14.11 is usually called the symmetrical Laue case. A monochromatic primary beam is transmitted through a thin slice of crystal, and at the correct angular setting there is a diffracted beam from the set of planes perpendicular to the surface of the slice. If the crystal slice is thin and highly imperfect, the measured intensities of the reflected and transmitted beams are of the form shown by Fig. 14.12. At the correct Bragg law angle θ_0, there is a reflected peak, and at the same angular position there is a small dip in the intensity of the transmitted beam because of the energy diverted into the reflected beam. This is a well-known classical observation, and it does not cause any surprise since it is just what would be expected from elementary reasoning.

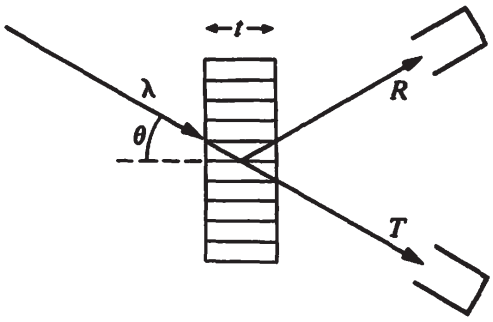

Fig. 14.11 The arrangement for symmetrical Laue reflection.

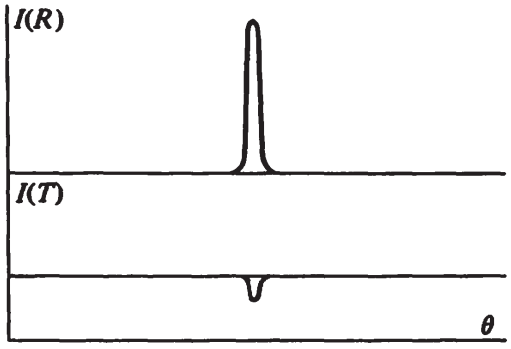

Fig. 14.12 Variation of the reflected and transmitted intensities for the symmetrical Laue case when the crystal is highly imperfect.

Next suppose that the crystal slice is highly perfect and rather thick. As an example let $\mu t = 20$, where μ is the linear absorption coefficient and t is the thickness. Under these conditions everything should be killed by the absorption factor $\exp[-20/\cos\theta]$, and we would not expect to observe

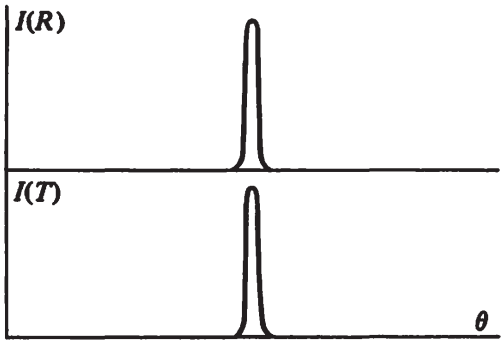

Fig. 14.13 Variation of the reflected and transmitted intensities for the symmetrical Laue case for a thick and highly perfect crystal.

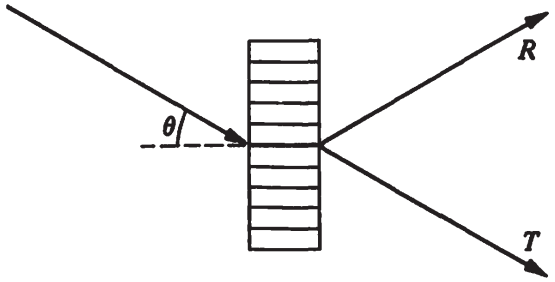

Fig. 14.14 Emergence of the reflected and transmitted beams at a point directly opposite the entrance position for symmetrical Laue reflection in a thick perfect crystal.

either a reflected or transmitted beam. However, what is observed in this case is shown by Fig. 14.13. At any arbitrary angle the intensities of the transmitted and reflected beams are zero as expected, but at the Bragg law angle θ_0, there is a strong reflected beam and simultaneously a strong transmitted beam of about equal intensity, both of these beams appearing in spite of an absorption factor such as $\exp[-20/\cos\theta]$. This surprising experimental fact is called the "Borrmann effect" or sometimes the "anomalous transmission effect." It was discovered by Borrmann[17] and first interpreted by von Laue.[18] An additional curious fact is illustrated by Fig. 14.14. When the crystal is at the Bragg law setting, so that reflected and transmitted beams exist, the point of emergence can be determined by making several film recordings at different distances from the crystal. It is found that for both beams the point of emergence is directly opposite the entrance point, suggesting that the effective combination of the two beams has traveled through the crystal parallel to the diffracting planes.

To treat the symmetrical Laue case for a perfect crystal, we follow the method of Borie[12] and consider Fresnel diffraction by a set of planes other than the Bragg planes. This same procedure had been used previously in connection with other problems by Howie and Whelan,[19] Kato,[20] and Hirsch.[21] We restrict ourselves to a crystal containing only one kind of atom. The Bragg planes of spacing d are represented by the horizontal dashed lines of Fig. 14.15(a). Since the diffraction by this set of planes is independent of the repetition within a single plane, we can choose a repetition distance a in the plane of the figure and a repetition distance b perpendicular to the figure, subject only to the restriction $ab = 1/M$, where M is the number of atoms per unit area in the plane. The diffracting atoms are represented by the black dots of Fig. 14.15(a), and they have been placed in such a way that they define a set of vertical atomic layers represented by the solid lines. These vertical layers of atoms are parallel to the surface of the crystal.

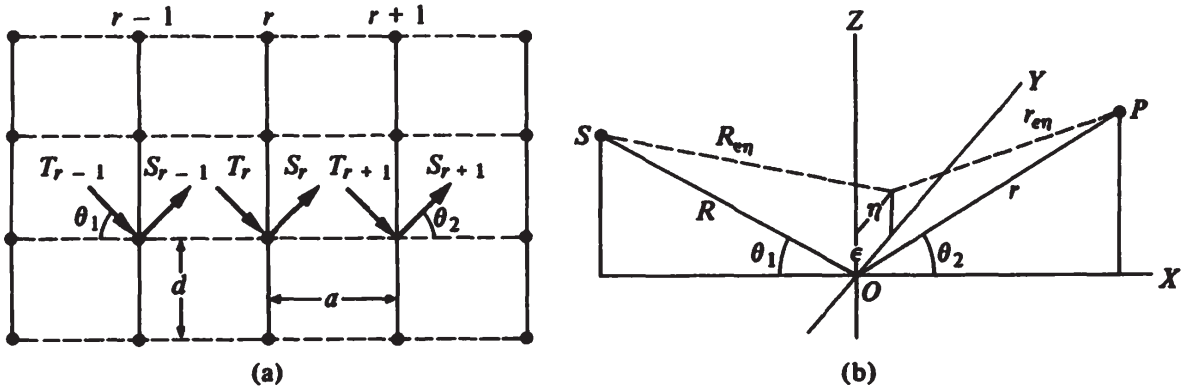

Fig. 14.15 (a) The Borie method for treating the symmetrical Laue case. The horizontal dashed lines represent the Bragg planes. The vertical solid lines represent a set of planes which are parallel to the surface of the crystal. (b) Path lengths for a position ϵ and η in one of the vertical layers of Fig. 14.15(a). The x-ray source is S and the point of observation is P.

The essential feature in Borie's treatment is to now consider Fresnel diffraction by one of these vertical atomic layers rather than by the horizontal Bragg planes. The primary and reflected beams make angles θ_1 and θ_2 with the Bragg planes, and hence angles $(90 - \theta_1)$ and $(90 - \theta_2)$ with the vertical plane. Following the procedure of Section 14.2, we let ϵ and η be coordinates in one of the vertical planes with ϵ vertical and η perpendicular to the plane of the paper as illustrated by Fig. 14.15(b). With the same approximations,

$$R_{\epsilon\eta} = R - \epsilon \sin\theta_1 + \frac{\epsilon^2 \cos^2\theta_1 + \eta^2}{2R},$$

$$r_{\epsilon\eta} = r - \epsilon \sin\theta_2 + \frac{\epsilon^2 \cos^2\theta_2 + \eta^2}{2r}.$$

Letting $R \gg r$, the total path length becomes

$$R_{\epsilon\eta} + r_{\epsilon\eta} = R + r - \epsilon(\sin\theta_1 + \sin\theta_2) + \frac{\epsilon^2 \cos^2\theta_2 + \eta^2}{2r}.$$

In a vertical layer, atoms exist only at positions $\epsilon = nd$, and we now fix the value of θ_2 relative to that of θ_1 by the relation

$$d(\sin\theta_1 + \sin\theta_2) = \lambda. \tag{14.56}$$

The value of $\epsilon(\sin\theta_1 + \sin\theta_2)$ at positions occupied by atoms will be $n\lambda$, and this drops out in setting up an integral similar to Eq. (14.2). The integrals are evaluated in the usual way, and we obtain an expression similar to that of Eq. (14.6) for the instantaneous value of the electric field in the

radiation scattered by a single vertical layer:

$$E_p = E_0(ig)e^{2\pi i/\lambda[ct-(R+r)]},$$

where

$$g = \left(\frac{e^2}{mc^2}\right)\frac{M'\lambda f(\theta_1 + \theta_2)}{\cos\theta_2}.$$

We are purposely using the letter g rather than the Darwin q to emphasize that g has to do with the vertical atomic layers. Since M' is the number of atoms per unit area in a vertical plane, $M'/a = N$, where N is the number of atoms per unit volume. We shall be interested in g only for the case that θ_1 and θ_2 are nearly equal to the Bragg law angle θ, and hence g can be expressed in the simpler form

$$g = \left(\frac{e^2}{mc^2}\right)\frac{\mathrm{Na}\lambda f(2\theta)}{\cos\theta}. \tag{14.57}$$

The vertical atomic layers in Fig. 14.15(a) are numbered by the index r, and with the abbreviations

$$\phi_1 = \frac{2\pi a\cos\theta_1}{\lambda}, \qquad \phi_2 = \frac{2\pi a\cos\theta_2}{\lambda}, \tag{14.58}$$

we now write the two difference equations:

$$S_r = T_r(ig) + S_{r-1}(1 + ig_0)e^{-i\phi_2}, \tag{14.59}$$

$$T_{r+1} = T_r(1 + ig_0)e^{-i\phi_1} + S_{r-1}(ig)e^{-i(\phi_1+\phi_2)}. \tag{14.60}$$

From Eq. (14.60) we obtain

$$S_{r-1} = \frac{T_{r+1} - T_r(1 + ig_0)e^{-i\phi_1}}{(ig)e^{-i(\phi_1+\phi_2)}}, \qquad S_r = \frac{T_{r+2} - T_{r+1}(1 + ig_0)e^{-i\phi_1}}{(ig)e^{-i(\phi_1+\phi_2)}},$$

and substituting these in Eq. (14.59) we obtain an equation involving only the T_r:

$$T_{r+2} + T_r e^{-i(\phi_1+\phi_2)}[g^2 + (1 + ig_0)^2] = T_{r+1}(1 + ig_0)(e^{-i\phi_1} + e^{-i\phi_2}).$$

With the trial solution

$$T_r = T_0 x^r, \tag{14.61}$$

the equation in the T_r reduces to a quadratic equation in x:

$$x^2 + [g^2 + (1 + ig_0)^2]e^{-i(\phi_1+\phi_2)} = x(1 + ig_0)(e^{-i\phi_1} + e^{-i\phi_2}).$$

With the representation

$$\phi_1 = \phi + \Delta\phi, \qquad \phi_2 = \phi - \Delta\phi, \qquad \phi_1 + \phi_2 = 2\phi, \tag{14.62}$$

we can make the simplification

$$e^{-i\phi_1} + e^{-i\phi_2} = e^{-i\phi}2\cos\Delta\phi,$$

and the quadratic equation reduces to

$$x^2 - xe^{-i\phi}(1 + ig_0)2\cos\Delta\phi + [g^2 + (1 + ig_0)^2]e^{-i2\phi} = 0.$$

With the abbreviation

$$u = [g^2 + (1 + ig_0)^2 \sin^2\Delta\phi]^{1/2}, \tag{14.63}$$

the two solutions are given by

$$\begin{aligned} x_1 &= e^{-i\phi}[(1 + ig_0)\cos\Delta\phi + iu], \\ x_2 &= e^{-i\phi}[(1 + ig_0)\cos\Delta\phi - iu]. \end{aligned} \tag{14.64}$$

To use both solutions, we generalize Eq. (14.61) and write

$$T_r = T_0(C_1x_1^r + C_2x_2^r). \tag{14.65}$$

From the condition that $T_r = T_0$ when $r = 0$, it follows that $C_1 + C_2 = 1$. Since $S_{-1} = 0$, it follows from Eq. (14.60) that $T_1 = T_0(1 + ig_0)\exp[-i\phi_1]$ and combining this with Eq. (14.65), we obtain

$$C_1x_1 + C_2x_2 = (1 + ig_0)e^{-i\phi_1}.$$

With this additional relation between C_1 and C_2, we find

$$\begin{aligned} 2C_1 &= 1 - \sin\Delta\phi(1 + ig_0)/u, \\ 2C_2 &= 1 + \sin\Delta\phi(1 + ig_0)/u. \end{aligned} \tag{14.66}$$

Combining Eqs. (14.65) and (14.66), we obtain a general expression for the electric field in the primary beam:

$$T_r = \frac{T_0}{2}\{[1 - \sin\Delta\phi(1 + ig_0)/u]x_1^r + [1 + \sin\Delta\phi(1 + ig_0)/u]x_2^r\}. \tag{14.67}$$

It is convenient to represent the electric field in the reflected beam by means of $S_{r-1}e^{-i\phi}$, since the position represented is the same as that of T_r. With appropriate substitutions for T_{r+1} and T_r, we obtain from Eq. (14.60)

$$S_{r-1}e^{-i\phi} = \frac{T_0g}{2u}(x_1^r - x_2^r). \tag{14.68}$$

Although there is a great deal of interest in the general case where the Bragg law is only approximately satisfied ($\Delta\phi$ is small), we shall now restrict ourselves to the special case where the Bragg law is exactly satisfied. Setting $\theta_1 = \theta_2 = \theta$ and $\Delta\phi = 0$, Eqs. (14.67) and (14.68) reduce to

$$T_r = \frac{T_0}{2}e^{-i\phi r}\{(1 + ig_0 + ig)^r + (1 + ig_0 - ig)^r\}, \tag{14.69}$$

$$S_{r-1}e^{-i\phi} = \frac{T_0}{2}e^{-i\phi r}\{(1 + ig_0 + ig)^r - (1 + ig_0 - ig)^r\}. \tag{14.70}$$

With appropriate representation by exponentials, the two equations reduce to

$$T_r = \frac{T_0}{2} e^{-i\phi r}\{e^{i(g_0+g)r} + e^{i(g_0-g)r}\}, \tag{14.71}$$

$$S_{r-1}e^{-i\phi} = \frac{T_0}{2} e^{-i\phi r}\{e^{i(g_0+g)r} - e^{i(g_0-g)r}\}. \tag{14.72}$$

We consider first the case of negligible absorption, where the imaginary parts of g_0 and g can be neglected. For this case, Eqs. (14.71) and (14.72) can be written

$$\begin{aligned} T_r &= T_0 e^{-i\phi r} e^{ig_0 r} \cos gr, \\ S_{r-1}e^{-i\phi} &= T_0 e^{-i\phi r} e^{ig_0 r}(i) \sin gr. \end{aligned} \tag{14.73}$$

Multiplying by the complex conjugate, we obtain the corresponding intensities of the transmitted and reflected beams:

$$\begin{aligned} I_r(T) &= I_0 \cos^2 gr, \\ I_r(S) &= I_0 \sin^2 gr. \end{aligned} \tag{14.74}$$

This is the familiar effect for which Ewald coined the name "Pendellösung Effect." The intensity oscillates with increasing r; at one position, $I_r(T)$ is a maximum and $I_{r_\perp}(S)$ is zero, and at another position $I_r(T)$ is zero and $I_r(S)$ is a maximum. In terms of a horizontal distance x from the entrance face of the crystal, $r = x/a$. From Eq. (14.57),

$$gr = \left(\frac{e^2}{mc^2}\right)\frac{N\lambda f(2\theta)Px}{\cos\theta},$$

where $P = 1$ or $P = \cos 2\theta$ depending on whether E_0 is perpendicular or parallel to the plane of primary and reflected beams. From one maximum to the next in $I_r(T)$, the value of gr changes by π, and the corresponding separation Δx is given by

$$\Delta x = \frac{\pi \cos\theta}{(e^2/mc^2)N\lambda f(2\theta)P}. \tag{14.75}$$

By proper use of a crystal slice which has a slight taper, the different Pendellösung maxima can be observed, and a value obtained for Δx. We then have the interesting possibility of determining the value of the scattering factor $f(2\theta)$ from a measured distance between Pendellösung fringes.

We next consider the case of a thick crystal with an absorption coefficient which is much too large to be neglected. Both g_0 and g have imaginary parts and we write

$$g = g' + ig'', \qquad g_0 = g_0' + ig_0'',$$

where g'' and g_0'' are the imaginary parts of g and g_0. As a good approximation we can assume that the imaginary part of the scattering factor is

independent of the scattering angle, so that $\Delta f''(2\theta) = \Delta f''(0)$. We now consider the two cases for E_0 parallel or perpendicular to the plane of the primary and reflected beams.

CASE I. E_0 parallel:

$$g = \left(\frac{e^2}{mc^2}\right)\frac{Na\lambda f(2\theta)\cos 2\theta}{\cos\theta},$$

$$g_0 = \left(\frac{e^2}{mc^2}\right)\frac{Na\lambda f(0)}{\cos\theta}.$$

For Case I, it follows that $g'' = g_0'' \cos 2\theta$.

CASE II. E_0 perpendicular:

$$g = \left(\frac{e^2}{mc^2}\right)\frac{Na\lambda f(2\theta)}{\cos\theta}$$

$$g_0 = \left(\frac{e^2}{mc^2}\right)\frac{Na\lambda f(0)}{\cos\theta}$$

For Case II, it follows that $g'' = g_0''$.

Expressing g'' in terms of g_0'', the two exponential terms of Eqs. (14.71) and (14.72) take the following forms.

CASE I. E_0 parallel:

(Ia) $$e^{i(g_0+g)r} = e^{i(g_0'+g')r}e^{-g_0''(1+\cos 2\theta)r}; \tag{14.76}$$

(Ib) $$e^{i(g_0-g)r} = e^{i(g_0'-g')r}e^{-g_0''(1-\cos 2\theta)r}. \tag{14.77}$$

CASE II. E_0 perpendicular:

(IIa) $$e^{i(g_0+g)r} = e^{i(g_0'+g')r}e^{-g_0''2r}; \tag{14.78}$$

(IIb) $$e^{i(g_0-g)r} = e^{i(g_0'-g')r}e^{-g_0''(1-1)r}. \tag{14.79}$$

In Eqs. (14.76) through (14.79), the exponential factors involving g_0'' represent an absorption of the beam. For intermediate values of $\cos 2\theta$ which are not too close to $+1$ or -1, and for large values of r, it is evident that for cases Ia, Ib, and IIa, the beams will be eliminated by absorption. For IIb, the effective absorption is zero, and this beam will persist even for large values of r. Retaining only the component IIb, Eqs. (14.71) and (14.72) reduce to

$$\begin{aligned} T_r &= \frac{T_0}{2}e^{-i\phi r}e^{i(g_0'-g')r}, \\ S_{r-1}e^{-i\phi} &= -\frac{T_0}{2}e^{-i\phi r}e^{i(g_0'-g')r}. \end{aligned} \tag{14.80}$$

Multiplying by the complex conjugate, we obtain

$$|T_r|^2 = |T_0|^2/4 \qquad |S_{r-1}e^{-i\phi}|^2 = |T_0|^2/4. \tag{14.81}$$

An unpolarized primary beam of intensity I_0 can be considered as two beams of intensity $I_0/2$ with mutually perpendicular polarization. It is only the perpendicular component which produces the beams represented by Eq. (14.81), and hence the intensities of the transmitted and reflected beams are given by

$$I_r(T) = I_0/8, \qquad I_r(S) = I_0/8, \tag{14.82}$$

where I_0 is the intensity of a highly parallel unpolarized primary beam which makes the exact Bragg law angle. The transmitted and reflected beams predicted by Eq. (14.82) will exist even for a rather thick crystal, and these are the beams which represent the Borrmann effect. In practice, the intensities are a little less than $I_0/8$, because we have neglected the spacial extent and temperature vibration of the atoms, and the fact that the primary beam is never perfectly monochromatic and parallel.

Throughout this chapter, the discussion has been in terms of a transmitted beam and a reflected beam. However, they are not independent since each one is continually modifying the other. At any point in the crystal, it is the "wave field" or resultant of the electric fields of the two waves which is the really fundamental quantity. For the conditions, represented by Eqs. (14.80), it is a simple matter to set up an expression for the wave field.

We represent a position in the crystal by the coordinates x and y, where x is the horizontal distance from the entrance face, and y is the distance above the reference Bragg plane of Fig. 14.15(a). Let the propagation vector for the T-wave be $\mathbf{k}$, with magnitude $|\mathbf{k}| = 2\pi/\lambda$, and components $+k_x$ and $-k_y$. For the S-wave the magnitude of the propagation vector is the same, but the components are $+k_x$ and $+k_y$. The electric field in the two waves at position xy is then represented by

$$\begin{aligned} T(x, y) &= \frac{T_0}{2} e^{-i(k_x x - k_y y)}, \\ S(x, y) &= -\frac{T_0}{2} e^{-i(k_x x + k_y y)}. \end{aligned} \tag{14.83}$$

To see that Eqs. (14.80) and (14.83) are equivalent, we can compare $T(x, 0)$ and T_r. Setting $y = 0$, and using the fact that $k_x = (2\pi/\lambda)\cos\theta$, Eq. (14.83) leads to

$$T(x, 0) = \frac{T_0}{2} e^{-i(2\pi x/\lambda)\cos\theta}.$$

Since $\phi = (2\pi/\lambda)a \cos\theta$, it is of the order of magnitude of 2π, whereas $(g_0' - g')$ is of the order of 10^{-5}. Neglecting the term $\exp[i(g_0' - g')r]$, Eq. (14.80) becomes

$$T_r = \frac{T_0}{2} e^{-i(2\pi x/\lambda)\cos\theta}$$

and hence is identical to the $T(x, 0)$ obtained from Eq. (14.83).

The resultant electric field is given by the sum of $T(x, y)$ and $S(x, y)$

$$E(x, y) = iT_0 e^{-ik_x x} \sin k_y y.$$

Using the relations

$$k_x = (2\pi/\lambda)\cos\theta, \qquad k_y = (2\pi/\lambda)\sin\theta = \pi/d,$$

and bringing out explicitly the time dependence which is contained in T_0, we express the wave field in the following form:

$$E(x, y) = i\,|T_0| \exp\left[2\pi i\left(\nu t - \frac{x\cos\theta}{\lambda}\right)\right] \sin\frac{\pi y}{d}. \qquad (14.84)$$

The wave field has nodes at levels y which are a multiple of d, and hence $E(x, y)$ is zero at each of the Bragg planes of Fig. 14.15(a). This is another way of explaining the Borrmann effect. Since there are nodes with zero intensity at the positions of the atomic planes, the atoms are in regions of nearly zero intensity, absorption is largely eliminated, and the wave field can persist through a thick crystal. It is evident that the Borrman effect will be observed only from reflections for which all atoms are on the planes with spacing d. If there are additional atoms at positions between the layers, these atoms will not be at intensity nodes. For this case the absorption will not be eliminated, and the wave field will be rapidly extinguished. Apart from the nodes in the y-direction, Eq. (14.84) represents a traveling wave which propagates in the x-direction. It is for this reason that the beams emerge from the crystal at a position which is opposite the entrance point as illustrated by Fig. 14.14.

When a crystal is set to give a transmitted and a reflected beam by means of the Borrmann effect, both beams are highly polarized. This is readily demonstrated with the arrangement shown schematically by Fig. 14.16. Radiation from a copper target tube is partially monochromated with a Ni filter and collimated by a small aperture A. It is convenient to use a Ge crystal about 0.5 mm thick, which has been cut so that the 220-planes are perpendicular to the face of the slice. When the crystal is set at the correct Bragg law angle θ_0, there will be a transmitted and a reflected beam, both of them highly polarized with E perpendicular to the plane of the incident and reflected beams. To show that the transmitted beam is highly polarized, it can be reflected from a crystal which has a set of planes for which the 2θ-angle

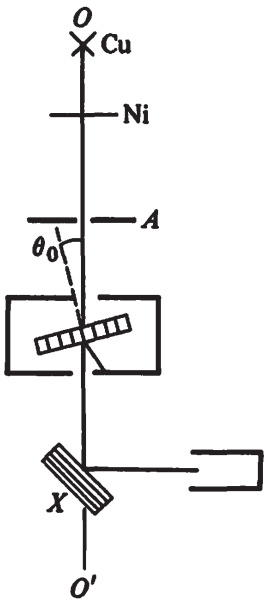

Fig. 14.16 Experimental arrangement for showing that the transmitted beam in Borrmann reflection is highly polarized. With Cu$K\alpha$ radiation it is convenient to use a highly perfect Ge crystal about 0.5 mm thick, cut for reflection by the 220 planes.

is close to 90°. Although not very close, it is possible to use 400 of LiF for which $2\theta = 100°$. The Ge crystal is fixed in a cylindrical holder, so that it can be rotated about the OO'-axis. At the position shown, and also at the 180° position, there will be a strong beam reaching the counter, while at the two 90° positions the reading is practically zero. Set up in this way, the Ge crystal is a convenient polarizer,[22] and it plays a role which is very similar to that of a sheet of Polaroid.

In the Borrmann effect, the transmitted and reflected beams are almost perfect beams, they are highly monochromatic, highly parallel, and highly polarized. There is sufficient intensity for simple experiments, but unfortunately not enough for some of the more elaborate experiments which suggest themselves.

14.9 ASYMMETRIC BRAGG REFLECTION

We now consider Bragg reflection from a crystal whose external surface makes an angle α with the Bragg planes. As illustrated by Fig. 14.17, the primary and reflected beams make angles $\theta + \alpha$ and $\theta - \alpha$ with the external surface. This problem has considerable practical importance in connection

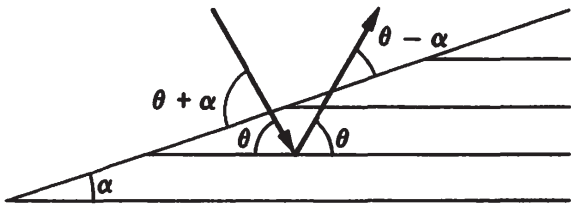

Fig. 14.17 Illustration of asymmetric Bragg reflection where the crystal surface makes an angle α with the Bragg planes.

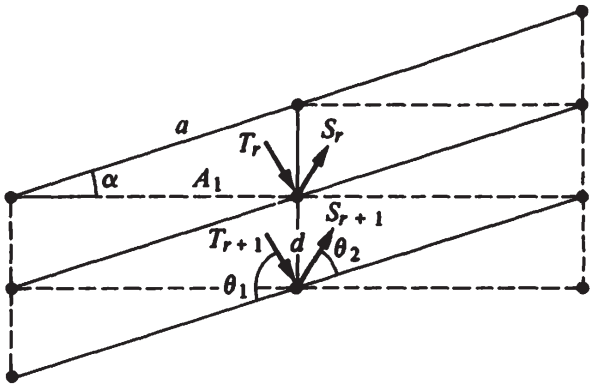

Fig. 14.18 Asymmetric Bragg reflection. The horizontal dashed lines represent the Bragg planes. The slanting solid lines represent a set of planes which are parallel to the surface of the crystal.

with double crystal spectrometer measurements of the reflecting power width of a perfect crystal, and it also illustrates a more generalized application of the Darwin equations. To handle the problem, we make use of the procedure used by Borie[12] in his treatment of the symmetrical Laue case. We restrict ourselves to a simple crystal containing only one kind of atom, and we assume that absorption is small enough relative to attenuation to be neglected.

In Fig. 14.18 the Bragg planes are horizontal, with spacing d. The diffraction from each Bragg plane is independent of the repetitions within the plane as long as M, the number of atoms per unit area, is maintained constant. Hence we can choose a repetition A_1 in the plane of the figure, and A_2 perpendicular to the figure, subject only to the condition that $A_1A_2 = 1/M$. For convenience we choose $A_1 = d/\tan\alpha$. The lattice points are represented by the black dots, and it is evident that these define a set of tilted planes which are parallel to the surface of the crystal. The primary and reflected rays make angles θ_1 and θ_2 with the tilted planes.

We now apply Fresnel diffraction to one of the tilted planes, but with the condition $\theta_1 \neq \theta_2$. Following the procedure of Section 14.2, we can write

$$R_{\epsilon\eta} = R + \epsilon\cos\theta_1 + \frac{\epsilon^2\sin^2\theta_1 + \eta^2}{2R},$$

$$r_{\epsilon\eta} = r - \epsilon\cos\theta_2 + \frac{\epsilon^2\sin^2\theta_2 + \eta^2}{2r}.$$

Introducing the condition $R \gg r$, the sum is given by

$$R_{\epsilon\eta} + r_{\epsilon\eta} = R + r + \epsilon(\cos\theta_1 - \cos\theta_2) + \frac{\epsilon^2\sin^2\theta_2 + \eta^2}{2r}.$$

In the tilted planes, atoms occur only at positions $\epsilon = na$, where $a = A_1/\cos\alpha$, and hence if we introduce the restriction

$$\cos\theta_1 - \cos\theta_2 = \lambda/a, \tag{14.85}$$

the term $\epsilon(\cos\theta_1 - \cos\theta_2)$ becomes $n\lambda$ and drops out in representing E_p by an equation similar to Eq. (14.2). The Fresnel integrals are evaluated in the usual way, and we obtain an equation similar to Eq. (14.6):

$$E_{1'} = E_0(iq_2)e^{(2\pi i/\lambda)[ct-(R+r)]},$$

where

$$q_2 = \left(\frac{e^2}{mc^2}\right)\frac{M'\lambda f(\theta_1+\theta_2)}{\sin\theta_2}.$$

For the tilted planes, M' is the number of atoms per unit area, and $d' = d\cos\alpha$ is the planar spacing. Since $M'/d' = N$ is the number of atoms per unit volume, q_2 can be expressed in terms of the usual q defined by Eq. (14.5) for the case of symmetrical reflection at an angle θ_0 by the Bragg planes:

$$q_2 = \frac{q\cos\alpha\sin\theta_0}{\sin\theta_2}. \tag{14.86}$$

Introduce the two abbreviations:

$$\phi_1 = \frac{2\pi d}{\lambda}\sin(\theta_1-\alpha), \qquad \phi_2 = \frac{2\pi d}{\lambda}\sin(\theta_2+\alpha). \tag{14.87}$$

Considering diffraction by the tilted planes of Fig. 14.18, we now set up difference equations similar to those of Eqs. (14.14) and (14.15):

$$S_r = T_r(iq_2) + S_{r+1}(1+iq_{02})e^{-i\phi_2}, \tag{14.88}$$

$$T_{r+1} = T_r(1+iq_{01})e^{-i\phi_1} + S_{r+1}(iq_1)e^{-i(\phi_1+\phi_2)}. \tag{14.89}$$

The parameter q_2 is given by Eq. (14.86), and by similar reasoning,

$$q_1 = \frac{q\cos\alpha\sin\theta_0}{\sin\theta_1}, \qquad q_{01} = \frac{q_0\cos\alpha\sin\theta_0}{\sin\theta_1}, \qquad q_{02} = \frac{q_0\cos\alpha\sin\theta_0}{\sin\theta_2}. \tag{14.90}$$

From Eq. (14.89), we obtain

$$S_{r+1} = \frac{T_{r+1} - T_r(1+iq_{01})e^{-i\phi_1}}{(iq_1)e^{-i(\phi_1+\phi_2)}}, \qquad S_r = \frac{T_r - T_{r-1}(1+iq_{01})e^{-i\phi_1}}{(iq_1)e^{-i(\phi_1+\phi_2)}}. \tag{14.91}$$

Substituting these expressions in Eq. (14.88), we obtain an equation involving only the T_r. With the trial solution

$$T_r = T_0x^r, \tag{14.92}$$

the equation in T_r reduces to the following quadratic equation in x:

$$1 + q_1q_2e^{-i(\phi_1+\phi_2)} + (1 + iq_{01})(1 + iq_{02})e^{-i(\phi_1+\phi_2)} = (1 + iq_{01})e^{-i\phi_1}x^{-1} + (1 + iq_{02})e^{-i\phi_2}x \quad (14.93)$$

For the primary beam we now define an angle θ_{01} by the relation

$$\frac{2\pi d \sin \theta_{01}}{\lambda} = m\pi + q_{01}. \quad (14.94)$$

Setting $\theta_1 = \theta_{01} + \Delta\theta_1 + \alpha$ and combining with Eq. (14.87), we obtain

$$\phi_1 = \frac{2\pi d}{\lambda} \sin (\theta_{01} + \Delta\theta_1).$$

It will turn out that θ_{01} is the Bragg law angle for the primary beam with correction for the index of refraction, and $\Delta\theta_1$ is the angle between the primary beam direction and the exact Bragg law direction with refraction correction. For small values of $\Delta\theta_1$, the value of ϕ_1 differs but little from the left-hand side of Eq. (14.94), and we can write

$$\phi_1 = \frac{2\pi d}{\lambda} \sin (\theta_{01} + \Delta\theta_1) = m\pi + q_{01} + v_1. \quad (14.95)$$

From Eqs. (14.94) and (14.95), it follows that

$$v_1 = \frac{2\pi d}{\lambda} \cos \theta_{01} \Delta\theta_1, \quad (14.96)$$

$$e^{-\phi_1} = e^{-i(m\pi+q_{01}+v_1)} = (-1)^m(1 - iq_{01} - iv_1). \quad (14.97)$$

Similarly we define an angle θ_{02} for the reflected beam by the relation

$$\frac{2\pi d \sin \theta_{02}}{\lambda} = m\pi + q_{02}. \quad (14.98)$$

Setting $\theta_2 = \theta_{02} + \Delta\theta_2 - \alpha$, and combining with Eq. (14.87), we obtain

$$\phi_2 = \frac{2\pi d}{\lambda} \sin (\theta_{02} + \Delta\theta_2) = m\pi + q_{02} + v_2,$$

where

$$v_2 = \frac{2\pi d}{\lambda} \cos \theta_{02} \Delta\theta_2, \quad (14.99)$$

$$e^{-i\phi_2} = e^{-i(m\pi+q_{02}+v_2)} = (-1)^m(1 - iq_{02} - iv_2). \quad (14.100)$$

Combining Eqs. (14.97) and (14.100) with Eq. (14.93), and with appropriate dropping of small quantities, the quadratic equation reduces to

$$1 + q_1q_2 + (1 - iv_1)(1 - iv_2) = (-1)^m\{(1 - iv_1)x^{-1} + (1 - iv_2)x\}. \quad (14.101)$$

With the representation

$$v_1 = v + \Delta v, \qquad v_2 = v - \Delta v, \qquad v_1 + v_2 = 2v,$$

we can write

$$\begin{aligned}(1 - iv_1) &= e^{-iv_1} = (1 - iv)e^{-i\Delta v},\\ (1 - iv_2) &= e^{-iv_2} = (1 - iv)e^{i\Delta v}.\end{aligned} \tag{14.102}$$

By using these expressions, Eq. (14.101) reduces to

$$1 - q_1q_2 + (1 - iv)^2 = (-1)^m(1 - iv)\{xe^{i\Delta v} + (xe^{i\Delta v})^{-1}\}. \tag{14.103}$$

To solve Eq. (14.103), it is convenient to introduce the representation

$$xe^{i\Delta v} = (-1)^m(1 - \eta). \tag{14.104}$$

Since η is small, $(1 - \eta)^{-1}$ can be expanded and we obtain

$$xe^{i\Delta v} + (xe^{i\Delta v})^{-1} = (-1)^m\{1 - \eta + 1 + \eta + \eta^2 + \cdots\} = (-1)^m(2 + \eta^2).$$

With the simplification, Eq. (14.103) reduces to

$$1 + q_1q_2 + (1 - iv)^2 = (1 - iv)(2 + \eta^2),$$

and the value of η is given by

$$\eta = \pm(q_1q_2 - v^2)^{1/2}.$$

Introducing the value of η in Eq. (14.104), we obtain an expression for x:

$$x = e^{-i\Delta v}(-1)^m[1 - (\pm)(q_1q_2 - v^2)^{1/2}]. \tag{14.105}$$

From Eqs. (14.91) and (14.92) it follows that $S_{r+1} = xS_r$. Using this relation in Eq. (14.88), we obtain an expression for S_r, and by setting $r = 0$, we find

$$\frac{S_0}{T_0} = \frac{iq_2}{1 - x(1 + iq_{02})e^{-i\phi_2}}. \tag{14.106}$$

With the value of x from Eq. (14.105), and the use of Eqs. (14.100) and (14.102), this reduces to

$$\frac{S_0}{T_0} = \frac{iq_2}{1 - (1 - iv)[1 - (\pm)(q_1q_2 - v^2)^{1/2}]} = \frac{iq_2}{iv \pm (q_1q_2 - v^2)^{1/2}}. \tag{14.107}$$

In the middle region where $v^2 < q_1q_2$, the intensity ratio is given by

$$\frac{I_2}{I_1} = \left(\frac{S_0}{T_0}\right)\left(\frac{S_0}{T_0}\right)^* = \left[\frac{iq_2}{iv \pm (q_1q_2 - v^2)^{1/2}}\right]\left[\frac{-iq_2}{-iv \pm (q_1q_2 - v^2)^{1/2}}\right] = \frac{q_2}{q_1}. \tag{14.108}$$

From Eqs. (14.86) and (14.90), it follows that $q_2/q_1 = \sin\theta_1/\sin\theta_2$, and hence

$$\frac{I_2}{I_1} = \frac{\sin\theta_1}{\sin\theta_2}. \tag{14.109}$$

For the case illustrated by Fig. 14.18, $\sin\theta_1 > \sin\theta_2$ and Eq. (14.109) predicts a reflected intensity which is greater than the primary intensity. At first sight this might seem to be absurd, but it must be remembered that the geometry of Fig. 14.18 results in a cross-sectional area ratio of the two beams $A_2/A_1 = \sin\theta_2/\sin\theta_1$. In the middle region the power in the reflected beam $P_2 = I_2A_2$ is equal to the power in the primary beam $P_1 = I_1A_1$, and this is perfectly reasonable.

For the middle region, v is confined between the limits $v(\max) = \pm(q_1q_2)^{1/2}$, and from Eqs. (14.86) and (14.90) this can be expressed as

$$v(\max) = \pm\frac{q\cos\alpha\sin\theta_0}{(\sin\theta_1\sin\theta_2)^{1/2}}. \tag{14.110}$$

We now wish to express $v(\max)$ in angular units. From Eqs. (14.96) and (14.99),

$$v = (v_1 + v_2)/2 = \frac{\pi d\cos\theta_0}{\lambda}(\Delta\theta_1 + \Delta\theta_2). \tag{14.111}$$

Since θ_1 and θ_2 must satisfy Eq. (14.85), the changes $\Delta\theta_1$ and $\Delta\theta_2$ are related by

$$\sin\theta_1\,\Delta\theta_1 - \sin\theta_2\,\Delta\theta_2 = 0. \tag{14.112}$$

Using Eq. (14.112) to express $\Delta\theta_2$ in terms of $\Delta\theta_1$, Eq. (14.111) becomes

$$v = \frac{\pi d\cos\theta_0}{\lambda}\left(1 + \frac{\sin\theta_1}{\sin\theta_2}\right)\Delta\theta_1 = \frac{2\pi d\cos\theta_0\sin\theta_0\cos\alpha}{\lambda\sin\theta_2}\Delta\theta_1. \tag{14.113}$$

Equating Eqs. (14.110) and (14.113), we obtain the limits of the middle region in terms of the variation in angle of the primary beam

$$\Delta\theta_1(\max) = \pm\frac{q\lambda}{2\pi d\cos\theta_0}\left(\frac{\sin\theta_2}{\sin\theta_1}\right)^{1/2}. \tag{14.114}$$

Going back to Eq. (14.112) and expressing $\Delta\theta_1$ in terms of $\Delta\theta_2$, we obtain a similar expression for the limits of the middle region in terms of the variation in angle of the reflected beam:

$$\Delta\theta_2(\max) = \pm\frac{q\lambda}{2\pi d\cos\theta}\left(\frac{\sin\theta_1}{\sin\theta_2}\right)^{1/2}. \tag{14.115}$$

For symmetrical Bragg reflection where the crystal surface is parallel to the Bragg planes, the middle region is limited to variations in angle of

either the primary or reflected beams by the amount

$$\Delta\theta_s(\max) = \pm \frac{q\lambda}{2\pi d \cos\theta_0}.$$

For symmetrical reflection we call w_s the angular width of the middle region, and for asymmetric reflection we call w_1 the angular width of the primary beam in the middle region and w_2 the angular width of the reflected beam in the middle region. The angular widths for asymmetric reflection are then given by

$$w_1 = w_s(\sin\theta_2/\sin\theta_1)^{1/2}, \tag{14.116}$$

$$w_2 = w_s(\sin\theta_1/\sin\theta_2)^{1/2}. \tag{14.117}$$

For the case illustrated by Fig. 14.18, $\theta_2 < \theta_1$ and hence the angular width of the reflected beam is greater than that for symmetrical Bragg reflection, but the cross-sectional area of the beam is smaller. For the primary beam the angular width of reflection is smaller than that for symmetrical reflection, and by cutting the crystal so as to make θ_2 very small, w_1 can be made as small as desired. This has an important application for the double-crystal spectrometer measurement which is illustrated by Fig. 14.7. If crystal B is cut so as to make w_1 very small, a measurement of I as a function of the rocking angle ϕ gives directly the angular variation of the reflecting power curve of crystal A alone. Applications of this possibility have been made by Renninger[23] and Kohra.[24]

REFERENCES

1. C. G. Darwin, *Phil. Mag.*, **27**, 315, 675 (1914).
2. P. P. Ewald, *Ann Physik* **49**, 1, 117 (1916); **54**, 519 (1917).
3. M. von Laue, *Ergeb. Exakt. Naturw.*, **10**, 133 (1931).
4. R. W. James, *Optical Principles of the Diffraction of X-Rays*, G. Bell and Sons, London, 1950.
   R. W. James, *Solid State Physics*, Vol. 15, Academic Press, New York, 1963.
5. W. H. Zachariasen, *Theory of X-Ray Diffraction in Crystals*, John Wiley and Sons, Inc., New York, 1945.
6. P. B. Hirsch, *Acta Cryst.*, **5**, 176 (1952), and P. B. Hirsch and G. N. Ramachandran, *Acta Cryst.*, **3**, 187 (1950).
7. N. Kato, *J. Phys. Soc. Japan*, **7**, 397 (1952).
8. G. Borrmann, *Trends in Atomic Physics*, Interscience Publishers, Inc., New York, 1959.
9. K. Kohra, *X-Ray Crystallography* (Maruzen Co. Ltd., Japan 1961), Vol. II, 9, p. 849.
10. A. Authier, *Bull. Soc. Franc. Mineral. Crist.*, **84**, 51 (1961).

11. B. W. Batterman and H. Cole, *Rev. Mod. Phys.*, **36**, 681 (1964).
12. B. S. Borie, *Acta Cryst*, **21**, 470 (1966).
13. W. H. Zachariasen, *Acta Cryst*, **23**, 558 (1967).
14. J. E. White, *J. Appl. Phys.*, **21**, 855 (1950).
15. J. A. Prins, *Zeit f. Physik*, **63**, 477 (1930).
16. M. Renninger, *Zeit f. Krist*, **89**, 344 (1934).
17. G. Borrmann, *Zeit. f. Physik*, **127**, 297 (1950).
18. M. von Laue, *Acta. Cryst.*, **2**, 106 (1949).
19. A. Howie and M. J. Whelan, *Proc. Roy. Soc.*, **A263**, 217 (1961).
20. N. Kato, *Acta Cryst.* **16**, 276 (1963).
21. P. B. Hirsch, A. Howie, R. B. Nicholson, D. W. Pashley, and M. J. Whelan. *Electron Microscopy of Thin Crystals*, Butterworth and Co., Ltd., London (1965), Chap. VIII, p. 196.
22. H. Cole, F. W. Chambers, C. Wood, *J. Appl. Phys.*, **32**, 1942 (1961).
23. M. Renninger, *Z. Naturforsch.* **16a**, 1110 (1961).
24. K. Kohra, *J. Phys. Soc. Japan*, **17**, 589 (1962).

PROBLEMS

14.1 Following the method of Darwin, *Phil. Mag.*, **43**, 800 (1922), we investigate quantitatively the magnitude of primary extinction by considering Bragg reflection in a crystal which is perfect but very thin. The layers have a spacing d and there are only p-layers. We start out by assuming only one kind of atom, and we restrict ourselves to a primary beam which is polarized with E_0 perpendicular to the plane of the primary and reflected beams. We neglect all absorption and hence neglect the imaginary parts of q and q_0.

If there are p-layers in the crystal, there will be layers from $r = 0$ to $r = p - 1$. At $r = p$, there is no layer, and hence $S_p = 0$. To handle this case, it is best to eliminate the T_r from the difference equations and obtain a difference equation in S_r. We then try a solution of the form

$$S_r = S_0\left(\frac{x^{r-p} - x^{p-r}}{x^{-p} - x^{p}}\right)$$

which has the desired properties: $S_r = S_0$ for $r = 0$, and $S_r = 0$ for $r = p$. We solve the quadratic equation by setting $x = (-1)^m(1 - \eta)$, where η is small. Later it will be convenient to write this as $x = (-1)^m e^{-\eta}$. We can make approximations such as

$$\frac{\sinh(p\eta - \eta)}{\sinh(p\eta)} = 1 - \eta\coth(p\eta).$$

a) Show that

$$\frac{S_0}{T_0} = \frac{iq}{iv + \eta\coth(p\eta)} \quad \text{where} \quad \eta = \pm(q^2 - v^2)^{1/2}.$$

b) For the middle region where $v^2 < q^2$, obtain the intensity ratio I/I_0.

c) With relations such as $\coth(ix) = -i\cot(x)$ show that the expression for I/I_0 in (b) applies over the whole range of v.

The primary beam has a cross-sectional area A_0 and it is wholly intercepted by the crystal. In terms of the angular variable $\epsilon = \theta - \theta_0 = v\lambda/(2\pi d\cos\theta)$, the integrated reflection is given by

$$\frac{E\omega}{P_0} = \int \frac{I}{I_0}\, d\epsilon.$$

d) Obtain an expression for the integrated reflection $E\omega/P_0$. Generalize to make N the number of unit cells per cc, and F the structure factor per cell.

$$\int_{-\infty}^{+\infty} \frac{dy}{y^2 + (1-y^2)\coth^2[A(1-y^2)^{1/2}]} = \pi \tanh A.$$

For an ideally imperfect crystal, and polarization with E_0 perpendicular to the plane of the primary and reflected beams, the integrated intensity can be obtained from Eq. (4.6):

$$E = \frac{I_0}{\omega}\left(\frac{e^2}{mc^2}\right)^2 \frac{\lambda^3 N^2 F^2}{\sin 2\theta}\,(\delta V).$$

The effective volume δV can be expressed in terms of the cross-sectional area of the primary beam A_0, and the thickness t in terms of the crystal.

e) Obtain an expression for the ratio $(E\omega/P_0)$(Perfect) to $(E\omega/P_0)$(Imperfect).

f) If the reflection is 200 NaCl, what is the maximum thickness t for $(E\omega/P_0)$ (Perfect) and $(E\omega/P_0)$(Imperfect) to differ by not more than one percent? For 200 NaCl; $f(\text{Na}) + f(\text{Cl}) = 21.9$. The value obtained for t can be taken as the maximum size of the "mosaic blocks" or "crystallites" for primary extinction to be negligible in the 200-reflection from NaCl.

14.2 For the 220-reflection from Germanium using Cu$K\alpha$ radiation, compute

a) The attenuation coefficients $\langle\tau\rangle$ of Eq. (14.39);

b) The reflection width $\Delta\theta = 2.12s$ of Eq. (14.40);

c) The curves I/I_0 vs. η for 220 $\parallel$ and 220 $\perp$ corresponding to Fig. 14.10.

14.3 Consider the Symmetrical Laue Case for 200 of NaCl using Cu$K\alpha$ $\lambda = 1.542$ A. Assume that the primary beam is highly parallel and is polarized with E_0 perpendicular to the plane of the primary and reflected beams so that $P = 1$ and $g'' = g_0''$. If θ is the exact Bragg law angle, let the primary beam make an angle $\theta_1 = \theta - \epsilon$, where ϵ is very small, and hence $\Delta\phi = [2\pi(a/\lambda)\sin\theta]\epsilon$. Since $\Delta\phi$ is small,

$$u^2 = g^2 + (\Delta\phi)^2,$$

$$x_1 = e^{-i\phi}(1 + ig_0 + iu), \qquad x_2 = e^{-i\phi}(1 + ig_0 - iu).$$

Since g and g_0 are complex, we write

$$u^2 = (g' + ig'')^2 + (\Delta\phi)^2 = Z^2 e^{i2\gamma} = Z^2(\cos 2\gamma + i\sin 2\gamma).$$

Equating real and imaginary parts, we express Z^4 and $\tan 2\gamma$ in terms of g', g'', and $\Delta\phi$. We then express u by

$$u = Ze^{i\gamma} = Z\cos\gamma + iZ\sin\gamma,$$

$$N(\text{Na} + \text{Cl}) = 22.3 \times 10^{21}\,\text{cm}^{-3},$$

$$f'(\text{Na}) + f'(\text{Cl}) = 21.9, \qquad \Delta f''(\text{Na}) + \Delta f''(\text{Cl}) = 0.90,$$

$$\left(\frac{e^2}{mc^2}\right)\frac{N\lambda}{\cos\theta} = 100.9\,\text{cm}^{-1}, \qquad \frac{\sin\theta}{\lambda} = 0.177 \times 10^8\,\text{cm}^{-1}.$$

Neglect any temperature effect.

We wish to obtain an expression for the intensity of the reflected beam. Starting with Eq. (14.68) and multiplying by the complex conjugate,

$$[(X_1^r) - (X_2^r)][(X_1^r)^* - (X_2^r)^*] = (X_1^r)(X_1^r)^* + (X_2^r)(X_2^r)^* - [(X_1^r)(X_2^r)^* + (X_2^r)(X_1^r)^*].$$

From the numerical data, it will turn out that of the three terms on the right, two are so small that they can be dropped. From the data, it will also turn out that we can write $\sin\gamma = (\frac{1}{2})\tan 2\gamma$.

a) With additional approximations, justified by the data, show that

$$\frac{I_r(S)}{I_0/4} = \frac{1}{1 + (k_1\epsilon'')^2}\exp\left[-k_2 t\left(1 - \frac{1}{[1 + (k_1\epsilon'')^2]^{1/2}}\right)\right],$$

where t is the crystal thickness in cms, and ϵ'' is the angle ϵ in seconds.

Determine the coefficients k_1 and k_2.

b) Compute $I_r(S)/(I_0/4)$ for $\epsilon'' = 0, 1, 2, 3$ seconds and for thicknesses $t = 0.5$ mm and $t = 1.0$ mm. Plot $I_r(S)/(I_0/4)$ against ϵ'' for the two thicknesses.

c) In Borrmann reflection, what is the general effect of increasing the thickness of the crystal?

Appendix I

THE KINEMATICAL INTEGRATED INTENSITY BY FRESNEL DIFFRACTION

In deriving Eq. (3.6) for the intensity from a single crystal, we assumed that the crystal was small enough to treat the primary and diffracted beams by the plane-wave approximation. However, the restrictions imposed by the plane-wave approximation disappear when we change from an intensity to the integrated intensity E, since the errors in the peak height and the peak width cancel one another to give a correct peak area. It is now of interest to carry through the derivation using Fresnel integrals so as to show that Eq. (4.6) is independent of the plane-wave approximation.

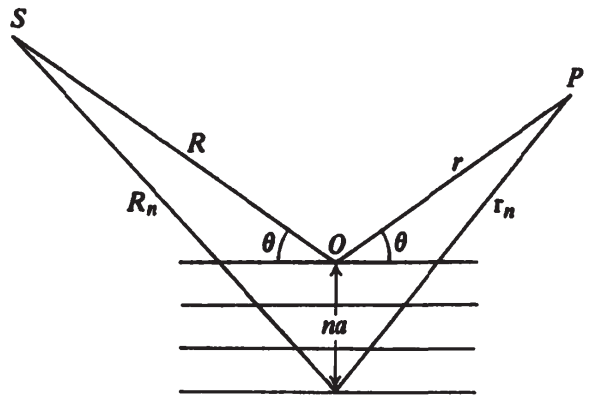

Fig. A.I.1 Geometry used in computing the integrated intensity from a crystal by Fresnel diffraction. The horizontal lines represent the diffracting planes.

The diffracting crystal is shown by Fig. AI.1. To simplify the treatment, we assume that the crystal contains only one kind of atom, and that there are N layers of spacing a, with M atoms per unit area in each layer. Radiation diverges from the source S, and the diffracted radiation is measured at a point P on the receiving surface. The distances R and r are to a point O in the top layer which is chosen so that the two beams make equal angles θ with the diffracting layer. We consider a primary beam which is polarized with electric field normal to the plane of the paper, and with amplitude E_0 at the position of the crystal. Using Fresnel diffraction, the instantaneous value

of the electric field at P which is due to all the atoms in the top layer is given by Eq. (14.3):

$$E_P = \frac{iE_0M\lambda R}{(R + r)\sin\theta\, mc^2}\frac{e^2f}{}\, e^{(2\pi i/\lambda)[ct-(R+r)]}.$$

The nth layer is at a distance na below the surface of the crystal, and we let R_n and r_n be the corresponding path lengths as illustrated by Fig. AI.1.

$$R_n^2 = R^2 + (na)^2 + 2Rna\sin\theta = (R + na\sin\theta)^2 + (na)^2\cos^2\theta$$

$$r_n^2 = r^2 + (na)^2 + 2rna\sin\theta = (r + na\sin\theta)^2 + (na)^2\cos^2\theta$$

Correct to quadratic terms in na, the total path for the nth layer is given by

$$R_n + r_n = R + r + 2na\sin\theta + \cos^2\theta(na)^2/\rho,$$

where $\rho = 2Rr/(R + r)$. The instantaneous field at P due to scattering from the whole crystal is obtained by summing over the layers:

$$E_P = \frac{iE_0M\lambda Re^2f}{(R + r)\sin\theta mc^2}\, e^{(2\pi i/\lambda)[ct-(R+r)]}\sum_{n=0}^{N-1} e^{-(2\pi i/\lambda)[2na\sin\theta-\cos^2\theta(na)^2/\rho]}.$$

We now set $\theta = \theta_0 + \epsilon$, where θ_0 is the correct Bragg law angle and ϵ is a small departure. For small ϵ, we can make the approximation $\sin\theta = \sin\theta_0 + \epsilon\cos\theta_0$, and since $2na\sin\theta_0 = \lambda$, we can drop this term. The exponent in the sum now varies slowly with n and we can replace the sum by an integral:

$$E_P = \frac{iE_0R\lambda Me^2f}{(R + r)\sin\theta_0 mc^2}\, e^{(2\pi i/\lambda)[ct-(R+r)]}\int_{n=0}^{N} e^{-(2\pi i/\lambda)[2na\epsilon\cos\theta_0+\cos^2\theta_0(na)^2/\rho]}. \tag{AI.1}$$

By completing the square, the integral in Eq. (AI.1) can be put into the form

$$e^{(2\pi i\rho\epsilon^2/\lambda)}\int_{n=0}^{N} e^{-i(\pi/2)(4/\lambda\rho)(\rho\epsilon+na\cos\theta_0)^2}\, dn.$$

With the change in variable

$$v = \frac{2}{\sqrt{\lambda\rho}}(\rho\epsilon + na\cos\theta_0), \qquad dv = \frac{2}{\sqrt{\lambda\rho}}a\cos\theta_0\, dn.$$

Equation (AI.1) is expressed in terms of a Fresnel integral:

$$E_P = \frac{iE_0RM\lambda^{3/2}\rho^{1/2}e^2f}{(R + r)a\sin 2\theta mc^2}\, e^{(2\pi i/\lambda)[ct-(R+r)+\rho\epsilon^2]}\int_s^{s+u} e^{-i(\pi/2)v^2}\, dv,$$

where

$$s = 2\epsilon\sqrt{\rho/\lambda}, \qquad u = \frac{2}{\sqrt{\lambda\rho}}Na\cos\theta_0. \tag{AI.2}$$

Multiplying by the complex conjugate, and adding a polarization factor to allow for an unpolarized primary beam, we obtain the intensity at the point of observation:

$$I_P = I_0 \frac{e^4}{m^2c^4}\left(\frac{1+\cos^2 2\theta}{2}\right)\frac{R^2\lambda^3M^2\rho f^2}{(R+r)^2a^2\sin^2 2\theta}\int_s^{s+u} e^{-i(\pi/2)v^2}\,dv\int_s^{s+u} e^{i(\pi/2)w^2}\,dw \tag{AI.3}$$

To calculate the total diffracted energy E when the crystal rotates at velocity ω, it is convenient to think of a receiving surface perpendicular to the diffracted beam and at a small distance r from the crystal. If δV is the volume of the crystal, $\delta V/\mathrm{Na}$ is the area of the top face of the crystal. The effective area on the receiving surface which is illuminated by diffracted radiation is

$$A = \left(\frac{R+r}{K}\right)^2 \frac{\delta V}{Na}\sin\theta.$$

During the rotation, $\int I_p\,dt$ takes the same value at all points in the area A. Since $dt = d\epsilon/\omega$, the diffracted energy is given by

$$E = \left(\frac{R+r}{R}\right)^2 \frac{\delta V}{Na}\frac{\sin\theta}{\omega}\int I_p\,d\epsilon.$$

Combined with Eq. (AI.3), we can write the total diffracted energy E in the following form:

$$E = \frac{I_0e^4}{\omega m^2c^4}\left(\frac{1+\cos^2 2\theta}{2}\right)\frac{\lambda^3M^2\rho f^2\,\delta V}{2Na^3\sin 2\theta\cos\theta} \times\int\left\{\int_s^{s+u} e^{-i(\pi/2)v^2}\,dv\int_s^{s+u} e^{+i(\pi/2)w^2}\,dw\right\}d\epsilon. \tag{AI.4}$$

Using Eq. (AI.2), the triple integral which appears in Eq. (AI-4) can be put into the form

$$Y = \int_{-\infty}^{+\infty}\left\{\int_s^{s+u} e^{-i(\pi/2)v^2}\,dv\int_s^{s+u} e^{i(\pi/2)w^2}\,dw\right\}\frac{ds}{2\sqrt{\rho/\lambda}}.$$

The integral is readily evaluated by using the geometrical interpretation which is represented by Fig. AI.2. The variables v and w are shown as orthogonal axes, and the two integrals within the bracket cover the square of side u. By taking a new set of axes x and y at 45° to v and w, we can write the relations

$$v + w = x\sqrt{2}, \qquad w - v = y\sqrt{2}, \qquad dv\,dw = dx\,dy.$$

Since

$$e^{-i(\pi/2)v^2}e^{i(\pi/2)w^2} = e^{-i(\pi/2)(v^2-w^2)} = e^{i\pi xy},$$

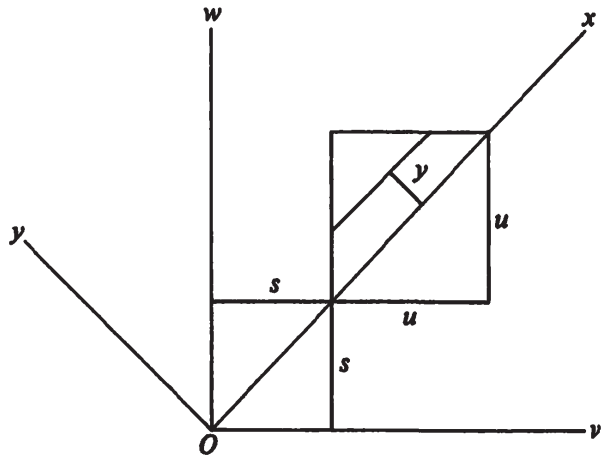

Fig. AI.2 Geometrical interpretation which is used to evaluate the triple integral appearing in Eq. (AI.4).

the integrals within the bracket can be changed to an integration over the square in terms of dx and dy:

$$Y = \frac{1}{2\sqrt{\rho/\lambda}} \int_{-\infty}^{+\infty} \left\{ \int_{\text{Sq}} \int_{\text{Sq}} e^{i\pi xy}\, dx\, dy \right\} ds.$$

A variation in s moves the square along the x-axis, and a change in s can be expressed by a change in x. Making the replacement $ds = dx/\sqrt{2}$, we first integrate between $x = -X$ and $x = X$, and then later let X go to infinity:

$$Y(X) = \frac{1}{\sqrt{2\rho/\lambda}} \left\{ \int_{\text{Sq}} \int_{\text{Sq}} \frac{\sin \pi Xy}{\pi y}\, dx\, dy \right\}.$$

At a distance y from the x-axis, the length intercepted by the square is $(u\sqrt{2} - 2\,|y|)$, and $Y(X)$ reduces to

$$Y(X) = \frac{2}{\sqrt{2\rho/\lambda}} \int_0^{u/\sqrt{2}} (u\sqrt{2} - 2y) \frac{\sin \pi Xy}{\pi y}\, dy.$$

Letting $\pi Xy = z$, the expression becomes

$$Y(X) = \frac{2}{\pi\sqrt{2\rho/\lambda}} \int_0^{\pi X u/\sqrt{2}} \left(u\sqrt{2} - \frac{2z}{\pi X} \right) \frac{\sin z}{z}\, dz.$$

Now letting X go to infinity, we obtain

$$Y = \frac{2u}{\pi\sqrt{\rho/\lambda}} \int_0^{\infty} \frac{\sin z}{z}\, dz = \frac{u}{\sqrt{\rho/\lambda}}.$$

With the value of u from Eq. (AI.2), our expression becomes $Y = 2N(a/\rho)\cos\theta$. Substituting this value for Y in Eq. (AI.4), and letting

$a/M = v_0$ where v_0 is the volume per atom, we obtain an expression for the diffracted energy:

$$E = \frac{I_0}{\omega}\left(\frac{e^4}{m^2c^4}\right)\frac{\lambda^3\,\delta V f^2}{v_0^2}\left(\frac{1+\cos^2 2\theta}{2\sin 2\theta}\right). \tag{AI.5}$$

To generalize this result, it is merely necessary to replace the scattering factor f by the structure factor F_T and the volume per atom v_0 by the volume per cell v_a. Equation (AI.5) then becomes identical to Eq. (4.6). By having carried through the derivation of Eq. (AI.5) using Fresnel diffraction, we have proved that the total diffracted energy given by Eq. (4.6) is independent of the assumption that the crystal was small enough to make the plane-wave approximation.

Appendix II

Wavelengths (in Angstroms) of Some Characteristic Emission Lines and Absorption Edges*

Element	Z	$K\alpha$ (weighted average)†	$K\alpha_2$ Strong	$K\alpha_1$ Very strong	$K\beta_1$ Weak	K edge	$L\alpha_1$ Very strong	L_{III} edge
Na	11		11.909	11.909	11.617			
Mg	12		9.8889	9.8889	9.558	9.5117		
Al	13		8.33916	8.33669	7.981	7.9511		
Si	14		7.12773	7.12528	6.7681	6.7446		
P	15		6.1549	6.1549	5.8038	5.7866		
S	16		5.37471	5.37196	5.03169	5.0182		
Cl	17		4.73050	4.72760	4.4031	4.3969		
A	18		4.19456	4.19162	....	3.8707		
K	19		3.74462	3.74122	3.4538	3.43645		
Ca	20		3.36159	3.35825	3.0896	3.07016		
Sc	21		3.03452	3.03114	2.7795	2.7573		
Ti	22		2.75207	2.74841	2.51381	2.49730		
V	23		2.50729	2.50348	2.28434	2.26902		
Cr	24	2.29092	2.29351	2.28962	2.08480	2.07012		
Mn	25		2.10568	2.10175	1.91015	1.89636		
Fe	26	1.93728	1.93991	1.93597	1.75653	1.74334		
Co	27	1.79021	1.79278	1.78892	1.62075	1.60811		
Ni	28		1.66169	1.65784	1.50010	1.48802		
Cu	29	1.54178	1.54433	1.54051	1.39217	1.38043	13.357	13.2887
Zn	30		1.43894	1.43511	1.29522	1.28329	12.282	12.1309
Ga	31		1.34394	1.34003	1.20784	1.19567	11.313	
Ge	32		1.25797	1.25401	1.12889	1.11652	10.456	
As	33		1.17981	1.17581	1.05726	1.04497	9.671	9.3671
Se	34		1.10875	1.10471	0.99212	0.97977	8.990	8.6456
Br	35		1.04376	1.03969	0:93273	0.91994	8.375	
Kr	36		0.9841	0.9801	0.87845	0.86546		
Rb	37		0.92963	0.92551	0.82863	0.81549	7.3181	6.8633
Sr	38		0.87938	0.875214	0.78288	0.76969	6.8625	6.3868
Y	39		0.83300	0.82879	0.74068	0.72762	6.4485	5.9618
Zr	40		0.79010	0.78588	0.701695	0.68877	6.0702	5.5829
Nb	41		0.75040	0.74615	0.66572	0.65291	5.7240	5.2226
Mo	42	0.71069	0.713543	0.70926	0.632253	0.61977	5.40625	4.9125
Tc	43		0.6793	0.6749	0.6014	0.5891		
Ru	44		0.64736	0.64304	0.57246	0.56047	4.84552	4.3689
Rh	45	0.61470	0.617610	0.613245	0.54559	0.53378	4.59727	4.1296
Pd	46		0.589801	0.585415	0.52052	0.50915	4.36760	3.9081
Ag	47		0.563775	0.559363	0.49701	0.48582	4.15412	3.6983
Cd	48		0.53941	0.53498	0.475078	0.46409	3.95628	3.5038
In	49		0.51652	0.51209	0.454514	0.44387	3.77191	3.3244
Sn	50		0.49502	0.49056	0.435216	0.42468	3.59987	3.1559

* Reprinted from *International Tables for X-Ray Crystallography*, Volume III, with the permission of the Editorial Commission of the International Tables.
† In averaging, $K\alpha_1$ is given twice the weight of $K\alpha_2$.

Appendix II (*cont.*)

Element	Z	$K\alpha$ (weighted average)	$K\alpha_2$ Strong	$K\alpha_1$ Very strong	$K\beta_1$ Weak	K edge	$L\alpha_1$ Very strong	L_{III} edge
Sb	51		0.47479	0.470322	0.417060	0.40663	3.43915	2.9999
Te	52		0.455751	0.451263	0.399972	0.38972	3.28909	2.8554
I	53		0.437805	0.433293	0.383884	0.37379	3.14849	2.7194
Xe	54		0.42043	0.41596	0.36846	0.35849	....	2.5924
Cs	55		0.404812	0.400268	0.354347	0.34473	2.8920	2.4739
Ba	56		0.389646	0.385089	0.340789	0.33137	2.7752	2.3628
La	57		0.375279	0.370709	0.327959	0.31842	2.6651	2.2583
Ce	58		0.361665	0.357075	0.315792	0.30647	2.5612	2.1639
Pr	59		0.348728	0.344122	0.304238	0.29516	2.4627	2.0770
Nd	60		0.356487	0.331822	0.293274	0.28451	2.3701	1.9947
Il	61		0.3294	0.3207	0.28209	....	2.2827	
Sm	62		0.31365	0.30895	0.27305	0.26462	2.1994	1.8445
Eu	63		0.30326	0.29850	0.26360	0.25551	2.1206	1.7753
Gd	64		0.29320	0.28840	0.25445	0.24680	2.0460	1.7094
Tb	65		0.28343	0.27876	0.24601	0.23840	1.9755	1.6486
Dy	66		0.27430	0.26957	0.23758	0.23046	1.90875	1.579
Ho	67		0.26552	0.26083	....	0.22290	1.8447	1.5353
Er	68		0.25716	0.25248	0.22260	0.21565	1.78428	1.48218
Tu	69		0.24911	0.24436	0.21530	0.2089	1.7263	1.4328
Yb	70		0.24147	0.23676	0.20876	0.20223	1.6719	1.38608
Lu	71		0.23405	0.22928	0.20212	0.19583	1.61943	1.34135
Hf	72		0.22699	0.22218	0.19554	0.18981	1.56955	1.29712
Ta	73		0.220290	0.215484	0.190076	0.18393	1.52187	1.25511
W	74		0.213813	0.208992	0.184363	0.17837	1.47635	1.21546
Re	75		0.207598	0.202778	0.178870	0.17311	1.43286	1.17700
Os	76		0.201626	0.196783	0.173607	0.16780	1.39113	1.14043
Ir	77		0.195889	0.191033	0.168533	0.16286	1.35130	1.10565
Pt	78		0.190372	0.185504	0.163664	0.15816	1.31298	1.07239
Au	79		0.185064	0.180185	0.158971	0.15344	1.27639	1.03994
Hg	80		....	....	....	0.14923	1.24114	1.00898
Tl	81		0.175028	0.170131	0.150133	0.14470	1.20735	0.97930
Pb	82		0.170285	0.165364	0.145980	0.14077	1.17504	0.95029
Bi	83		0.165704	0.160777	0.141941	0.13706	1.14385	0.92336
Th	90		0.137820	0.132806	0.117389	0.11293	0.95598	0.76062
U	92		0.130962	0.125940	0.111386	0.1068	0.91053	0.72216

Appendix III

Mass Absorption Coefficients μ_m of the Elements (Z = 1 to 83) for a Selection of Wavelengths (Values given in italics are of low accuracy)

(Reprinted from *International Tables for X-Ray Crystallography*, Vol. III, with the permission of the Editorial Commission of the International Tables.)

Target radiation λ(A)		Ag		Rh		Mo		Cu		Co		Fe		Cr		Ti	
		$K\bar{\alpha}$ 0.5608	$K\beta_1$ 0.4970	$K\bar{\alpha}$ 0.6147	$K\beta_1$ 0.5456	$K\bar{\alpha}$ 0.7107	$K\beta_1$ 0.6323	$K\bar{\alpha}$ 1.5418	$K\beta_1$ 1.3922	$K\bar{\alpha}$ 1.7902	$K\beta_1$ 1.6208	$K\bar{\alpha}$ 1.9373	$K\beta_1$ 1.7565	$K\bar{\alpha}$ 2.2909	$K\beta_1$ 2.0848	$K\bar{\alpha}$ 2.7496	$K\beta_1$ 2.5138
Absorber		μ_m (cm²/g)															
H	1	*0.371*	*0.366*	*0.375*	*0.370*	*0.380*	*0.376*	*0.435*	*0.421*	*0.464*	*0.443*	*0.483*	*0.459*	*0.545*	*0.507*	*0.658*	*0.595*
He	2	*0.195*	*0.190*	*0.199*	*0.194*	*0.207*	*0.200*	*0.383*	*0.333*	*0.491*	*0.414*	*0.569*	*0.474*	*0.813*	*0.661*	*1.26*	*1.01*
Li	3	*0.187*	*0.177*	*0.197*	*0.185*	*0.217*	*0.200*	*0.716*	*0.571*	*1.03*	*0.804*	*1.25*	*0.978*	*1.96*	*1.52*	*3.26*	*2.53*
Be	4	*0.229*	*0.208*	*0.251*	*0.224*	*0.298*	*0.258*	*1.50*	*1.15*	*2.25*	*1.71*	*2.80*	*2.13*	*4.50*	*3.44*	7.64	5.88
B	5	*0.279*	*0.244*	*0.314*	*0.270*	*0.392*	*0.327*	*2.39*	*1.81*	*3.63*	*2.74*	*4.55*	*3.44*	7.38	5.61	12.6	9.67
C	6	*0.400*	*0.333*	*0.469*	*0.383*	*0.625*	*0.495*	*4.60*	*3.44*	7.07	5.31	8.90	6.69	14.5	11.0	24.8	19.1
N	7	*0.544*	*0.433*	*0.658*	*0.515*	*0.916*	*0.700*	7.52	5.60	11.6	8.70	14.6	11.0	23.9	18.2	41.0	31.5
O	8	*0.740*	*0.570*	*0.916*	*0.696*	*1.31*	*0.981*	11.5	8.52	17.8	13.3	22.4	16.8	36.6	27.8	62.5	48.1
F	9	*0.976*	*0.732*	*1.23*	*0.913*	*1.80*	*1.32*	16.4	12.2	25.4	19.0	32.1	24.0	52.4	39.8	89.4	68.8
Ne	10	*1.31*	*0.969*	*1.67*	*1.22*	*2.47*	*1.80*	22.9	17.0	35.4	26.5	44.6	33.5	72.8	55.3	124	95.4
Na	11	*1.67*	*1.22*	*2.15*	*1.56*	*3.21*	*2.32*	30.1	22.3	46.5	34.8	58.6	44.0	95.3	72.5	162	125
Mg	12	*2.12*	*1.54*	*2.73*	*1.97*	*4.11*	*2.96*	38.6	28.7	59.5	44.6	74.8	56.3	121	92.4	204	158
Al	13	*2.65*	*1.90*	*3.42*	*2.45*	5.16	*3.71*	48.6	36.2	74.8	56.2	93.9	70.9	152	116	255	198
Si	14	*3.28*	*2.35*	*4.25*	*3.04*	6.44	*4.61*	60.6	45.1	93.3	70.1	117	88.3	189	144	315	245
P	15	*4.01*	*2.85*	5.20	*3.71*	7.89	5.64	74.1	55.2	114	85.5	142	108	229	175	381	297
S	16	*4.84*	*3.44*	6.29	*4.48*	9.55	6.82	89.1	66.5	136	103	170	129	272	209	450	352
Cl	17	5.77	*4.09*	7.51	5.34	11.4	8.14	106	79.0	161	122	200	152	318	246	*522*	410
A	18	6.81	*4.82*	8.87	6.29	13.5	9.62	123	92.4	187	142	232	177	366	284	*593*	469
K	19	8.00	5.66	10.4	7.39	15.8	11.3	143	107	215	164	266	204	417	325	*667*	*531*
Ca	20	9.28	6.57	12.1	8.58	18.3	13.1	162	122	243	186	299	231	463	363	*728*	*585*
Sc	21	10.7	7.57	13.9	9.89	21.1	15.1	184	139	273	210	336	260	*513*	405	*794*	*643*
Ti	22	12.3	8.70	16.0	11.4	24.2	17.3	208	158	308	237	377	293	*571*	453	98.4	75.8
V	23	14.0	9.91	18.2	12.9	27.5	19.7	233	178	343	266	419	327	68.4	*502*	116	89.6
Cr	24	15.8	11.2	20.6	14.6	31.1	22.3	260	199	381	296	463	363	79.8	60.7	135	104
Mn	25	17.7	12.6	23.0	16.4	34.7	24.9	285	219	414	323	57.2	395	93.0	70.8	157	122

Fe	26	19.7	14.0	25.6	18.2	38.5	27.7	308	238	52.8	349	66.4	50.0	108	82.2	182	141
Co	27	21.8	15.5	28.3	20.2	42.5	30.6	313	257	61.1	45.8	76.8	57.8	125	95.0	210	163
Ni	28	24.1	17.1	31.1	22.3	46.6	33.7	45.7	275	70.5	52.8	88.6	66.7	144	109	242	187
Cu	29	26.4	18.8	34.1	24.4	50.9	36.9	52.9	39.3	81.6	61.2	103	77.3	166	127	280	217
Zn	30	28.8	20.6	37.2	26.7	55.4	40.2	60.3	44.8	93.0	69.7	117	88.0	189	144	318	246
Ga	31	31.4	22.4	40.4	29.1	60.1	43.7	67.9	50.5	105	78.4	131	98.9	212	162	356	276
Ge	32	34.1	24.4	43.8	31.6	64.8	47.3	75.6	56.2	116	87.3	146	110	235	180	393	306
As	33	36.9	26.5	47.3	34.2	69.7	51.1	83.4	62.1	128	96.2	160	121	258	198	430	335
Se	34	39.8	28.6	50.9	36.9	74.7	54.9	91.4	68.1	140	105	175	133	281	216	467	364
Br	35	42.7	30.8	54.6	39.7	79.8	58.8	99.6	74.4	152	115	190	144	305	234	*503*	394
Kr	36	45.8	33.1	58.3	42.5	84.9	62.8	108	80.7	165	124	206	156	327	252	*538*	422
Rb	37	48.9	35.4	62.2	45.5	90.0	66.9	117	87.3	177	134	221	168	351	271	*573*	451
Sr	38	52.1	37.8	66.0	48.4	95.0	70.9	125	94.0	190	144	236	180	373	289	*606*	479
Y	39	55.3	40.3	69.9	51.5	100	75.0	134	101	203	154	252	193	396	308	*638*	*506*
Zr	40	58.5	42.8	73.7	54.5	15.9	79.0	143	108	216	165	268	205	419	326	*669*	*533*
Nb	41	61.7	45.3	77.4	57.5	17.1	82.9	153	115	230	175	284	218	441	345	*699*	*559*
Mo	42	64.8	47.8	81.1	60.5	18.4	13.1	162	123	243	186	300	231	463	363	*727*	*584*
Tc	43	67.9	50.3	13.0	63.5	19.7	14.1	172	131	257	197	316	244	485	382	*753*	*609*
Ru	44	10.7	52.8	13.9	66.4	21.1	15.1	183	139	272	209	334	259	*509*	403	*784*	*637*
Rh	45	11.5	55.2	14.9	10.6	22.6	16.2	194	148	288	222	352	274	*534*	424	*814*	*665*
Pd	46	12.3	57.5	15.9	11.3	24.1	17.3	206	157	304	235	371	289	*559*	446	*845*	*694*
Ag	47	13.1	9.29	17.0	12.1	25.8	18.5	218	166	321	248	391	305	*586*	468	*876*	*723*
Cd	48	14.0	9.91	18.2	12.9	27.5	19.7	231	176	338	262	412	322	*613*	492	*908*	*753*
In	49	14.9	10.6	19.4	13.8	29.3	21.0	243	186	356	277	432	339	*638*	*514*	*935*	*781*
Sn	50	15.9	11.3	20.6	14.7	31.1	22.3	256	197	373	291	451	356	*662*	*536*	*957*	*805*
Sb	51	16.9	12.0	21.9	15.6	33.1	23.8	270	207	391	306	472	373	*688*	*559*	*1100*	*832*
Te	52	17.9	12.7	23.3	16.6	35.0	25.2	282	218	407	320	490	389	*707*	*578*	*557*	*899*
I	53	19.0	13.5	24.6	17.6	37.1	26.7	294	228	422	333	*506*	404	*722*	*594*	214	*919*
Xe	54	20.1	14.3	26.1	18.6	39.2	28.2	306	238	436	346	*521*	418	*763*	*609*	245	*511*
Cs	55	21.3	15.1	27.5	19.7	41.3	29.8	318	248	450	358	*534*	431	*793*	*621*	274	215

(cont.)

Appendix III (*cont.*)

Target radiation $\lambda(A)$		Ag $K\bar{\alpha}$ 0.5608	Ag $K\beta_1$ 0.4970	Rh $K\bar{\alpha}$ 0.6147	Rh $K\beta_1$ 0.5456	Mo $K\bar{\alpha}$ 0.7107	Mo $K\beta_1$ 0.6323	Cu $K\bar{\alpha}$ 1.5418	Cu $K\beta_1$ 1.3922	Co $K\bar{\alpha}$ 1.7902	Co $K\beta_1$ 1.6208	Fe $K\bar{\alpha}$ 1.9373	Fe $K\beta_1$ 1.7565	Cr $K\bar{\alpha}$ 2.2909	Cr $K\beta_1$ 2.0848	Ti $K\bar{\alpha}$ 2.7496	Ti $K\beta_1$ 2.5138
Absorber						μ_m (cm²/g)											
Ba	56	22.5	16.0	29.1	20.8	43.5	31.4	330	258	463	370	*546*	444	*461*	*661*	302	237
La	57	23.7	16.9	30.6	21.9	45.8	33.2	341	268	475	382	*557*	456	202	*681*	329	259
Ce	58	25.0	17.8	32.3	23.1	48.2	34.9	352	278	486	394	*601*	468	219	*409*	356	281
Pr	59	26.3	18.8	34.0	24.4	50.7	36.7	363	288	497	405	*359*	479	236	183	381	302
Nd	60	27.7	19.8	35.7	25.7	53.2	38.6	374	298	*543*	416	*379*	*519*	252	196	405	322
Pm	61	29.1	20.8	37.6	27.0	55.9	40.6	386	308	*327*	428	172	*538*	268	209	429	342
Sm	62	30.6	21.9	39.5	28.4	58.6	42.6	397	319	*344*	*461*	182	*328*	284	222	452	361
Eu	63	32.2	23.0	41.4	29.8	61.5	44.8	*425*	329	156	*478*	193	*344*	299	234	473	379
Gd	64	33.8	24.2	43.5	31.3	64.4	47.0	*439*	340	165	*295*	203	157	314	247	495	397
Tb	65	35.5	25.4	45.6	32.9	67.5	49.2	*273*	352	173	*309*	214	165	329	259	*516*	415
Dy	66	37.2	26.6	47.8	34.5	70.6	51.6	*286*	*369*	182	140	224	173	344	271	*536*	433
Ho	67	39.0	27.9	50.0	36.1	73.9	54.0	128	*231*	191	146	234	181	359	283	*555*	450
Er	68	40.8	29.3	52.4	37.9	77.3	56.6	134	*242*	199	153	245	190	373	295	*574*	466
Tm	69	42.8	30.7	54.9	39.7	80.8	59.2	140	*252*	208	160	255	198	387	307	*592*	483
Yb	70	44.8	32.2	57.4	41.5	84.5	61.9	146	111	217	167	265	206	401	319	*610*	499
Lu	71	46.8	33.6	60.0	43.4	88.2	64.7	153	116	226	174	276	215	416	331	*628*	*515*
Hf	72	48.8	35.1	62.5	45.3	91.7	67.4	159	121	235	181	286	223	430	343	*645*	*532*
Ta	73	50.9	36.7	65.1	47.3	95.4	70.2	166	126	244	189	297	232	444	355	*662*	*547*
W	74	53.0	38.2	67.8	49.3	99.1	73.1	172	132	253	196	308	241	458	368	*679*	*563*
Re	75	55.2	39.8	70.4	51.2	103	75.9	179	137	262	204	319	250	473	380	*696*	*579*
Os	76	57.3	41.4	73.1	53.2	106	78.7	186	143	272	212	330	259	487	393	*712*	*595*
Ir	77	59.4	42.9	75.6	55.2	110	81.4	193	148	282	219	341	269	*502*	406	*729*	*611*
Pt	78	61.4	44.5	78.0	57.1	113	83.9	200	154	291	228	353	278	*517*	419	*745*	*628*
Au	79	63.1	45.8	80.0	58.7	115	86.0	208	160	302	236	365	288	*532*	432	*761*	*644*
Hg	80	64.7	47.1	81.8	60.2	117	87.9	216	166	312	245	377	298	*547*	446	*777*	*660*
Tl	81	66.2	48.4	83.5	61.7	119	89.5	224	172	323	253	389	309	*563*	460	*794*	*677*
Pb	82	67.7	49.8	85.0	63.2	120	91.0	232	179	334	262	402	319	*579*	474	*810*	*694*
Bi	83	69.1	51.1	86.1	64.6	120	92.0	240	185	346	272	415	330	*596*	489	*827*	*712*

Appendix IV

Atomic Scattering Factors*

$(\sin\theta)/\lambda(A^{-1})$		0.0	0.1	0.2	0.3	0.4	0.5	0.6	0.7	0.8	0.9	1.0	1.1	1.2	1.3	1.4	1.5
H	1	1.0	0.81	0.48	0.25	0.13	0.07	0.04	0.02	0.02	0.01	0.01					
He	2	2.0	1.83	1.45	1.06	0.74	0.52	0.36	0.25	0.18	0.13	0.10	0.07	0.05	0.04	0.03	0.03
Li	3	3.0	2.22	1.74	1.51	1.27	1.03	0.82	0.65	0.51	0.40	0.32	0.26	0.21	0.16		
Be	4	4.0	3.07	2.07	1.71	1.53	1.37	1.20	1.03	0.88	0.74	0.62	0.52	0.43	0.37		
B	5	5.0	4.07	2.71	1.99	1.69	1.53	1.41	1.28	1.15	1.02	0.90	0.78	0.68	0.60		
C	6	6.0	5.13	3.58	2.50	1.95	1.69	1.54	1.43	1.32	1.22	1.11	1.01	0.91	0.82	0.74	0.66
N	7	7.0	6.20	4.60	3.24	2.40	1.94	1.70	1.55	1.44	1.35	1.26	1.18	1.08	1.01		
O	8	8.0	7.25	5.63	4.09	3.01	2.34	1.94	1.71	1.57	1.46	1.37	1.30	1.22	1.14		
F	9	9.0	8.29	6.69	5.04	3.76	2.88	2.31	1.96	1.74	1.59	1.48	1.40	1.32	1.25		
Ne	10	10.0	9.36	7.82	6.09	4.62	3.54	2.79	2.30	1.98	1.76	1.61	1.50	1.42	1.35	1.28	1.22
Na	11	11.0	9.76	8.34	6.89	5.47	4.29	3.40	2.76	2.31	2.00	1.78	1.63	1.52	1.44	1.37	1.31
Na^+	11	10.0	9.55	8.39	6.93	5.51	4.33	3.42	2.77	2.31	2.00	1.79	1.63	1.52	1.44	1.37	1.30
Mg	12	12.0	10.50	8.75	7.46	6.20	5.01	4.06	3.30	2.72	2.30	2.01	1.81	1.65	1.54		
Al	13	13.0	11.23	9.16	7.88	6.77	5.69	4.71	3.88	3.21	2.71	2.32	2.05	1.83	1.69	1.57	1.48
Si	14	14.0	12.16	9.67	8.22	7.20	6.24	5.31	4.47	3.75	3.16	2.69	2.35	2.07	1.87	1.71	1.60
P	15	15.0	13.17	10.34	8.59	7.54	6.67	5.83	5.02	4.28	3.64	3.11	2.69	2.35	2.10	1.89	1.75
S	16	16.0	14.33	11.21	8.99	7.83	7.05	6.31	5.56	4.82	4.15	3.56	3.07	2.66	2.34		
Cl	17	17.0	15.33	12.00	9.44	8.07	7.29	6.64	5.96	5.27	4.60	4.00	3.47	3.02	2.65		
Cl^-	17	18.0	16.02	12.20	9.40	8.03	7.28	6.64	5.97	5.27	4.61	4.00	3.47	3.03	2.65	2.35	2.11
A	18	18.0	16.30	12.93	10.20	8.54	7.56	6.86	6.23	5.61	5.01	4.43	3.90	3.43	3.03		
K	19	19.0	16.73	13.73	10.97	9.05	7.87	7.11	6.51	5.95	5.39	4.84	4.32	3.83	3.40	3.01	2.71
Ca	20	20.0	17.33	14.32	11.71	9.64	8.26	7.38	6.75	6.21	5.70	5.19	4.69	4.21	3.77	3.37	3.03

(*cont.*)

* Reprinted from *International Tables for X-Ray Crystallography*, Vol. III, with the permission of the Editorial Commission of the International Tables. The values for elements 1–36 are computed from self-consistent or variational wave functions, while those for elements 37–92 are obtained from the Thomas-Fermi-Dirac statistical model. For values corresponding to ionized states, reference should be made to the International Tables.

Appendix IV (*cont.*)

$(\sin\theta)/\lambda(A^{-1})$		0.0	0.1	0.2	0.3	0.4	0.5	0.6	0.7	0.8	0.9	1.0	1.1	1.2	1.3	1.4	1 5
Sc	21	21.0	18.72	15.39	12.39	10.12	8.60	7.64	6.98	6.45	5.96	5.48	5.00	4.53	4.09	3.68	3.31
Ti	22	22.0	19.41	16.07	13.20	10.83	9.12	7.98	7.22	6.65	6.19	5.72	5.29	4.84	4.41	4.01	3.64
V	23	23.0	20.47	17.03	14.03	11.51	9.63	8.34	7.48	6.86	6.39	5.94	5.53	5.10	4.71	4.30	3.93
Cr	24	24.0	21.93	18.37	15.01	12.22	10.14	8.72	7.75	7.09	6.58	6.14	5.74	5.34	4.94	4.55	4.18
Mn	25	25.0	22.61	19.06	15.84	13.02	10.80	9.20	8.09	7.32	6.77	6.32	5.93	5.54	5.18	4.80	4.45
Fe	26	26.0	23.68	20.09	16.77	13.84	11.47	9.71	8.47	7.60	6.99	6.51	6.12	5.74	5.39	5.03	4.69
Co	27	27.0	24.74	21.13	17.74	14.68	12.17	10.26	8.88	7.91	7.22	6.70	6.29	5.91	5.58	5.23	4.90
Ni	28	28.0	25.80	22.19	18.73	15.56	12.91	10.85	9.33	8.25	7.48	6.90	6.47	6.08	5.75	5.41	5.09
Cu	29	29.0	27.19	23.63	19.90	16.48	13.65	11.44	9.80	8.61	7.76	7.13	6.65	6.25	5.90	5.57	5.25
Zn	30	30.0	27.92	24.33	20.77	17.42	14.51	12.16	10.37	9.04	8.08	7.37	6.84	6.42	6.07	5.73	5.43
Ga	31	31.0	28.65	24.92	21.47	18.26	15.38	12.95	11.02	9.54	8.46	7.64	7.05	6.58	6.21	5.88	5.58
Ge	32	32.0	29.52	25.53	22.11	19.02	16.19	13.72	11.68	10.08	8.87	7.96	7.29	6.77	6.37	6.02	5.72
As	33	33.0	30.47	26.20	22.69	19.69	16.95	14.48	12.37	10.67	9.34	8.32	7.57	6.98	6.54	6.17	5.86
Se	34	34.0	31.43	26.91	23.24	20.28	17.63	15.20	13.06	11.27	9.83	8.71	7.86	7.21	6.72	6.31	5.99
Br	35	35.0	32.43	27.70	23.82	20.84	18.27	15.91	13.78	11.93	10.41	9.19	8.24	7.51	6.95	6.51	6.16
Kr	36	36.0	33.44	28.53	24.40	21.34	18.82	16.54	14.44	12.57	10.97	9.66	8.62	7.81	7.19	6.70	6.31
Rb	37	37.0	34.11	28.97	24.75	21.29	18.55	16.30	14.47	12.94	11.66	10.58	9.65	8.84	8.14	7.53	6.99
Sr	38	38.0	35.06	29.83	25.51	21.96	19.15	16.84	14.96	13.39	12.07	10.95	9.99	9.16	8.44	7.80	7.24
Y	39	39.0	36.01	30.68	26.28	22.64	19.76	17.39	15.46	13.84	12.48	11.32	10.34	9.48	8.73	8.08	7.50
Zr	40	40.0	36.96	31.54	27.04	23.32	20.37	17.94	15.95	14.29	12.89	11.70	10.68	9.80	9.03	8.36	7.76
Nb	41	41.0	37.91	32.40	27.81	24.01	20.98	18.49	16.45	14.74	13.31	12.08	11.04	10.13	9.33	8.64	8.02
Mo	42	42.0	38.86	33.25	28.57	24.69	21.60	19.04	16.95	15.20	13.73	12.46	11.39	10.45	9.64	8.92	8.29
Tc	43	43.0	39.81	34.12	29.34	25.38	22.21	19.60	17.46	15.65	14.15	12.85	11.74	10.78	9.94	9.21	8.55
Ru	44	44.0	40.76	34.98	30.12	26.07	22.83	20.16	17.96	16.12	14.57	13.24	12.10	11.11	10.25	9.49	8.82

Rh	45	45.0	41.72	35.84	30.89	26.76	23.46	20.72	18.47	16.58	14.99	13.63	12.46	11.45	10.56	9.78	9.09
Pd	46	46.0	42.67	36.70	31.67	27.46	24.08	21.28	18.98	17.05	15.42	14.02	12.82	11.78	10.87	10.07	9.37
Ag	47	47.0	43.63	37.57	32.44	28.16	24.71	21.85	19.50	17.52	15.85	14.42	13.19	12.12	11.19	10.37	9.64
Cd	48	48.0	44.58	38.44	33.22	28.85	25.34	22.42	20.02	17.99	16.28	14.81	13.56	12.46	11.51	10.66	9.92
In	49	49.0	45.5	39.3	34.0	29.6	26.0	23.0	20.5	18.5	16.7	15.2	13.9	12.8	11.8	11.0	10.2
Sn	50	50.0	46.5	40.2	34.8	30.3	26.6	23.6	21.1	18.9	17.2	15.6	14.3	13.2	12.1	11.3	10.5
Sb	51	51.0	47.5	41.1	35.6	31.0	27.2	24.1	21.6	19.4	17.6	16.0	14.7	13.5	12.5	11.6	10.8
Te	52	52.0	48.4	41.9	36.4	31.7	27.9	24.7	22.1	19.9	18.0	16.4	15.1	13.8	12.8	11.9	11.0
I	53	53.0	49.4	42.8	37.1	32.4	28.5	25.3	22.6	20.4	18.5	16.8	15.4	14.2	13.1	12.2	11.3
Xe	54	54.0	50.3	43.7	37.9	33.1	29.2	25.9	23.2	20.9	18.9	17.2	15.8	14.5	13.4	12.5	11.6
Cs	55	55.0	51.3	44.5	38.7	33.8	29.8	26.5	23.7	21.3	19.4	17.7	16.2	14.9	13.8	12.8	11.9
Ba	56	56.0	52.3	45.4	39.5	34.5	30.4	27.0	24.2	21.8	19.8	18.1	16.6	15.3	14.1	13.1	12.2
Ta	73	73.0	68.6	60.4	53.1	46.9	41.7	37.3	33.6	30.4	27.7	25.4	23.3	21.6	20.0	18.6	17.4
W	74	74.0	69.5	61.3	54.0	47.6	42.3	37.9	34.1	30.9	28.2	25.8	23.7	21.9	20.3	18.9	17.7
Re	75	75.0	70.5	62.2	54.8	48.3	43.0	38.5	34.7	31.4	28.7	26.3	24.2	22.3	20.7	19.3	18.0
Os	76	76.0	71.5	63.1	55.6	49.1	43.7	39.1	35.3	32.0	29.1	26.7	24.6	22.7	21.1	19.6	18.3
Ir	77	77.0	72.4	64.0	56.4	49.8	44.4	39.7	35.8	32.5	29.6	27.1	25.0	23.1	21.4	19.9	18.6
Pt	78	78.0	73.4	64.9	57.2	50.6	45.0	40.3	36.4	33.0	30.1	27.6	25.4	23.5	21.8	20.3	18.9
Au	79	79.0	74.4	65.8	58.0	51.3	45.7	41.0	37.0	33.5	30.6	28.0	25.8	23.9	22.2	20.6	19.3
Hg	80	80.0	75.3	66.7	58.8	52.1	46.4	41.6	37.5	34.1	31.1	28.5	26.3	24.3	22.5	21.0	19.6
Tl	81	81.0	76.3	67.6	59.7	52.8	47.1	42.2	38.1	34.6	31.6	29.0	26.7	24.7	22.9	21.3	19.9
Pb	82	82.0	77.2	68.5	60.5	53.6	47.8	42.9	38.7	35.1	32.1	29.4	27.1	25.1	23.3	21.7	20.3
Bi	83	83.0	78.2	69.3	61.3	54.3	48.5	43.5	39.3	35.7	32.6	29.9	27.5	25.5	23.6	22.0	20.6
Th	90	90.0	85.0	75.6	67.1	59.6	53.3	47.9	43.3	39.4	36.1	33.1	30.5	28.3	26.3	24.5	22.9
U	92	92.0	86.9	77.4	68.7	61.1	54.7	49.2	44.5	40.5	37.1	34.0	31.4	29.1	27.0	25.2	23.6

Appendix V

Dispersion Corrections for Atomic Scattering Factors

Atom	Cu$K\alpha$ radiation (λ = 1.542 Å)					Mo$K\alpha$ radiation (λ = 0.7107 Å)						
	$\Delta f'$		$\Delta f''$				$\Delta f'$			$\Delta f''$			
	$(\sin\theta)/\lambda$ =		$(\sin\theta)/\lambda$ =				$(\sin\theta)/\lambda$ =			$(\sin\theta)/\lambda$ =			
	0	0.6	0	0.4	0.6		0.0	0.9	1.3	0.0	0.6	0.9	1.3
10 Ne	0.1	0.1	0.2	0.1	0.1	10 Ne	0.0	0.0	0.0	0.0	0.0	0.0	0.0
11 Na	0.1	0.1	0.2	0.2	0.2	11 Na	0.0	0.0	0.0	0.1	0.1	0.1	0.0
12 Mg	0.1	0.1	0.3	0.2	0.2	12 Mg	0.0	0.0	0.0	0.1	0.1	0.1	0.1
13 Al	0.2	0.1	0.3	0.3	0.3	13 Al	0.1	0.1	0.0	0.1	0.1	0.1	0.1
14 Si	0.2	0.2	0.4	0.4	0.4	14 Si	0.1	0.1	0.1	0.1	0.1	0.1	0.1
15 P	0.2	0.2	0.5	0.5	0.5	15 P	0.1	0.1	0.1	0.2	0.2	0.1	0.1
16 S	0.3	0.3	0.6	0.6	0.6	16 S	0.1	0.1	0.1	0.2	0.2	0.2	0.1
17 Cl	0.3	0.3	0.7	0.7	0.7	17 Cl	0.1	0.1	0.1	0.2	0.2	0.2	0.2
18 A	0.3	0.3	0.9	0.9	0.8	18 A	0.1	0.1	0.1	0.3	0.3	0.2	0.2
19 K	0.3	0.3	1.1	1.1	1.0	19 K	0.2	0.2	0.1	0.3	0.3	0.3	0.3
20 Ca	0.3	0.3	1.4	1.4	1.3	20 Ca	0.2	0.2	0.2	0.4	0.4	0.3	0.3
21 Sc	0.3	0.3	1.6	1.6	1.5	21 Sc	0.2	0.2	0.2	0.5	0.5	0.4	0.4
22 Ti	0.2	0.2	1.9	1.9	1.8	22 Ti	0.3	0.2	0.2	0.6	0.6	0.5	0.5
23 V	0.1	0.1	2.3	2.3	2.2	23 V	0.3	0.3	0.2	0.7	0.7	0.6	0.6
24 Cr	−0.1	−0.1	2.6	2.6	2.5	24 Cr	0.3	0.3	0.3	0.8	0.8	0.7	0.7
25 Mn	−0.5	−0.5	3.0	2.9	2.9	25 Mn	0.4	0.3	0.3	0.9	0.9	0.8	0.7
26 Fe	−1.1	−1.1	3.4	3.3	3.3	26 Fe	0.4	0.3	0.3	1.0	0.9	0.9	0.8
27 Co	−2.2	−2.2	3.9	3.8	3.8	27 Co	0.4	0.3	0.3	1.1	1.0	1.0	0.9
28 Ni	(−3.1)	(−3.1)	0.6	0.6	0.5	28 Ni	0.4	0.3	0.3	1.2	1.1	1.1	1.0
29 Cu	−2.1	−2.1	0.7	0.7	0.6	29 Cu	0.3	0.3	0.3	1.4	1.3	1.3	1.2
30 Zn	−1.7	−1.7	0.8	0.7	0.7	30 Zn	0.3	0.3	0.2	1.6	1.5	1.5	1.4
31 Ga	−1.5	−1.5	0.9	0.8	0.8	31 Ga	0.2	0.2	0.2	1.7	1.6	1.6	1.5
32 Ge	−1.3	−1.3	1.1	1.0	0.9	32 Ge	0.2	0.2	0.2	1.9	1.8	1.8	1.7
33 As	−1.2	−1.2	1.2	1.1	1.0	33 As	0.1	0.1	0.1	2.2	2.1	2.0	1.9
34 Se	−1.0	−1.1	1.3	1.2	1.1	34 Se	−0.1	−0.1	−0.1	2.4	2.3	2.2	2.1
35 Br	−0.9	−1.0	1.5	1.4	1.3	35 Br	−0.3	−0.3	−0.3	2.6	2.5	2.4	2.3
36 Kr	−0.9	−1.0	1.7	1.6	1.5	36 Kr	−0.6	−0.6	−0.6	2.9	2.8	2.7	2.6
37 Rb	−0.8	−0.9	1.9	1.8	1.7	37 Rb	−0.9	−0.9	−0.9	3.2	3.1	3.0	2.9
38 Sr	−0.7	−0.8	2.1	2.0	1.8	38 Sr	−1.4	−1.4	−1.5	3.6	3.5	3.4	3.2
39 Y	−0.7	−0.8	2.3	2.2	2.0	39 Y	−2.3	−2.3	−2.4	3.9	3.8	3.7	3.5
40 Zr	−0.6	−0.7	2.5	2.4	2.2	40 Zr	−2.8	−2.8	−2.9	0.8	0.7	0.6	0.6
41 Nb	−0.6	−0.7	2.8	2.6	2.5	41 Nb	−2.1	−2.1	−2.2	0.9	0.8	0.6	0.5
42 Mo	−0.5	−0.6	3.0	2.8	2.7	42 Mo	−1.7	−1.7	−1.8	0.9	0.8	0.7	0.6
43 Tc	−0.5	−0.6	3.3	3.1	3.0	43 Tc	−1.4	−1.5	−1.5	1.0	0.9	0.8	0.6
44 Ru	−0.5	−0.6	3.6	3.4	3.3	44 Ru	−1.2	−1.3	−1.3	1.1	1.0	0.8	0.7
45 Rh	−0.5	−0.6	4.0	3.8	3.6	45 Rh	−1.1	−1.2	−1.3	1.2	1.1	0.9	0.8
46 Pd	−0.5	−0.6	4.3	4.1	3.9	46 Pd	−1.0	−1.1	−1.2	1.3	1.2	1.0	0.8
47 Ag	−0.5	−0.6	4.7	4.5	4.3	47 Ag	−0.9	−1.0	−1.1	1.4	1.3	1.1	0.9
48 Cd	−0.6	−0.7	5.0	4.8	4.6	48 Cd	−0.8	−0.9	−1.0	1.6	1.4	1.3	1.1
49 In	−0.6	−0.8	5.4	5.2	5.0	49 In	−0.7	−0.8	−0.9	1.7	1.5	1.4	1.2
50 Sn	−0.7	−0.9	5.8	5.6	5.4	50 Sn	−0.6	−0.8	−0.9	1.9	1.7	1.5	1.3
51 Sb	−0.8	−1.0	6.3	6.1	5.8	51 Sb	−0.6	−0.8	−0.9	2.0	1.8	1.6	1.4
52 Te	−0.9	−1.1	6.7	6.5	6.2	52 Te	−0.5	−0.7	−0.8	2.2	2.0	1.8	1.5
53 I	−1.1	−1.3	7.2	6.9	6.7	53 I	−0.5	−0.7	−0.8	2.4	2.2	1.9	1.7
54 Xe	−1.4	−1.6	7.8	7.5	7.2	54 Xe	−0.4	−0.6	−0.8	2.5	2.3	2.1	1.8
55 Cs	−1.7	−1.9	8.3	8.0	7.7	55 Cs	−0.4	−0.6	−0.8	2.7	2.5	2.3	2.0
56 Ba	−2.1	−2.3	8.9	8.6	8.3	56 Ba	−0.4	−0.6	−0.8	3.0	2.8	2.5	2.2

* Reprinted from *International Tables for X-Ray Crystallography*, Vol. III, with the permission of the Editorial Commission of the International Tables.

Appendix V (*cont.*)

Atom	$\Delta f'$		$\Delta f''$			Atom	$\Delta f'$			$\Delta f''$			
	$(\sin\theta)/\lambda =$		$(\sin\theta)/\lambda =$				$(\sin\theta)/\lambda =$			$(\sin\theta)/\lambda =$			
	0	0.6	0	0.4	0.6		0.0	0.9	1.3	0.0	0.6	0.9	1.3
70 Yb	−7	−8	5	4	4	70 Yb	−0.5	−0.8	−0.9	6.7	6.3	5.9	5.4
71 Lu	−7	−7	5	5	4	71 Lu	−0.6	−0.9	−1.0	7.0	6.6	6.1	5.6
72 Hf	−6	−7	5	5	4	72 Hf	−0.7	−1.0	−1.1	7.3	6.9	6.4	5.9
73 Ta	−6	−6	6	5	5	73 Ta	−0.8	−1.1	−1.2	7.6	7.2	6.7	6.2
74 W	−6	−6	6	5	5	74 W	−1.0	−1.3	−1.4	8.0	7.6	7.1	6.5
75 Re	−5	−6	6	6	5	75 Re	−1.2	−1.5	−1.6	8.3	8.0	7.5	6.9
76 Os	−5	−6	7	6	6	76 Os	−1.4	−1.7	−1.8	8.8	8.4	7.9	7.3
77 Ir	−5	−6	7	7	6	77 Ir	−1.7	−2.0	−2.1	9.2	8.8	8.3	7.7
78 Pt	−5	−5	8	7	7	78 Pt	−1.9	−2.2	−2.3	9.6	9.1	8.7	8.1
79 Au	−5	−5	8	8	7	79 Au	−2.2	−2.5	−2.6	10.1	9.6	9.2	8.5
80 Hg	−5	−5	9	8	8	80 Hg	−2.6	−2.9	−3.0	10.6	10.1	9.7	9.0
81 Tl	−4	−5	9	9	8	81 Tl	−3.2	−3.5	−3.6	11.2	10.7	10.2	9.5
82 Pb	−4	−5	10	9	9	82 Pb	−3.8	−4.1	−4.2	11.7	11.2	10.7	9.9
83 Bi	−4	−5	10	10	9	83 Bi	−4.5	−4.8	−4.9	11.2	11.7	11.1	10.3
84 Po	−4	−5	11	10	10	84 Po	−5.3	−5.5	−5.6	12.8	12.3	11.7	10.8
90 Th	−4	−5	15	14	13	90 Th	−6	−7	−7	9	8	7	7
91 Pa	−4	−5	16	15	14	91 Pa	−7	−7	−7	9	8	8	7

Appendix VI

Compton-scattering Intensities $\mathscr{I}_{inc}/R$ with Exchange Terms based on Hartree-Fock Wave Functions*

R is the recoil factor: $R = (\nu'/\nu)^3$. $\mathscr{I}_{inc}$ is the atomic incoherent intensity expressed in electronic units.

Atom or ion	$(\sin\theta)/\lambda(A^{-1})$										Number of electrons
	0.05	0.1	0.2	0.3	0.4	0.5	0.6	0.7	0.9	1.1	
Li^+		0.126	0.448	0.841	1.201	1.477	1.669	1.794	1.921	1.968	2
Li		1.047	1.441	1.829	2.187	2.466	2.661	2.789	2.919	2.976	3
Be		1.465	2.228	2.494	2.770	3.036	3.273	3.465	3.726	3.864	4
B	0.439	1.381	2.779	3.264	3.510	3.731	3.945	4.144	4.467	4.684	5
C		1.030	2.511	3.532	4.027	4.432	4.672	4.879	5.223	5.484	6
N		1.050	2.824	4.075	4.780	5.177	5.438	5.639	5.970	6.247	7
N^-		1.721	3.856	5.172	5.859	6.226	6.462	6.650	6.974	7.248	8
O^+		0.630	2.049	3.430	4.363	4.901	5.220	5.439	5.769	6.042	7
O		0.970	2.797	4.305	5.271	5.841	6.185	6.417	6.758	7.036	8
O^-		1.531	3.741	5.330	6.310	6.870	7.203	7.428	7.763	8.030	9
F		0.861	2.706	4.464	5.718	6.482	6.934	7.221	7.584	7.854	9
F^-		1.346	3.540	5.296	6.534	7.330	7.827	8.148	8.550	8.837	10
Ne		0.816	2.539	4.255	5.628	6.627	7.315	7.772	8.314	8.641	10
Na^+		0.560	1.893	3.428	4.817	5.909	6.728	7.314	8.027	8.430	10
Na		1.504	2.883	4.417	5.802	6.895	7.718	8.308	9.025	9.429	11
Al^+		1.57	3.10	4.24	5.42	6.51	7.44	8.21	9.29	9.92	12
Al		2.28	4.03	5.20	6.38	7.48	8.42	9.19	10.28	10.92	13
Si^{+4}		0.24	0.93	1.89	2.96	4.00	4.95	5.74	6.91	7.64	10
Si		2.46	4.57	5.76	6.82	7.85	8.79	9.60	10.82	11.59	14
Cl^-		2.68	5.94	8.14	9.55	10.54	11.38	12.16	13.50	14.52	18
K^+		1.50	4.30	6.66	8.41	9.65	10.57	11.33	12.65	13.73	18
Ca^{++}		1.21	3.69	6.01	7.82	9.16	10.16	10.95	12.26	13.36	18
Ca		3.09	5.65	7.95	9.77	11.14	12.15	12.95	14.25	15.35	20
Sc^+	0.52	1.74	4.53	7.00	8.99	10.52	11.66	12.53	13.89	15.00	20
Ti^+		1.54	4.03	6.25	8.25	9.97	11.38	12.52	14.19	15.40	21
V^{+2}		1.11	3.48	5.83	7.91	9.69	11.16	12.35	14.10	15.36	21
Cr^+	0.46	1.62	4.50	7.11	9.35	11.23	12.74	13.93	15.66	16.90	23
Mn^+		1.59	4.57	7.28	9.62	11.67	13.36	14.74	16.76	18.15	24
Mn		2.92	5.78	8.44	10.75	12.74	14.39	15.74	17.75	19.15	25
Fe^{+2}	0.32	1.19	3.74	6.38	8.69	10.67	12.34	13.71	15.73	17.13	24
Fe^+	0.44	1.57	4.53	7.25	9.60	11.63	13.33	14.72	16.75	18.14	25
Fe		2.49	5.47	8.01	10.34	12.34	14.02	15.44	17.53	19.00	26
Co^{+2}	0.31	1.17	3.72	6.40	8.77	10.82	12.58	14.04	16.22	17.72	25
Co^+	0.43	1.54	4.51	7.28	9.68	11.77	13.56	15.05	17.24	18.74	26
Ni^{+2}	0.31	1.14	3.69	6.40	8.82	10.93	12.76	14.31	16.67	18.29	26
Ni^+	0.41	1.50	4.47	7.28	9.72	11.86	13.73	15.30	17.67	19.29	27
Cu^{+2}	0.30	1.12	3.66	6.39	8.85	11.02	12.92	14.55	17.06	18.81	27
Cu^+	0.40	1.45	4.42	7.26	9.73	11.92	13.85	15.51	18.06	19.82	28
Cu		1.99	5.26	8.15	10.70	12.90	14.82	16.46	19.02	20.80	29
Zn^{+2}		1.11	3.64	6.39	8.87	11.07	13.01	14.71	17.39	19.29	28
Ge		1.59	4.75	7.39	10.02	12.54	14.73	16.59	19.59	21.90	32

* Reprinted from *International Tables for X-Ray Crystallography*, Vol. III, with the permission of the Editorial Commission of the International Tables.

INDEX

INDEX

Absorption coefficients μ_m, table, 366
Angles between planar normals, cubic, table, 81
Antiphase domains, 216
  Effect on peak shape in reciprocal space, 219
  Effect on powder pattern integral breadths, 223
  Integrated intensity independent of antiphase domains, 217
Asymmetric Bragg reflection by Darwin method, 348
  Intensity of reflection, 353
  Width of reflection, 354
Atomic scattering factor f, 10
  Table, 369
AUTHIER, A, 316
AVERBACH, B. L., 195, 241, 269
Axial divergence error, 70

BADEN-POWELL, 177
BATTERMAN, B., 190, 316
BEARDEN, J. A., 68
Bernal chart, 89
BERTAUT, F., 267, 271
BJURSTROM, T., 62
Blackening of film, B, 54
BORIE, B., 167, 198, 199, 241, 316, 340, 349
BORN, M., 178
Born-von Karman theory, 187
BORRMANN, G., 316, 340
Borrmann effect, 340, 346
Bragg and Williams long-range order parameter, 208
Bragg law in vector form, 18
Bragg reflection in perfect crystals, 316
  Attenuation coefficient, 328
  Darwin difference equations, 321
  Integrated intensity, negligible absorption, 326
  Integrated intensity, small reflecting power, 334
  Reflecting power, including absorption, 335
  Thick crystal, negligible absorption, 324
  Width of reflection, 329
Bravais lattices, 22
Breit-Dirac factor, 12
Brillouin zone, 158
BUERGER, M. J., 92
Buerger precession camera, 90
BUNN, C. W., 62

CARTZ, L., 203
Cauchy relations, 152
CHIPMAN, D. R., 190, 200, 213, 214, 240
CHRISTIAN, J. W., 299
COCHRAN, W., 100, 111
COHEN, M. U., 70
COLE, H., 175, 316
Complex conjugate ϵ^*, 7
Complex exponential, use of, 6
Compton intensities, table, 374
Convergence factor, 127, 137
COWLEY, J. M., 215, 230, 235, 236
Cowley short-range order parameter, 229
Crystal axes, definition, 15
Crystallographic planes hkl, 16
CURIEN, H., 188

DARWIN, C. G., 315
DAUBEN, C. H., 12
DAVEY, W. P., 62
DEBYE, P., 123, 151, 189, 190
Debye temperature factor, 38
  With two kinds of atoms, 61
Debye scattering equation, 117
DELAUNAY, J., 153
Dispersion of elastic waves, 176
Dispersion correction to scattering factors, 10
  Table, 372
Double crystal spectrometer, 328
DUMOND, J. W. M., 260
Dynamical theory of x-ray diffraction, 315

EDMUNDS, I. G., 222
Elastic moduli for cubic crystals, table, 153
Elastic waves in cubic crystals, 152
Electron unit for intensities, 1
EWALD, P. P., 315
Ewald sphere, 19
Extinction, correction for, 332
  Primary, 331
  Secondary, 332

FAXEN, H., 151
Faulting in BCC metals, 305
  Particle size and fault probabilities from Fourier coefficients, 311
Faulting in FCC metals, 275
  Deformation fault, 275
  Deformation faulting from peak shifts, 288
  Difference equation for deformation and twin faulting, 280
  Effects of faulting on peak broadening, 291
  Growth or twin fault, 275
  Twin faulting from peak asymmetry, 294
Faulting in HCP metals, 298
  Difference equation for deformation and growth faulting, 300
  Particle size and fault probabilities from Fourier coefficients, 303
Fiber diagrams as rotation patterns, 92
FINBAK, C., 135
FOREMAN, A. J. E., 186
Fourier analysis of size and strain broadening, 264
  Use of fictitious quantities, 273
Fourier inversion with Beevers-Lipson strips, 131
Fourier series methods, 105
  Representation of the electron density, 108
Fresnel integrals, 144
Fresnel treatment for amorphous sample, 142
Fundamental reflections, 210

Gaussian probability, 36
GEROLD, V., 206
GEVERS, R., 300
Gnomonic projection, 77
Greninger chart, 79
GUENTERT, O. J., 305
GUINIER, A., 206, 312
GUTTMAN, L., 206

HARKER, D., 111
Harker-Patterson sections, 114
Harmonic oscillator, energy, 162
HERBSTEIN, F. H., 195
HINDE, R. M., 222
HIRSCH, P. B., 305, 316, 340
Hook effect, 272
HOWIE, A., 340
HUANG, K., 241, 244
HULL, A. W., 62
Hull-Davey hexagonal chart, 63

Index of refraction, 320
Integral breadth, definition, 225
Integrated intensity
  Diffractometer powder briquet, 49
  Extended face imperfect crystal, 46
  Kinematical theory by Fresnel diffraction, 359
  Laue pattern reflections, 50
  Powder sample bathed in beam, 49
  Small crystal rotated, 44

Instrumental broadening corrections, 257
Convolution relation, 258
Rachinger correction for α_2, 260
Stokes correction, 258
Intensity
Definition, 3
From a small crystal, 29
Intensity of modified scattering per atom, 10
Table, 374
Interatomic force constants FCC, 183
Aluminum, table, 187
Interference function, 262
International Tables for X-Ray Crystallography, 12, 96
Inversion temperature for TDS, 201

JACOB, C. W., 100
JACOBSEN, E. H., 188
JAMES, R. W., 12, 151, 189, 316
JONES, F. W., 227

KASPER, J. S., 111
KATO, N., 316, 340
KEATING, D. T., 139, 214, 215, 237
KOHRA, K., 316, 354

LAUE, M. von, 315, 340
Laue equations, 31
Laue monotonic scattering, 229
Laue pattern
Transmission, 75
Back reflection, 77
LAVAL, J., 151
LIPSON, H., 66, 100, 111, 206, 222
LOMER, W. M., 186
Long-range order in binaries, 208
Experimental determination of order parameters, 211
Measured LRO for Cu_3Au, 213
Measured LRO for β Cu Zn, 214
Shift in peak position with order, 215
Structure factors for partial LRO, 209
Lorentz-polarization factor
Powder sample, 49
Single crystal rotated, 44
Lucite standard, 172

MAVEL, G., 124
MENKE, H., 123
MERING, J., 221, 278
Microphotometering of film, 53
Miller indices, 16
MOSS, S. C., 237, 240
MOZZI, R. L., 149
Multiple scattering in amorphous samples, 145
Multiplicity factor, 47

NILSSON, N., 201
NIX, F. C., 206, 208
Norman method for standardizing, 141

OLMER, P., 166
OTTE, H. M., 305

Pair function, 138
Area under a pair function, 140
PARRISH, W., 67
Particle size broadening
Scherrer equation, 253
Method of Stokes and Wilson, 254
Separation of particle size and distortion broadening, 269
PASKIN, A., 200
PATERSON, M. S., 278
PATTERSON, A. L., 112
Patterson function, 112
Pendellosung effect, 344
Perfect crystal theory, 315
PHILLIPS, J. C., 188
Polarization
Compton scattering, 5
Unmodified scattering, 4
Polarization factor
Crystal monochromated beam, 13
Unpolarized primary beam, 4
Powder patterns, interpretation
Hexagonal pattern, 65
Orthorhombic pattern, 66
Rock salt pattern, 57
Powder diffractometer, 55
Peak area, quantitative expression, 57
Recording of rock salt pattern, 55
Powder pattern power theorem, 262

Precision axial lengths from powder patterns
By diffractometer recording, 70
By film recording, 68
Index of refraction correction, 72
PRINS, J. A., 123, 335

RACHINGER, W. A., 260
Radial distribution function, 120
Reciprocal vectors, definition, 16
Reciprocal lattice, 17
RENNINGER, M., 339, 354
ROBERTS, B. W., 241, 244
Rocking curve, 329
Rotation pattern, simple, 85
Indexing of rotation patterns, 88
Layer line equation, 86
Sphere of reflection construction, 87

Scattering by amorphous samples
Applied to crystalline powder, 119
Approximate method for more than one kind of atom, 132
Exact method for more than one kind of atom, 135
Gas of polyatomic molecules, 117
Sample with one kind of atom, 120
Simple liquid, application, 123
Scattering of x-rays
Classical scattering by a free electron, 1
Phase change of 180°, 8
Scattering factor per electron, 9
SCHERRER, P., 251
Scherrer particle size equation, 253
SCHOMAKER, V., 135
Secular equation, 180
Sharpening factor, 137
SHOCKLEY, W., 206, 208
Short-range order, 227
Cowley SRO parameters, 229
Cowley SRO parameters for Cu_3Au, 236
Effect of temperature vibration on SRO intensities, 237
Experimental measurement of SRO intensities, 245
Laue monotonic scattering, 229
SRO from powder patterns, 229
SRO from single crystals, 232
Size effect in disordered binaries, 241
SNEDDON, I. N., 128
Space group, definition, 95
Hermann-Mauguin notation, 96
Space group Cmcm, 96
Use in determination of Uranium structure, 100
Spacing formulae, 20
Sphere of reflection (Ewald sphere), 19
STOKES, A. R., 254, 258, 264
Straumanis powder camera, 52
Structure factor F, 28
For body-centered lattice, 33
For Bragg reflection, 31
For copper structure, 34
For face-centered lattice, 32
For HCP structure, 34
For rock salt structure, 33
For tungsten structure, 34
For zinc blende structure, 34
Superstructure reflections, 210
SYKES, C., 227
Symmetrical back reflection focusing camera, 53
Symmetrical Laue case, perfect crystal, 339
Borrmann effect, 340, 346
Method of Borie, 340
Polarization of beams, 347

TARASOV, L. P., 124
TDS correction to Bragg peak, 199
Temperature effect on intensity from crystal, 37
TEMPLETON, D. H., 12
Termination satellites, 127
Thomson scattering equation, 4
TOURNARIE, M., 71
Transformation of axes and indices, 24

Unit cell, definition, 15
Unmodified scattering by an atom, 8
Uranium, structure determination, 100

VAN HOVE, L., 188
Vanishings (*see* Structure factor *F*)

WAGNER, C. N. J., 294, 298
WALKER, C. B., 169, 173, 187, 188, 237
WALLER, I., 151
WAREKOIS, E. P., 278, 290
WARREN, B. E., 100, 124, 149, 170, 175, 194, 241, 264, 269, 270, 278, 290, 305
WASER, J., 135
Wavelengths of emission lines and absorption edges, 364
Weissenberg pattern, 89
WHELAN, M. J., 340
WHITE, J. E., 332
WOOSTER, W. A., 176

ZACHARIASEN, W. H., 316, 332
ZERNICKE, F., 123
Zone axis, 76

A CATALOG OF SELECTED

DOVER BOOKS

IN SCIENCE AND MATHEMATICS

Math–Decision Theory, Statistics, Probability

ELEMENTARY DECISION THEORY, Herman Chernoff and Lincoln E. Moses. Clear introduction to statistics and statistical theory covers data processing, probability and random variables, testing hypotheses, much more. Exercises. 364pp. 5⅜ x 8½. 0-486-65218-1

STATISTICS MANUAL, Edwin L. Crow et al. Comprehensive, practical collection of classical and modern methods prepared by U.S. Naval Ordnance Test Station. Stress on use. Basics of statistics assumed. 288pp. 5⅜ x 8½. 0-486-60599-X

SOME THEORY OF SAMPLING, William Edwards Deming. Analysis of the problems, theory and design of sampling techniques for social scientists, industrial managers and others who find statistics important at work. 61 tables. 90 figures. xvii +602pp. 5⅜ x 8½. 0-486-64684-X

LINEAR PROGRAMMING AND ECONOMIC ANALYSIS, Robert Dorfman, Paul A. Samuelson and Robert M. Solow. First comprehensive treatment of linear programming in standard economic analysis. Game theory, modern welfare economics, Leontief input-output, more. 525pp. 5⅜ x 8½. 0-486-65491-5

PROBABILITY: AN INTRODUCTION, Samuel Goldberg. Excellent basic text covers set theory, probability theory for finite sample spaces, binomial theorem, much more. 360 problems. Bibliographies. 322pp. 5⅜ x 8½. 0-486-65252-1

GAMES AND DECISIONS: INTRODUCTION AND CRITICAL SURVEY, R. Duncan Luce and Howard Raiffa. Superb nontechnical introduction to game theory, primarily applied to social sciences. Utility theory, zero-sum games, n-person games, decision-making, much more. Bibliography. 509pp. 5⅜ x 8½. 0-486-65943-7

INTRODUCTION TO THE THEORY OF GAMES, J. C. C. McKinsey. This comprehensive overview of the mathematical theory of games illustrates applications to situations involving conflicts of interest, including economic, social, political, and military contexts. Appropriate for advanced undergraduate and graduate courses; advanced calculus a prerequisite. 1952 ed. x+372pp. 5⅜ x 8½. 0-486-42811-7

FIFTY CHALLENGING PROBLEMS IN PROBABILITY WITH SOLUTIONS, Frederick Mosteller. Remarkable puzzlers, graded in difficulty, illustrate elementary and advanced aspects of probability. Detailed solutions. 88pp. 5⅜ x 8½. 65355-2

PROBABILITY THEORY: A CONCISE COURSE, Y. A. Rozanov. Highly readable, self-contained introduction covers combination of events, dependent events, Bernoulli trials, etc. 148pp. 5⅜ x 8¼. 0-486-63544-9

STATISTICAL METHOD FROM THE VIEWPOINT OF QUALITY CONTROL, Walter A. Shewhart. Important text explains regulation of variables, uses of statistical control to achieve quality control in industry, agriculture, other areas. 192pp. 5⅜ x 8½. 0-486-65232-7

Math–Geometry and Topology

ELEMENTARY CONCEPTS OF TOPOLOGY, Paul Alexandroff. Elegant, intuitive approach to topology from set-theoretic topology to Betti groups; how concepts of topology are useful in math and physics. 25 figures. 57pp. 5⅜ x 8½. 0-486-60747-X

COMBINATORIAL TOPOLOGY, P. S. Alexandrov. Clearly written, well-organized, three-part text begins by dealing with certain classic problems without using the formal techniques of homology theory and advances to the central concept, the Betti groups. Numerous detailed examples. 654pp. 5⅜ x 8½. 0-486-40179-0

EXPERIMENTS IN TOPOLOGY, Stephen Barr. Classic, lively explanation of one of the byways of mathematics. Klein bottles, Moebius strips, projective planes, map coloring, problem of the Koenigsberg bridges, much more, described with clarity and wit. 43 figures. 210pp. 5⅜ x 8½. 0-486-25933-1

THE GEOMETRY OF RENÉ DESCARTES, René Descartes. The great work founded analytical geometry. Original French text, Descartes's own diagrams, together with definitive Smith-Latham translation. 244pp. 5⅜ x 8½. 0-486-60068-8

EUCLIDEAN GEOMETRY AND TRANSFORMATIONS, Clayton W. Dodge. This introduction to Euclidean geometry emphasizes transformations, particularly isometries and similarities. Suitable for undergraduate courses, it includes numerous examples, many with detailed answers. 1972 ed. viii+296pp. 6⅛ x 9¼. 0-486-43476-1

PRACTICAL CONIC SECTIONS: THE GEOMETRIC PROPERTIES OF ELLIPSES, PARABOLAS AND HYPERBOLAS, J. W. Downs. This text shows how to create ellipses, parabolas, and hyperbolas. It also presents historical background on their ancient origins and describes the reflective properties and roles of curves in design applications. 1993 ed. 98 figures. xii+100pp. 6½ x 9¼. 0-486-42876-1

THE THIRTEEN BOOKS OF EUCLID'S ELEMENTS, translated with introduction and commentary by Sir Thomas L. Heath. Definitive edition. Textual and linguistic notes, mathematical analysis. 2,500 years of critical commentary. Unabridged. 1,414pp. 5⅜ x 8½. Three-vol. set.
Vol. I: 0-486-60088-2 Vol. II: 0-486-60089-0 Vol. III: 0-486-60090-4

SPACE AND GEOMETRY: IN THE LIGHT OF PHYSIOLOGICAL, PSYCHOLOGICAL AND PHYSICAL INQUIRY, Ernst Mach. Three essays by an eminent philosopher and scientist explore the nature, origin, and development of our concepts of space, with a distinctness and precision suitable for undergraduate students and other readers. 1906 ed. vi+148pp. 5⅜ x 8½. 0-486-43909-7

GEOMETRY OF COMPLEX NUMBERS, Hans Schwerdtfeger. Illuminating, widely praised book on analytic geometry of circles, the Moebius transformation, and two-dimensional non-Euclidean geometries. 200pp. 5⅜ x 8¼. 0-486-63830-8

DIFFERENTIAL GEOMETRY, Heinrich W. Guggenheimer. Local differential geometry as an application of advanced calculus and linear algebra. Curvature, transformation groups, surfaces, more. Exercises. 62 figures. 378pp. 5⅜ x 8½. 0-486-63433-7

History of Math

THE WORKS OF ARCHIMEDES, Archimedes (T. L. Heath, ed.). Topics include the famous problems of the ratio of the areas of a cylinder and an inscribed sphere; the measurement of a circle; the properties of conoids, spheroids, and spirals; and the quadrature of the parabola. Informative introduction. clxxxvi+326pp. 5⅜ x 8½.
0-486-42084-1

A SHORT ACCOUNT OF THE HISTORY OF MATHEMATICS, W. W. Rouse Ball. One of clearest, most authoritative surveys from the Egyptians and Phoenicians through 19th-century figures such as Grassman, Galois, Riemann. Fourth edition. 522pp. 5⅜ x 8½. 0-486-20630-0

THE HISTORY OF THE CALCULUS AND ITS CONCEPTUAL DEVELOPMENT, Carl B. Boyer. Origins in antiquity, medieval contributions, work of Newton, Leibniz, rigorous formulation. Treatment is verbal. 346pp. 5⅜ x 8½. 0-486-60509-4

THE HISTORICAL ROOTS OF ELEMENTARY MATHEMATICS, Lucas N. H. Bunt, Phillip S. Jones, and Jack D. Bedient. Fundamental underpinnings of modern arithmetic, algebra, geometry and number systems derived from ancient civilizations. 320pp. 5⅜ x 8½. 0-486-25563-8

A HISTORY OF MATHEMATICAL NOTATIONS, Florian Cajori. This classic study notes the first appearance of a mathematical symbol and its origin, the competition it encountered, its spread among writers in different countries, its rise to popularity, its eventual decline or ultimate survival. Original 1929 two-volume edition presented here in one volume. xxviii+820pp. 5⅜ x 8½. 0-486-67766-4

GAMES, GODS & GAMBLING: A HISTORY OF PROBABILITY AND STATISTICAL IDEAS, F. N. David. Episodes from the lives of Galileo, Fermat, Pascal, and others illustrate this fascinating account of the roots of mathematics. Features thought-provoking references to classics, archaeology, biography, poetry. 1962 edition. 304pp. 5⅜ x 8½. (Available in U.S. only.) 0-486-40023-9

OF MEN AND NUMBERS: THE STORY OF THE GREAT MATHEMATICIANS, Jane Muir. Fascinating accounts of the lives and accomplishments of history's greatest mathematical minds–Pythagoras, Descartes, Euler, Pascal, Cantor, many more. Anecdotal, illuminating. 30 diagrams. Bibliography. 256pp. 5⅜ x 8½. 0-486-28973-7

HISTORY OF MATHEMATICS, David E. Smith. Nontechnical survey from ancient Greece and Orient to late 19th century; evolution of arithmetic, geometry, trigonometry, calculating devices, algebra, the calculus. 362 illustrations. 1,355pp. 5⅜ x 8½. Two-vol. set. Vol. I: 0-486-20429-4 Vol. II: 0-486-20430-8

A CONCISE HISTORY OF MATHEMATICS, Dirk J. Struik. The best brief history of mathematics. Stresses origins and covers every major figure from ancient Near East to 19th century. 41 illustrations. 195pp. 5⅜ x 8½. 0-486-60255-9

Physics

OPTICAL RESONANCE AND TWO-LEVEL ATOMS, L. Allen and J. H. Eberly. Clear, comprehensive introduction to basic principles behind all quantum optical resonance phenomena. 53 illustrations. Preface. Index. 256pp. 5⅜ x 8½. 0-486-65533-4

QUANTUM THEORY, David Bohm. This advanced undergraduate-level text presents the quantum theory in terms of qualitative and imaginative concepts, followed by specific applications worked out in mathematical detail. Preface. Index. 655pp. 5⅜ x 8½. 0-486-65969-0

ATOMIC PHYSICS (8th EDITION), Max Born. Nobel laureate's lucid treatment of kinetic theory of gases, elementary particles, nuclear atom, wave-corpuscles, atomic structure and spectral lines, much more. Over 40 appendices, bibliography. 495pp. 5⅜ x 8½. 0-486-65984-4

A SOPHISTICATE'S PRIMER OF RELATIVITY, P. W. Bridgman. Geared toward readers already acquainted with special relativity, this book transcends the view of theory as a working tool to answer natural questions: What is a frame of reference? What is a "law of nature"? What is the role of the "observer"? Extensive treatment, written in terms accessible to those without a scientific background. 1983 ed. xlviii+172pp. 5⅜ x 8½. 0-486-42549-5

AN INTRODUCTION TO HAMILTONIAN OPTICS, H. A. Buchdahl. Detailed account of the Hamiltonian treatment of aberration theory in geometrical optics. Many classes of optical systems defined in terms of the symmetries they possess. Problems with detailed solutions. 1970 edition. xv + 360pp. 5⅜ x 8½. 0-486-67597-1

PRIMER OF QUANTUM MECHANICS, Marvin Chester. Introductory text examines the classical quantum bead on a track: its state and representations; operator eigenvalues; harmonic oscillator and bound bead in a symmetric force field; and bead in a spherical shell. Other topics include spin, matrices, and the structure of quantum mechanics; the simplest atom; indistinguishable particles; and stationary-state perturbation theory. 1992 ed. xiv+314pp. 6⅛ x 9¼. 0-486-42878-8

LECTURES ON QUANTUM MECHANICS, Paul A. M. Dirac. Four concise, brilliant lectures on mathematical methods in quantum mechanics from Nobel Prize-winning quantum pioneer build on idea of visualizing quantum theory through the use of classical mechanics. 96pp. 5⅜ x 8½. 0-486-41713-1

THIRTY YEARS THAT SHOOK PHYSICS: THE STORY OF QUANTUM THEORY, George Gamow. Lucid, accessible introduction to influential theory of energy and matter. Careful explanations of Dirac's anti-particles, Bohr's model of the atom, much more. 12 plates. Numerous drawings. 240pp. 5⅜ x 8½. 0-486-24895-X

ELECTRONIC STRUCTURE AND THE PROPERTIES OF SOLIDS: THE PHYSICS OF THE CHEMICAL BOND, Walter A. Harrison. Innovative text offers basic understanding of the electronic structure of covalent and ionic solids, simple metals, transition metals and their compounds. Problems. 1980 edition. 582pp. 6⅛ x 9¼. 0-486-66021-4

HYDRODYNAMIC AND HYDROMAGNETIC STABILITY, S. Chandrasekhar. Lucid examination of the Rayleigh-Benard problem; clear coverage of the theory of instabilities causing convection. 704pp. 5⅜ x 8¼. 0-486-64071-X

INVESTIGATIONS ON THE THEORY OF THE BROWNIAN MOVEMENT, Albert Einstein. Five papers (1905–8) investigating dynamics of Brownian motion and evolving elementary theory. Notes by R. Fürth. 122pp. 5⅜ x 8½. 0-486-60304-0

THE PHYSICS OF WAVES, William C. Elmore and Mark A. Heald. Unique overview of classical wave theory. Acoustics, optics, electromagnetic radiation, more. Ideal as classroom text or for self-study. Problems. 477pp. 5⅜ x 8½. 0-486-64926-1

GRAVITY, George Gamow. Distinguished physicist and teacher takes reader-friendly look at three scientists whose work unlocked many of the mysteries behind the laws of physics: Galileo, Newton, and Einstein. Most of the book focuses on Newton's ideas, with a concluding chapter on post-Einsteinian speculations concerning the relationship between gravity and other physical phenomena. 160pp. 5⅜ x 8½. 0-486-42563-0

PHYSICAL PRINCIPLES OF THE QUANTUM THEORY, Werner Heisenberg. Nobel Laureate discusses quantum theory, uncertainty, wave mechanics, work of Dirac, Schroedinger, Compton, Wilson, Einstein, etc. 184pp. 5⅜ x 8½. 0-486-60113-7

ATOMIC SPECTRA AND ATOMIC STRUCTURE, Gerhard Herzberg. One of best introductions; especially for specialist in other fields. Treatment is physical rather than mathematical. 80 illustrations. 257pp. 5⅜ x 8½. 0-486-60115-3

AN INTRODUCTION TO STATISTICAL THERMODYNAMICS, Terrell L. Hill. Excellent basic text offers wide-ranging coverage of quantum statistical mechanics, systems of interacting molecules, quantum statistics, more. 523pp. 5⅜ x 8½. 0-486-65242-4

THEORETICAL PHYSICS, Georg Joos, with Ira M. Freeman. Classic overview covers essential math, mechanics, electromagnetic theory, thermodynamics, quantum mechanics, nuclear physics, other topics. First paperback edition. xxiii + 885pp. 5⅜ x 8½. 0-486-65227-0

PROBLEMS AND SOLUTIONS IN QUANTUM CHEMISTRY AND PHYSICS, Charles S. Johnson, Jr. and Lee G. Pedersen. Unusually varied problems, detailed solutions in coverage of quantum mechanics, wave mechanics, angular momentum, molecular spectroscopy, more. 280 problems plus 139 supplementary exercises. 430pp. 6½ x 9¼. 0-486-65236-X

THEORETICAL SOLID STATE PHYSICS, Vol. 1: Perfect Lattices in Equilibrium; Vol. II: Non-Equilibrium and Disorder, William Jones and Norman H. March. Monumental reference work covers fundamental theory of equilibrium properties of perfect crystalline solids, non-equilibrium properties, defects and disordered systems. Appendices. Problems. Preface. Diagrams. Index. Bibliography. Total of 1,301pp. 5⅜ x 8½. Two volumes. Vol. I: 0-486-65015-4 Vol. II: 0-486-65016-2

WHAT IS RELATIVITY? L. D. Landau and G. B. Rumer. Written by a Nobel Prize physicist and his distinguished colleague, this compelling book explains the special theory of relativity to readers with no scientific background, using such familiar objects as trains, rulers, and clocks. 1960 ed. vi+72pp. 5⅜ x 8½. 0-486-42806-0

A TREATISE ON ELECTRICITY AND MAGNETISM, James Clerk Maxwell. Important foundation work of modern physics. Brings to final form Maxwell's theory of electromagnetism and rigorously derives his general equations of field theory. 1,084pp. 5⅜ x 8½. Two-vol. set. Vol. I: 0-486-60636-8 Vol. II: 0-486-60637-6

QUANTUM MECHANICS: PRINCIPLES AND FORMALISM, Roy McWeeny. Graduate student-oriented volume develops subject as fundamental discipline, opening with review of origins of Schrödinger's equations and vector spaces. Focusing on main principles of quantum mechanics and their immediate consequences, it concludes with final generalizations covering alternative "languages" or representations. 1972 ed. 15 figures. xi+155pp. 5⅜ x 8½. 0-486-42829-X

INTRODUCTION TO QUANTUM MECHANICS With Applications to Chemistry, Linus Pauling & E. Bright Wilson, Jr. Classic undergraduate text by Nobel Prize winner applies quantum mechanics to chemical and physical problems. Numerous tables and figures enhance the text. Chapter bibliographies. Appendices. Index. 468pp. 5⅜ x 8½. 0-486-64871-0

METHODS OF THERMODYNAMICS, Howard Reiss. Outstanding text focuses on physical technique of thermodynamics, typical problem areas of understanding, and significance and use of thermodynamic potential. 1965 edition. 238pp. 5⅜ x 8½. 0-486-69445-3

THE ELECTROMAGNETIC FIELD, Albert Shadowitz. Comprehensive undergraduate text covers basics of electric and magnetic fields, builds up to electromagnetic theory. Also related topics, including relativity. Over 900 problems. 768pp. 5⅜ x 8¼. 0-486-65660-8

GREAT EXPERIMENTS IN PHYSICS: FIRSTHAND ACCOUNTS FROM GALILEO TO EINSTEIN, Morris H. Shamos (ed.). 25 crucial discoveries: Newton's laws of motion, Chadwick's study of the neutron, Hertz on electromagnetic waves, more. Original accounts clearly annotated. 370pp. 5⅜ x 8½. 0-486-25346-5

EINSTEIN'S LEGACY, Julian Schwinger. A Nobel Laureate relates fascinating story of Einstein and development of relativity theory in well-illustrated, nontechnical volume. Subjects include meaning of time, paradoxes of space travel, gravity and its effect on light, non-Euclidean geometry and curving of space-time, impact of radio astronomy and space-age discoveries, and more. 189 b/w illustrations. xiv+250pp. 8⅜ x 9¼. 0-486-41974-6

STATISTICAL PHYSICS, Gregory H. Wannier. Classic text combines thermodynamics, statistical mechanics and kinetic theory in one unified presentation of thermal physics. Problems with solutions. Bibliography. 532pp. 5⅜ x 8½. 0-486-65401-X

Paperbound unless otherwise indicated. Available at your book dealer, online at **www.doverpublications.com**, or by writing to Dept. GI, Dover Publications, Inc., 31 East 2nd Street, Mineola, NY 11501. For current price information or for free catalogues (please indicate field of interest), write to Dover Publications or log on to **www.doverpublications.com** and see every Dover book in print. Dover publishes more than 500 books each year on science, elementary and advanced mathematics, biology, music, art, literary history, social sciences, and other areas.

(continued from front flap)

INTRODUCTION TO QUANTUM MECHANICS WITH APPLICATIONS TO CHEMISTRY, Linus Pauling and E. Bright Wilson, Jr. (64871-0)

SURVEY OF PHYSICAL THEORY, Max Planck. (67867-9)

THE PHILOSOPHY OF SPACE AND TIME, Hans Reichenbach. (60443-8)

BOUNDARY AND EIGENVALUE PROBLEMS IN MATHEMATICAL PHYSICS, Hans Sagan. (66132-6)

STATISTICAL THERMODYNAMICS, Erwin Schrodinger. (66101-6)

PRINCIPLES OF ELECTRODYNAMICS, Melvin Schwartz. (65493-1)

ELECTROMAGNETIC FIELD, Albert Shadowitz. (65660-8)

PARTIAL DIFFERENTIAL EQUATIONS OF MATHEMATICAL PHYSICS, S.L. Sobolev. (65964-X)

PRINCIPLES OF STATISTICAL MECHANICS, Richard C. Tolman. (63896-0)

LIGHT SCATTERING BY SMALL PARTICLES, H.C. van de Hulst. (64228-3)

UNDERSTANDING THERMODYNAMICS, H.C. Van Ness. (63277-6)

MATHEMATICAL ANALYSIS OF PHYSICAL PROBLEMS, Philip R. Wallace. (64676-9)

STATISTICAL PHYSICS, Gregory H. Wannier. (65401-X)

X-RAY DIFFRACTION, B.E. Warren. (66317-5)

SPACE—TIME—MATTER, Hermann Weyl. (60267-2)

Paperbound unless otherwise indicated. Available at your book dealer, online at **www.doverpublications.com**, or by writing to Dept. 23, Dover Publications, Inc., 31 East 2nd Street, Mineola, NY 11501. For current price information or for free catalogs (please indicate field of interest), write to Dover Publications or log on to **www.doverpublications.com** and see every Dover book in print. Each year Dover publishes over 500 books on fine art, music, crafts and needlework, antiques, languages, literature, children's books, chess, cookery, nature, anthropology, science, mathematics, and other areas.

Manufactured in the U.S.A.

X-RAY DIFFRACTION

B.E. Warren

Basic diffraction theory has numerous important applications in solid-state physics and physical metallurgy, and this graduate-level text is the ideal introduction to the fundamentals of the discipline. Development is rigorous (throughout the book, the treatment is carried far enough to relate to experimentally observable quantities) and stress is placed on modern applications to nonstructural problems such as temperature vibration effects, order-disorder phenomena, crystal imperfections, the structure of amorphous materials, and the diffraction of x-rays in perfect crystals.

Contents include: X-Ray Scattering by Atoms * Crystal Axes and the Reciprocal Lattice * Diffraction by a Small Crystal * The Integrated Intensity * The Powder Method * The Laue Method * The Rotation Method * The Use of Space Groups in Structure Determination * Fourier Series Methods in Structure Determinations * Scattering by Noncrystalline Forms of Matter * The Effect of Temperature Vibration on X-Ray Diffraction * X-Ray Studies of Order-Disorder * Diffraction by Imperfect Crystals * Perfect Crystal Theory

Carefully selected problems have been included at the end of each chapter to help the student test his grasp of the material. Professor Warren, a recognized authority on the use of x-rays to probe the structure of matter, is Professor Emeritus of Physics, Massachusetts Institute of Technology.

Unabridged, corrected Dover (1990) republication of the edition published by Addison-Wesley Publishing Company, Inc., Reading, Mass., 1969. Preface. Problems. Six Appendixes (including tables of values). Bibliographies. 146 black-and-white illustrations. x + 381pp. 5⅜ × 8½. Paperbound.

ALSO AVAILABLE

DIFFUSE X-RAY REFLECTIOINS FROM CRYSTALS, W. A. Wooster. 212pp. 5⅜ x 8½. 69641-3

THEORETICAL SOLID STATE PHYSICS, VOL. I: PERFECT LATTICES IN EQUILIBRIUM: VOL. II: NON-EQUILIBRIUM AND DISORDER, William Jones and Norman H. March. Total of 1301pp. 5⅜ x 8½. 65015-4 65016-2

See every Dover book in print at
www.doverpublications.com

ISBN 0-486-66317-5

51895

9 780486 663173

$18.95 IN USA
$28.50 IN CANADA

Cover design by Paul E. Kennedy